# Spallation Neutron Source (SNS) Front End and Linac Course

*Abstract:* This is a course presented at the US Particle Accelerator School in Madison, Wisconsin, June 21-25, 2004, titled "Spallation Neutron Source (SNS) Front End and Linac". The course was comprised of 14 lectures. The lecturers were Thomas P. Wangler, LANL, James Billen, LANL, and Roderich Keller, LBNL.

June 2, 2004

Dear student,

In this e-mail we are attaching the preliminary material for the USPAS course "SNS Front End and Linac" in Madison, June 21-25, 2004. The assignments before class begins are indicated in red.

For an overview of the SNS, **please read the paper "Status of the Spallation Neutron Source" by Norbert Holtkamp,** presented at the 2003 Particle Accelerator Conference to be found at http://accelconf.web.cern.ch/accelconf/p03/PAPERS/MOAL003.PDF. This is not really up to date in terms of the present status, but is the most recent overview paper I could find.

Additional publications and information on SNS may be found at http://www.sns.gov/documentation/pubs.htm.

A detailed parameter list for the SNS may be found at http://www.sns.gov/documentation/100000000-PL0001-R11.pdf. I recommend printing this. It will probably be useful during our course.

Attached is Chapter 1 of the textbook "RF Linear Accelerators". The complete textbook will be distributed at the first class period. Sections 1.1 through 1.5 constitute a brief overview of the linear accelerator field. Sections 1.6 through 1.14 covers some basic introductory material for the course.

Notice the problems at the end of Chapter 1**. The first homework assignment consists of the four problems, 1-1, 1-7, 1-8, and 1-9. After reading the appropriate Chapter 1 material, please look these problems over and try your best to work them before the first class,** since this material is fundamental to the course. We will be collecting the problems and they will be counted as part of the homework.

We look forward to seeing you in Madison.

Tom Wangler, Jim Billen, and Roderich Keller

# US Particle Accelerator School

## *The SNS-1 – Front End and Linac*

# The SNS Front End (Linac Injector)

## Rod Keller

Senior Team Leader, Front-End Systems
for the Spallation Neutron Source (SNS)

E. O. Lawrence Berkeley National Laboratory

**Madison, WI, June 21, 2004**

# Spallation Neutron Source (SNS)



Front End

- Accelerator based, pulsed-beam neutron source
- Being built at Oak Ridge, TN, for the US Dept. of Energy by **a collaboration of six US laboratories**
- 1.4 MW average proton-beam power
- $ 1.4 B total project cost
- 7+ years construction

| | |
|---|---|
| **H$^-$ Linac injector (front end) with 2.5-MeV RFQ** | **LBNL** |
| 1 GeV Linear Accelerator (Linac) | LANL |
|    ■ Superconducting cavities for Linac | TJNAF |
| Proton Storage Ring and Beam Transfer Lines | BNL |
| Liquid-mercury Spallation Target and Conv. Facilities | ORNL |
| 5 Experimental Stations | ANL/ORNL |

# SNS Front End (FE)

## Ancillary Systems

## Beamline Elements

Instrumentation racks   RF waveguide   IS/LEBT HV enclosure
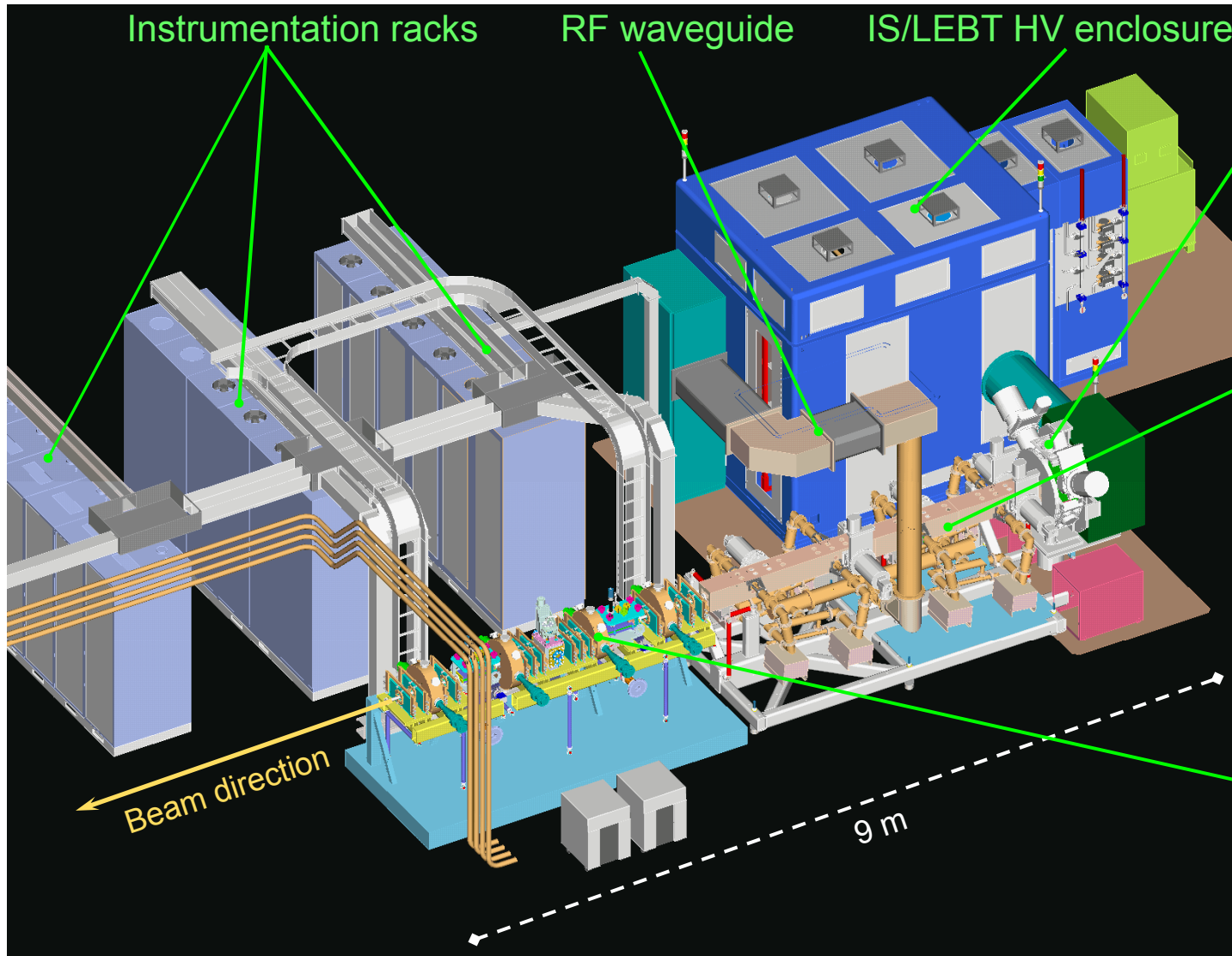
**Ion Source (IS) and Low-Energy Beam Transport (LEBT)**

Create ~50 mA pulsed H- ion beam 1 ms - 60 Hz

**Radio-Frequency Quadrupole (RFQ) accelerator**

Accelerate beam to 2.5 MeV

**LEBT/ MEBT**

Chop beam into 650 ns mini pulses

**Medium-Energy Beam transport (MEBT)**

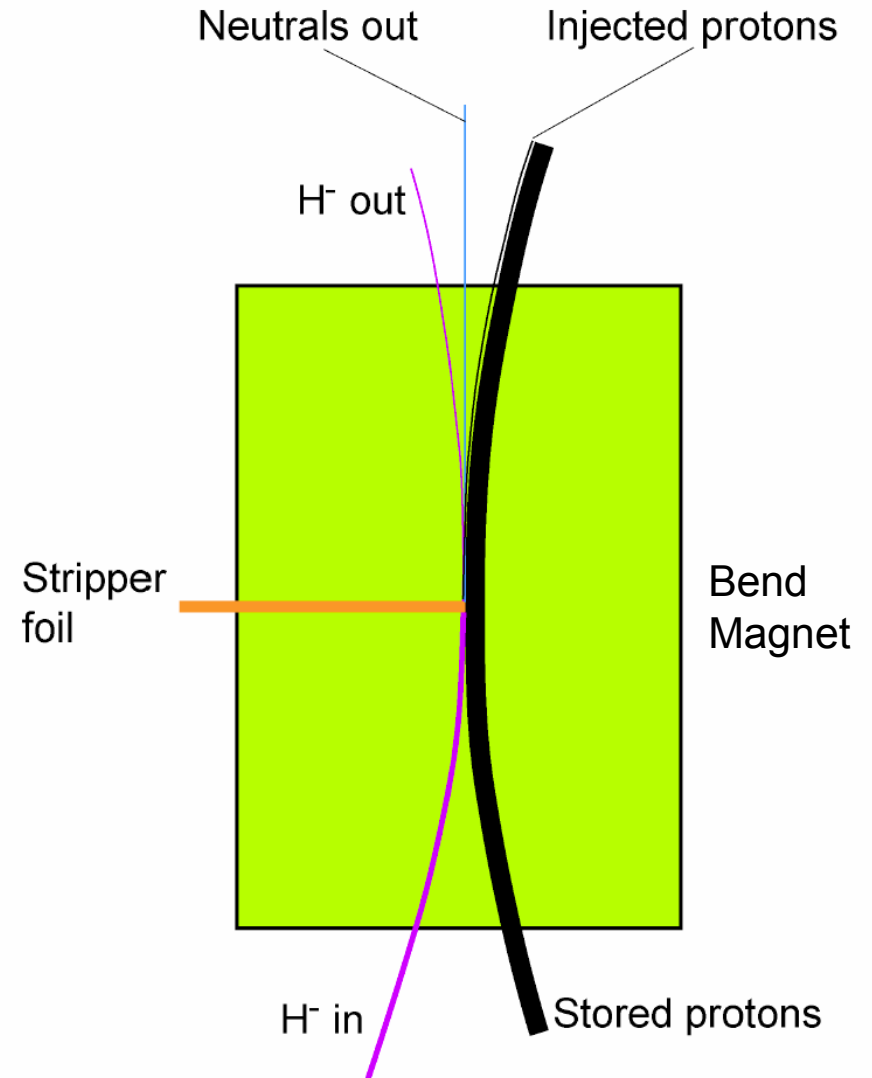Match 38 mA beam into Linac

Beam direction

9 m

# SNS Front End
## Nominal Performance Parameters

| | |
|---|---|
| Ion species | H$^-$ |
| **MEBT output energy (keV)** | **2500** |
| *LEBT output energy (keV)* | *65* |
| H$^-$ pulse current | |
| **MEBT output (mA)** | **38** |
| *Nominal ion-source output (mA),* assuming 80% RFQ transmission | *50* |
| Output normalized transverse rms emittance ($\pi$ mm mrad) | 0.27 |
| *Output longitudinal rms emittance ($\pi$ MeV deg) at 402.5 MHz* | *0.126* |
| Macro pulse length (ms) | 1 |
| Duty factor (%) | 6 |
| Repetition rate (Hz) | 60 |
| *1.06-MHz mini-pulse chopper system:* | |
| *LEBT rise, fall time (ns)* | *50* |
| *MEBT rise, fall time (ns)* | *10* |
| *Off/on beam-current ratio* | *$10^{-4}$* |
| Time of nominal operation between ion-source services (days) | 21 |

- ❑ H⁻ ion source proper (plasma generator)
  - ▪ Negative ions are needed to facilitate injection into the storage ring utilizing the charge-exchange process
    - Charge-exchange rates for protons to neutral atoms or back to H⁻ are very low at 1-GeV energy
  - ▪ Production of negative ions is much more difficult than that of positive ions
    - Cross sections for formation are low
    - Loss mechanisms are strong
    - Requires substantial power density in ion-source discharge
      - ▪ Reduces ion source lifetime
  - ▪ Two main processes of H- production
    - Surface production (about 90%)
    - Volume production (10% or less)

Neutrals out     Injected protons

H⁻ out

Stripper foil     Bend Magnet

H⁻ in     Stored protons

**Principle of Charge-Exchange Injection**

- ❑ Key features of plasma generator
  - ▪ Two-chamber discharge vessel
  - ▪ Discharge in main chamber is sustained by pulsed 2-MHz rf and confined by multi-cusp magnet array
    - • Power delivered by internal porcelain-coated copper antenna
      - ▪ About 1 kW rf power needed for 1 mA of H⁻ beam
    - • Auxiliary, low-power, c.w. 13.56-MHz rf maintains low-density plasma and facilitates ignition of main discharge pulses
      - ▪ 2-frequency rf allows optimizing the main discharge parameters for H⁻ production
  - ▪ Magnetic dipole filter keeps high-energy electrons from entering the second discharge chamber where H⁻ ions are being produced
    - • Low-energy electrons are needed to produce H⁻ ions via vibrationally excited molecules
    - • High-energy electrons and neutral hydrogen atoms destroy H⁻ ions
  - ▪ H⁻ production chamber ("cesium collar") is coated with a thin layer of cesium atoms
    - • Collar can be externally heated and/or plasma-heated
    - • Cesium is contained in the form of cesium chromate in stainless-steel 'getter wires'
    - • About 1/2 monolayer is optimal
    - • Coating has to be replenished after about 8 hrs
    - • Sputtered porcelain from antenna coating condenses on source surfaces and deteriorates the H⁻ production rate over days of operation
  - ▪ H⁻ output current is about 3 times higher with optimal cesium coating than without cesium
    - ⟶ **Surface production is the dominant generation process**
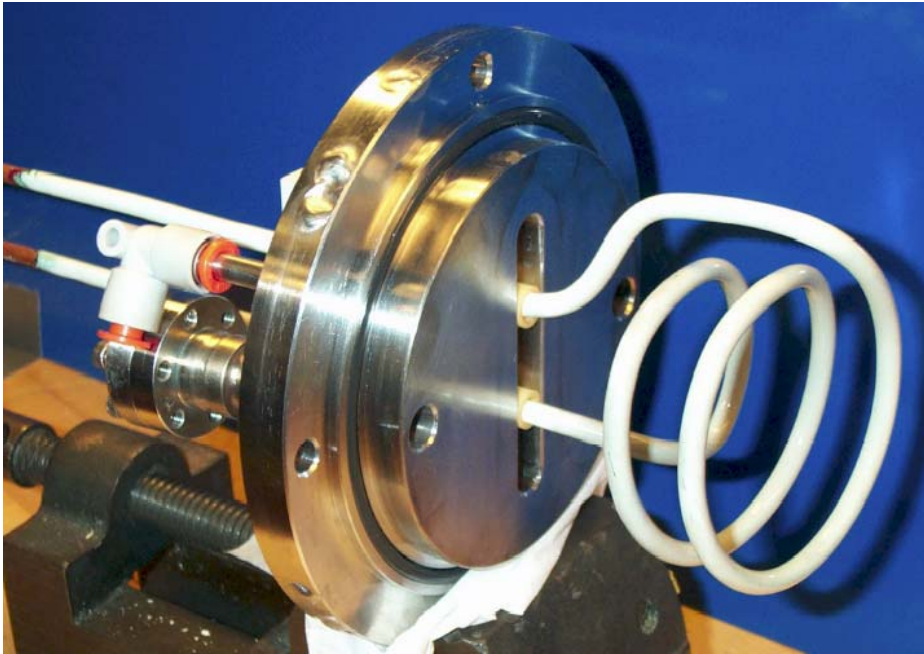  - ▪ Free 'survival' path length for H⁻ ions inside the collar is a few mm

# LEBT Tank, Ion Source, and RF Matcher
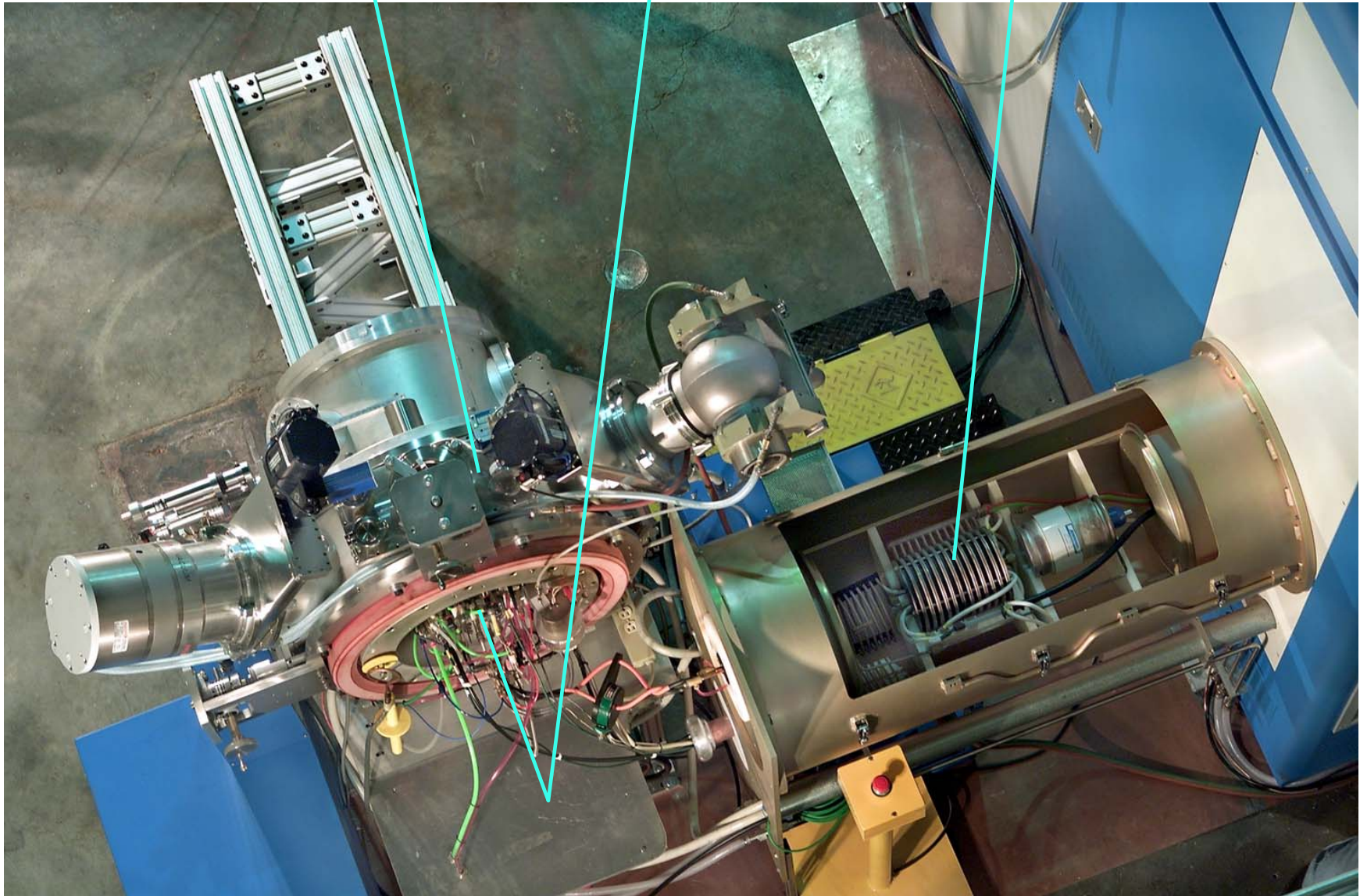
# Plasma Production in Ion Source
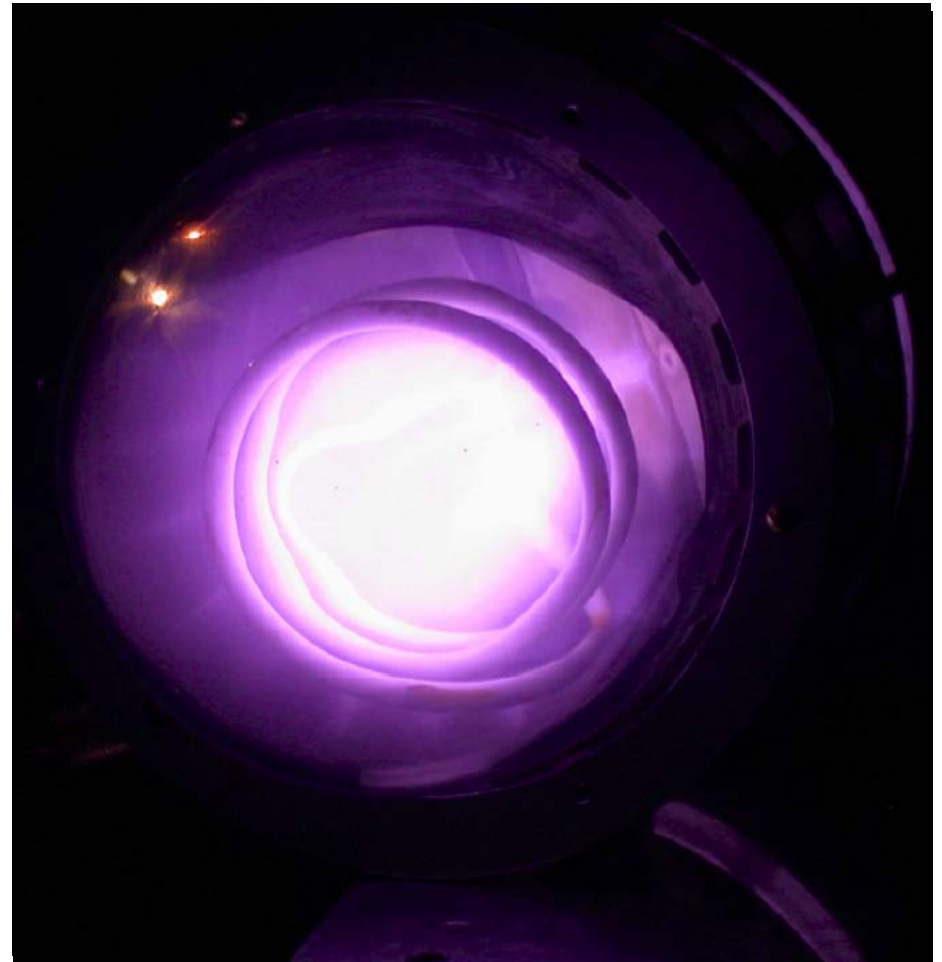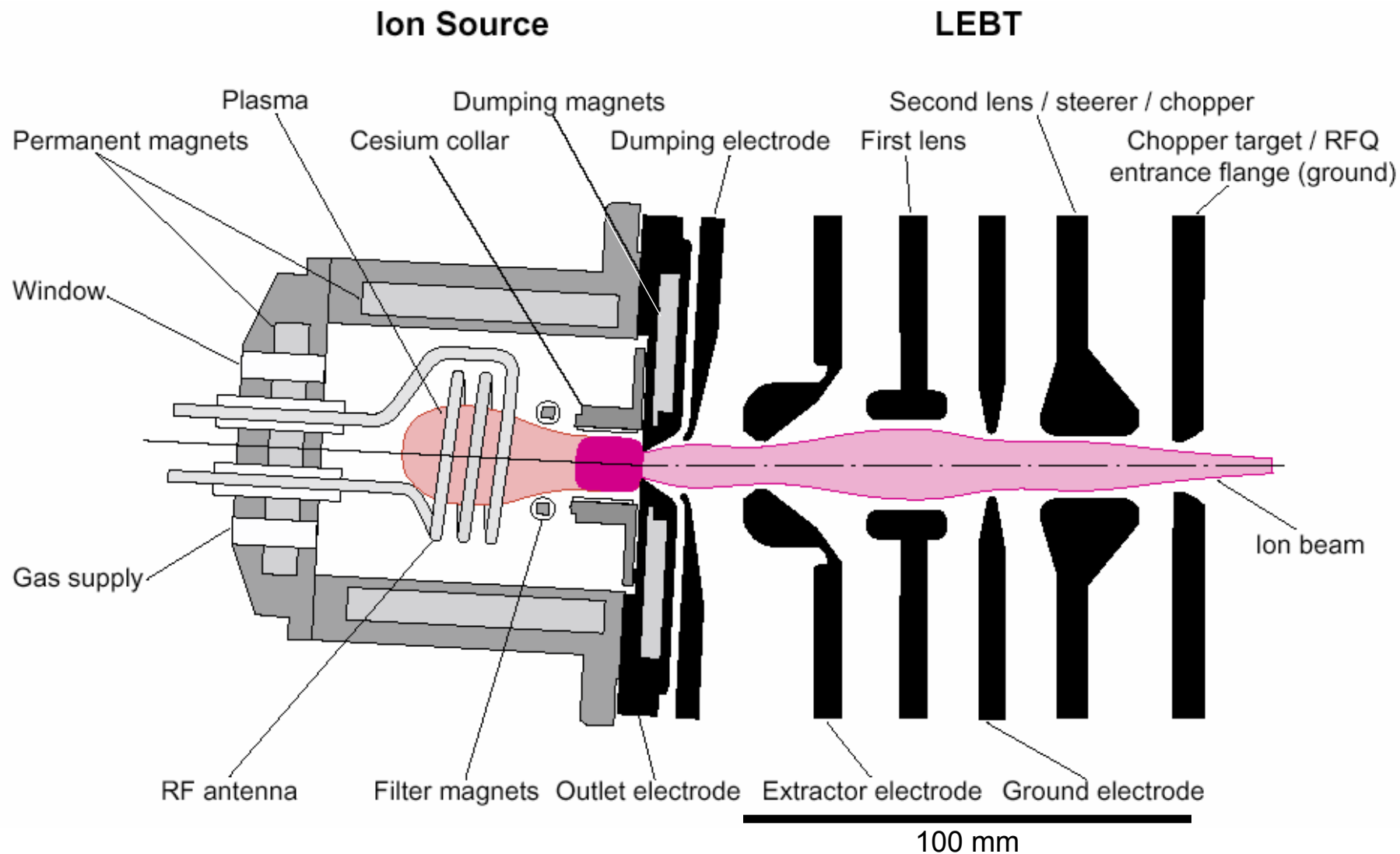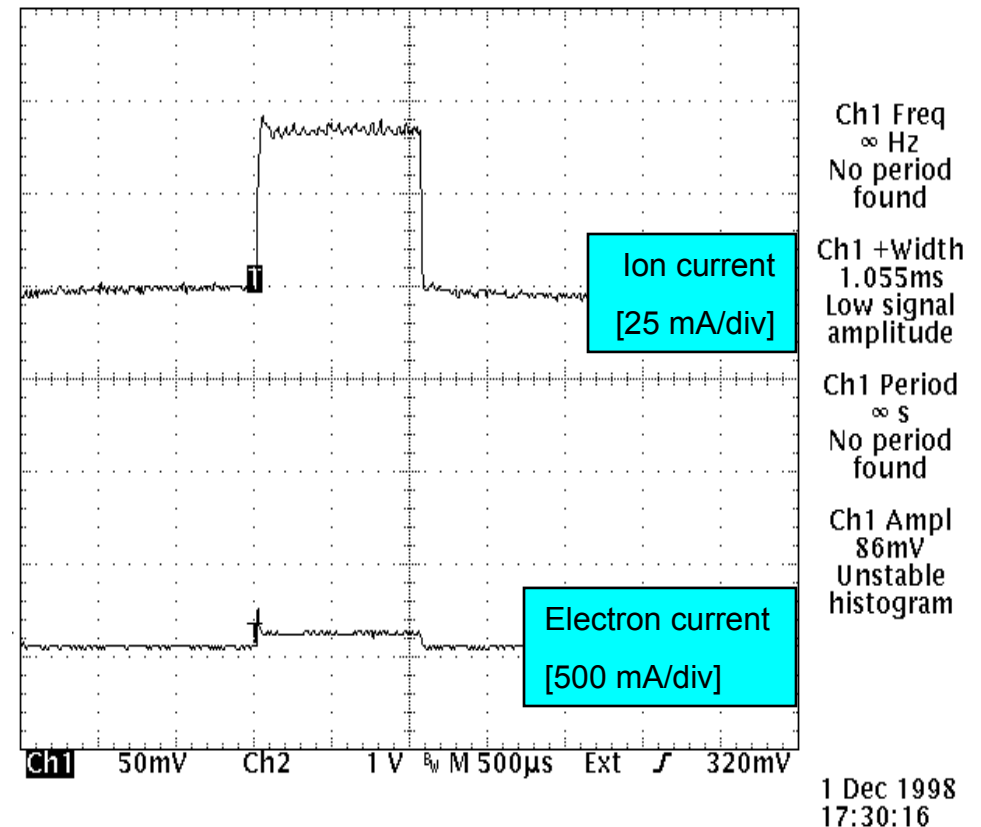


RF antenna

RF-sustained plasma

# Ion Source and LEBT Layout



Beam outline is schematic only (see simulation on P. 18.) Filter- and dumping-magnet fields are orthogonal to the illustration plane and anti-parallel to each other.

# Beam Formation (1)

- High voltage (65 kV) applied between the outlet electrode of the plasma generator and the extractor electrode
- Positive ions are pushed back into the ion-source plasma
- H⁻ ions (desired) and electrons (parasitic) are extracted from the ion source plasma
  - With well-cesiated surfaces, about 2 times more electrons than ions
  - Electron removal from beam by magnetic dipole field
    - Most electrons deposited at low energy inside 'dumping electrode'
    - Some electrons still reach the extractor electrode
  - Additional electron space-charge in the extraction gap adversely affects beam quality
- Up to 70 mA H⁻ beam current measured in peak of pulse signal
  - Using two-chamber Faraday cup with electron deflector
  - Conducted helium test



Ch1 Freq ∞ Hz No period found

Ch1 +Width 1.055ms Low signal amplitude

Ch1 Period ∞ s No period found

Ch1 Ampl 86mV Unstable histogram

Ion current [25 mA/div]

Electron current [500 mA/div]

Ch1   50mV   Ch2   1 V   M 500µs   Ext   320mV

1 Dec 1998 17:30:16

**Demonstration of 43 mA H- current in presence of 90 mA electron current**

# Beam Formation (2)

- Balance between plasma pressure and extraction field strength leads to 'matched beam' conditions
  - Boundary layer between plasma and beam is planar or only slightly curved
    - Radius of curvature much larger than extraction gap-width
  - Divergence half-angle of the beam after leaving the extraction system is of the order of 20 mrad
- Matched beams in space-charge limited conditions tend to follow a modified Child/Langmuir law

$$I_{beam} = const. \times \frac{\sqrt{q/_A}\, U^{3/2}}{d^2}$$

  where the constant is mostly determined by the outlet aperture area and the allowed divergence angle
- To avoid severe distortions of the emittance shape, the aspect ratio of the extraction gap (S=r/d) is practically limited to S ≤ 1
  - H⁻ beam formation is further affected by the space charge of extracted electrons; in the case of the SNS Front End, this space charge is asymmetrically distributed in the extraction gap
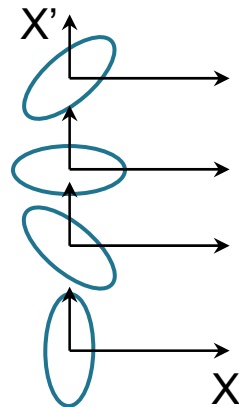
# Emittance for Beginners

❑ Beam quality (or rather its opposite, the degree of non-laminarity) is characterized by the **emittance** of any two-dimensional particle distribution {x/x'}, {y/y'} (transverse) or {E/$\phi$} (longitudinal) in a given plane orthogonal to the beam axis

- ▪ Transverse emittances quantify the geometrical beam properties
  - • Sharpness of focus or resolution of image
  - • Spread of trajectory angles
  - • Amount of halo
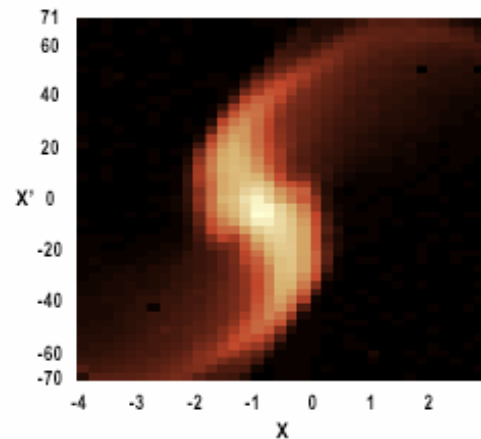  - • Effects of aberrations of the of beam-optical elements

❑ Main emittance properties

- ▪ Size
- ▪ General orientation

    - • Diverging
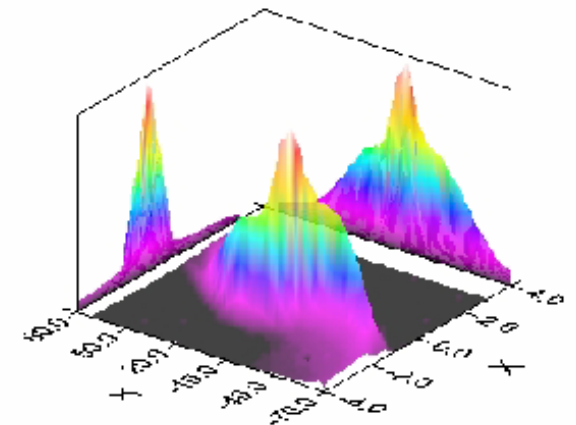    - • Parallel
    - • Converging
    - • Focused



**Beam Parameters:**

| | | |
|---|---|---|
| Current = | 50.00 | mA |
| Energy = | 65.00 | keV |
| M/Q = | 1.00 | |

- ▪ Shape
  - • Degree of contortion

# Emittance Size

- ❑ Effective emittance
  - ▪ Only the area actually covered by beam particles
  - ▪ How fine is the resolution?
- ❑ Encompassing emittance
  - ▪ Which geometrical shape to choose?
- ❑ RMS size
  - ▪ See expressions on P. 15

X'

X

- ❑ The effective emittance of a beam does not decrease during its transport unless the beam is accelerated or particles are lost
- ❑ The effective, normalized emittance of an accelerated beam does not decrease unless particles are lost
- ❑ Beam-optical elements allow to trade off beam diameter vs. divergence angle
  - ▪ Rotation or shearing of emittance shape
  - ▪ Effective size is conserved (at best!)
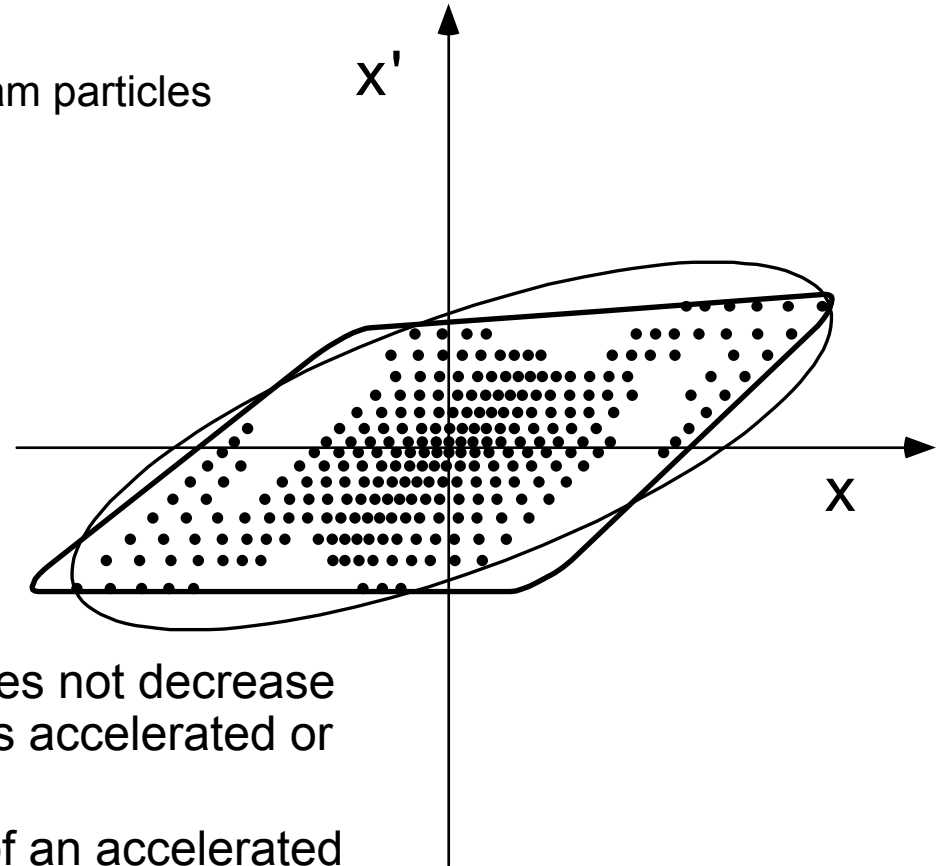
# Representation of Emittances by Encompassing Ellipses

- ❑ Ellipse equations
    - "Analytical" parameters

$$x' = \pm \frac{B}{A} \sqrt{A^2 - B^2} + Cx$$

    - Twiss parameters

$$\gamma\, x^2 + 2\alpha\, x\, x' + \beta\, x'^2 = \varepsilon$$

$$with \quad \beta\gamma - \alpha^2 = 1 \quad and \quad \beta,\, \gamma \geq 0$$

# Representation of Emittances by RMS Ellipse Quantities

RMS size

$$\varepsilon_{rms} = \left( \langle x_i^2 \rangle \langle x_i'^2 \rangle - \langle x_i \, x_i' \rangle^2 \right)^{1/2}$$

Typically, an rms ellipse encompasses about 40% of the entire distribution

RMS shape (Twiss) parameters

$$\beta = \langle x_i^2 \rangle / \varepsilon \qquad \gamma = \langle x_i'^2 \rangle / \varepsilon \qquad \alpha = - \langle x_i \, x_i' \rangle / \varepsilon$$

4 RMS size

$$\varepsilon_{4rms} = 4 \, \varepsilon_{rms}$$

The emittance size as defined here represents the product A x B of the main ellipse half-axes.

However, it is also very common, to refer to the **ellipse area** as the emittance size.
For clarification, the factor $\pi$ is often inserted before the dimension, e. g. [ $\pi$ mm mrad ], to indicate that the given numerical value for the size represents the half-axes product.

# Emittance Formulae

- Normalized emittance  $\varepsilon_n = \beta_{rel}\,\gamma_{rel}\,\varepsilon_{abs}$  ( = const. in 'normal' cases)

- Relativistic parameters $\beta_{rel}$, $\gamma_{rel}$  – no relation to Twiss parameters $\alpha$, $\beta$, $\gamma$ ! –

  - Ion beams  $\beta_{rel} = v/c = 1.460\ 10^{-3}\ (\zeta U_{kV}/\ A)^{1/2}$

  - Relativistic electron beams  $\gamma_{rel} = 1.9558\ U_{MV}$

- Lower limit to emittance due to ion temperature

  - Round aperture  $\varepsilon_{rms} = 0.0653\ r\ (kT/A)^{1/2}$  [mm mrad ]
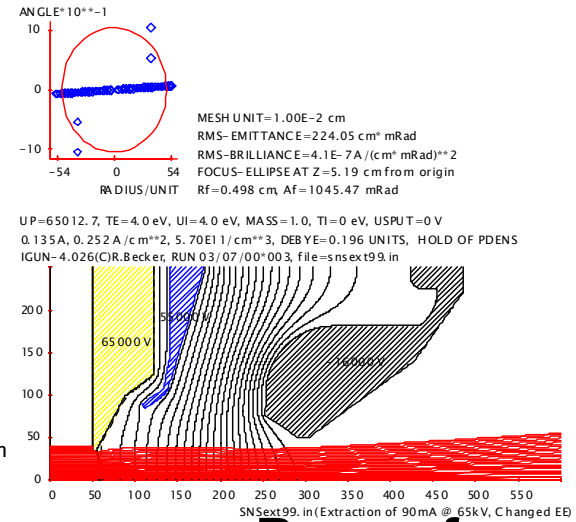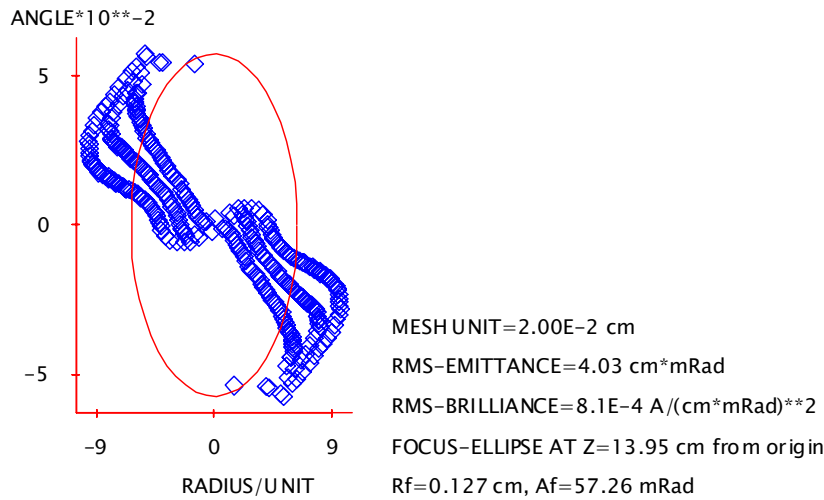  - Slit  $\varepsilon_{rms} = 0.0377\ s\ (kT/A)^{1/2}$  [mm mrad ]

# LEBT (Low-Energy Beam Transport) Design
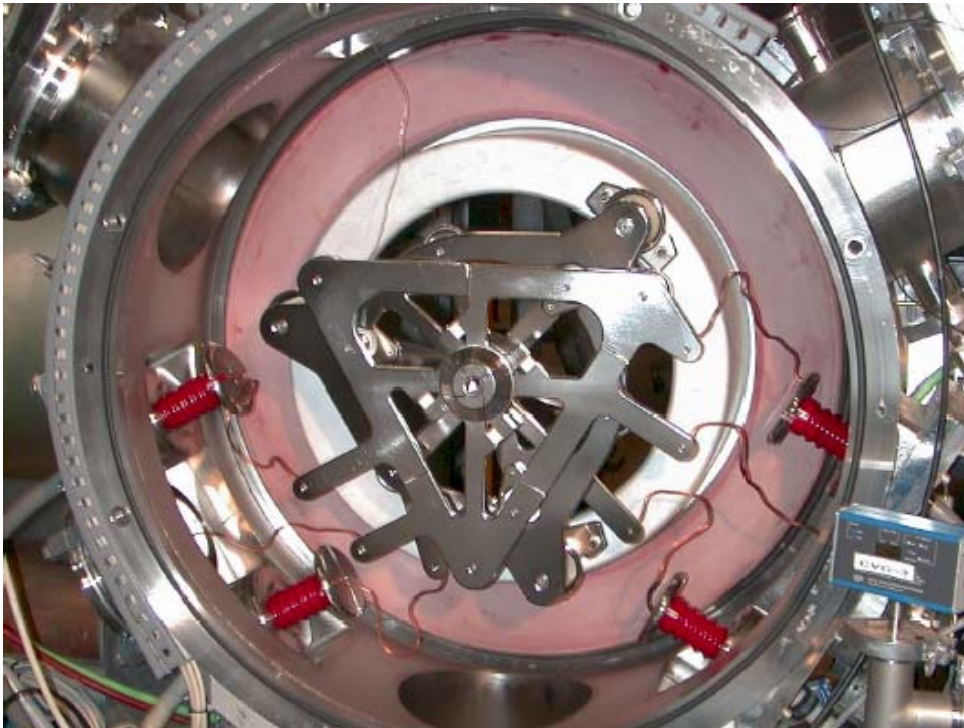


*View of LEBT from downstream side*

- ❑ All-electrostatic design with two einzel lenses
  - ▪ Eliminates time variations of space-charge compensation
- ❑ Second einzel lens is split into four quadrants
  - ▪ Electrostatic steering
  - ▪ Pre-chopping
- ❑ Ion source and LEBT can be mechanically shifted with respect to RFQ axis
  - ▪ Facilitates two-parameter steering
- ❑ Last LEBT ground electrode (not shown in this picture) coincides with RFQ entrance wall
  - ▪ Integrated chopper target/current detector
- ❑ Highly 'transparent' electrode-support structure enhances effective pumping speed

# LEBT Beam Simulation

ANGLE*10**−2



MESH UNIT=2.00E−2 cm

RMS−EMITTANCE=4.03 cm*mRad

RMS−BRILLIANCE=8.1E−4 A/(cm*mRad)**2

FOCUS−ELLIPSE AT Z=13.95 cm from origin

Rf=0.127 cm, Af=57.26 mRad

RADIUS/UNIT

ANGLE*10**−1



MESH UNIT=1.00E−2 cm
RMS−EMITTANCE=224.05 cm* mRad
RMS−BRILLIANCE=4.1E−7 A/(cm* mRad)**2
FOCUS−ELLIPSE AT Z=5.19 cm from origin
Rf=0.498 cm, Af=1045.47 mRad

RADIUS/UNIT

UP=65012. 7, TE=4.0 eV, UI=4.0 eV, MASS=1.0, TI=0 eV, USPUT=0 V
0.135A, 0.252 A/cm**2, 5. 70E11/cm**3, DEBYE=0.196 UNITS,  HOLD OF PDENS
IGUN−4.026(C)R.Becker, RUN 03/07/00*003, file=snsext99.in

65000 V

SNSext99. in(Extraction of 90mA @ 65kV, Changed EE)

## Emittance at LEBT exit

## Beam formation

6.50E−2 A, 10.000 A/cm**2, 0/cm**3, DEBYE=0 UNITS,  TRACE IONS

IGUN−4.026(C)R.Becker, RUN 03/07/00*020, file=snslb79k.in



−10000 V
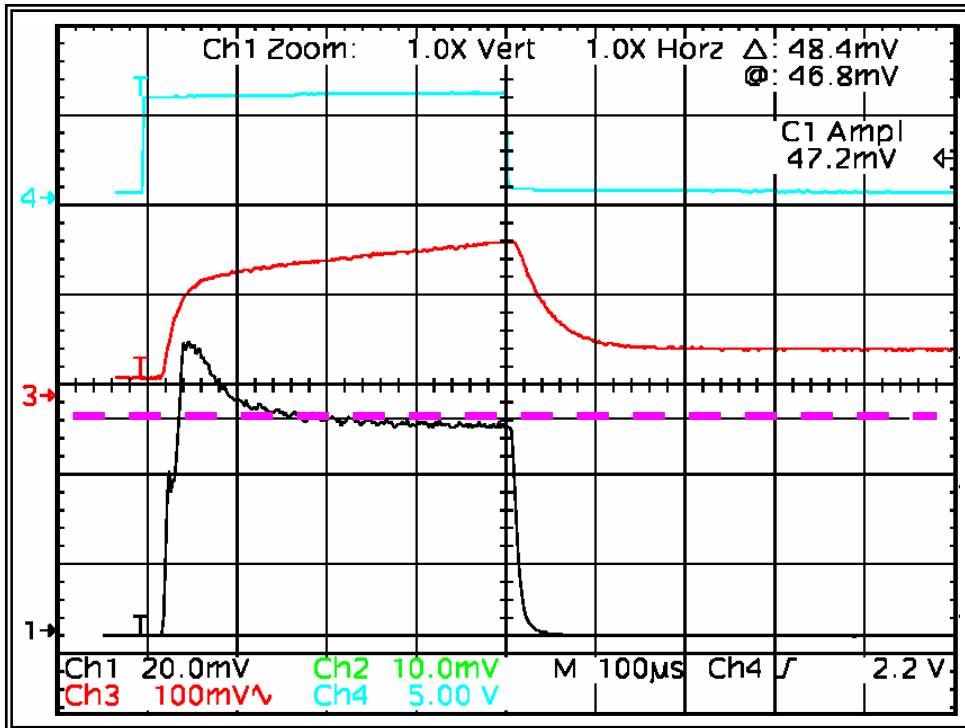
−16000 V

48000 V

0 V

45000 V

0 V
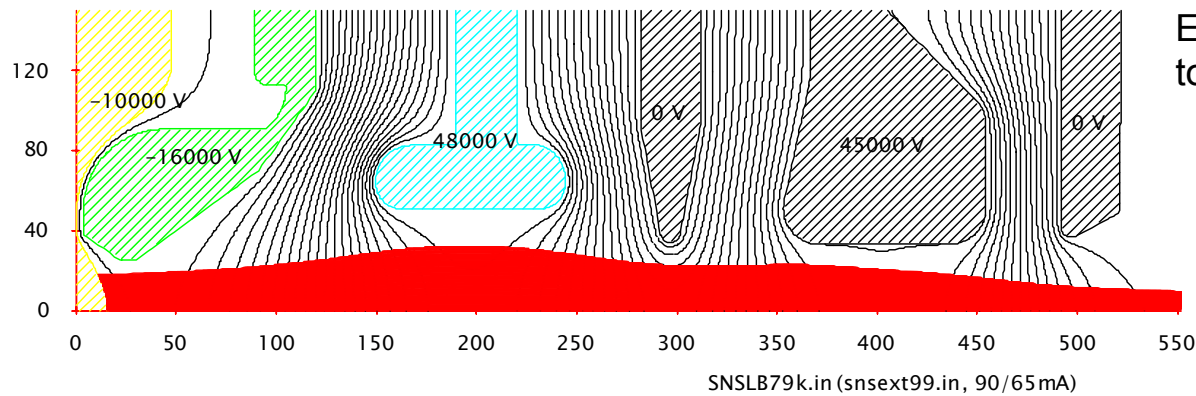
Electrode potentials apply
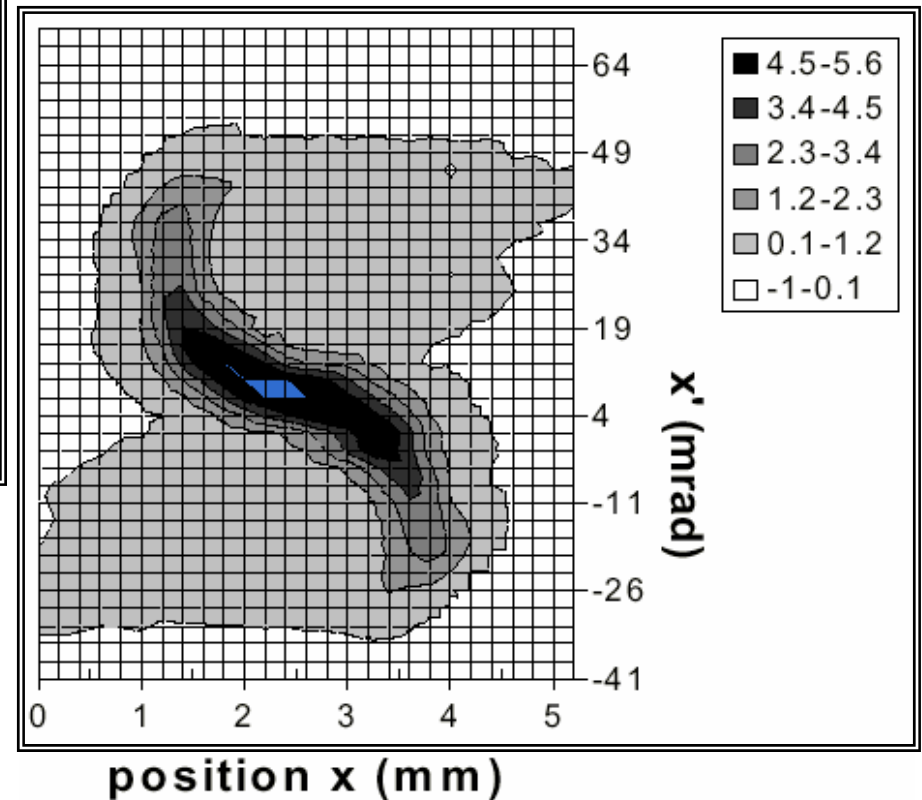to positive-ion extraction!

SNSLB79k.in(snsext99.in, 90/65mA)

## Beam in LEBT (For absolute scale, see P. 9)

# Measured Beam at LEBT Exit



50 mA average current

Vertical LEBT rms emittance at 33 mA: 0.186 mm mrad

# Beam Chopping into Mini Pulses

- ❑ Necessary to allow Ring extraction-kicker magnet to rise to nominal excitation while avoiding beam spill on Ring extraction septum
  - ▪ Spill would lead to septum activation
- ❑ Pre-chopping in LEBT
  - ▪ 8 fast switches apply deflection voltages to 4 segments of second einzel lens
    - • Two adjacent segments have same polarity - steer at 45° angles w.r.t. main axes
    - • Polarities rotate by 90° between subsequent chopping pulses
    - • A fraction of the beam is dumped on the RFQ entrance aperture
      - ▪ Aperture is isolated to permit current monitoring
    - • The remainder of the beam is dumped on the RFQ walls, between vanes
  - ▪ Eliminates most of the beam current between mini pulses
  - ▪ Not quite fast enough for overall specification (25 ns rise/fall time)
  - ▪ Not quite complete enough ($10^{-3}$ of total current)
- ❑ Cleanup chopping in MEBT (Chopper provided by Los Alamos Nat. Lab.)
  - ▪ Traveling-wave chopper excitation
  - ▪ Meander-shaped conductor on chopper plates
  - ▪ 10 ns rise/fall time demonstrated for switching waveforms
  - ▪ Original MEBT design had chopper/anti-chopper pair
    - • Anti-chopper was supposed to direct partially-chopped beam back on axis
    - • Anti-chopper now eliminated, replaced by diagnostics and halo scrapers
  - ▪ High-power chopper target

# LEBT Chopper Results



Beam current 24 mA with an uncertainty of +0.4 mA
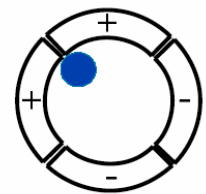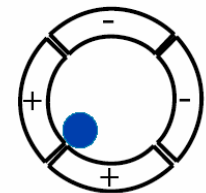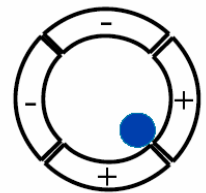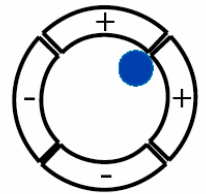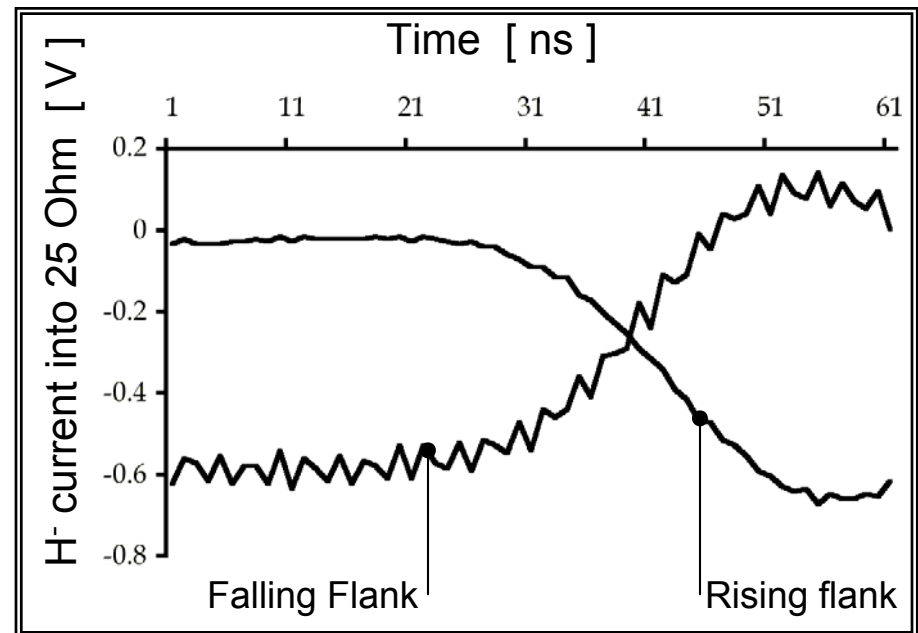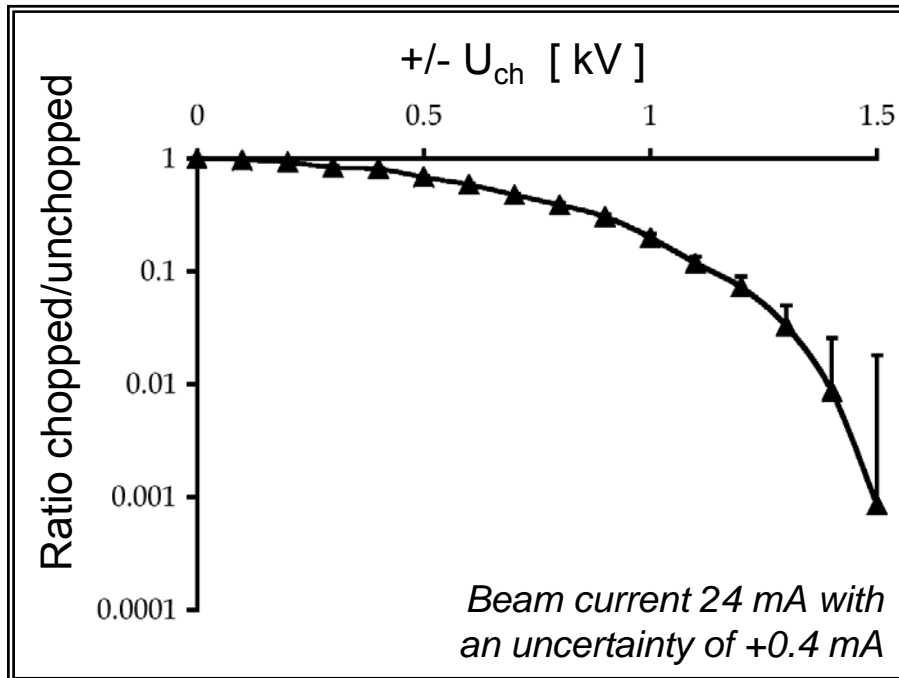
LEBT chopper commissioned at 6% duty factor with beam

# SNS Front End
## IS/LEBT Commissioning Summary

- Measured up to 50 mA of beam current
- Electron dumping at low energy works, but not perfectly
  - Minor electron spill on extractor electrode requires active cooling
- LEBT emittance acceptable
- Achieved matching Twiss parameters for injection into RFQ
- Suitability of electrostatic focusing method proven
- Chopping performance better than required

# RFQ Principle

- ❑ RFQ (Radio-Frequency Quadrupole accelerator) combines transverse and longitudinal focusing (bunching) with acceleration in a common structure
  - ▪ Interleaving electrode bulges create transverse quadrupole and longitudinal dipole fields
    - • "Two-dimensional zipper"
  - ▪ Electrical rf fields are relevant for beam transport
- ❑ Principal functions of the RFQ structure
  - ▪ Radial matcher
    - • Shape beam coming from LEBT
  - ▪ Buncher
    - • Create micro-bunches for efficient transport to Linac
  - ▪ Accelerator
    - • Bring beam to nominal Linac injection energy

➙ Details in Tom Wangler's part of this lecture series

# RFQ Technical Characteristics
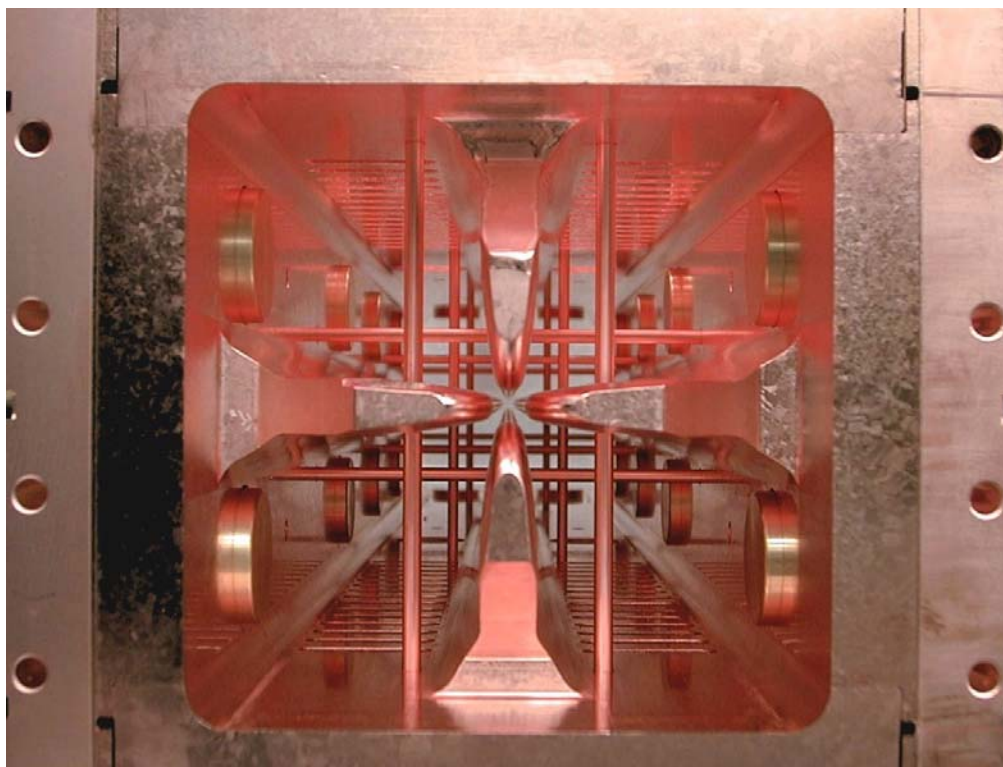


SNS RFQ seen from the LEBT side

- 4-vane RFQ with $\pi$-mode stabilizers
  - Brazed hybrid structure
    - GlidCop® outside for stiffness
    - OFE copper inside for conductivity
  - 4 modules with 3.72-m total length
    - Joined without flanges using bolt pockets and barrel nuts
- 402.5 MHz resonant frequency
  - Imposed by Linac rf frequency
- 640 kW pulsed power needed to achieve nominal gradient without beam
  - 8 power couplers
  - 80 fixed tuners
  - Dynamic tuning implemented by adjusting wall-to-vanetip temperature difference
  - 2.5 min. needed to reach stable operation from cold start

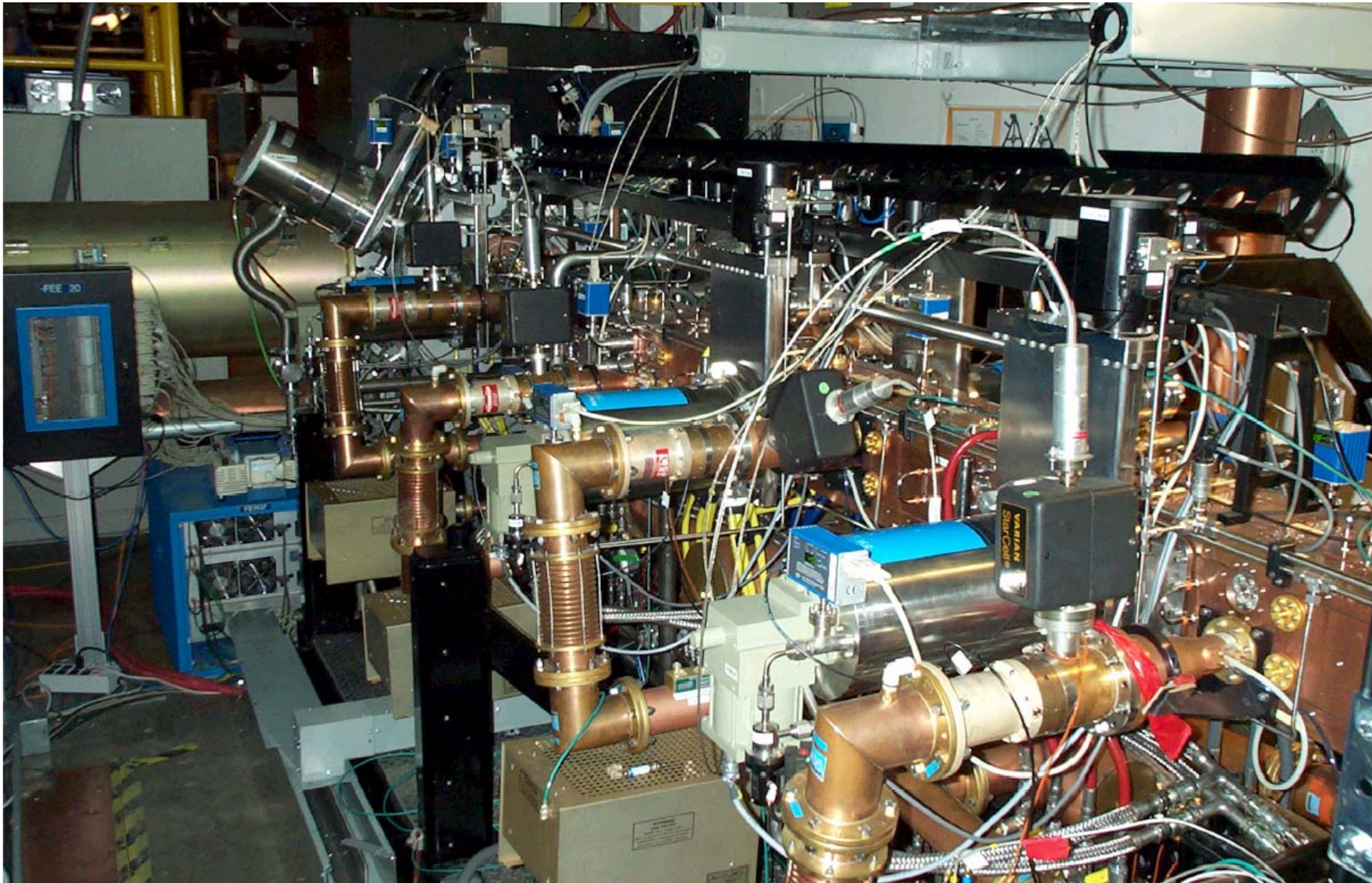# RFQ Beam Energy vs. Length
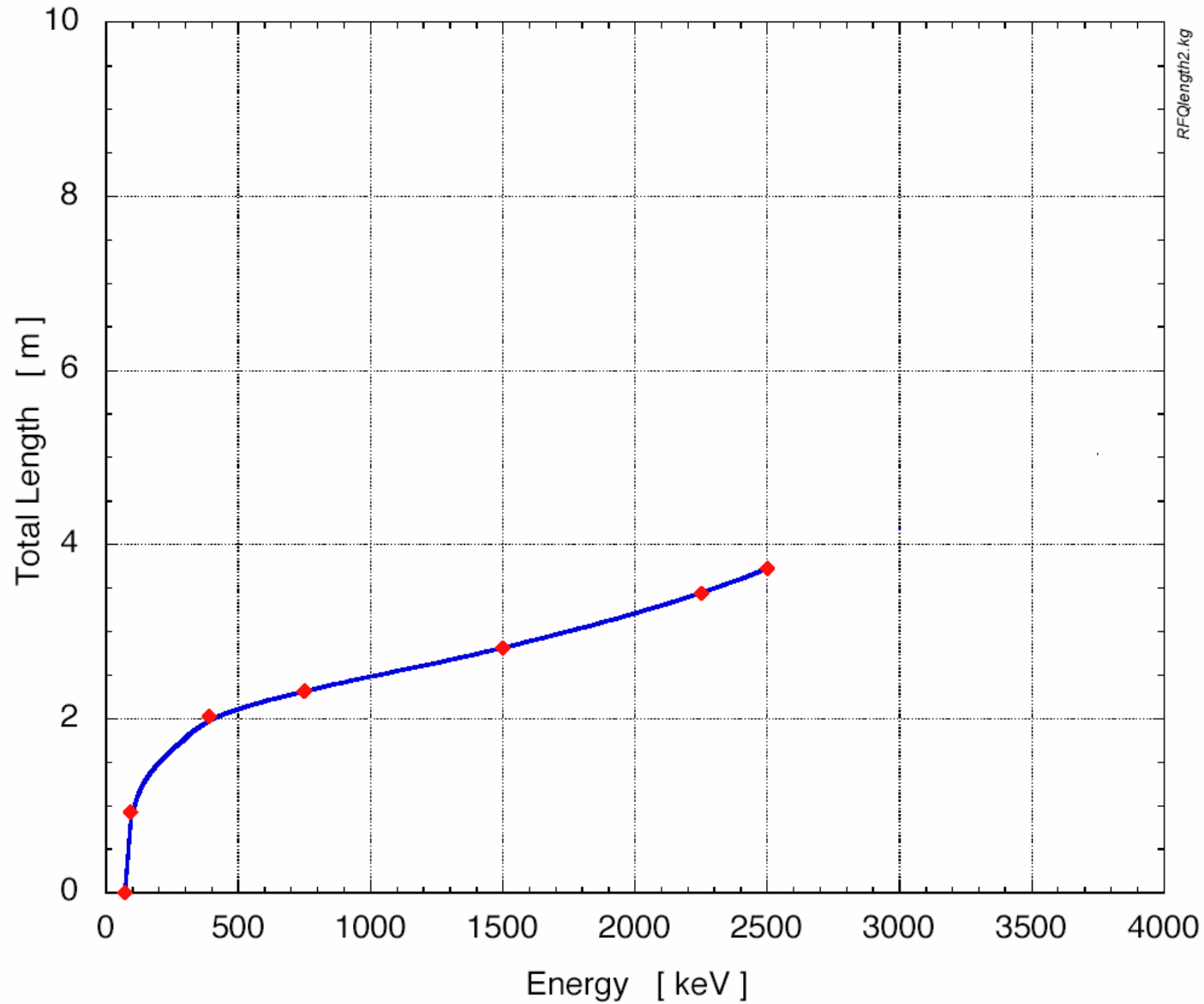
# RFQ Module #3 – Two of Four Vanes

QuickTime™ and a
TIFF (LZW) decompressor
are needed to see this picture.

QuickTime™ and a
TIFF (LZW) decompressor
are needed to see this picture.

←——————————— Beam direction
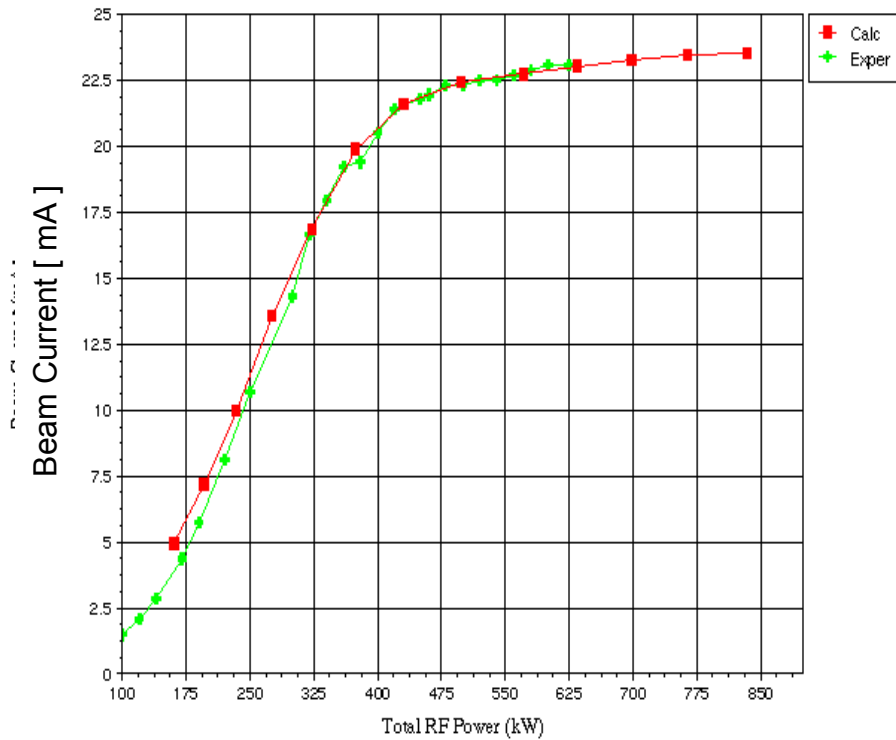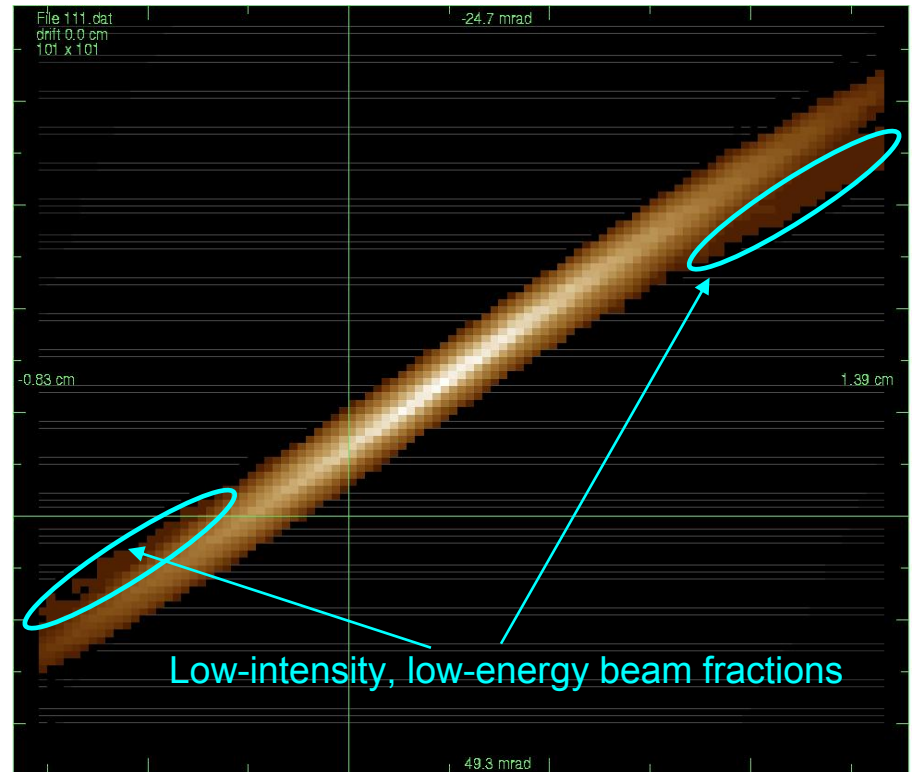
# RFQ Commissioning Results



Transmission vs. RF Power Level



Measured 22-mA Vertical Emittance

0.325 $\pi$ mm mrad

# RFQ – Table of Measured Twiss Parameters

| | Current [mA] | Emittance [$\pi$-mm-mrad] | $\alpha$ | $\beta$ [ m ] |
|---|---|---|---|---|
| Horizontal | 14.0 | 0.210 | -11.86 | 5.40 |
| | 21.8 | 0.272 | -12.91 | 6.47 |
| | 32.0 | 0.282 | -12.75 | 6.47 |
| Expected | 20.0 | 0.296 | -11.13 | 5.32 |
| Vertical | 13.4 | 0.204 | -6.69 | 2.52 |
| | 21.8 | 0.286 | -6.94 | 2.62 |
| | 29.8 | 0.298 | -6.00 | 2.29 |
| Expected | 20.0 | 0.254 | -8.17 | 3.15 |

Corrections applied for low-energy particles and slit scattering

# RFQ Commissioning Summary

- ❏ Commissioned at low duty factor with beam
  - ▪ 32 mA current reached during RFQ commissioning with intentionally 'relaxed' ion-source extraction gap
  - ▪ No emittance distortions visible
    - • Input emittance wings are clipped
  - ▪ Over 90% transmission with ~35-mA input beam

- ❏ Reliably supported MEBT commissioning

# MEBT Functions

- ❑ Match 2.5-MeV beam from RFQ exit to chopper target
  - ▪ Flat shape needed at target for fast rise/fall times
- ❑ Match unchopped beam from chopper target
  to Linac entrance
- ❑ Preserve 402.5-MHz bunch structure
- ❑ Accommodate beam diagnostics elements
- ❑ Keep emittance growth at minimum

# SNS Front End
# MEBT Technical Characteristics

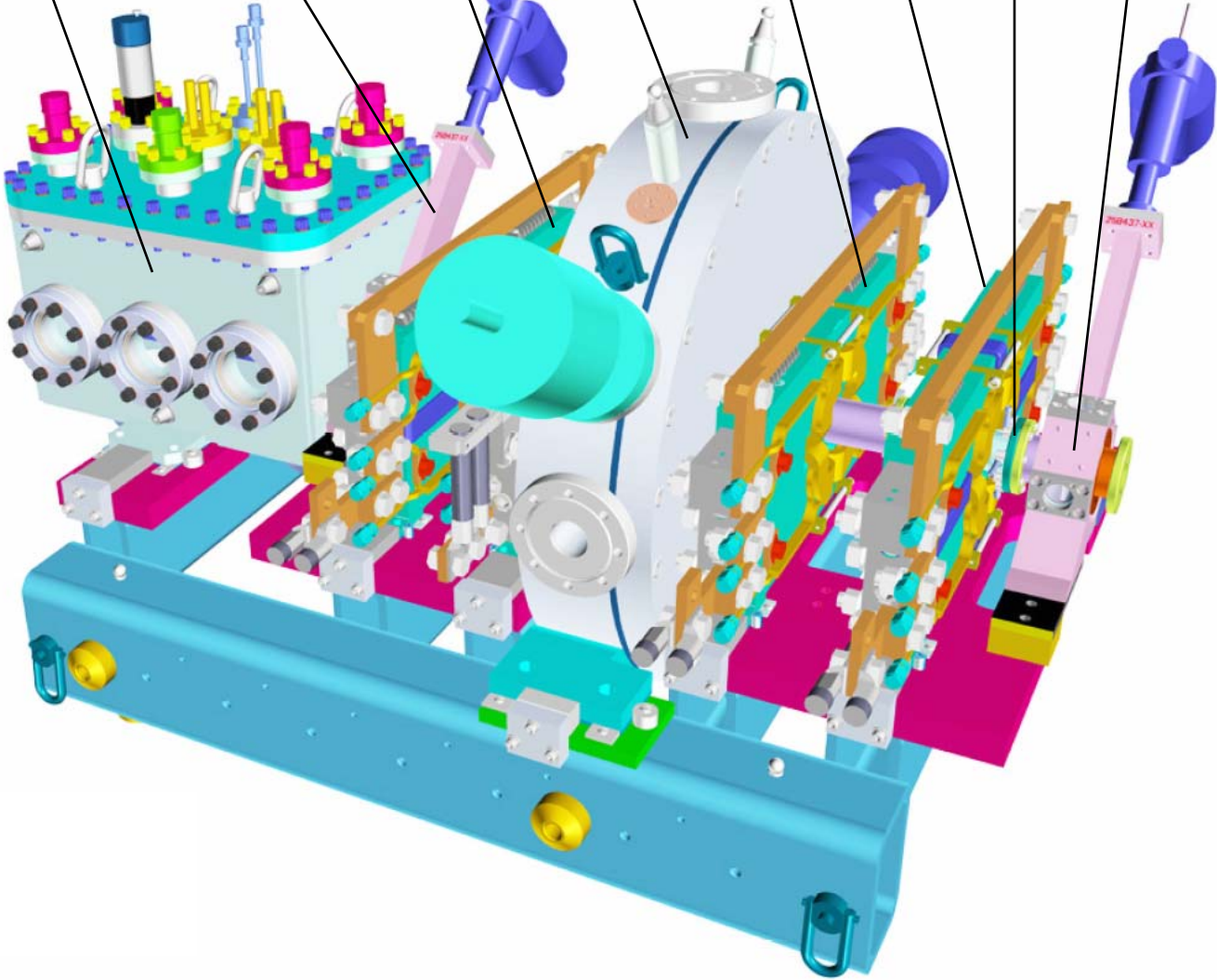- ❑ Beamline elements arranged on 3 rafts supported by common frame using 6-strut systems
    - ▪ Ease of alignment and suitability for shipment
- ❑ 14 quadrupole magnets (LANL design)
- ❑ 4 rebunchers (402.5-MHz)
- ❑ Chopper/anti-chopper pair
    - ▪ Unchopped beam is guided back to beamline axis
- ❑ High-power chopper target
    - ▪ 400 kW/cm$^2$ peak power density
    - ▪ Molybdenum-coated TZM material
- ❑ On-line diagnostics
    - ▪ Beam-current monitors
    - ▪ Profile monitors
        - • Wire scanners (BNL design, standard monitors)
        - • BNL laser profile monitor (R&D test)
    - ▪ Beam-position monitors
        - • Also used for phase measurements
- ❑ Off-line emittance device

**Quadrupole**

**Rebuncher**

**Chopper**

**Chopper Target**
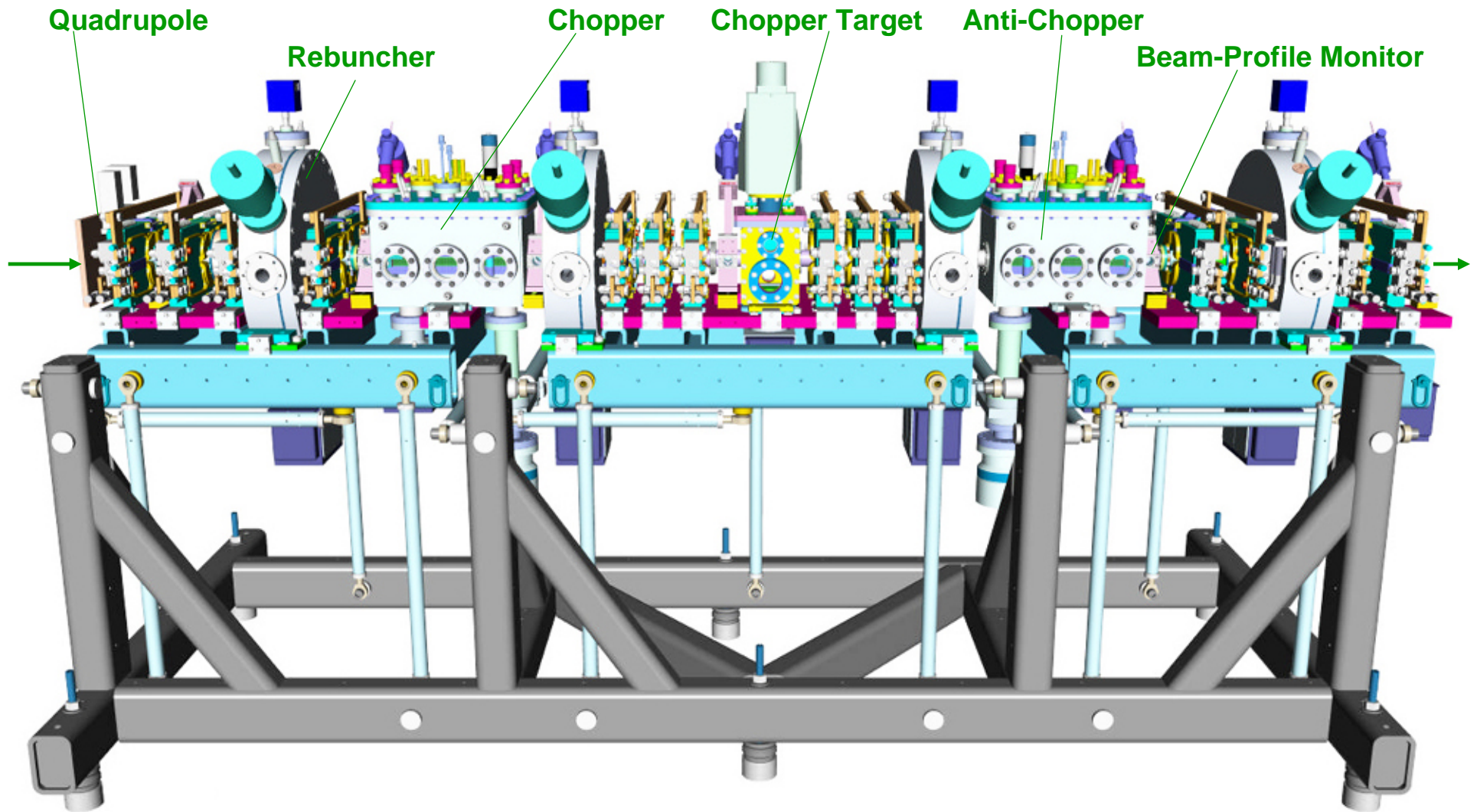
**Anti-Chopper**

**Beam-Profile Monitor**

Anti-chopper   Profile Monitor   Quad   Rebuncher   Quad   Quad   BCM   Profile Monitor

# SNS Front End
## MEBT Beam Dynamics
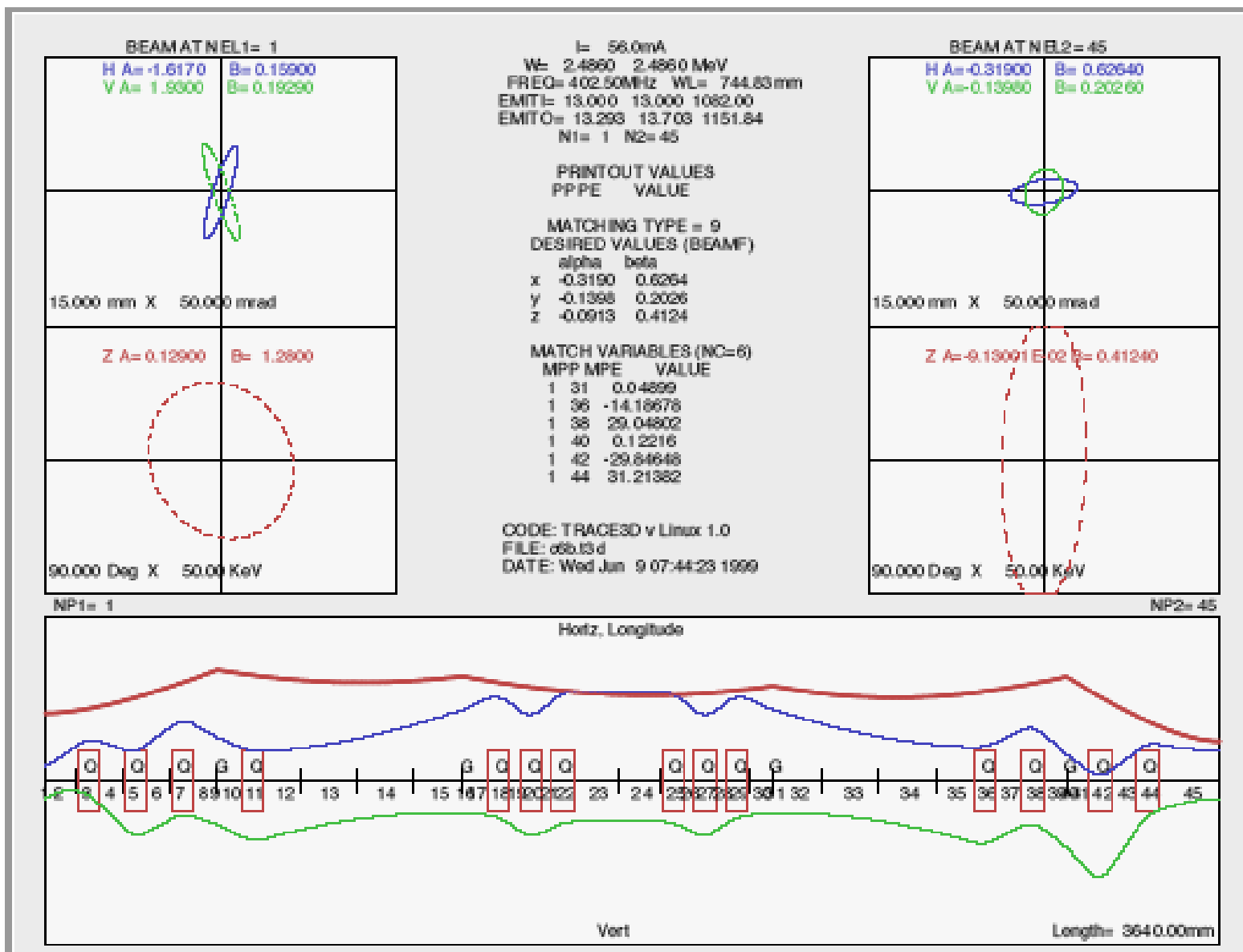
# MEBT Installation at LBNL in 2002



Feb. 21

March 31

# MEBT Chopper Target



Cooling water

Dimensions in inches

Incoming beam, deflected by chopper
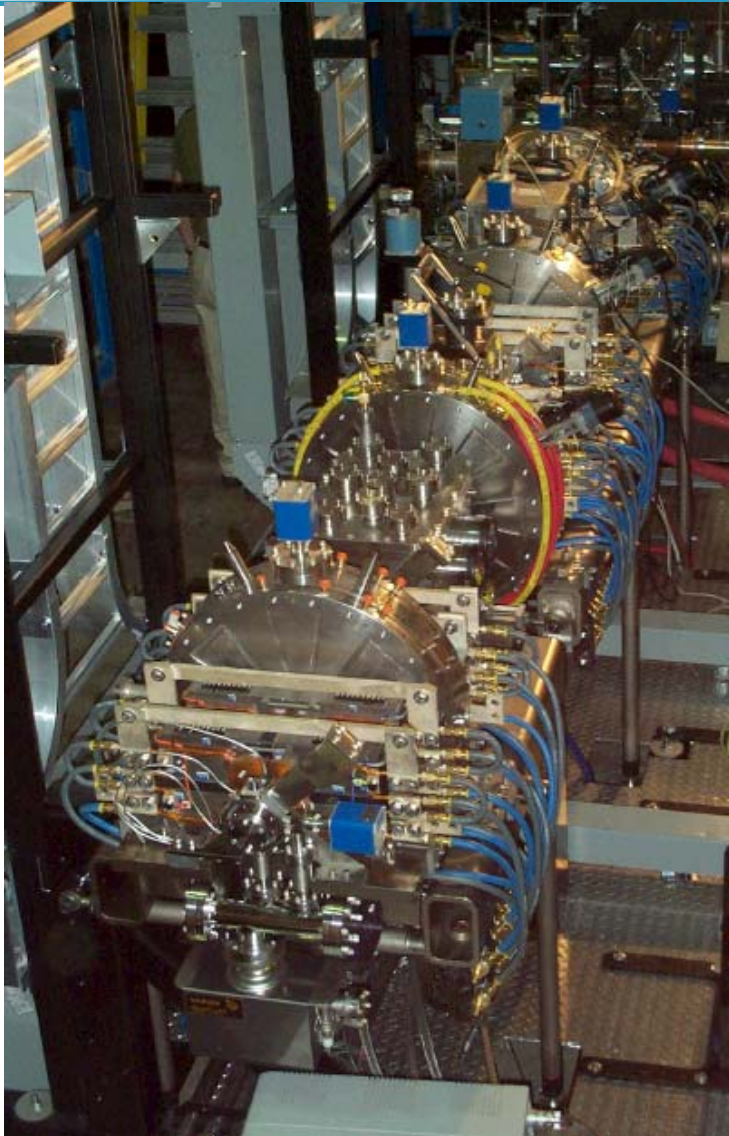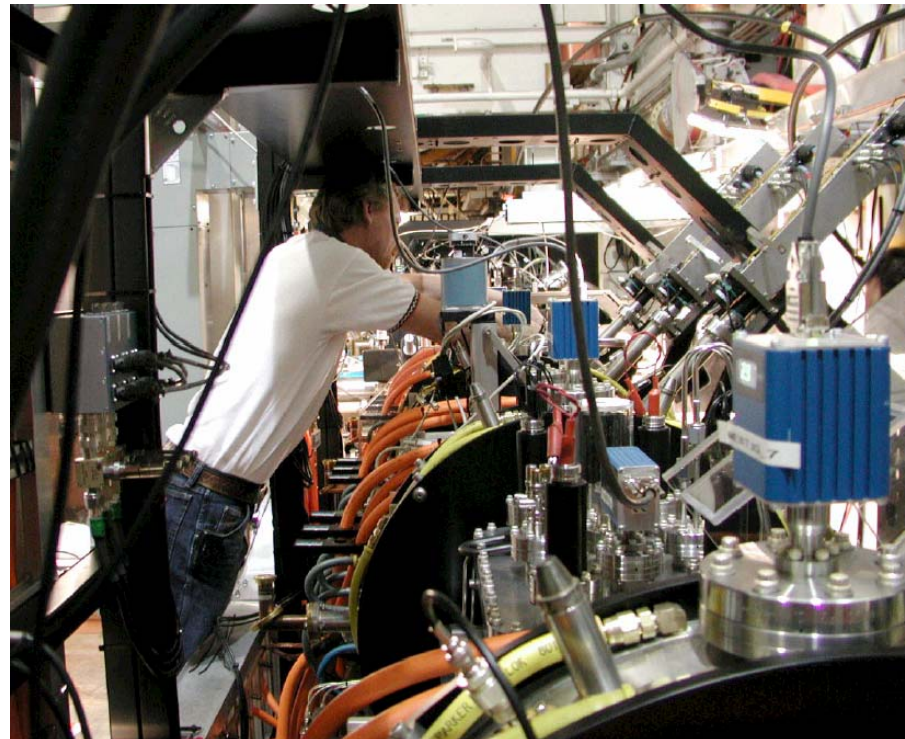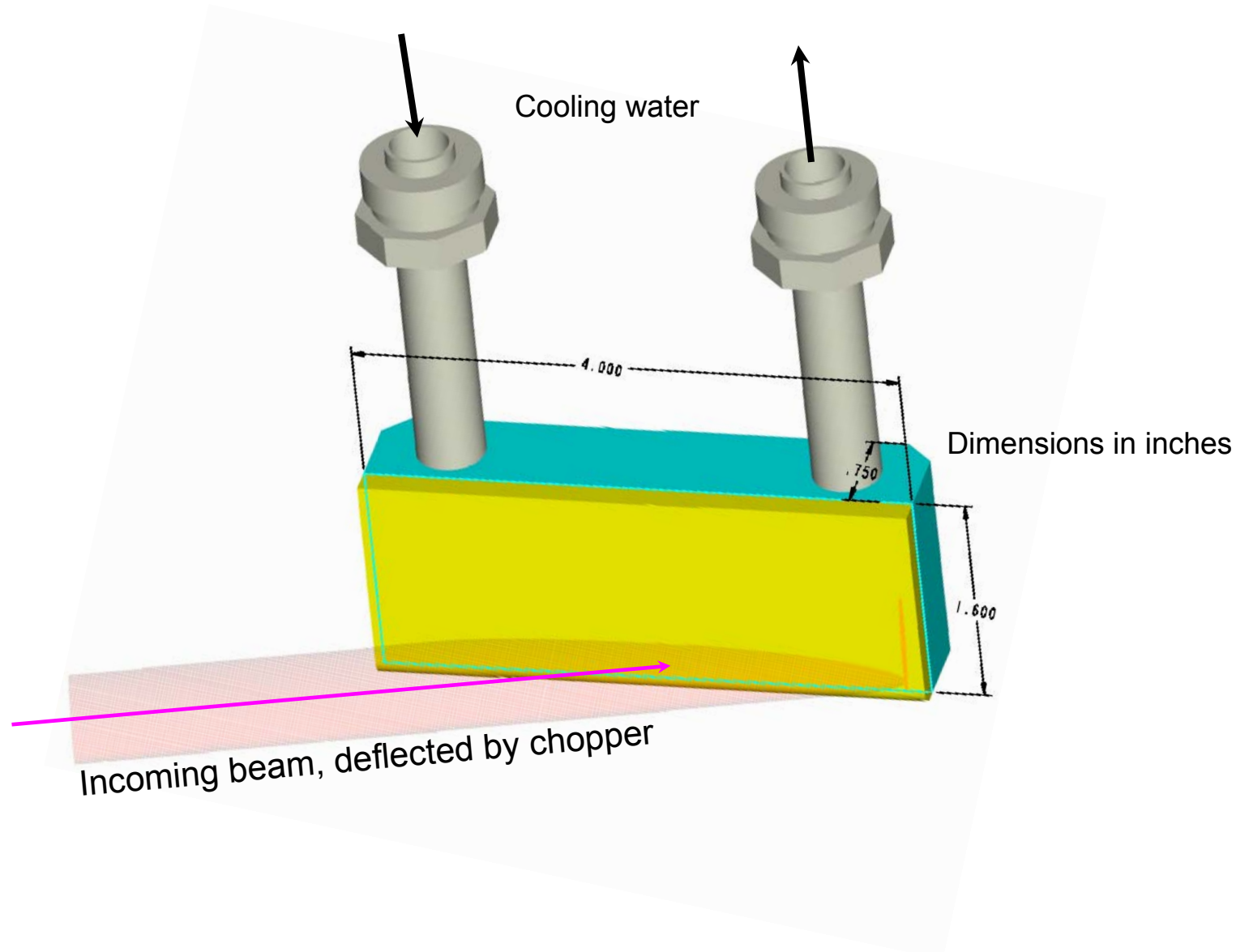
# MEBT Components
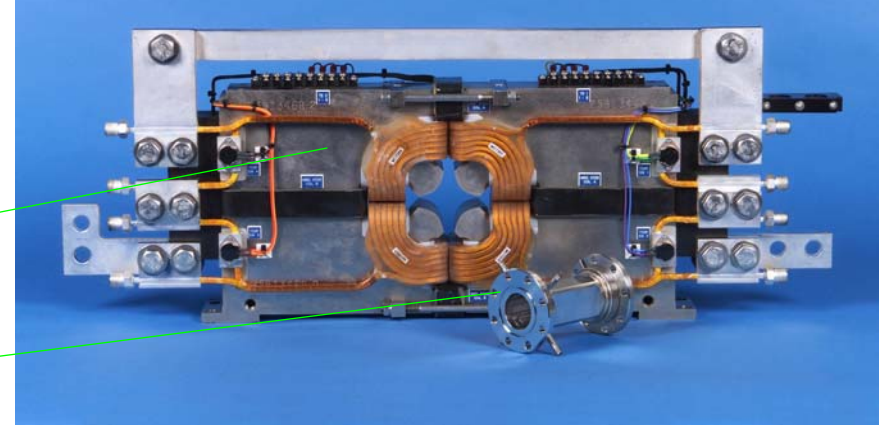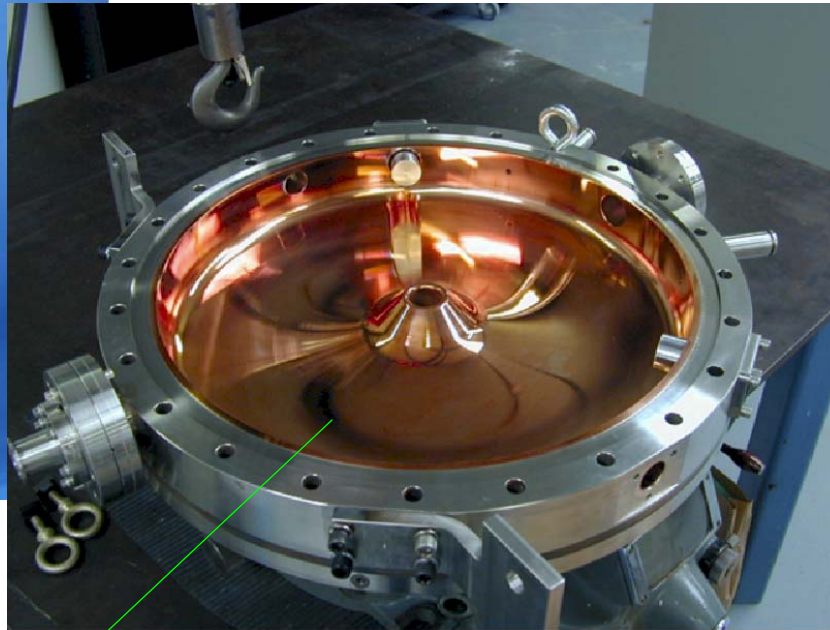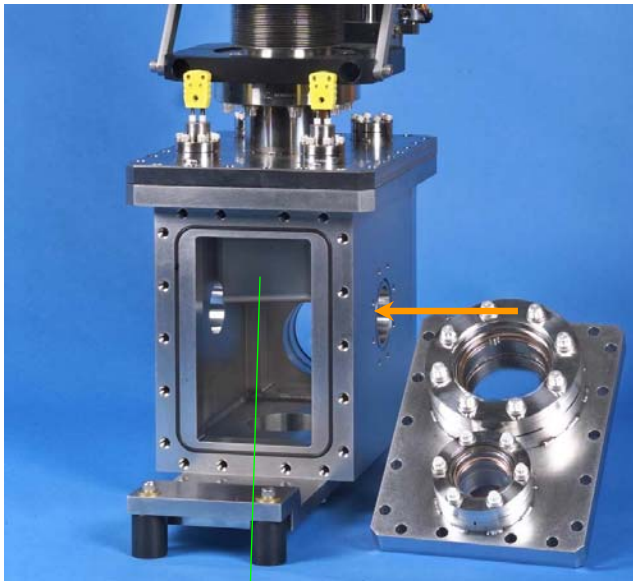


Chopper Target

Rebuncher Cavity

Quadrupole Magnet
    with Beam-Position Monitor

# Example of MEBT Emittance
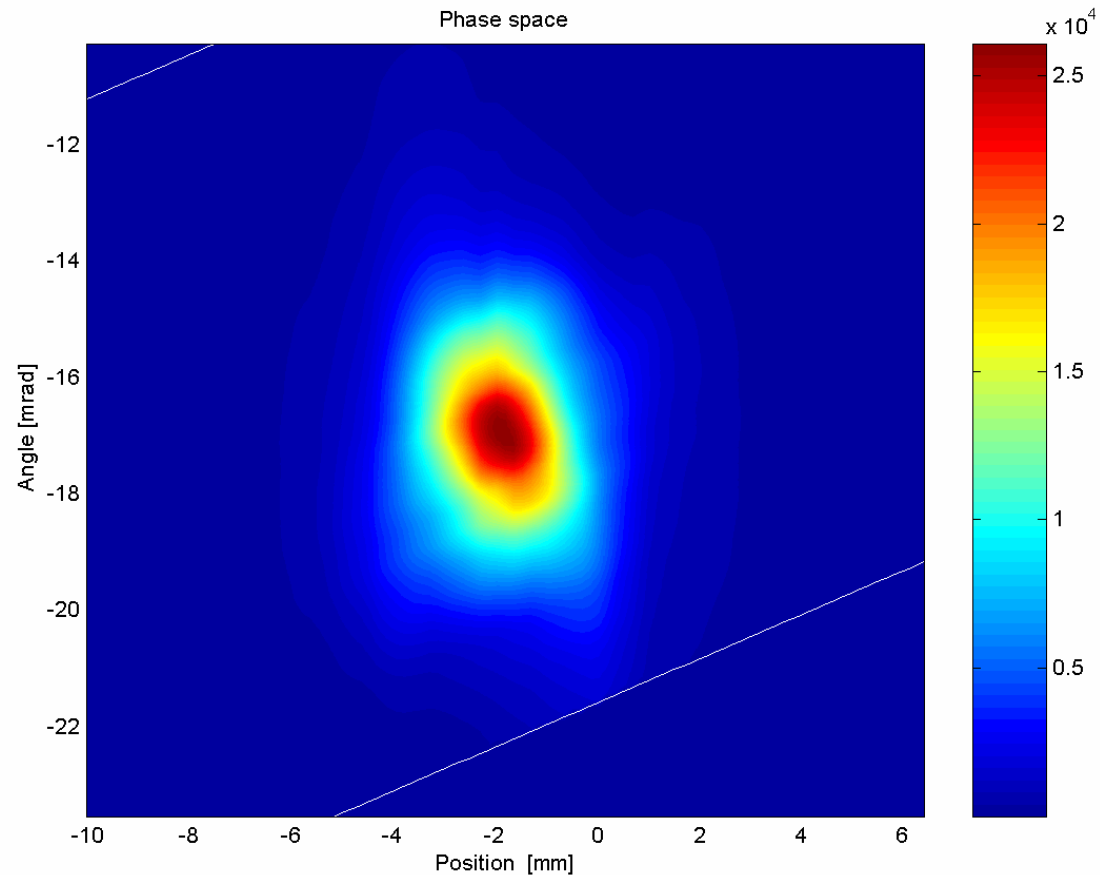


$\varepsilon = 0.23\ \pi$ mm mrad $\qquad\qquad \alpha = 0.08$

$\beta = 0.79$ m $\qquad\qquad\qquad$ I = 20 mA

*Twiss parameters measured at defining slit (0.5 m downstream of MEBT exit)*

# Measured MEBT Beam Emittances

- Performed horizontal and vertical emittance measurements
- Results were satisfactory at slightly less than nominal current
- Halo scraping will further reduce rms size

| Current | rms size | Condition |
|---------|----------|-----------|
| [ mA ] | [ $\pi$ mm mrad ] | |
| 24 | 0.276 | hor-unbunched |
| 33.4 | 0.281 | hor-unbunched |
| 27 | 0.261 | vert-unbunched |
| 27 | 0.270 | vert-bunched |

*Nominal values hor. and vert.: 0.270 $\pi$ mm mrad*

0.281 $\pi$ mm mrad rms

*Outline around halo was manually traced*
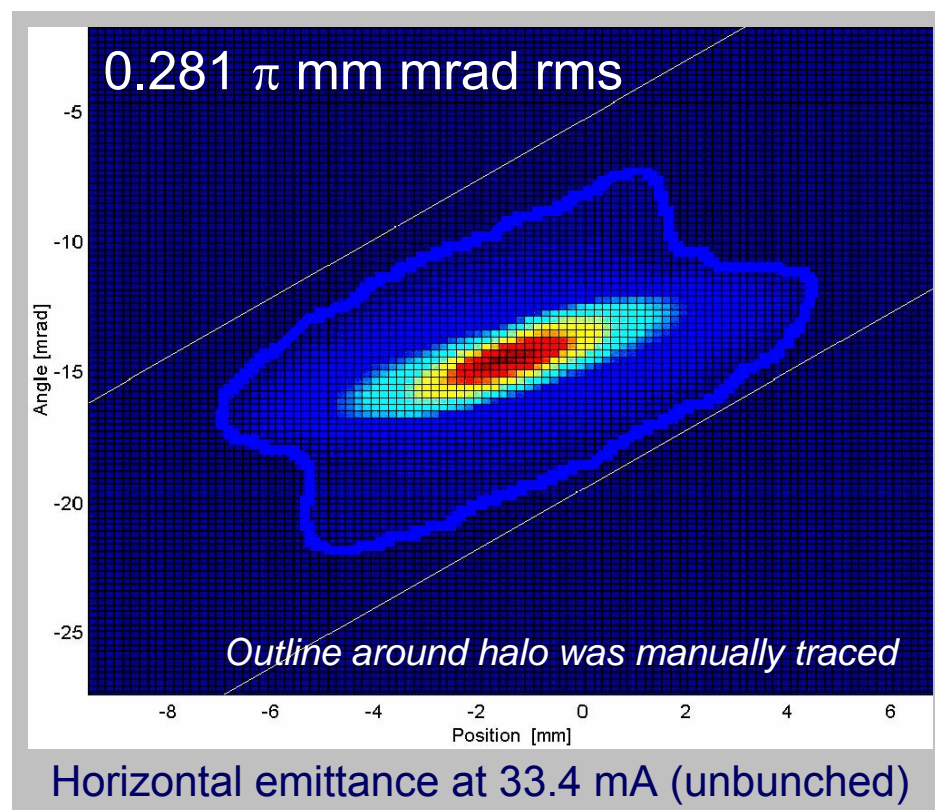
Horizontal emittance at 33.4 mA (unbunched)

# MEBT Wire Scanner Results
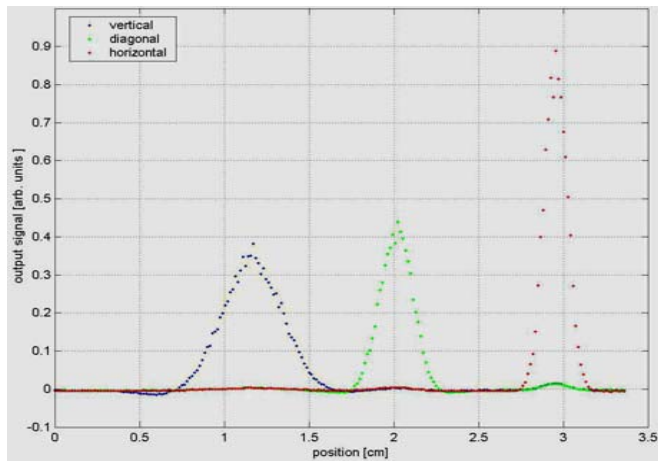


Wire Scanner sample
display



Interface flange to
diagnostic box

One set of hardware
to take x and y profiles

Linear bearing to
support fork motion

Beam scanning zone
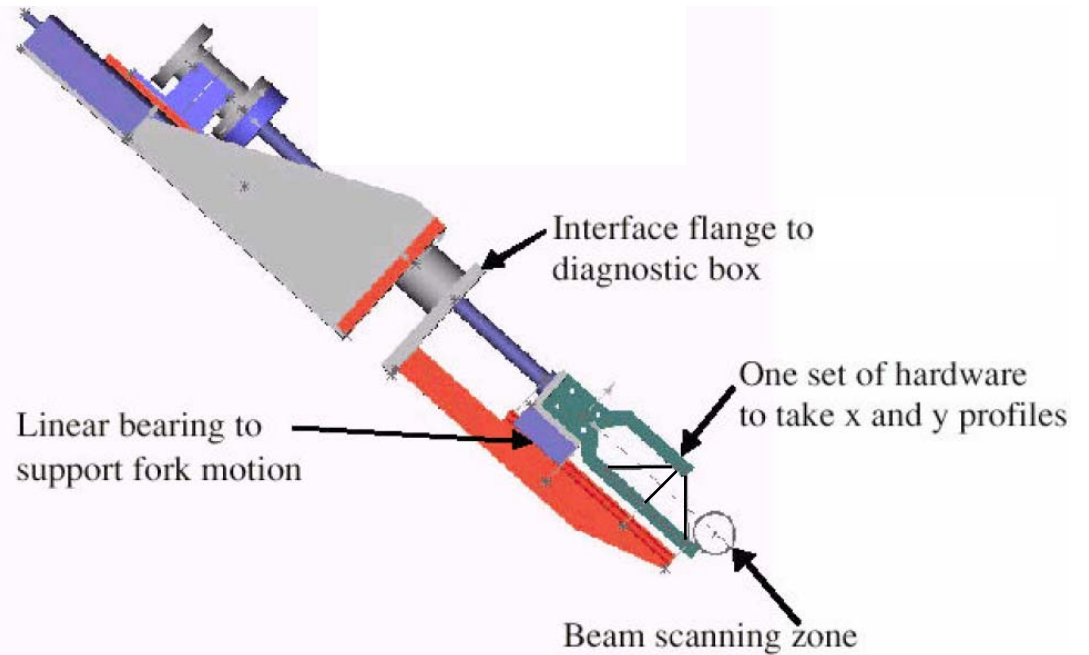
### Relative deviations between measured and simulated beam widths

| WS # | 1 | 2 | 3 | 4 | 5 | StDev |
|------|-----|------|-----|------|-----|-------|
| dx [ % ] | 5.8 | -1.8 | 1.4 | -7.6 | 4.6 | 5.4 |
| dy [ % ] | 4.5 | -6 | 4.2 | 0 | 2.2 | 4.3 |

*Design accuracy of wire scanners: 5%*

# MEBT Diagnostics Commissioning

- ❑ **All diagnostics elements produced usable signals**
    - ▪ 2 Beam-Current Monitors
    - ▪ 6 Beam-Position Monitors
    - ▪ 5 Wire Scanners
        - • Beam sensitivity to quadrupole tuning verified
        - • Measured profiles fit Trace-3d simulation results well
        - • Wire scanner hardware will benefit from remake
    - ▪ BNL's Laser Profile-Monitor demonstrated
        - • Results not used for MEBT characterization

# SNS Front End
## Maximum Beam-Current Demonstration

- Nearly all of the RFQ and MEBT commissioning was performed using a 'relaxed' ion-source extraction gap
  - Better suited to match about 30 mA beam to the RFQ
  - Successfully transported up to 36 mA beam current through MEBT with relaxed gap

- Changed ion-source extraction gap to nominal width for last day of commissioning

- Achieved 50 mA of transported beam current through MEBT on first try
  - **Nearly 30% more than nominal SNS beam-current goal of 38 mA, needed for 1.44 MW average beam power**
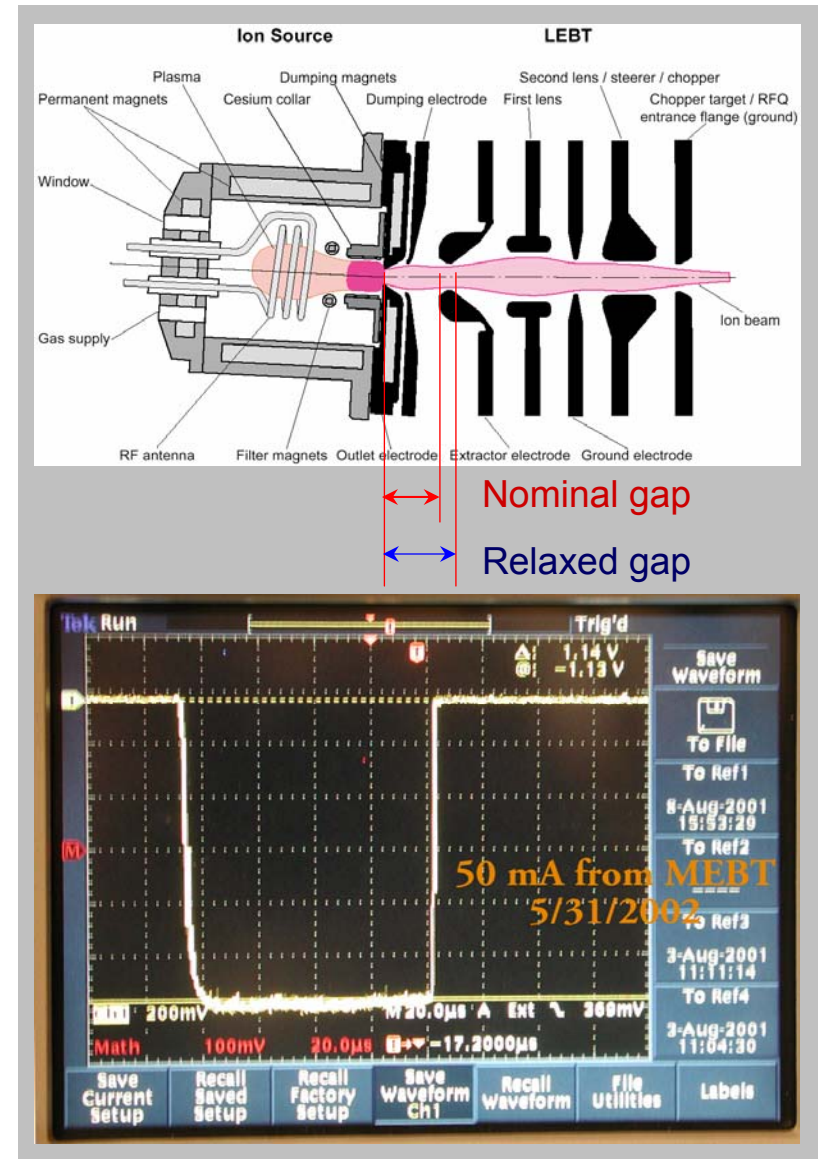
|  |  | Nominal | Achieved | Remark |
|---|---|---|---|---|
| **SNS** |  |  |  |  |
| Pulse repetition rate | Hz | 60 | 60 |  |
| Proton pulse length | $\mu$s | 0.695 | (0.69) | Pre-chopper only |
| Linac beam macropulse duty factor | % | 6 | (6) | Front End only |
|  |  |  |  |  |
| **FRONT END** |  |  |  |  |
| Ion type |  | H⁻ | H⁻ |  |
| Output peak current | mA | 38 | 50 |  |
|  |  |  |  |  |
| **ION SOURCE AND LEBT** |  |  |  |  |
| Output energy | keV | 65 | 65 |  |
| Output peak current | mA | 48 | > 50 |  |
| Estimated output rms norm H & V emittance | $\pi$ mm-mrad | 0.20 | (.223) | @ 33 mA |
| Ion source lifetime | weeks | 3 | in reach |  |
| Ion source replacement time | hours | 2 | plausible | Achieved with prototype |

|  |  | Nominal | Achieved | Remark |
|---|---|---|---|---|
| **RFQ ACCELERATOR** |  |  |  |  |
| Output peak current | mA | 38 | (50) | Not directly measured |
| Output energy | MeV | 2.5 | 2.5 |  |
| Expected output rms norm H & V emittance | $\pi$ mm-mrad | 0.21 | (0.29) | @ 30 mA |
| Expected output rms L emittance | $\pi$ MeV-deg | 0.10 | not measured |  |
|  |  |  |  |  |
|  |  |  |  |  |
| **MEBT** |  |  |  |  |
| Output peak current | mA | 38 | 50 |  |
| Expected output rms norm H & V emittance with errors | $\pi$ mm-mrad | 0.27 | (0.29) | @ 33 mA, calc. for bunched beam |
| Expected output rms L emittance with errors | $\pi$ MeV-deg | 0.13 | not measured |  |
|  |  |  |  |  |
|  |  |  |  |  |
| **CHOPPING SYSTEM** |  |  |  |  |
| Full rise/fall time | ns | 10 | (10) | Power switch |
|  |  |  | 25 | *LEBT chopping only* |
| Post chopper off/on beam-current ratio |  | $1.0 \times 10^{-4}$ | not measured |  |

# MEBT Commissioning Summary

- Very good beam performance up to full duty factor
  - Achieved matching Twiss parameters for Linac injection
  - With intentionally 'relaxed' ion-source extraction gap
    - 9 mA on very first pulse
    - Increased to 36 mA within 2 weeks
  - No steering needed in entire MEBT for optimum transmission
  - Emittance sizes satisfactory
  - A maximum of 50 mA transported current was reached on last day with nominal extraction gap
    - **~30% higher than requirement**
- Performed round-the-clock beam test over one week
  - Duty factor raised from ~1 to 3% with 25 mA transmitted beam current
  - Identified and resolved a few hardware flaws
- Operated the entire Front End at 6% duty factor with beam (25 mA)
- All diagnostics elements produced usable signals
  - Wire profile scans fit simulated data very well
  - BNL's Laser Profile Monitor demonstrated

# SNS Front End
## FE Re-commissioning at the SNS Site
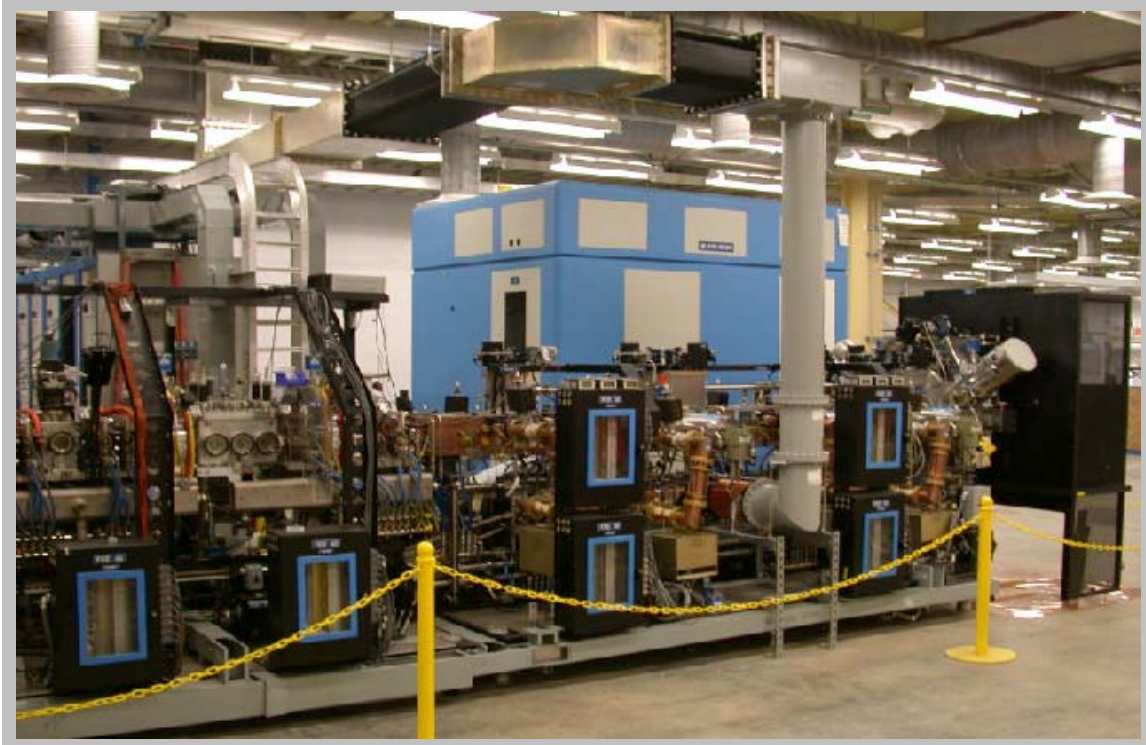


Front End at the
SNS site in Oak Ridge

❑ Work performed in Dec. 14, 2002 - Jan. 31, 2003 by SNS staff
led by A. Aleksandrov
- Assistance by LBNL staff to a minor degree
- Demonstrated most key performance parameters
- Repeated 50 mA beam current result
- Measured beam parameters for a wider range of operating conditions
than could be done at LBNL

# FE Re-commissioning at the SNS Site



Emittance and orbit correction

- IS,LEBT and MEBT settings were optimized at 28mA then current was varied by changing IS RF power. Measured in one run (blue points)
- 38mA not fully optimized due to QV6-9 power supply problem
- 51 mA not optimized (single measurement)

Emittance vs. beam current



Vertical, bunched, 38mA

normalized r.m.s. = 0.30 $\pi$ mm mrad

Horizontal, bunched, 30mA

normalized r.m.s. = 0.24 $\pi$ mm mrad

Emittance near nominal current

# Main Contributors to SNS Front-End Work



*About half of the FES team with the system nearly completed, April 2002 at Berkeley Lab*

**LBNL**

B. Abraham

J. Ayers

P. Bach

K. Barat

D. Cheng

P. Cull

A. Demello

R. DiGennaro

L. Doolittle

D. Fong

D. Garfield

R. Gough

J. Greer

A. Harris

M. Hoff

R. Keller

T. Kuneli

M. Leitner

K. N. Leung

S. Lewis

C. Lionberger

C. C. Lo

P. Luft

R. McGill

M. Monroy

D. Oshatz

D. Peterson

J. Pruyn

A. Ratti

M. Regis

J. Reijonen

D. Ruiz

T. Schenkel

J. W. Staples

D. Syversrud

M. Szajbler

W. Tabler

R. Thomae

S. Virostek

N. Ybarrolaza

R. Yourd

A. Zachoszcz

**ORNL**

A. Aleksandrov

P. Gibson

T. Shea

M. Stockli

R. Welton

Additional staff from

**LBNL**

**ORNL**

**LANL**

**BNL**

R. Keller, R. W. Thomae, M. P. Stockli, and R. F. Welton
**Status of the SNS H- Ion Source and Low-Energy Beam Transport System**
ICFA-HB2002 workshop, April 8-12, 2002, Paper wed-sh-keller, Fermi National Accelerator Lab

R. Keller
**The SNS Front End, an Injector for a High-power Hydrogen-ion Accelerator**
25th International Power Modulator Conference and 2002 High Voltage Workshop, Los Angeles, IEEE 02CH37381, pp. 671 – 673 (2002)

A. Ratti, J.J. Ayers, L. Doolittle, J.B. Greer, R. Keller, S. Lewis, C. Lionberger, M. Monroy, J. Pruyn, J. W. Staples, D. Syversrud, R. Thomae, and S. Virostek; A. Aleksandrov for the SNS Accelerator Physics Group and T. Shea for the SNS Beam Diagnostics Collaboration
**Results of the SNS Front-End Commissioning at Berkeley Lab**
Linac 2002, Kyong-ju, Korea (2002)

A. Aleksandrov
**Commissioning of the Spallation Neutron Source Front End Systems**
2003 Particle Accelerator Conference, paper MOPB002, Portland, OR (2003)

M. Stockli, ed.
**Production and Neutralization of Negative Ions and Beams**
AIP Conf. Proceedings Vol. 639 (2002) American Institute of Physics, Melville, NY (2002)

# The SNS-1, Front End and Linac

## Tom Wangler, Jim Billen, Roderich Keller

# Course Preliminaries and SSN Overview

# The SNS-1, Front End and Linac(1)

Madison, Wisconsin, June 21-25

Jim Billen, LANL; Roderich Keller, LBNL, and Tom Wangler, LANL

- Introductions
- Prerequisites, Text, Course Description
- Plan of the Course (50% basic principles, 50% SNS specific material)
- Class Times (9:00am-12:00pm; 1:30pm-4:30pm)
- Office Hours (following the afternoon session)
- Homework problems (essential part of the course; please work together)
- Final exam (problems similar to the homework)
- Grade basis (50% homework, 50% final). Material covered for problems and exam will emphasize basic the principles.

# The SNS-1, Front End and Linac (2)

- Instructors: Tom Wangler, Jim Billen, Roderich Keller

- Prerequisites:  Electrodynamics, Particle Dynamics

- Text:  Introduction to Linear Accelerators book plus handouts

- Course Description: This is a 1-week course on the SNS accelerator including the basic accelerator physics and accelerator technology that are required for understanding the SNS accelerator and its design.

# Plan of the Course (1)

- **Monday**
  -Introductions and Course Preliminaries (Tom Wangler)
  -Overview of the SNS Project and the SNS Accelerator (Tom Wangler)
  -SNS Front End(Roderich Keller)
  -Introduction to RF Linacs (Tom Wangler)

- **Tuesday**
  -Introduction to RF Linacs Continued (Tom Wangler)
  -RF Linac Structures (Tom Wangler)
  -SNS Linac Design and DTL  Tuning (Jim Billen)

- **Wednesday**
  -RF Linac Structures Continued (Tom Wangler)
  -SNS Linac Design and CCL Tuning (Jim Billen)
  -RF Linac Beam Dynamics (Tom Wangler)

# Plan of the Course (2)

- **Thursday**
  - RF Linac Beam Dynamics Continued (Tom Wangler)
  - RFQ Video (Tom Wangler)
  - SNS Material on Superconducting Cavities (Tom Wangler)
  - SNS Material on Beam Dynamics (Tom Wangler)
- **Friday**
  - Pre-Final Exam Review
  - Final Exam – 2 hours

# Problem Assignments

| Set | Due | Problems |
|-----|-----|----------|
| 1[1] | Tuesday (Wednesday at the latest) | 1.1, 1.7, 1.8, 1.9 |
| 2 | Tuesday | Three injector problems and 2.2 from the book |
| 3 | Wednesday | 2.3, 2.4, 2.9 |
| 4 | Thursday | 4.6, 6.1, 6.2, 6.4 |
| 5[2] | Friday | 7.1, 7.3, 8.1, 8.5 |

The numbered problems are from the book.

{1} The first problem set can be turned in at any time before noon Wednesday
{2} Not required; may be turned in by Friday for extra credit
• We encourage you to work all the assigned problems.
• We have emphasized problems that allow you to compute numerical values.
  Be sure to check whether your results make sense (i.e. do they have proper units and do the numerical values have a reasonable magnitude).
• Problems are due at the afternoon meeting on the due dates.
• We will hand out solutions to the problems.
• Course grade will be based 50% on problems and 50% on the final exam.
• We encourage students to work together on the problems.
• Final exam will consist of 4 problems very much like those assigned.

# Overview of the SNS Project and the SNS accelerator

Tom Wangler

*Thanks to Norbert Holtkamp for many of the viewgraphs used in this section.*

# Spallation Neutron Source

Highest beam power

worldwide under construction

Stepping stone to next generation

spallation sources



- **The SNS will begin operation in 2006**

- **At 1.4 MW it will be ~8x ISIS, the world's leading pulsed spallation source**

- **The peak thermal neutron flux will be ~50-100x ILL**

- **5000 hours per year at an availability of >90% ......      !!!!!!!!!!! (~ in 2009)**

# The Spallation Neutron Source Partnership

| Description | | Accelerator |
|---|---|---|
| Project Support | 75.7 | |
| Front End Systems | 20.8 | 20.8 |
| Linac Systems | 304.9 | 304.9 |
| Ring & Transfer System | 147.3 | 147.3 |
| Target Systems | 106.4 | |
| Instrument Systems | 63.3 | |
| Conventional Facilities | 355.3 | |
| Integrated Control Syst | 59.6 | 59.6 |
| BAC | 1,133.3 | |
| Contingency | 59.4 | |
| TEC | 1,192.7 | |
| R&D | 101.2 | 81.0 |
| Pre-Operations | 117.8 | 94.2 |
| TPC | 1,411.7 | 707.8 |



SNS-ORNL Accelerator systems: ~167 M$

Front-End Systems (Lawrence Berkeley) ~20 M$

Accumulator Ring (Brookhaven) ~113 M$

~106 M$ Target (Oak Ridge)

Linac (Los Alamos and Jefferson) ~177 M$ ~60 M$

Instrument ~63 M$ Systems (Argonne and Oak Ridge)

99-06976F/arb

Lawrence Berkeley

Argonne

Brookhaven

Jefferson

Los Alamos
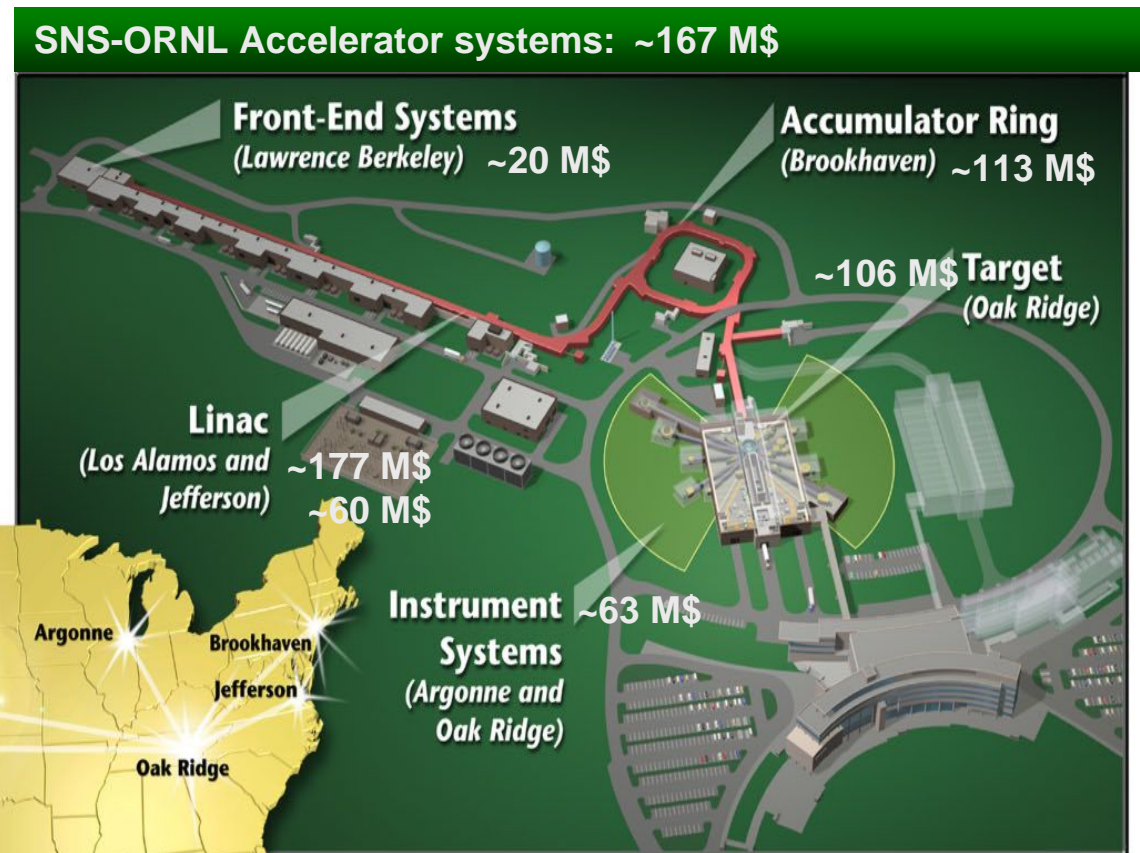
Oak Ridge

*At peak : ~500 People worked on the construction of the SNS accelerator*

- *Project ~70 % complete*
- *Completed as early as Dec '05*

Oak Ridge, TN

35° 49' N , 83° 59' W

# Motivation for the Spallation Neutron Source

- Neutrons are an important probe technique for the study of material science.

- A more powerful pulsed neutron source was needed. Pulsed neutrons have the advantage of allowing time-resolved experiments where the energy of the incident neutrons
  can be obtained from time-of-flight.

- A high intensity pulsed source can be obtained by spallation of heavy targets from a pulsed proton beam with kinetic energy of about 1 GeV.

- Experimenters want about 1-$\mu$sec pulses at about 60 Hz with as many neutrons per pulse as possible.

- What is the best technical approach to produce the desired spallation neutron source has been the subject of several studies and the rf linac-accumulator/compressor ring was chosen.

# Basic Concept of the Spallation Neutron Source

**H- source & Front End**

**Rf linac**

**Stripper foil** Converts H- to H+

**Accumulator/ Compressor Ring**

**Spallation Target**

**Neutrons for experiments**
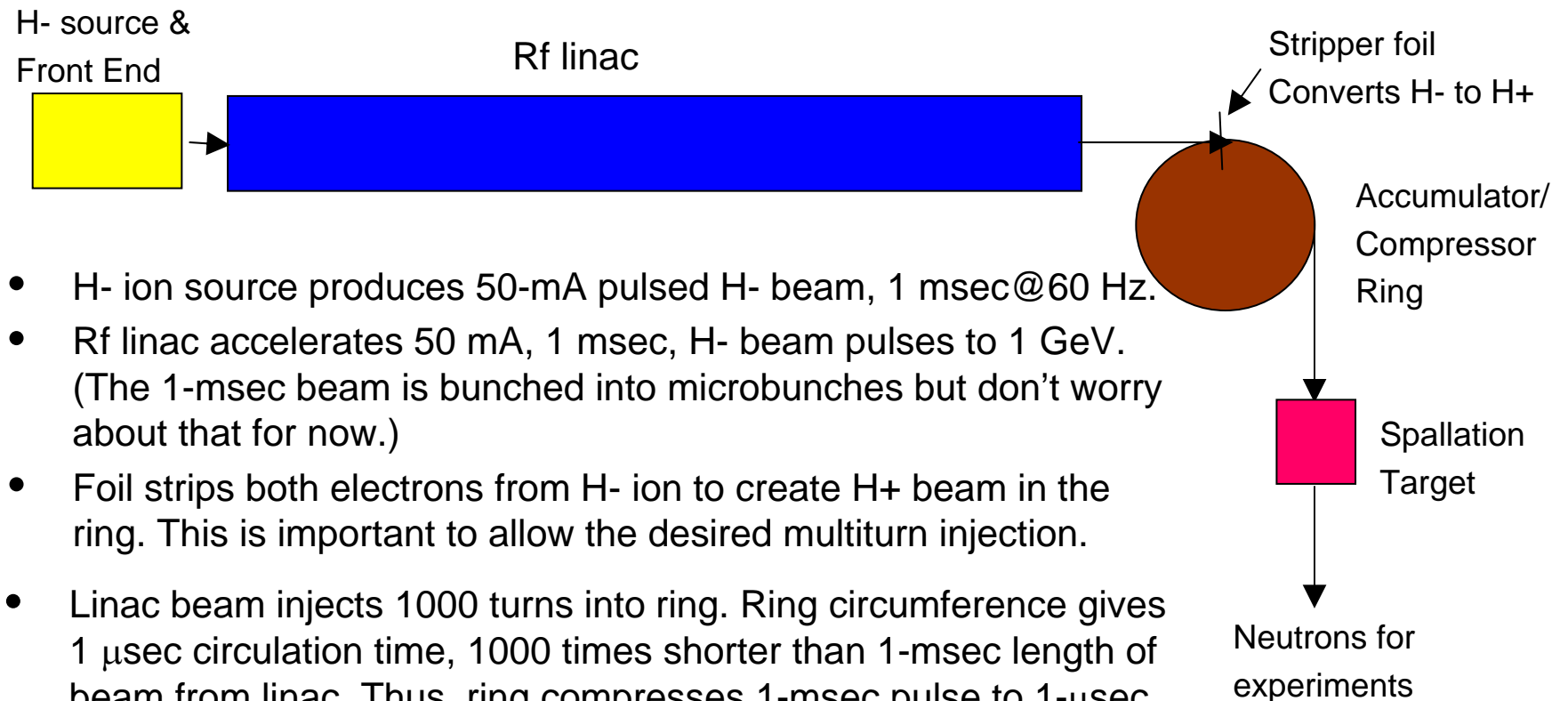
- H- ion source produces 50-mA pulsed H- beam, 1 msec@60 Hz.
- Rf linac accelerates 50 mA, 1 msec, H- beam pulses to 1 GeV. (The 1-msec beam is bunched into microbunches but don't worry about that for now.)
- Foil strips both electrons from H- ion to create H+ beam in the ring. This is important to allow the desired multiturn injection.

- Linac beam injects 1000 turns into ring. Ring circumference gives 1 $\mu$sec circulation time, 1000 times shorter than 1-msec length of beam from linac. Thus, ring compresses 1-msec pulse to 1-$\mu$sec pulse.
- After 1-msec of injection into ring, 1-$\mu$sec H+ beam is extracted in 1 turn and transported to spallation neutron target.
- High Z spallation target makes 30 neutrons per incident proton.
- Neutrons may be moderated to lower energies as required, and then transported to experiments

# Primary Concern: *Uncontrolled Beam Loss*

- Hands-on maintenance: no more than 100 mrem/hour residual activation (4 h cool down, 30 cm from surface)
- 1 Watt/m uncontrolled beam loss for linac & ring
- Less than $10^{-6}$ fractional beam loss per tunnel meter at 1 GeV; $10^{-4}$ loss for ring
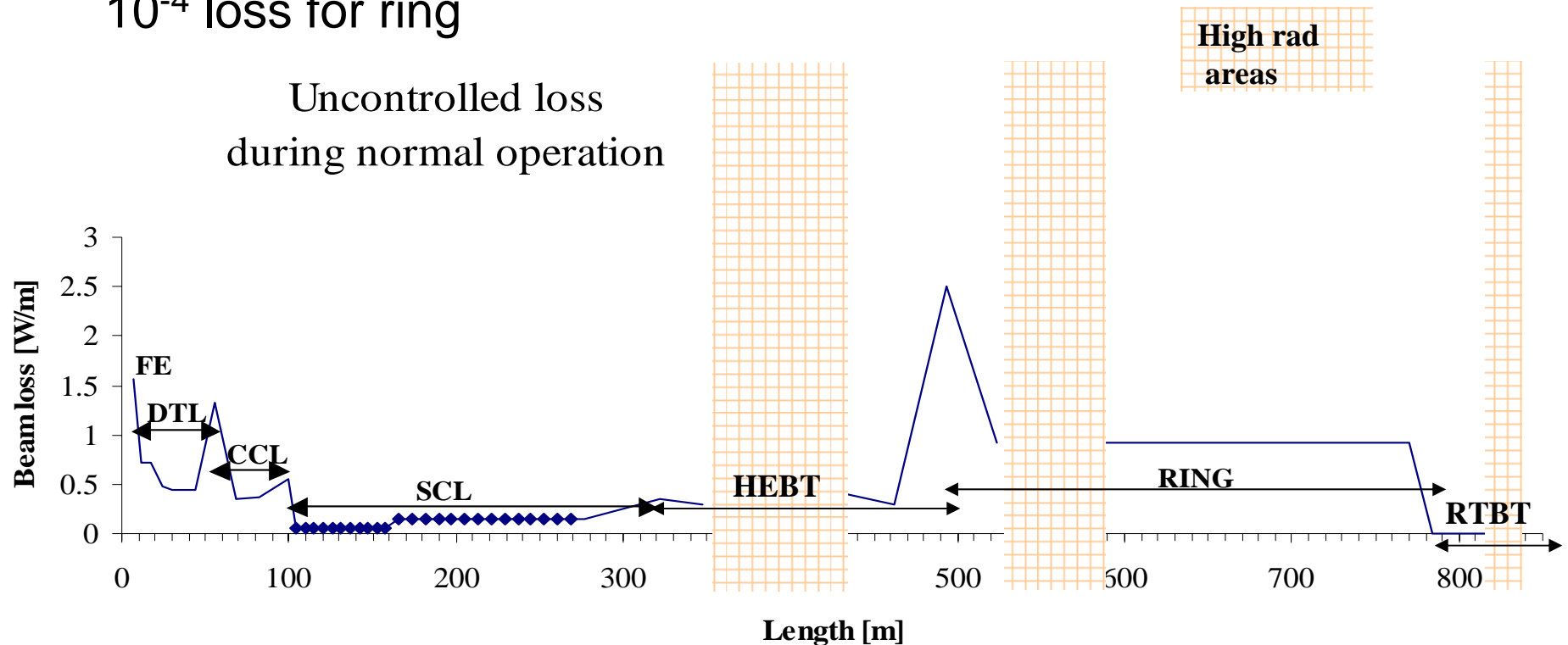
## Chopping of the H- beam is an important requirement for reducing beam loss during beam extraction in the ring.

- Beam extraction requires turn-on of fast extraction magnets in the ring.
- To avoid beam loss in the ring during extraction, a beam free gap in the ring is provided, which is roughly 1/3 of the ring circumference.
- The idea is to turn on the extraction magnets at the time when the beam-free gap arrives at the magnets.
- A beam free gap in the ring is provided by introducing beam chopper systems in the front end and in the linac to remove about 1/3 $\mu$sec of the beam.
- SNS has a 2-stage chopping system.

# Major SNS Facility Parameters



**402.5 MHz** ← → **805 MHz** ← →

| Injector | RFQ | DTL | CCL | SRF, β=0.61 | SRF, β=0.81 | HEBT | To Ring |

Injector — 2.5 MeV — 86.8 MeV — 186 MeV — 387 MeV — 1000 MeV
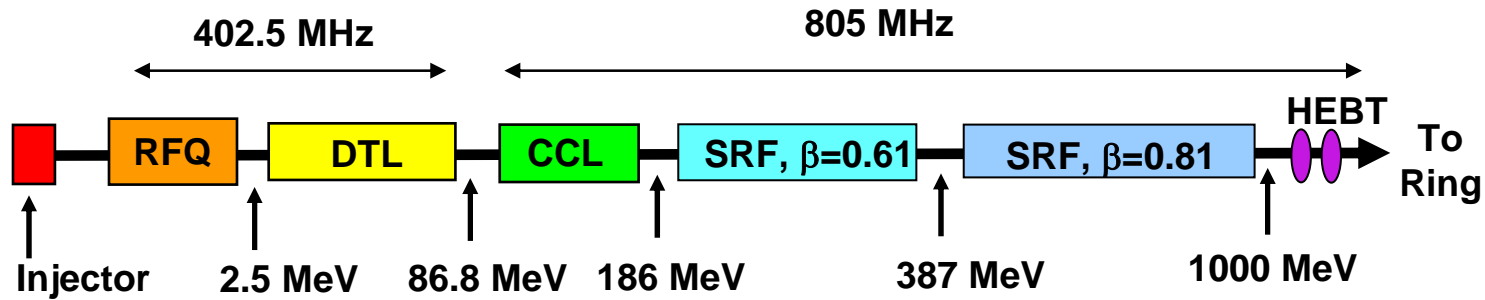
1  RFQ
6  DTL Tanks
4  CCL Modules

11  Medium-β Cryomodules - 3 Nb cavities each
12  High-β      Cryomodules - 4 Nb cavities each

1.0 GeV Ring
Up to 1.3 GeV

Target
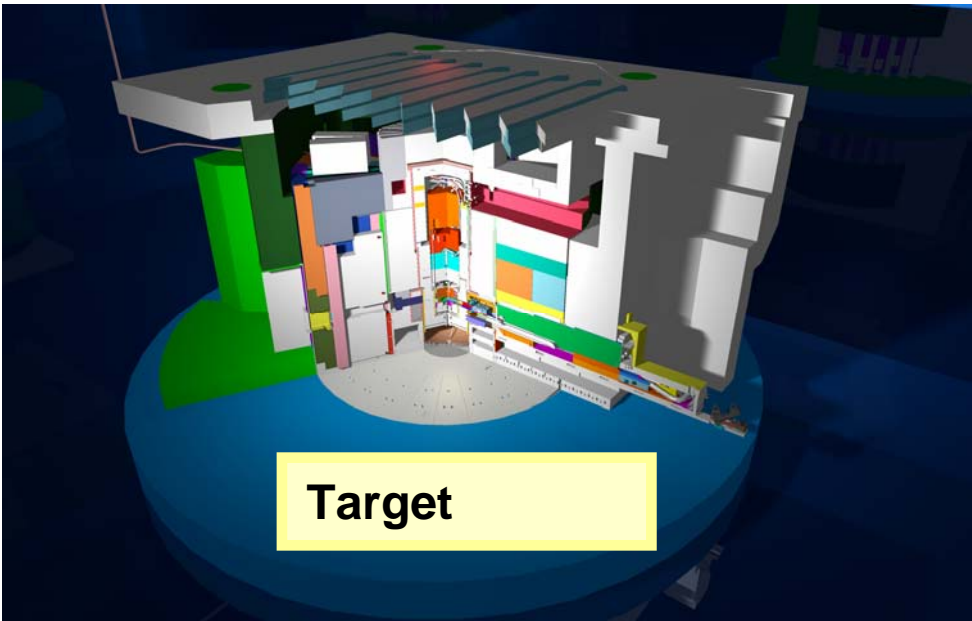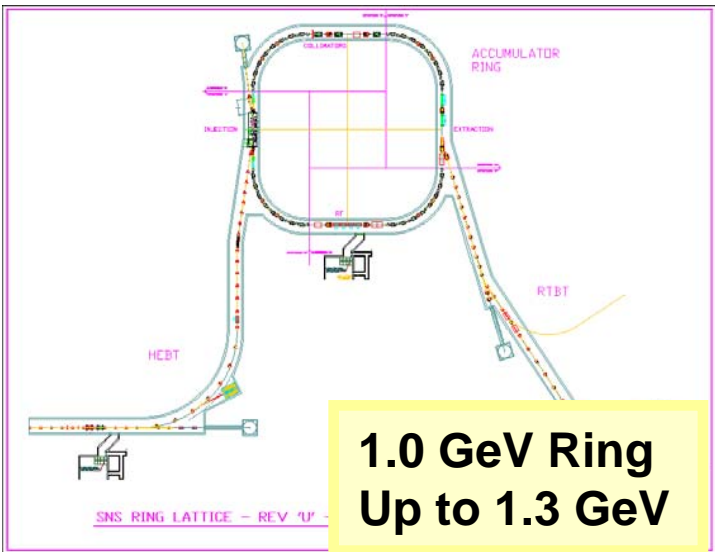
# Some nomenclature for accelerator beam systems

- Front end = H- ion source, LEBT, RFQ, MEBT
  -**LEBT**=low energy beam transport system that matches and injects beam into the RFQ.
  -**RFQ**=radiofrequency quadrupole, the first linac structure.
  -**MEBT**=medium energy transport system that matches and injects beam into the DTL.

- Linac = DTL, CCL, SCL(medium $\beta$), SCL(high $\beta$)
  -**DTL**=drift tube linac, which includes 6 tanks or modules
  -**CCL**=coupled-cavity linac, more specifically the side-coupled linac, which includes 4 modules.
  - **SCL(medium $\beta$)=**superconducting linac which includes 11 cryomodules with three $\beta$=0.61 6-cell cavities each.
  -**SCL(high $\beta$)=**superconducting linac which includes 12 cryomodules with four $\beta$=0.81 6-cell cavities each.

- Ring = accumulator/compressor ring, and RTBT
  -RTBT=ring-to-target beam transport system

# LBNL: Design And Built Front End
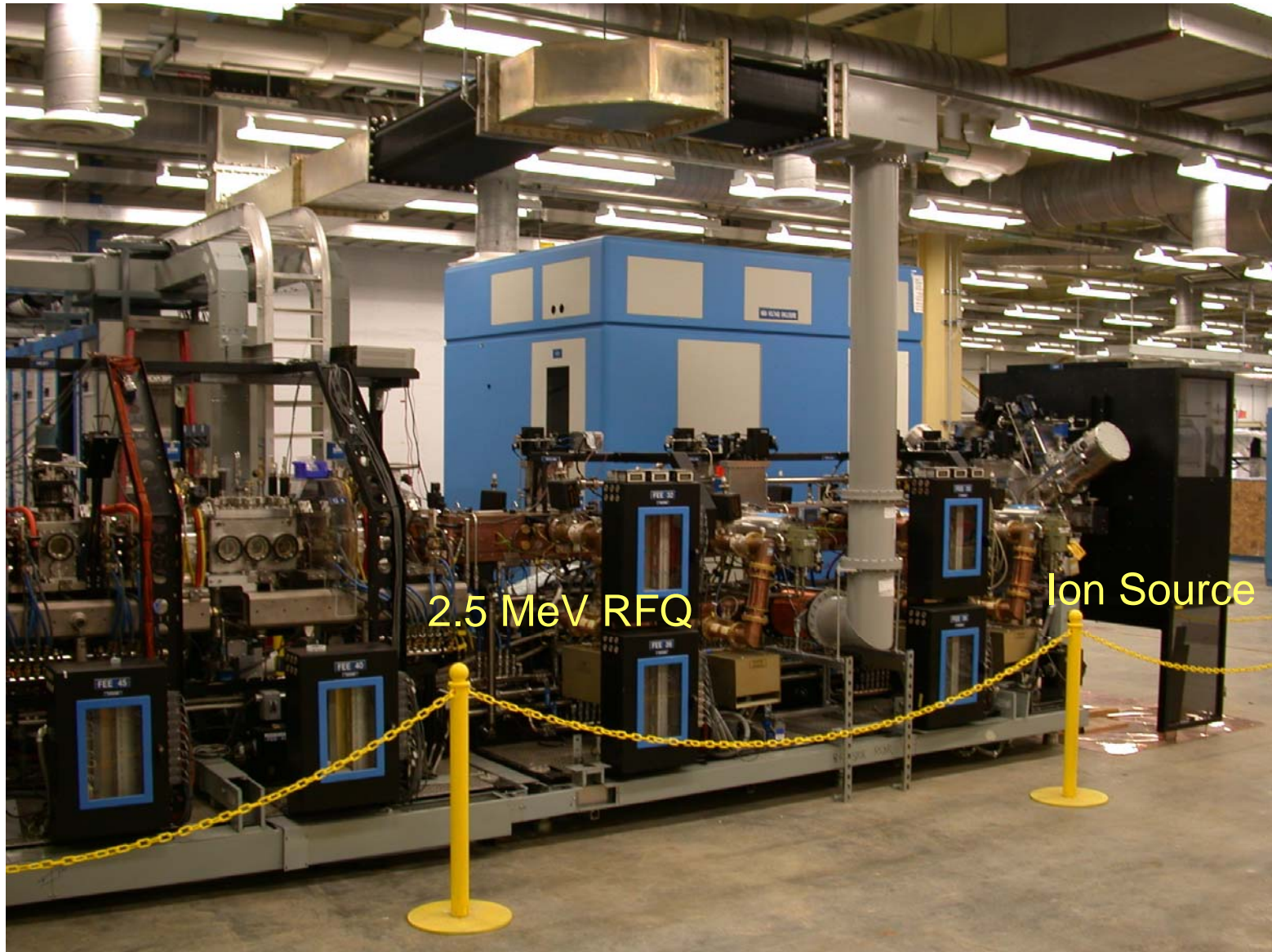
# Drift Tube Linac


DTL 1 in the tunnel …


DTL 3 …


Here it goes …

# Coupled-Cavity Linac (CCL) Construction by LANL done in Industry

- Contract awarded to Industry

- Hot model operated at 130% of peak field and 190% average power



*E*
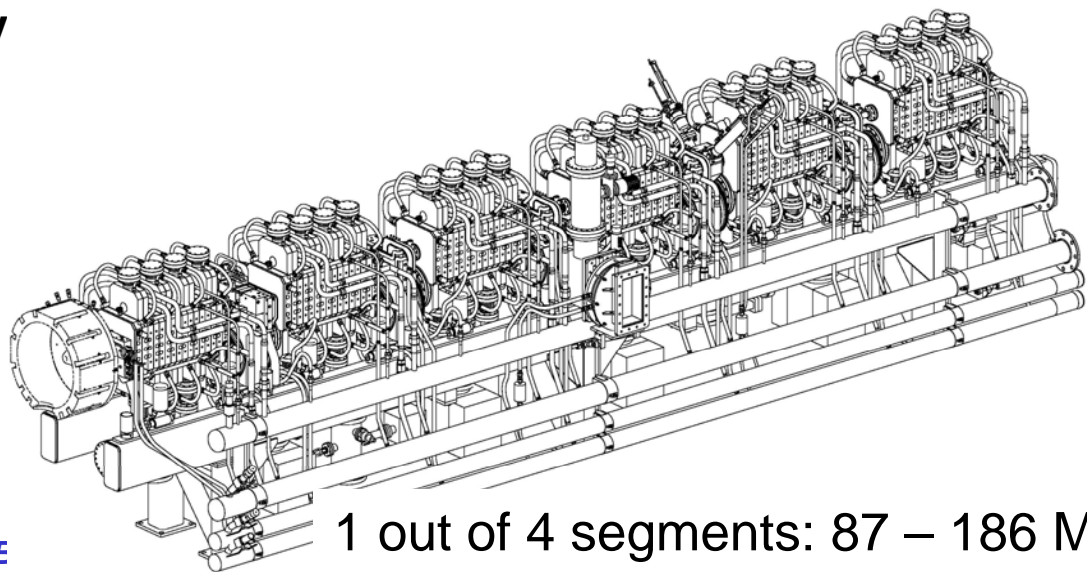
1 out of 4 segments: 87 – 186 MeV





*Production Segments*

# JLAB: The Superconducting Linac

### Superconducting RF Advantages:

1. **Flexibility ➔ gradient and energy are not fixed**
2. **More power efficient ➔ lower operational cost**
3. **High cavity fields ➔ less real estate**
4. **Better vacuum ➔less gas stripping**
5. **Large aperture ➔ less aperture restrictions ➔ reduced beam loss ➔reduced activation**



Medium β

~ No ε growth

DTL+CCL

$\varepsilon_{rms}(\pi$ cm-mrad)

W (MeV)

$\varepsilon_x$
$\varepsilon_y$
$\varepsilon_z$
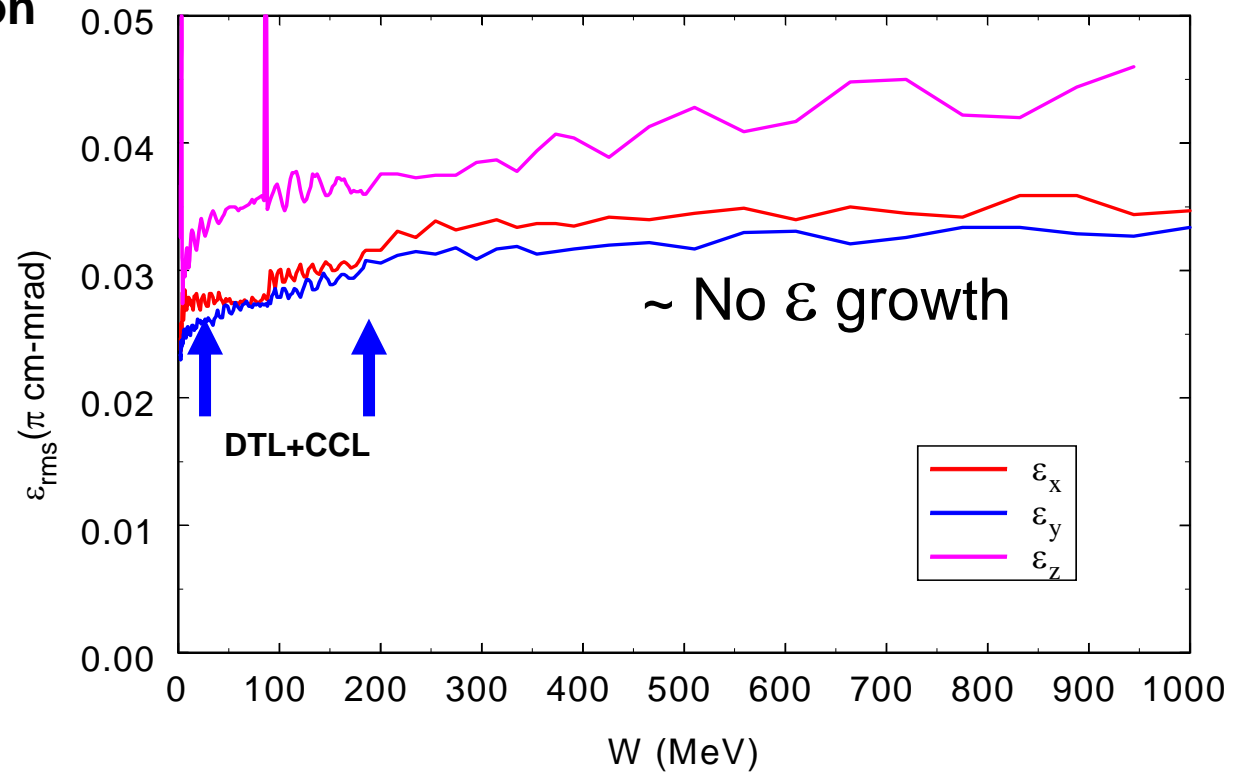
# Performance of SC Cavities in Medium β Cryomodule

**Production Cavities used for First 4 Medium Beta Cryomodules**
**Gradient @ Q0 = 5 * 10E9**

Medium Beta
Specification

Best TESLA Cavity
R&D High Beta Electro-Polished
Production Medium Beta

R&D will make them better !!!

# 

\#

Gradient MV/m
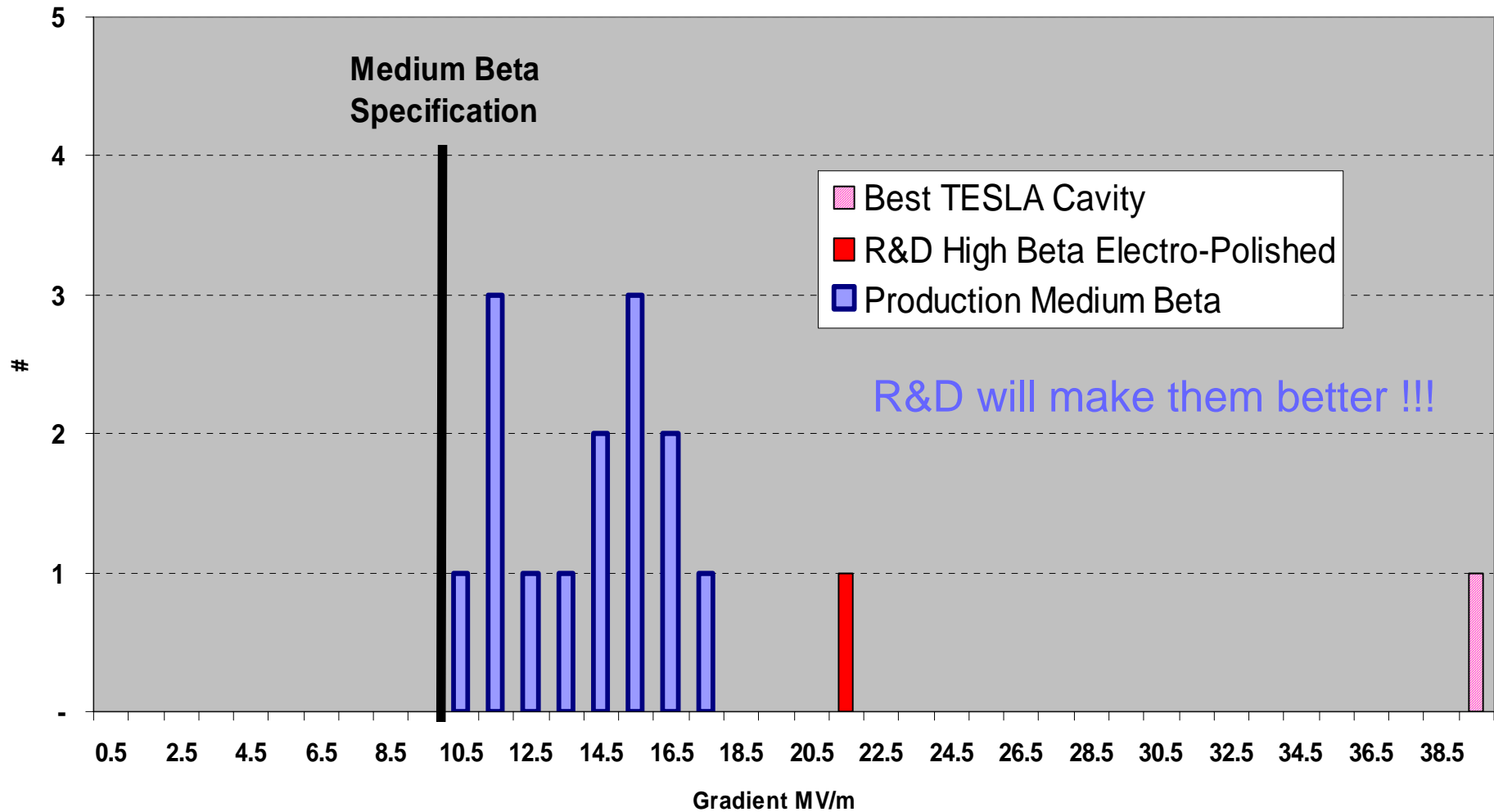
# BNL: The Accumulator Ring and Transfer Lines

| | | |
|---|---|---|
| Nr of injected turns | | 1060 |
| Ring revolution frequency | MHz | 1.058 |
| Ring filling fraction | % | 68 |
| **Ring transverse emittance 99%** | **$\pi$mm mrad** | **240** |
| **Ring transverse acceptance** | **$\pi$mm mrad** | **480** |
| **Space charge Tune shift** | **$\Delta Q_{x,y}$** | **0.15** |
| Peak Current | 52 | A |
| HEBT / RTBT Length | m | 170 / 150 |
| Ring Circumference | m | 248 |
| RTBT transverse acceptance | $\pi$mm mrad | 480 |
| Beam size on target (HxV) | mm x mm | 200x70 |

**Totals:**
**235 Low Power Bipolar Supplies (< 5 kW)**
**24 Medium Power Bipolar Supplies (5-50 kW)**
**101 Medium Power Supplies (5-50 kW)**
**42 High Power Supplies (>50 kW)**
**22 Kicker Power Supplies**

Baseline: 1.0 GeV, 2 MW
Designed and built for 1.3 GeV
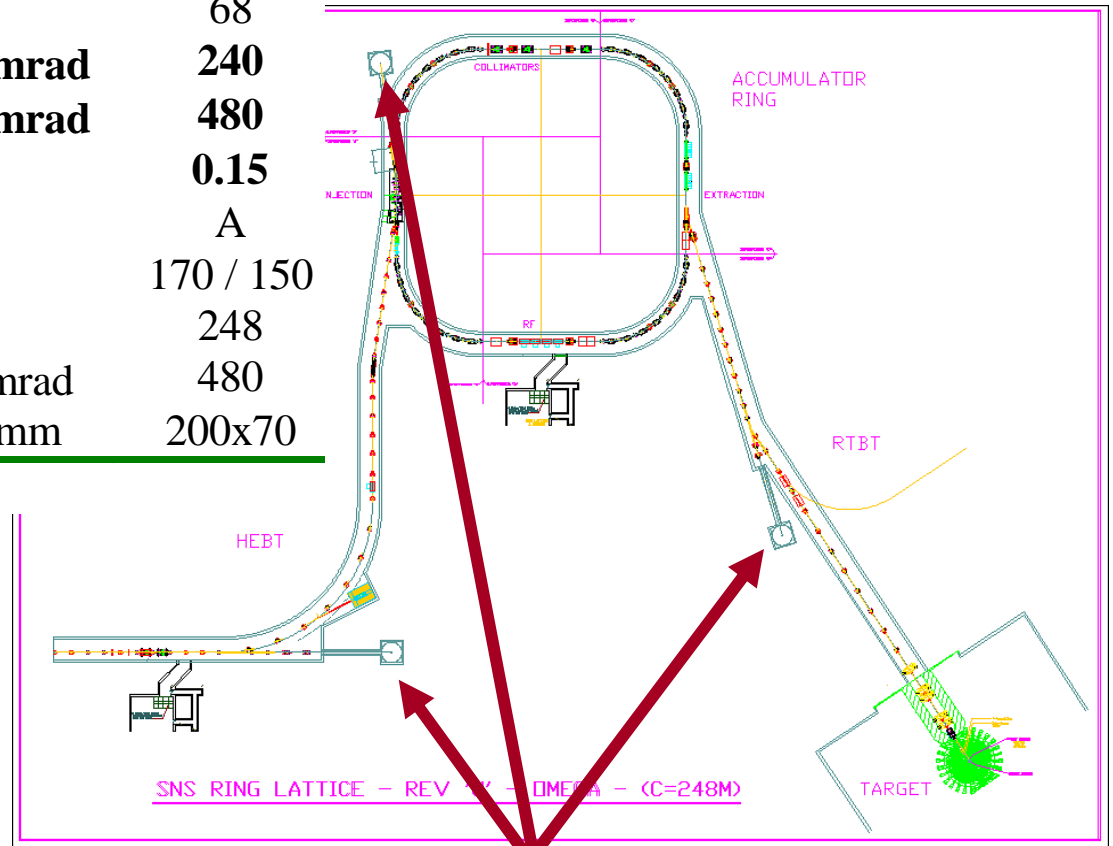


Several commissioning beam dumps

# 1% of the Reference Beam Misses the Injection Foil
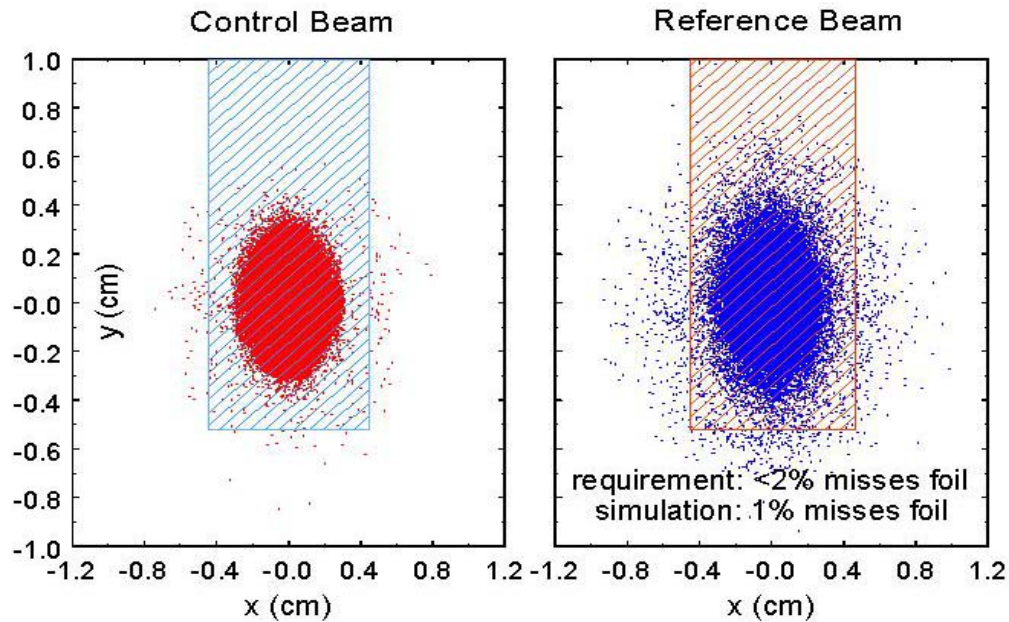


- Transverse Jitter at the Foil is a Function of Quad Vibrations in the linac& Increases the Effective Emittance

- This drives tolerance for mechanical design
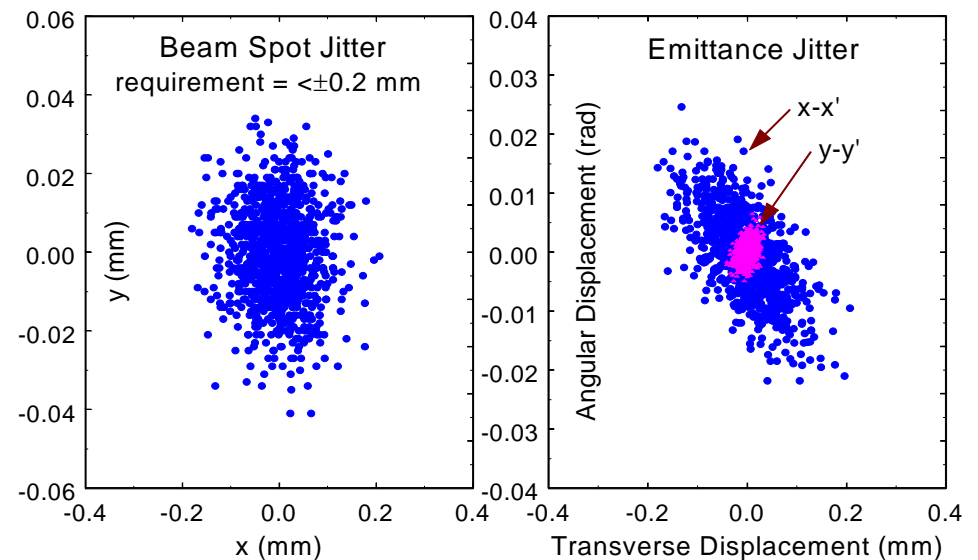
# A 20-Year Plan- The Long Term Future for SNS

| | Baseline | Upgrade | Ultimate |
|---|---|---|---|
| Kinetic energy, $E_k$ [MeV] | 1000 | 1300 | 1400 |
| Beam power on target, $P_{max}$ [MW] | 1.4 | 3.0 | 5.0 |
| Chopper beam-on duty factor [%] | 68 | 70 | 70 |
| Linac beam macro pulse duty factor [%] | 6.0 | 6.0 | 6.0 |
| Average macropulse H- current [mA] | 26 | 42 | 65 |
| Peak Current from front end system | 38 | 59 | 92 |
| Linac average beam current [mA] | 1.6 | 2.5 | 3.9 |
| SRF cryo-module number (med-beta) | 11 | 11 | 11 |
| SRF cryo-module number (high-beta) | 12 | 12 + 8 (+1 reserve) | 12 + 8 (+1 reserve) |
| Number of SRF cavities | 33+48 | 33+80 (+4 reserve) | 33+80 (+4 reserve) |
| Peak gradient, $E_p$ ($\beta$=0.61 cavity) [MV/m] | 27.5 (+/- 2.5) | 27.5 (+/- 2.5) | 27.5 (+/- 2.5) |
| Peak gradient, $E_p$ ($\beta$=0.81 cavity) [MV/m] | 35 (+2.5/-7.5) | 31 | 34 |
| Ring injection time [ms] / turns | 1.0 / 1060 | 1.0 / 1100 | 1.0 / 1110 |
| Ring rf frequency [MHz] | 1.058 | 1.098 | 1.107 |
| Ring bunch intensity [$10^{14}$] | 1.6 | 2.5 | 3.8 |
| Ring space-charge tune spread, $\Delta Q_{sc}$ | 0.15 | 0.15 | 0.2 |
| Pulse length on target [ns] | 695 | 691 | 683 |

# Introduction to RF Linacs

Tom Wangler

# RF linacs compared with other types of accelerators

- In DC accelerators the energy gain is limited by the maximum applied voltage, which is limited by electric breakdown.

- In RF accelerators (linacs, synchrotrons, cyclotrons) the final energy can exceed the maximum voltage, which can be applied repeatedly to the beam. **The final energy is limited only by economics.**

- Synchrotrons are limited to low beam currents by beam instabilities associated with the repetitive cycling of the beam from turn to turn through unavoidable focusing lattice errors.

- Cyclotrons are not pulsed but are limited to low beams currents by weak focusing and same inherent circular machine instabilities.

- Linacs can deliver high beam currents because they can provide strong focusing to confine the beam and are not subject to circular machine instabilities.

# Advantages of RF linacs

- **SUMMARY: Linacs are capable of delivering beams with high energy, high intensity, and good beam quality (small emittance).**

- Maximum energy not limited by electric breakdown.

- Strong focusing can be provided.

- Single pass device means beam is not subject to repetitive error conditions which cause destructive resonances as in circular machines.

- No power loss from synchrotron radiation for electron linacs.

- Natural orbit is a straight line making injection and extraction easier.

- No limit to duty factor.

# Block diagram of an RF linac system
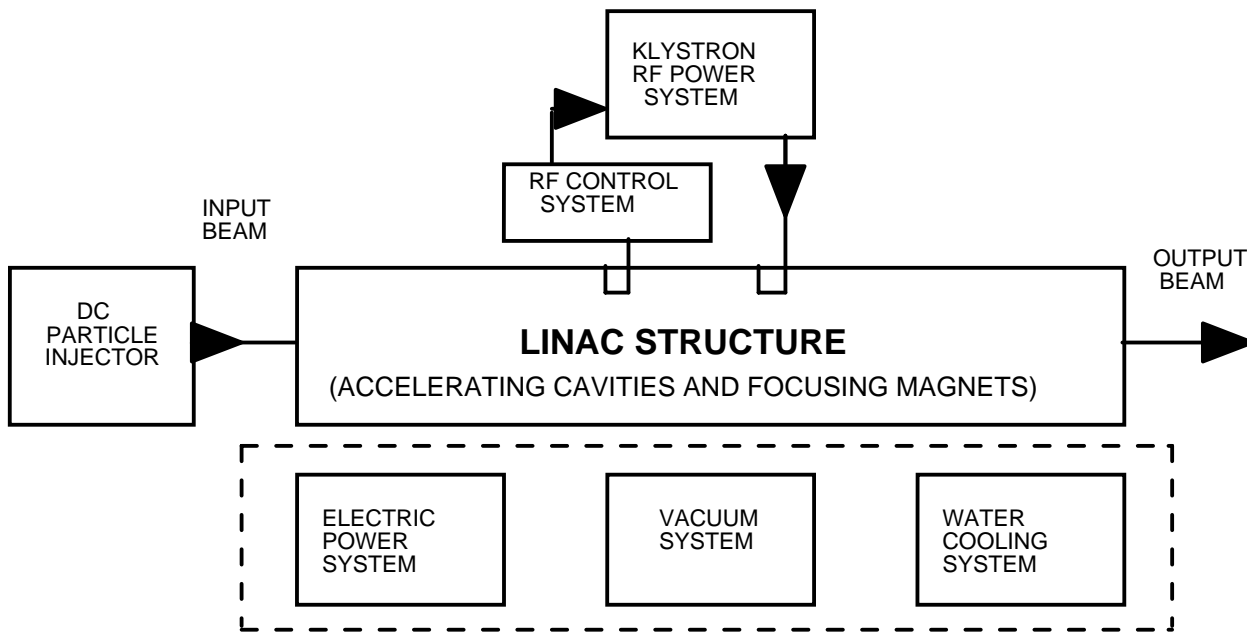
# Units

---

- We use SI or MKS units with two notable exceptions.
- Magnetic flux density B is sometimes given in Gauss. The SI unit (Tesla) is also used. **1T=$10^4$ Gauss.**
- Beam kinetic energy is expressed in units derived from the electron volt (eV), such as keV, MeV, or GeV, instead of Joules.

  1eV=energy acquired by a particle with electronic charge 1.602 X $10^{-19}$ C accelerated through 1 Volt.

  **1.602 X $10^{-19}$ J/eV**

# Relativistic Particle Dynamics

- Nonrelativistic (Newton's Laws)

$$Kinetic\ energy = mv^2 / 2$$

$$Momentum = mv$$

$$Force = \frac{d\vec{p}}{dt} = m\frac{d\vec{v}}{dt}$$

- Relativistic (Einstein) is more general.

$$Velocity = \beta = v / c$$

$$Relativistic\ mass\ factor = \gamma = \frac{1}{\sqrt{1-\beta^2}}$$

$$Rest\ energy = mc^2$$

$$Kinetic\ energy = W = (\gamma - 1)mc^2$$

$$Total\ energy = U = W + mc^2 = \gamma mc^2$$

$$Momentum = \vec{p} = \gamma m\vec{v}$$

$$Force = \vec{F} = \frac{d\vec{p}}{dt} = m\frac{d(\gamma\vec{v})}{dt}$$

# Relativistic particle dynamics (continued)

- When $\beta \ll 1$ the relativistic formulas reduce to the nonrelativistic ones. Thus

$$\gamma \to 1 + \beta^2 / 2$$

$$p \to mv$$

$$W \to mv^2 / 2$$

$$U \to mc^2 + mv^2 / 2$$

- Lorentz force is the force on a charged particle in an electromagnetic field:

$$\vec{F} = q\left(\vec{E} + \vec{v} \times \vec{B}\right)$$

# Electromagnetic Theory

- Maxwell's equations are the laws that relate the time and spatial dependence of the electric (E) and magnetic (B) fields to the charges and currents.

- We use E and B more than we use currents and voltages because:

  a) The fields determine the force on the charged particles in the beam.

  b) In microwave structures the fields are the measured quantities rather than currents and voltages.

# Maxwell's Equations in Vacuum

$$\nabla \bullet \vec{E} = \rho / \varepsilon_0 \quad Gauss's\,law$$

$$\nabla \bullet \vec{B} = 0$$

$$\nabla \times \vec{E} = -\frac{\partial \vec{B}}{\partial t} \quad Faraday's\,law$$

$$\nabla \times \vec{H} = \vec{j} + \varepsilon_0 \frac{\partial \vec{E}}{\partial t} \quad Ampere's\,law$$

$$\vec{B} = \mu_0 \vec{H}$$

*Wave equations are derived from Maxwell's equations.*

$$\nabla^2 \vec{E} - \frac{1}{c^2}\frac{\partial^2 E}{\partial t^2} = 0, \quad \nabla^2 \vec{H} - \frac{1}{c^2}\frac{\partial^2 \vec{H}}{\partial t^2} = 0$$

*Boundary conditions at a perfect conductor* :

$$E_{normal} = \sigma / \varepsilon_0 \qquad (\sigma = surface\,ch\arg e\,per\,unit\,area)$$

$$E_{parallel} = 0$$

$$H_{normal} = 0$$

$$H_{parallel} = K \quad \left(K = surface\,current\,per\,unit \perp length\right)$$

# RF power dissipation on a nonperfect conductor

- Consider a plane conducting surface (a good approximation for curved surface if radius of curvature is >> skin depth).



- Average power dissipation on surface with area $A=\ell^2$ is

$$P = \frac{R_s I^2}{2} = \frac{R_s (H\ell)^2}{2} = \frac{R_s H^2 A}{2} \rightarrow P = \frac{R_s}{2}\int H^2 dA$$

  using $H=I/\ell$, and $R_s$ is called the surface resistance.
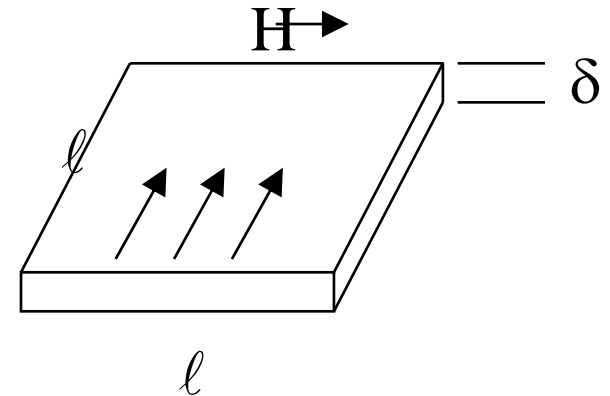
- Using $B=\mu_0 H$ we can also write a general result (for both normal conducting and superconducting cases):

$$P = \frac{R_s}{2}\int \left(\frac{B}{\mu_0}\right)^2 dA$$

- The Ohmic power loss depends on the RF surface magnetic field.

- This result is valid for both normal conductors and superconductors. What is different about these is $R_s$.

# Normal-conducting surface resistance

•There are Ohmic losses

in the non-perfect conductor.

•Skin effect: RF currents are
confined near surface.

•These "surface" currents produce
an H field that cancels the
applied H field inside the conductor.
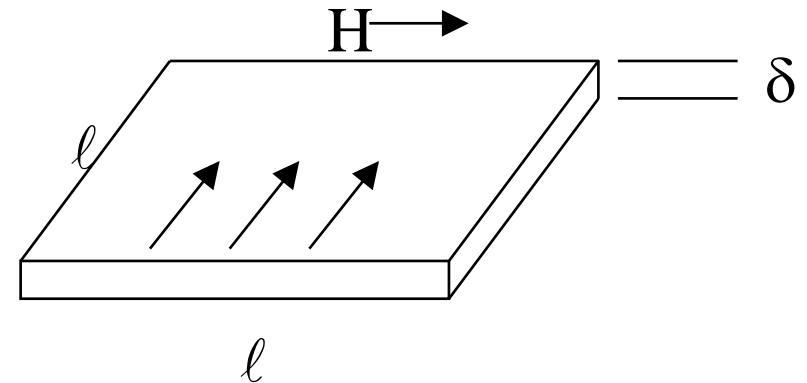


• Naive derivation: Assume the skin-effect resistance is the same
as the DC resistance, as if the current associated with H is uniformly
distributed over the skin depth $\delta$. (Actually the current really falls off
exponentially with depth into the conductor.)

The surface resistance is: $\quad R_s = \dfrac{1}{\sigma}\dfrac{\ell}{\ell\delta} = \dfrac{1}{\sigma\delta}$

• A rigorous treatment shows this is the correct result (normal conductor)

$$\delta = \sqrt{\dfrac{2}{\mu_0\sigma\omega}} \qquad and\ \ R_s = \sqrt{\dfrac{\mu_0\omega}{2\sigma}}$$

# Superconducting niobium rf surface resistance

$$R_s(\Omega) \cong 9 \times 10^{-5} \frac{f(GHz)^2}{T(K)} e^{-\alpha \frac{T_c}{T}} + R_{residual}$$

$\alpha$=1.92, $T_c$=9.2K, $R_{residual}$=residual resistance (typically 10 n$\Omega$.

$R_s$ for superconducting niobium is roughly $10^{-5}$ times that of copper.

# Proton Linac Beam Dynamics

- Proton linacs are designed for sustained acceleration of a single particle called the synchronous or reference particle.

- To accelerate high-intensity beams, two things must be done.
  1) Create beam bunches centered on the synchronous particle. On average, the other (non-synchronous) particles see accelerating fields like those seen by the synchronous particle.
  2) Provide focusing in all three planes to counteract the defocusing effects such as the space-charge forces.

# A bunched beam must be injected into an rf linac and the cavities are phased to provide acceleration and longitudinal focusing of the beam.
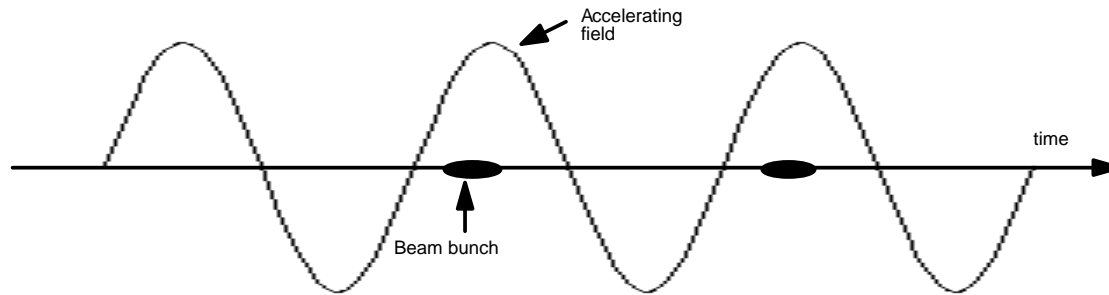


Fig. 1.2b. Beam bunches in an RF linac.

# Bunching

- Bunching of a DC beam can be done with buncher cavities installed in front of the linac. Particles bunch about the stable -90 deg phase.

- In many modern linacs bunching is done adiabatically in the RFQ.
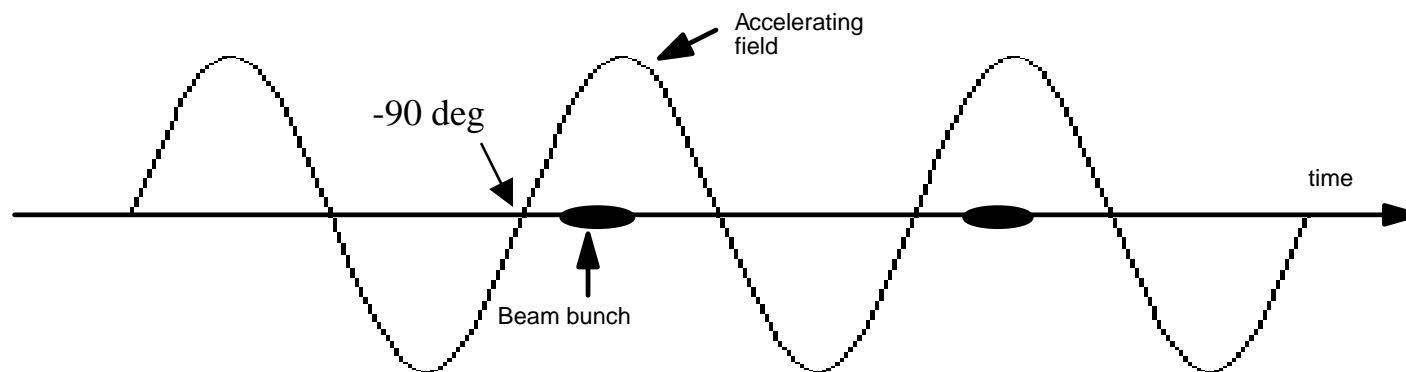


Fig. 1.2b. Beam bunches in an RF linac.

# Focusing

---

- Focusing really means confinement in presence of defocusing effects of emittance and space charge.

- Longitudinal focusing is achieved by injecting the beam into each accelerating cavity before the $E_z$ field reaches the peak.

- Early particles see a smaller $E_z$ field and later particles see a larger field. This produces longitudinal oscillations about the synchronous phase, i.e. phase stability.

- Transverse focusing can be achieved by providing magnetic lenses such as quadrupole magnets, which can be used in pairs to confine the beam in both transverse planes.

- Transversely focused particles oscillate about the beam axis. These are known as betatron oscillations.

# Time structure of linac beam

---

- Time structure of a pulsed linac beam consists of micropulses within macropulses.

- Micropulse length is beam-bunch time duration which is some fraction of an rf period. For SNS the beam is bunched at 402.5 MHz for 2.5 nsec RF period. The RF system is too slow to see the micropulses.

- Macropulse length is the time duration containing a string of beam bunches. For SNS this is 1 msec, which contains 400,000 of the 2.5 nsec micropulses.

- Beam choppers, such as used in SNS, remove a few hundred nsec of beam from the macropulse about every microsecond synchronized to provide a beam free gap in the ring. For SNS this is a 0.250 $\mu$sec gap every 0.955 $\mu$sec.

- Chopping may be said to produce "mini" pulses. There are 40,000 chopper minipulses per macropulse.

# Starting point for RF accelerating structures is the pillbox cavity operating in TM$_{010}$ mode.
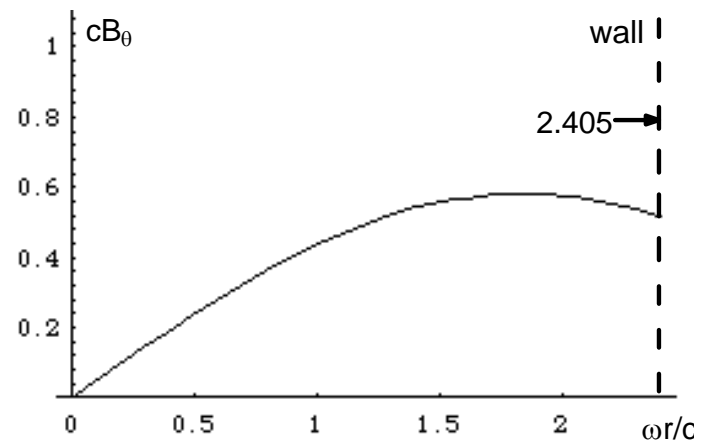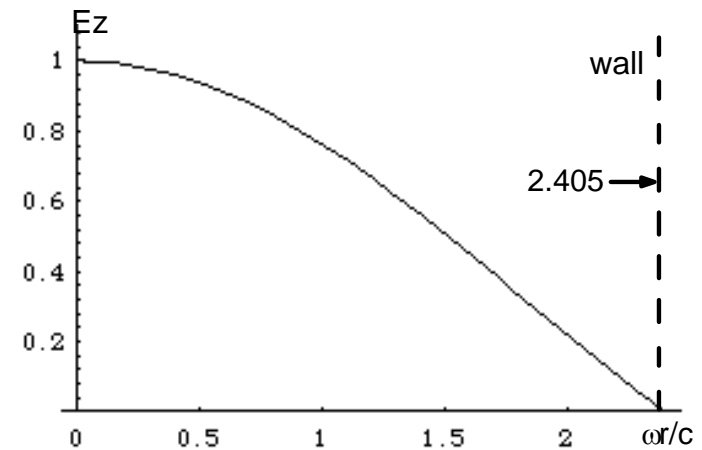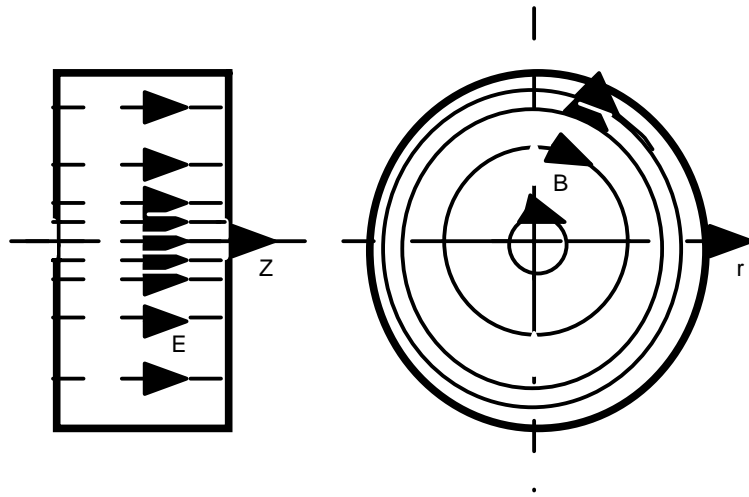


$$E_z = E_0 J_0(2.405 r / R)\cos(\omega t)$$

$$B_\theta = -\frac{E_0}{c} J_1(2.405 r / R)\sin(\omega)$$

$$Cavity\ radius = R = 2.405\lambda / 2\pi$$

# Pillbox cavity(1)

- Most cavity resonators are derived from the simple cylindrical or pillbox cavity.

- Simple geometry with conducting end plates on each end of a conducting cylinder with radius $R_c$. Apertures for beam are ignored.

- Fortunately, an analytic solution exists for the pillbox cavity.

- Assume azimuthally symmetric trial solution with longitudinal field given by:

$$E_z(r, z, t) = R(r)e^{j\omega t}$$

- The solution must satisfy the wave equation with the condition that Ez=0 at r=$R_c$.

$R_c$
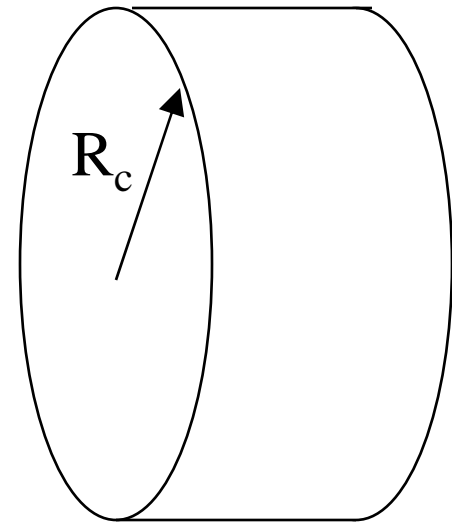
# Pillbox cavity(2)

- Wave equation in cylindrical coordinates (azimuthal symmetry):

$$\frac{\partial^2 E_z}{\partial z^2} + \frac{1}{r}\frac{\partial E_z}{\partial r} + \frac{\partial^2 E_z}{\partial r^2} - \frac{1}{c^2}\frac{\partial^2 E_z}{\partial t^2} = 0$$

- Substituting the trial solution we find that R(r) satisfies the Bessel Equation of order zero. The magnetic field is obtained from Ampere's law.
- The nonzero field components are:

$$E_z(r,t) = E_0 J_0(k_r r)\cos(\omega t)$$

$$B_\theta(r,t) = -\frac{E_0}{c} J_1(k_r r)\sin(\omega t), \qquad k_r = 2\pi/\lambda$$

- To satisfy the boundary condition that $E_z=0$ at $r=R_c$, we need $k_r R_c=2.405$. This fixes resonant frequency as:

$$\omega_c = k_r c = 2.405c/R_c$$

# Bessel functions of argument x
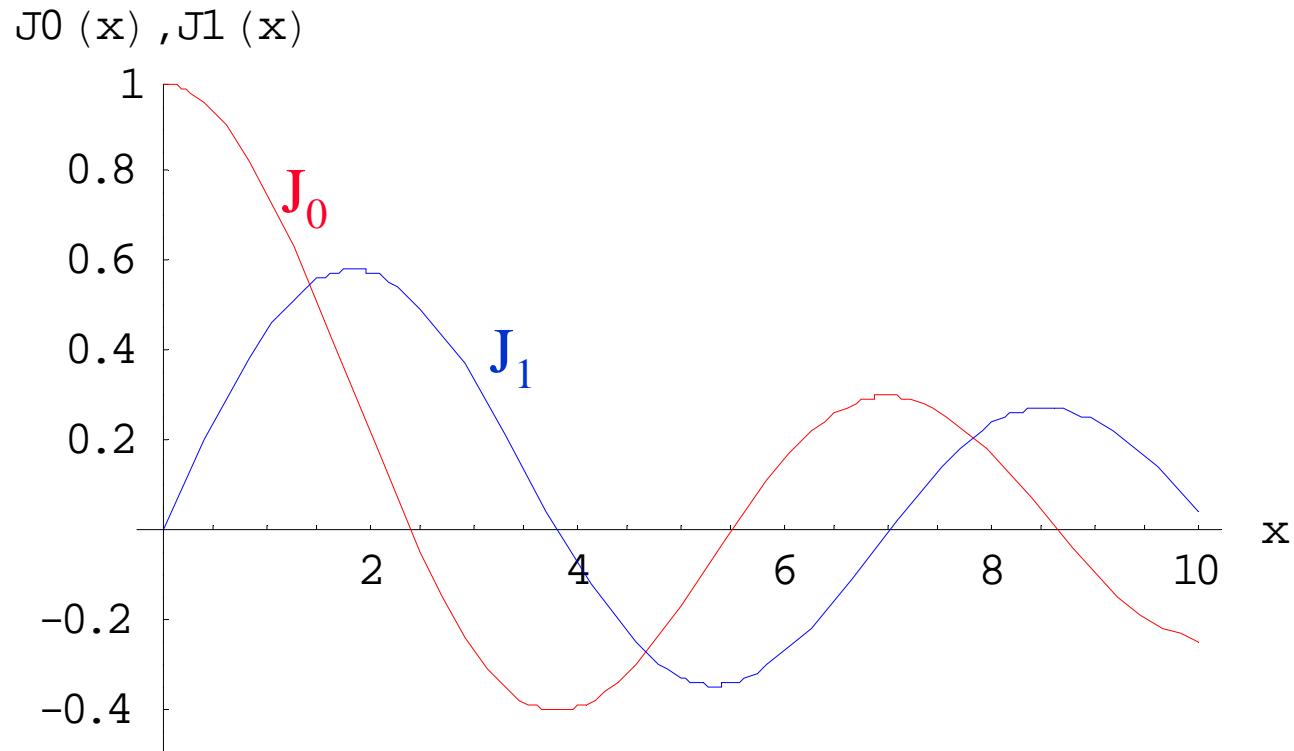


An important number is the value of x that gives the first zero of $J_0$.
This is x=2.405 for the first $J_0(x)=0$.

# Pillbox cavity (3)

- Cavity radius is given by $R_c = 2.405\lambda/2\pi$. This also follows from $k_r R_c = 2.405$.

- Note that $E_{max}$ is at $r=0$.

- $B_{max}$ is at $J_{1,max} = 0.5819$, which occurs at $k_r r = 1.842$ on each end wall.

- The result is $B_{max} = 0.5819 E_0/c$, which occurs at $r=0.842$.

- Note that the electric and magnetic fields are 90 deg out of phase.

# Electric and magnetic field lines for a pillbox cavity excited in a $TM_{010}$ resonant mode.



Fig. 1.12b. Fields for a $TM_{010}$ mode of a cylindrical (pillbox) cavity resonator.

# Radial dependence of electric and magnetic fields in TM$_{010}$ pillbox cavity
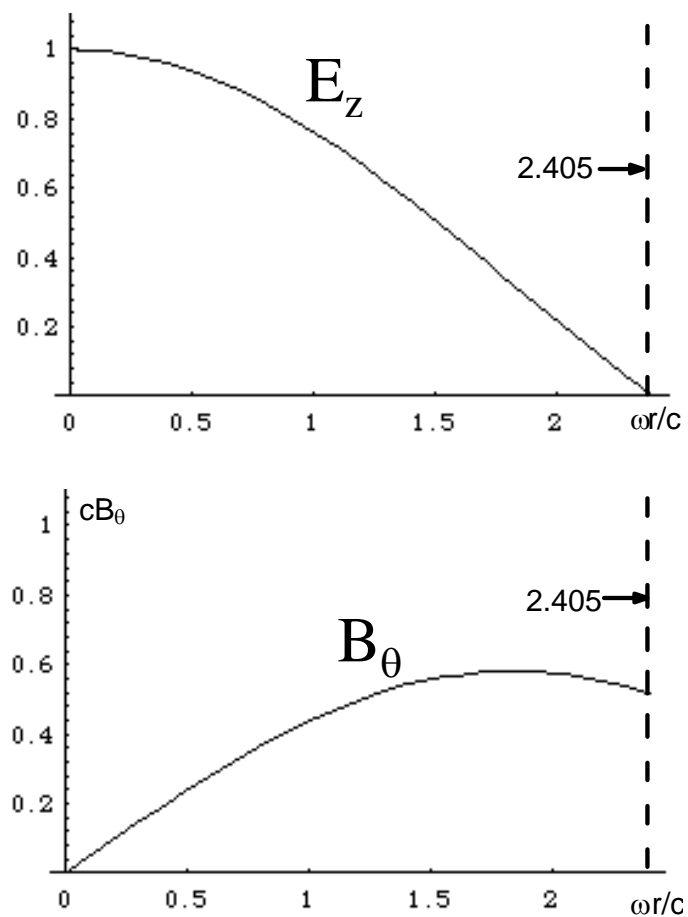


Fig. 1.12a.        Fields for a TM$_{010}$ mode of a cylindrical (pillbox) cavity resonator.

The radial field distributions are shown graphically in Figs. 1.12a and b. To satisfy the boundary condition, the resonant frequency of this mode must be $\omega_c = k_r c = 2.405c / R_c$, which is independent of the cavity length. The mode is called a transverse magnetic mode, because the z-compone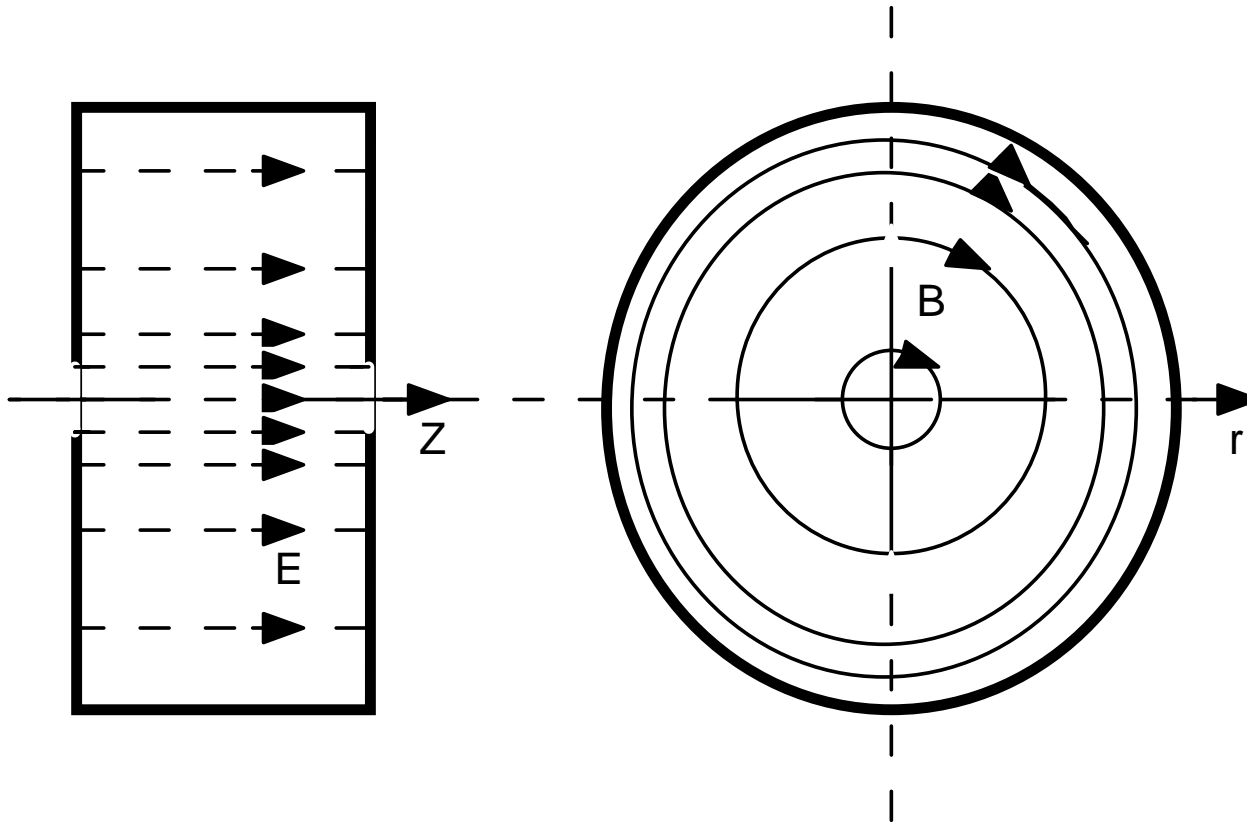nt of the magnetic field is zero, and in the conventional nomenclature the mode is called a $TM_{010}$ mode for reasons that will be explained shortly. The total electromagnetic stored energy can be calculated from the peak electric stored energy, and the result is

$$U = \frac{\pi \varepsilon_0 \ell R_c^2}{2} E_0^2 J_1^2 (2.405).$$

(3)

The average power dissipated on the cylindrical walls and the end walls is

$$P = \pi R_c R_S E_0^2 \left( \frac{\varepsilon_0}{\mu_0} \right) J_1^2 (2.405)(\ell + R_c).$$

(4)

The quality factor is

$$Q = \frac{\omega_C U}{P} = \frac{2.405 \sqrt{\mu_0 / \varepsilon_0}}{2R_S} \frac{1}{1 + R_c / \ell}.$$

(5)

The electric field is maximum at $r = 0$, where $J_0$ is maximum. Two useful values of $J_1$ are the maximum value, which is $J_1(1.841)=0.5819$, and the value of $J_1$ at the cylindrical wall, which is $J_1(2.405) = 0.5191$. The magnetic field is maximum at $k_r R = 0.7655$, where $J_1(k_r R)$ is maximum. Therefore, $B_{max} / E_{max} = 0.5819 / c = 19.4G / MV / m$.

# There are an infinite number of other modes. There is a mode nomenclature for transverse magnetic (TM) modes of a cylindrical cavity.

- $\text{TM}_{mnp}$ where m, n, p corresponds to $\theta$, r, z.
- m = number of full period variations in $\theta$ of the field components.
- n = number of zeros of axial field component Ez in the radial direction in range $0 < r \le R_c$ excluding r=0.
- p = number of half period variations in z of the field components.

## 1.13 Cylindrical Resonator Transverse Magnetic Modes

Other transverse magnetic modes exist with the same radial Bessel-function solution, corresponding to fitting a half-integer number of guide wavelengths within the length $\ell$. We label the different longitudinal modes with the index p, and adopt the conventional nomenclature $TM_{01p}$, p = 1,2,3, ... . The dispersion relation is the same as for a uniform waveguide, except that the longitudinal wave number is restricted to those discrete values required to satisfy the boundary conditions at the two ends. The modes lie on the curve given by $\omega^2 / c^2 = k_r^2 + k_z^2$, where $k_r = 2.405 / R_c$ , and $k_z = 2\pi / \lambda_g = \pi p / \ell$. Then the dispersion relation becomes a discrete spectrum of points that are sprinkled on a hyperbolic curve, as shown in Fig. 1.13a . The $TM_{010}$ mode, discussed in Section 1.12, is the lowest mode with p = 0. The dispersion relation gives the resonant frequency of this mode as the cut-off frequency $\omega_c = k_r c = 2.405c / R_c$.
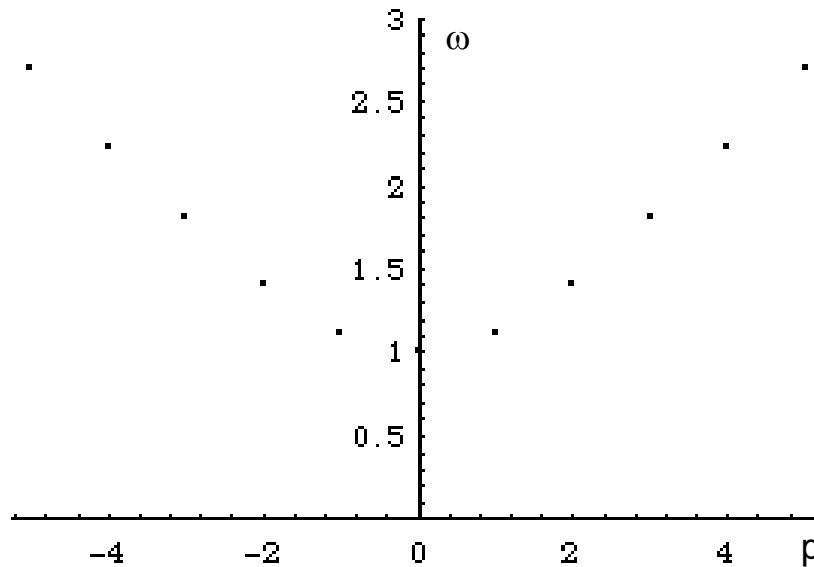


Fig. 1.13a The dispersion curve for the $TM_{01p}$ family of modes of a circular cylindrical cavity.

There exist additional transverse magnetic modes of a cylindrical cavity, corresponding to different radial and azimuthal solutions. The general expressions for the field components is

$$E_z = E_0 J_m(k_{mn}r)\cos m\theta \cos(p\pi z / \ell)\exp[j\omega t] \ ,$$

$$E_r = -\frac{p\pi}{\ell}\frac{a}{x_{mn}} E_0 J'_m(k_{mn}r)\cos m\theta \sin(p\pi z / \ell)\exp[j\omega t] \ ,$$

$$E_\theta = -\frac{p\pi}{\ell}\frac{ma^2}{x_{mn}^2 r} E_0 J_m(k_{mn}r)\sin m\theta \sin(p\pi z / \ell)\exp[j\omega t] \ ,$$

$$B_z = 0 \ ,$$

$$B_r = -j\omega \frac{ma^2}{x_{mn}^2 rc^2} E_0 J_m(k_{mn}r)\sin m\theta \cos(p\pi z / \ell)\exp[j\omega t] \ ,$$

$$B_\theta = -j\omega \frac{a}{x_{mn}c^2} E_0 J'_m(k_{mn}r)\cos m\theta \cos(p\pi z / \ell)\exp[j\omega t] \ ,$$

(1)

The general dispersion relation is $\omega^2 / c^2 = k_{mn}^2 + k_z^2$, where $k_{mn} = x_{mn} / R_c$, and $k_z = 2\pi / \lambda_{guide} = p\pi / \ell$, $p = 0, 1, 2, \ldots$. Some values of the zeros of the Bessel functions, $x_{mn}$, are given in Table 1.13a. The nomenclature of the $TM_{mnp}$ modes is defined as follows. The subscript m (m = 0, 1, 2, ...) is the number of full period variations in $\theta$ of the field components. The subscript n (n = 1, 2, 3, ...) is the number of zeros of the axial field component in the radial direction in the range $0 < r \le R_c$, excluding r = 0. The subscript p (p = 0,1,2,...) is the number of half period variations in z of the fields.

Table 1.13a    Zeros of $J_m(x)$,

| m | $x_{m1}$ | $x_{m2}$ | $x_{m3}$ |
|---|----------|----------|----------|
| 0 | 2.405 | 5.520 | 8.654 |
| 1 | 3.832 | 7.016 | 10.173 |
| 2 | 5.136 | 8.417 | 11.620 |

### 1.14 Cylindrical Resonator Transverse Electric Modes

Likewise there exist additional transverse electric modes of a cylindrical cavity, corresponding to solutions with zero axial component of the electric field. The general field-component expressions for the transverse electric modes are:

$$B_z = B_0 J_m(k_{mn}r)\cos m\theta \sin(p\pi z / \ell)\exp[j\omega t] ,$$

$$B_r = \frac{p\pi}{\ell} \frac{a}{x'_{mn}} B_0 J'_m(k_{mn}r)\cos m\theta \cos(p\pi z / \ell)\exp[j\omega t] ,$$

$$B_\theta = -\frac{p\pi}{\ell} \frac{ma^2}{x'^2_{mn}r} B_0 J_m(k_{mn}r)\sin m\theta \cos(p\pi z / \ell)\exp[j\omega t] ,$$

$$E_z = 0 ,$$

(1)

$$E_r = j\omega \frac{ma^2}{x'^2_{mn}r} B_0 J_m(k_{mn}r)\sin m\theta \sin(p\pi z / \ell)\exp[j\omega t] ,$$

$$E_\theta = j\omega \frac{a}{x'_{mn}} B_0 J'_m(k_{mn}r)\cos m\theta \sin(p\pi z / \ell)\exp[j\omega t] .$$

The general dispersion relation is $\omega^2 / c^2 = k^2_{mn} + k^2_z$ , where $k_{mn} = x'_{mn} / R_c$ , and $k_z = 2\pi / \lambda_{guide} = p\pi / \ell, \ p = 0, 1, 2, ....$ The $x'_{mn}$ are the zeros of the derivatives of the Bessel functions, and are given in Table 1.14a. The nomenclature of the TE$_{mnp}$ modes is defined as follows. The subscript m (m = 0, 1, 2, ...) is the number of full period variations in $\theta$ of the field components. The subscript n (n = 1, 2, 3, ...) is the number of zeros of the axial field component in the radial direction in the range $0 < r \leq R_c$, excluding r = 0. The subscript p (p = 0,1,2,...) is the number of half period variations in z of the fields.

Table 1.14a     Zeros of $J'_m$

| m | $x'_{m1}$ | $x'_{m2}$ | $x'_{m3}$ |
|---|---|---|---|
| 0 | 3.832 | 7.016 | 10.174 |
| 1 | 1.841 | 5.331 | 8.536 |
| 2 | 3.054 | 6.706 | 9.970 |

# Electromagnetic Modes of Cavities

**Most commonly used modes of single-cell cavities**

• **TM$_{010}$** "Transverse magnetic" nomenclature for lowest mode
of pillbox cavity, and the most commonly used mode for acceleration
in topologically equivalent cavities, including <u>DTL</u>, <u>CCDTL</u>, <u>CCL</u>,
and <u>superconducting elliptical cavities</u>. Indices specify azimuthal, radial,
and longitudinal field variations.

• **TE$_{210}$** "Transverse electric" nomenclature for quadrupole
mode of pillbox cavity. This mode, perturbed by the vane geometry,
is the main mode used in the <u>RFQ</u>. The end geometry of the RFQ
must be "tuned" carefully to produce the field distribution of
this mode over the length of the vanes.

• **TM$_{11n}$**, n=0,1,... "Transverse magnetic" nomenclature for lowest
deflecting modes of pillbox cavity. These modes can be excited by
beam and may lead to beam-breakup instability.

# Electromagnetic Modes of Multicell Cavity Structures

**Definition: Multicell cavities consist of an array of single-gap cavities called cells. Below are listed the most commonly used modes (structure modes) of multicell cavities in standing-wave operation.**

• **0-mode**          Zero-degree phase shift from cell to cell, so fields in adjacent cells are in phase. Best example is <u>DTL</u>.

• **π-mode**          180-degree phase shift from cell to cell, so fields in adjacent cells are out of phase. Best example is multicell <u>superconducting cavities</u>.

• **π/2 mode**          90-degree phase shift from cell to cell. In practice these are biperiodic structures with two kinds of cells, accelerating cavities and coupling cavities. The <u>CCL</u> operates in a π/2 structure mode. This is the preferred mode for very long multicell cavities, because of very good field stability.

# Particle Acceleration in a Gap

---

• First we give exact equations of motion for numerical solution. This allows accurate solution in general case, but not as much insight.

• Second, we deduce general properties of the motion by expressing the energy gain in the **approximation that the velocity is constant** throughout the accelerating gap. This procedure is a good approximation for protons, heavy ions, and relativistic electrons.

# RF acceleration in a gap

• Assume a TM$_{010}$-like mode of a cavity with beam holes, which will introduce a non-zero component for E$_r$. The only non-zero components will be E$_z$, E$_r$, and B$_\theta$. Lorentz force components are:

$$\frac{dp_z}{dt} = q\left[E_z(r,z)\cos(\omega t + \phi)\right] + v_r B_\theta(r,z)\sin(\omega t + \phi)$$

$$\frac{dp_r}{dt} = q\left[E_r(r,z)\cos(\omega t + \phi)\right] - v_z B_\theta(r,z)\sin(\omega t + \phi)$$

# Exact Equations of Motion

- One can solve numerically:

$$\frac{d\vec{p}}{dt} = q\left[\vec{E}\sin(\omega t + \phi) + \vec{v} \times \vec{B}\cos(\omega t + \phi)\right]$$

$$\frac{d\vec{r}}{dt} = \vec{v}$$

- Time origin can be when particle at entrance to cavity.
- Calculation is suitable for arbitrary structures and even for low energy electrons where β can increase from near 0 to near 1 in a single gap.
- PARMELA code uses step-by-step numerical integration of equations of motion through the fields obtained from an electromagnetic field solver code like SUPERFISH.

## Conventional (approximate) treatment based on the assumption that the velocity is constant in accelerating cell.

---

• Consider particle moving along z axis of cavity excited in a standing wave where axial electric field is

$$E_z(z, t) = E(z)\cos(\omega t + \phi)$$

$$t = \int_0^z dz / v(z)$$
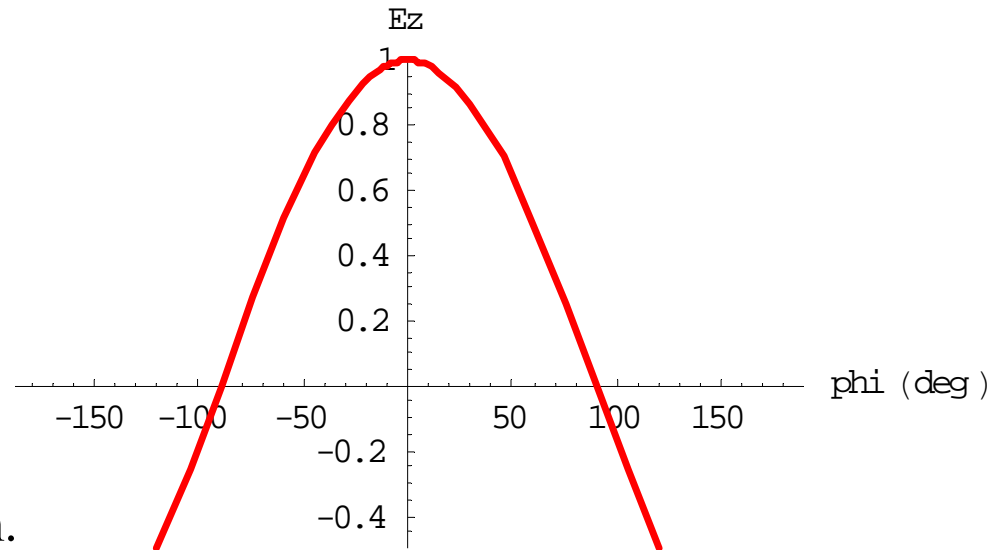
where t=0 when particle is at center of cell where z=0.

• Often E(z) is nearly an even function about z =0. For simplicity we assume this.

# Phase Convention

$$E_z = E_{z0}\cos(phi), \quad phi = \omega t$$



- $\phi$ is phase of field when particle arrives at gap center (t=z=0). When $\phi$=0 (t=0), the field is maximum.

- **$\phi$ is called phase of the particle, but is actually the phase of the field when the particle is at the center of the cell.**
- Examples:

$\phi$ =-30 degrees means particle arrives at center of cell 30 degrees before the peak.

$\phi$ =+30 degrees means particle arrives at center of cell 30 degrees after the peak.

# Acceleration or Energy Gain in an RF Gap

- Exact result:

$$\Delta W = q \int_{-L/2}^{L/2} E(z) \cos\left( \omega \int_{0}^{z} \frac{dz}{v(z)} + \phi \right) dz$$

The integrand is the electric field seen by the particle. L is chosen large enough to contain all the field.

- Need v(z) for an exact solution, which we don't know. For approximate solution assume constant velocity within the gap. (This is OK except for low-velocity electrons.) Then

$$\Delta W \cong q \int_{-L/2}^{L/2} E(z) \cos\left( \frac{\omega z}{v} + \phi \right) dz$$

# Energy Gain in Symmetric Cavity

- Assume symmetric cavity where E(z)=E(-z) is an even function. Use trigonometric identity:

$$E(z)\cos(\frac{\omega z}{v} + \phi) = E(z)\cos(\frac{\omega z}{v})\cos\phi - E(z)\sin(\frac{\omega z}{v})\sin\phi$$

- Second term is product of an even function of z times an odd function of z, which integrates to zero. Thus,

$$\Delta W = q\cos\phi \int_{-L/2}^{L/2} E(z)\cos\left(\frac{\omega z}{v}\right)dz$$

# Energy Gain and Transit-Time Factor

Write:

$$\Delta W = q \int_{-L/2}^{L/2} E(z)\cos(\frac{2\pi z}{\beta\lambda})dz = q\left[\int_{-L/2}^{L/2} E(z)dz\right]\left[\frac{\int_{-L/2}^{L/2} E(z)\cos(\frac{2\pi z}{\beta\lambda})dz}{\int_{-L/2}^{L/2} E(z)dz}\right]^{*}$$

Define:

$$E_0 \equiv \frac{1}{L}\int_{-L/2}^{L/2} E(z)dz, \quad \text{axial (spatial) average field}$$

$$T \equiv \frac{\int_{-L/2}^{L/2} E(z)\cos(\frac{2\pi z}{\beta\lambda})dz}{\int_{-L/2}^{L/2} E(z)dz}, \quad \text{axial transit} - \text{time factor}$$

* Note that you must select an interval where $\int_{-L/2}^{L/2} E(z)dz \neq 0$

# Linac Energy-Gain Formula(Panofsky)

$$\Delta W = q E_0 L T (\cos \phi)$$

---

• $V_0 = E_0 L$ is voltage gain of a particle if the gap voltage was fixed in time at its maximum value.

• The $\cos\phi$ factor accounts for actual phase of the field when the particle arrives at the gap electrical center.

• The transit-time factor T accounts for time variation of field while particle moves through gap. T depends on particle velocity and field distribution. **A compact axial distribution increases T.**

• Transit-time factor may be defined as ratio of voltage actually seen by particle to the voltage that would be seen if value at gap center was fixed during transit-time of particle across the gap. T<1.

# Example: Pillbox cavity with no beam holes

• Electric field is uniform within gap and zero outside.
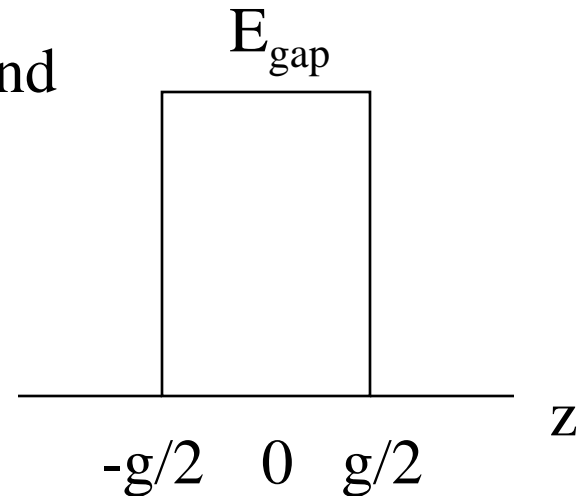


$$E_0 = \frac{1}{g} \int_{-g/2}^{g/2} E_z(z)dz = E_g$$

$$T = \frac{\int_{-g/2}^{g/2} E_z(z)\cos(2\pi z / \beta\lambda)dz}{\int_{-g/2}^{g/2} E_z(z)dz} = \frac{1}{g} \int_{-g/2}^{g/2} \cos(2\pi z / \beta\lambda)dz$$

$$or \boxed{\; T = \frac{\sin(\pi g / \beta\lambda)}{\pi g / \beta\lambda} \;}$$

# βλ = distance particle travels in one rf period

- β=v/c and λ=c/f.

- In one RF period τ, a particle travels a distance

$$\Delta z = v\tau = (\beta c)(\lambda/c) = \beta\lambda.$$

- Thus, $\omega z/v = 2\pi z / \beta\lambda$.

For g/(beta*lambda)=integer, T=0 and no net acceleration.
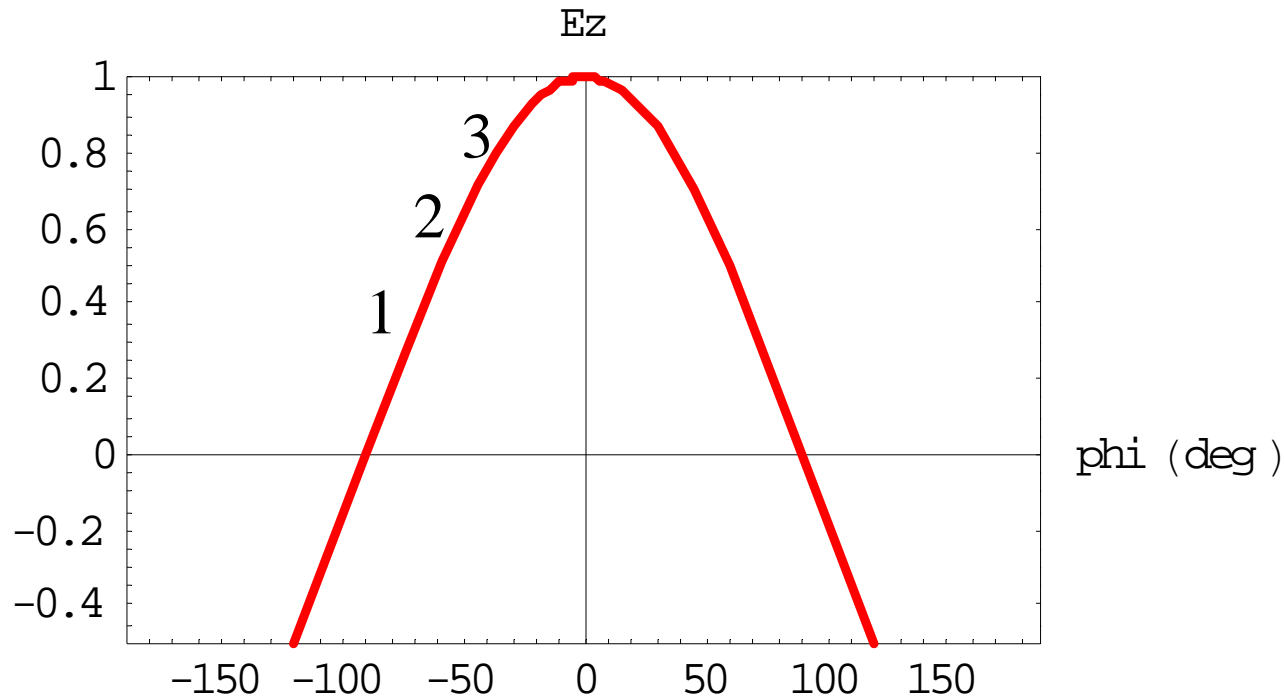T is large only for g<(beta*lambda/2).
T=0.9 for g= beta*lambda /4.
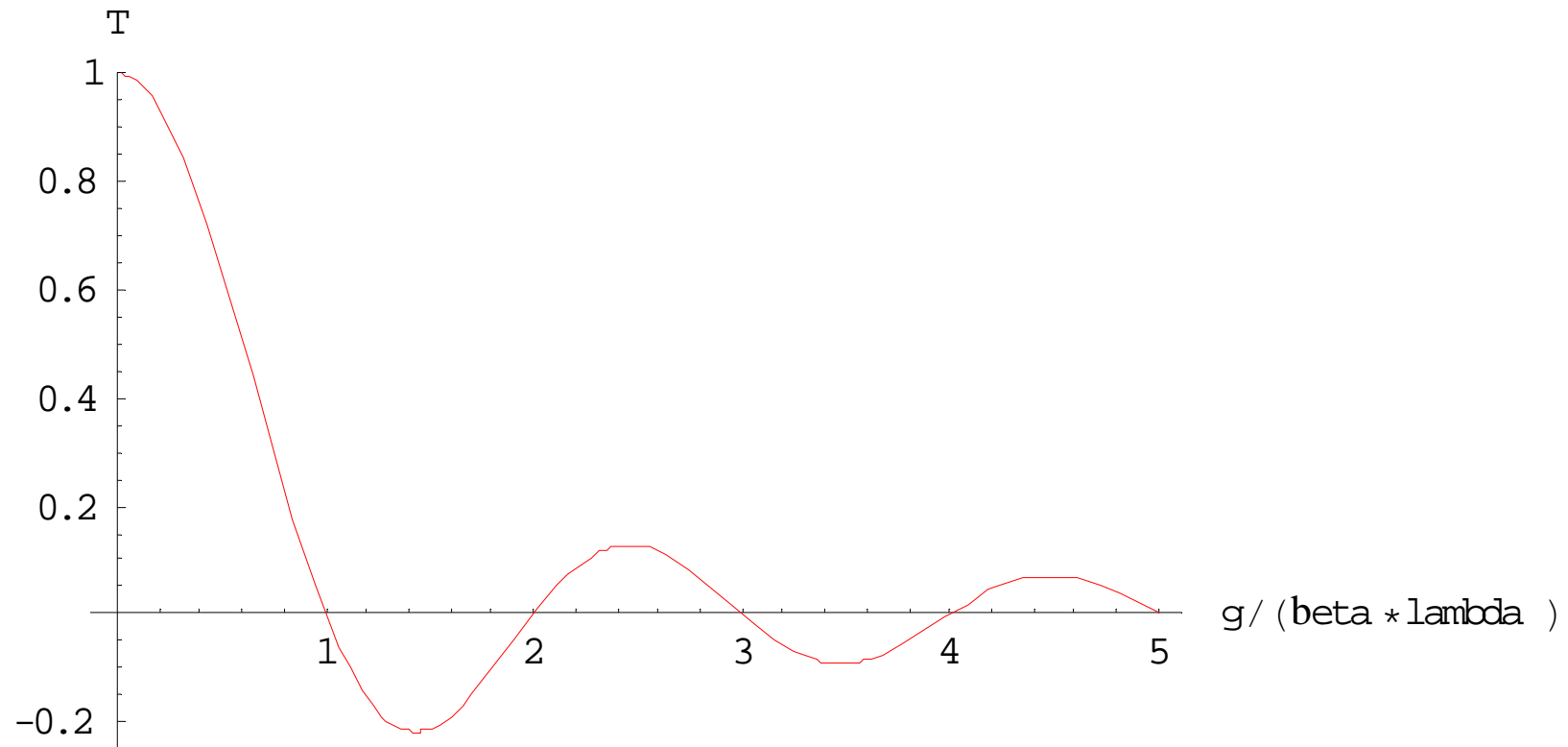
# Physical explanation of transit-time factor



1: Field when particle is at entrance of gap.
2: Field when particle is at middle of gap.
3: Field when particle is at exit of gap.
**With a sinusoidal accelerating field the average field in the gap
is always less than the field seen at gap center because of the curvature
Of the cosine function.**

# Better Model for Transit-Time Factor of a Gap in a Single-Gap Cavity or a DTL

- Assume gap axial electric field is uniform at radius r=a, where a is aperture, and is zero outside gap. At r=0, the field can penetrate into the beam bore hole, which reduces T on axis.

- Result

$$T = \frac{J_0(2\pi a / \lambda)}{I_0(2\pi a / \gamma\beta\lambda)} \frac{\sin(\pi g / \beta\lambda)}{\pi g / \beta\lambda}$$
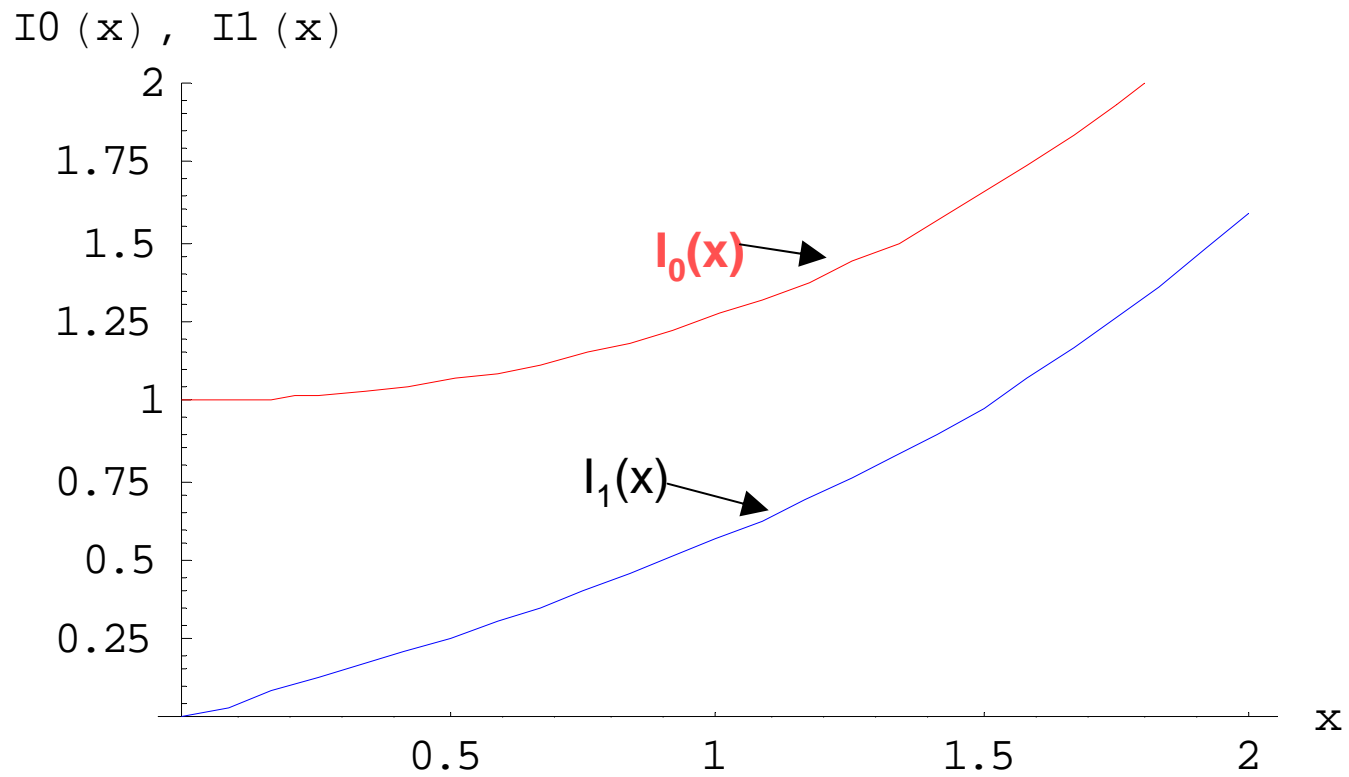
$$= \text{aperture factor} \times \text{gap factor.}$$

$$\text{Usually } 2\pi a / \lambda << 1, \text{ so } J_0 \cong 1.$$

- Aperture factor accounts for field penetration into bore.
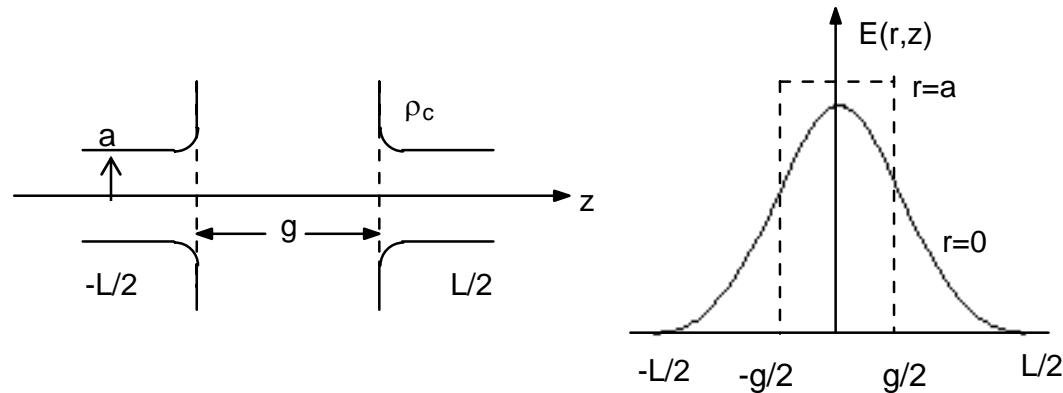
# Modified Bessel Functions $I_0(x)$ and $I_1(x)$



$$I_0(x) \cong 1 + x^2/4 + \ldots$$

# Basic principles - Acceleration in a gap



$$E_0 \equiv \frac{1}{L}\int_{-L/2}^{L/2} E(0,z)dz, \quad E_0 T \ called \ accelerating \ gradient.$$

$$Transit-time\ factor\ (r=0): T = \frac{J_0(2\pi a/\lambda)}{I_0(2\pi a/\gamma\beta\lambda)}\frac{\sin(\pi g/\beta\lambda)}{\pi g/\beta\lambda} \le 1$$

$$aperture \qquad gap$$

$$J_0(x) \cong 1 - x^2/4 + ... \qquad I_0(x) \cong 1 + x^2/4 + ...$$

# Better Model for Transit-Time Factor of a Gap in a π-Mode Multicell Structure

---

• If the multicell structure is excited in a structure mode such that the field must reverse sign between adjacent accelerating cells (e.g. CCL, or multicell superconducting cavities), a better model comes from assuming a **cosine field distribution**, which goes to zero at each end of each cell.

• This gives the simple result that **T=π/4=0.785**.  Even for large bore radius, the field can't leak far into the bore tube, because the boundary condition (Dirichlet) forces the field to zero. This keeps the transit time factor relatively large even for large bore radii.

# Example: "Elliptical" superconducting cavity with TM$_{010}$-like mode for individual cells and $\pi$-mode for structure.
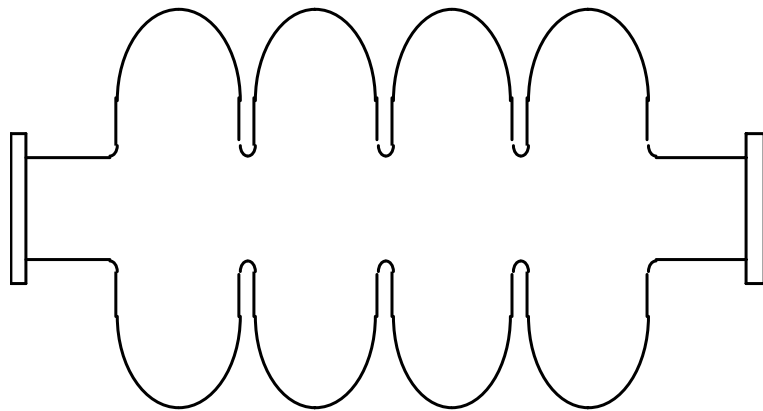


$\pi$ (structure) mode
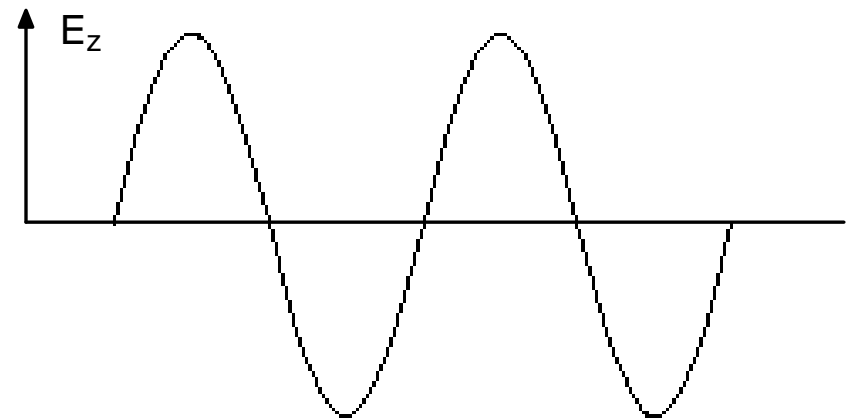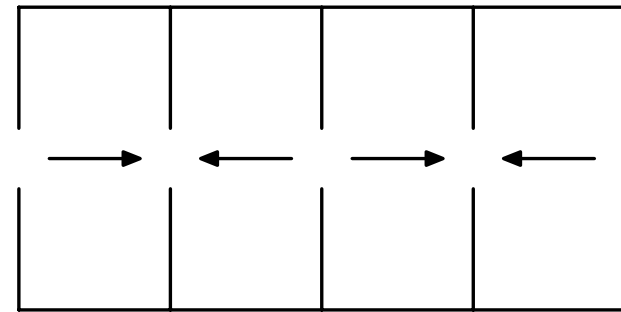
# Definition: Electrical Center of Gap

Even if E(z) is not an even function about the mechanical center of the cavity, our result for ΔW is still valid if z=0 is chosen as the electrical center defined by the condition

$$\int_{-L/2}^{L/2} E(z)\sin\left(\frac{\omega z}{v}\right)dz = 0.$$

# Most General Transit-Time Factor Result

• If we choose a coordinate system whose origin is not at the electrical center of gap, we still can write:

$$\Delta W = qLE_0 T \cos\phi$$

where

$$T = \frac{\int\limits_{-L/2}^{L/2} E(z)\cos(\omega z/v)\,dz}{\int\limits_{-L/2}^{L/2} E(z)\,dz} - \tan(\phi)\frac{\int\limits_{-L/2}^{L/2} E(z)\sin(\omega z/v)\,dz}{\int\limits_{-L/2}^{L/2} E(z)\,dz}$$

• This has acquired a dependence on $\phi$ and is more complicated. We will keep origin at electrical center where second term vanishes.

# Transit-time Factor for Multicell Cavities

---

• Previous transit-time factor treatment was for single-gap case. Now we treat a multigap cavity.

• We can calculate T assuming constant velocity throughout all the cells of the cavity.

• One finds that T is a product of T(single gap) times a synchronism factor, which depends on number of cells.

• The smaller the number of cells the broader the velocity acceptance of T.

• Thus if number of cells is small enough, a given cavity can be used over a broad velocity range.

Example of transit-time factor versus velocity β showing the velocity acceptance. As the number of cells per cavity increases, the curves get narrower, and the velocity acceptance decreases.
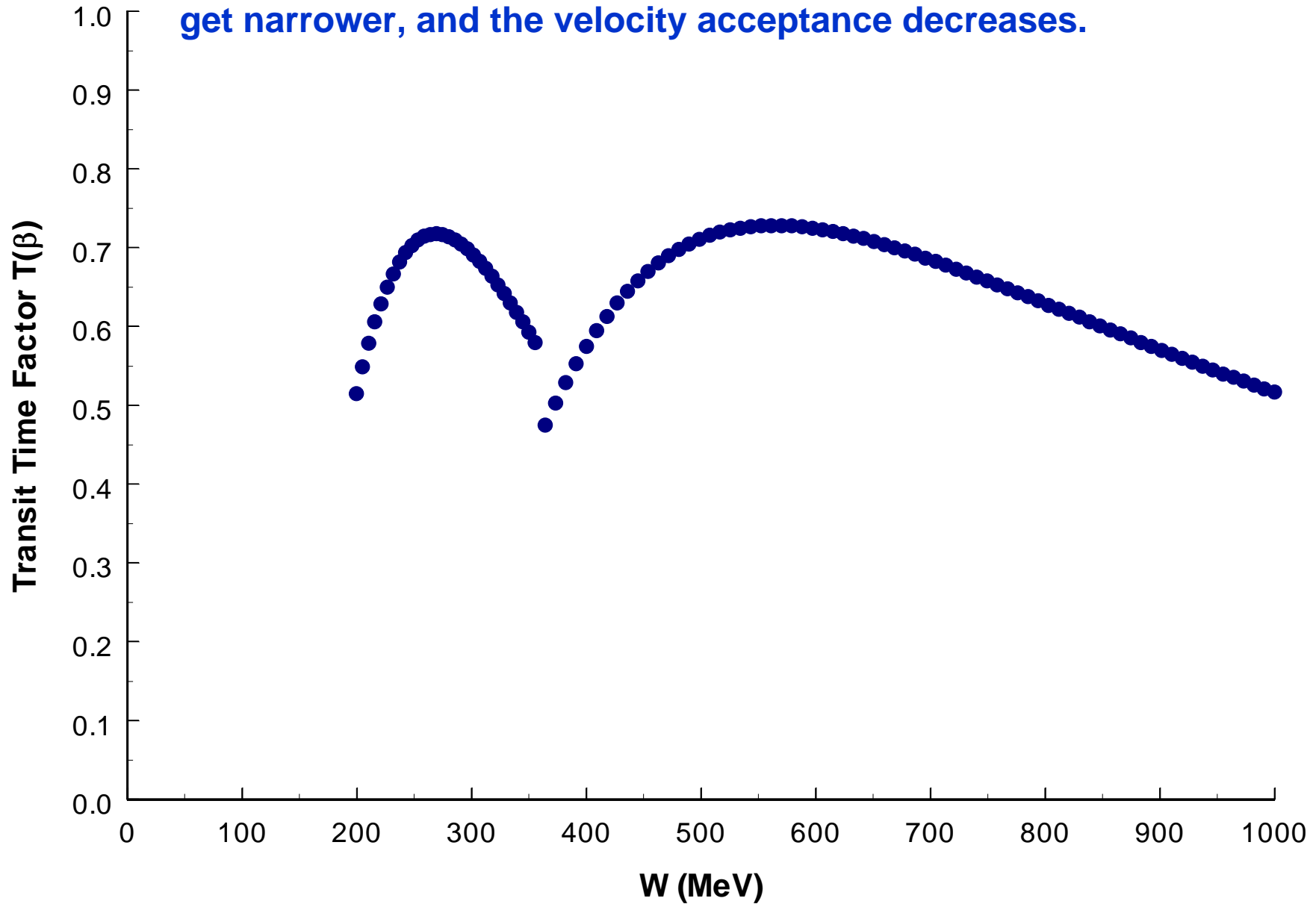
# Figures of Merit for RF Power Efficiency

- Quality factor Q definition is well established:

$$Q = \frac{\omega \times Stored\ energy}{Average\ power\ dissipation}$$

- But shunt impedance to be defined next is a more useful figure of merit for accelerator efficiency characterization.

# Basic Accelerator Shunt Impedance Definition

- Begin with basic "shunt impedance" figure of merit for axial voltage squared per unit dissipated power. Require figure of merit be independent of field level.

$$r_s (M\Omega) \equiv \frac{V_0^2}{P} = \frac{(E_0 \ell)^2}{P} \quad , \qquad V_0 = \int_{-L/2}^{L/2} E_z(z)\, dz$$

$$where\, P = average\, power\, dissipated\, over\, RF\ period$$

- Notice no factor of 2 in denominator. Sometimes people define it with factor of 2 so be careful!

# Effective Shunt Impedance Definition (1)

---

- Next we would like to define the figure of merit to measure **the actual energy gain of a particle** instead of just the axial voltage. At peak of electric accelerating field:

$$\Delta W_{peak} = qE_0 T\ell = q\sqrt{r_s T^2 P} \ \ sin\,ce \ E_0 = \sqrt{r_s P}/\ell.$$

- Thus, $r_s T^2$ determines $\Delta W_{peak}$. Define" **effective shunt impedance**"

$$r(M\Omega) \equiv r_s T^2 = \frac{(E_0 T\ell)^2}{P}$$

- $r_s$ and $r$ are important definitions for a single accelerating cavity.

# Effective Shunt Impedance Per Unit Length (2)

- For multicell structures **we want figures of merit that are also independent of length.** Both r and $r_s$ are scale linearly with cavity length since:

$$r \propto r_s = \frac{(E_0 T \ell)^2}{P} = \frac{(E_0 T \ell)^2}{\frac{R_s}{2} \int H^2 dA} \propto \frac{\ell^2}{\ell} = \ell$$

- Define **shunt impedance per unit length**:

$$Z(M\Omega / m) \equiv \frac{r_s}{\ell} = \frac{E_0^2}{P / \ell}$$

# Effective Shunt Impedance Per Unit Length and RF Power Efficiency (3)

- Define "**effective shunt impedance per unit length**":

$$ZT^2 \, (M\Omega / m) = \frac{r}{\ell} = \frac{\left(E_0 T\right)^2}{P / \ell}$$

- **$ZT^2$ measures efficiency of acceleration, independent of field level and cavity length.** Larger $ZT^2$ means more energy gain for a given power per unit length.

- If you determine $ZT^2$ from an electromagnetic field-solver code like SUPERFISH, you can calculate $P/\ell$ at any $E_0 T$.

# More on RF Power Losses and RF Efficiency Definitions

- Quality Factor: $Q_0 = \omega U / P_{walls}$ , where $\omega$ is angular frequency, U is stored energy, and $P_{walls}$, called P earlier, is average power dissipated per period in Ohmic losses in cavity walls. Cavity time constant $\tau = 2Q_0/\omega$.

- $r/Q_0$, $r_s/Q_0$ , $Z/Q_0$ , or $ZT^2/Q_0$ are useful because they are independent of the surface resistance. These are generically called "**r over Q**".

- Beam power, $P_{beam} = IW/q$

- $P_{tot} = P_{walls} + P_{beam}$; i.e. total rf power delivered to cavity = Ohmic power loss in walls +power delivered to beam.

- $\varepsilon_s$ = Structure efficiency= $P_{beam} / P_{tot}$ (also known as "beam loading")

- $\varepsilon_{op}$ = RF operating efficiency = $P_{tot} / P_{ac}$ (includes Rf generator efficiency, HVDC conversion efficiency, waveguide losses, and reflections from coupler mismatch, and cavity detuning effects.)

- $\varepsilon_{tot}$ = Overall RF efficiency = $\varepsilon_s \, \varepsilon_{op}$ = $P_{beam} / P_{ac}$

# How to Improve on the Pillbox Cavity Shape

• Beam holes added to a pillbox cavity reduces T and the concentration of the axial field.

• **One can add noses for radial concentration of electric field**. This increases $r_s/Q_0$ and $Z/Q_0$.

• The noses can be adjusted to reduce the gap and raise T. Too small a gap increases the capacitance, which increases wall currents and increases Ohmic power dissipation. Also peak surface electric field will increase. **Optimum nose geometry can be chosen to maximize $r/Q_0$ and $ZT_2/Q_0$**, consistent with limiting the peak surface electric field.

• Finally, $Q_0$ can be maximized by minimizing the surface area to volume ratio. This leads to **spherical geometry** for outer surface.

**Improving the pillbox cavity model.**
**Add beam holes; add noses to raise transit-time**
**factor; spherical outer wall to reduce surface area.**
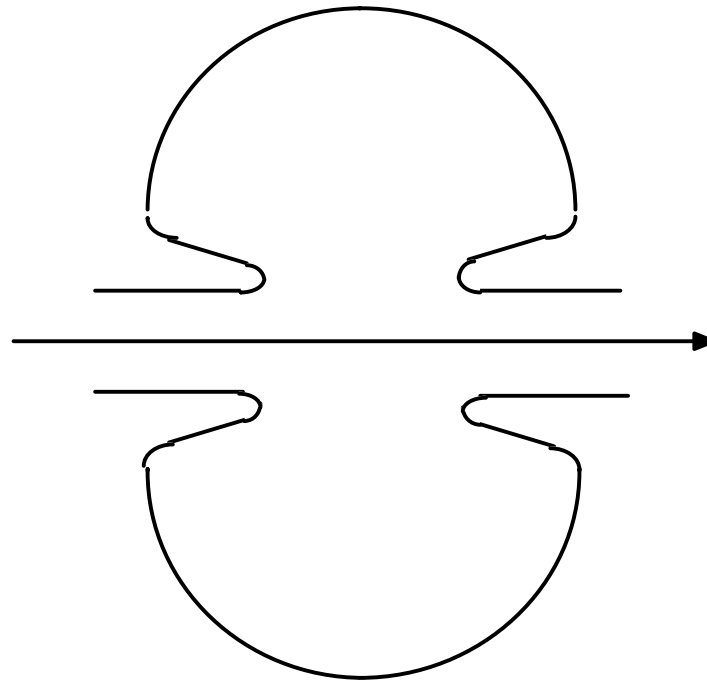


These cells can be combined to form a multicell structure
to provide higher "real-estate" accelerating gradient and
allowing for use of higher power klystrons (an economic advantage).

# Superconducting Cavity Shapes for High-β Particles

• Because of reduced RF losses, efficiency is often less important than controlling peak surface electric and magnetic fields, which limit the performance.

• The spherical or elliptical cavity without noses has significant advantages for acceleration of high-β particles.

      1) Minimal multipacting.

      2) Easy to access surfaces and drain chemicals during chemical processing.

      3) Low peak surface electric and magnetic fields.

# Example: "Elliptical" superconducting cavity with TM$_{010}$-like mode for individual cells and $\pi$-mode for structure.

$\pi$ (structure) mode

$E_z$
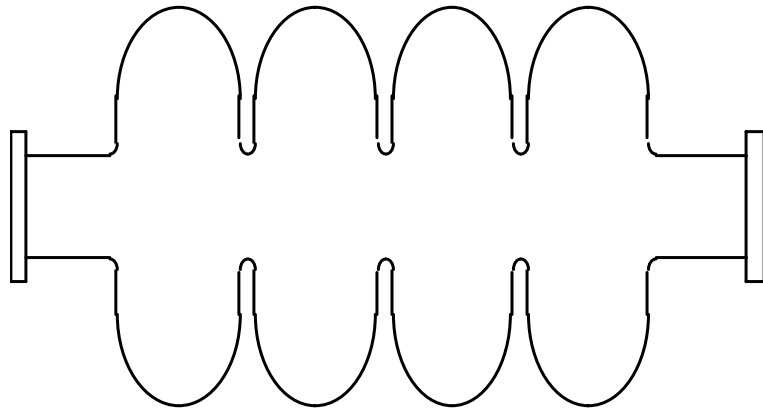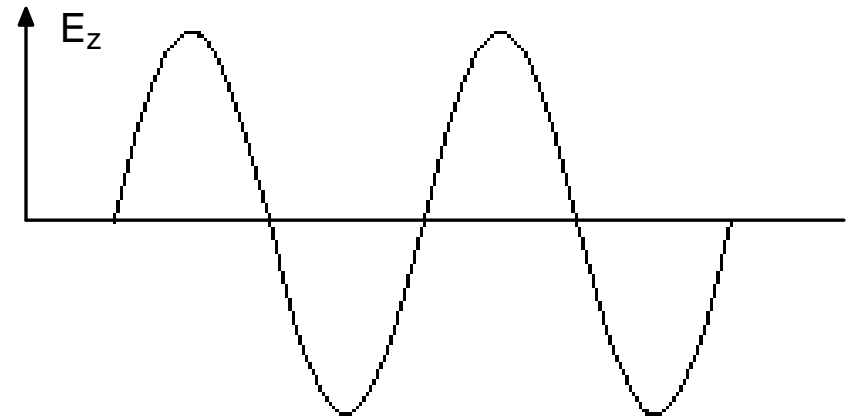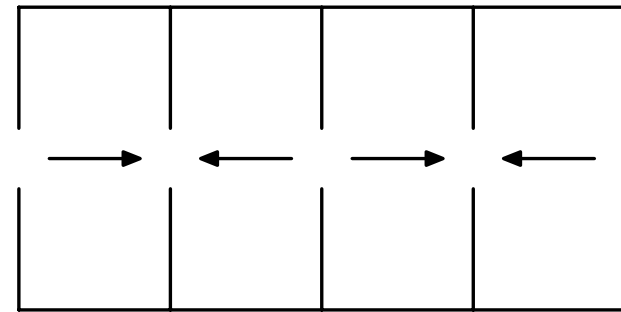
• In this case no noses to reduce peak electric fields and to facilitate drainage of fluids.

# Scaling of cavity parameters with frequency(1)

- Suppose we compare linacs with different frequencies f=c/λ, but with the energy gain ΔW and the same length L.
- Assume all structure dimensions including the apertures scale proportional to the wavelength.

$$diameter \propto \lambda$$

$$cell\ length \propto \lambda$$

$$fields \propto \lambda^0$$

$$surface\ area \propto \lambda L \propto \lambda$$

$$cavity\ volume \propto \lambda^2 L \propto \lambda^2$$

$$stored\ energy \propto field^2 \times volume \propto \lambda^2$$

# Scaling of cavity parameters with frequency (2)

- Scaling of RF surface resistance:

$$R_s \propto \begin{cases} f^{1/2} & normal\ conducting \\ f^2 & superconducting\,(BCS\ theory) \end{cases}$$

- Power dissipation:

$$P \cong \frac{R_s}{2} H^2 A \propto \begin{cases} f^{-1/2} & normal\ conducting \\ f & superconducting\,(BCS\ theory) \end{cases}$$

Higher frequency reduces power loss for normal conducting structures but increases power loss for superconducting structures.

# Scaling of parameters with frequency (3)

- Shunt impedance and quality factor scaling:

$$ZT^2 = \frac{(E_0 T)^2}{P/L} \propto \begin{cases} f^{1/2}, & normal\ conducting \\ f^{-1}, \sup erconducting\ (BCS) \end{cases}$$

$$Q = \frac{\omega U}{P} \propto \begin{cases} f^{-1/2}, & normal\ conducting \\ f^{-2}, & \sup erconducting\ (BCS) \end{cases}$$

- Note: If aperture is fixed, independent of wavelength, one finds that $ZT^2$ is insensitive to frequency.
- The peak surface electric field generally increases with frequency.
- For normal conducting case the empirical Kilpatrick law is used for peak surface electric field.
- For the superconducting case smaller surface area produces less field emission and an empirical formula for peak surface electric field is:

$$E_{peak\ surface} \propto (surface\ area)^{-1/4} \propto f^{1/4}$$

# Electron-Loading Effects

• Electrons can be removed from cavity walls by electric fields and can be accelerated absorbing energy from the electromagnetic field.

• This is an additional load for the RF system and is called electron loading.

• Electron loading can limit the fields and produce x-rays when electrons strike the cavity walls.

Three effects can be identified: (1) **multipacting,** (2) **field emission**, and (3) **rf electric breakdown**.

# Multipacting (also called multipactoring)

• Multipacting is a discharge (usually low voltage) that loads the RF system and prevents RF fields from building up.

• Electrons emitted from one surface cross a gap in an odd multiple of rf half cycles and produce secondary electrons that return to the first surface after the field reverses.

• A resonant condition for electron transit-time between two surfaces must be satisfied.

• Secondary electron coefficient must exceed unity.

$$V \sin(\omega t)$$

$x_0$

e-
primary

secondary
emission

$x=0$      $x=x_0$
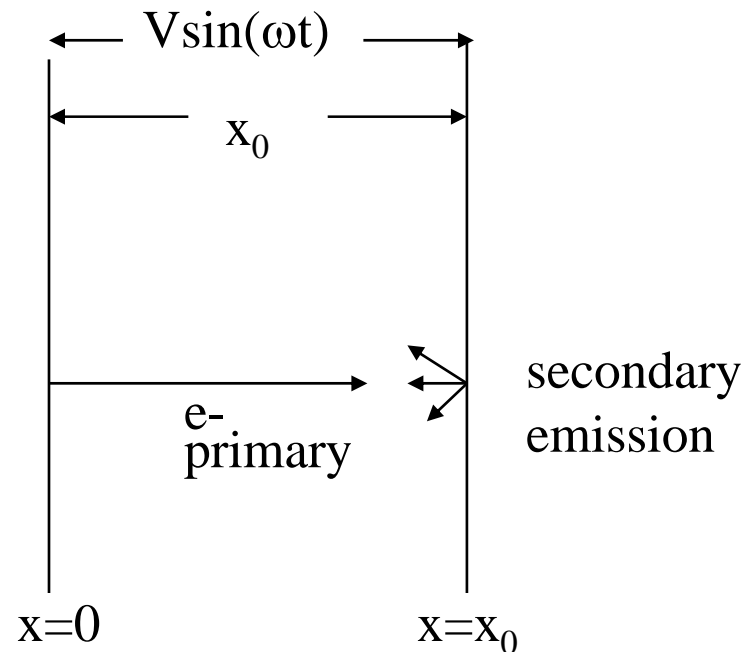
# Multipacting – Classical Two-Point Theory
## (Hatch and Williams, Phys. Rev. 112(1958)68)

• As given by Hatch, NIM 41 (1966)261.
-Multipacting=multiple impacting
-multipactor (noun)
-multipact (verb)
-multipacting or multipactoring (present participle)
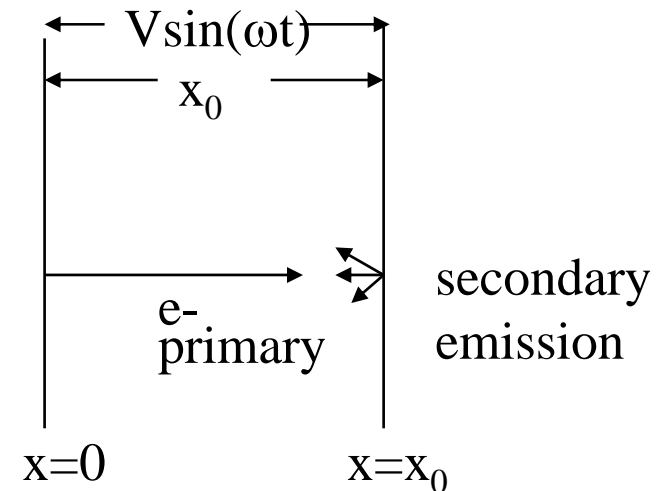


• Consider an AC electric field perpendicular to two plane metal surfaces with a field strength such that an electron originating from one surface takes exactly ½ a period to cross the gap.

•Suppose it knocks out several secondary electrons from the second surface. These will return to the first surface in next half RF period, where they knock out several more electrons.

•The process will continue until the avalanche or discharge is limited by the electron space charge.

# Two Point Multipacting (2)

• There are multiple resonant voltage levels since what is required is that electrons go a distance $x_0$ in an integral number of half RF periods.

• Results of the theory are that multipacting can occur at voltages $V=E_0 x_0$ between:

$$V_{\max} = \frac{m\omega^2 x_0^2}{2e}, \ and$$

$$V_{\min}(n) = \frac{m\omega^2 x_0^2}{e} \frac{1}{\sqrt{(2n+1)^2 \pi^2 + 4}}, \quad n = 0, 1, 2, .., \infty$$

• n is the order of the level defined by $t_{\text{transit}}=(n+1/2)T/2$, where $T=2\pi/\omega$.

• The maximum electric field for multipacting to occur for gap $x_0$ is:

$$E_{\max} = \frac{V_{\max}}{x_0} = \frac{m\omega^2 x_0}{2e}$$

• There is no minimum field below which multipacting can not occur.

# Two Point Multipacting (3)
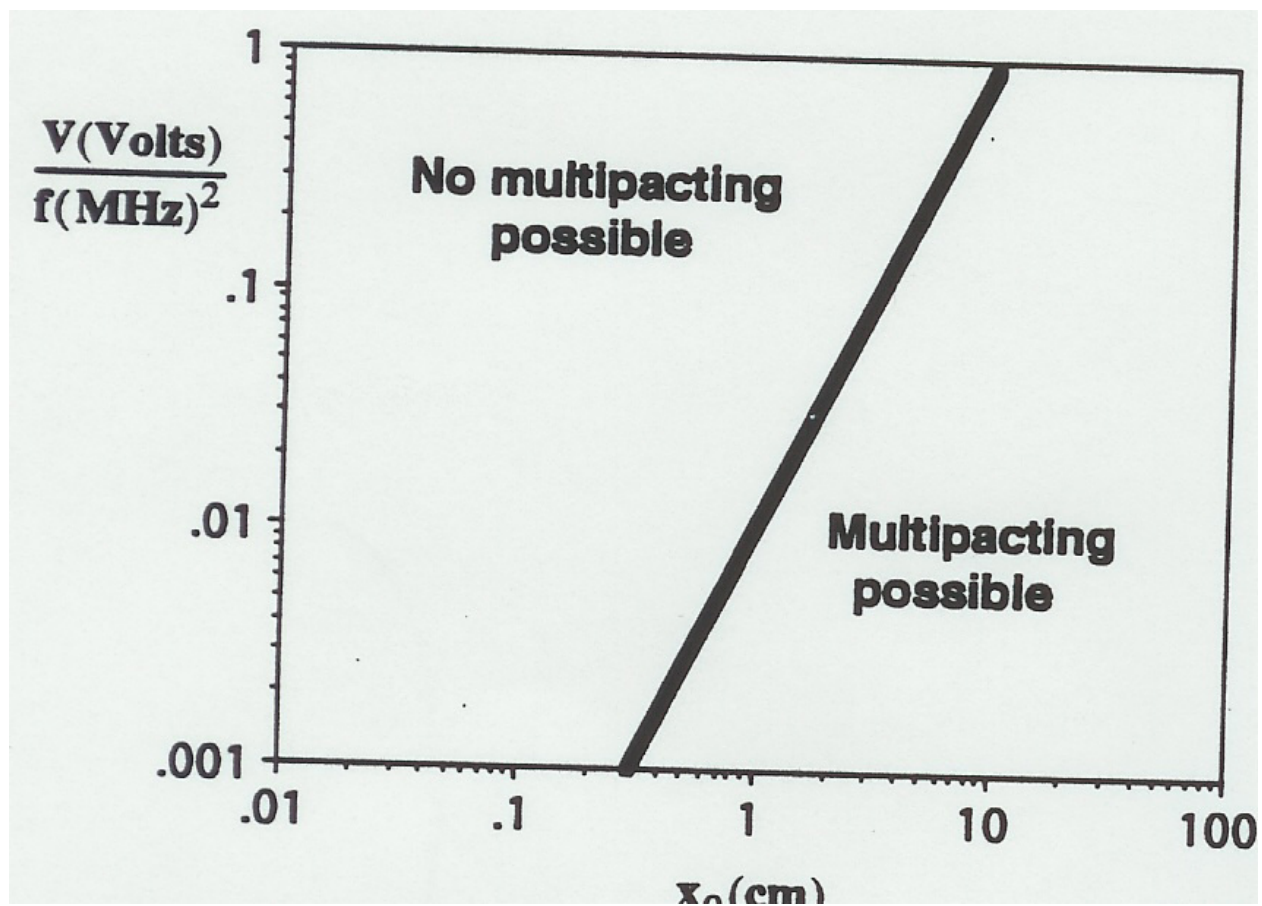


The curves $V_{max}/f^2$ versus $x_0$ is plotted versus $x_0$.

# Two Point Multipacting (4)

- The secondary electron coefficient must exceed unity for multipacting to occur.

- Multipacting often occurs at low electric fields when raising the cavity fields to operating levels.

- The simple theory does not include magnetic fields.

- DC Magnetic fields perpendicular to the surfaces can enhance multipacting, whereas magnetic fields parallel to the surfaces can supress multipacting.

- Overcoupling to reduce the cavity time constant can supress the effect by bringing the field through the multipacting region before the multipacting resonance can build up.

# Two Point Multipacting (5)

- Keeping surfaces thoroughly clean and oil free by use of oil-free vacuum pumps can suppress the effect by keeping the secondary electron coefficient small.

- RF conditioning helps by letting the multipactor discharge "burn" until the secondary electron coefficient decreases enough.

- The most serious multipacting situation arises when multipacting occurs near the operating level of an accelerating cavity.

- Multipacting has occurred in the low-field coupling cavities of coupled-cavity linacs, exacerbated in electron machines by solenoidal DC magnetic focusing.

- Surface coatings can reduce the secondary emission coefficient (titanium, and titanium nitride).

# Single Point Multipacting Summary.

- Multipacting requires two conditions:
  1) Kinematic – electrons must go from surface to surface in the right amount of time to sustain the resonance.
  2) Physical – The secondary electron coefficient must exceed unity.

- For a strong troublesome multipacting level, there usually must be sufficient symmetry or uniformity in the geometry and in the fields to involve enough electrons from a large surface area.

# Single-Point Multipacting

- This was discovered in superconducting cavities, where it occurs at the outer wall (magnetic-field region) of cavities operating in the $TM_{010}$ mode.

- Electrons are emitted and return to the same surface where they knock out secondary electrons and build up a discharge.

- The time between surface hits is an integer multiple of an RF period.

- One point multipacting can occur only if the electrons impact the surface with sufficient energy so secondary electron coefficient exceeds unity.

- The theory yields an expression for the impact energy:

$$W_{impact} = 7.6 \times 10^3 \left[ \frac{E_\perp (MV/m)}{f(GHz)} \right]^2$$

# Single-point multipacting showing typical location and trajectories of first three orders
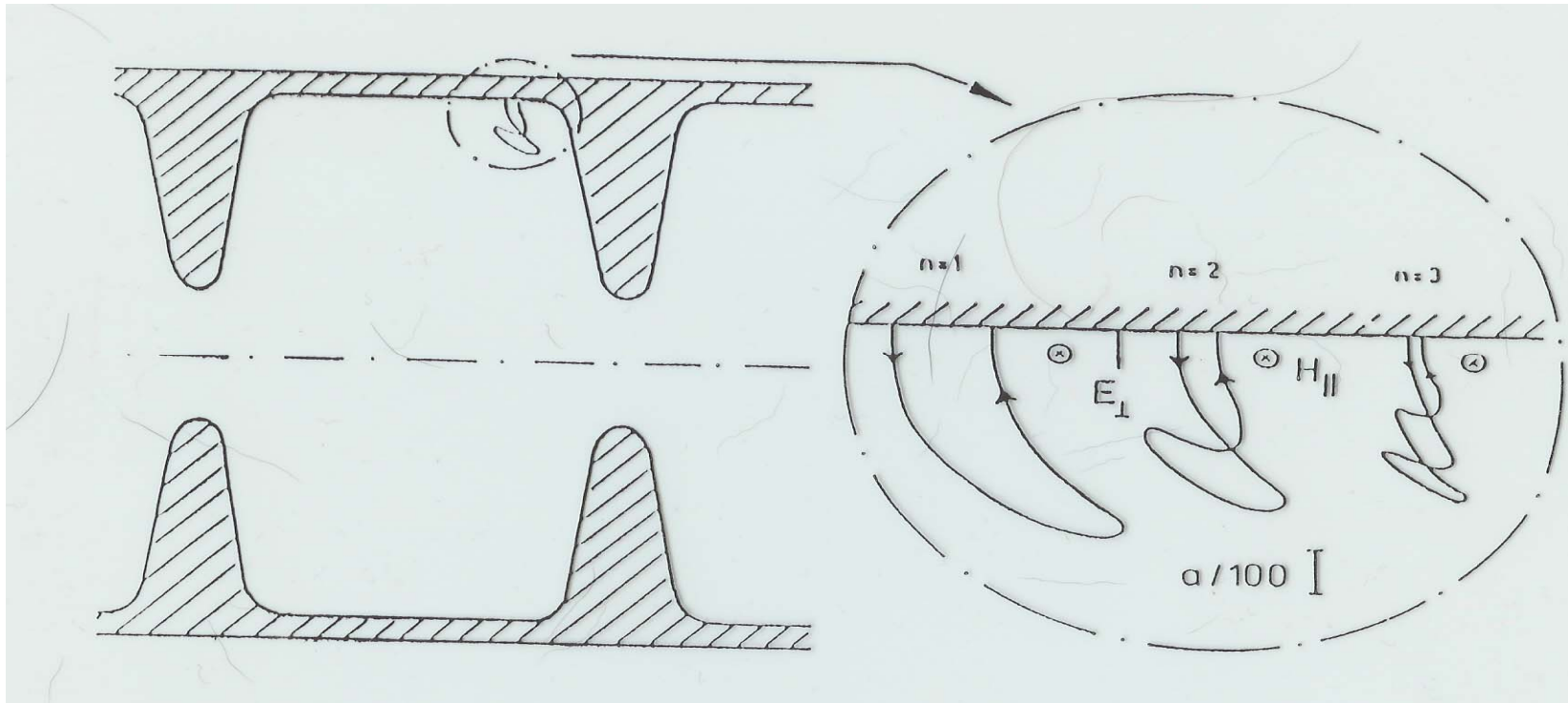
# Secondary emission versus impact energy
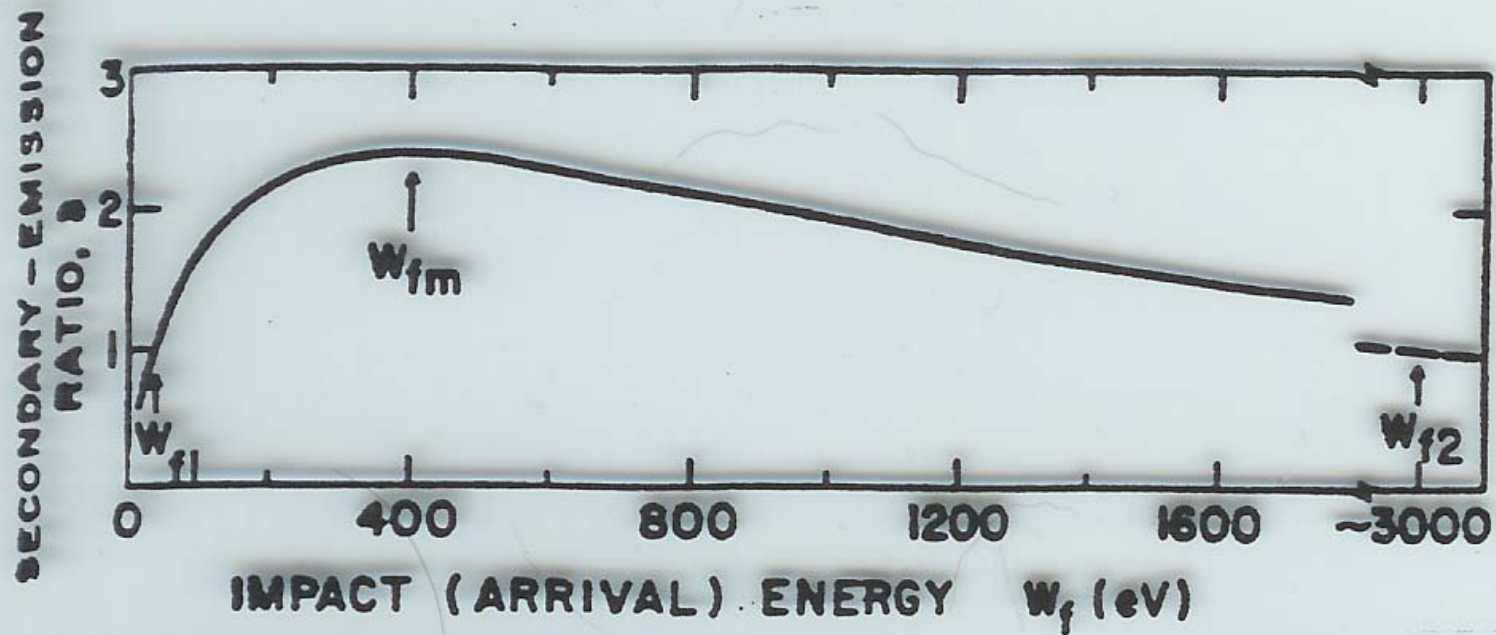


Fig. 2. Secondary-emission yield curve for aluminum

# Single-Point Multipacting-Possible Supression Methods

- Design cavity with small enough $E_\perp$ at surface that secondary electron coefficient is less than unity.

- Elliptical cavity design with spherical outer shape usually eliminates strong one-point multipacting. Electrons drift towards the equator where $E_\perp$ is nearly zero and secondary electron coefficient is less than 1.

# Electron Field Emission

• Field emission occurs in both normal conducting and superconducting cavities and limits the performance of superconducting cavities.

• In the presence of a strong E field, electrons are emitted from cavity surfaces and from **dust particles** on cavity walls. Electrons gain energy in RF fields and are accelerated into cavity walls, generating heat and x-rays. This **reduces the Q of superconducting** cavities at high fields.

• The most important rule for controlling field emission in superconducting cavities is **cleanliness.**

• Statistically it is more likely to have field emission sites on larger surface areas. Thus, smaller cavities tend to achieve larger fields.

# Classical Electron Field Emission

•Fowler Nordheim Law:

$$j(A/m^2) \propto \frac{E^2}{\Phi} \exp\left[\frac{-a\Phi^{3/2}}{E}\right], \text{ where } E \text{ is the electric field}$$

$$\text{and } \Phi \text{ is the work function. For niobium } \Phi = 4.3 \ eV.$$

• In practice E is not the ideal surface field $E_s$ but is a surface field enhanced value $E=\beta E_s$, where $\beta$ is a field-enhancement factor which can be as large as $\beta=250$.

• Even so the onset of field emission in superconducting cavities occurs at lower than expected fields. It is believe that this is caused by presence of low work-function dust particles with sharp protrusions.

• The most important rule for suppressing field emission is cleanliness; rinsing in ultrapure water, assembly in dust-free airflow systems.

• Statistically, the probability of field emission is expected to increase with the surface area exposed to high fields. Approximate scaling law:

$$E_{peak} \propto (surface\,area)^{-1/4}$$

# RF Electric Breakdown

---

• For normal-conducting cavities, field emission loading is not as easily observed. This may be the result of large Ohmic power dissipation in cavity which masks field-emission effects.

• **At sufficiently high fields normal-conducting cavities suffer electric breakdown or sparking.**

• The detailed mechanism is not well understood, but probably is initiated by field emission. It has been suggested that protons are also involved in the discharge.

# Kilpatrick Criterion on RF Breakdown

- About 40 years ago, W. D. Kilpatrick analyzed the data on rf breakdown, and proposed the conditions that would avoid rf breakdown.

- The results were expressed by T.J.Boyd in a convenient formula:

$$f(MHz) = 1.64 E_K^2 e^{-8.5/E_\kappa}$$

where f is the frequency, and $E_K$ is called the Kilpatrick limit. The equation must be solved iteratively for $E_K$.

- The criterion is based on experimental results that were obtained in an era before clean vacuum systems were prevalent. The criterion is **conservative** by today's standards.
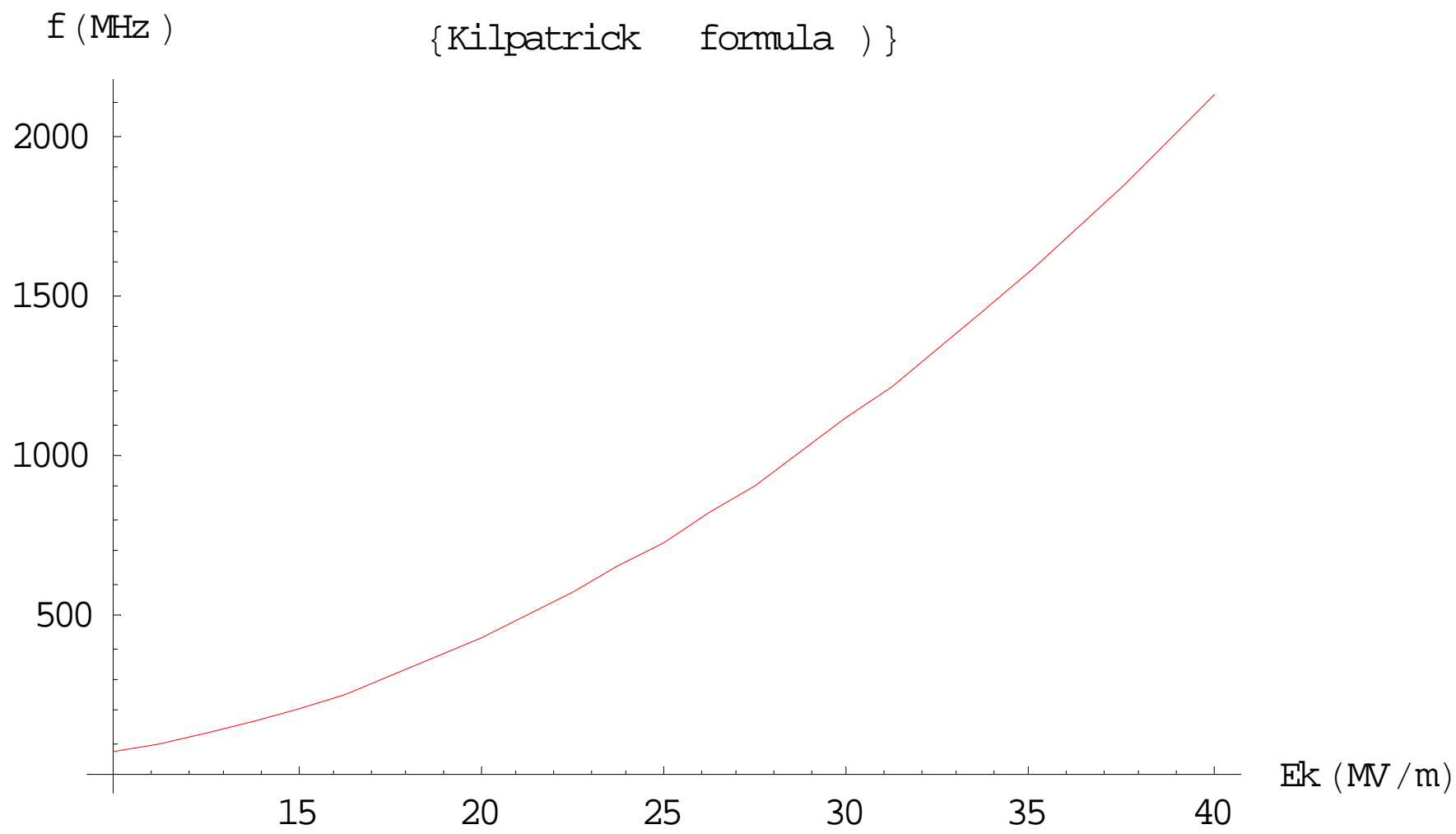
# Bravery Factor Modification

---

• To apply the Kilpatrick criterion to modern normal conducting structures, we introduce a bravery factor. Replace $E_K$ by $E_s = b\, E_K$ , where Es is the peak surface electric field, and b is the bravery factor.

• Typical values range from **1.5<b<2.0**. CW RFQs are usually designed using b=1.8. Larger values are used for pulsed accelerators with pulse lengths less than 1 msec.

• Notice **$E_K$ increases with increasing frequency**. Below 1 GHz, one finds approximately

$$E_K \propto f^{0.4}$$

# Peak Magnetic Field Limits

---

• Maximum power/surface area is limited by ability to provide cooling and increases as $B^2$ since

$$P / A \cong \frac{R_s}{2} \left( \frac{B_s}{\mu_0} \right)^2$$

• For water-cooled cavities an approximate limit for conventional cooling systems is 20 W/cm$^2$.

• Superconducting cavities will quench if B is too large. The effective rf critical field is 2400 Gauss for Nb. **Because of normal conducting defects, real Nb cavities can quench for B as low as 500 to 1000 Gauss, depending on the thermal conductivity of the niobium material .**

# Basic Parameters of an RF Cavity System

$$Stored\ Energy: U = \frac{1}{4} \int\limits_{vol} \left( \frac{B^2}{\mu_0} + \varepsilon_0 E^2 \right) dV$$

$$Unloaded\ Q:\ Q_0 = \frac{\omega U}{P_c},\ where\ P_c\ is\ the\ time\ average\ power\ dissipation$$

$$External\ Q: Q_{ext} = \frac{\omega U}{P_{ext}},\ where\ P_{ext}\ is\ the\ radiated\ power$$

*from the cavity through input coupler when generator is off.*

$$Loaded\ Q: Q_L = \frac{\omega_0 U}{P_c + P_{ext}},\ \frac{1}{Q_L} = \frac{1}{Q_0} + \frac{1}{Q_{ext}}$$

$$Q_L\ det\,er\min es\ cavity\ time\ cons\tan t;\ \tau = 2Q_L / \omega.$$

# Waveguide to Cavity Coupling

Waveguide to Cavity Coupling Parameter $\beta$

$$\beta \equiv \frac{Q_0}{Q_L}$$

The $l \arg er$ $\beta$ the greater the coupling.

Three coupling regimes :

$\beta < 1$ is called undercoupled case.

$\beta = 1$ is called critical coupling case (matched case with generator on giving zero reflected power from input coupler.

$\beta > 1$ is called overcoupled case.

# Cavity Perturbations

(This will turn out to provide a practical means to measure the fields.)

- On resonance the time-averaged electric stored energy equals the time-averaged magnetic stored energy.

- If a perturbation is introduced the balance is upset. The resonant frequency will shift to restore the balance.

- We want to calculate this resonant frequency shift.

# Adiabatic Invariants of an Oscillator.

---

• Consider an oscillator where some parameter changes at a rate that is slow compared with an oscillator period.
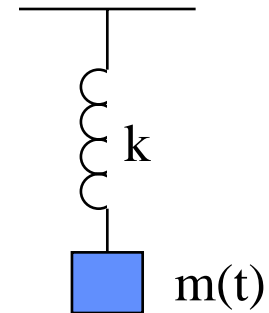
*For a Hamiltonian system (frictionless)*

$$I \equiv \iint dq\,dp / 2\pi = Area / 2\pi = cons\tan t$$

*where q = displacement, and p = momentum*

Enclosed phase space area is constant although the shape may change.
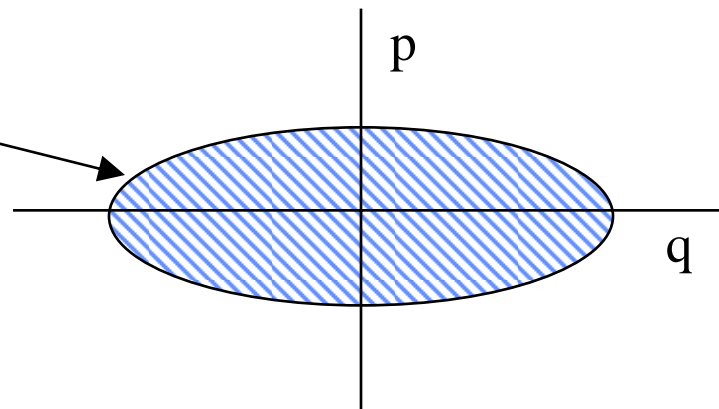
# Adiabatic Invariant for a Simple Harmonic Oscillator

$$H(q, p) = \frac{p^2}{2m} + \frac{m\omega_0^2 q^2}{2} = U \ \ where$$

$$U = total \ energy = cons\tan t$$

$$\left(\frac{p}{p_0}\right)^2 + \left(\frac{q}{q_0}\right)^2 = 1$$

$$p_0 = \sqrt{2mU}, \ \ q_0 = \sqrt{2U/m\omega_0^2}$$

$$Then \ I = \frac{Area}{2\pi} = \frac{\pi q_0 p_0}{2\pi} = \frac{U}{\omega_0} = cons\tan t$$
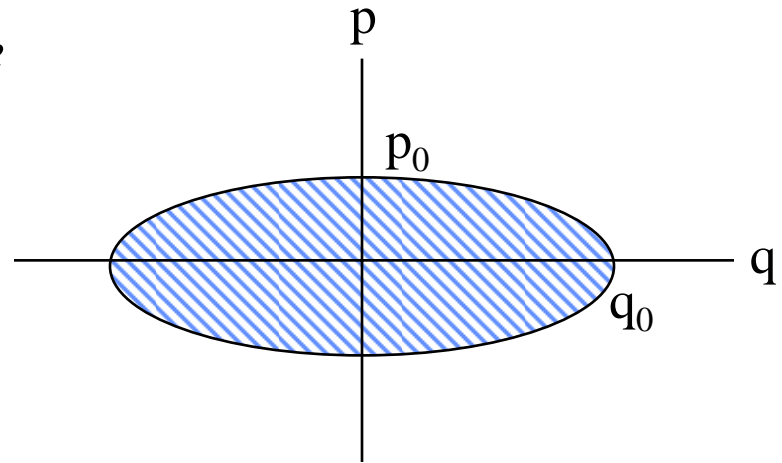
# Adiabatic Invariant for Simple Harmonic Oscillator

$$I = \frac{U}{\omega_0} = cons \tan t$$

$$or \ U \propto \omega_0$$

$$or \ \frac{\Delta \omega_0}{\omega_0} = \frac{\Delta U}{U}$$

• This is known as the Boltzmann-Ehrenfest Theorem. (Boltzmann in 1911 and Ehrenfest in 1914.
• Adiabatic processes can be pictured as going from one equilibrium state to another since the change is very slow. This is a general result applying to any two equilibrium states.

# Slater Perturbation Theorem

• Slater proved a similar theorem for two equilibrium states in an electromagnetic cavity. If a small volume $\Delta V$ is removed from a cavity, for example by pushing in the walls:

$$\frac{\Delta \omega_0}{\omega_0} = \frac{\Delta U_E - \Delta U_M}{U}, \quad where \ U = U_E + \Delta U_M,$$

$$\Delta U_E = \frac{\varepsilon_0}{4} \int_{\Delta V} E^2 dV \ is \ the \ time \ averaged \ stored \ electric \ energy$$

$removed, \ and \ E \ is \ the \ unperturbed \ electric \ field.$

$$\Delta U_H = \frac{\mu_0}{4} \int_{\Delta V} H^2 dV \ is \ the \ time \ averaged \ stored \ magnetic \ energy$$

$removed, \ and \ H \ is \ the \ unperturbed \ magnetic \ field.$

$\Delta V \ is \ the \ volume \ removed.$

# Slater Result for an LC Circuit

- The theorem is easier to remember by using an LC oscillator picture.

$$\omega_0 = 1/\sqrt{LC}$$

- Removing volume from the magnetic field region reduces L and raises $\omega_0$.

- Removing volume from the electric field region reduces the capacitive gap and raises C. This lowers $\omega_0$.

# Cavity Field Measurements from the Slater Theorem

• If a small spherical bead is introduced into a cavity, the resonant frequency will shift.

$$\frac{\Delta\omega_0}{\omega_0} = -\frac{3\Delta V}{4U}\left[\frac{\varepsilon_r - 1}{\varepsilon_r + 2}\varepsilon_0 E^2 + \frac{\mu_r - 1}{\mu_r + 2}\mu_0 H^2\right]$$

$\Delta V = bead\ volume$

$U = unperturbed\ stored\ energy$

$E, H = unperturbed\ fields$

$\varepsilon_r = dielectric\ cons\tan t\ relative\ to\ vacuum$

$\mu_r = magnetic\ permeability\ relative\ to\ vacuum$

# Dielectric and Metallic Beads

- Dielectric Bead

$$\mu_r = 1$$

$$\varepsilon_r = 9 \, for \; sapphire$$

$$\frac{\Delta\omega_0}{\omega_0} = -\frac{3\Delta V}{4U}\frac{\varepsilon_r - 1}{\varepsilon_r + 2}\varepsilon_0 E^2, \quad independent \; of \; H$$

- Metallic bead

$$\mu_r \to 0 \; for \; diamagnetic \; metal$$

$$\varepsilon_r = 1 - j\frac{\sigma}{\varepsilon_0\omega_0} \to -j\infty \; for \; perfect \; conductor$$

$$\frac{\Delta\omega_0}{\omega_0} = -\frac{3\Delta V}{4U}\left[\varepsilon_0 E^2 - \frac{\mu_0 H^2}{2}\right], \; depends \; on \; both \; E \; and \; H.$$

# Typical Bead-Pull Setup for Measurement of Cavity Field Distribution.
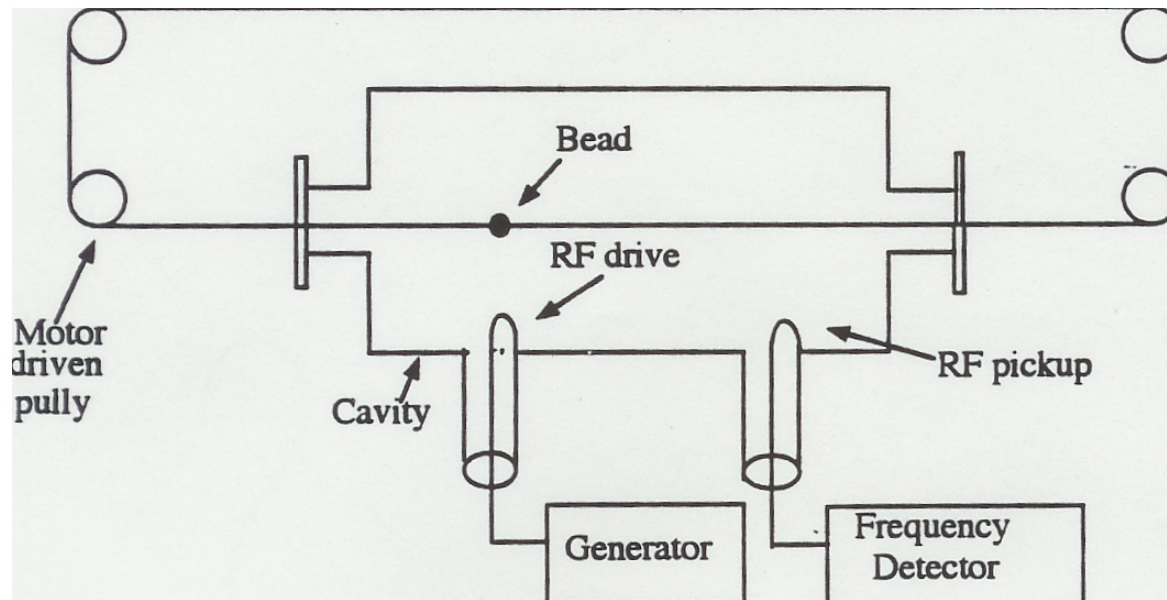


• The Slater result provides the basis for measuring RF electric and magnetic fields as a function of position. A small spherical beam, usually metallic, is moved through the cavity. At each position the bead displaces some field and produces a measurable resonant frequency shift. This allows measurement of the relative $E^2$ or $B^2$. Absolute field measurements are also possible.

# Principles of Accelerating Structures for the SNS

Tom Wangler

# Accelerating Structures for SNS

• In a proton linac, different accelerating structures are used in different velocity ranges. The main issues that determine this are **RF power efficiency** and beam **focusing**.

• The **SNS linac accelerating structures are:**

\***Radiofrequency Quadrupole** (**RFQ**)-strong rf electric focusing from 0.065 to 2.5 MeV.

\***Drift-Tube Linac** (**DTL**) from 2.5 to 87 MeV-high efficiency and strong magnetic focusing in intermediate velocity range.

\***Coupled-Cavity Linac** (**CCL**) from 87 to 186 MeV. High efficiency for these velocities.

\***Superconducting Linac** (**SCL $\beta$=0.61**) from 186 to 387 MeV.

\***Superconducting Linac** (**SCL $\beta$=0.81**) from 387 to 1000 MeV.

# Radiofrequency Quadrupole (RFQ)
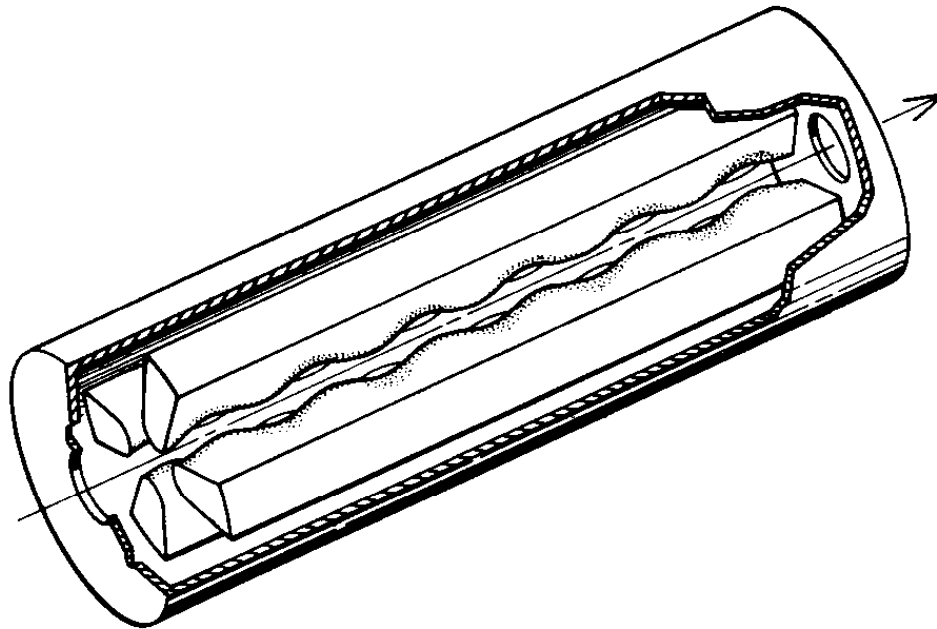


Fig.1.2f.  The radiofrequency quadrupole (RFQ), used for acceleration of low-velocity ions, consists of four vanes mounted within a cylindrical cavity. The cavity is excited in an electric quadrupole mode in which the RF electric field is concentrated near the vane tips to produce a transverse RF electric-restoring force for particles that are off axis. The modulation of the vane tips produces a longitudinal electric-field component that accelerates the beam along the axis.

- **The RFQ was invented by Kapchinskiy and Tepliakov,**
- **I.M.Kapchinskiy and V.A.Tepliakov, Prib.Tekh.Eksp. 2,19-22(1970)**

# Radiofrequency quadrupole (RFQ) for particles with $\beta < 0.1$
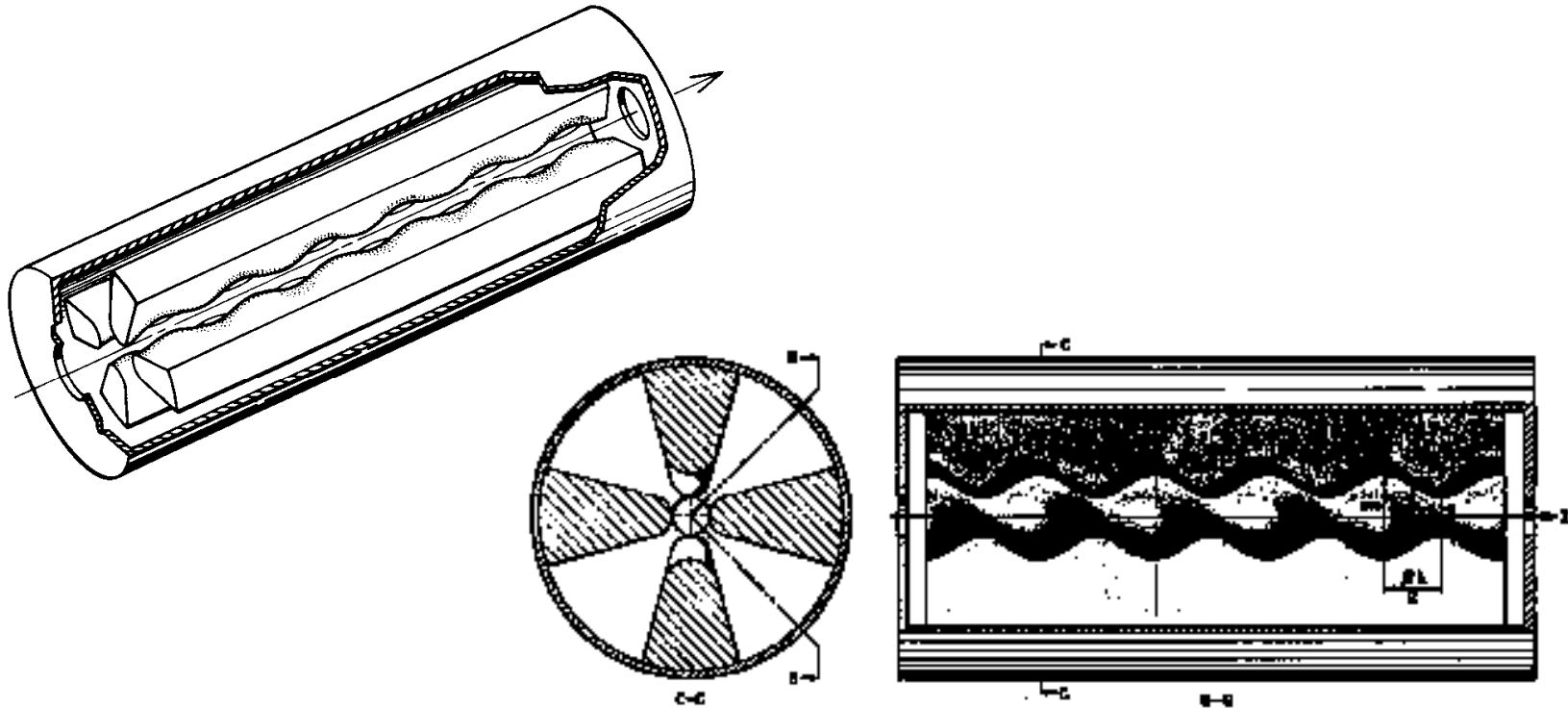


- Has a $TE_{210}$-like field pattern that produces **rf electric quadrupole fields**.
- The RFQ provides rf electric field for **bunching, acceleration, and transverse rf electric quadrupole focusing.**

# Four-vane Radiofrequency-Quadrupole (RFQ) linac



E field region

B field region
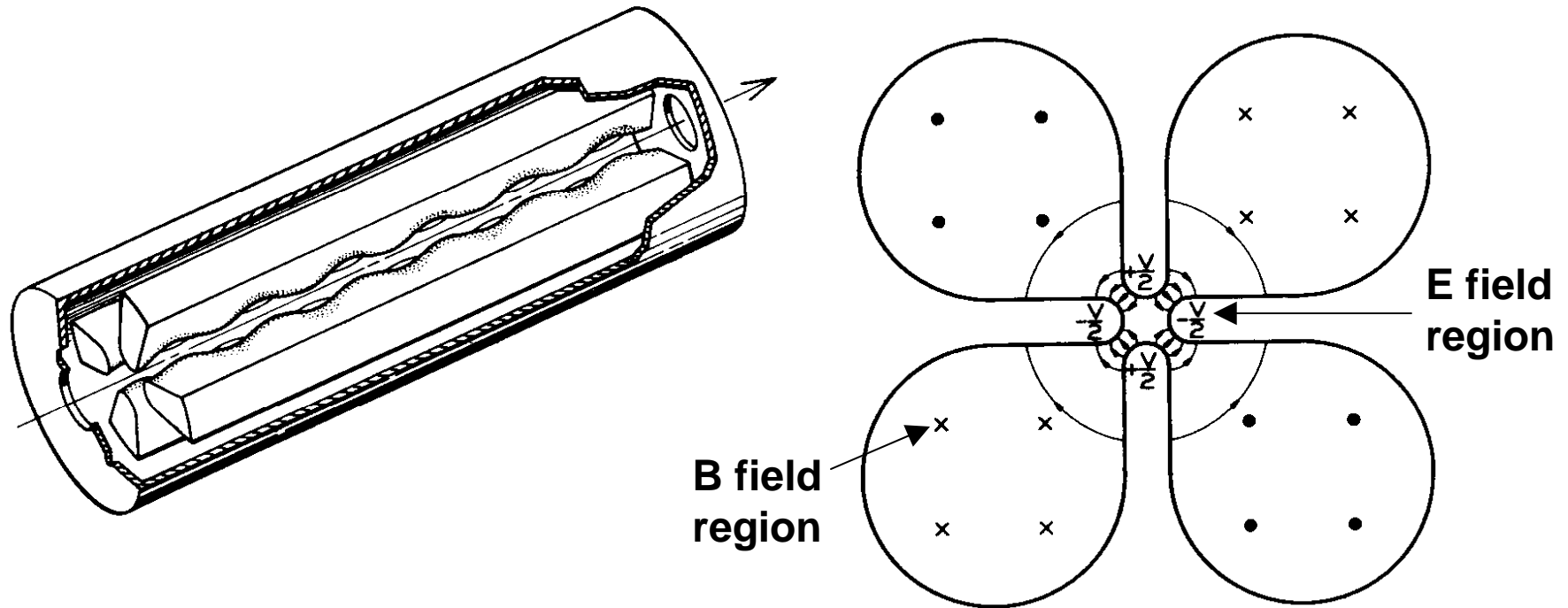
- The four vanetips (poletips) are excited with rf electric quadrupole voltages to focus the beam transversely.

# Views of a four-vane RFQ unit cell
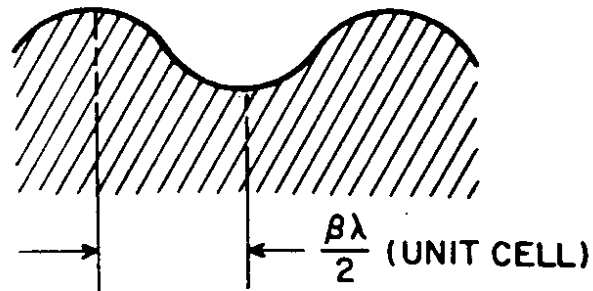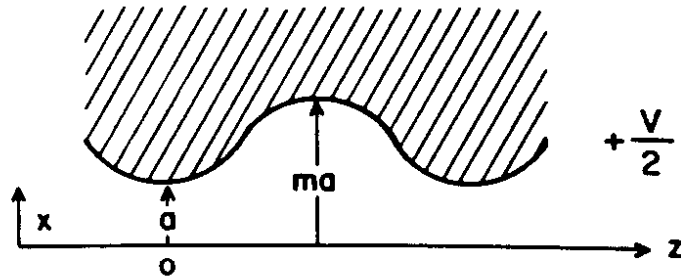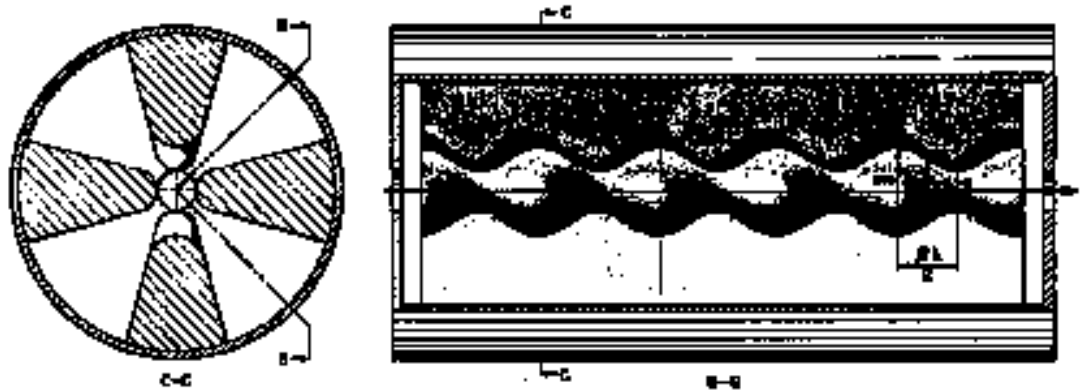
# Two-Term RFQ Potential Function, Solution to Laplace's Equation, Provides An Analytic Solution for the Electric Fields

$$U(r, \theta, z, t) = \frac{V_0}{2}\left[ X\left[\frac{r}{a}\right]^2 \cos(2\theta) + A\, I_0(kr)\cos(kz) \right]\sin(\omega t + \phi),$$ ← **Potential**

$$X = \frac{I_0(ka) + I_0(kma)}{m^2 I_0(ka) + I_0(kma)},$$ ← **Focusing efficiency**

$$A = \frac{m^2 - 1}{m^2 I_0(ka) + I_0(kma)}.$$ ← **Acceleration efficiency**
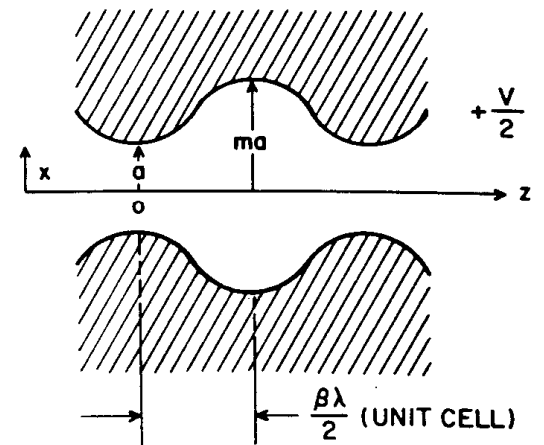


**Electric Field Components are derived from potential.** →

$$E_x = -\frac{XV_0}{a^2}x - \frac{kAV_0}{2}I_1(kr)\frac{x}{r}\cos(kz),$$

$$E_y = \frac{XV_0}{a^2}y - \frac{kAV_0}{2}I_1(kr)\frac{y}{r}\cos(kz),$$

$$E_z = \frac{kV_0 A}{2}I_0(kr)\sin(kz),$$

**Quadrupole focusing plus rf defocusing.**

**Acceleration**

# Modified Bessel Functions $I_0(x)$ and $I_1(x)$
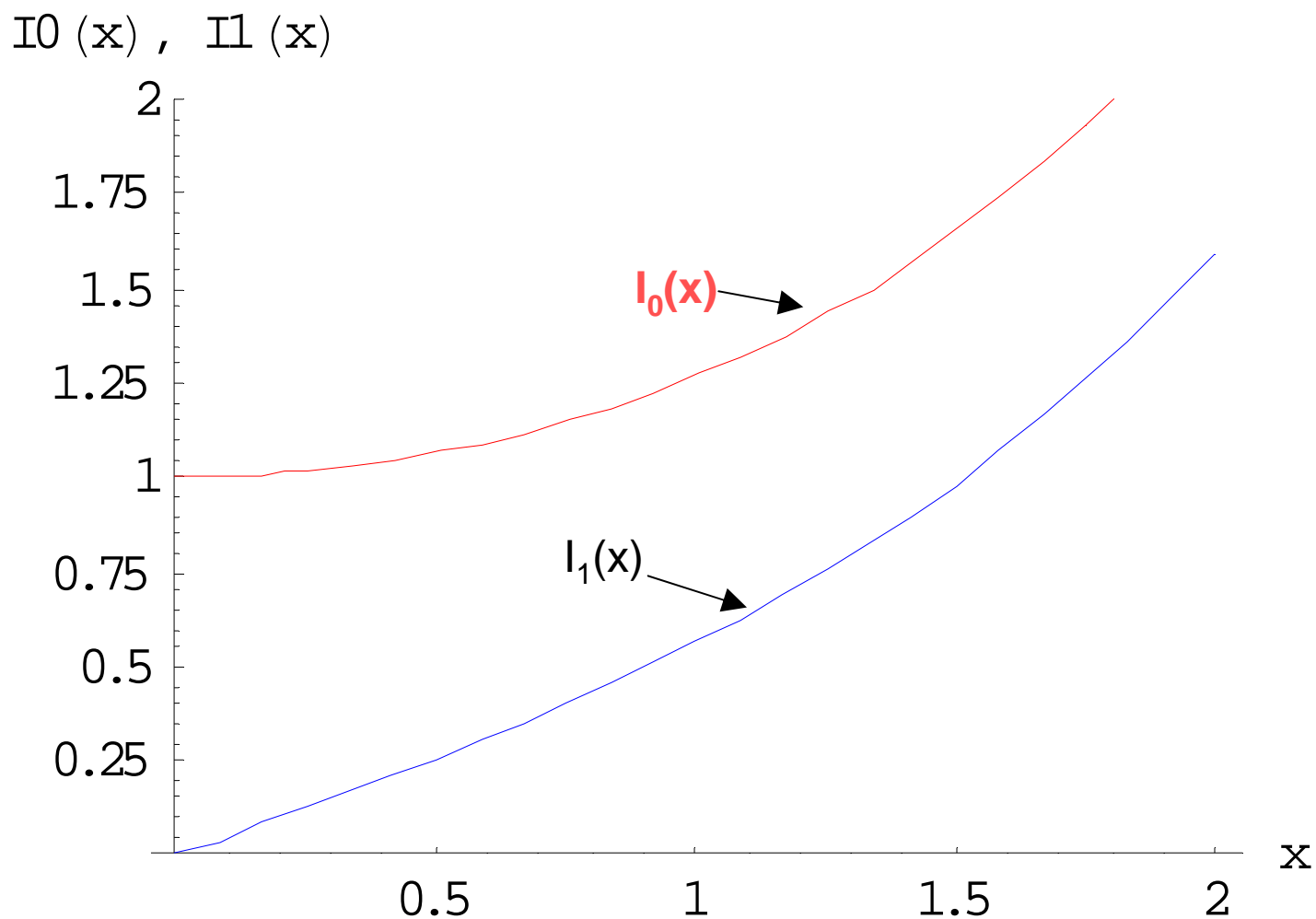


$I_0(x) \cong 1 + x^2/4 + ..., \ I_1(x) \cong 1 + x/2 + ....$

# Synchronous acceleration in the RFQ is the really the same as for other linac structures

$$\Delta W = q \ E_0 T I_0(kr) \ \ell \cos \ \phi_s$$

$k = 2\pi/\beta_s\lambda$, and $\ell = \beta_s\lambda/2$ is the length of the unit cell.

$$E_0 = \frac{1}{\ell} \int_0^{\ell} E_z dz = \frac{2A \ V_0}{\beta\lambda} .$$

⟵ **Interpretation: A is the fraction of the intervane voltage $V_0$ that is applied across a cell of length $\beta\lambda/2$.**

• **Note that $E_0$ decreases as $\beta$ increases. Thus the acceleration becomes less efficient with increasing $\beta$.**

$$T = \frac{\int_0^{\ell} E_z \sin(kz) \ dz}{\int_0^{\ell} E_z dz} = \frac{\pi}{4} .$$
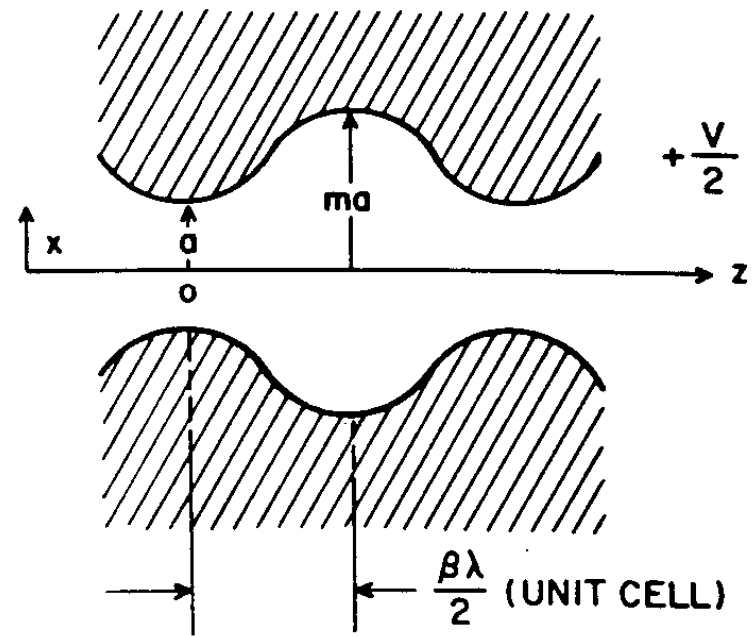
# Poletips of an RFQ with adiabatic bunching
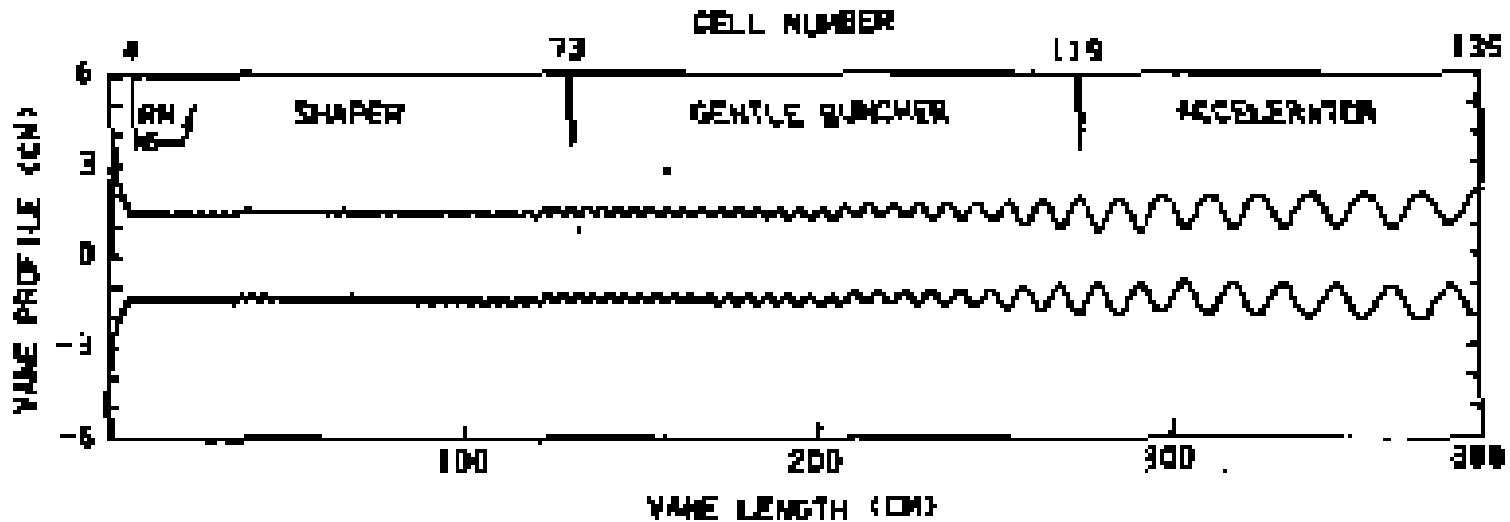


- Transverse dimensions are magnified compared with longitudinal ones.

- Beam goes from left to right.

- Four sections: Radial Matching, Shaper, Gentle Buncher, Accelerator Section. Note changing cell geometry.

- Bunching is started in the shaper. Adiabatic bunching is done in gentle-buncher section.

# Adiabatic bunching in the RFQ combines the functions of bunching and acceleration and increases the current limit.

- The invention of the RFQ made major improvement in the current limit for ion RF linacs.

- The modulation parameter m is gradually increased to turn on the accelerating field.

- The cell lengths are gradually adjusted to increase the synchronous phase from -90 degree (bunching only) to about -30 degrees (good acceleration while maintaining longitudinal focusing).

- **This adiabatic bunching approach allows the phase length of the bunch to decrease while maintaining a nearly constant bunch length in real space.**

- This **avoids longitudinal compression of the bunch** and undesirable increase of the transverse space charge force.

# Proof-of-Principle RFQ –1980
## 30-mA proton beam, 100 keV to 640 keV, 425 MHz
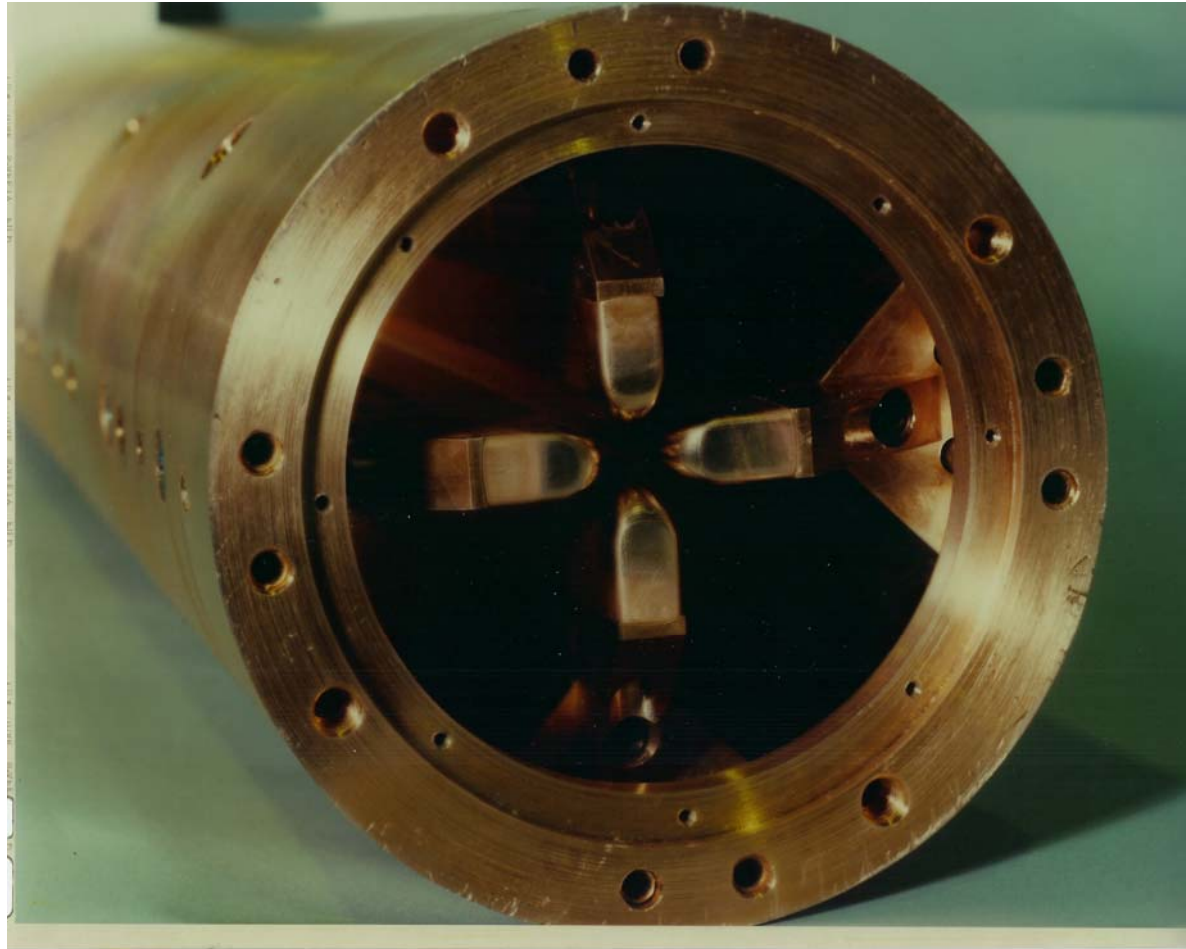


~15 cm

# ATS RFQ – 1985
## 100 mA protons, 100 kev to 2 MeV, 425 MHz
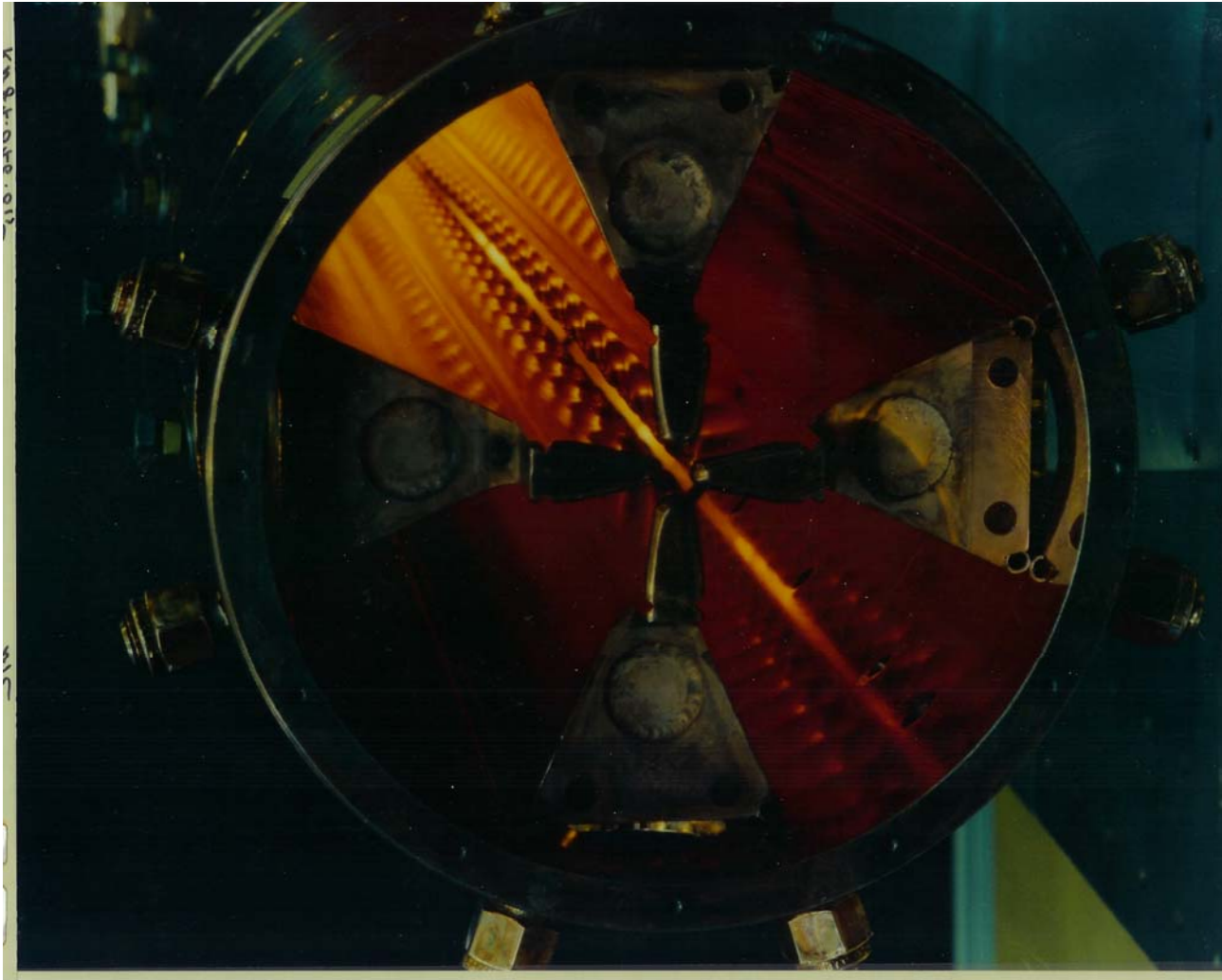
# Beam Aboard A Rocket (BEAR) RFQ – 1989
## 30 mA H⁻, 425 MHz, 30 keV to 1 MeV



BEAR RFQ LINAC
LOS ALAMOS AT-1 / GRUMMAN / GAR
MARCH 1988

# APT RFQ 1999

## 100-mA protons CW, 75 keV to 6.7 MeV, 350 MHz, 8-m long

# SNS H⁻ RFQ
## 65 keV to 2.5 MeV, 402.5 MHz
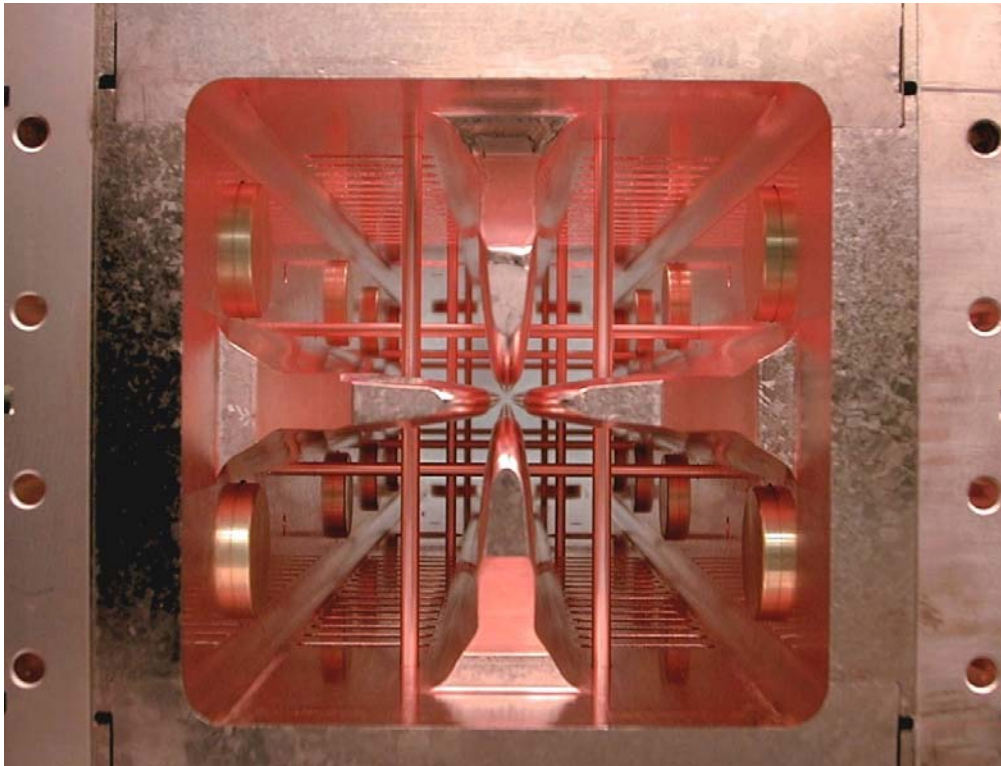


SNS RFQ seen from the LEBT side

- 4-vane RFQ with $\pi$-mode stabilizers
  - 4 modules with 3.72-m total length
- 402.5 MHz resonant frequency
- 640 kW pulsed power needed to achieve nominal gradient without beam
  - 8 power couplers
  - 80 fixed tuners
  - Dynamic tuning implemented by adjusting wall-to-vanetip temperature difference
  - 2.5 min. needed to reach stable operation from cold start

# Three linac structures are used to accelerate the H⁻ beam from 2.5 to 1000 MeV



DTL    CCL    SRF

*The SNS Linac consists of a drift-tube linac (DTL), a coupled-cavity linac (CCL), followed by a superconducting RF (SRF) linac with beta =0.61 (medium beta) and beta=0.81 (high beta) cavities.*
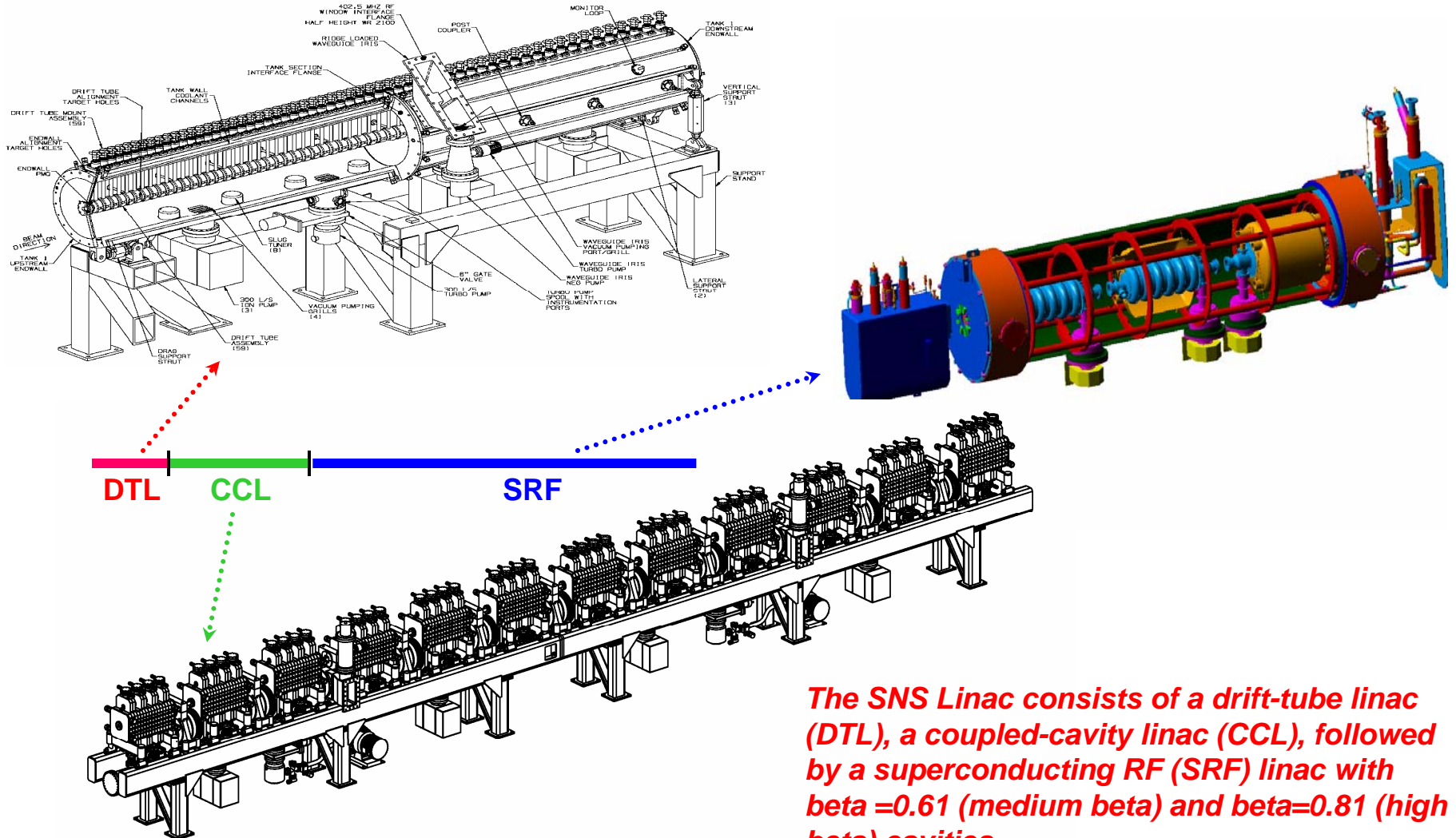
# Alvarez Drift-Tube Linac for medium-velocity particles ($\beta \approx 0.05$ to 0.5) is really a long $TM_{010}$ pillbox cavity with drift tubes to shield the particles when the field has the wrong polarity.
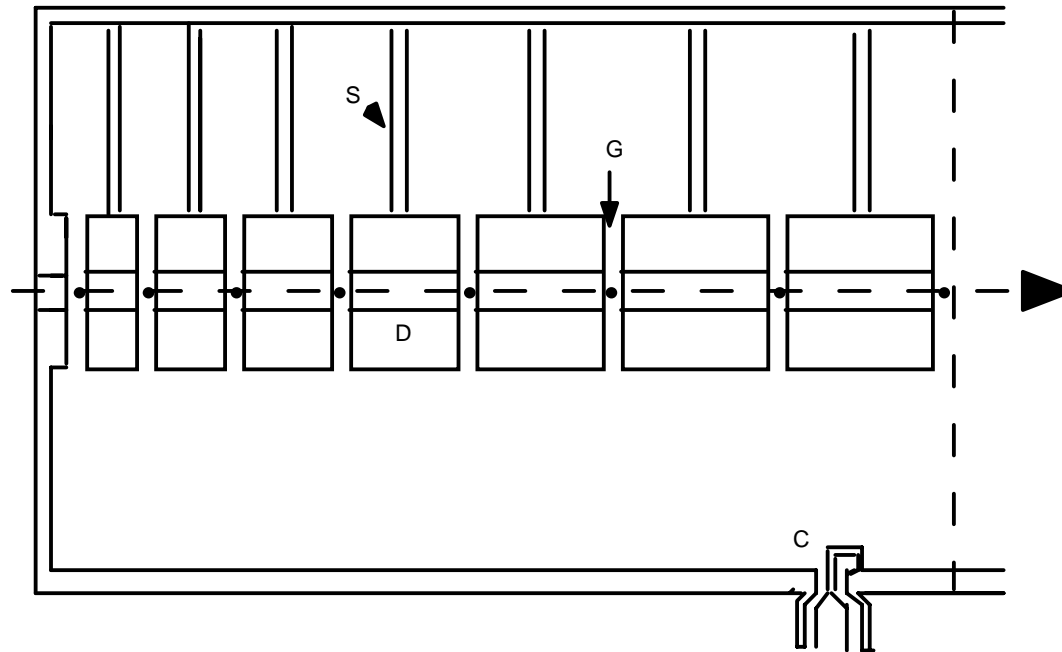


- Field has same polarity in all gaps.
- Intercell walls removed improving efficiency.
- Called a zero mode.
- Designed for fixed velocity profile.
- Focusing quadrupoles in drift-tubes.

# The Alvarez Drift-Tube Linac (DTL) is a pillbox cavity with drift tubes.

• DTL is a multicell cavity obtained by installing drift tubes
in a long pillbox cavity operating in a $TM_{010}$ mode.

• Motivation: When pillbox cavity length $>\beta\lambda/2$, acceleration becomes
inefficient (or zero) because acceleration and deceleration tend to
cancel.

• The idea is to introduce hollow drift tubes to shield the beam
from the decelerating fields, dividing cavity into **cells of length $\beta\lambda$**.
As $\beta$ increases, cell lengths increase.

• Electric fields in gaps remain everywhere in phase, called 0 mode,
which means zero phase change from cell to cell.

# Drift-tube linac works well for velocity range 0.05<β<0.5.
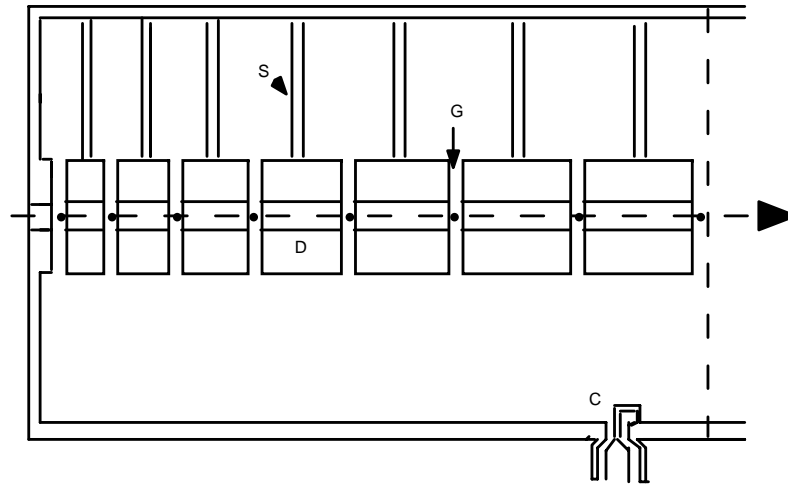


- For β>0.5 the gap lengths have increased so much that gap factor (in transit-time factor) decreases. Coupled -cavity structure is more efficient.
- For β<0.05 the aperture factor (in transit time factor) drops.
- For β<0.05 quadrupole magnets in the drift-tube become short and focusing weakens. The RFQ structure is superior.

# Alvarez DTL Characteristics

- DTL can be tuned to make $E_0$ constant for all cells.

- Drift tubes can contain focusing quadrupole magnets.

- Drift tubes are supported by stems, which carry no net current. They are needed only for mechanical support.

- The field distribution in a long DTL cavity becomes sensitive to fabrication errors. Compensation for the errors is obtained by use of post couplers.

# Three linac structures are used to accelerate the H⁻ beam from 2.5 to 1000 MeV
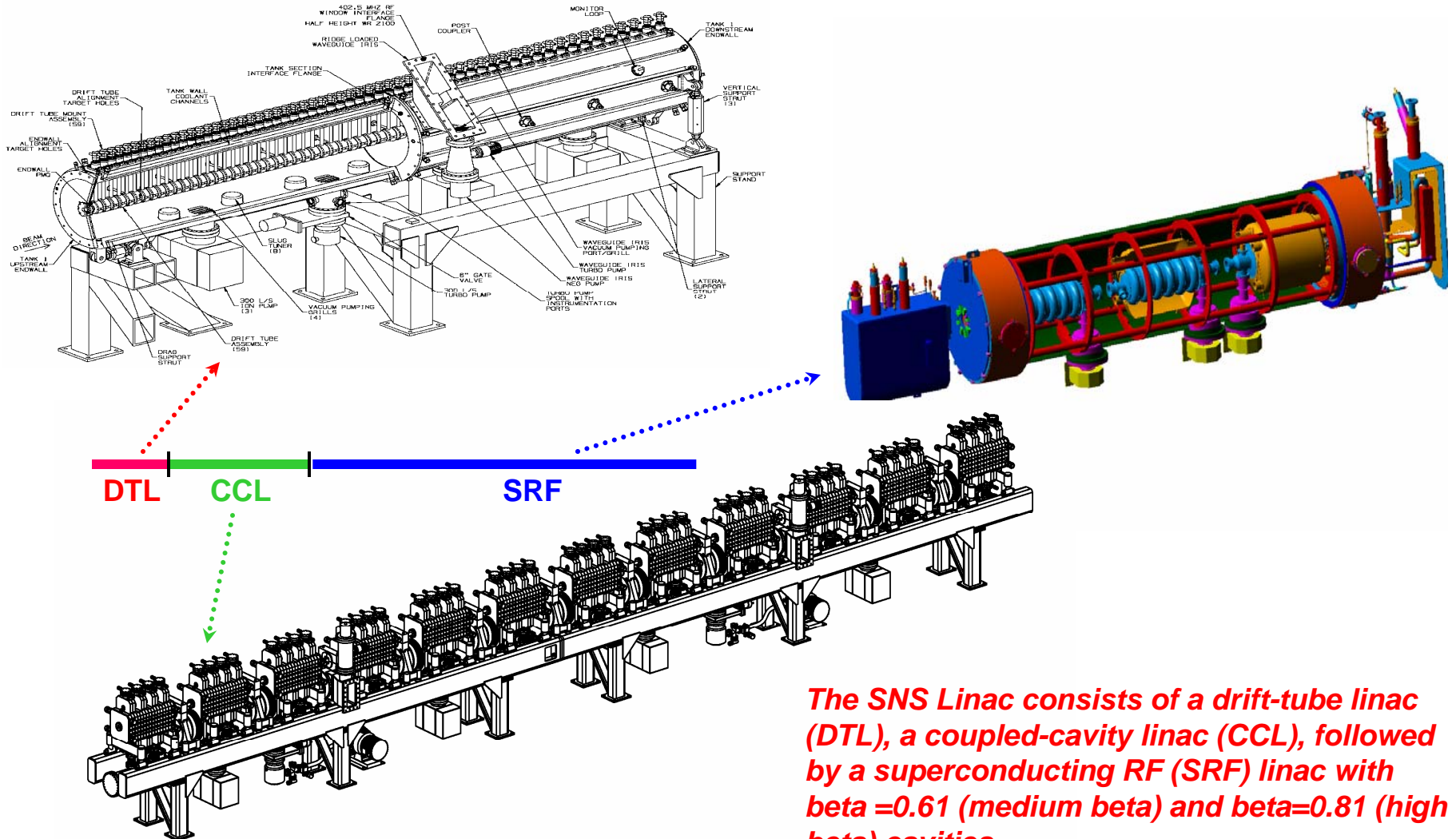


*The SNS Linac consists of a drift-tube linac (DTL), a coupled-cavity linac (CCL), followed by a superconducting RF (SRF) linac with beta =0.61 (medium beta) and beta=0.81 (high beta) cavities.*

# After the DTL comes the Coupled Cavity Linac (CCL)

---

• The coupled-cavity linac consists of an array of single-gap cavities or cells, that are electromagnetically coupled together to form a multicell accelerating structure.

• The cells may be coupled either magnetically through slots in outer wall or electrically through the beam aperture ( as in superconducting cavities).

• Each accelerating cell is excited in a nominal $TM_{010}$ mode.

• There are different kinds of CCLs; the kind used in SNS (and in the LANSCE linac is the side-coupled linac (SCL).

•Main motivation: For high $\beta > 0.4$, we want long multicell accelerating structures that can be driven by a single high power klystron.

# Coupled Cavity Linacs

- Each cell is excited in a $TM_{010}$-like mode.

- But resonant frequency errors of the individual cells in long multicell structures can lead to distorted and unstable field distributions.

- How to build long multicell structures that give stable field distributions and high power efficiency.

- A solution was found in the 1960's for the high energy structure of the 800-MeV LAMPF linac, called the"side-coupled linac structure".

# Three Coupled Oscillator Problem

- Begin with a simple problem to get a feeling for the physics of coupled oscillators.

- First look at the normal-mode solutions (normal modes are the steady state harmonic solutions) of **three identical electrical oscillators with no power losses.**

- We will associate the oscillators with cavities and the currents with fields.

- Write Kirchoff's equations with no losses and solve for the three normal modes, their characteristic resonant frequencies, and corresponding eigenvectors (field distributions).

- Next, we will introduce **cavity frequency errors** and use perturbation theory to see how the frequencies and field distributions are modified.

- Finally, introduce **power losses** (add an RF generator to supply the losses) and see how this affects the field distribution.

# Complex Exponential Notation

- Harmonic time dependence is represented by $\exp(j\omega t)$

- Recall $Re[\exp(j\omega t)]=Re[\cos(\omega t)+j\sin(\omega t)=\cos(\omega t)$

- If $B=A\exp(j\phi)$, it means the phase of B is larger than the phase of A by $\phi$.

- Another relationship: $\exp(j\pi/2)=\cos(\pi/2)+j\sin(\pi/2)=j$. Thus j represents a phase increase of $\pi/2$.

- Thus $j\exp(j\omega t)=\exp(j[\omega t+\pi/2]$.

# Coupled Circuit Model for three oscillators
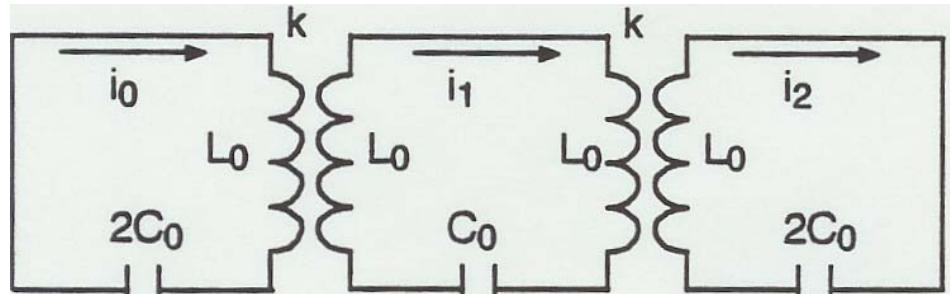


$$i_0 \left[ j\Omega L_0 + \frac{1}{2 j\Omega C_0} \right] + i_1 \underbrace{j\Omega k L_0}_{M} = 0, \ cell \ 0$$

$$i_0 \underbrace{j\Omega k L_0}_{M} + i_1 \left[ j2\Omega L_0 + \frac{1}{j\Omega C_0} \right] + i_2 \underbrace{j\Omega k L_0}_{M} = 0, \ cell \ 1$$

$$i_1 \underbrace{j\Omega k L_0}_{M} + i_2 \left[ j\Omega L_0 + \frac{1}{j2\Omega C_0} \right] = 0, \ cell \ 2$$

$$\omega_0 = \frac{1}{\sqrt{2 L_0 C_0}} = cell \ resonant \ frequency \ (when \ no \ coupling)$$

$\Omega = angular \ frequency \ of \ the \ \text{mod} e$

$$k = \frac{M}{L} = \text{int} ercell \ coupling \ strength \ k << 1$$

*Typically for accelerator cavities* $(k \approx 0.05)$.

# Solve for the Three Normal Modes

• Procedure is to solve the eigenvalue problem. The three Kirchoff's equations can be expressed in the following form.

$$\underset{\substack{matrix \\ operator}}{\underline{L}} \underset{\substack{eigen- \\ vector}}{X_q} = \frac{1}{\underset{\substack{eigen- \\ value}}{\Omega_q^2}} X_q, \quad q = 0,1,2 \ is \ \mathrm{mod} e \ number$$

 • Eigenvector components give the currents (fields) in each cell. We find

$$L = \begin{bmatrix} \dfrac{1}{\omega_0^2} & \dfrac{k}{\omega_0^2} & 0 \\[2ex] \dfrac{k}{2\omega_0^2} & \dfrac{1}{\omega_0^2} & \dfrac{k}{2\omega_0^2} \\[2ex] 0 & \dfrac{k}{\omega_0^2} & \dfrac{1}{\omega_0^2} \end{bmatrix}, \quad X_q = \begin{bmatrix} x_0 \\ x_1 \\ x_2 \end{bmatrix}, \quad x_n = i_n \sqrt{2L_0}, \quad n = 0,1,2 \ cell$$
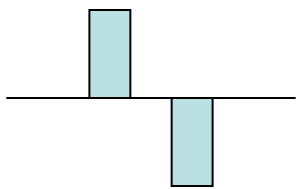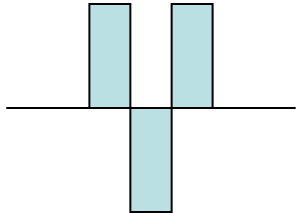
• Want solutions for $X_q$ and $\Omega_q$. There will be 3 solutions (3 modes).

# Eigenvalue Problem Results

- Three normal modes

| $q$ | $\mathrm{mod}\,e$ | $\Omega_q$ | $X_q$ | |
|---|---|---|---|---|
| 0 | 0 | $\dfrac{\omega_0}{\sqrt{1+k}}$ | $\begin{bmatrix} 1 \\ 1 \\ 1 \end{bmatrix}$ | |
| 1 | $\dfrac{\pi}{2}$ | $\omega_0$ | $\begin{bmatrix} 1 \\ 0 \\ -1 \end{bmatrix}$ | |
| 2 | $\pi$ | $\dfrac{\omega_0}{\sqrt{1-k}}$ | $\begin{bmatrix} 1 \\ -1 \\ 1 \end{bmatrix}$ | |

$$\frac{\Omega_\pi - \Omega_0}{\Omega_{\pi/2}} = \frac{\dfrac{\omega_0}{\sqrt{1-k}} - \dfrac{\omega_0}{\sqrt{1+k}}}{\omega_0} \cong k$$

# Perturbation Theory

- Suppose the cells are slightly different, i.e. suppose we introduce errors.

- In the unperturbed case all the cells have the same frequency $\omega_0$.

- In the perturbed case the three frequencies will be slightly different and experimentally we don't have any way to define the unperturbed frequency.

- Let's make it easy for ourself. No generality is lost in the perturbed case by defining the unperturbed frequency $\omega_0$ to equal the average of the two end cell frequencies.

- Then the two end cell frequency errors are $-\delta\omega_0$ and $+\delta\omega_0$. The middle cell frequency error is called $\delta\omega_1$.
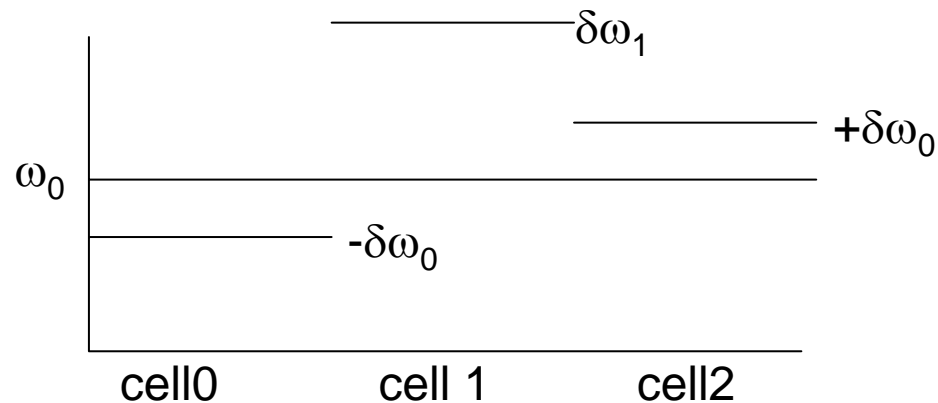
# Perturbation Theory—First Order

$$P = \begin{bmatrix} \delta\left(\dfrac{1}{\omega_0^2}\right) & k\delta\left(\dfrac{1}{\omega_0^2}\right) & 0 \\[2em] \dfrac{k}{2}\delta\left(\dfrac{1}{\omega_1^2}\right) & \delta\left(\dfrac{1}{\omega_1^2}\right) & \dfrac{k}{2}\delta\left(\dfrac{1}{\omega_1^2}\right) \\[2em] 0 & -k\delta\left(\dfrac{1}{\omega_0^2}\right) & -\delta\left(\dfrac{1}{\omega_0^2}\right) \end{bmatrix}, \quad perturbation\ matrix$$

Three parameters matter.

$$\Delta\left(\frac{1}{\Omega_q^2}\right) = X_q P X_q, \quad eigenvalue\ correction;\ q = 0,1,2$$

$$\Delta X_q = \sum_{r \neq q} a_{qr} X_r, \quad eigenvector\ correction,\ q = 0,1,2$$

$$a_{qr} = \frac{X_q P X_r}{\dfrac{1}{\Omega_r^2} - \dfrac{1}{\Omega_q^2}}$$

$$\delta\left(\frac{1}{\omega_0^2}\right) = -2\frac{\delta\omega_0}{\omega_0^3}$$

$$\delta\left(\frac{1}{\omega_1^2}\right) = -2\frac{\delta\omega_1}{\omega_1^3}$$

$$k$$

- Note coefficients $a_{qr}$ are larger for modes r close in frequency to mode q.

# Perturbation Theory Results

| $q$ | $\text{mod}\,e$ | $\Omega_q$ | $X_q$ | |
|---|---|---|---|---|
| 0 | 0 | $\dfrac{\omega_0}{\sqrt{1+k}}\sqrt{1+\dfrac{\delta\omega_1}{\omega_1}}$ | $\begin{bmatrix} 1+\dfrac{1+k}{2k}\left(\dfrac{\delta\omega_1}{\omega_0}-4\dfrac{\delta\omega_0}{\omega_0}\right) \\[2mm] 1-\dfrac{1+k}{2k}\dfrac{\delta\omega_1}{\omega_0} \\[2mm] 1+\dfrac{1+k}{2k}\left(\dfrac{\delta\omega_1}{\omega_0}+4\dfrac{\delta\omega_0}{\omega_0}\right) \end{bmatrix}$ | • Corrections Are linear in the errors. |
| 1 | $\dfrac{\pi}{2}$ | $\dfrac{\omega_0}{\sqrt{1-4\dfrac{\delta\omega_0^2}{\omega_0^2}}}$ | $\begin{bmatrix} 1+\dfrac{4}{k^2}\dfrac{\delta\omega_1}{\omega_0}\dfrac{\delta\omega_0}{\omega_0}-\dfrac{2}{k^2}\dfrac{(\delta\omega_0)^2}{\omega_0^2} \\[2mm] -\dfrac{2\delta\omega_0}{k\omega_0} \\[2mm] -1+\dfrac{4}{k^2}\dfrac{\delta\omega_1}{\omega_0}\dfrac{\delta\omega_0}{\omega_0}-\dfrac{2}{k^2}\dfrac{(\delta\omega_0)^2}{\omega_0^2} \end{bmatrix}$ | • Corrections for are quadratic in The errors. |
| 2 | $\pi$ | *next page* | | |

# Perturbation Theory Results (2)

| $q$ | $\mathrm{mod}\,e$ | $\Omega_q$ | $X_q$ |
|---|---|---|---|
| 2 | $\pi$ | $\dfrac{\omega_0}{\sqrt{1-k}}\sqrt{1+\dfrac{\delta\omega_1}{\omega_0}}$ | $\begin{bmatrix} 1-\dfrac{1-k}{2k}\left(\dfrac{\delta\omega_1}{\omega_0}-4\dfrac{\delta\omega_0}{\omega_0}\right) \\[2mm] -1-\dfrac{1-k}{2k}\dfrac{\delta\omega_1}{\omega_0} \\[2mm] 1-\dfrac{1-k}{2k}\left(\dfrac{\delta\omega_1}{\omega_0}+4\dfrac{\delta\omega_0}{\omega_0}\right) \end{bmatrix}$ |

• Corrections are linear in the errors.

• Notice there are first order corrections to frequency and eigenvectors in the 0 and $\pi$ modes.

• We have included second order terms for $\pi/2$ mode when the first order terms were zero.

• Notice the $\pi/2$ mode is different from the other two modes. The frequency and end cell amplitudes have only second order corrections. Thus, the $\pi/2$ mode amplitudes are very insensitive to cell frequency errors.

# Effects of Power Dissipation in Steady State

• Now turn off cell frequency errors, turn on power loss and turn on the generator to supply the power loss and look at the steady-state solution. Assume the generator is in cell 0. The results are:

| $q$ | $\mathrm{mode}$ | $X_q$ | |
|-----|-----------------|-------|--|
| 0 | 0 | $\begin{bmatrix} 1 \\ \exp\left(-j3\sqrt{1+k}/kQ\right) \\ \exp\left(-j4\sqrt{1+k}/kQ\right) \end{bmatrix}$ | *power flow phase shift* |
| 1 | $\dfrac{\pi}{2}$ | $\begin{bmatrix} 1 \\ \exp\left(-j\pi/2\right) \\ -1+2/(kQ)^2 \end{bmatrix}$ | *power flow droop in end cell* |
| 2 | $\pi$ | $\begin{bmatrix} 1 \\ \exp\left(-j3\sqrt{1-k}/kQ\right) \\ \exp\left(-j4\sqrt{1-k}/kQ\right) \end{bmatrix}$ | *power flow phase shift* |

• **Power flow droop and power flow phase shift are so named because 1/Q is proportional to power P.**

# Effects of Power Loss from Perturbation Theory

- For the 0 and $\pi$ modes one sees phase shifts in cells downstream of the drive point that are first order in 1/kQ, called power-flow phase shifts.

- The $\pi/2$ mode is different. The nominally excited cells (end cells in this case) have no power flow phase shift.

- The nominally excited cells in the $\pi/2$ mode have a second order amplitude correction, called power flow droop. Because it is second order this effect is generally small.

# Summary of the Three Coupled Oscillator Problem

- The analysis reveals sensitivity to cell frequency errors for the usual 0 and $\pi$ modes.

- 0 and $\pi$ mode currents (fields) are sensitive to cell resonant frequency errors. Errors distort the nominally uniform field distributions for these modes.

- Power flow from the generator to the cells in the array causes phase shifts from the nominal phases in the 0 and $\pi$ mode.

- The nominally-excited cells in the $\pi/2$ mode are insensitive to both effects.

- Question: How will these results carry over to the general problem of N coupled oscillators?

# Results for N+1 Coupled Oscillators
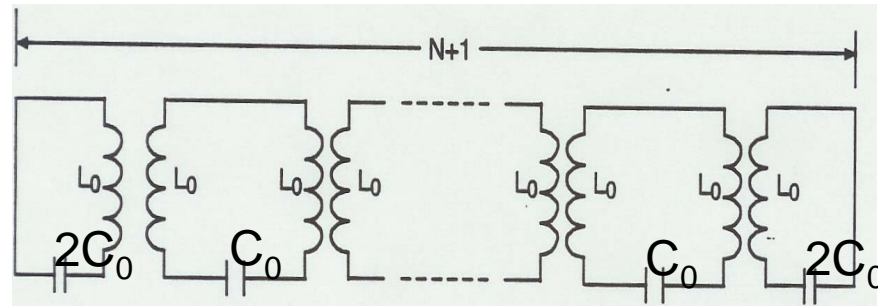


• Dispersion curve (normal mode frequency $\Omega$ versus phase advance per cell $\pi q/N$.

$$\Omega_q = \frac{\omega_0}{\sqrt{1 + k\cos(\pi q / N)}}, \quad q = \mathrm{mode\ number}$$

$$q = 0 \ is \ zero \ \mathrm{mod}e, \ q = N/2 \ is \ \pi/2 \ \mathrm{mod}e,$$

$$q = N \ is \ \pi \ \mathrm{mod}e$$

$$\frac{\pi q}{N} \ is \ phase \ advance \ per \ cell \ of \ a \ traveling \ wave.$$

• Eigenvectors (fields):
$$X_{q,n} = \cos\left(\frac{\pi q n}{N}\right) e^{j\Omega t}$$

$$n = 0,1,2,....,N, \quad n \ is \ oscillator \ number$$

$$q = 0,1,2,.....,N, \quad q = \mathrm{mode\ number}$$

# Example: Dispersion Curve (Normal Mode Spectrum) for 7 Coupled Oscillators
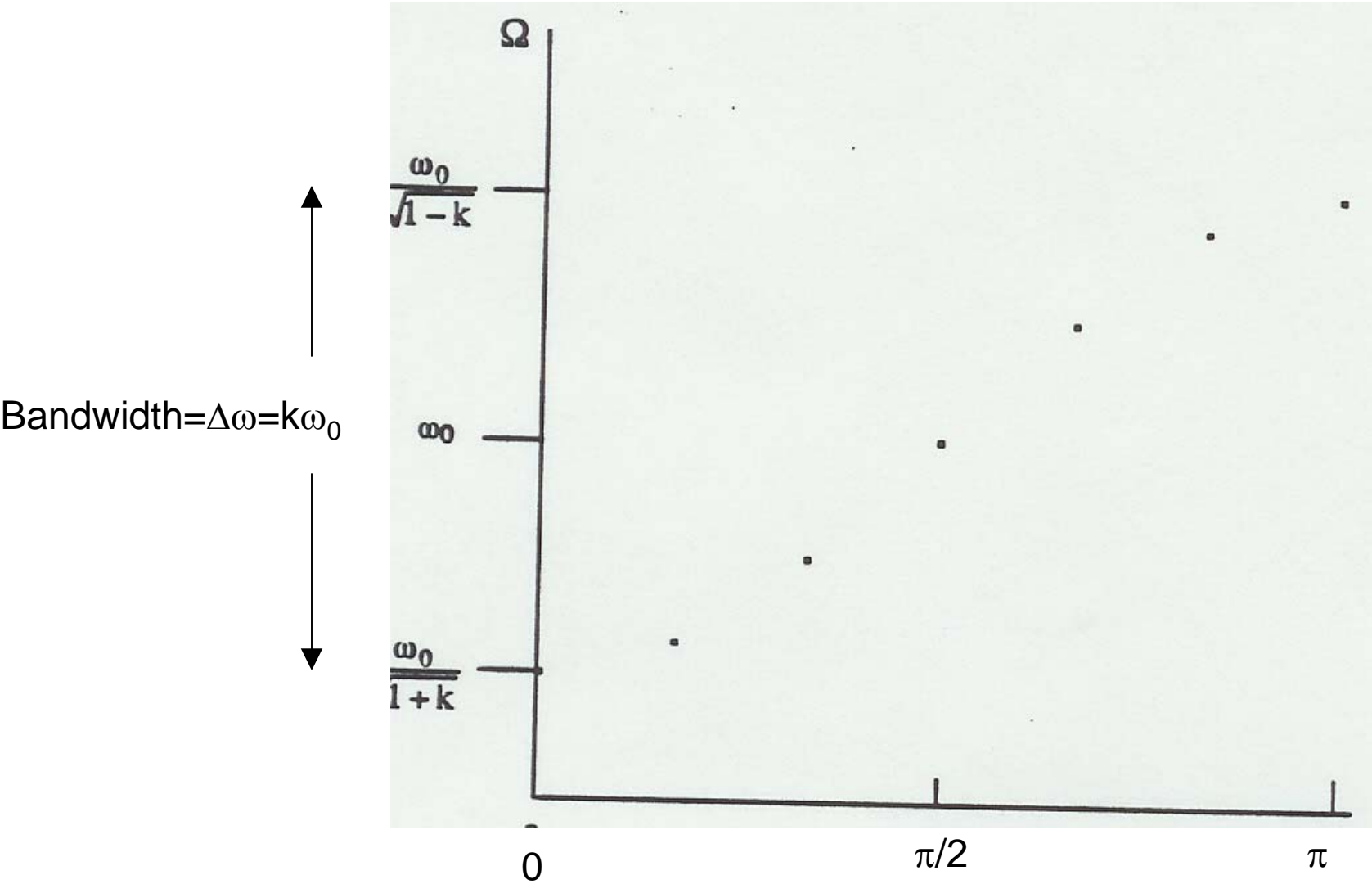
# Discussion of 0 and $\pi$ normal modes in the general case

- Zero and $\pi$ modes have high efficiency if cell spacing is $\beta\lambda$ for zero mode or $\beta\lambda/2$ for $\pi$ mode. Then the beam can get maximum acceleration from every cell.

- But the zero and $\pi$ mode field distributions are sensitive to cell frequency errors.

- Important effect: When the power is dissipated in the walls or when power is delivered to the beam, a cell-to-cell phase shift occurs. The integrated phase shift increases the farther a cell is from the drive point. This is called **power-flow phase shift.**

- **This means that the phases of the cells would depend on the beam current, which would not be good.**

# How to use the $\pi/2$ mode for acceleration

- The $\pi/2$ mode has unique properties that are related fundamentally to its central location in the mode spectrum.

- Field in the nominally excited cells are **insensitive to cell frequency errors.**

- We can use this mode for an accelerating structure if we use the excited cells for **accelerating cells**, and design these cells with a spacing $\beta\lambda/2$ as you would for $\pi$ mode.

# How to use the $\pi/2$ mode for acceleration.(2)

- The problem is **poor efficiency** if the beam passes through the nominally unexcited cells, since these cells do not contribute any acceleration.

- (For example consider a periodic array of cells with equal cell lengths for all cells. In a given structure length the $\pi/2$ mode structure must have twice the field in the excited cells to deliver the same energy to the beam as the $\pi$ mode. Then twice as much power is dissipated in the $\pi/2$ mode than for the $\pi$ mode.)

- **Solution:** We could improve the efficiency of the $\pi/2$ mode by using different cells for the accelerating and coupling cells. This allows us to configure the coupling cells to have less influence on the beam.

- An attractive solution is to move the unexcited cells completely off to the side resulting in the side-coupled structure.

# Evolution to $\pi/2$ normal mode of the side-coupled structure



$\beta\lambda/2$

$\pi/2$ mode of periodic structure

biperiodic on-axis-coupled structure
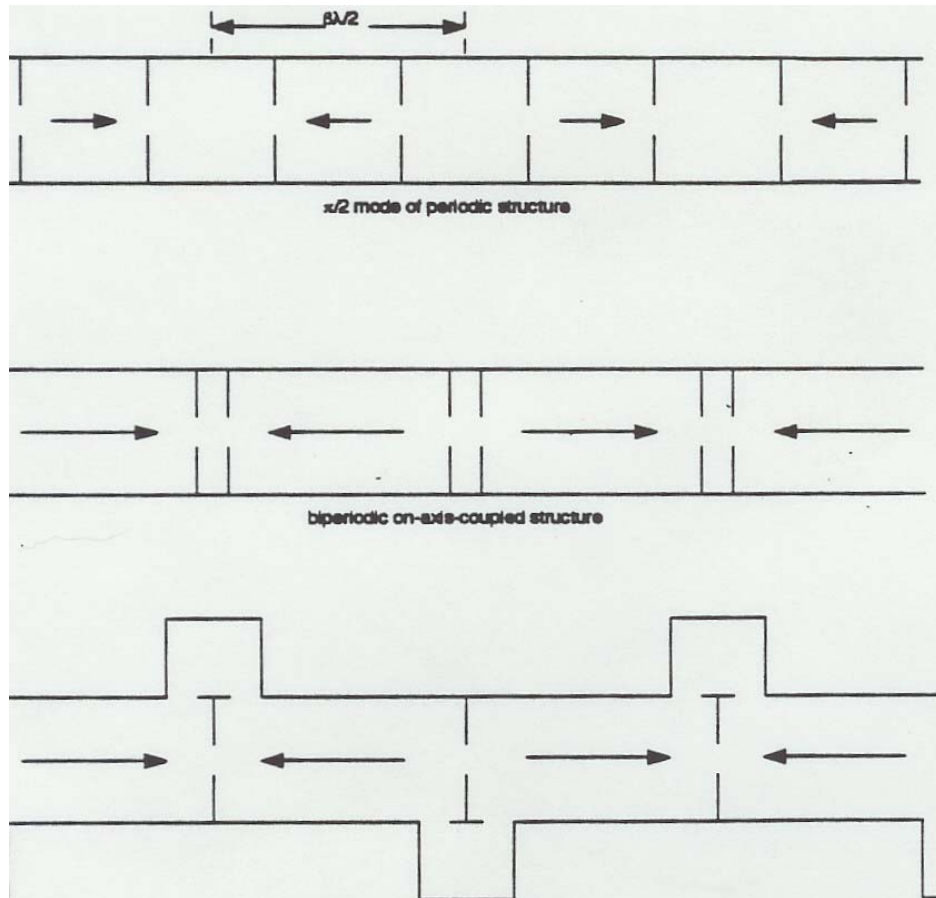
- $\pi/2$ mode of a periodic structure. Half the space is inactive due to the unexcited coupling cells.

- Decrease the inactive volume of the coupling cells to improve the efficiency.

- Remove the coupling cavities to the sides so beam sees only the accelerating cells in a $\pi$-mode configuration, whereas electrically the structure is in a $\pi/2$ mode.

# Side-Coupled Linac Structure Showing Accelerating Cells and Coupling Cells
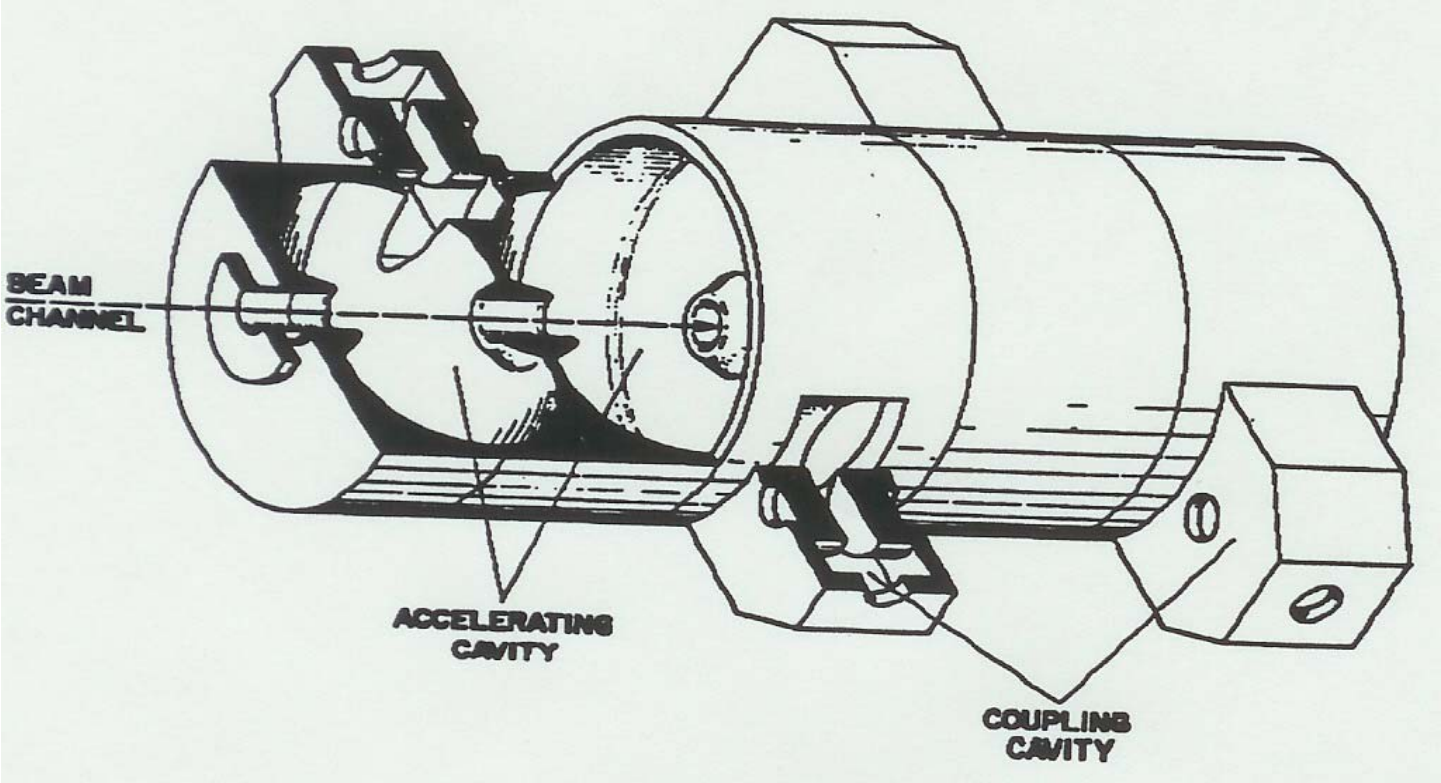
# Dispersion Curve for a Biperiodic Structure

- Dispersion curve relates mode frequencies $\Omega$ to phase advance per cell $\pi q/2N$, q=1, 2, …., 2N for mode q.

$$k^2 \cos^2\left(\frac{\pi q}{2N}\right) = \left[1 - \frac{\omega_a^2}{\Omega_q^2}\right]\left[1 - \frac{\omega_c^2}{\Omega_c^2}\right], \quad q = 0,1,2,...,2N \,(\mathrm{mod}\,e)$$

- $\pi/2$ mode corresponds to q=N. Then cos($\pi$q/2N)=0. Two solutions are $\Omega=\omega_a$, and $\Omega=\omega_c$.

- Dispersion relation has a discontinuity at $\pi/2$ with a stopband between the upper and lower passbands, unless $\omega_a=\omega_c$.

- **Theory shows that for the desired $\pi/2$ mode behavior, you must tune the cavities so $\omega_a=\omega_c$, which removes the stopband.**

# Dispersion Curve for a Biperiodic Coupled-Cavity Linac Structure
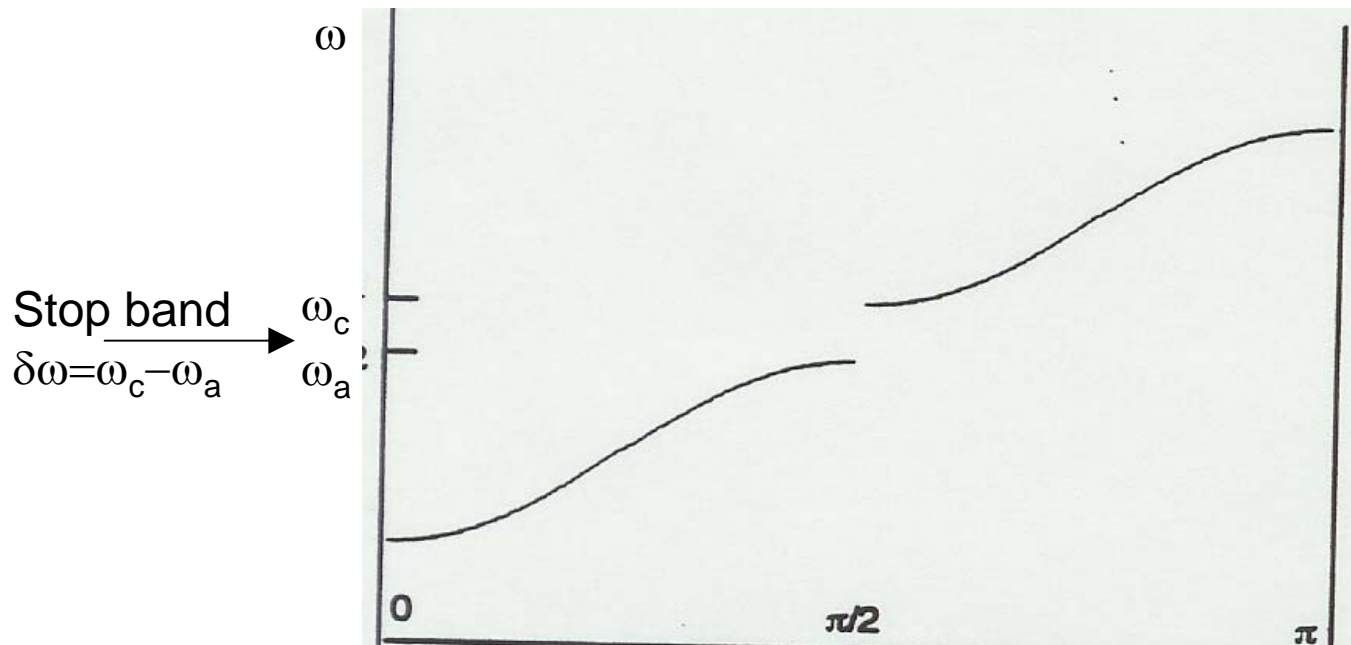


- A biperiodic structure consists of accelerating cells with resonant frequency $\omega_a$, and coupling cells with resonant frequency $\omega_c$.

- In general we anticipate that for a real structure, systematic fabrication errors will result in $\omega_a$ unequal to $\omega_c$ so before tuning we can expect to see a stop band as shown. Theory says we will want to tune to close this stop band.

# Field Distribution in Biperiodic Structure

- **Accelerating Cells:**

  *Label accelerating cells with an index $n \le m$.*

  $n = cell\ index,\ and\ m = drive\ cell\ index,\ n = 0, 1, 2, .... m$

  $$X_{2n} = (-1)^{n-m} X_{2m} \left[ 1 - \frac{2(m^2 - n^2)}{k^2 Q_a Q_c} \right] \exp\left[ j \frac{4(m^2 - n^2)}{k^2 Q_a} \frac{\delta\omega}{\omega_a} \right]$$

  *where stopband is $\delta\omega = \omega_a - \omega_c$*

- **Coupling Cells:**

  *Label coupling cells with an index $n < m$,   $n = 0, 1, 2, ..., m-1$*

  $$X_{2n+1} = (-1)^{n-m} X_{2m} \left[ \frac{2n+1}{k Q_a} \right] \exp^{j\pi/2}$$

- **Two effects included in this model**
1) **Finite stopband $d\omega = \omega_a - \omega_c$**
2) **Power flow effects**

# More Detail of Modes in a Side-Coupled Linac Structure

- **Example: 9 cells and 9 modes, 5 accelerating cells and 4 coupling cells**



Upper $\pi/2$ mode can be excited

Lower $\pi/2$ mode forbidden because of boundary condition
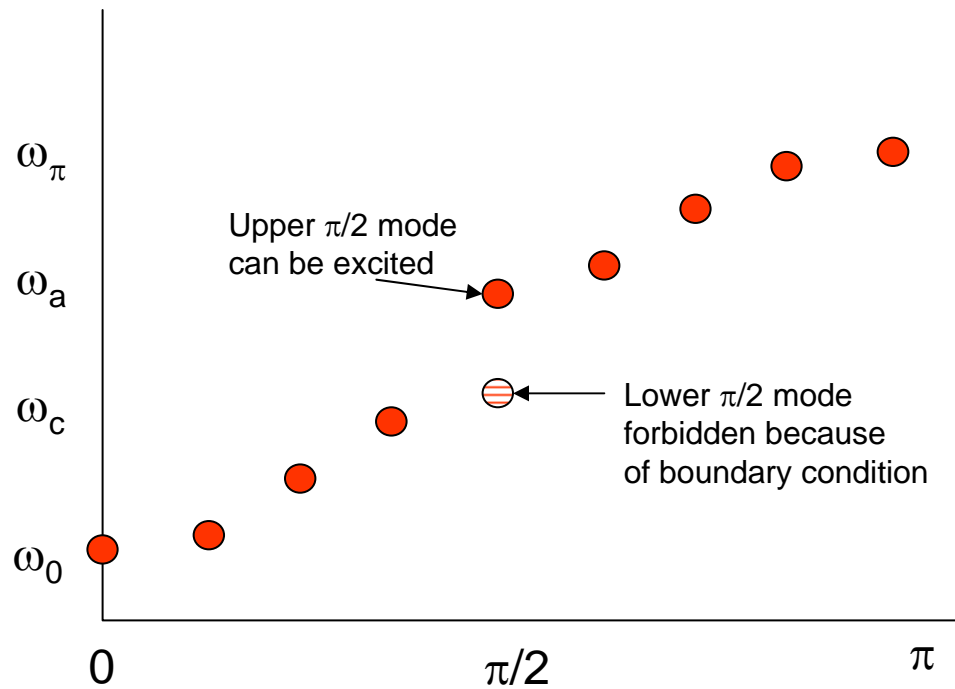
- Zero-mode:
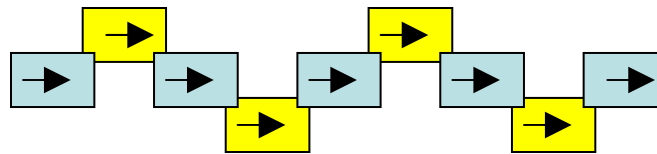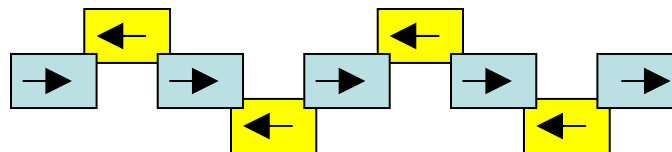
- $\pi$ mode

# Physical picture of allowed and forbidden π/2 modes
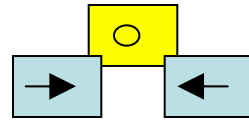


- The above coupling cell is unexcited because it is being driven by two excited cells with equal and opposite amplitudes.
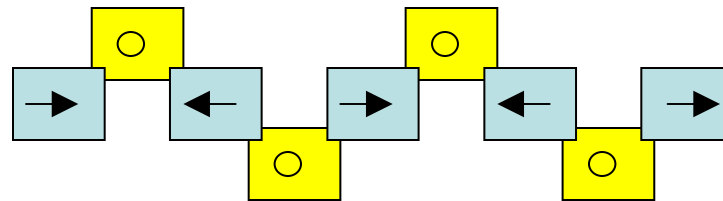


- The above mode is allowed, since each unexcited coupling cell has equal and opposite drive signals required to make it unexcited.
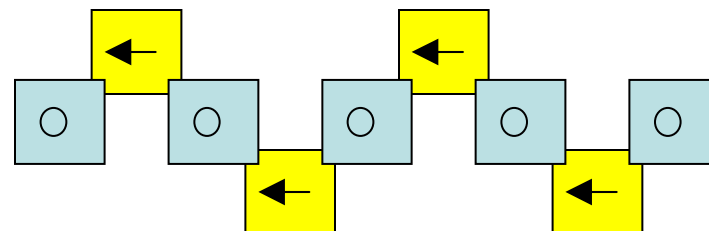


- This mode is forbidden, since the unexcited end cells have a nonzero driving amplitude and therefore can't be unexcited.

# Biperiodic cell nomenclature based on the published literature illustrated by an example



Cell numbers shown → [diagram of cells numbered 0–8 with drive cell and Klystron]

Drive cell with index n=m=4

Klystron
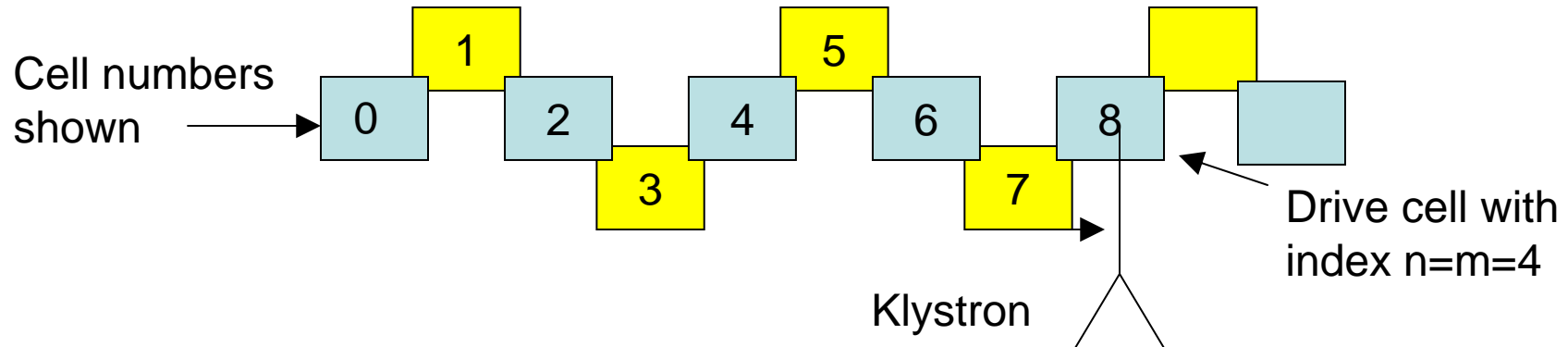
• Each cell has a **number** and an **index n**. Counting from one end, the accelerating cell numbers = 2n, where n=0,1,2…,m=4 (drive cell) and the coupling cell numbers are 2n+1, where n=0,1,2, …,m-1.

•The problem is that the formulas are given in terms of the cell index rather than the cell number.

• Usually the drive cell is at the middle, always an accelerating cell.

# How to identify the middle cell index which is usually the location of the drive cell

- Step 1: Equate 2m+1 to the total number of accelerating cavities where m is the drive cell index assumed to be at the middle.
- Step 2: Solve for drive cell index m.
- Step 3: The middle cell number is 2m.

- Example:
  5 accelerating cells and 4 coupling cells. Drive cell at center.
- Step 1: 2m+1=5
- Step 2: Middle cell index=m=2
- Step 3: The middle cell number=2m=4

# Example of power flow phase shift in accelerating cells when stop band is not closed

**33 accelerating cells, 32 coupling cells, m=16, drive cell number=32, $d\omega/\omega$=0.001, k=0.05, $Q_a$=10000, $Q_c$=1000**
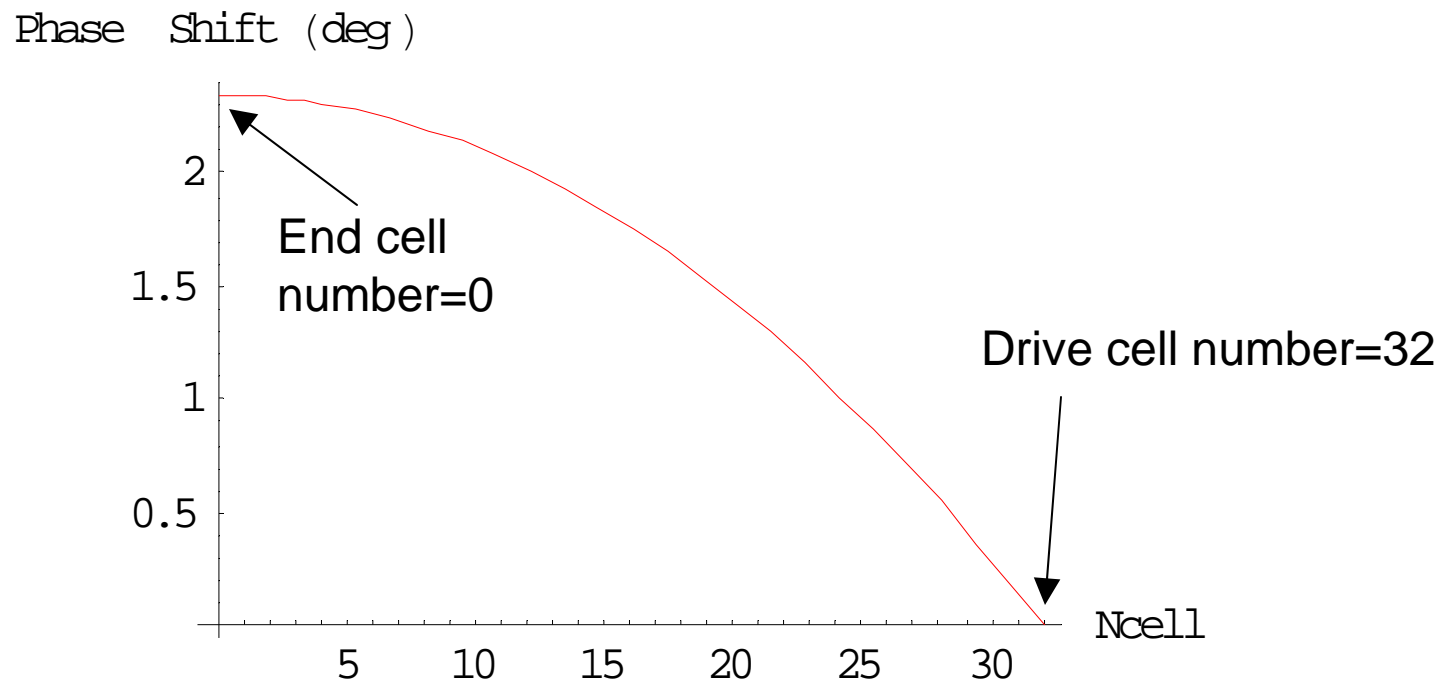
# Example of accelerating field amplitude (relative to drive cell amplitude)

**33 accelerating cells, m=16, drive cell number=32, dω/ω=0.001, k=0.05, Qa=10000, Qc=1000**
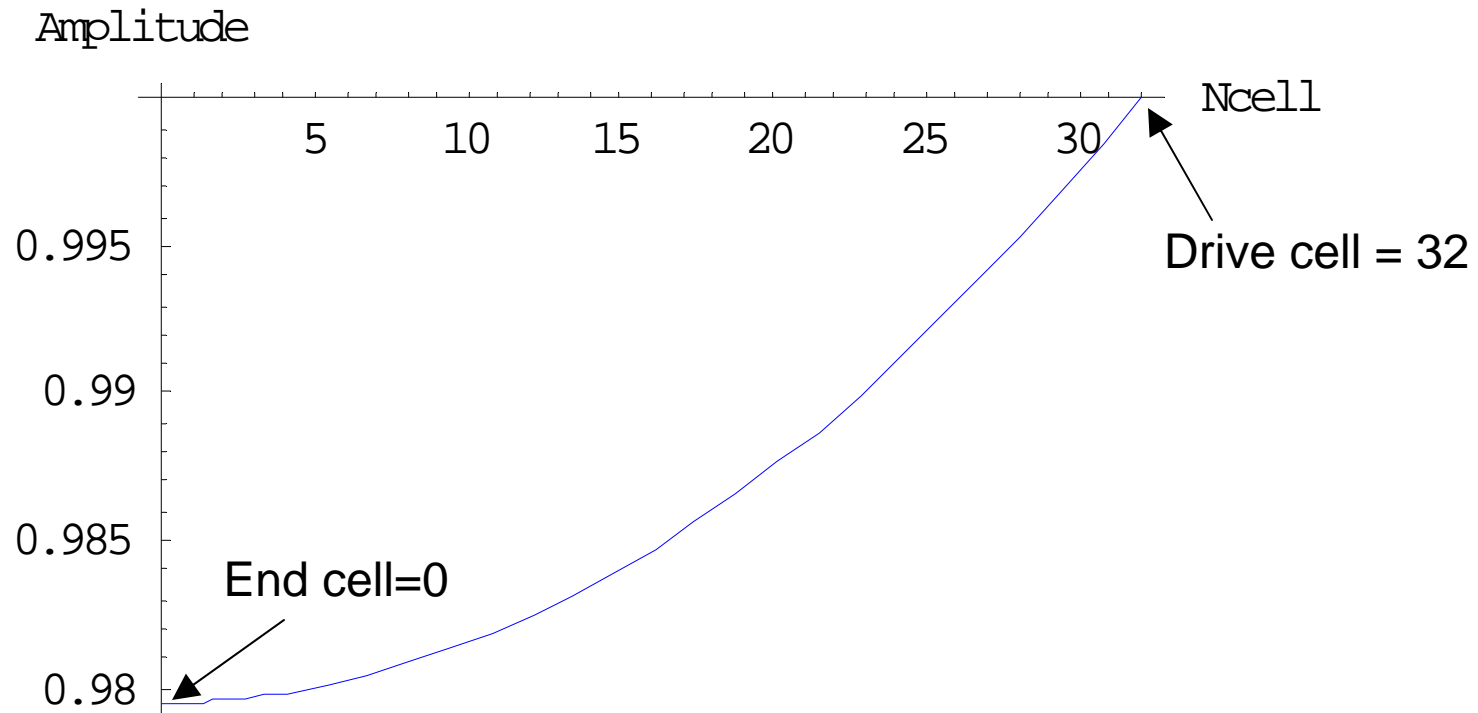
# Example of coupling cell amplitude (relative to drive cell amplitude)

**33 accelerating cells, m=16, drive cell number=32, dω/ω=0.001, k=0.05, Qa=10000, Qc=1000**
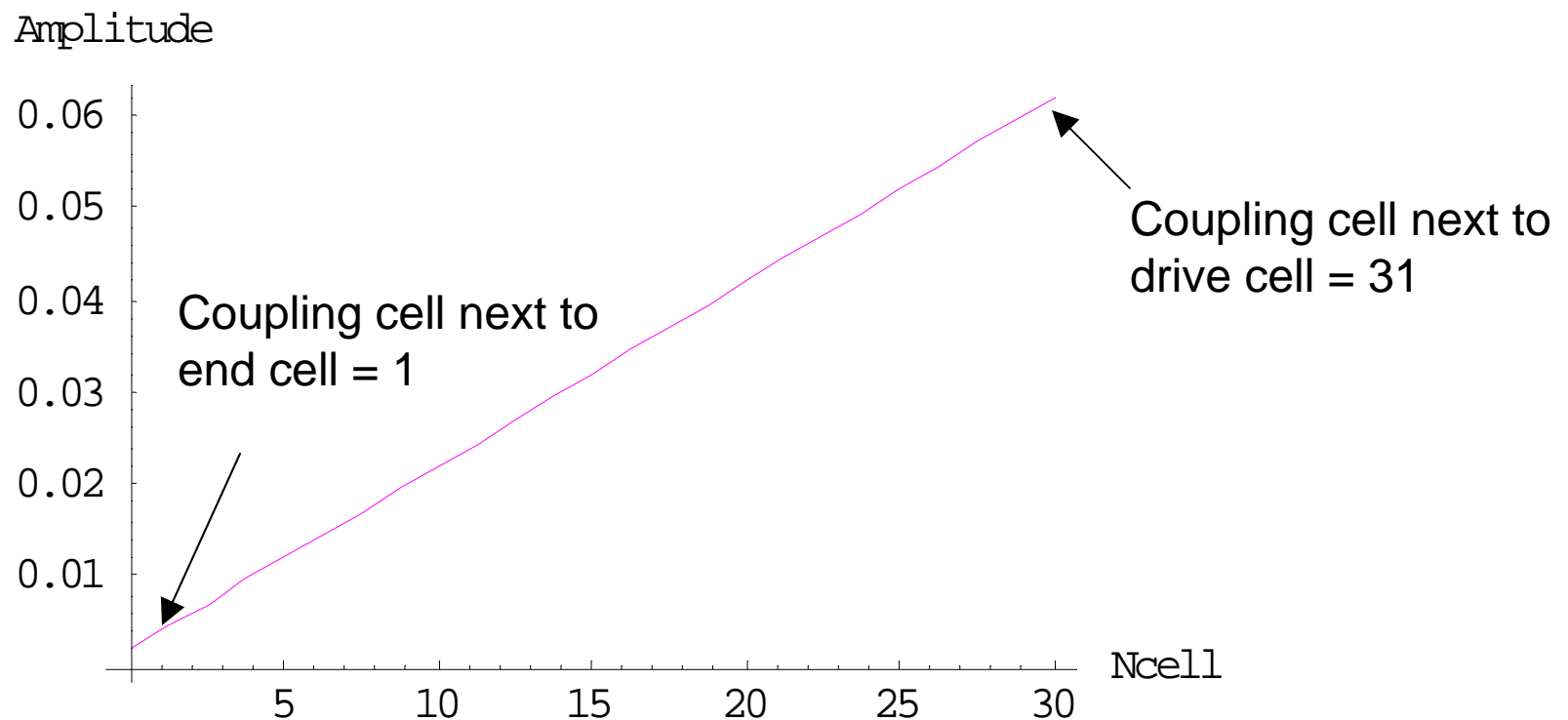
# Focusing is provided in a coupled-cavity linac by introducing a displaced cavity called a bridge coupler to make room for focusing lenses on the axis.
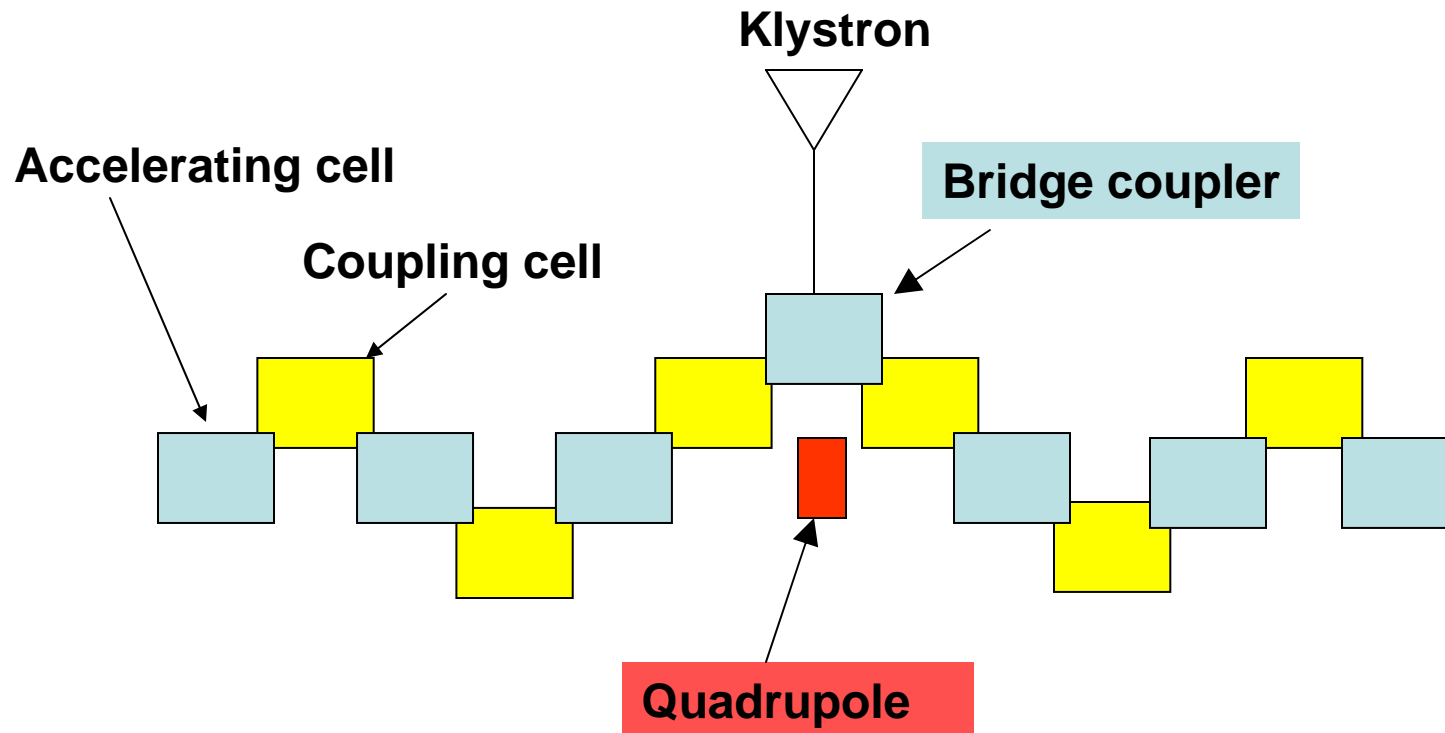


- The bridge coupler functions electrically as an excited cell like an accelerating cavity, but is off axis to make room for focusing quadrupoles.
- The bridge coupler may also be used for the drive cell, as shown in the figure.

# Ballpark error estimate

- Use pillbox cavity results. From $TM_{010}$ mode $\omega=\omega_c=2.405c/a$, $a=2.405\lambda/2\pi$.

$At\ 300MHz,\ \lambda = 1m, and\ a \cong 0.4m.$

$Assume\ k = 0.05\ is\ the\ intercell\ coupling\ strength.$

$Assume\ \delta a = 40\mu m\ radius\ error.$

$$\frac{\delta\omega}{\omega} = -\frac{\delta a}{a} = \frac{40\times10^{-6}}{0.4} = 10^{-4}$$

$$\frac{1}{k}\frac{\delta\omega}{\omega} = 2\times10^{-3}$$

# Resonant Coupling

- The general approach of stabilizing the field distribution of a multicell standing-wave cavity with respect to cell errors by using resonant oscillators as coupling elements is called resonant coupling.

- This enables construction of long multicell linac structures, providing advantages for simplicity and reduced cost for many linac applications..

- Examples:  Post couplers in DTL
             Side cavities for side-coupled linac

# Post couplers for field stabilization in long drift-tube linac structures
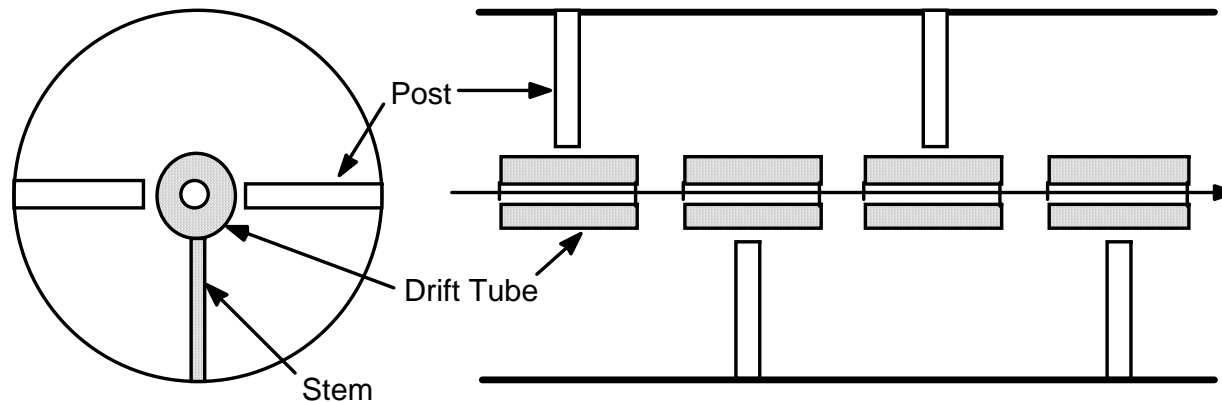


- Post couplers are $\lambda/4$ resonators that function like coupling cavities in coupled-cavity linacs operating in $\pi/2$ mode.

- Posts are nominally unexcited when tuned to the structure resonant frequency.

- Perturbations from fabrication errors excite posts in such a way that the axial acceleration fields remain nearly constant

# Three linac structures are used to accelerate the H⁻ beam from 2.5 to 1000 MeV
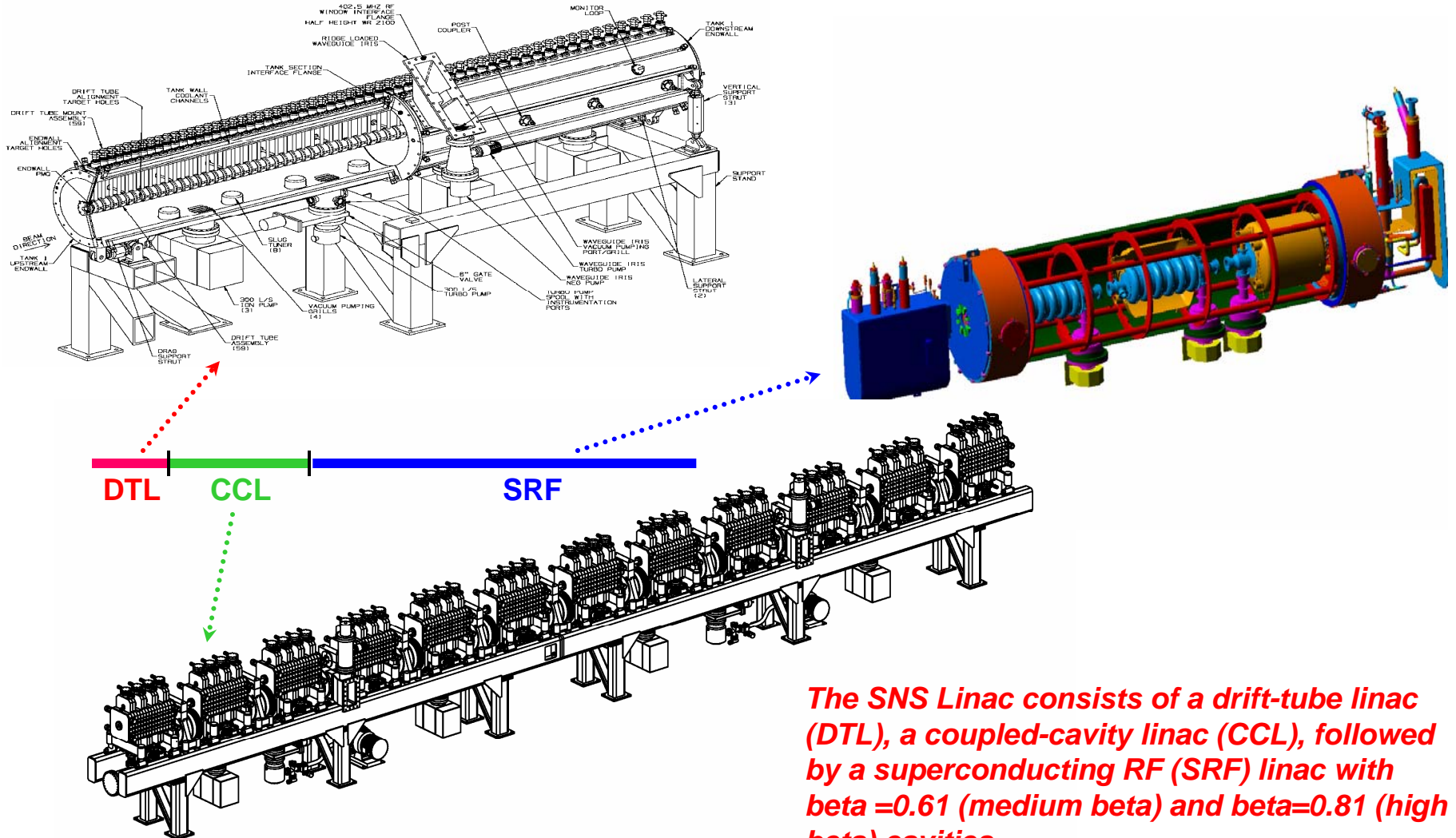


DTL    CCL    SRF

*The SNS Linac consists of a drift-tube linac (DTL), a coupled-cavity linac (CCL), followed by a superconducting RF (SRF) linac with beta =0.61 (medium beta) and beta=0.81 (high beta) cavities.*

## Superconducting (SC) trend in new high-power ion-linac projects.

- Technology progress is making SC more attractive.
  -Dramatic increase in **accelerating gradients**.
  -Higher power input **couplers**.
  -**Pulsed-beam experience** at TESLA Test Facility and soon at SNS.

- SNS (in 2006) is scheduled to become the first SC proton linac.

# Have Greatly Improved SC Cavity Performance



Comparison of CEBAF and TESLA Peak Surface Electric Fields
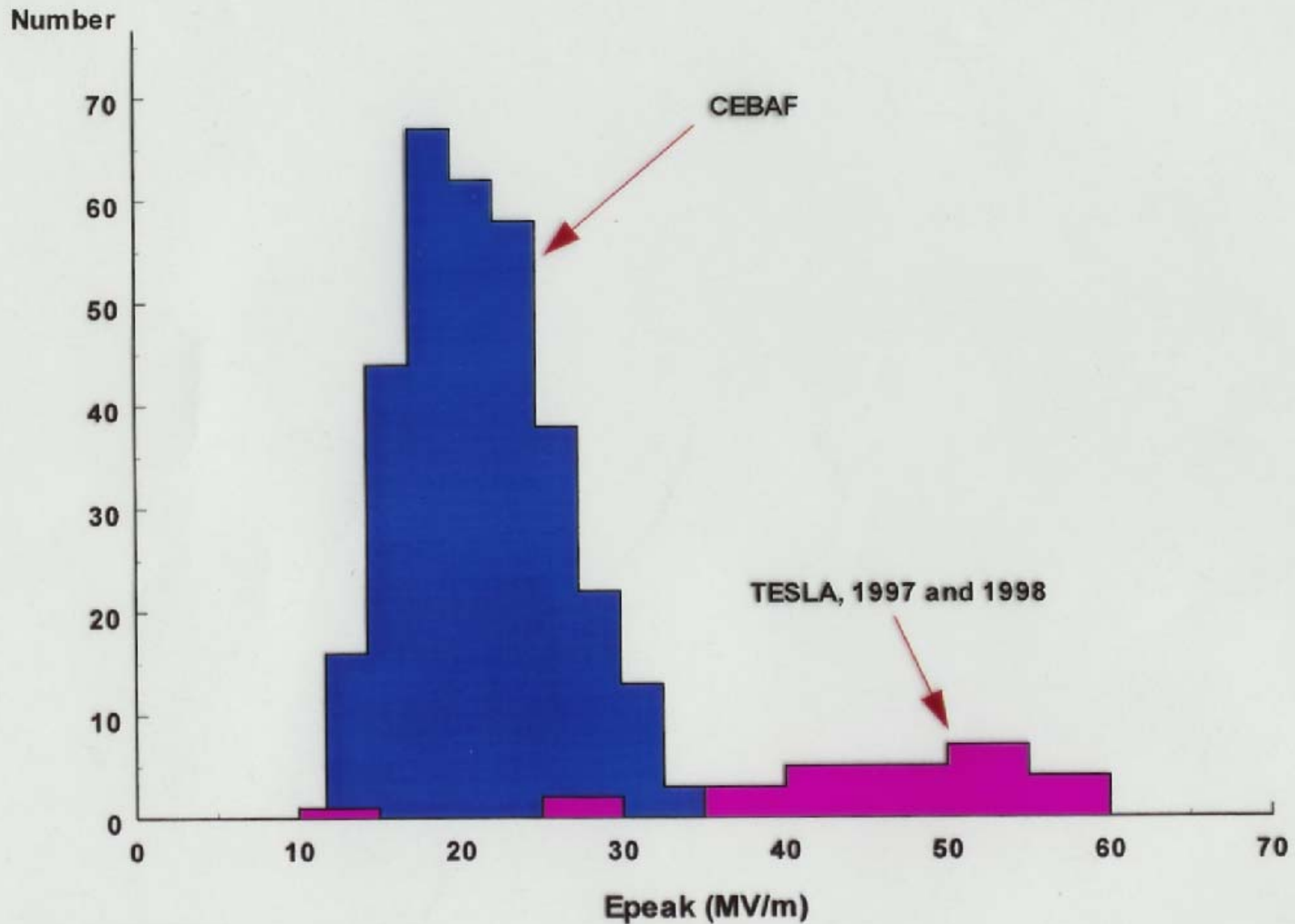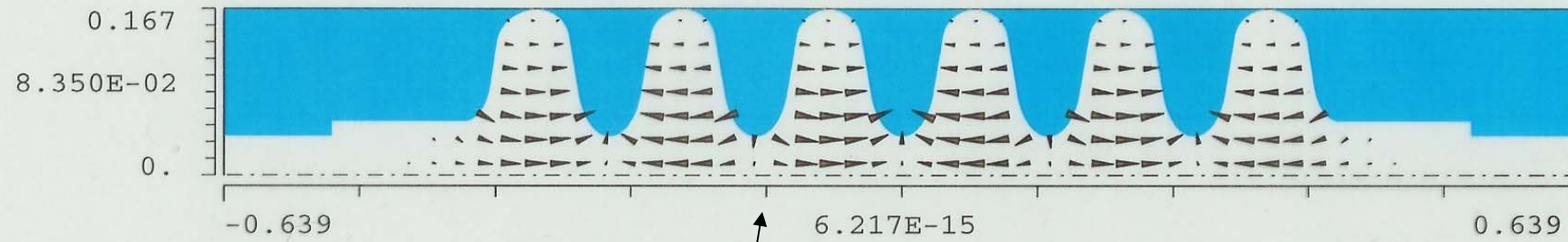
**Electric field lines**
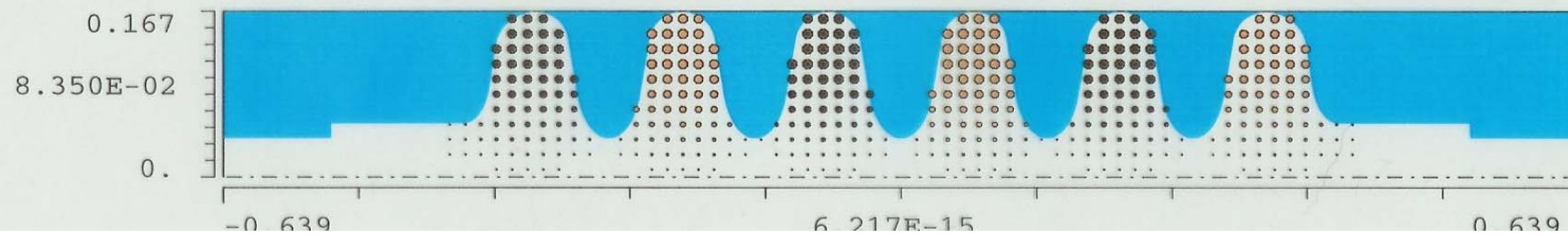
**Magnetic field lines**

# Superconducting accelerating structures

- **Superconducting accelerating structures are short with just a few cells per cavity.**
  -easier handling during chemical processing stage.
  -smaller surface area and ability to diagnose and correct for normal conducting impurities and field emission sites result in higher gradients.

- **Few cell structures have large velocity acceptance of the transit-time factor, which can be exploited in several ways:**
  -identical structures cover a given velocity range.
  -flexibility to reset phases and continue operation after loss of a module.

# SNS Superconducting Cavity Design Parameters

| Parameter | Medium $\beta$ | High $\beta$ |
|---|---|---|
| $\beta$ | 0.61 | 0.81 |
| No. of Cells | 6 | 6 |
| Epeak (MV/m) | 27.5 | 35 |
| Epeak/Eacc* | 2.71 | 2.19 |
| Bpeak/Eacc (Gauss/MV/m)* | 21.0 | 21.4 |
| Intercell Coupling k (%) | 1.61 | 1.61 |
| $Q_0$ at 2.1K | >5 X $10^9$ | >5 X $10^9$ |
| Active Length (m) | 0.682 | 0.906 |

* $E_{acc}$ is defined as $E_0 T$ where T is the maximum transit-time factor as a function of $\beta$.

Example of transit-time factor versus velocity β showing the velocity acceptance. As the number of cells per cavity increases, the curves get narrower, and the velocity acceptance decreases.
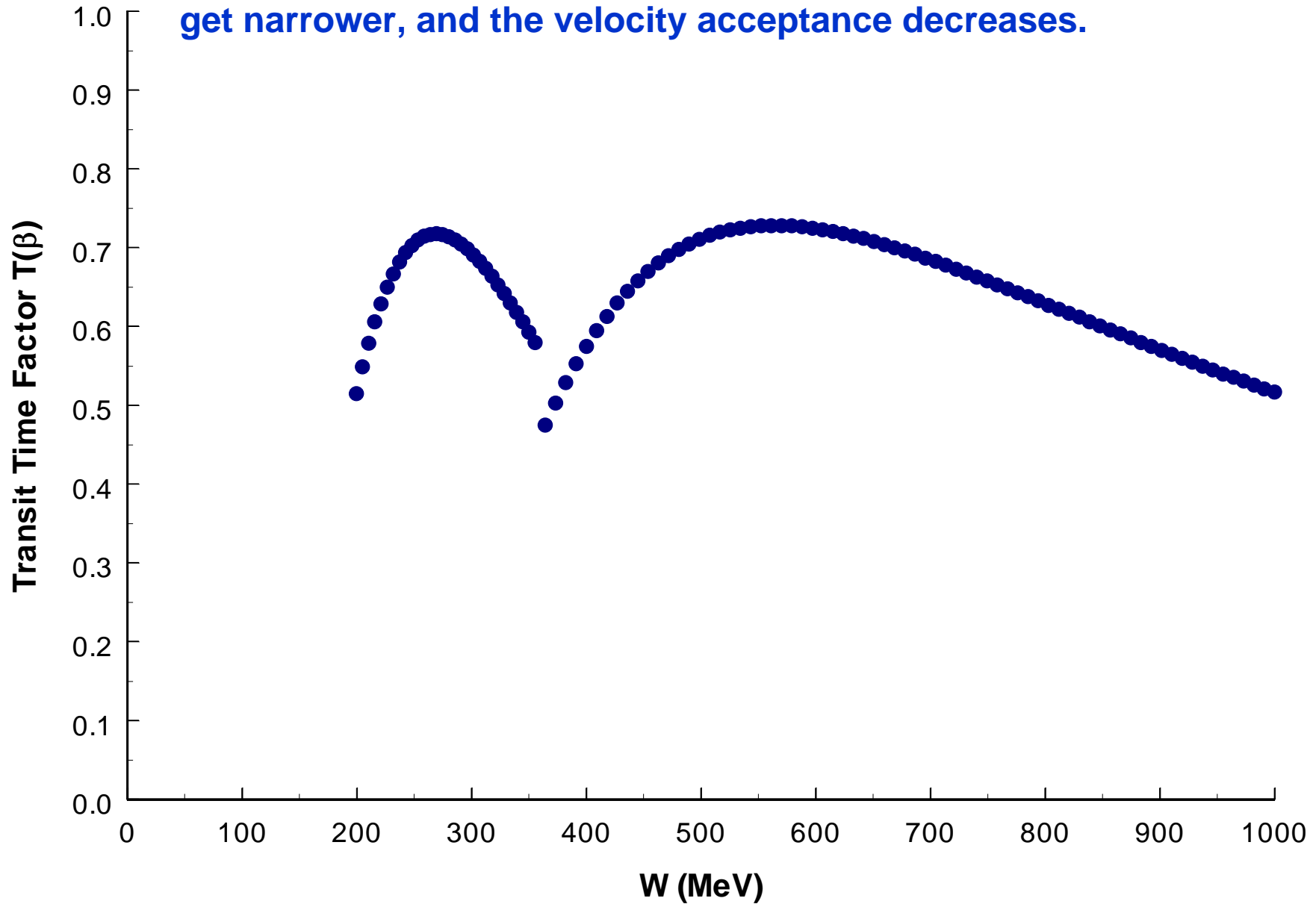
# Why use superconducting linacs?

- Disadvantages of copper linacs:
  -Large rf power dissipation results in
  1) high costs for rf system
  2) high operating costs for AC power
  3) cooling requirement limits accelerating gradient
  4) cavity design dominated by rf efficiency considerations

- Cryogenic cooling of normal conducting copper does not reduce the rf surface resistance enough to compensate for cryogenic refrigeration.

- The promise of superconducting rf technology is to provide the capability for high accelerating gradients (50 MV/m range) with low rf power for capital and operating costs.

# Consider the ultimate superconducting linac compared with a normal conducting linac. (CW case)

- Assume the accelerating gradient is limited by a critical magnetic field at about B=2000 Gauss.

- From pillbox cavity formula we have $B_{max}/E_{max}$=20 Gauss/MV/m.

- If $B_{max}$=2000 Gauss, $E_{max}$=100 MV/m and for a real cavity with beam apertures, $E_{acc}=E_0T=E_{max}/2$=50 MV/m.

- Assuming an superconducting enhancement factor of $10^5$, $ZT^2$=(50 M$\Omega$/m)X$10^5$=5X$10^6$ M$\Omega$/m.

- Then, a 1 GeV linac has length =1000 MeV/50 MV/m=20m.

- $P_{rf}=E_a^2L/(ZT^{2)}$=$(50)^2$20/(50X$10^6)$)=10 kW.

- For cryogenic efficiency = 0.001, $P_{ac}$=10 MW

- For normal conducting copper linac: If $E_a$=2 MV/m, a 1-GeV linac has L=500m. $P_{rf}=E_a^2L/ZT^2$=$(4)^2$500/50= 40 MW.  For 50% rf efficiency, $P_{ac}$=80 MW.

# Summary of the two linac designs

| | Conventional copper linac | Ultimate superconducting linac |
|---|---|---|
| $E_a = E_0 T$ | 2 MV/m | 50 MV/m |
| $L_{active}$ | 500m | 20m |
| $ZT^2$ | 50 M$\Omega$/m | $5 \times 10^6$ M$\Omega$/m |
| $P_{rf}$(wall loss) | 40 MW | 10 kW |
| $P_{ac}$ | 80 MW (rf system) | 10 MW (refrigerator) |

**A superconducting linac has the potential for large reductions in length, power, and costs.**

# History

- Superconductivity discovered by H. Kamerlingh Onnes (1911).
- Bardeen, Cooper, and Schrieffer (BCS) theory of superconductivity (1957).
- Electron acceleration in superconducting lead-plated cavity, Stanford, 1965.
- First accelerator projects with niobium superconducting cavities at Stanford, Karlsruhe, CERN, Argonne, Cornell, and Illinois (1970s).
- Solutions for practical problems that limited performance of early cavities for electron linacs; improved thermal conductivity and reduced multipacting with elliptical cavity geometry (1980s).
- Large scale superconducting accelerator projects built: LEP, HERA, TRISTAN, CEBAF,

  and planned: TESLA, and SNS (under construction).

# BCS Surface Resistance

$$R_s(\Omega) \cong 9 \times 10^9 \frac{f^2(GHz)}{T(K)} \exp\left[-\alpha \frac{T_c}{T}\right] + R_{residual}$$

• For niobium, $\alpha$=1.83 and $T_c$=9.2K.

• $R_s$ is about $10^{-5}$ lower than for room temperature copper.

• Frequency dependence is different than for normal-conducting case.
Lower frequencies have lower surface resistance for the superconducting case.

• Rresidual is the residual resistance determined by various imperfections
 in real material.

Superconducting RF Surface resistance of Niobium is $10^{-5}$ of that of normal-conducting copper

$R_S$ ($\Omega$)

$R_{res} = 4\,n\Omega$

$R_{BCS}$

$T_c/T$
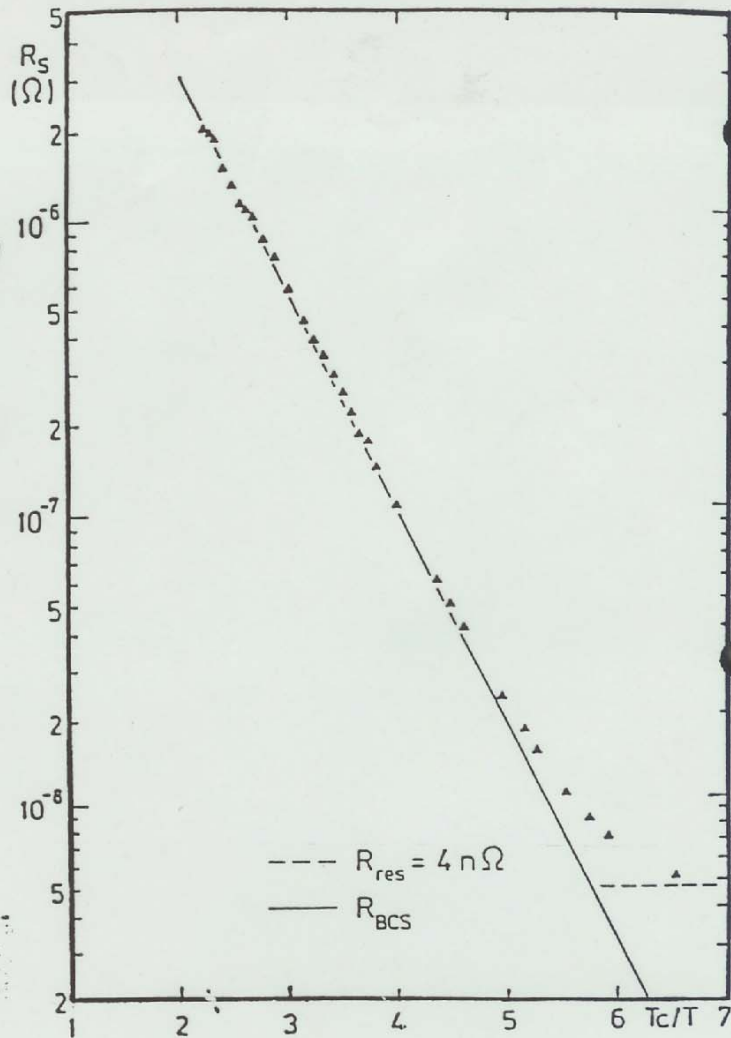
$R_S (cu) \sim 10^{-3} \Omega$

# Why superconducting RF surface resistance is not zero.

- Superconductors do <u>not</u> have zero AC surface resistance.

- Below the critical temperature ($T_c$=9.2K for Nb) there are both normal electrons that suffer Ohmic losses and Cooper pairs (superconducting electron pairs in a bound state).

- At T=0 there are only Cooper pairs, and at T=$T_c$ there are only normal unpaired electrons.

- Cooper pairs short out any DC potential difference and establish E=0 inside the superconductor.

- But Cooper pairs have finite mass and their inertia prevents them from responding instantly to time varying potential differences.

- Thus, AC potential differences are not completely shorted out by the Cooper pairs, so that residual normal electrons see fields, are accelerated, and dissipate energy through collisions.

- BCS theory describes the AC surface resistance as a function of temperature and frequency.

# Superconducting surface resistance (continued)

- We would expect the surface resistance to increase with increasing frequency because the inertial effect of the Cooper pairs would be relatively more important at higher frequency.

- We would expect the surface resistance to increase with increasing temperature because of the larger ratio of normal electrons to Cooper pairs at higher temperature.

# RF superconductivity physics and technology

- **Niobium**
  -Most commonly used material
  -Highest critical temperature of any element, $T_c$=9.2K
  -Cavities formed from thin niobium sheets
  -Electron beam welding in vacuum
  -Critical magnetic field about $B_c$=2400 Gauss, but quench can occur at lower B because of defects.

- **Cryogenic**
  -Cavities operate within a cryostat to maintain $T<T_c$=9.2K.
  -RF power dissipated on cavity walls is absorbed by liquid helium using cryogenic refrigeration system.
  -4K and 2K(superfluid He) are typical nominal operating temperatures. SNS operates at 2.1K.
  -Cryogenic efficiency is about 0.001. There is still a net gain from superconducting because $R_s$ improves by $10^5$.

# Performance Limitations for Superconducting Cavities

- **Electron multipacting:**
  -Single point multipacting problems overcome by going to cavity geometry with rounded or spherical shape – called elliptical structures.

- **Electron field emission:**
  -Caused by micron sized (dirt) particles on cavity surface. Need clean assembly conditions, chemical etching of surfaces, high pressure water rinse, high peak power processing.

- **Thermal instability (or quench):**
  -Normal-conducting defects heated by the rf field drive nearby niobium above critical temperature.
  -Solution was to improve purity of niobium thereby increasing the thermal conductivity.
  -RRR (called triple R) = residual resistivity ratio, a measure of the thermal conductivity, has improved from ~25 to ~250.

- **Microphonics**
- **Lorentz force detuning**

Thermal Breakdown
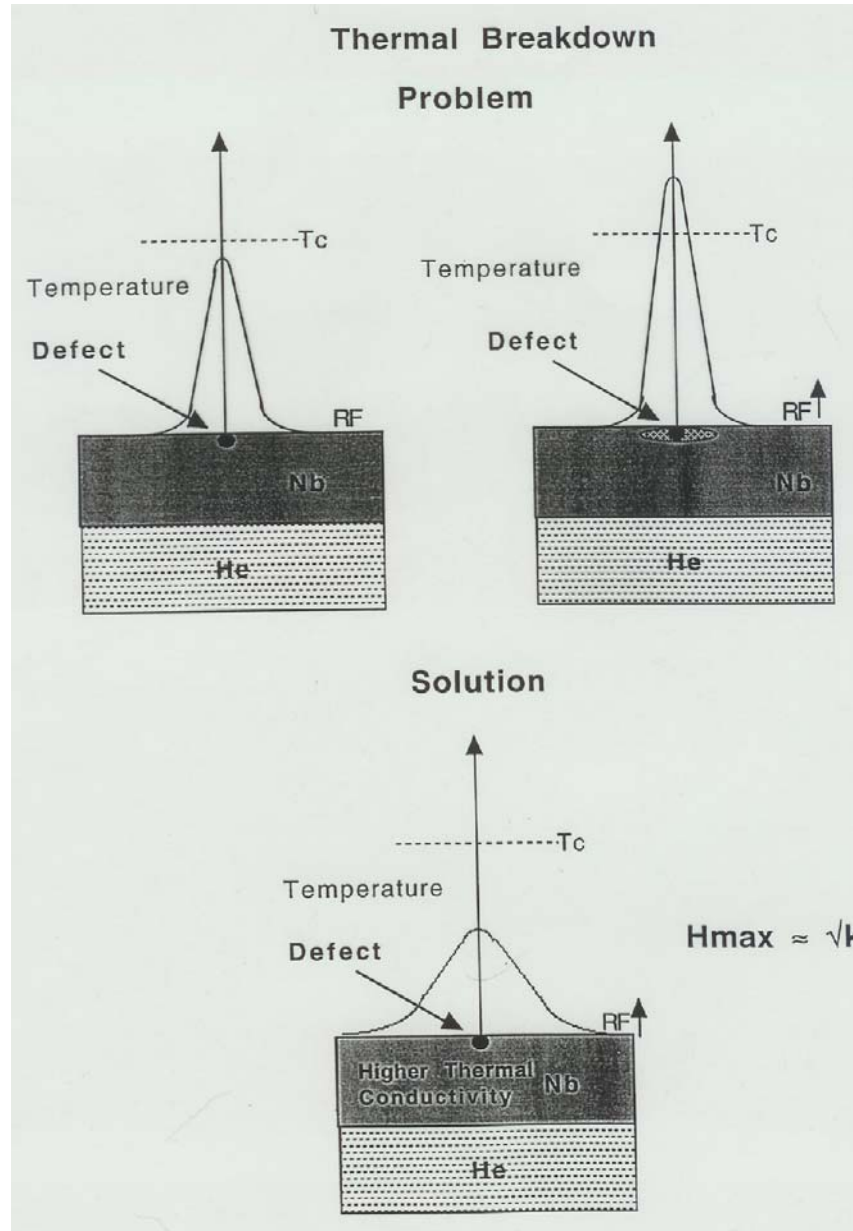
**• Increasing the thermal conductivity of Nb (measured by RRR) by an order of magnitude has played a major role in reducing the quench problem.**

# Microphonics

- Ambient acoustic noise (microphonics) excites mechanical vibrational modes of the cavity causing variations in the cavity resonant frequency.

- The magnitude of frequency variation depends on the ambient acoustic amplitudes and the stiffness of the cavity.

- The frequency variations cause phase variations and in a linac the phase must be synchronized with the beam (and the rf clock).

# Microphonics (2)

• The control system must compensate these phase variations either by providing for rapid retuning and/or adjusting the drive frequency. The phase variations must be kept small compared with the bandwidth.

• Microphonics is a more important issue for superconducting cavities because:
a) the loaded Q is higher for superconducting and bandwith is less.
b) SC cavities are made from thin walled material and are less stiff.

• Need to make stiff cavities to push mechanical frequencies as high as possible so they don't couple to the low frequency mechanical noise that have large amplitudes.

# Lorentz-Force Detuning

- The RF electric field interacts with wall charge and the RF magnetic field interacts with RF wall currents giving a Lorentz force on the cavity walls.

- The Lorentz force deforms the cavity (iris pulls in and outer wall pushes out) and shifts the resonant frequency. The static shift is

$$\Delta f = -KE_a^2, \; where \; typically \; K \approx few \, Hz/(MV/m)^2.$$

- A frequency tuner is needed to compensate for this shift.

- For a pulsed linac like SNS, one needs to be concerned with the transient or dynamic shift which causes phase variations. The SNS approach to this is a fast piezoelectric tuner to compensate.

# Advantages of the Superconducting Linac Design Approach

- Each section is built from **identical cavities** and covers a wide velocity range.

- **Reduced RF power** requirement because of $10^{-5}$ reduction in RF surface resistance.

- Reduced AC power requirement even including the low refrigeration efficiency of 0.001.

- **Larger bore size** becomes economically acceptable.

- Larger bore radius reduces risk of beam loss and relaxes alignment, steering, and focusing requirements, making it easier to commission and operate even with a high-power beam.

- **Higher gradient**.

- Short independently phased cavities provide advantages of **flexible operation** for a variety of off-normal conditions.

# Superconducting  Linac Overview

*Many vugraphs courtesy of Jean Delayen*

*Jefferson Lab*

# 805 MHz Elliptical Cavity Concept

Stiffening Rings

Titanium Bellows

2 - Phase Return Header

NbTi Dished Head

NbTi Dished Head

Field Probe

HOM Coupler

HOM Coupler

Fundamental Power Coupler

Medium Beta Cavity
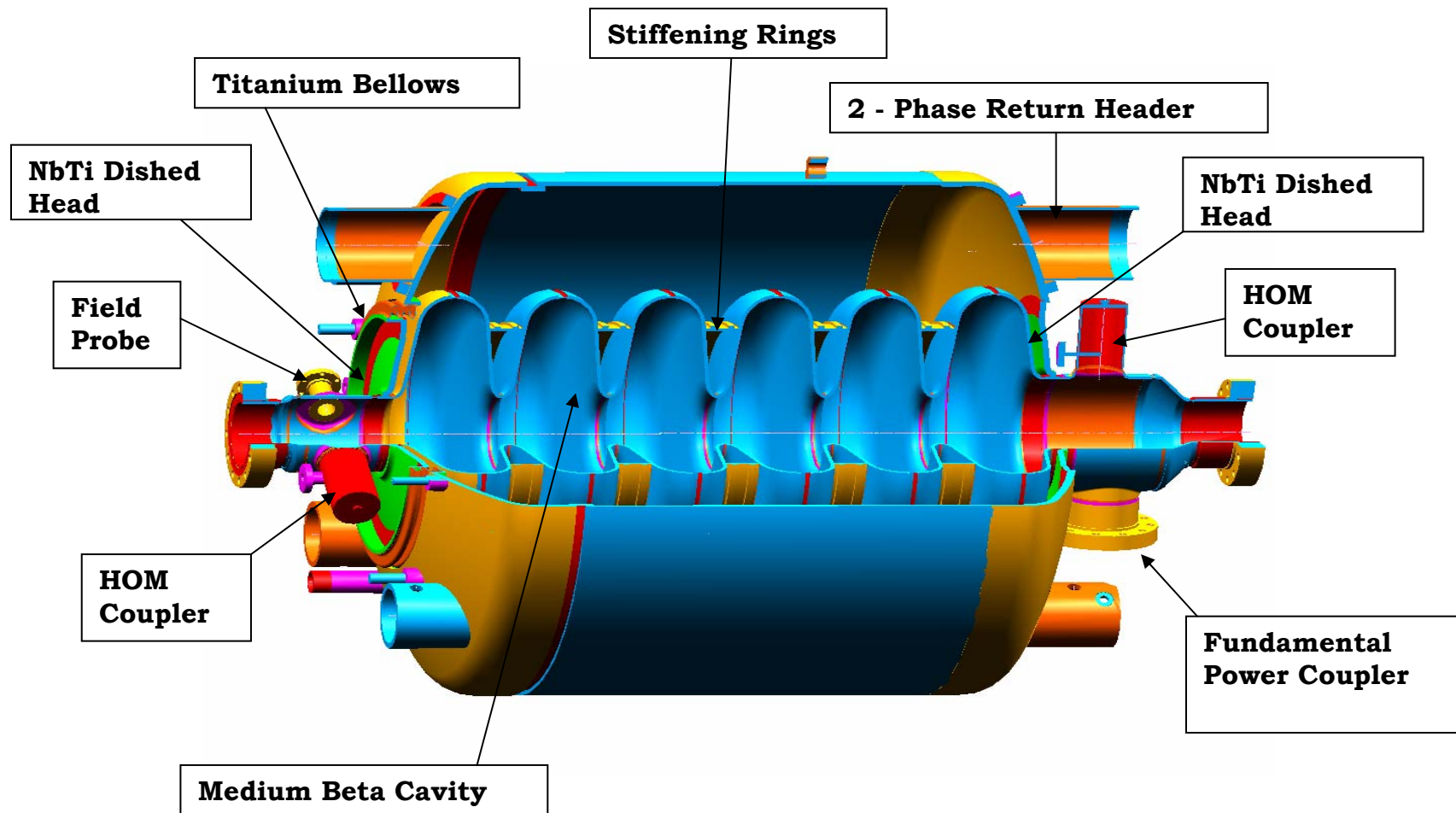
# SNS Cryomodule Concept
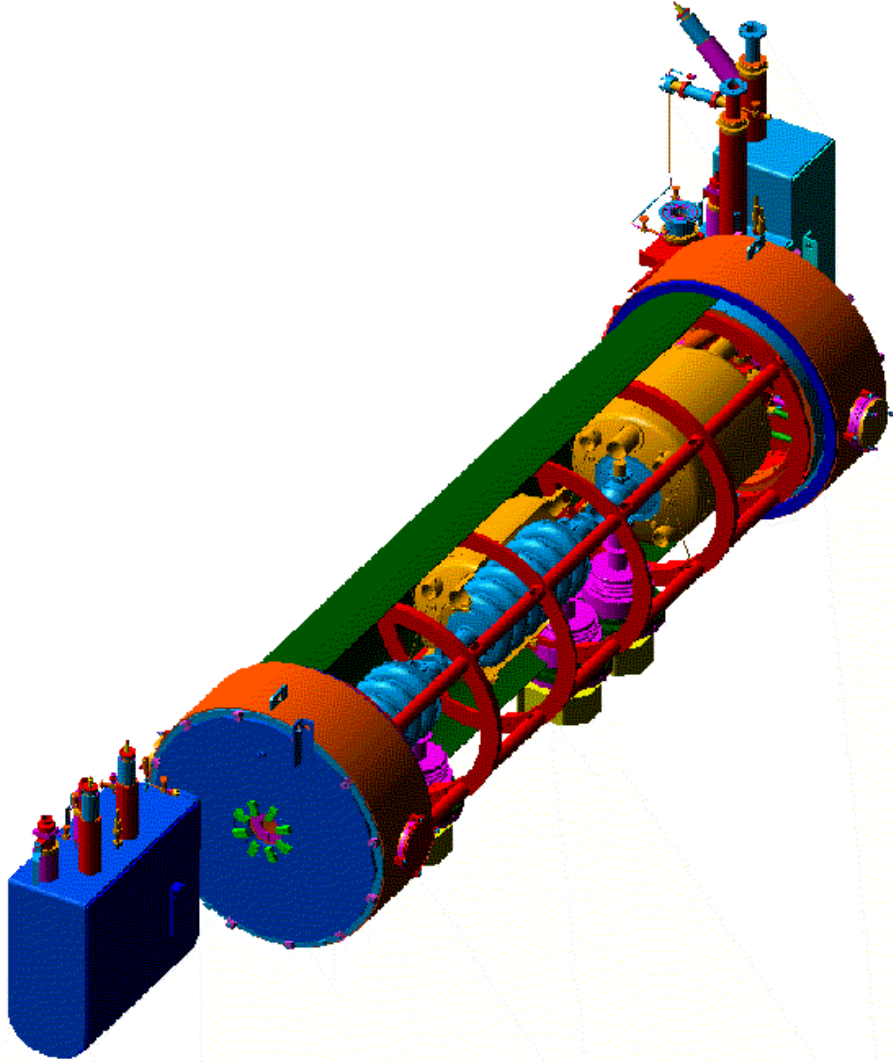
# SNS Cryomodules
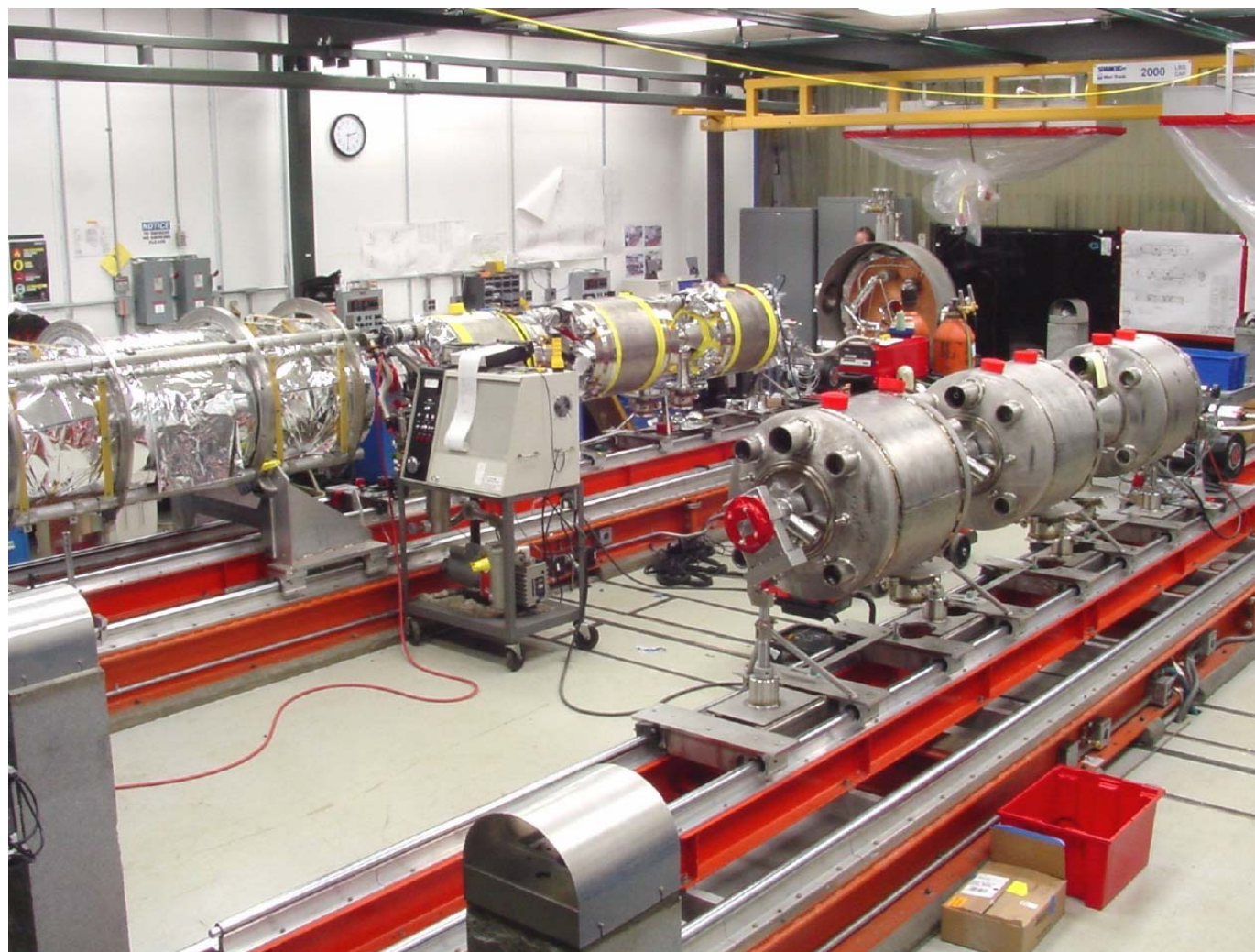
# Performance of Elliptical Cavities in VTA



SNS
SPALLATION NEUTRON SOURCE

Legend:
- ▲ MBspec
- ◆ HBspec
- ◇ MB01F
- ✕ MB02B
- + MB03A
- △ MB04F
- ⬤ mb05
- ■ MB06
- ◆ mb07a
- ▲ MB08
- ▼ mb09a
- ⊙ mb11
- ⧅ mb12
- ⊞ MB14
- ⬠ MB16B
- ⊡ MB17

Y-axis: Qo, from $10^9$ to $10^{11}$

X-axis: Eacc, from 0 to 20

*SNS Linac*

Jefferson Lab
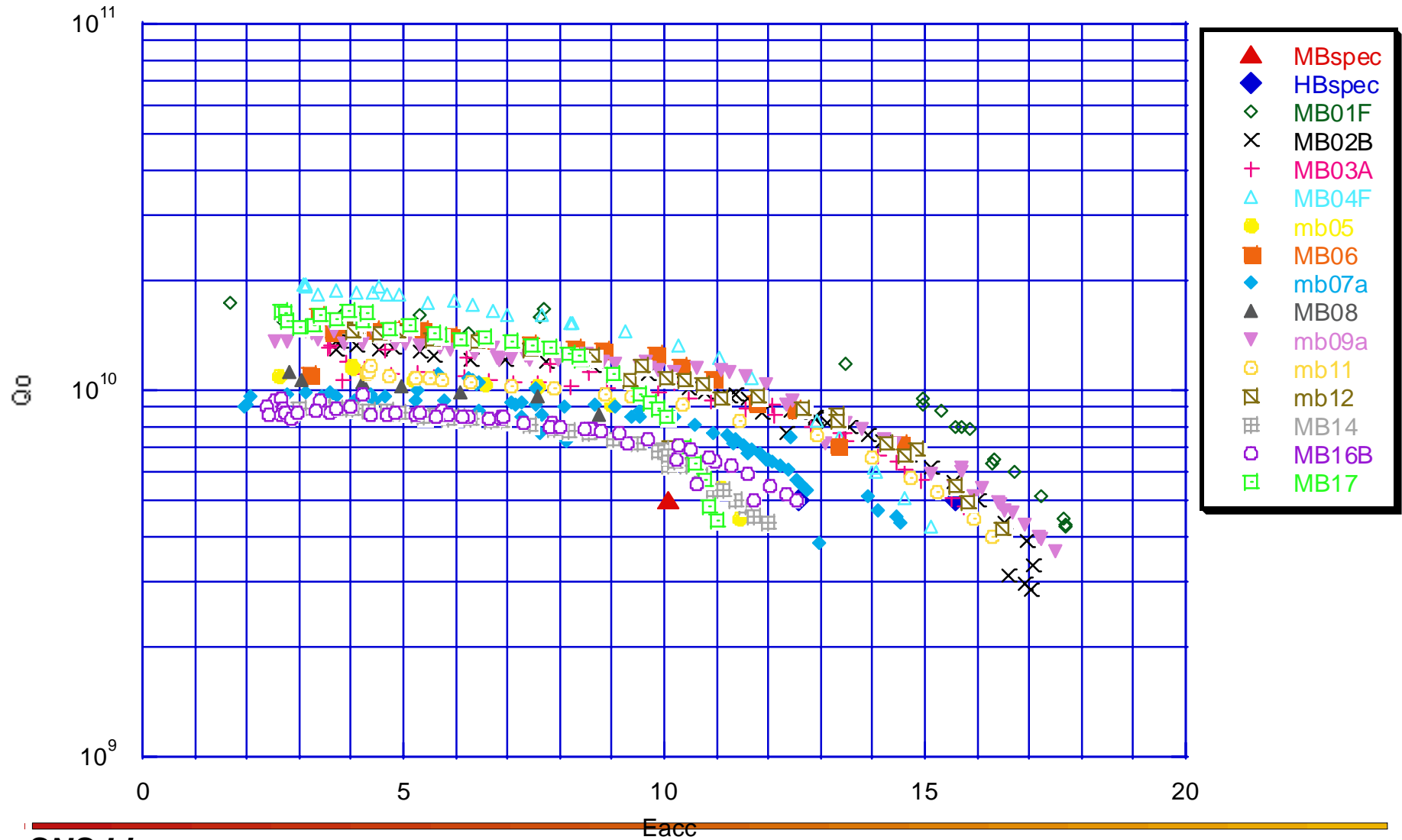
# Performance of High-β Cavities in VTA



Recent SNS High-β Cavity Performance

*March - April 2004*

Legend:
- Avg. Spec. (red diamond)
- Min. Spec. (blue diamond)
- HB10 (teal square)
- HB11 (purple square)
- HB12 (green triangle)
- HB13 (blue X)
- HB14 (orange +)
- HB15 (magenta open circle)
- HB16 (green open circle)
- HB17 (orange diamond)
- HB18 (navy diamond)

Y-axis: $Q_0$ (1.0E+08 to 1.0E+11)

X-axis: Gradient (MV/m) (0 to 25)

*SNS Linac*
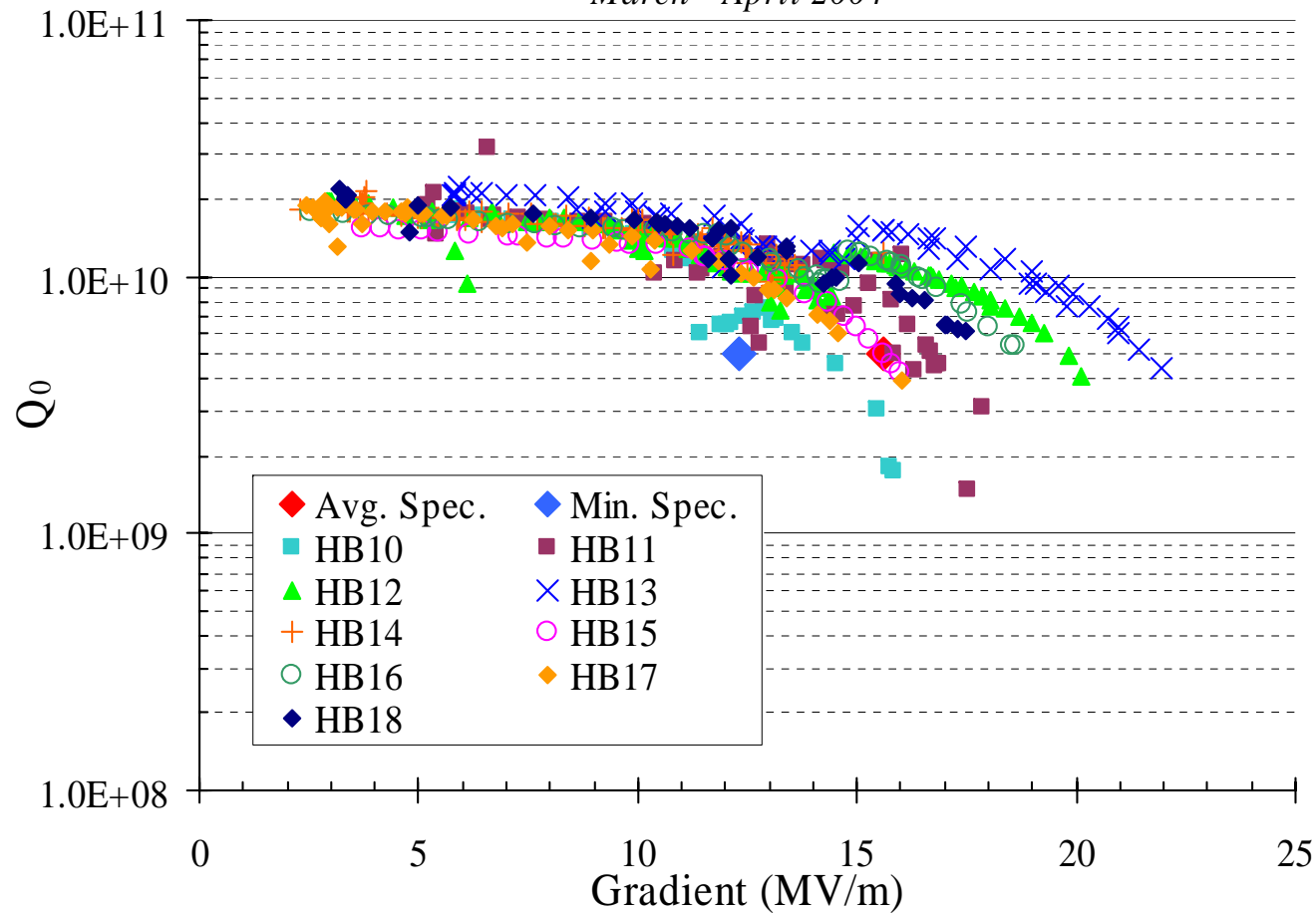
# Fundamental Power Coupler
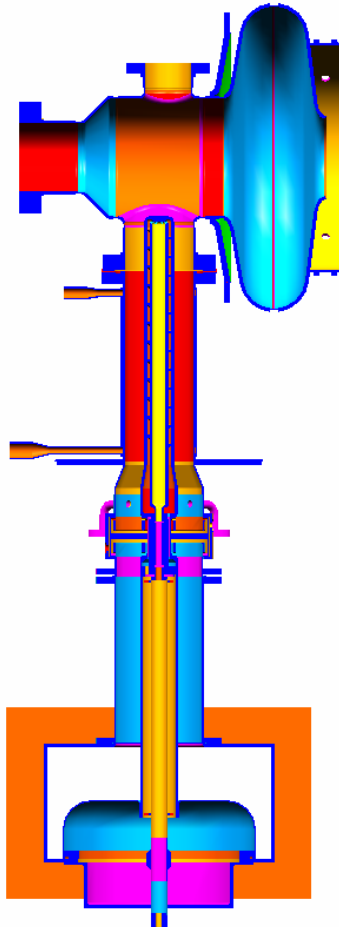


- Coupler scaled from KEKB coupler (508 to 805 MHz)

Specification: **550 kW** peak,
**48 kW** average

Coupler exceeded 2 MW peak power in tests at LANL

# Fundamental Power Coupler
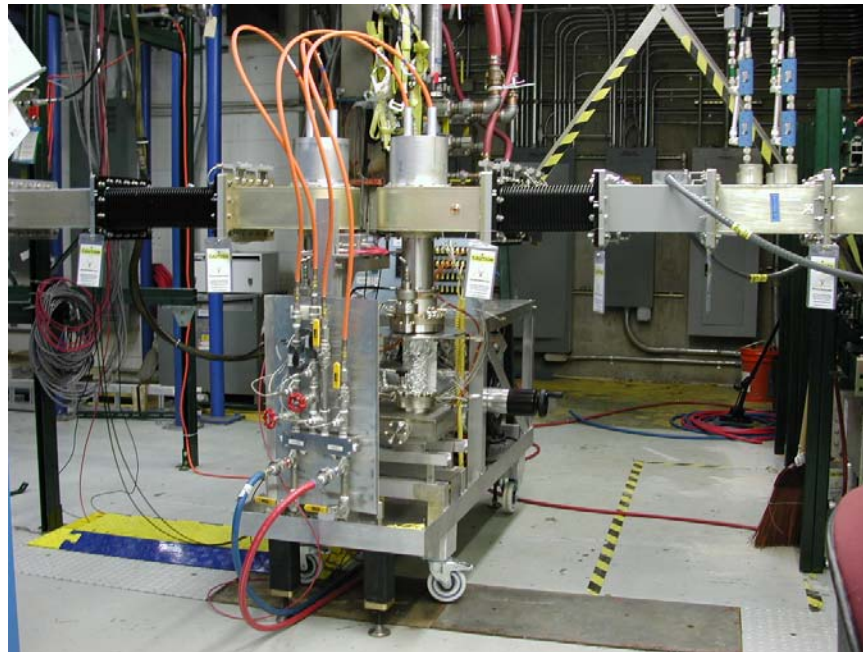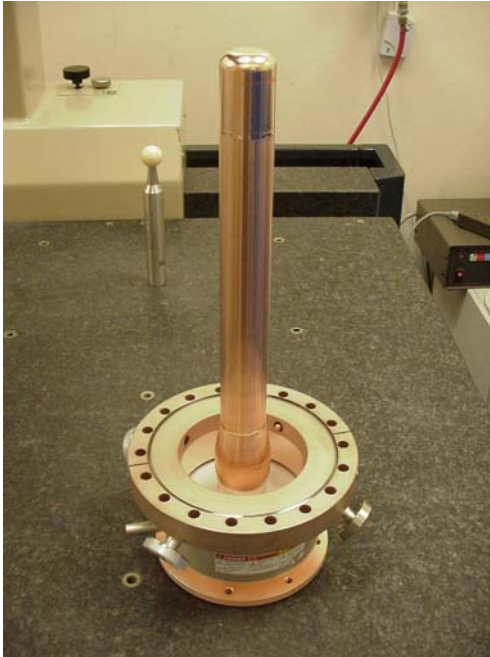
# Mechanical (TESLA/Saclay) and piezo tuners
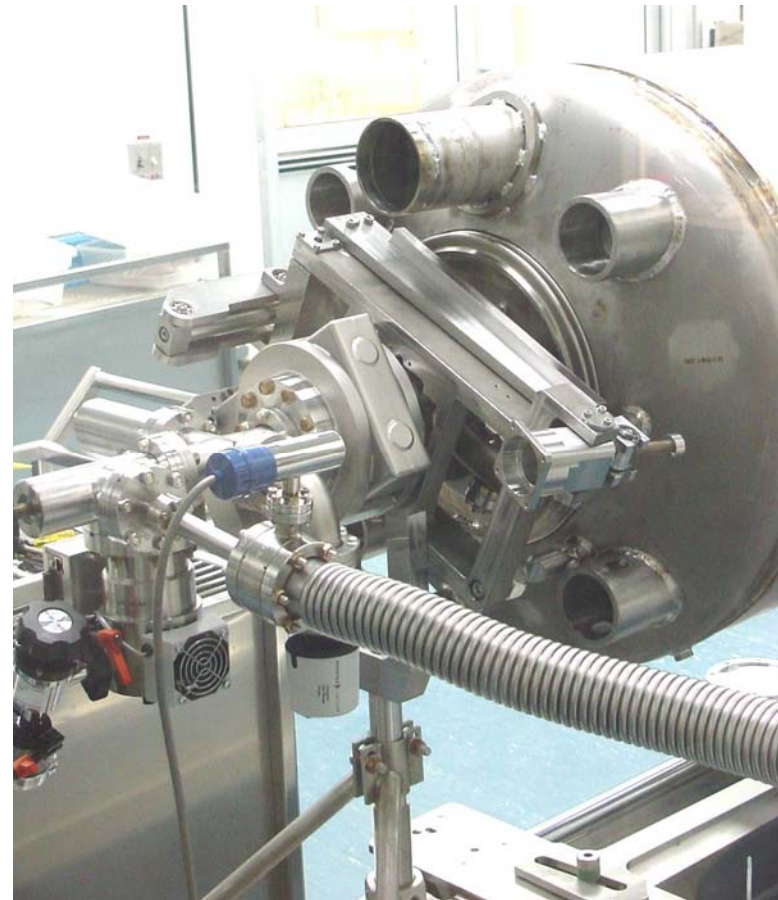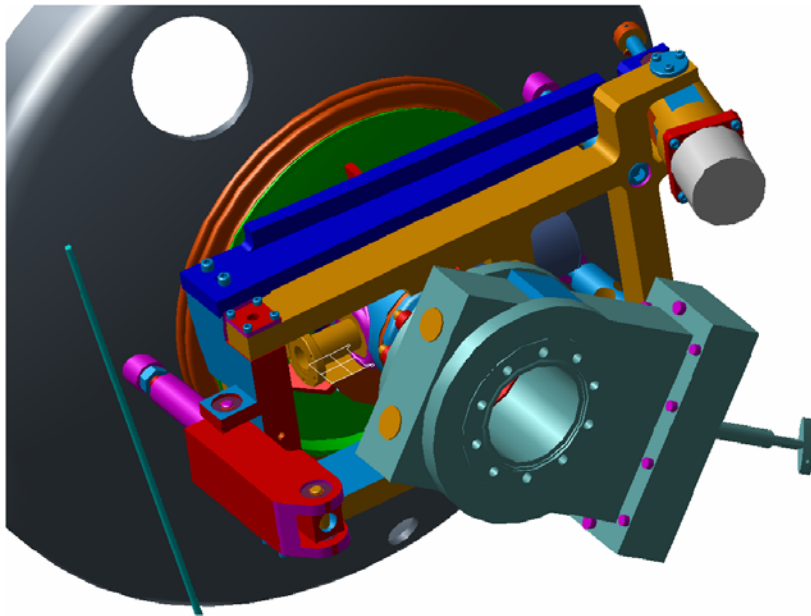
# Piezoelectric Tuner

- Piezoelectric devices exhibit mechanical motion in response to an electric voltage.

- A fast piezoelectric tuner will be used to compensate for dynamic Lorentz Force Detuning of the SNS cavities.

- This will be important for control of the cavity phase during the 1-msec beam pulse.

# Cavity Detuning versus Time
# Reduced by Factor of 3 with Piezoelectric Tuner

27.5 MV/m, 60 Hz, 1.3 ms

**Frequency Detuning (Hz)**

700
600
500
400
300
200
100
0
-100
-200
-300

12   12.5   13   13.5   14   14.5   15   15.5   16

BEAM

RF ON

Cavity Field Decay

**Time (ms)**

Piezo On
Piezo Off

*SNS Linac*
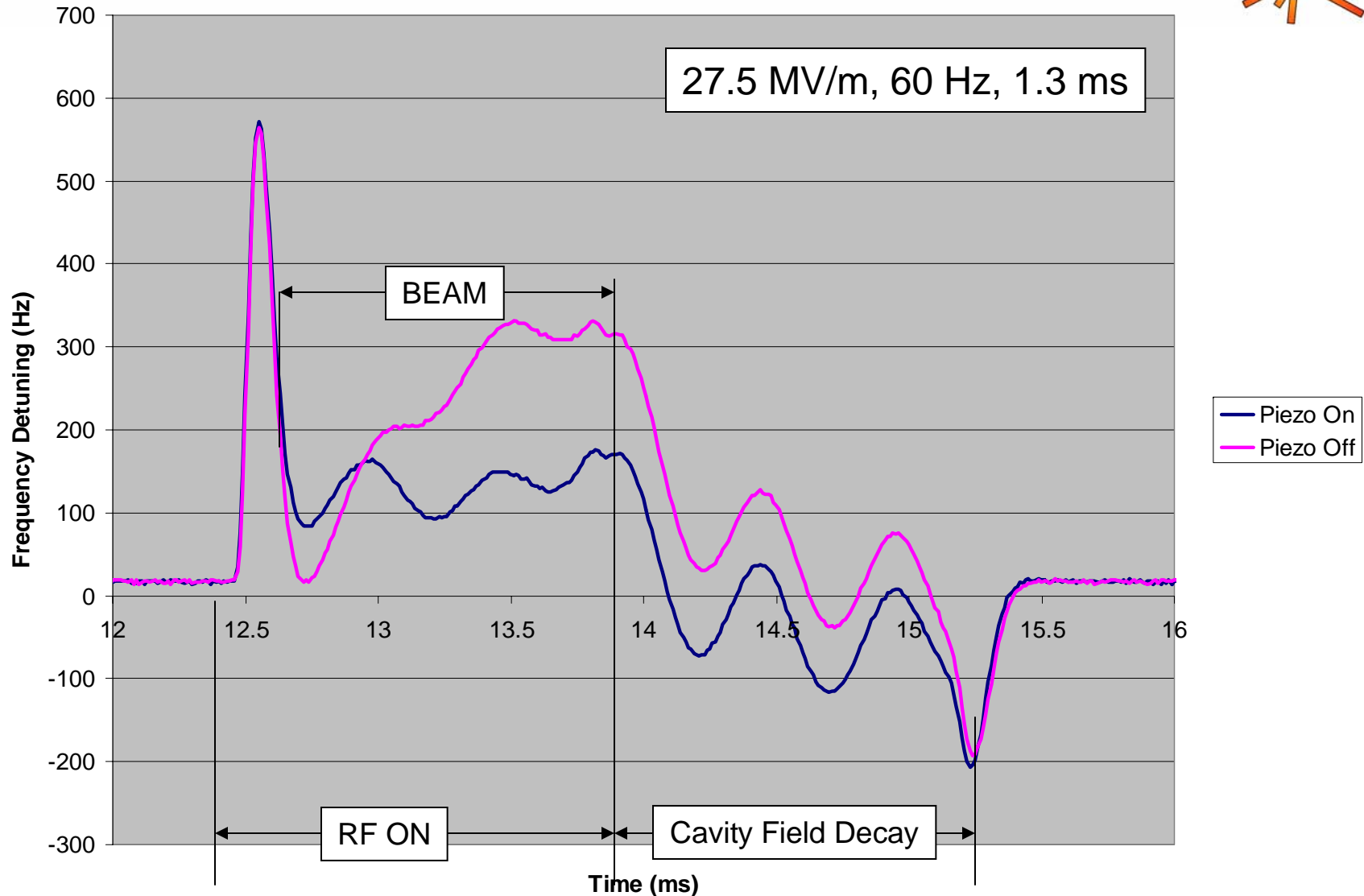
# Microphonics: Probability Density

**(Note: Slow drift has been removed)**

Baseline number
- SNS:                     17 Hz
- CEBAF & RIA: <3.5 Hz
  - Usually achieved
  - Sometimes exceeded
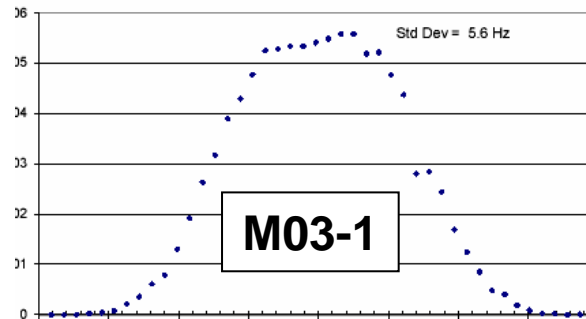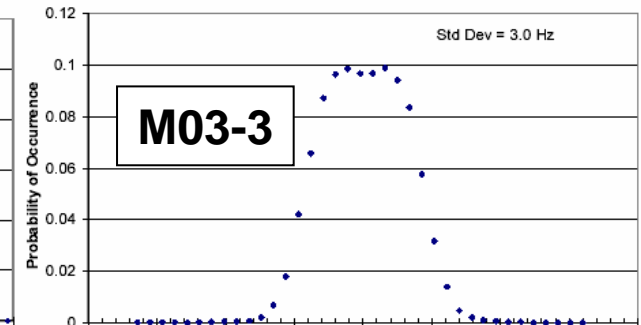
Substantial differences
- Between cavities
- Temporal

σ = 5.6Hz

σ = 3.0Hz

σ = 1.3Hz
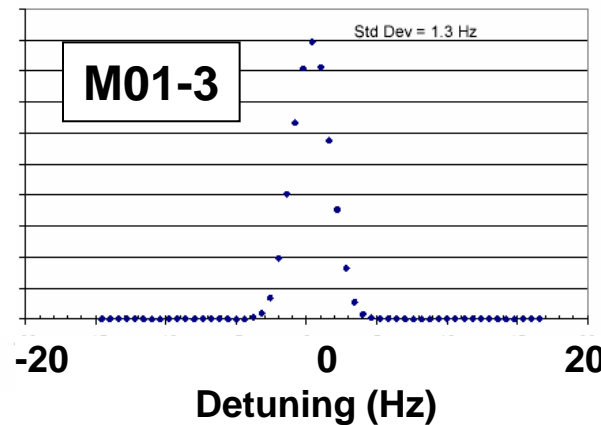
σ = 2.2Hz
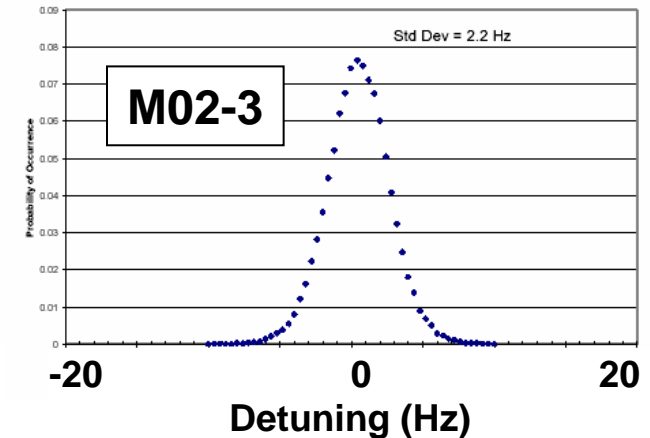
# SNS High Beta Performance

**Q$_0$ vs. E$_{acc}$**

▲ T=1.99K 30' RF & He Processing



**Electropolish**

Test #2

Old Design goal    New Design goal    VTA Performance goal

Q$_0$

E$_{acc}$ [MV/m]

*SNS Linac*
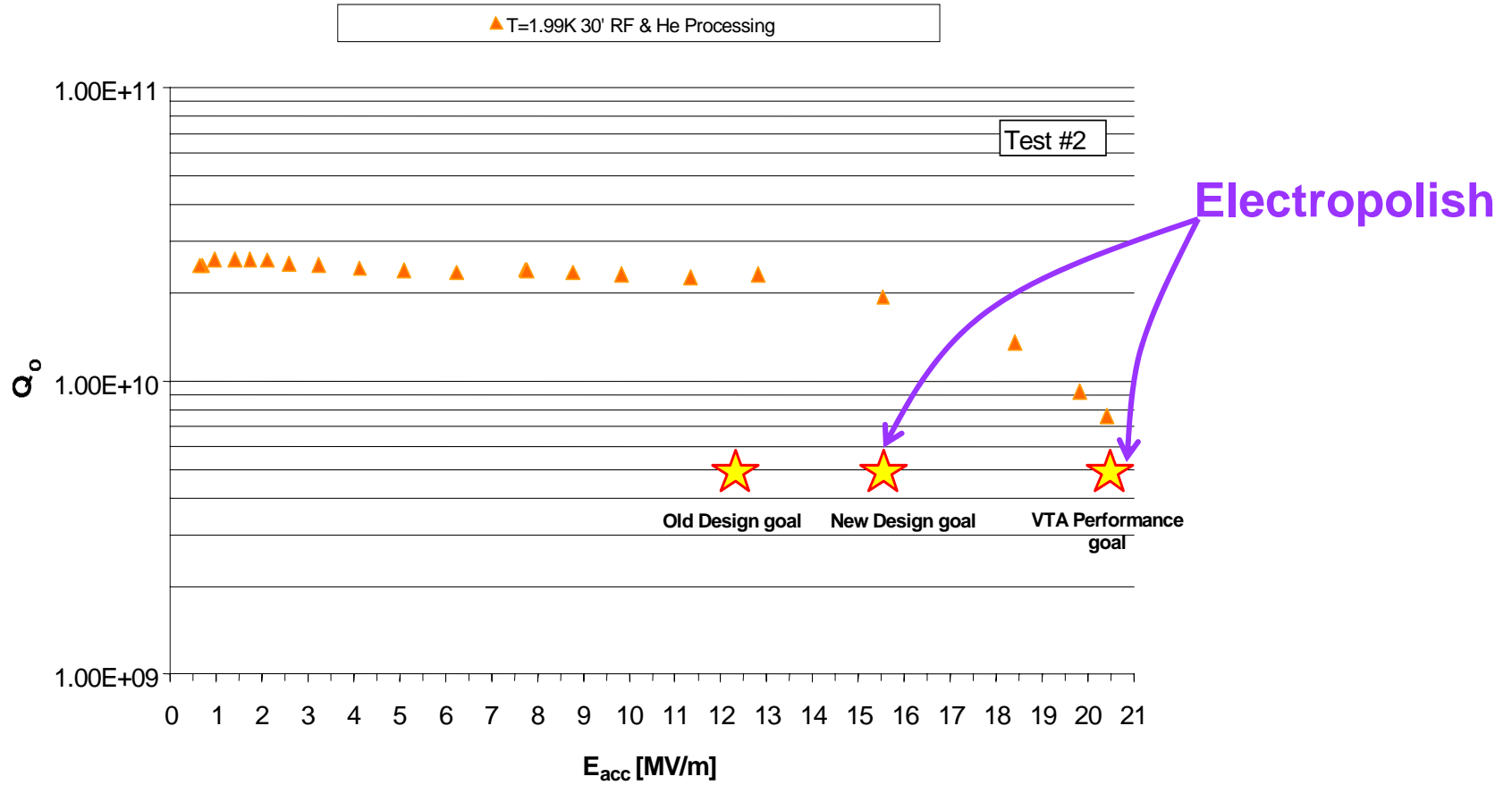
# Electropolishing will allow higher gradients for the high-beta superconducting cavities

- Electropolishing is an electrochemical removal process that removes a thin layer of metal including surface imperfections and embedded impurities.

- It is the reverse of electroplating and is an electrolytic removal of metal in an ionic solution with an applied voltage and current.

- It results in a smooth microscopic surface with no direction lines such as one gets with mechanical polishing and with the standard chemical polishing used for the medium beta cavities.

- Its use for superconducting cavities has resulted in reduced field emission and higher gradients.

- The decision to use electropolishing came just in time for application to the SNS high beta cavities

# Electropolishing of 7 – Cell Cavity



7-cell cavity JL7-2

SNS Linac
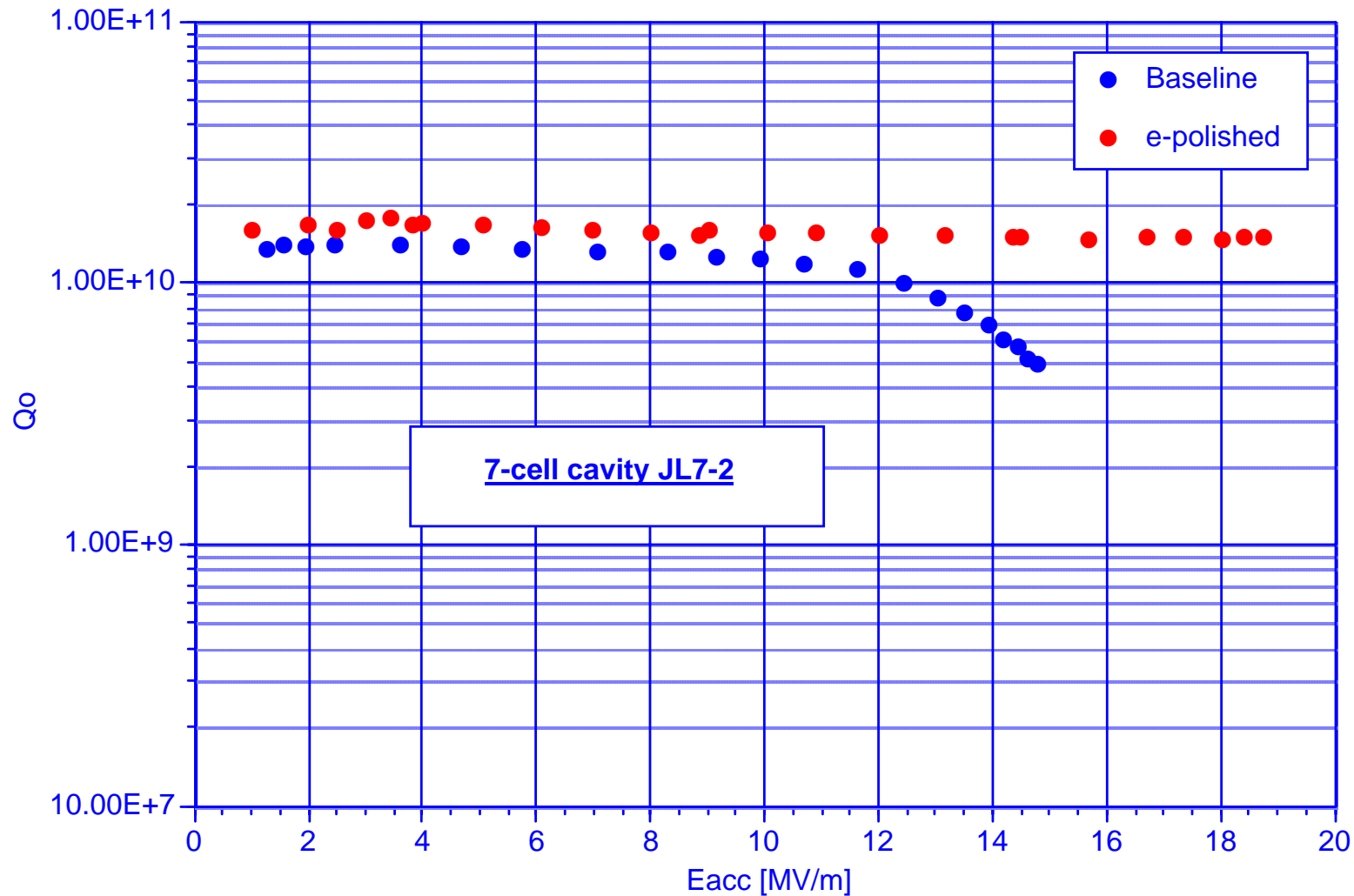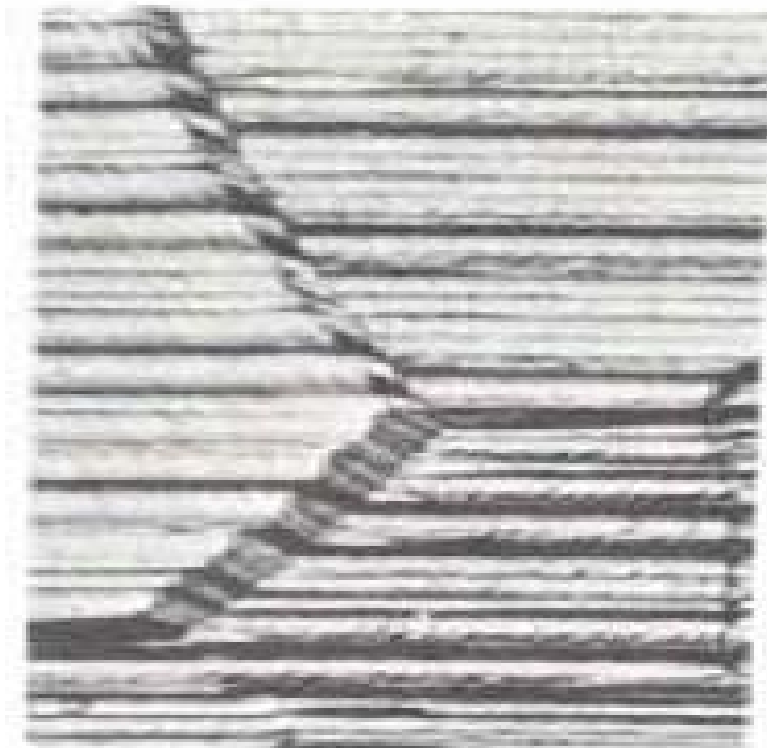
# Surface Texture

after chemical polishing
(HNO₃/HF)
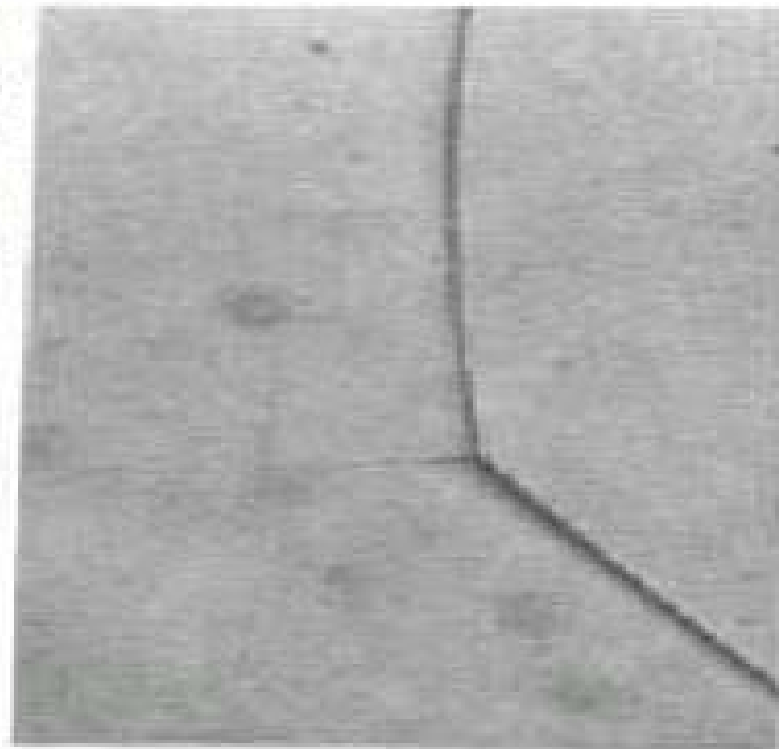
after electropolishing
(current oscillations)

BCP (used for medium beta)          EP (used for high beta)

# Surface Texture (Cont.)

**Chemically Polished
Grain Boundary**

**2μ**

**2μ**

**Electropolished Grain Boundary**
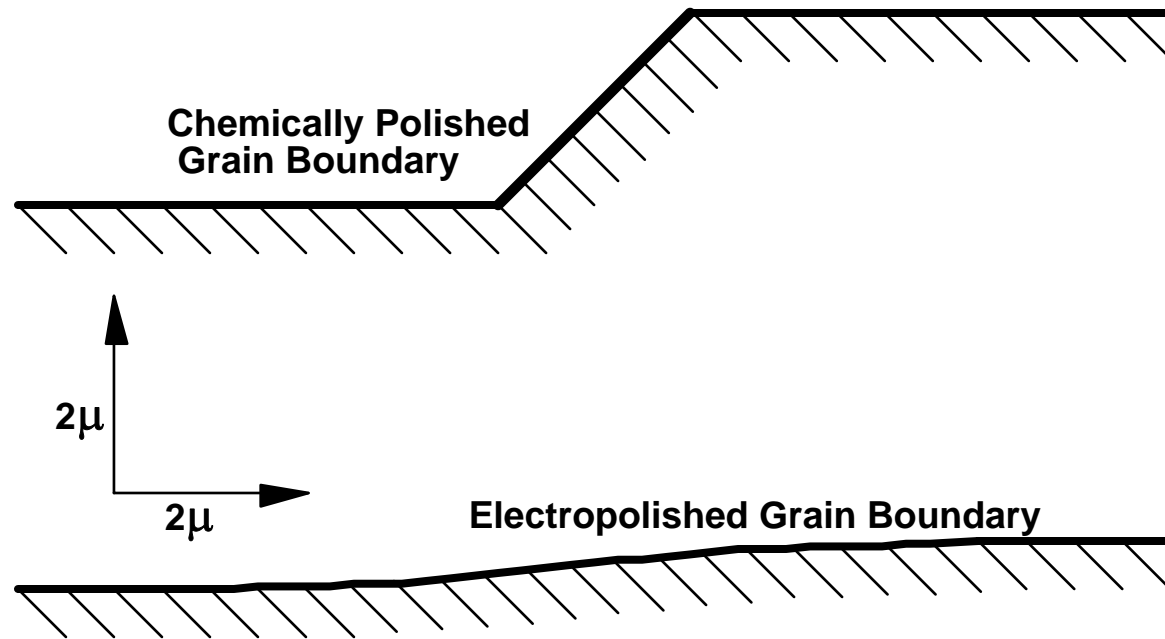
# SNS Beam Dynamics

## Tom Wangler

# Longitudinal focusing from operation on rising field



- Early particles see smaller field helping them to slow down.
- Late particles see larger field helping them to catch up.
- Stable particle is called the synchronous particle.
- Note linac phase convention with f=0 deg at crest.

# Longitudinal Dynamics

$$\frac{d(W - W_s)}{ds} = qE_0T(cos\,\phi - cos\,\phi_s)$$

$$\frac{d\phi}{ds} = -\frac{2\pi(W - W_s)}{mc^2\gamma_s^3\beta_s^3\lambda}$$

**Two coupled 1st order equations of longitudinal motion for $\phi$ and W-W_synchronous.**

$$\frac{d^2\phi}{ds^2} + \frac{2\pi qE_0T}{mc^2\gamma_s^3\beta_s^3\lambda}(cos\,\phi - cos\,\phi_s) = 0$$

**Equivalent 2nd order equation.**

Two coupled equations of motion for energy and phase and a combined 2nd order equation of motion.

# The sinusoidal RF-electric field makes the longitudinal focusing force nonlinear.
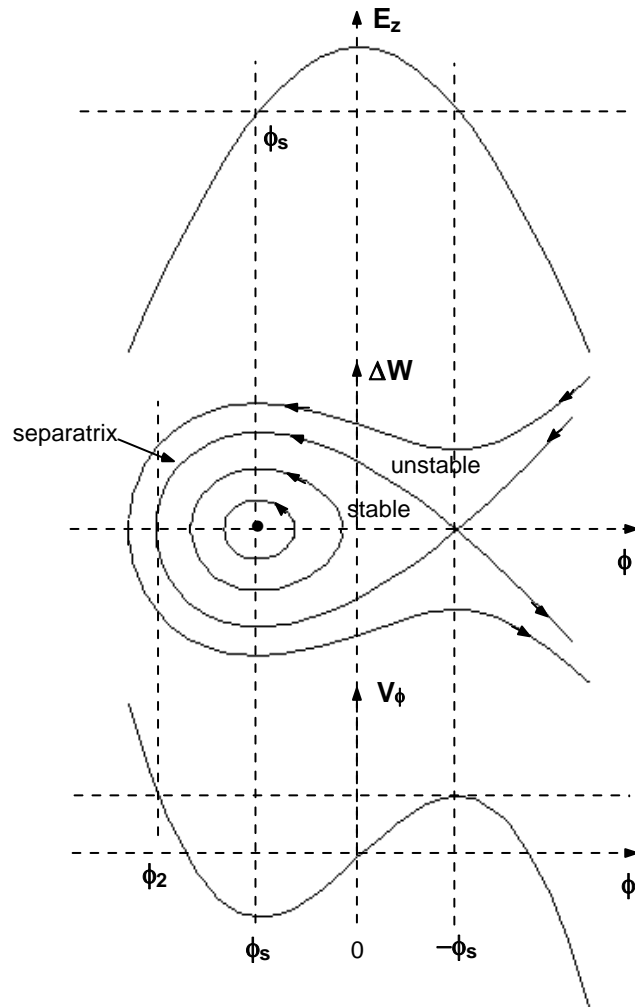


- There is a potential well centered on synchronous particle and a separatrix in phase $\phi$ versus energy $\Delta W = W - W_s$ phase-space defining the stable region.

- Analytic solution exists in approximation of weak accelerating field.

**Potential well. Typically $\phi_s$= -30 deg.**
**This potential well is also called the stable bucket.**

# Convenient variable change

$$w \equiv \Delta\gamma = \frac{W - W_s}{mc^2} \,, \quad A \equiv \frac{2\pi}{\beta_s^3 \gamma_s^3 \lambda} \,, \quad B \equiv \frac{qE_0 T}{mc^2}$$

$$w' \equiv \frac{dw}{ds} = B\left(\cos\phi - \cos\phi_s\right)$$

$$\phi' \equiv \frac{d\phi}{ds} = -Aw$$

*or*

$$\phi'' \equiv \frac{d^2\phi}{ds^2} = -AB\left(\cos\phi - \cos\phi_s\right)$$

*where*

$$AB = \frac{2\pi q E_0 T}{mc^2} \beta_s^3 \gamma_s^3 \lambda$$

# Potential Well (Stable bucket)

$$V_\phi = B\left(\sin\phi - \phi\cos\phi_s\right)$$

*The potential well (bucket) corresponds to*
$$-\pi < \phi_s < 0.$$

*Acceleration corresponds to* $-\pi/2 \le \phi_s \le \pi/2.$

*Simultaneous acceleration and potential well when*
$$-\pi/2 \le \phi_s < 0.$$

# Separatrix trajectory separates stable from unstable trajectories

$$\frac{Aw^2}{2} + B\left(\sin\phi - \phi\cos\phi_s\right) + B\left(\sin\phi_s - \phi_s\cos\phi_s\right) = 0$$

*Phase width $\psi$ of separatrix*

$$\tan\phi_s = \frac{\sin\psi - \psi}{1 - \cos\psi}, \ or$$

$$\psi \cong -3\tan\phi_s \cong -3\phi_s$$

# Maximum energy difference ΔW=W-W$_s$ of separatrix

The maximum occurs at $\phi=\phi_s$.

$$w_{\max} = \frac{\Delta W_{\max}}{mc^2} = \sqrt{\frac{2qE_0 T\beta_s^3\gamma_s^3\lambda}{\pi mc^2}\left(\phi_s\cos\phi_s - \sin\phi_s\right)}$$

# The area of the longitudinal ellipse is an adiabatic invariant

• If the acceleration rate is slow, the phase amplitude of all trajectories gradually decreases and the energy amplitudes gradually increase. This is referred to as phase damping.

$$Area = \pi \Delta W \Delta \phi = cons \tan t$$

$$\Delta \phi = \frac{cons \tan t}{\left(\beta_s \gamma_s\right)^{3/4}}$$

$$\Delta W = cons \tan t \times \left(\beta_s \gamma_s\right)^{3/4}$$

Phase damping of longitudinal beam ellipse

Phas

P
h
as

## If the actual accelerating gradient $E_0T$ is different from the design value $(E_0T)_{design}$, a different particle phase can satisfy the synchronous energy condition

$Since \, \Delta W = qE_0T \cos(\phi)L, \, we \, ma\text{int} ain \, correct \, \Delta W \, if$

$$E_0T \cos\phi = (E_0T)_{design} \cos\phi_s$$

$At \, \phi_s = 0 \, the \, accep\tan ce \, and \, the \, stable \, bucket \, vanishes.$

$For \, this \, case \, \cos\phi = 1 \, and \, this \, corresponds \, to \, the \, threshold$

$for \, for\min g \, a \, stable \, bucket. \, Thus, \, for \, a \, stable \, bucket$

$$(E_0T)_{threshold} = (E_0T)_{design} \cos\phi_s$$

# Separatrix for $\phi$=-90 degrees (no acceleration case) includes 360 degrees of phase.
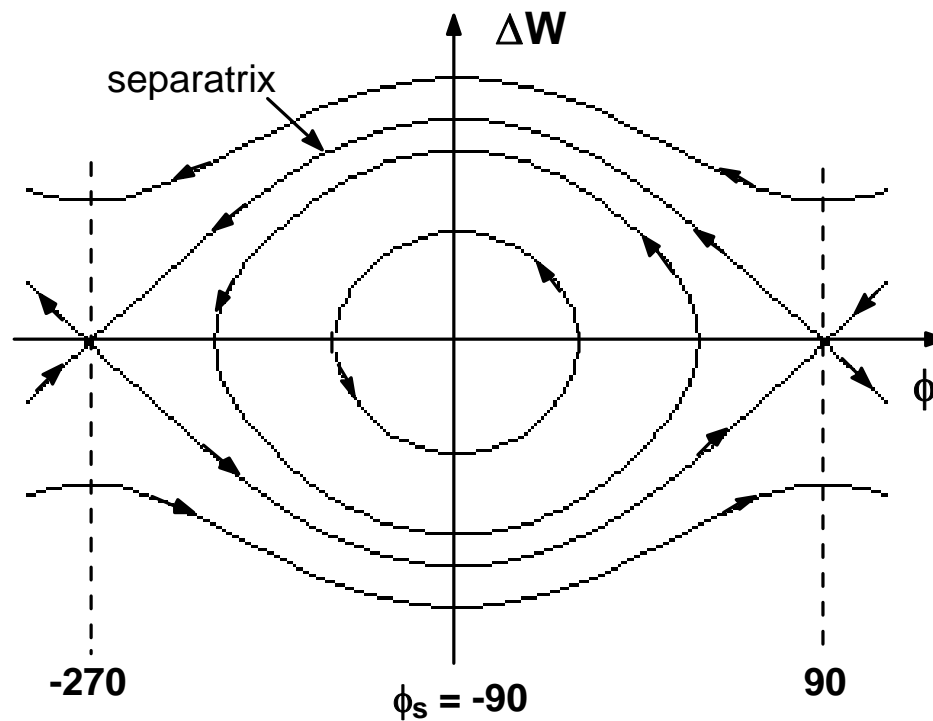
# Longitudinal phase space trajectories when acceleration is not negligible increases the longitudinal acceptance. (Golf club)
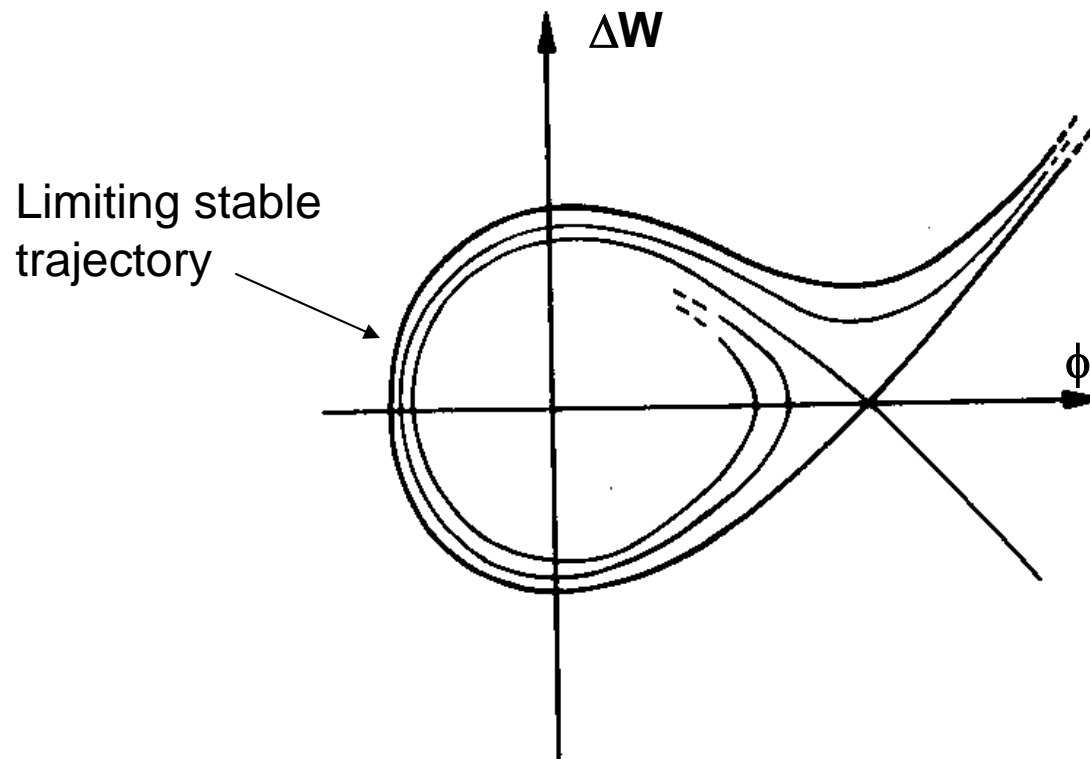
**Transverse effects of the accelerating field can be seen by looking at the transverse electric field lines at the entrance and exit of an accelerating gap.**
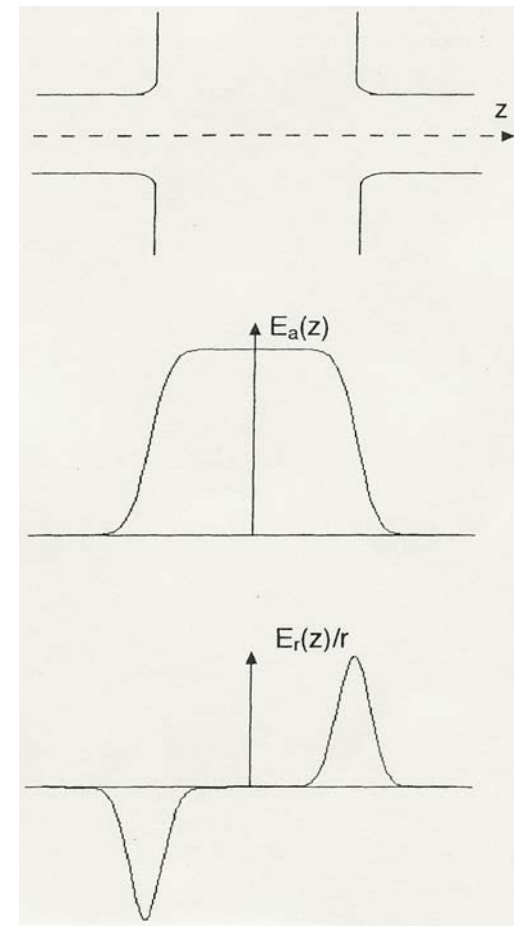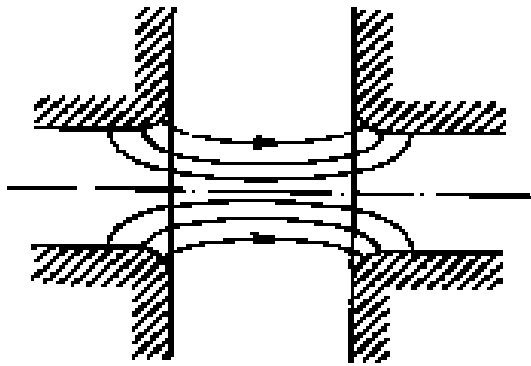
# Transverse RF Defocusing Force

- The radial fields are localized in the gap entrance and exit.

- If the field was constant in time the entrance (focusing) and exit (defocusing) radial effects would cancel.

- When the field increases with time as it must for longitudinal focusing, the exit (defocusing) radial field will be larger than the entrance (focusing) radial field. So we can expect a net radial RF defocusing force.

- An exception is for the case of very large fields when the velocity change of the particle becomes significant. Then, the particle spends less time in the gap exit region than in the entrance region, and you can get net radial focusing.

# Quadrupole focusing compensates for RF defocusing.
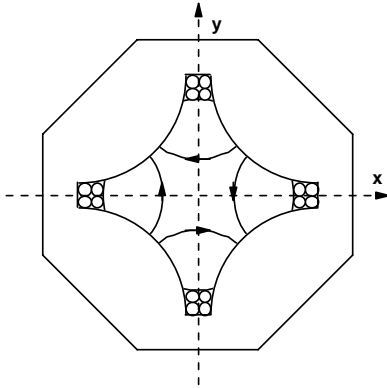


Quadrupole magnet cross section showing
magnetic field pattern.
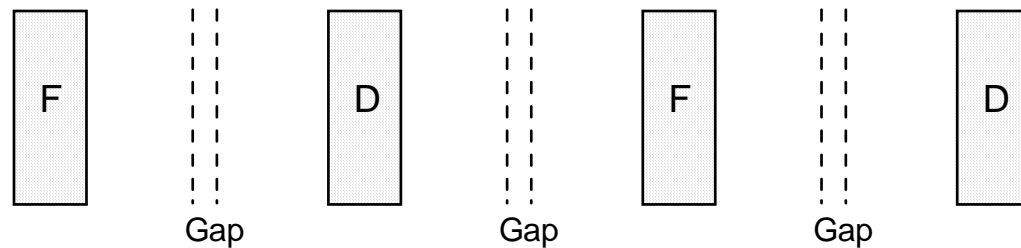


FODO quadrupole lattice with accelerating gaps between
lenses.

# Smooth approximation to linac focusing including quadrupole and radial RF defocusing forces

$$\frac{d^2 x}{ds^2} + k_0^2 x = 0$$

**Phase-advance
per unit length**

**Phase-advance
per period**

$$k_0^2 = \left[\frac{\sigma_0}{2L}\right]^2 \cong \left[\frac{qG\ell}{2mc\gamma\beta}\right]^2 - \frac{\pi q E_0 T \, sin(-\phi)}{mc^2 \lambda (\gamma\beta)^3}.$$

**Period
length**

**Quadrupole**

G=gradient
$\ell$=effective length

**RF defocus**

# Focusing in the SNS Linac

| SNS Linac Structure | Lattice Type | Period |
|---|---|---|
| RFQ | FD singlet-rf electric quads | $\beta\lambda$ (402.5 MHz) |
| DTL | FF0DD0 singlet-permanent magnet quads | $6\beta\lambda$ (402.5 MHz) |
| CCL | F0D0 singlet, one per bridge coupler, electromagnets | $13\beta\lambda$ (805 MHz) |
| Superconducting (medium $\beta$) | FD0 Doublet in warm intertank space-electromagnets | 1.7542m (805 MHz) |
| Superconducting (high $\beta$) | FD0 Doublet in warm intertank space-electromagnets | 1.8835m (805 MHz) |

# Multiparticle and High Intensity Effects in Proton Linacs

- **Beam Emittance**

-Emittance is the measure of area beam occupies in phase space.

-Is a defocusing effect in the sense that the spread of divergence angles causes beam particles to move apart unless compensated by focusing.


- **Space Charge Force**

-A real force that defocuses the beam particles.

-Can cause an effective emittance increase and beam halo formation.

-Is inherently a non-relativistic effect.

# RMS Description of a Beam

- An arbitrary phase space distribution can be described by an RMS ellipse.
- The Courant-Snyder ellipse parameters are defined from the second moments.

$$\tilde{\beta} = \left\langle x^2 \right\rangle / \varepsilon_{rms}$$

$$\gamma = \left\langle x'^2 \right\rangle / \varepsilon_{rms}$$

$$\alpha = -\left\langle xx' \right\rangle / \varepsilon_{rms}$$
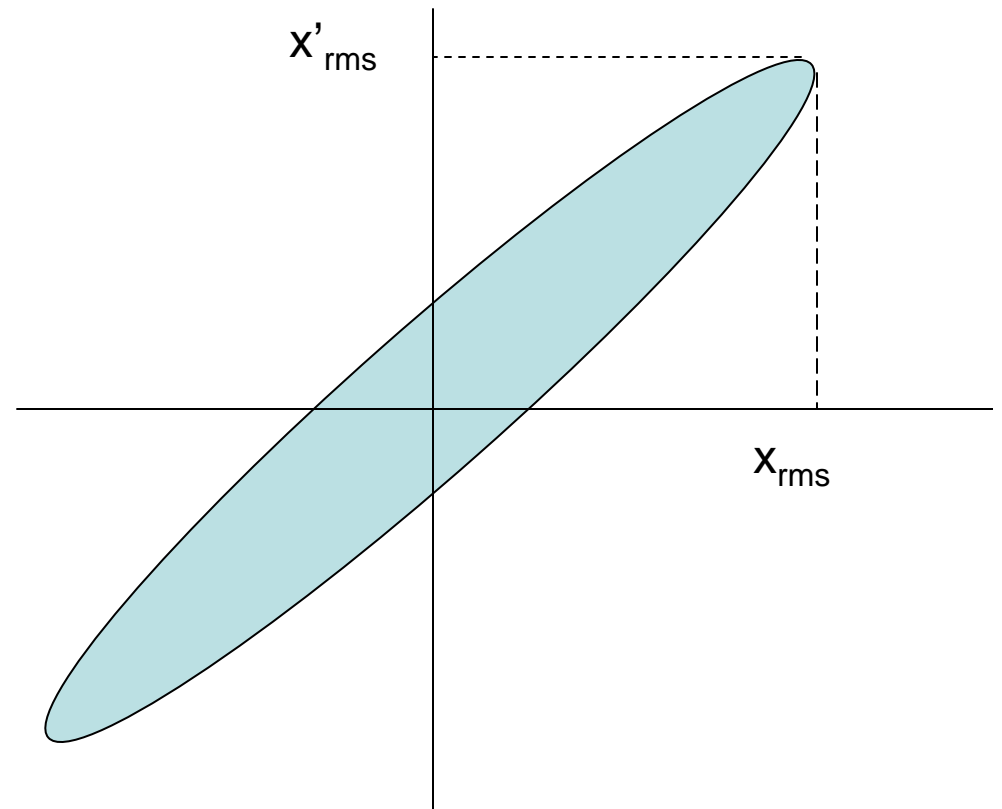
$$\varepsilon_{rms} = \sqrt{\left\langle x^2 \right\rangle \left\langle x'^2 \right\rangle - \left\langle xx' \right\rangle^2}$$

# RMS Emittance Definition

$$\varepsilon_{rms} = \sqrt{\left\langle x^2 \right\rangle \left\langle x'^2 \right\rangle - \left\langle xx' \right\rangle^2}$$

- Nonlinear forces (RF fields or aberrations in focusing elements or space-charge forces) can cause rms emittance growth which is usually irreversible.

- Nonlinear time-dependent forces (such as space-charge forces for mismatched beams) produce emittance growth and halo.

# Example: Upright RMS Ellipse
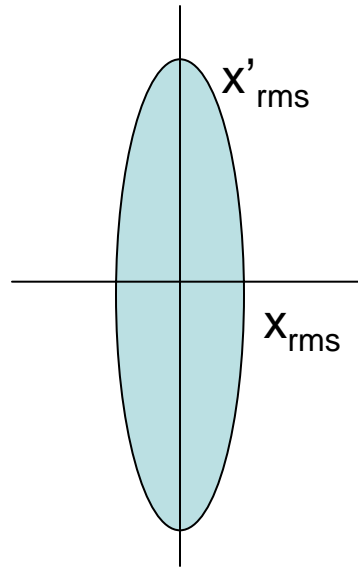


• In this case <xx'>=0 so:

$$\varepsilon_{rms} = \sqrt{\left\langle x^2 \right\rangle \left\langle x'^2 \right\rangle - \left\langle xx' \right\rangle^2} = \sqrt{\left\langle x^2 \right\rangle \left\langle x'^2 \right\rangle} = x_{rms} x'_{rms}$$

$$Area\ of\ ellipse = \pi x_{rms} x'_{rms}\ or$$

$$\varepsilon_{rms} = \frac{area\ of\ ellipse}{\pi}$$

# Transverse Emittance Normalized and Unnormalized

$$Normalized\ emit\tan ce: \varepsilon_n = \Delta x \Delta p_x / mc = \Delta x \Delta x' \beta \gamma$$

$$Unnormalized\ emit\tan ce: \varepsilon = \Delta x \Delta x'$$

• With acceleration, normalized emittance is conserved and unnormalized emittance decreases as $1/\beta\gamma$.

• Unnormalized emittance is what is generally measured in the laboratory.

•Typical units of normalized and unnormalized emittance are the same: meter-radians, cm-mradians, or mm-mradians.

# Space-charge or self-fields include electric and magnetic contributions

- Space-charge is primarily a non-relativistic effect.

- Electric space-charge force causes defocusing.

- Magnetic space-charge force is attractive, becomes significant at high velocities, where it nearly compensates for electric force.

- When the magnetic force and the relativistic mass effect are included, the electric field in the nonrelativistic equations of motion is reduced by a factor of $\gamma^3$.

# Calculating the Space Charge Force

- Need to describe the evolution of the beam distribution and the corresponding space-charge fields, including the nonlinear part that can cause emittance growth.

- The most reliable method is multiparticle simulation, where the standard approach is the particle-in-cell method.

# Rms emittance growth and beam halo are topics at the frontiers of beam-physics research

• Nonlinear space-charge forces in ion beams distort the phase space contours and produce rms emittance growth.

• The most useful emittance definition under these circumstances is the rms emittance, defined in terms of second moments as:

$$\varepsilon_{rms} = \beta\gamma\sqrt{\overline{x^2}\,\overline{x'^2} - \overline{xx'}^2}\ .$$

• Irreversible rms-emittance growth occurs as the phase-space distortion increases. Liouville's theorem is not violated.

• Nonlinear time-dependent space-charge forces, especially from rms mismatched beams, can produce halo with associated rms emittance growth.

# What are the most important space-charge induced emittance growth mechanisms?

- **Charge redistribution** of RMS matched beams results in transfer of space-charge field energy to thermal energy (emittance) is usually important only when tune depression ratio approaches zero, which is not the case for most RF linacs.

- **Energy transfer between degrees of freedom** (equipartitioning) is important only when coupling resonances are excited. Usually the tunes are changing to fast to sustain this.

- **Beam envelope instability** which usually can occur when $\sigma_0 > 90$ deg and $\sigma < 90$. Avoid by restricting $\sigma_0 < 90$ deg.

- **Rms beam mismatch** produces an extended halo is the beam is not matched.

# Emittance growth typically occurs at certain transitions

- Avoid changes in focusing channel where the focusing (phase advance per unit length) gets weaker.

- Avoid rms mismatch where additional energy in mismatch oscillations becomes available for emittance growth and halo formation.

- Avoid bunching beam so much that there is a significant change in the line charge density.

- Avoid transition where charge neutralization goes away, exposing beam to larger direct space charge force.

# Examples of Emittance-Growth Trouble Spots.

- RFQ injection (Charge neutralization goes away because of rf electric fields).

- RFQ initial bunching section (Line charge density increases).

- DTL, CCL, or superconducting linac injection (Focusing may get weaker in the new linac section, or beam may be rms mismatched)

# General strategy for controlling space-charge induced emittance growth and halo formation.

- Strong focusing in all planes for which emittance must be kept small.

- High frequencies so for a given average current, the charge is distributed over more bunches.

- Rms match the beam to minimize rms beam oscillations. Need good beam diagnostics, and adequate knobs to control beam parameters.

# What is beam halo? Example from simulation of mismatched beam in quadrupole-focusing channel.

## Mismatched beam develops larger amplitudes than matched beam.

### Matched Beam
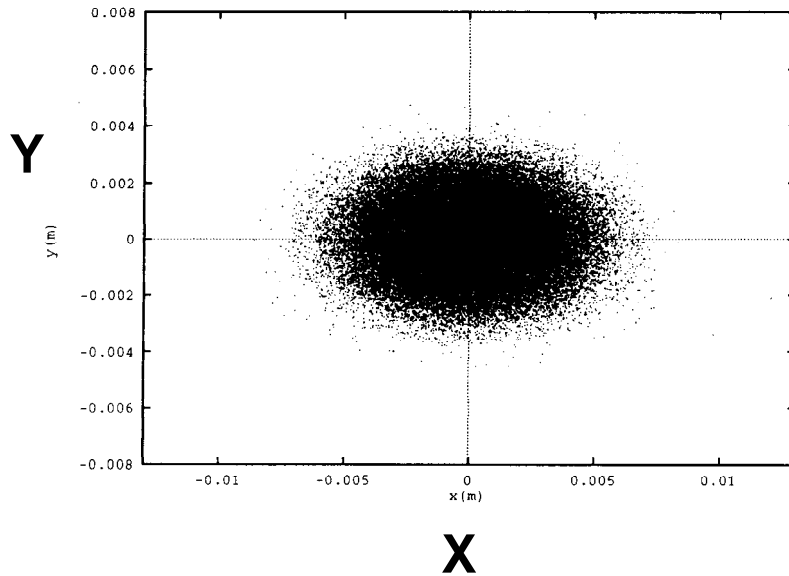
### Mismatched Beam
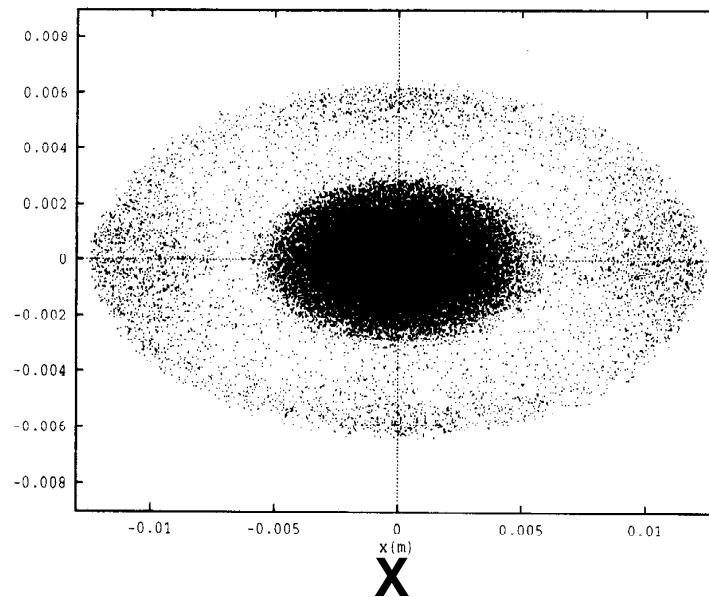
# Why beam halo is important.

- Halo can produce beam loss and activation that makes maintenance difficult and time-consuming.

- Control of beam halo and beam loss is necessary for high beam availability in high-power proton linacs.

**Computer simulations (1991) showed substantial halo is formed in mismatched beams and resulted in Free-Energy Model.**

*A. Cucchetti, M. Reiser, and T. Wangler, Proc. IEEE 1991 Part. Accel. Conf., p.251.*

---

- **Beam mismatch in presence of nonlinear space charge is a major source of halo.**

- **The mismatch creates free energy. Energy in mismatch oscillations can be converted into thermal energy of the beam [*M. Reiser, J. Applied Phys. 70, 1919 (1991)*].**

# **Particle-core model** incorporates a physical mechanism of halo growth.

---

- **Core dynamics:** Mismatch excites rms envelope modes (breathing and quadrupole modes) of uniform beam core.

- **Particle dynamics:** Space-charge of oscillating core modulates net focusing force and drives individual particles in parametric resonance when $f_{particle} = f_{mode}/2$.
  [*R. Gluckstern, Phys. Rev. Lett. 73, 1247 (1994)*].

- One finds that the resonant condition is satisfied for particles with amplitudes that lie outside the core.

- **Model predicts maximum halo particle amplitudes.**
  [*T.P.Wangler, K.R.Crandall, R.Ryne, and T.S.Wang, Phys. Rev. Special Topics-Accel and Beams.1, 084201 (1998)*].

- **Predictions of the model agreed with results from a recent beam halo experiment at Los Alamos.** *Phys. Rev. Letters, 89, 214802 (2002).*

# Evolution of the SNS Linac Design

# Design Choices

- Project-wide choices dictate some of the parameters that the cavity designer has to work with.
  - RF frequency
  - Beam current, focusing requirements
  - Energy range
  - Duty factor
- Choice of the rf structure is often based primarily on overall power efficiency and need for flexibility.
  - Independently powered cavities offers maximum flexibility at the expense more power supplies and a more complex control system.
  - Coupled structures with many cells locked together in phase reduces the number of rf systems and control system complexity.

# Optimizing the Design

- Everything affects everything else!
- System-wide studies are essential to guide choices.
- Studies must consider all aspects of the project.
  - Physics (beam dynamics, rf structures, diagnostics)
  - Engineering (materials, thermal, structural analysis,
  - Civil construction (site, physical plant, utilities)
  - Manufacturing
  - Installation
  - Commissioning
  - Operation
  - Maintenance
  - Cost and schedule

# SNS Design Evolved Over Many Years

- Early concepts settled on 2-MW beam power upgradeable to 4 MW by beam funneling at 20 MeV, using conventional room-temperature structures.
  - RFQ (402.5 MHz) to 2.5 MeV, followed by beam chopping.
  - DTL from 2.5 MeV to 20 MeV.
  - CCDTL (hybrid DTL and CCL) made funneling possible by doubling frequency at 20 MeV.
  - CCL is more efficient above 100 MeV, final energy 1 GeV.
- New management reduced project scope to 1-MW, no upgrade.
  - Design no longer needs the CCDTL.
  - DTL extended to ~87 MeV.

# The Upgrade Requirement Made Early Designs Very Complicated

- The 2-MW configuration has 70 rf modules and uses 35 klystrons.

- The 4-MW configuration has 48 rf modules and uses 42 klystrons.

- First 12 modules remain the same after the upgrade.

- After module 12 in the 2-MW configuration, there are 3 modules with 107 cavities, 19 modules with 89 cavities, and 37 modules with 71 cavities.

- After module 12 in the 4-MW configuration, there are 3 modules with 161 cavities, 7 modules with 143 cavities, 19 modules with 125 cavities, 6 modules with 107 cavities, and one 89-cavity module at the end.

# Between 1996 and 2000 the linac went through several design concepts.
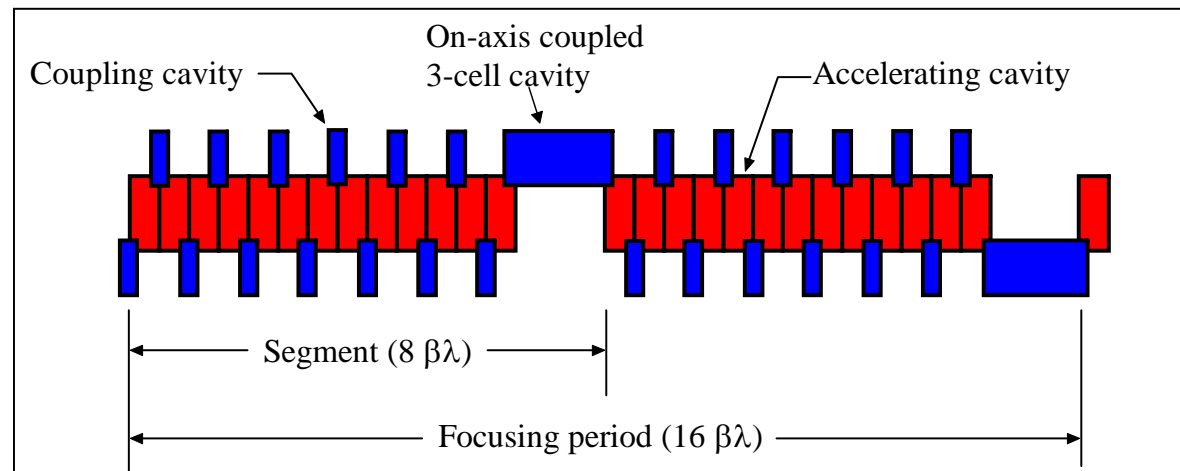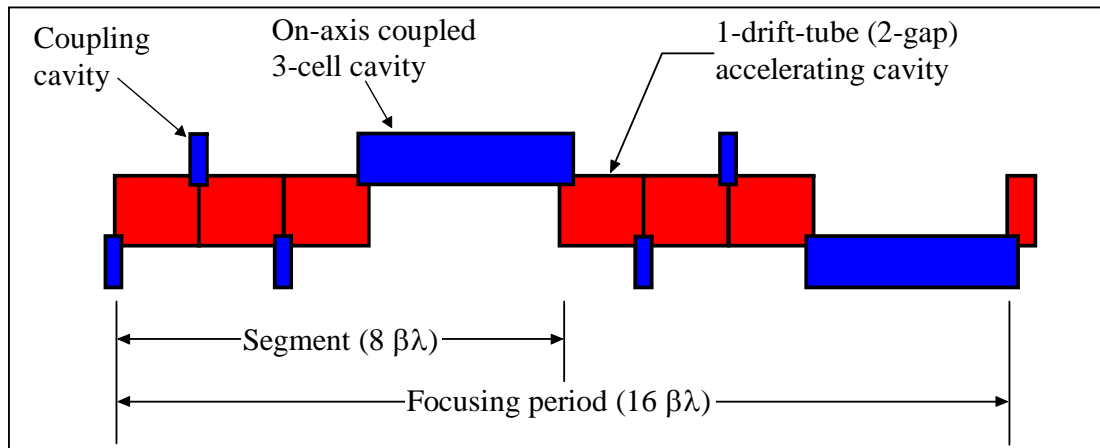
# Chopping Effect on Cavity Fields Had Major Influence on Structure Choices
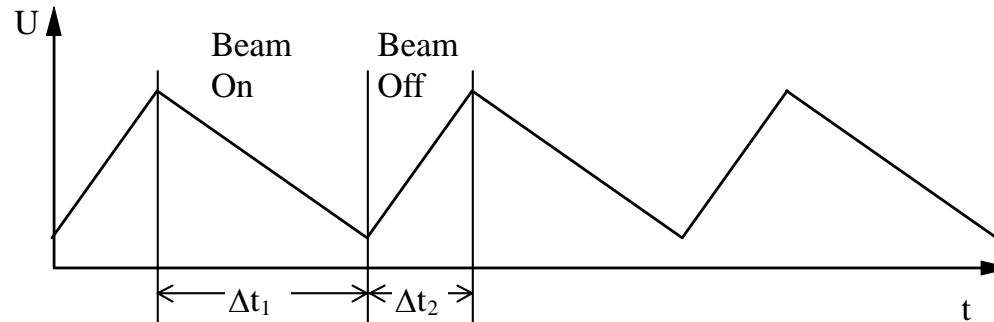


- For a constant power transmitted to the cavity, the stored energy rises and falls as the beam turns off and on. The corresponding change in accelerating field from peak to valley is

$$\frac{\Delta(E_0 T)}{E_0 T} = \frac{E_0 TL}{2U} \, I\cos\phi_s \, \frac{\Delta t_1 \Delta t_2}{\Delta t_1 + \Delta t_2}$$

- This effect favors a low-frequency structure (e.g., DTL at 402.5 MHz), which has large stored energy per unit length.

# Early SNS Design Used 3 Types of Room-Temperature Structures



402.5-MHz
DTL
Tank 1    Tank 2

805-MHz
CCDTL

805-MHz
CCL

2.5 MeV   10 MeV    20 MeV         (93 MeV)                    1 GeV

FOFODODO
Lattice
4 $\beta\lambda$ @ 402.5 MHz
8 $\beta\lambda$ @ 805 MHz

Continuous FODO
Lattice
16 $\beta\lambda$ @ 805 MHz

(soon to be changed to
11 $\beta\lambda$ @ 805 MHz)
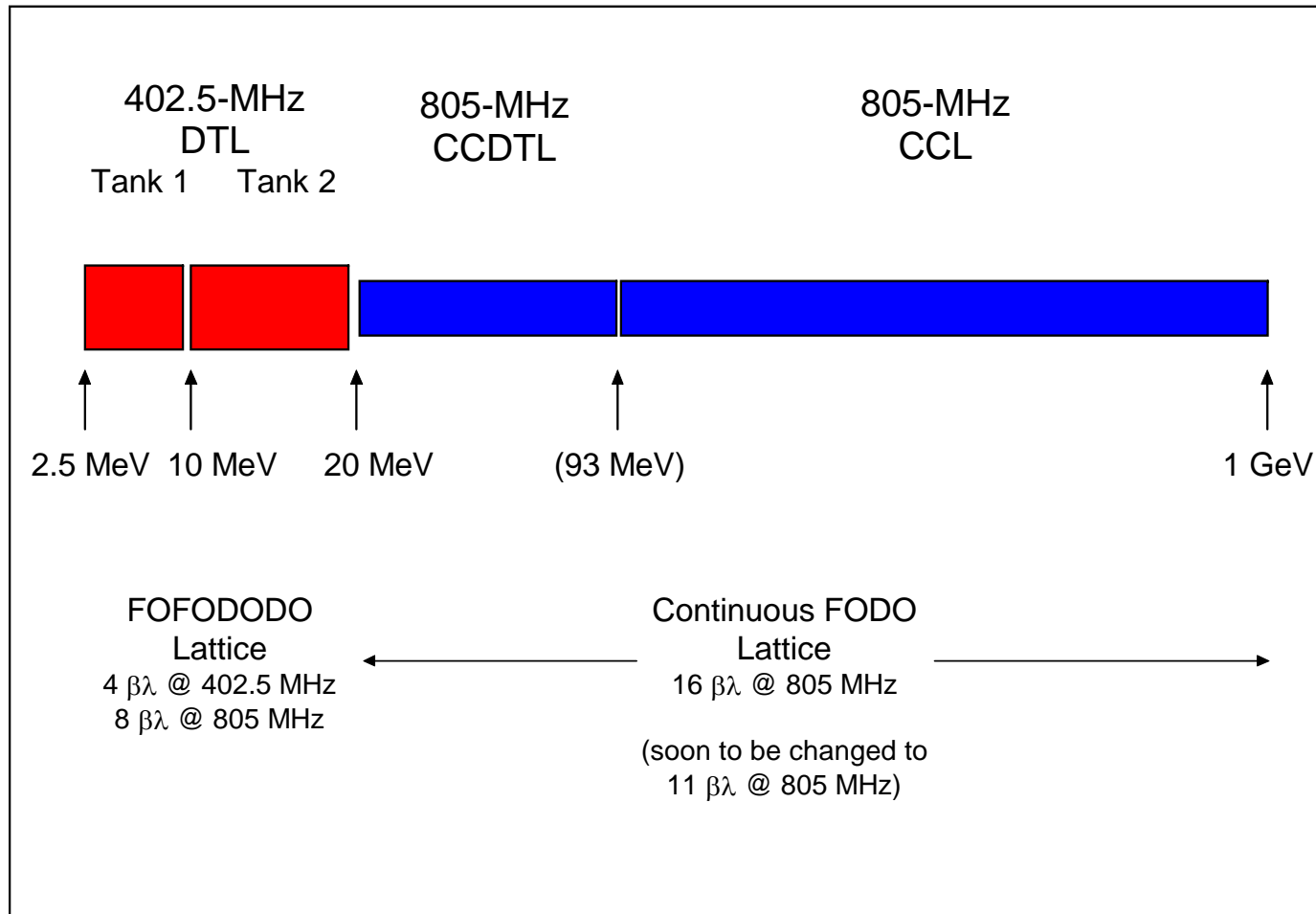
# Shunt impedance from early design studies
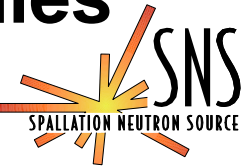
Numbers are bore radius in cm.
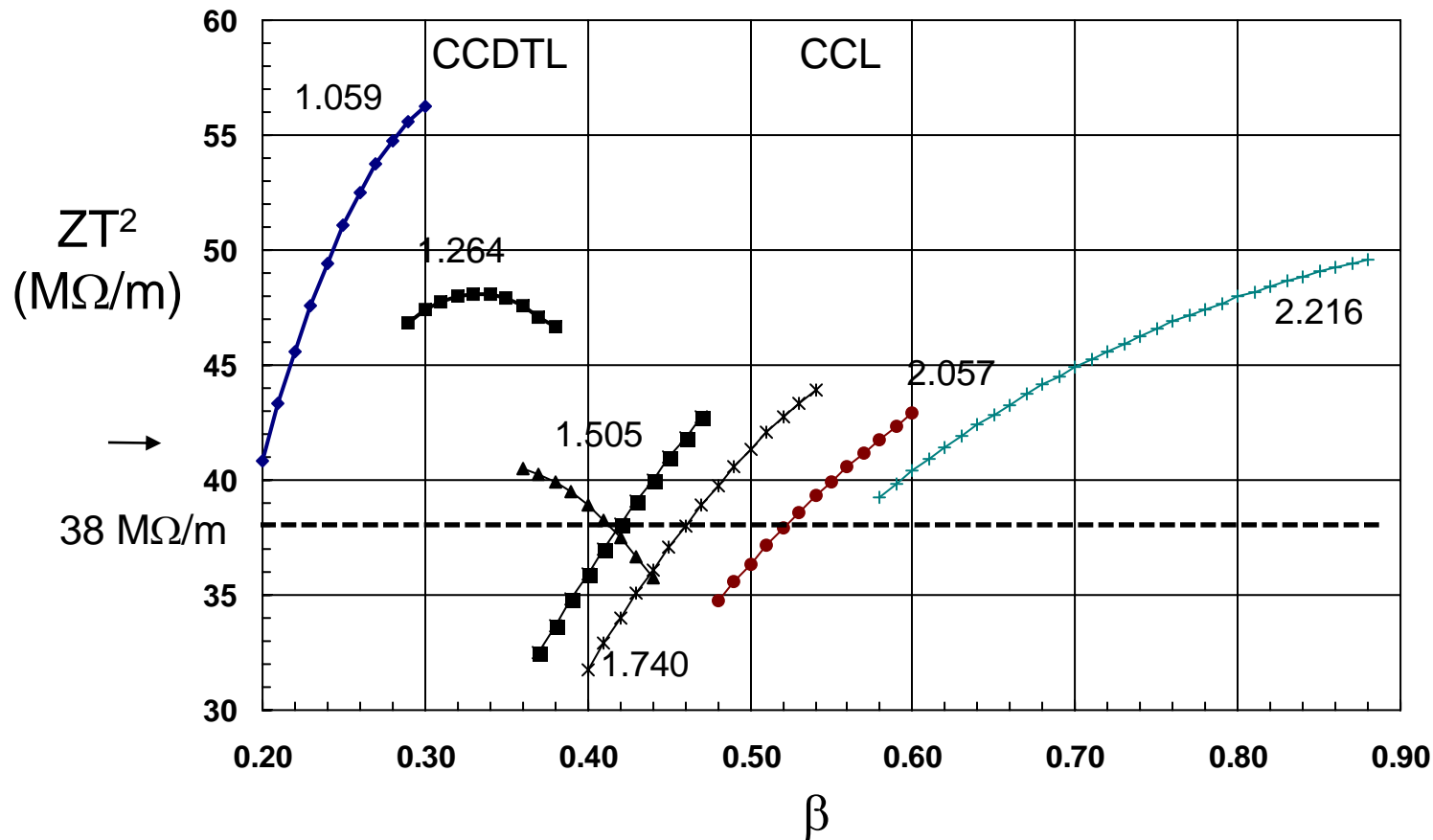
# Linac Design Summary in September 1998

- 52 klystrons at 1 MW beam power, 77 klystrons at 4 MW beam power.

- Modules 1 and 2 are CCDTL to 98.14 MeV.

- Modules 3, 4, and 5 are 8-cavity CCL to 190.33 MeV.

- Modules 6 to 26 are 10-cavity CCL to 1000.24 MeV.

- Total copper power = 79.04 MW.

- Total length of CCDTL and CCL = 452.71 m.

- Total number of segments = 343.

- Total number of cavities = 2518.

# Shunt Impedance, May 1999



DTL | CCDTL | CCL

$ZT^2$ (M$\Omega$/m)

$\beta$
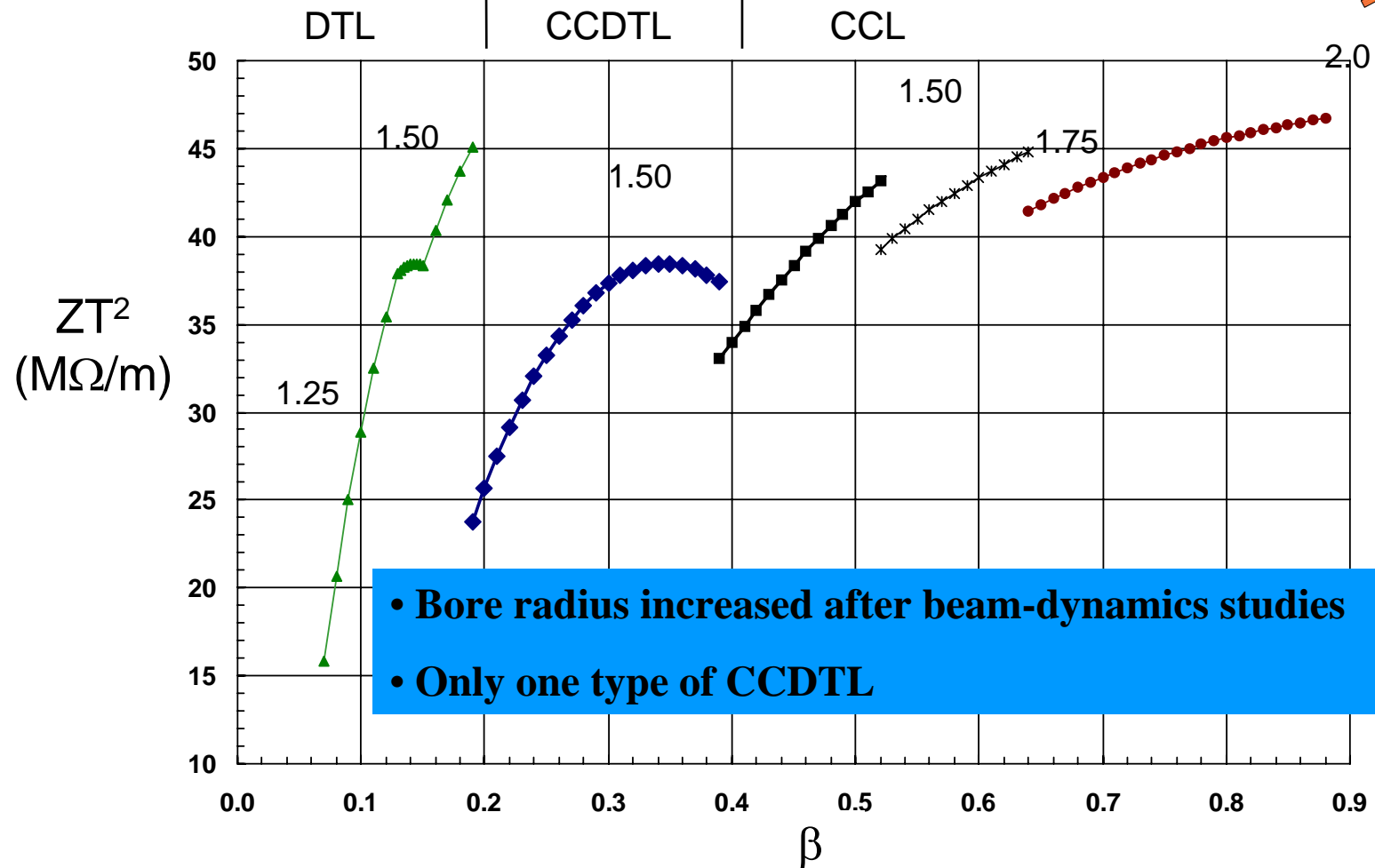
- Bore radius increased after beam-dynamics studies
- Only one type of CCDTL

# Baseline Architecture in March 2000
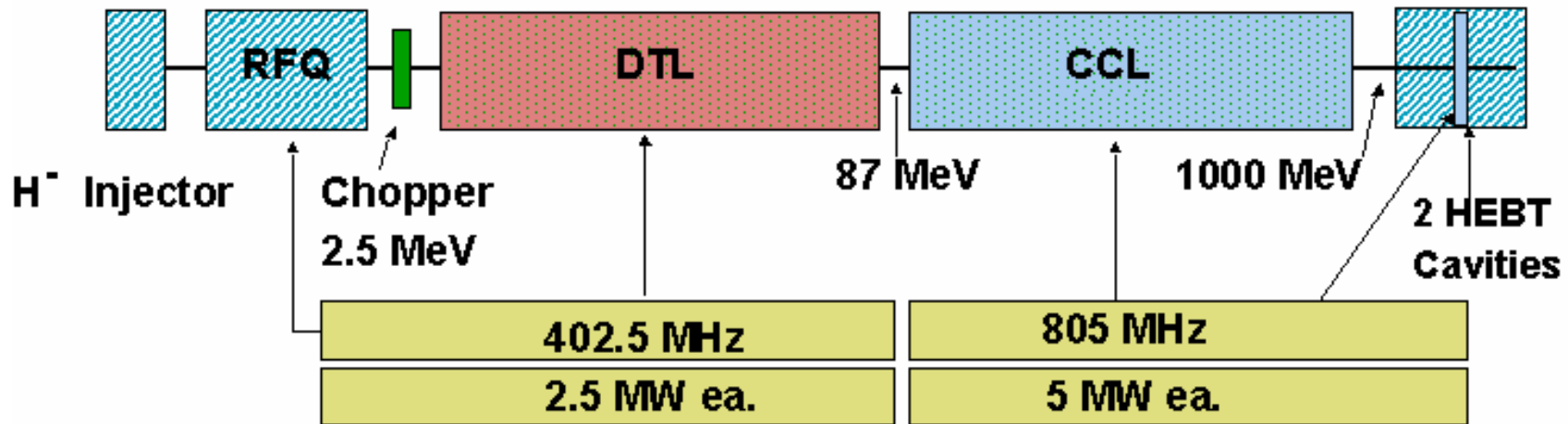


- **Project scope reduced to 1 MW (no upgrade).**

- **The baseline soon changed again to include superconducting cavities above ~200 MeV.**

# Lessons Learned

- Minimize the number of different structure types.

  - Each one requires a design team.

- Within each subsystem, minimize the number of different parts.

  - Power efficiency is not the whole story.

  - Drawing packages are expensive.

  - May allow easier recovery from manufacturing problems.

- Avoid major design changes after construction starts.

  - Unintended consequences will cost time and money.

- Monitor every step of the manufacturing process.

  - Beware of changes from methods used to build prototypes.

# DTL Cavity Design
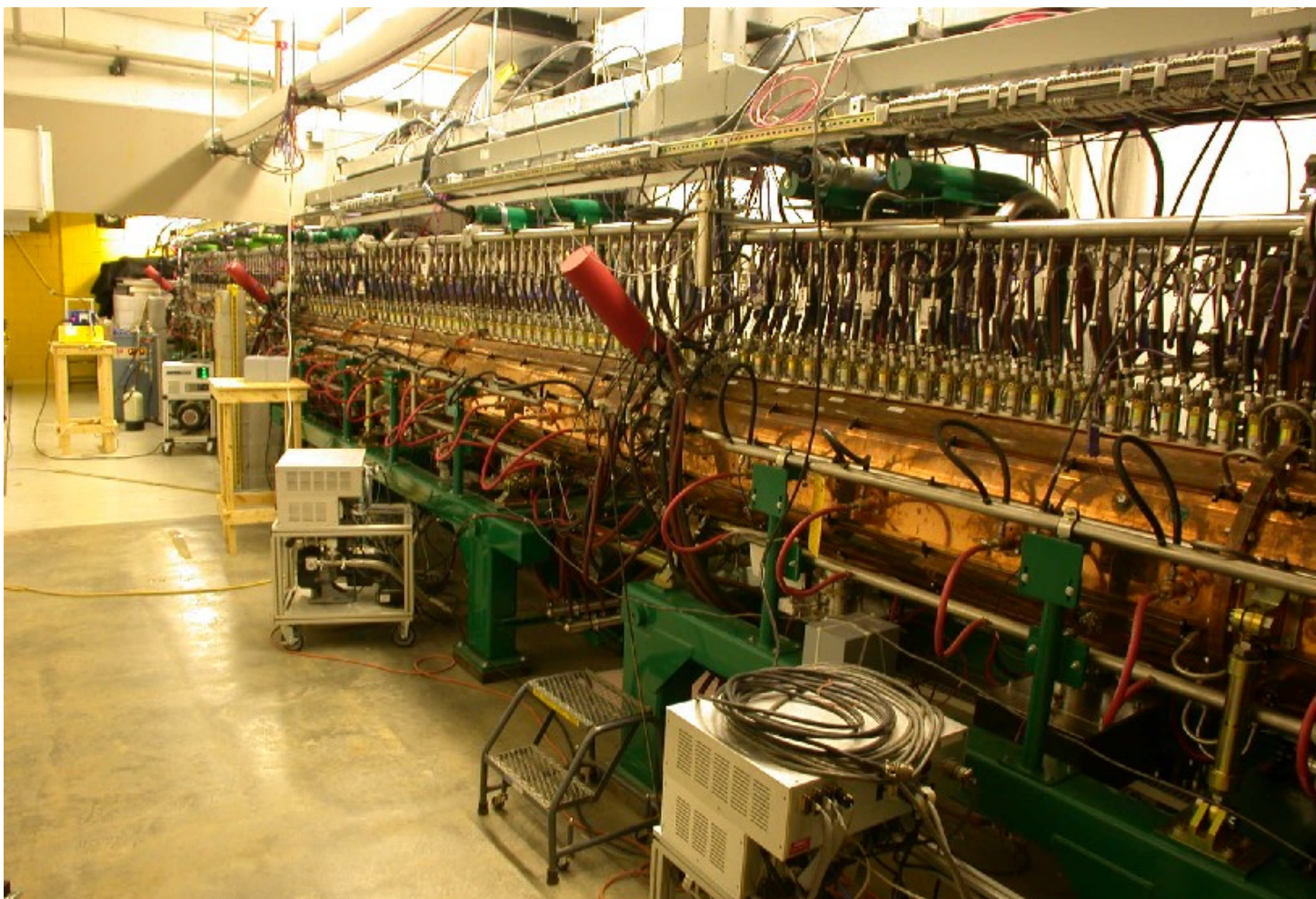
# Steps in DTL Design

- Physics design of representative cells
  - Frequency choice
  - Efficiency, peak surface fields
- Engineering design studies (thermal and structural analysis)
- Beam dynamics design and simulations using transit-time factor data from representative cells
  - Layout of cell lengths, $E_0$, number of tanks
- Design each cell determined from the beam-dynamics design
  - Drift-tube tables for engineering design
  - Compute tank power, Q, stored energy
  - $E_z$ data for tuning the structure
  - Frequency "budget" for each tank

# DTL Cell Geometry
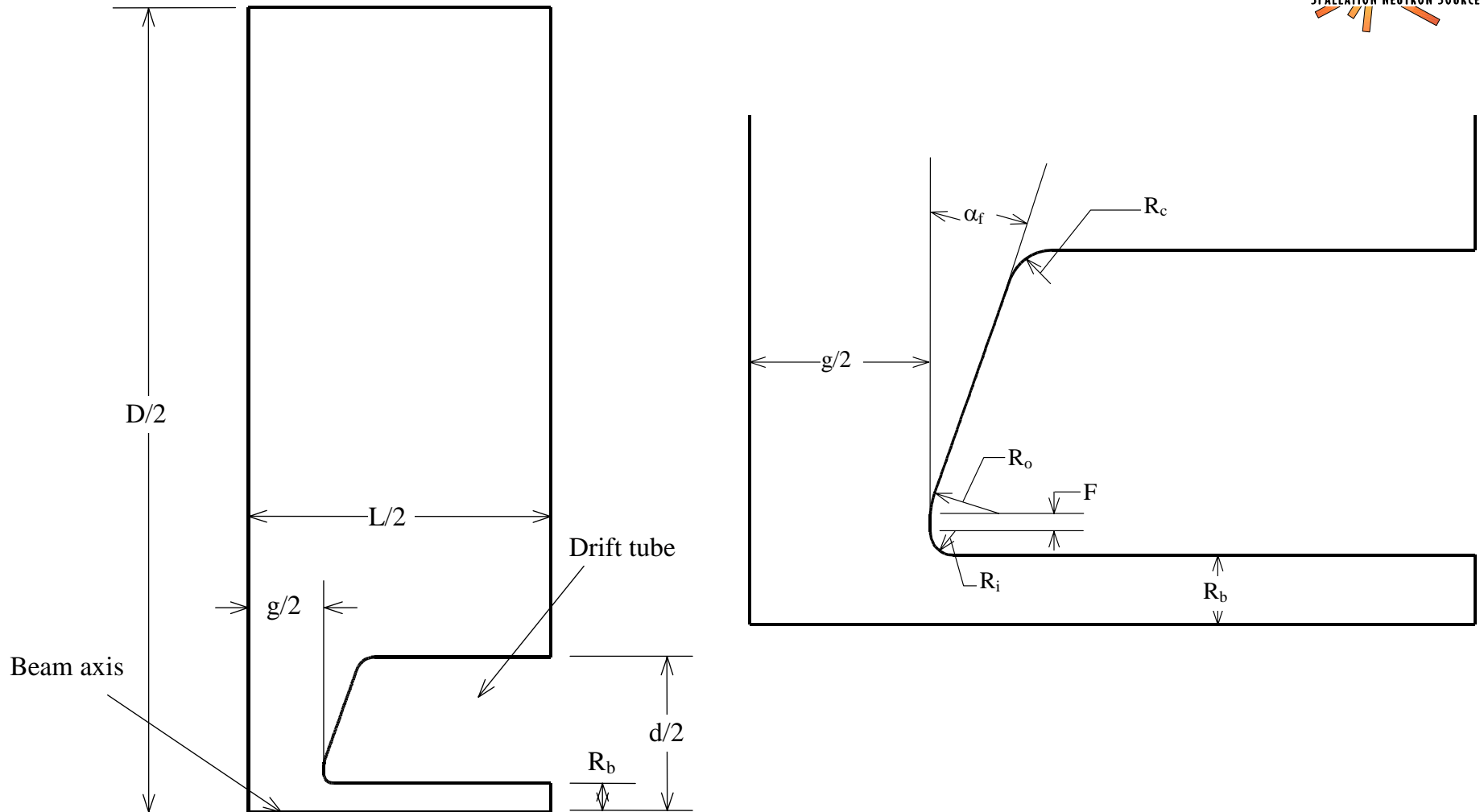
# DTL Cell Geometry Selections
# General Guidelines

- Cell length is 1 $\beta\lambda$ = distance traveled in 1 RF period.
- Drift tubes shield the beam from decelerating fields.
  - Beam-dynamics studies define required bore radius.
  - Metal in electric field region adds capacitance, lowers frequency.
  - Larger face angles reduce capacitance and length for magnets.
  - Cooling and magnet size (EMQ or PMQ?) sets drift-tube diameter.
  - Rounded corners reduce peak surface electric field.
- Tank diameter constrained by post stabilization.
- Tank length set by RF power supply (including beam power)
- Vary other parameters systematically to maximize $ZT^2$ .
  - Optimize cells at both ends of a tank, interpolate in between.

# Quadrupole Magnets

- SNS uses permanent magnet quadrupole (PMQ) in all 6 tanks.
  - No other choice at low $\beta$, except 2-$\beta\lambda$ DTL cells (inefficient).
  - Magnets consist of 16 pieces held in an aluminum fixture.
  - PMQs have very good field quality, uniformity among magnets.
- Early designs considered electromagnetic quadrupole (EMQ) starting at ~20 MeV where drift tubes are long enough.
  - Preserving this option is the reason for different tank and drift tube diameters for tanks 1-2 (43 & 9 cm) and tanks 3-6 (45 & 11 cm).
  - EMQs give flexibility, but increase complexity.
  - Require power supply, separate cooling loop for coils.
  - Probably cannot achieve PMQ field accuracy.

# Tank Diameter

- A pillbox cavity (containing no drift tubes) would have a diameter of 57 cm at 402.5 MHz.

- Drift tubes add capacitance and lower frequency.

- Must reduce tank diameter to maintain frequency.
  - SNS has D = 43 (tanks 1-2) and D = 45 (tanks 3-6)
  - Increased by ~0.5 cm for stems, post couplers, slug tuners,

- Post stabilization requires $(D - d)/2 \approx 0.95(\lambda/4)$.

  - Post couplers are quarter-wave resonators.
  - Capacitance between tip and drift tube accounts for some electrical length.
  - $(D - d)/2$ = distance from drift tube to tank wall.

# What's left to vary to optimize cells?

- Face angle $\alpha_f$
  - Can increase as cells lengthen
  - Larger $\alpha_f$ decreases gap and improves T
- Nose radii $R_i$ , $R_o$ and flat F
  - Small radii improves T, but increases $E_{peak}$
  - $R_i = R_o/3$ optimum for low $E_{peak}$
  - F also helps control $E_{peak}$
- Gap g
  - Usually vary g to tune the cell
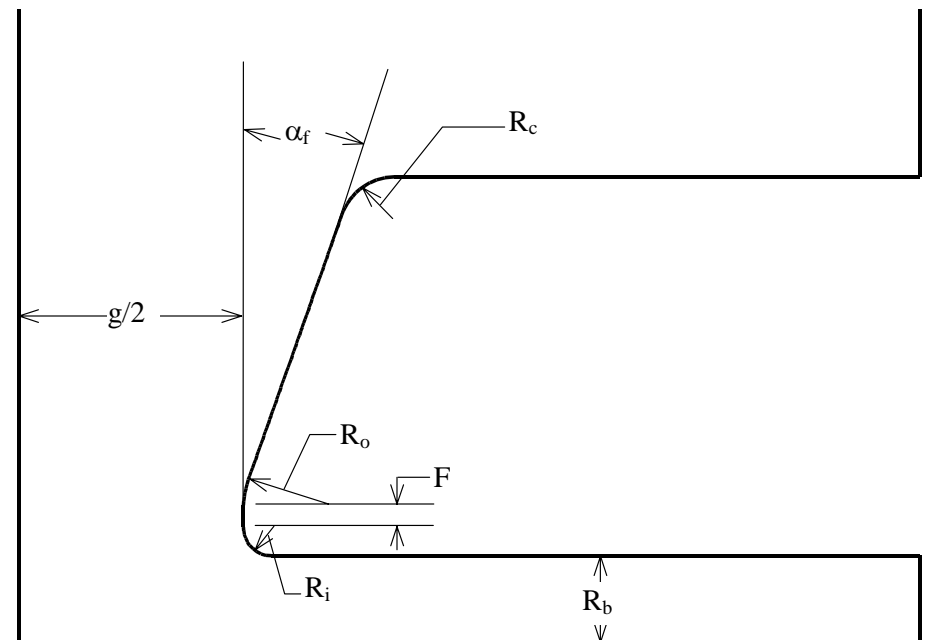
# Constraints on Peak Surface Fields

- When designing a cell geometry, one does not have complete freedom to choose many geometric dimensions.
- In addition, there are practical limits on the peak surface fields.
- Large surface magnetic fields lead to large power densities.
  - Usually not an issue, except for CW applications.
  - Hard to cool drift tubes that dissipate more than ~20 W/cm$^2$.
  - Use lower $E_0$.
- Largest surface electric fields occur on the drift-tube nose.
  - Conservative designs do not exceed ~1.6 Kilpatrick. (SNS is 1.3.)
  - Typically, ZT$^2$ continues to increase as $E_{peak}$ increases.
- Push close to the chosen limits, then stop.

# Parmila code uses transit-time-factor data to design the detailed cell layout

- Each cell is longer than the previous cell.
  - (exaggerated here)
- Though drift tubes are asymmetric in Parmila, stems are placed in the longitudinal center of the drift tubes when manufactured.
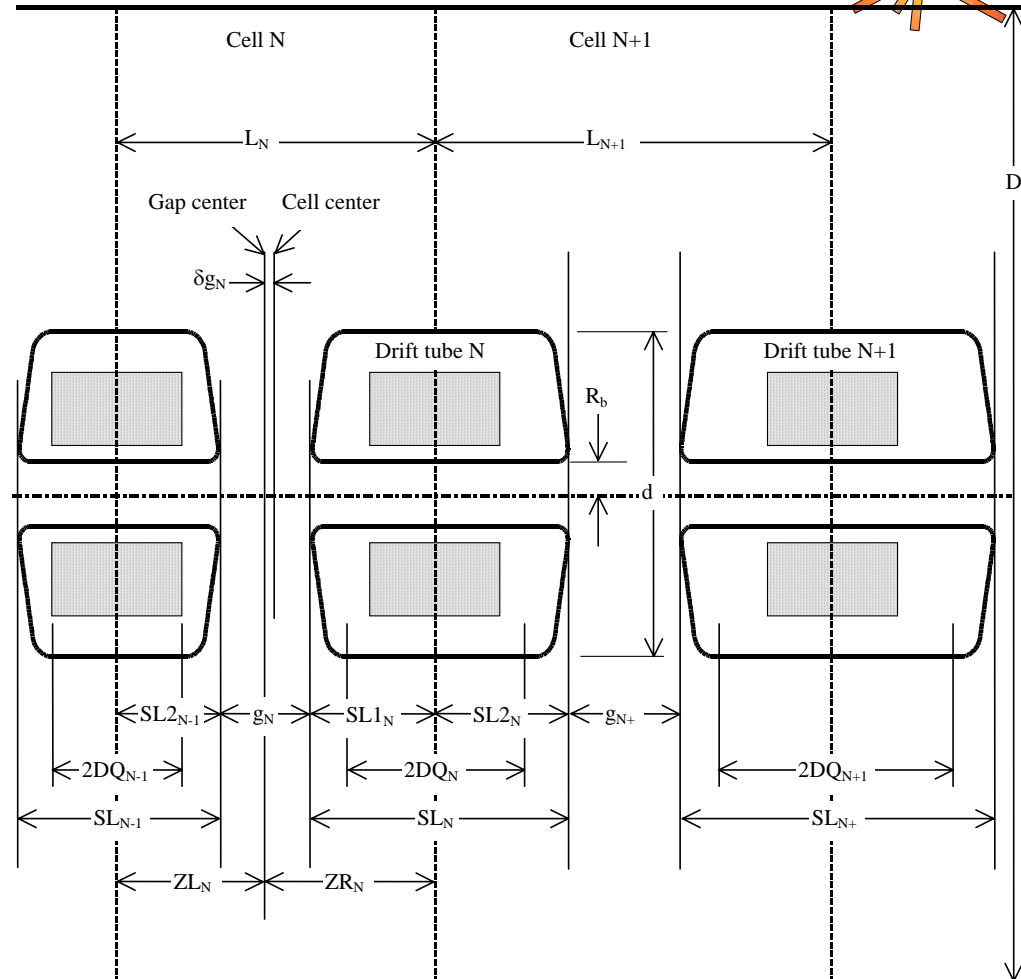
# Poisson Superfish Codes

- Static magnetic and electric fields and radio-frequency electromagnetic fields in either 2-D Cartesian coordinates or axially symmetric cylindrical coordinates.

- Uses triangular mesh fitted to the boundaries of different materials in the problem geometry.

- Original development in the 1960s by Ronald Holsinger and Klaus Halbach.

- Major improvements and additions in the mid 1990s by Lloyd Young and James Billen.

- Windows version now supported by Los Alamos Accelerator Code Group (laacg@lanl.gov).

# Program DTLfish

- Single program incorporates several Poisson Superfish codes to tune DTL cells.
  - Automesh - Triangular mesh generator
  - Fish – RF field solver
  - SFO – Postprocessor, cavity figures of merit, transit-time factors
- DTLfish runs Superfish repetitively to tune each cell to target frequency.
  - Can adjust tank diameter, drift-tube diameter, gap, or face angle.
  - Up to 100 jobs per input file.
- DTLcells – Companion program generates DTLfish input file containing all cells from Parmila design table.

# Properties of SNS DTL Tank 1

- Length = 4.1523 m, Diameter = 43.44 cm
- Drift-tube diameter = 9.0 cm
- 60 cells, 59 drift tubes, 19 post couplers
- Energy gain = 5.023 MeV
- Stored energy = 4.781 J
- Cavity power = 0.339 MW
- Beam power = 0.130 MW
- $ZT^2$ = 28.22 MW/m
- Unloaded Q (measured) = 39,148
- df/dT tank = +1.296 kHz/deg C
- df/dT drift tube = -8.681 kHz/deg C
- df/dT uniform T change= -7.385 kHz/deg C
- Eff. expansion coeff =18.348 x $10^{-6}$/deg C
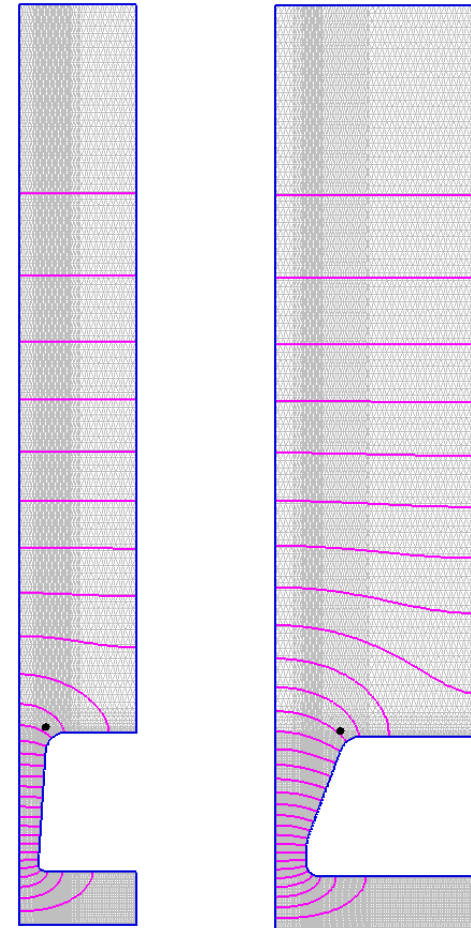
# Properties of SNS DTL Tank 2

- Length = 6.0634 m, Diameter = 43.4 cm
- Drift-tube diameter = 9.0 cm
- 48 cells, 47 drift tubes, 23 post couplers
- Energy gain = 15.362 MeV
- Stored energy = 16.767 J
- Cavity power = 1.058 MW
- Beam power = 0.397 MW
- $ZT^2$ = 45.25 MW/m
- Unloaded Q (measured) = 42,790
- df/dT tank = +0.452 kHz/deg C
- df/dT drift tube = -7.443 kHz/deg C
- df/dT uniform T change= -6.991kHz/deg C
- Eff. expansion coeff =17.370 x $10^{-6}$/deg C
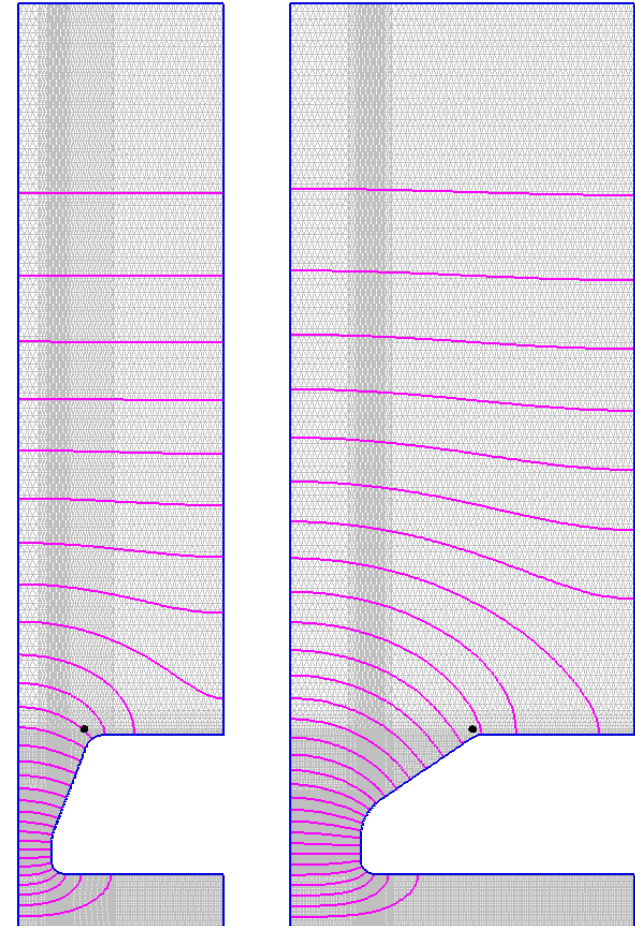
# Properties of SNS DTL Tank 3

- Length = 6.3241 m, Diameter = 45.38 cm
- Drift-tube diameter = 11.0 cm
- 34 cells, 33 drift tubes, 16 post couplers
- Energy gain = 16.880 MeV
- Stored energy = 21.84 J
- Cavity power = 1.277 MW
- Beam power = 0.597 MW
- $ZT^2$ = 43.54 MW/m
- Unloaded Q (measured) = 47,266
- df/dT tank = -1.375 kHz/deg C
- df/dT drift tube = -4.767 kHz/deg C
- df/dT uniform T change= -6.142 kHz/deg C
- Eff. expansion coeff =15.260 x $10^{-6}$/deg C
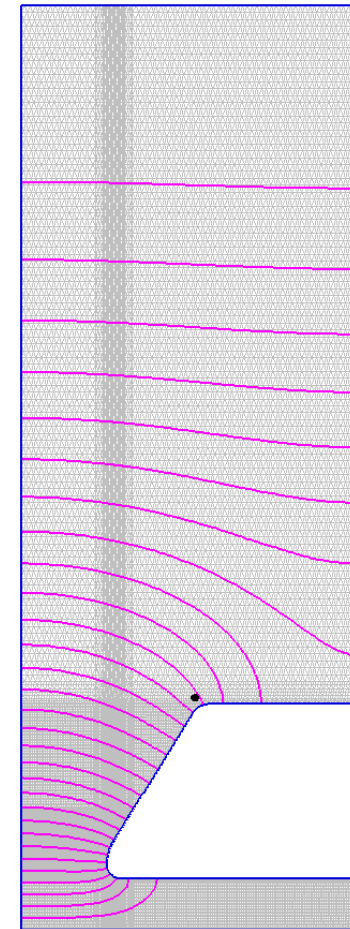
# Properties of SNS DTL Tank 4

- Length = 6.4105 m, Diameter = 45.38 cm
- Drift-tube diameter = 11.0 cm
- 28 cells, 27 drift tubes, 27 post couplers
- Energy gain = 16.771 MeV
- Stored energy = 22.225 J
- Cavity power = 1.292 MW
- Beam power = 0.593 MW
- $ZT^2$ = 41.91 MW/m
- Unloaded Q (measured) = 48,102
- df/dT tank = -1.624 kHz/deg C
- df/dT drift tube = -4.413 kHz/deg C
- df/dT uniform T change= -6.038 kHz/deg C
- Eff. expansion coeff =15.000 x $10^{-6}$/deg C
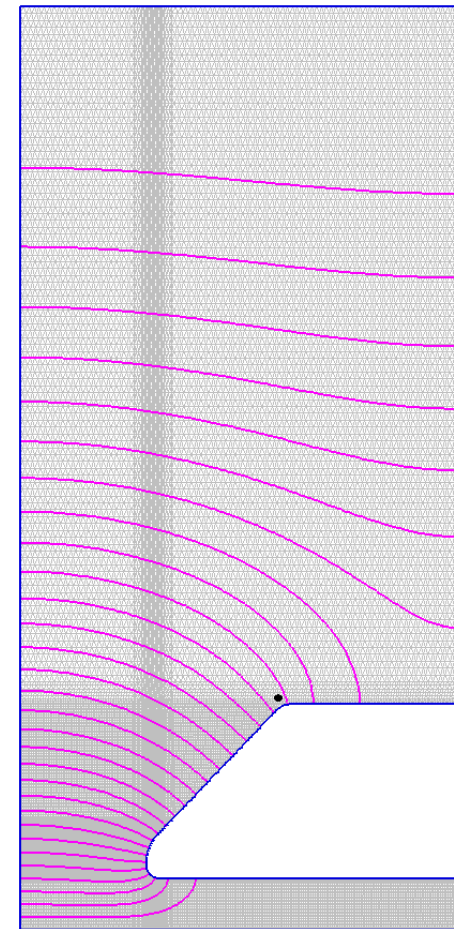
# Properties of SNS DTL Tank 5

- Length = 6.2941 m, Diameter = 45.38 cm
- Drift-tube diameter = 11.0 cm
- 24 cells, 23 drift tubes, 23 post couplers
- Energy gain = 16.284 MeV
- Stored energy = 22.046 J
- Cavity power = 1.284 MW
- Beam power = 0.576 MW
- $ZT^2$ = 40.83 MW/m
- Unloaded Q (measured) = 48.027
- df/dT tank = -1.773 kHz/deg C
- df/dT drift tube = -4.199 kHz/deg C
- df/dT uniform T change= -7.385 kHz/deg C
- Eff. expansion coeff =14.836 x $10^{-6}$/deg C
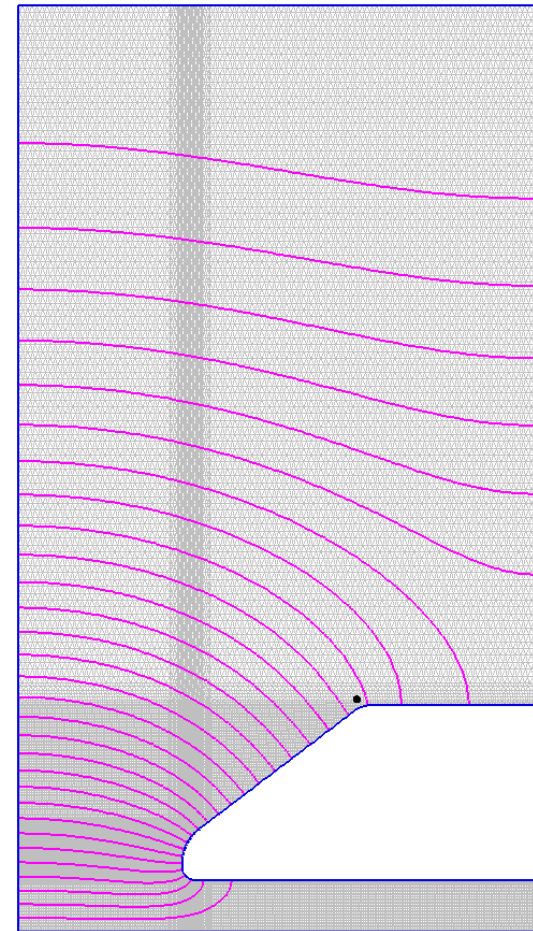
# Properties of SNS DTL Tank 6

- Length = 6.3454 m, Diameter = 45.38 cm
- Drift-tube diameter = 11.0 cm
- 22 cells, 21 drift tubes, 21 post couplers
- Energy gain = 14.306 MeV
- Stored energy = 21.474 J
- Cavity power = 1.254 MW
- Beam power = 0.506 MW
- $ZT^2$ = 39.03 MW/m
- Unloaded Q (measured) = 47,600
- df/dT tank = -1.863 kHz/deg C
- df/dT drift tube = -4.068 kHz/deg C
- df/dT uniform T change= -5.931 kHz/deg C
- Eff. expansion coeff =14.737 x $10^{-6}$/deg C
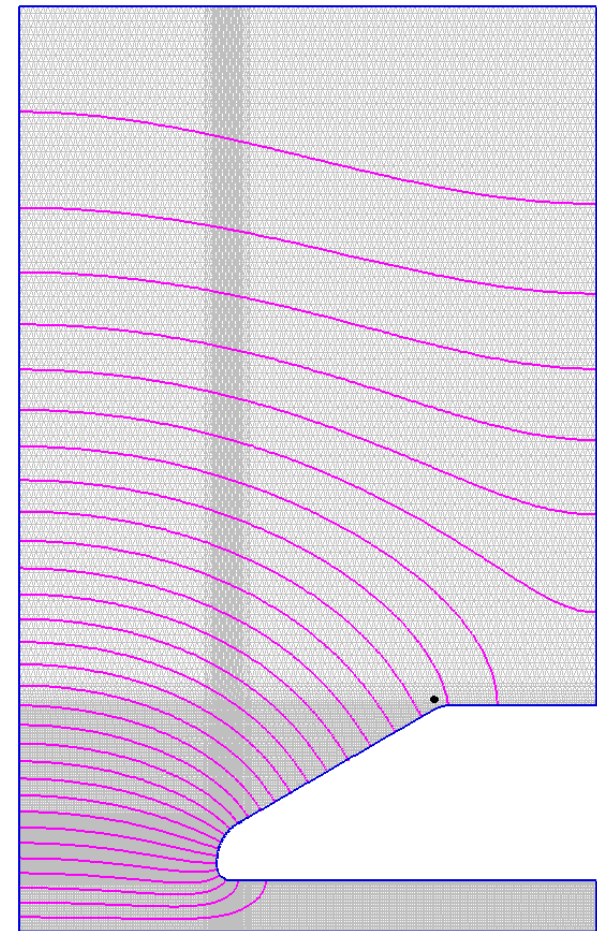
# Static Frequency Errors

- Manufacturing tolerances cause uncertainties in the frequency of the assembled DTL tank.

- Evaluate frequency effects in case of <u>systematic</u> errors in important dimensions (tank diameter, drift-tube lengths, diameters, face angles) to define realistic tolerances.

- Provide a means to statically tune over the expected range of frequency errors, even if they all contribute with like sign.
  - SNS uses 12 slug tuners per tank (9 in tank 1) evenly spaced along the tank bottom.
  - Older DTLs used "tuning bars" bolted next to the stems.
  - Slug tuners are much preferred and also allow adjustment of the longitudinal field distribution before post couplers are installed.

# SNS DTL Frequency Budget

- Slug tuners (11.4-cm diameter, 8 cm long) provide total tuning range of ~2.1 MHz.
  - All tuners moved together.
  - Tuner nominal position is inserted halfway.
- Tank radius tolerance = $\pm$0.010 inch gives $\Delta f = \pm$0.3 MHz.
- Drift-tube length and face-angle errors are more important in earlier tanks with shorter gaps. The following errors would each produce $\Delta f = \pm$0.25 MHz:
  - Tank 1.  $\Delta L = \pm$0.0012 inch, $\Delta\alpha_f = 0.07$ degree
  - Tank 3.  $\Delta L = \pm$0.0054 inch, $\Delta\alpha_f = 0.25$ degree
  - Tank 6.  $\Delta L = \pm$0.0086 inch, $\Delta\alpha_f = 0.47$ degree

# Dynamic Frequency Control

- In operation, resonant frequency must be 402.5 ± 0.01 MHz.
  - Some older DTLs used movable slug tuners.
  - SNS uses cooling-water temperature to maintain resonance.
  - Varying rf power distribution makes cavity temperature anisotropic.
- Because drift tubes are copper and tanks are steel (copper plated), each tank responds differently to temperature changes.
  - df/dT for tank temperature only changes sign from tank 2 to tank 3!
  - Effective coefficient of thermal expansion (in units of $10^{-6}$/deg C) ranges from 18.3 to 14.7 for tanks 1 to 6.
  - Corresponds to -7.3 kHz/deg C for tank 1 and -5.9 kHz/deg C for tank 6.

# Refinement in the DTL Design

- A multiple-tank DTL has mismatches (longitudinally and transversely) because of missing accelerating gaps between tanks.
  - Mismatches in focusing strength can degrade performance.
  - SNS has only $1-\beta\lambda$ drifts to minimize the effect, but it is still observable.
- We can compensate for the missing gap by increasing the focusing in gaps near a missing gap.
  - Longitudinal focusing term and the transverse rf defocus term are both proportional to $E_0 T\sin(-\phi)$.
  - Changing $E_0$ is difficult to achieve in a short length, but it easy to the synchronous phase $\phi$ more negative by moving the gap upstream.
  - But, we must move the gaps in a way that does not detune the tank.
- To make up for loss of acceleration, average $E_0$ increased ~1%.

# Final Design of the DTL Tanks
# Eliminates Mismatch Between Tanks

- Requirements satisfied when creating a new drift-tube table:

  - Final energy unchanged.

  - Longitudinal focusing strength in last cell unchanged.

  - Overall DTL length unchanged.

  - Same number of cells in each tank.

- Synchronous phase adjustments in three cells on both sides of a tank interface compensates for the missing rf gap.

  - Corrects both longitudinal focusing and transverse rf defocusing.

- Cavity field $E_0$ increased by ~1% to make up for the lost acceleration.

  - Tank lengths change a few mm.

  - Drift-tube dimensions change only slightly.

# Cell Length Adjustment
# Does Not Detune the Tank
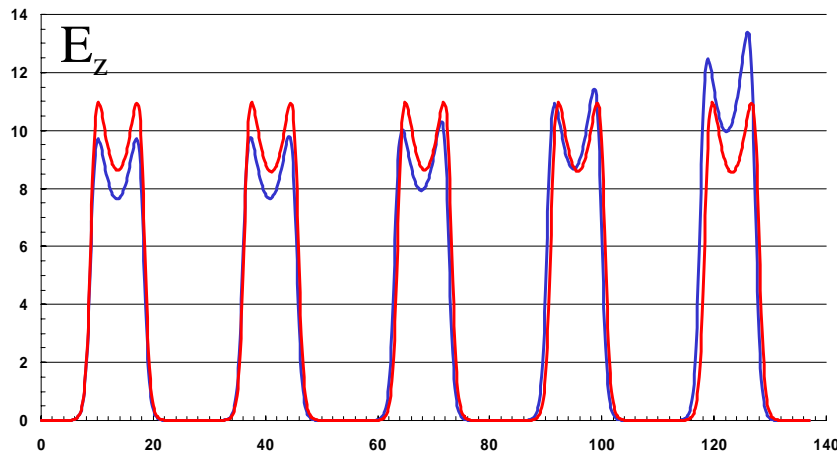


These Superfish calculations show resulting fields for two methods of shifting the last three gaps upstream (to the left)
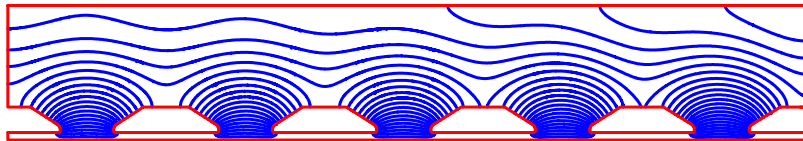
⬅ Moving the gap within a 360° cell detunes 5-cell example –400 kHz, and introduces a field tilt (blue curve).
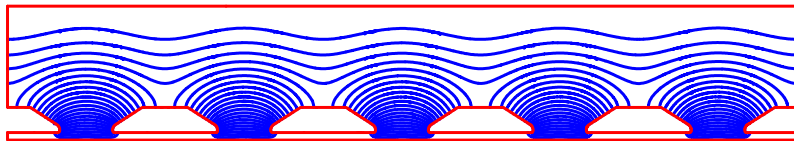
⬅ Making cells shorter than 360° preserves cell symmetry, tuning, and field flatness (red curve).

# Spatial Profile and Longitudinal Phase Space at the end of the DTL



SNS Linac                                                                    Los Alamos
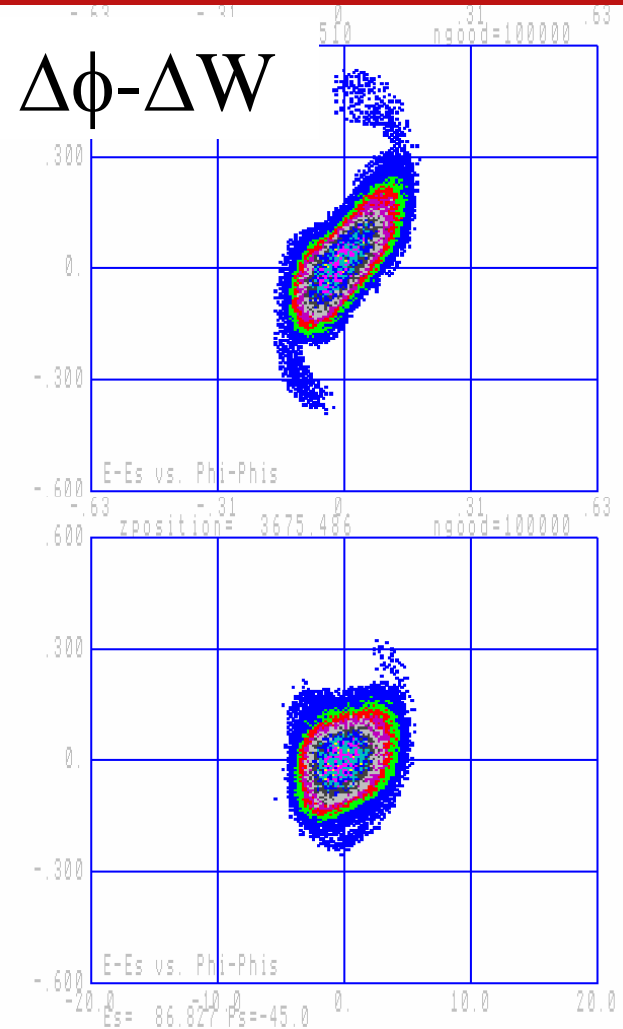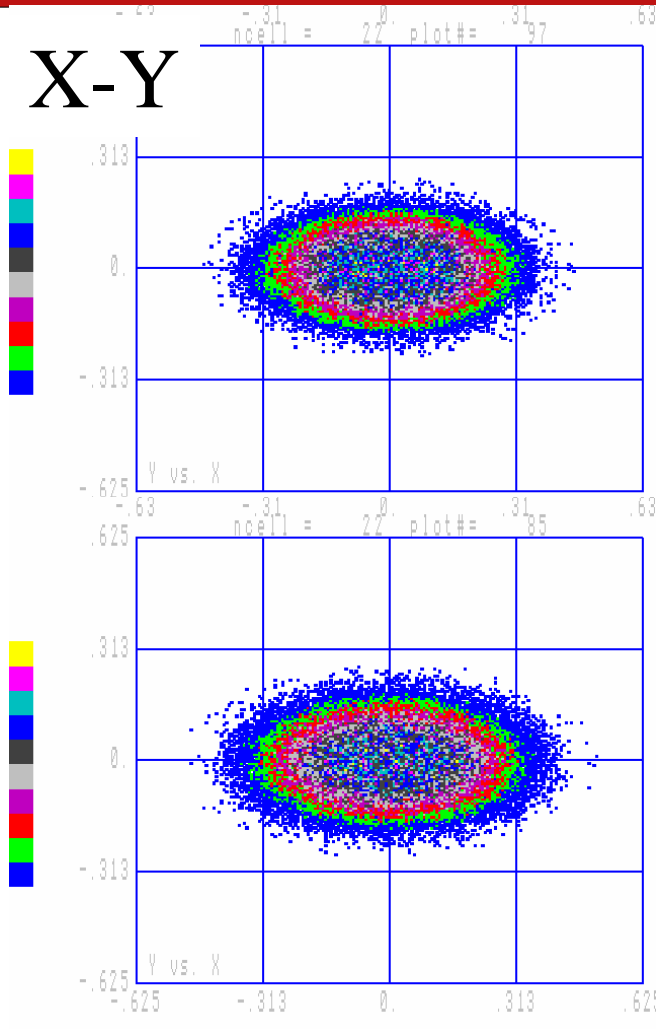
# DTL Cold Model to Verify the Cavity Design
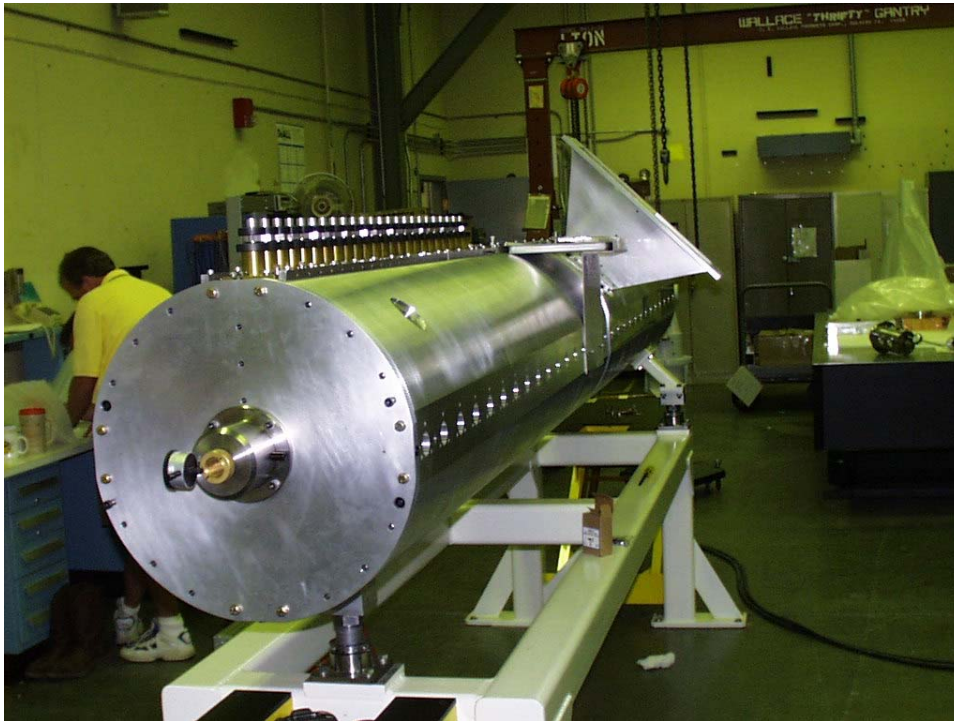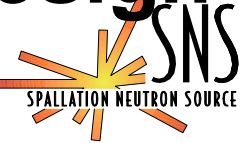
# Tank 1 Cold Model
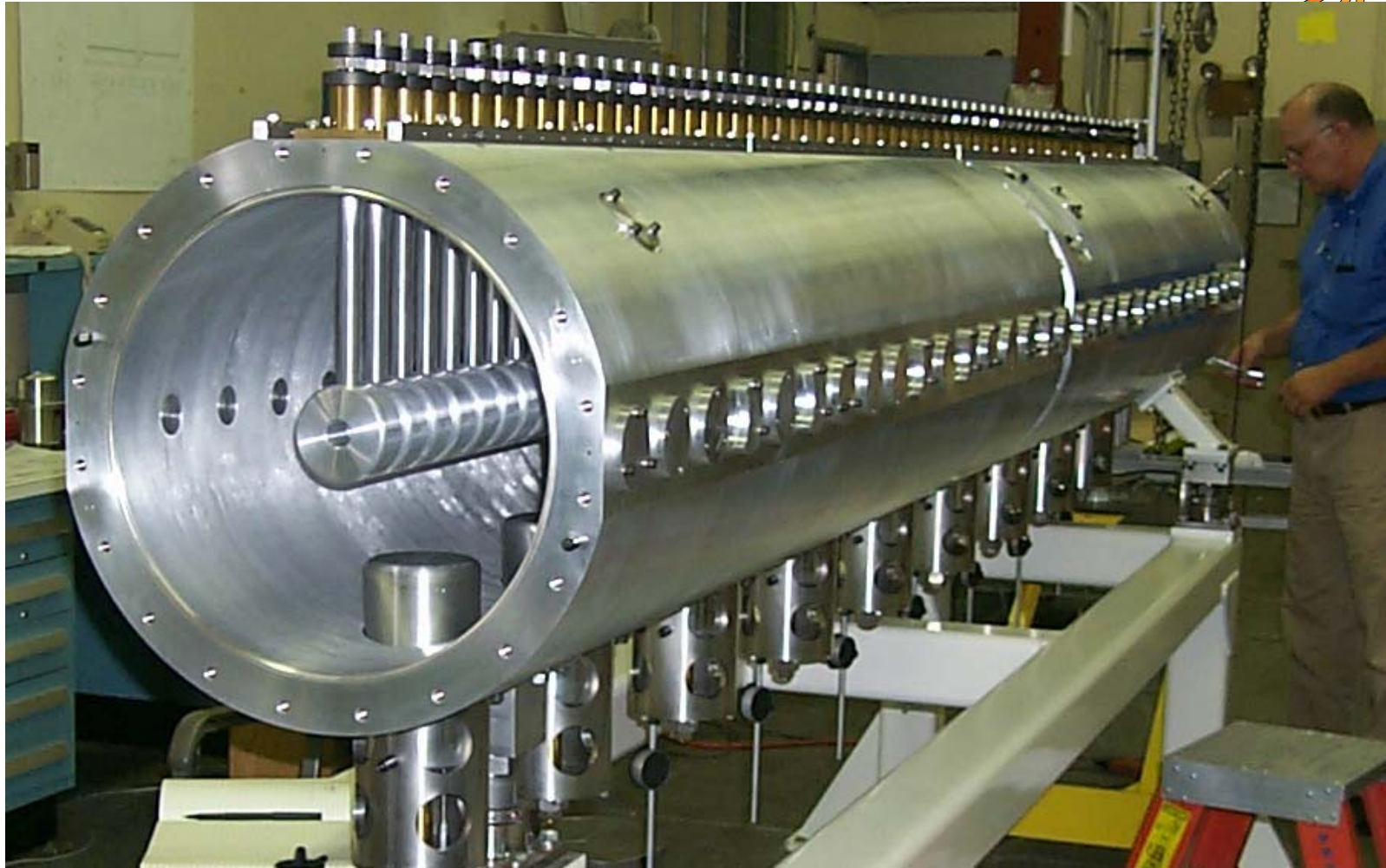
# Reasons for Building an Aluminum Model

- Provides a check on RF cavity calculations.
  - Verify that the tank frequency is correct.
  - Test stabilization using post couplers.
  - Measure the range of the slug tuners.
  - Cheap insurance that the copper structures will be tunable.
- Develop and test the measurement hardware.
  - Bead perturbation technique to measure fields.
  - Coupling measurements for sizing the iris.

# Superfish Cylindrically Symmetric Model



"slug tuner"



End-wall
tuning ring
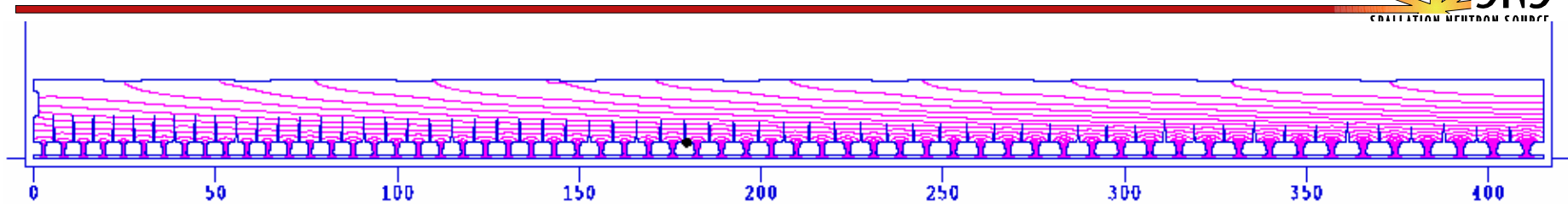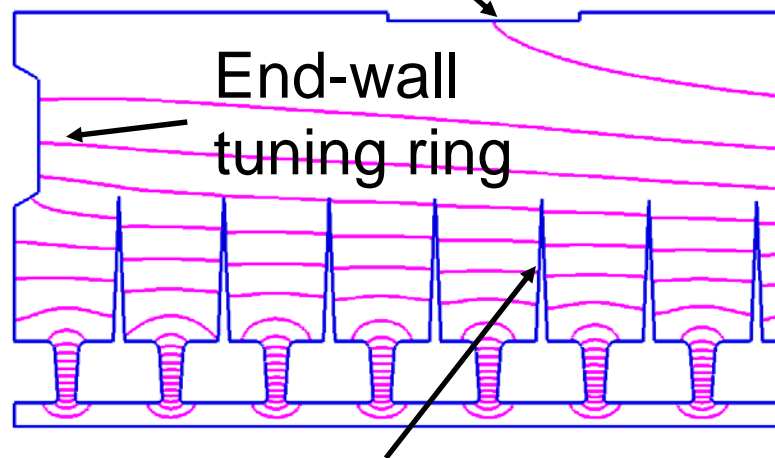
"stem + post coupler"

- Build a full-tank Superfish model of the a DTL.

- Add cylindrically symmetric features that reproduce frequency effects of stems, post couplers, and slug tuners at their longitudinal positions.

- Compare $E_z(z)$ to beadpull measurements.

# Field Measurements Agree with Symmetric-Model Calculations

Without no end-wall tuner the slight field ramp is from stems, which raise frequency of short cells more than long cells.

Wiggles from drift tube misalignments are also reproduced in the mathematical model.

The end-wall tuner increases the field ramp.



Superfish model compared with beadpull measurements

# Ring Tuner Establishes Ramped Field Distribution in Tank 1

- Post couplers remain nominally unexcited when they stabilize the tank's natural field distribution

"distributed" slug tuner (not realizable)



EO from Superfish runs at frequencies 402.400 compared to design

no ring

design field with tuning ring

# DTL Manufacturing and Tuning
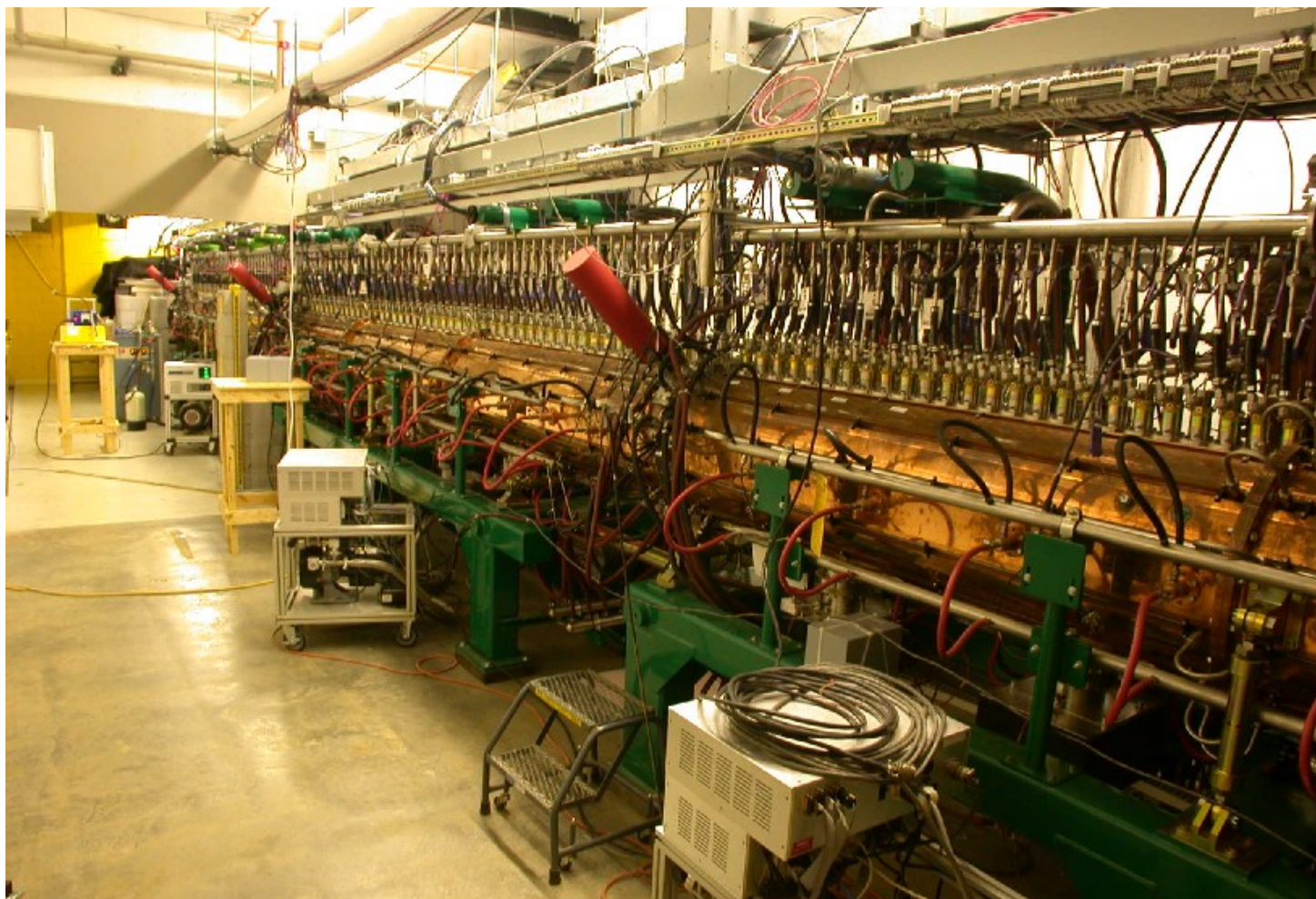
# Steps in DTL Installation

- Assemble tank sections and install drift tubes.

- Align drift tubes using laser tracker.

- Measure fields and stability using bead perturbation technique.
  - At this stage tank is equipped with adjustable aluminum slug tuners and post couplers.

- Measure final tuned dimensions of the aluminum parts.

- Finish machine copper (non-adjustable) slug and post couplers.

- Check fields and stability.

- Measure waveguide coupling factor and increase the iris size for design coupling.

# Copper Plating at GSI, Darmstadt

# Prepare tank sections after copper plating

- Steel tanks sections are machined in California, copper plated at GSI in Darmstadt.

- Three sections per DTL tank (2 in DTL tank 1)

# Tank O-ring Groove Modified
# After Copper Plating

- **Tank interface flange o-ring grooves have been modified for higher compression with larger cross-section o-rings.**

- **The measured dry-seal leak rates have been reduced from ~$10^{-5}$ torr-l/sec to less than ~$10^{-9}$ torr-l-sec.**



**DTL Tank Section**



.075 Increased Groove Width

.009 Increased Groove Depth

24.0° ±.5°

R (9.310)
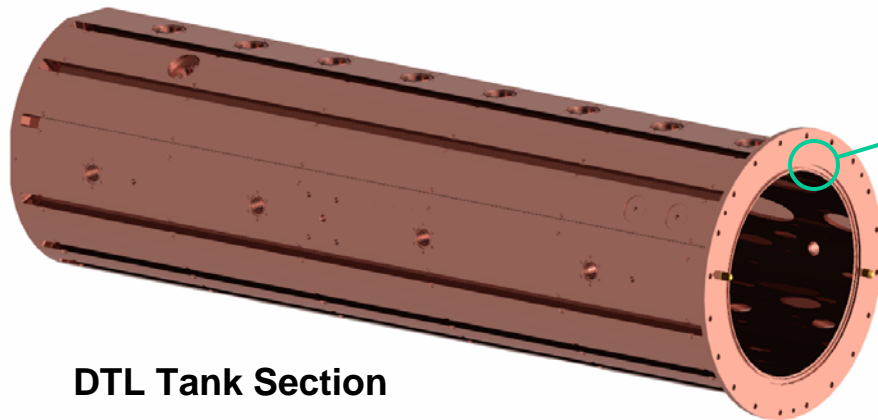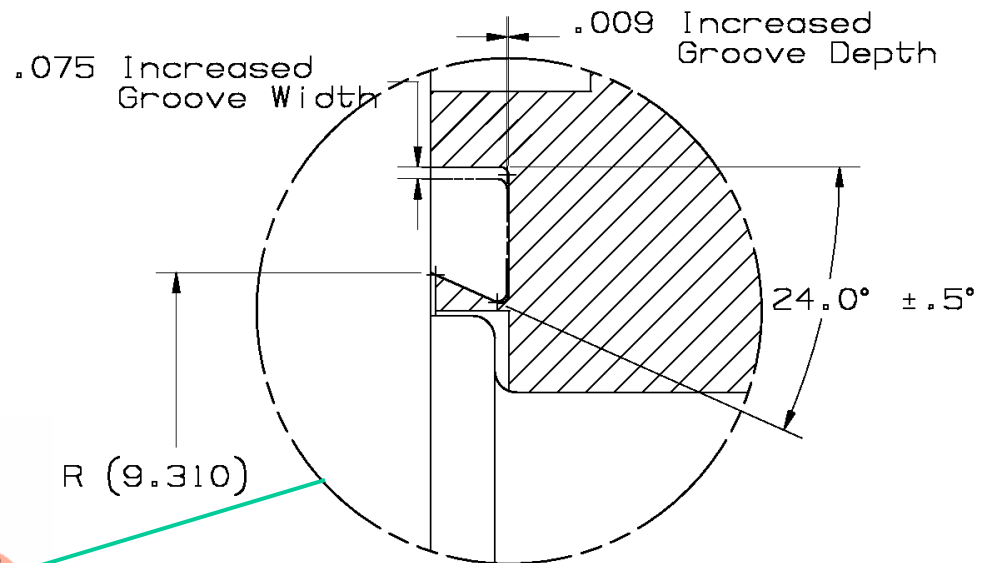
# Nickel Plating DTL Tank O-Ring Groove

- Larger o-ring and more compression than initial design allow dry assembly.

- Grooves were enlarged after plating of the tanks.

- Brush plating nickel onto re-machined groove to prevent rusting.

# DTL Tank Leak Testing in RATS

# DTL Tank Assembled on Frame
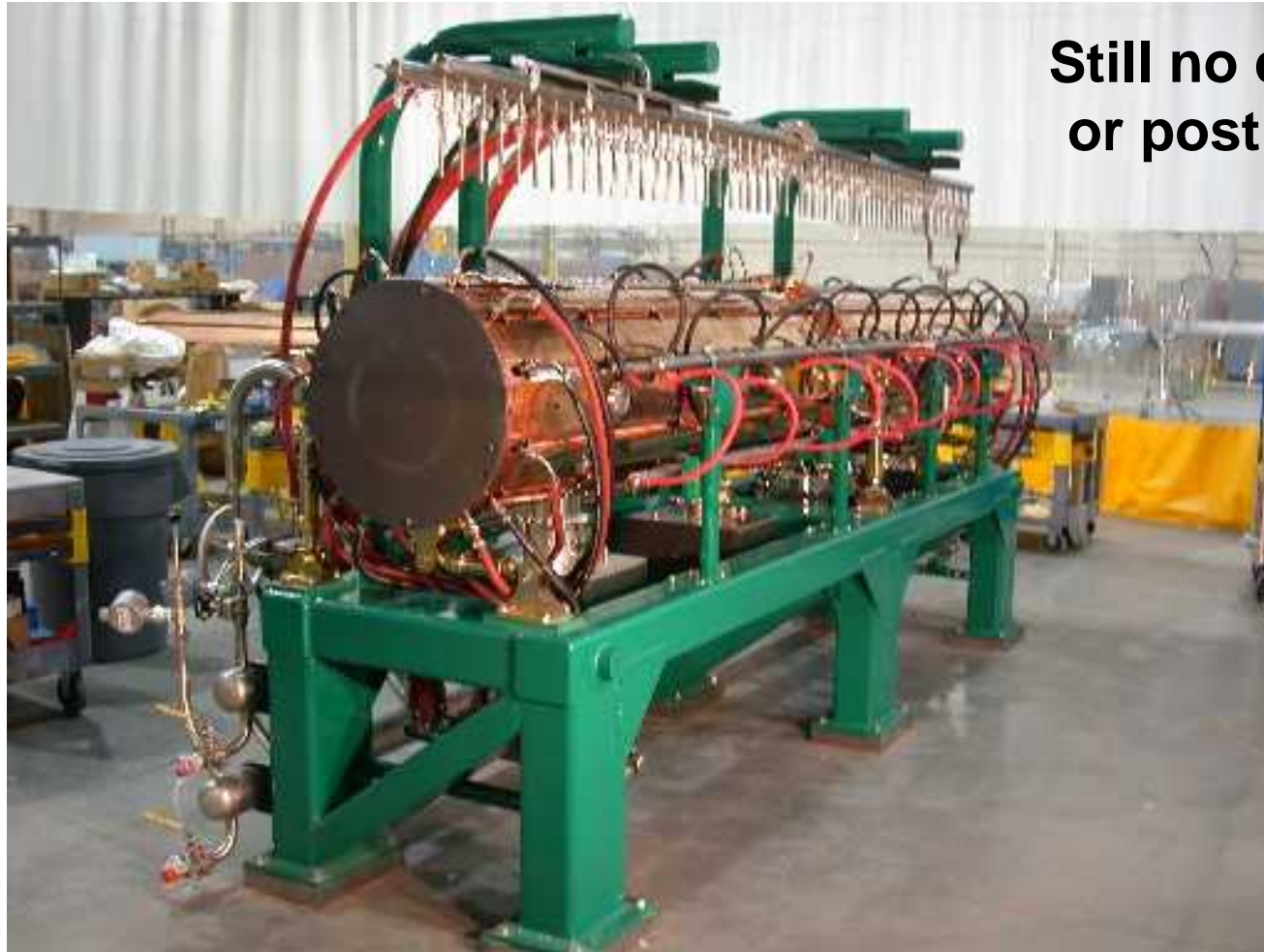
**Still no drift tubes
or post couplers**

# DTL Tank with Cooling Manifold Installed

# Preparing Drift Tubes for Installation

Drift tubes have a key slot that only allows quadrupole magnet insertion with the correct polarity. A final check is still prudent.
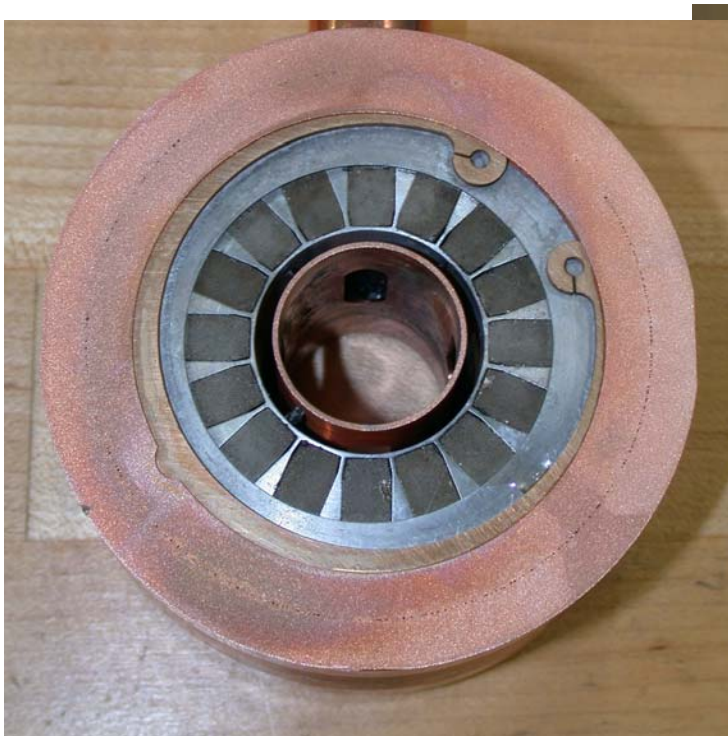
# All Drift Tubes Undergo Final Leak Testing

- Bore tube is open to vacuum.

- Water channels are pressurized with He gas while drift tube body is in vacuum chamber.

- These tests on tank-3 and tank-1 drift tubes uncovered major problems with the manufacturing process (more about this later).

# Rotating Coil Measures PMQ Field Strength and Multipole Components
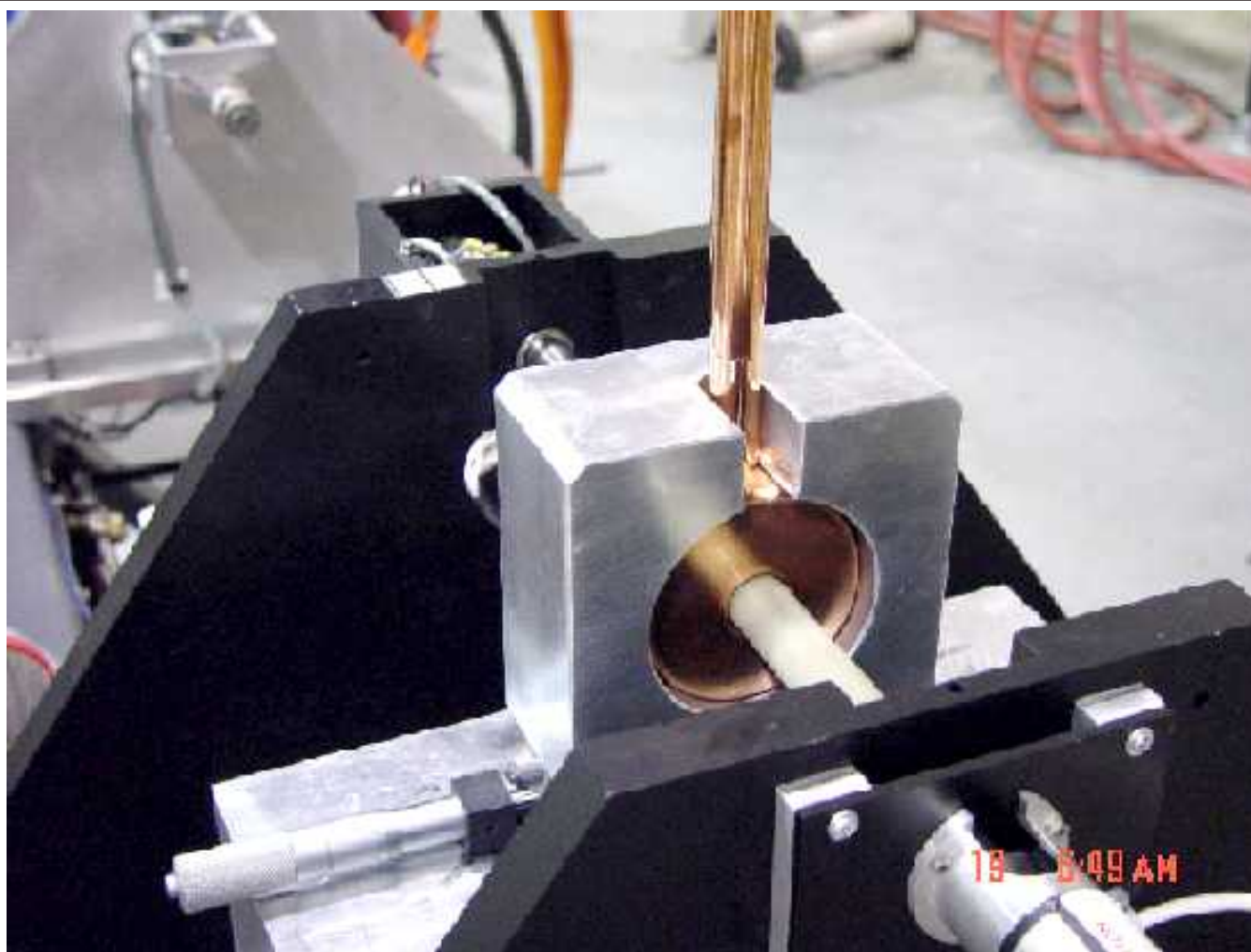
# AC Current Locates Magnetic Center

**Laser tracker measures geometric center and location of fiducials on both sides of the drift tube body.**

**Plumb wire**

**Corner cube**
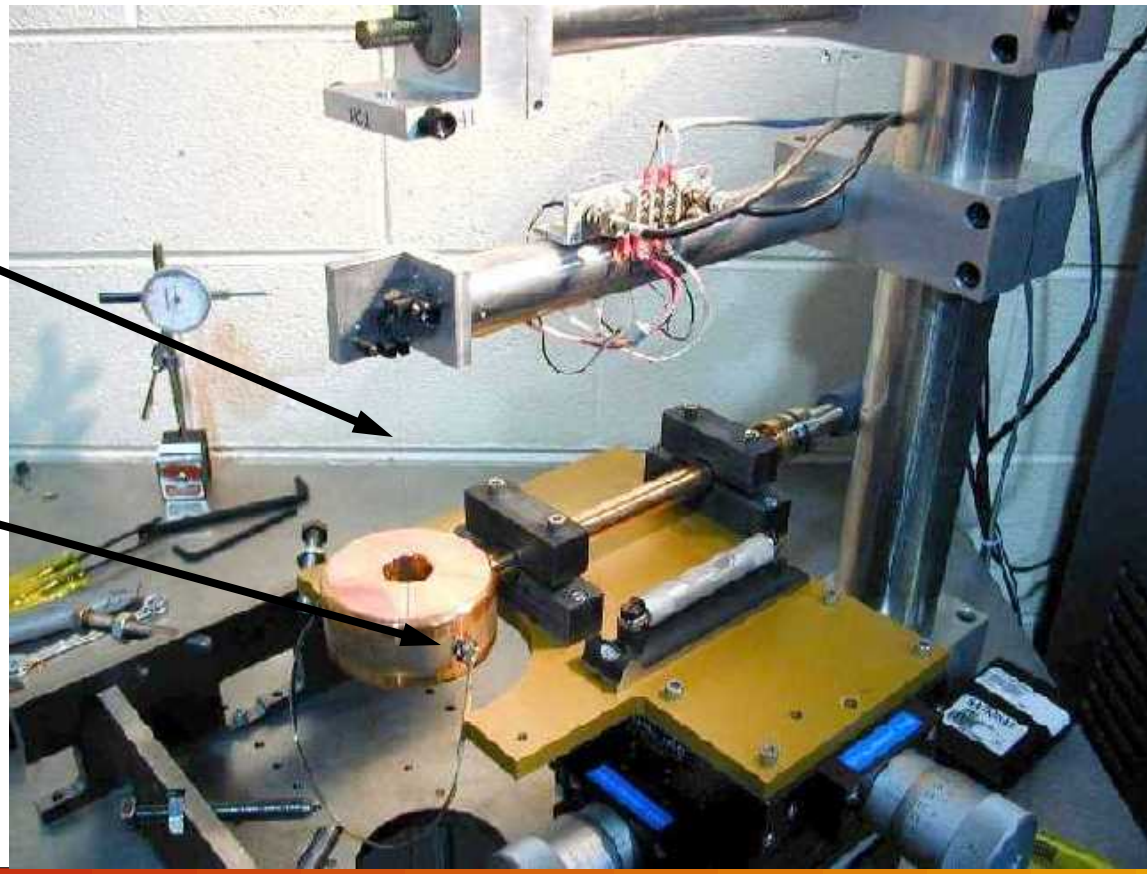
# Installing drift tubes
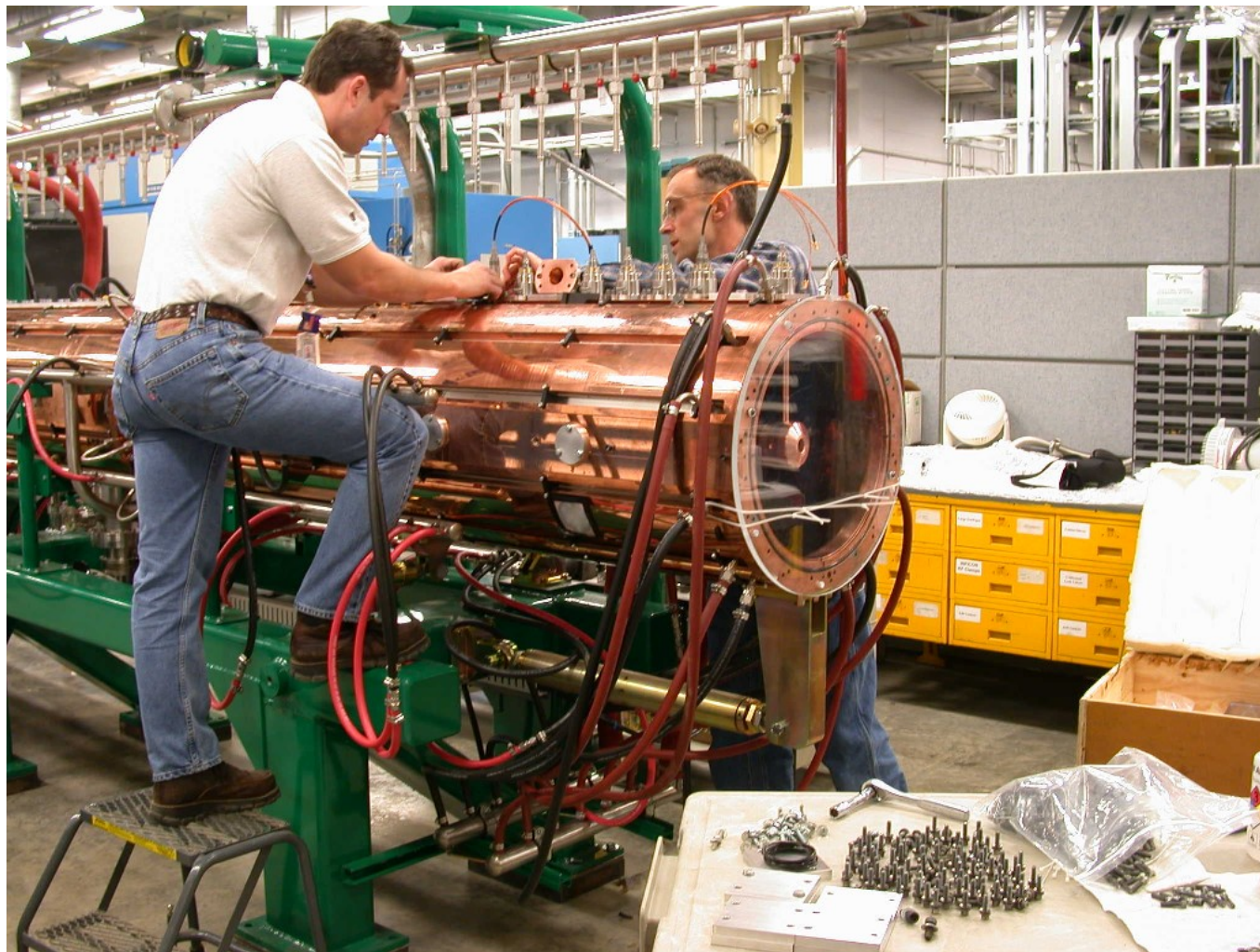
# Drift Tube Insertion from Tank End

**Far from an end, drift tubes are inserted through slug-tuner or pumping ports on the tank bottom.**

# Drift Tube Stem Has Double O-Ring and RF Seal

**Plastic wire wrap holds RF seal in place until seal is captured in the hole.**

# Adjusting Vertical Position of a Drift Tube

Adjusting screw is locked in place after alignment completed.

# Leak Test of Space Between O-Rings

# Aligning drift tubes with laser tracker

# Drift Tube Alignment

# Two Corner Cube Reflectors
# Held onto Drift Tube

**Corner cubes (in spherical tooling ball) fit into conical holes in drift tubes.**
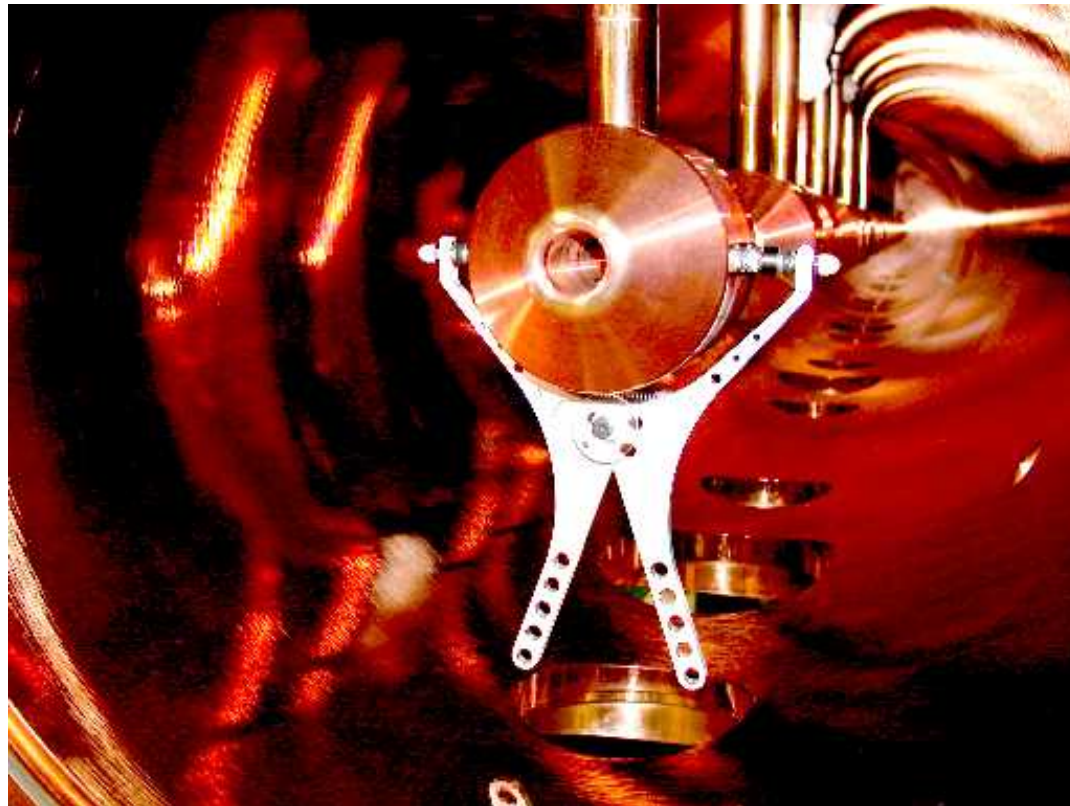
# Adjusting Drift Tube Transversely

# Stiffener Installed After Alignment

# DTL Tuning Activities

# Tuning Crew in Front-End Building

# Beadpull measurements

# Beadpull Applies Slater-Perturbation to Measure Axial Field Distribution

- A small object introduced into a resonant cavity disturbs the field distribution, and causes a shift in the resonant frequency.
  - The magnitude of the frequency shift is proportional to the stored energy displaced by the object.
  - For some shapes (e.g. spheres, cylinders), one can compute analytically a "shape factor" that accounts for distortion of the initial unperturbed field distribution.
  - For a sphere of volume $\Delta V$ in a cavity with total stored energy U:

$$\frac{\Delta \omega_0}{\omega_0} = -\frac{3\Delta V}{4U}\left[\frac{\varepsilon_r - 1}{\varepsilon_r + 2}\varepsilon_0 E^2 + \frac{\mu_r - 1}{\mu_r + 2}\mu_0 H^2\right]$$

# Application to a Metal Sphere

$$\frac{\Delta\omega_0}{\omega_0} = -\frac{3\Delta V}{4U}\left[\frac{\varepsilon_r - 1}{\varepsilon_r + 2}\varepsilon_0 E^2 + \frac{\mu_r - 1}{\mu_r + 2}\mu_0 H^2\right]$$

- For axial field measurements, we pull a hollow aluminum sphere through the cavity at constant speed, while a network analyzer under LabView control records the frequency at regular intervals.

  – For perfect conductors, $\varepsilon_r \to -j\infty$, and $\mu_r \to 0$:

$$\frac{\Delta\omega_0}{\omega_0} = -\frac{3\Delta V}{4U}\left(\varepsilon_0 E^2 - \frac{\mu_0 H^2}{2}\right)$$

- Although the magnetic field H = 0 on axis and is small nearby, the analysis of the data does take H into account to find $E_0$.

  – Rather than compute square roots of frequency shifts (very noisy!), the analysis code finds the peak height for each gap and multiplies by $E_0/\Delta f$ computed by Superfish for each cell.

# Comparing Tank 1 Calculated and Measured Frequency Shifts

Calculated

Measured
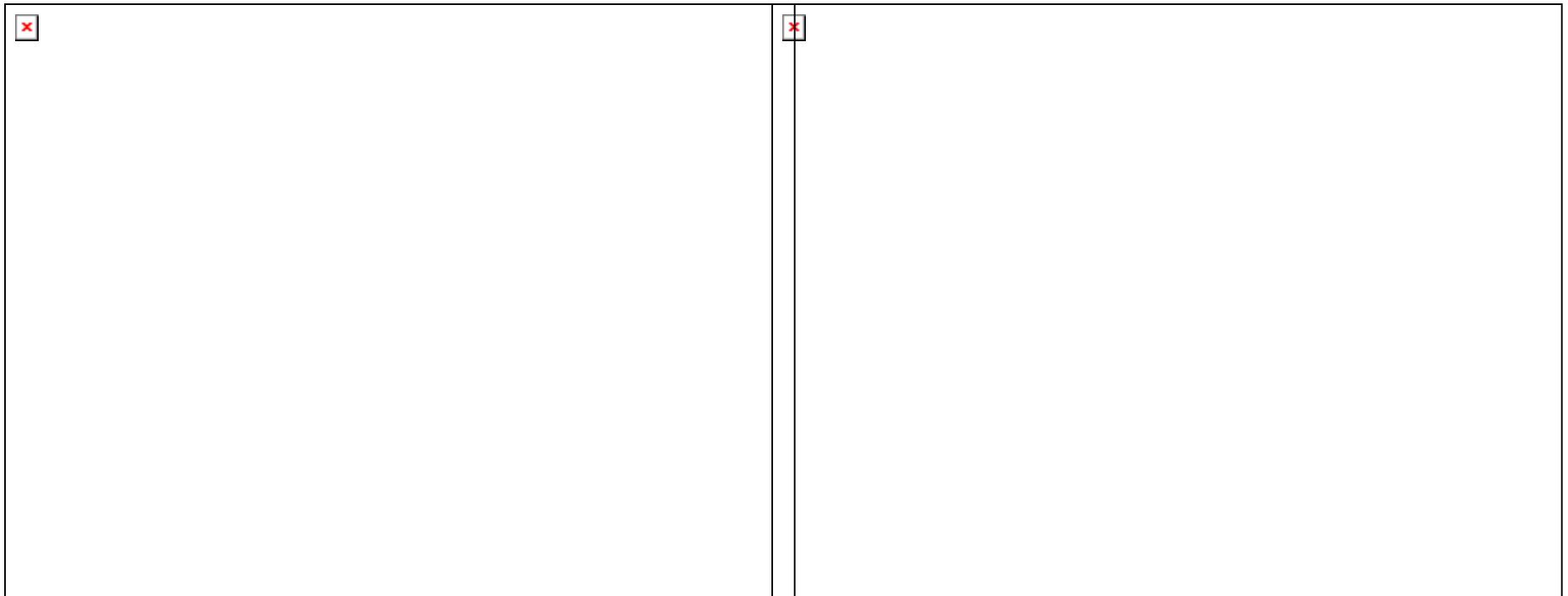
# Tank 1 Measured E₀ Divided by Design E₀
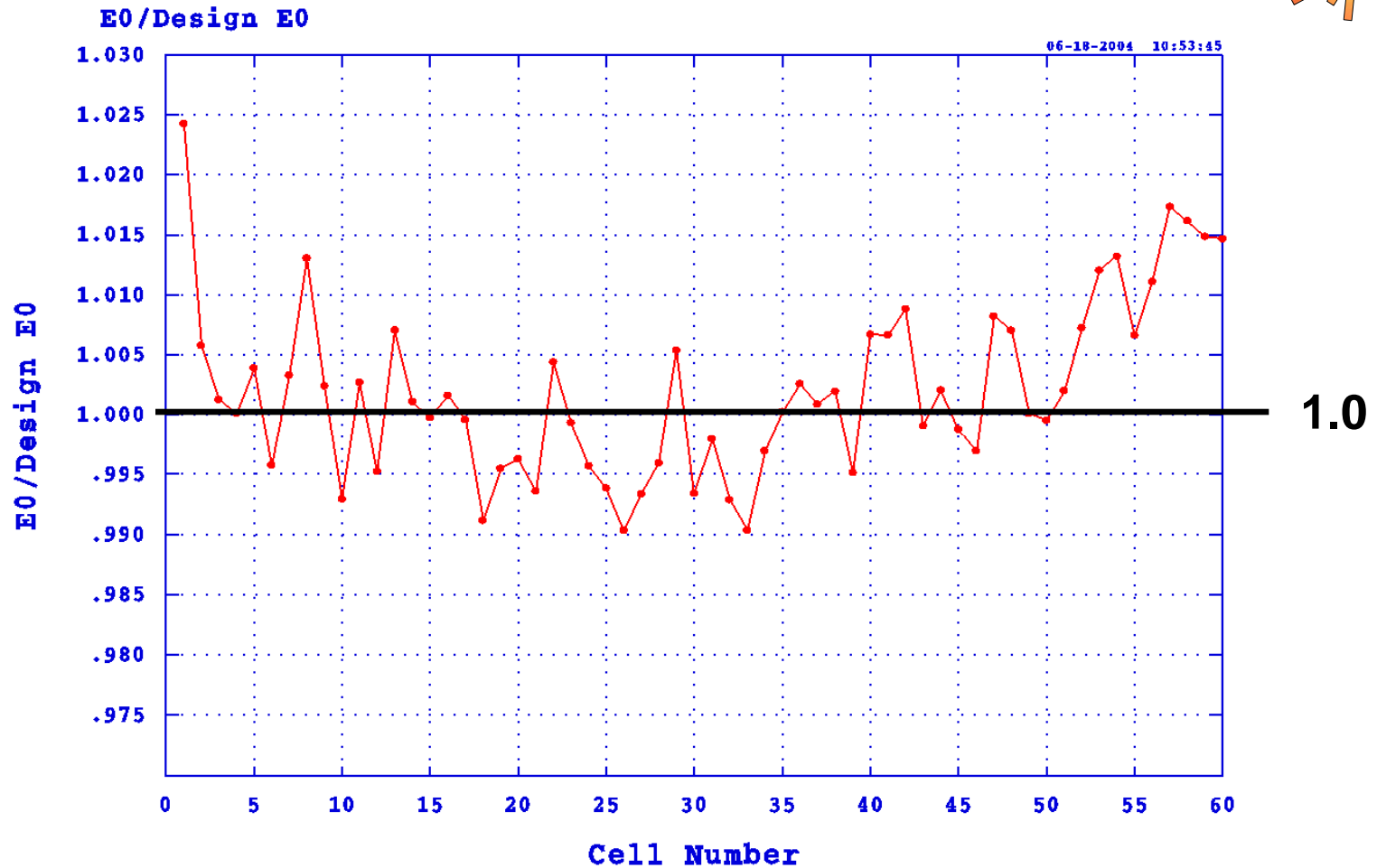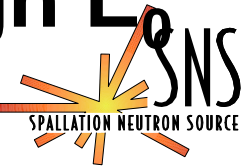
# Tilt Sensitivity Measures Field Stability

- Tilt Sensitivity measures (for every cell) the fractional change in field amplitude caused by deliberate frequency perturbations applied at the ends of the rf structure.

  - Requires two measurements (ideally at the same rf frequency) with different perturbations applied.

  - Conventional definition for each cell:

$$\text{Tilt Sensitivity} = \frac{E_{0,\text{Meas}1} - E_{0,\text{Meas}2}}{E_{0,\text{Average}}} \times \frac{1}{\Delta f_{\text{Meas}1} - \Delta f_{\text{Meas}2}}$$

$$\Delta f_{\text{Meas}1} = \Delta f_{\text{HE end cell,Meas}1} - \Delta f_{\text{LE end cell,Meas}1}$$

$$\Delta f_{\text{Meas}2} = \Delta f_{\text{HE end cell,Meas}2} - \Delta f_{\text{LE end cell,Meas}2}$$

# Applying the End-Cell Perturbations

$$\Delta f_{Meas1} = \Delta f_{HE\,end\,cell,Meas1} - \Delta f_{LE\,end\,cell,Meas1}$$

- Each beadpull measurement of a tilt-sensitivity pair may include perturbations at one end or both ends of the structure.
  - Maximize sensitivity with opposite-sign perturbations at both ends.
  - Sometimes it is not possible to apply perturbations of both signs.
- A frequency perturbation refers to a change in frequency applied to the end cell of the structure.
  - Not directly measurable. We can only see changes in frequency of the entire rf structure.
  - Analysis codes use stored-energy ratios derived from the measurement (if available) or design stored-energy ratios to compute the change applied to the individual end cell.

# E$_0$ for Two Tank-1 Perturbation Measurements

**Red: Tank Δf = -24 kHz applied at HE end**

**Green: Tank Δf = -17 kHz applied at LE end**

# Same Data Divided by Design E$_0$

**Red: Tank $\Delta f = -24$ kHz applied at HE end**

**Green: Tank $\Delta f = -17$ kHz applied at LE end**
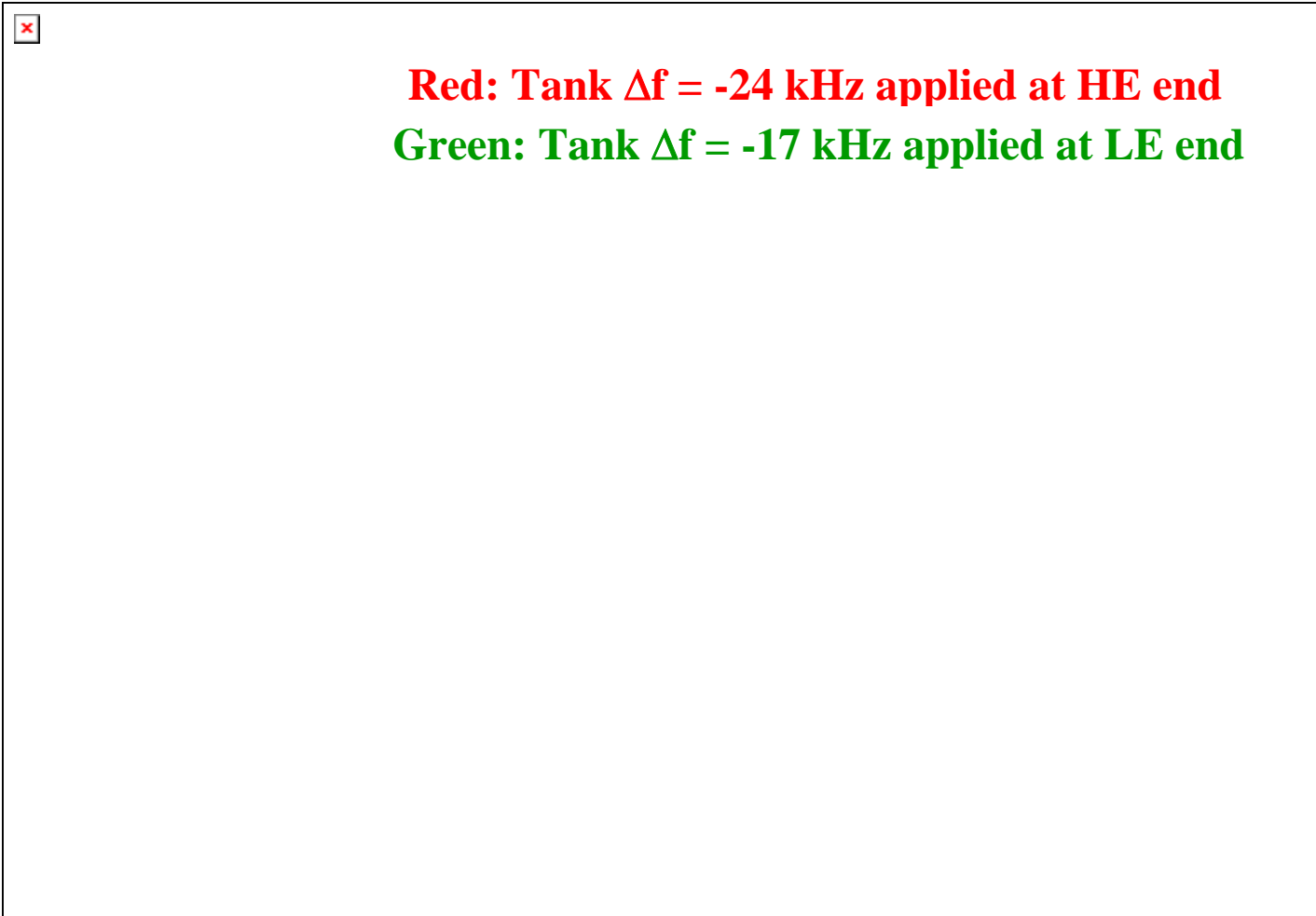
# Tilt Sensitivity Computed from Two Field Measurements
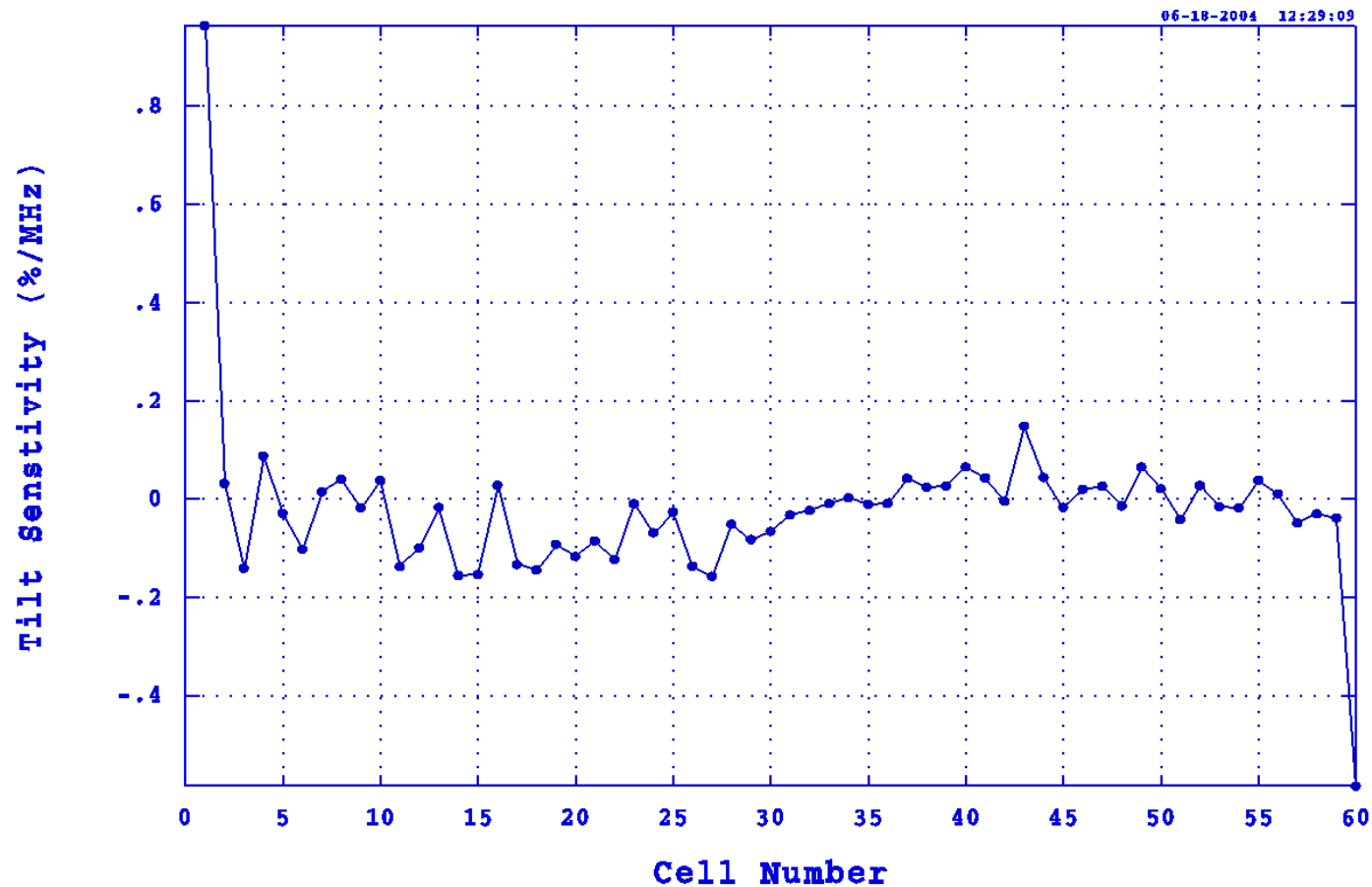


SNS Linac                                                                      Los Alamos

# Adjustable Aluminum Slug Tuners and Post Couplers

**Bend in post couplers allows adjustment of field cell to cell by rotating shaft.**

# Adjustable Aluminum Post Coupler

- Shaft slides in and out to tune frequency of the post.

- Disk on the tip increases capacitive coupling to drift-tube ends.

- Rotating the bent stem adjusts longitudinal field profile.

# Adjustable Aluminum Slug Tuner

- Raises cavity frequency as the tuner length increases.
- All tuners together provide a tuning range of ~2.1 MHz.
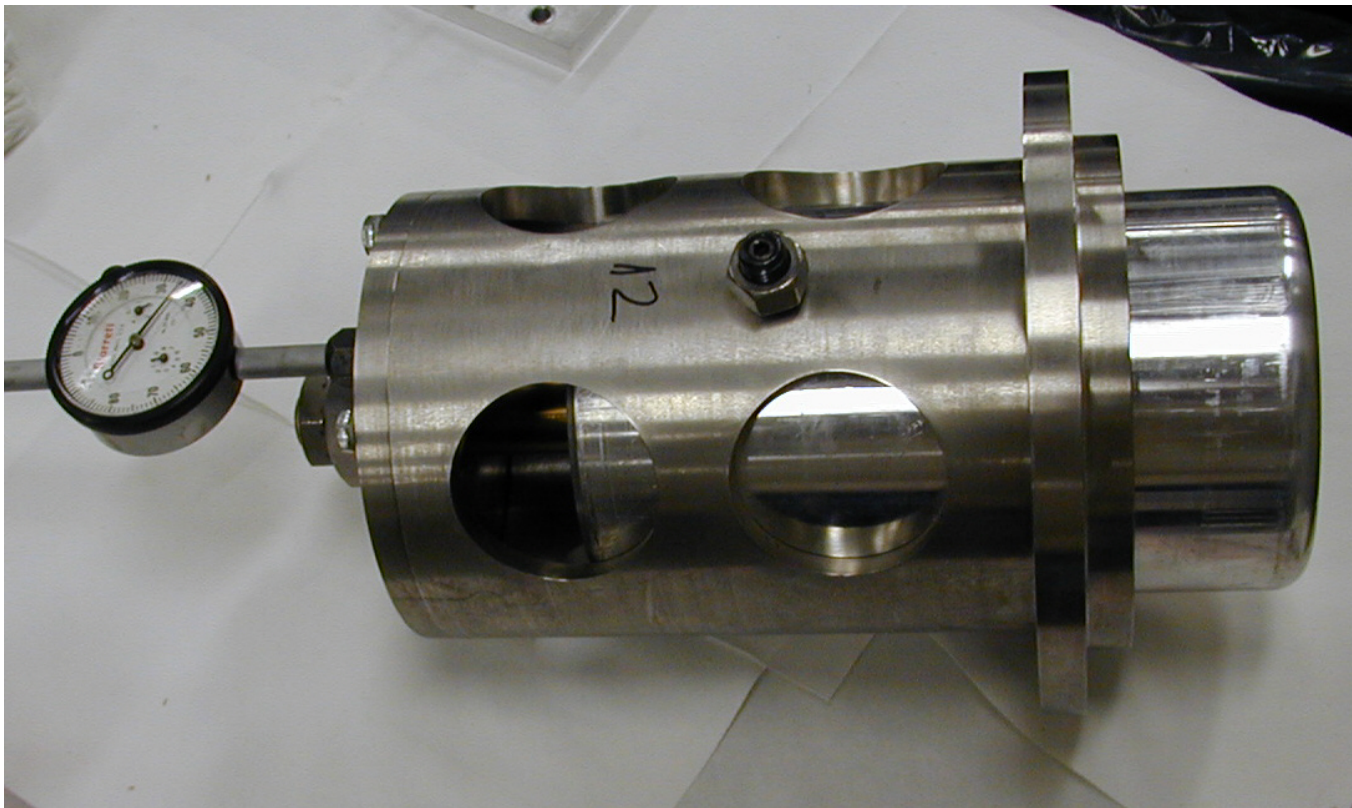
# DTL Tank 1



$E_o/E_{design}$
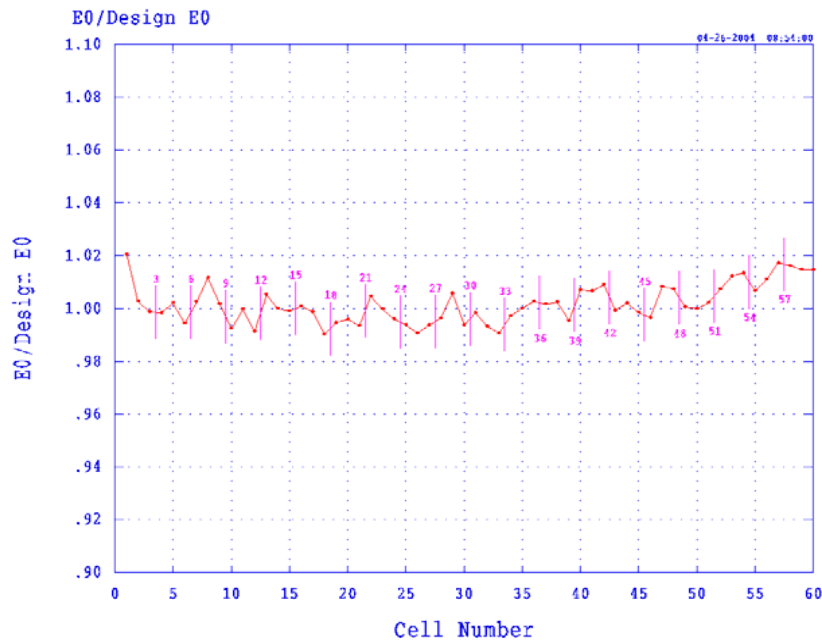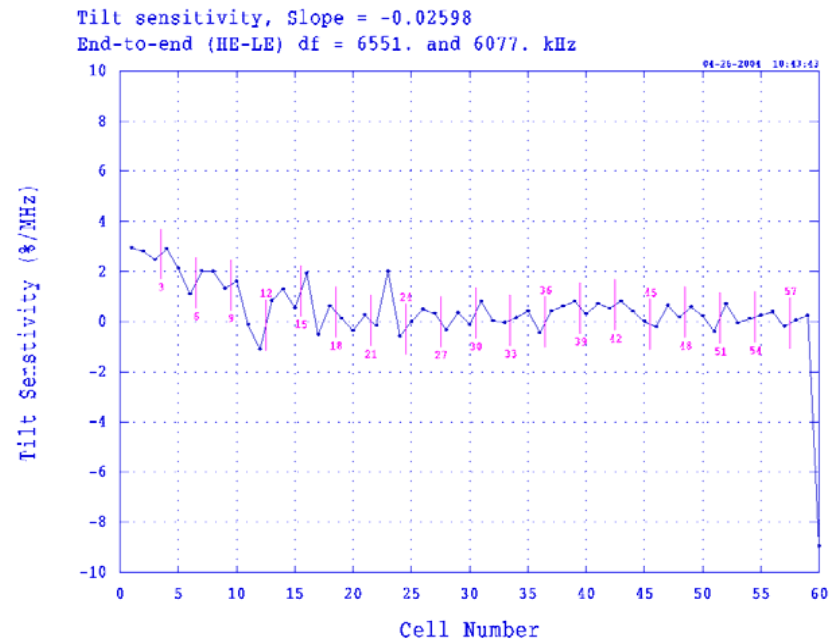
Tilt Sensitivity

$Q_o$=40,200    $Q_L$=12,100    $f_o$=402.5 MHz at 24.8 C

# DTL Tank 2



$E_o/E_{design}$
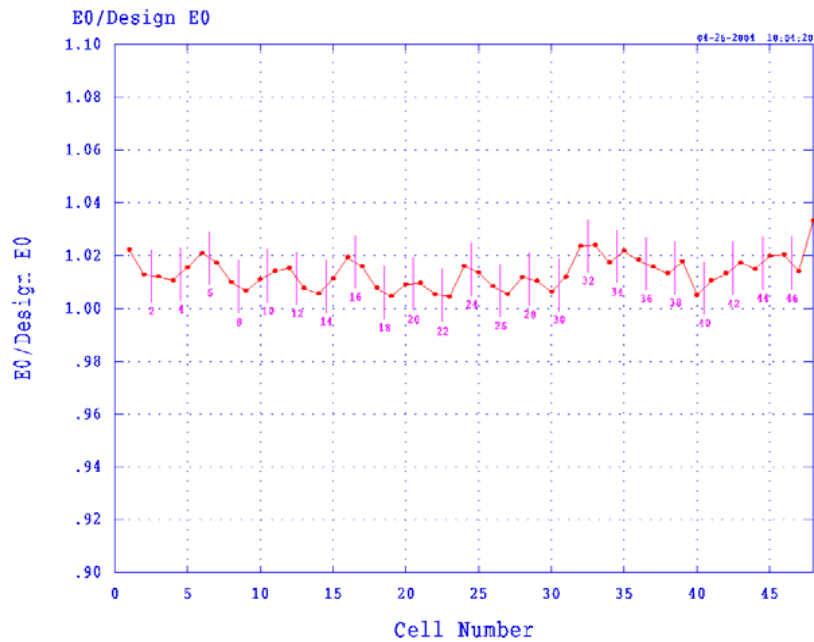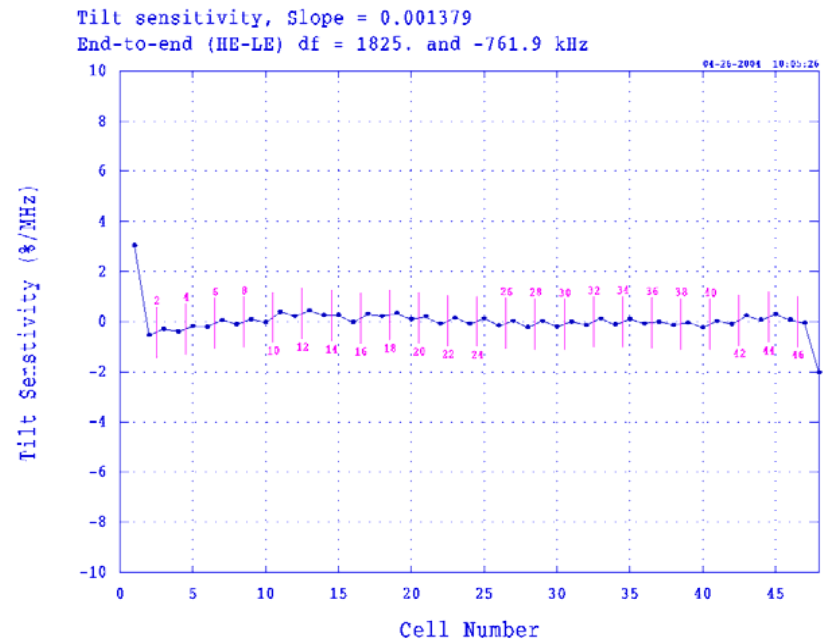
Tilt Sensitivity

$Q_o$=43,500   $Q_L$=18,100     $f_o$=402.5 at 21.2 C

# DTL Tank 3

$E_o/E_{design}$
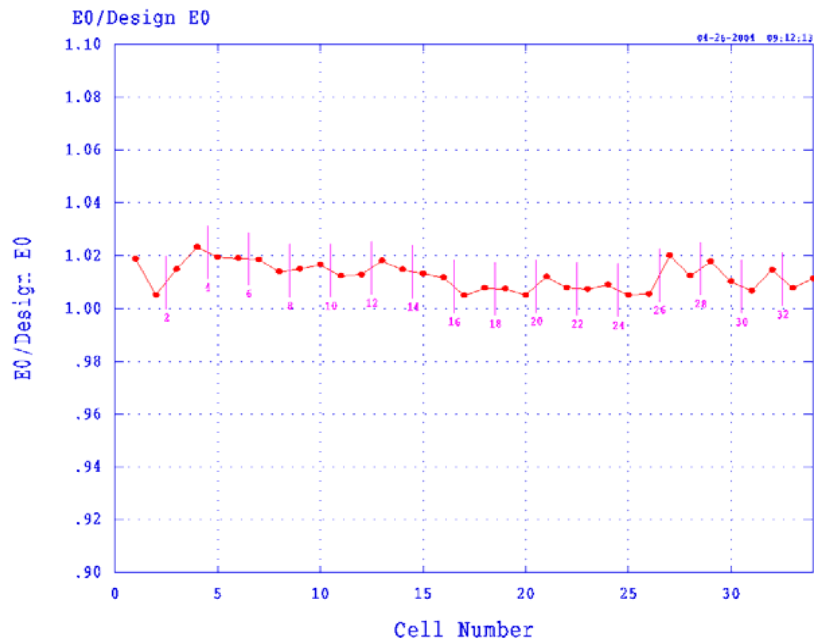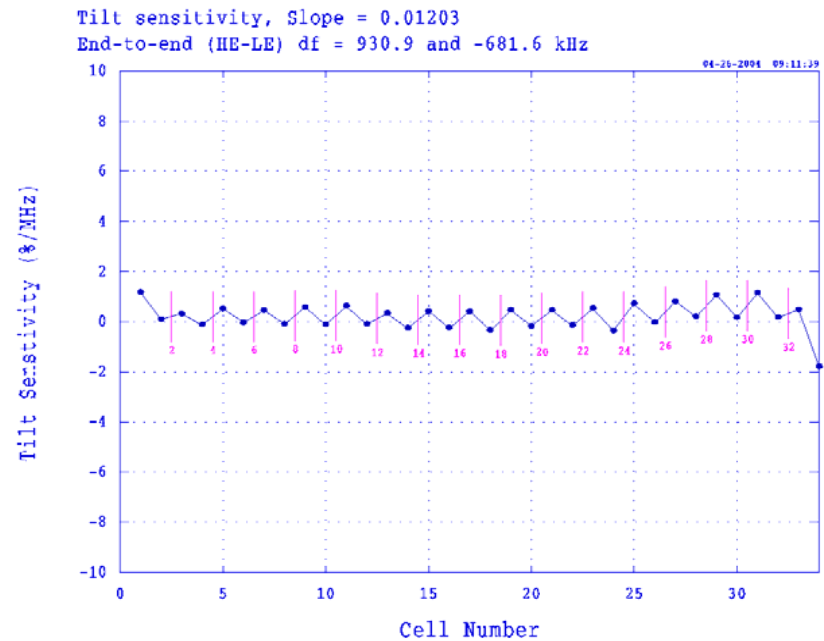
Tilt Sensitivity



$Q_o$=48,300    $Q_L$=17,700    $f_o$=402.5 MHz at 28.8 C

# DTL Tank 4

E$_o$/E$_{design}$
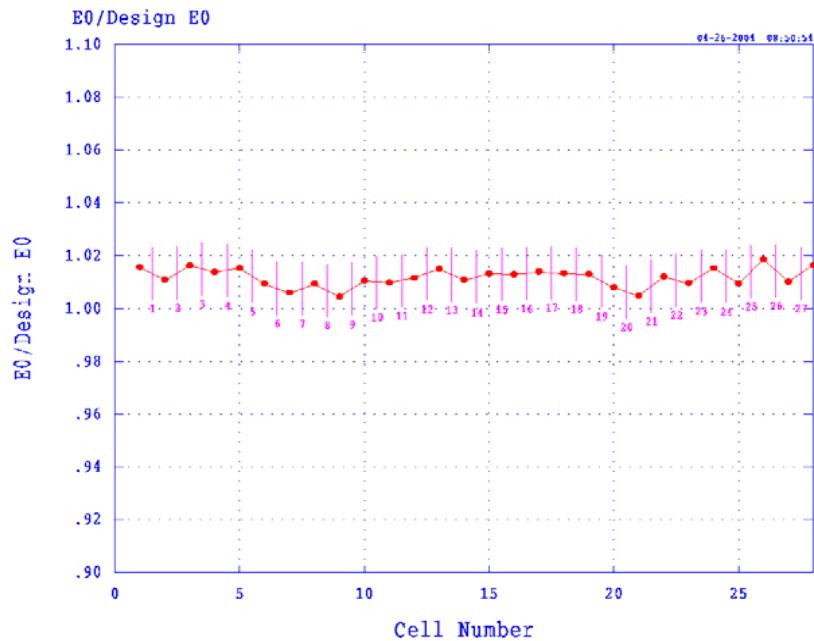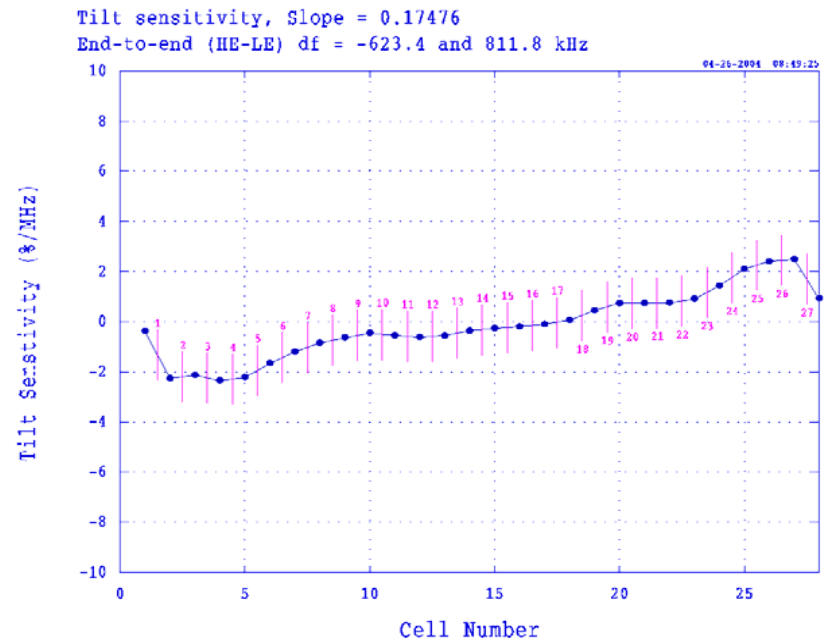
Tilt Sensitivity



Q$_o$=48,200     Q$_L$=17,700     f$_o$=402.5 at 18.9C

# DTL Tank 5

$E_o/E_{design}$
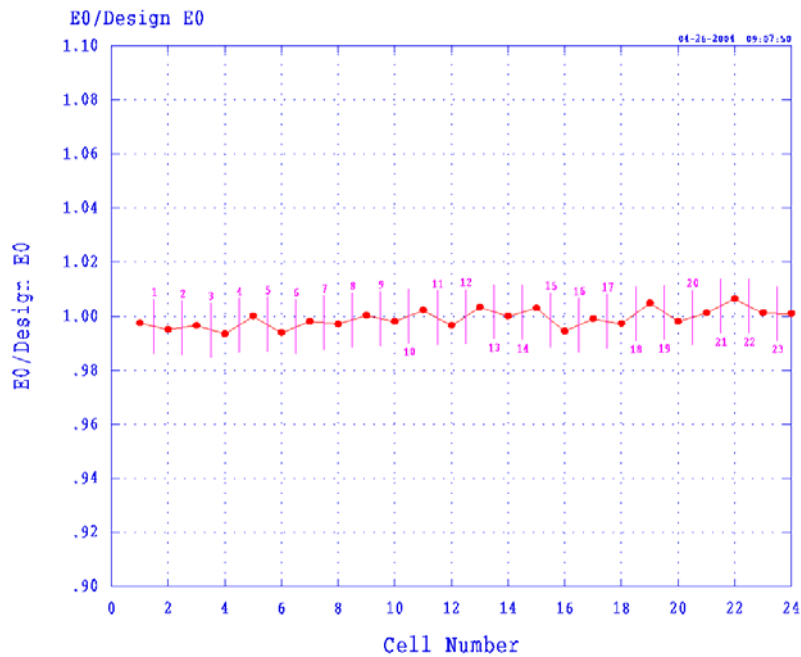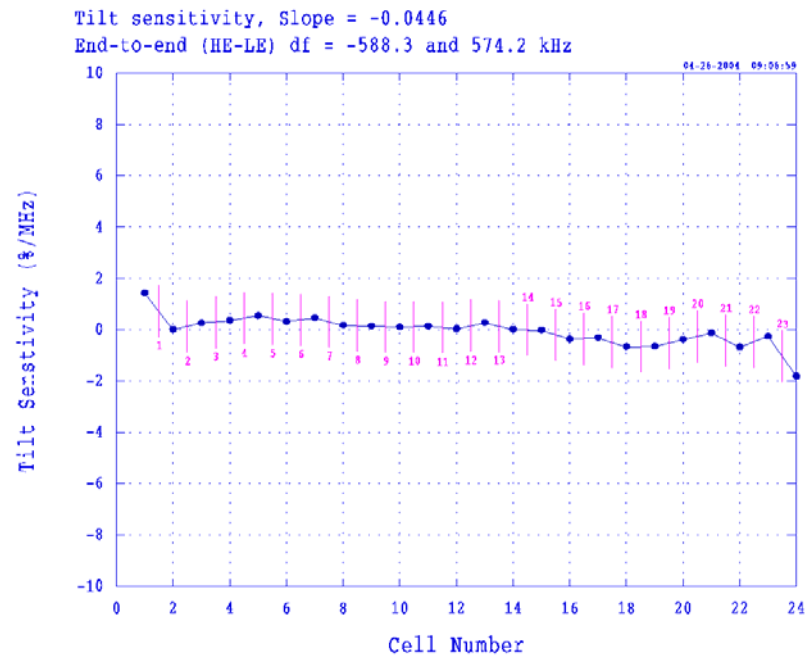
Tilt Sensitivity

# DTL Tank 6

$E_o/E_{design}$

Tilt Sensitivity



SNS Linac                                              Los Alamos
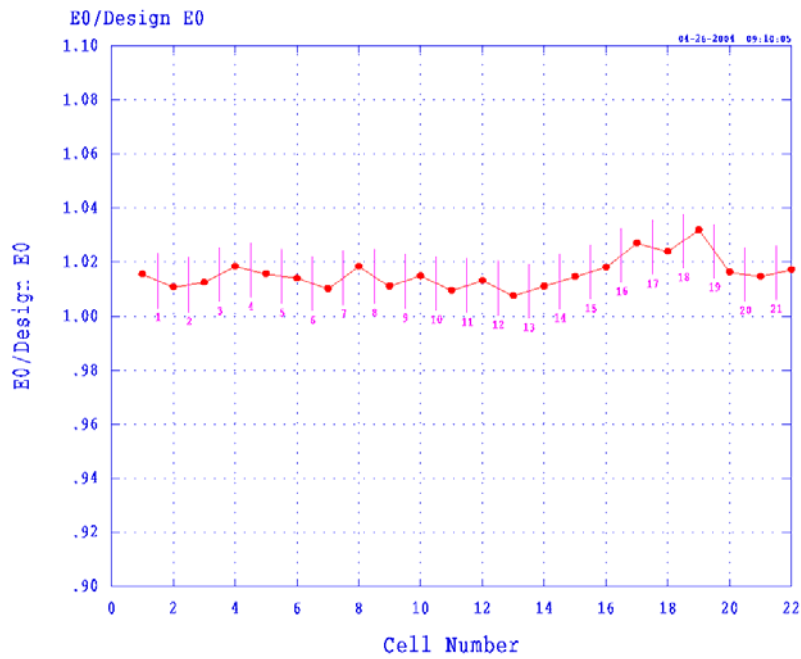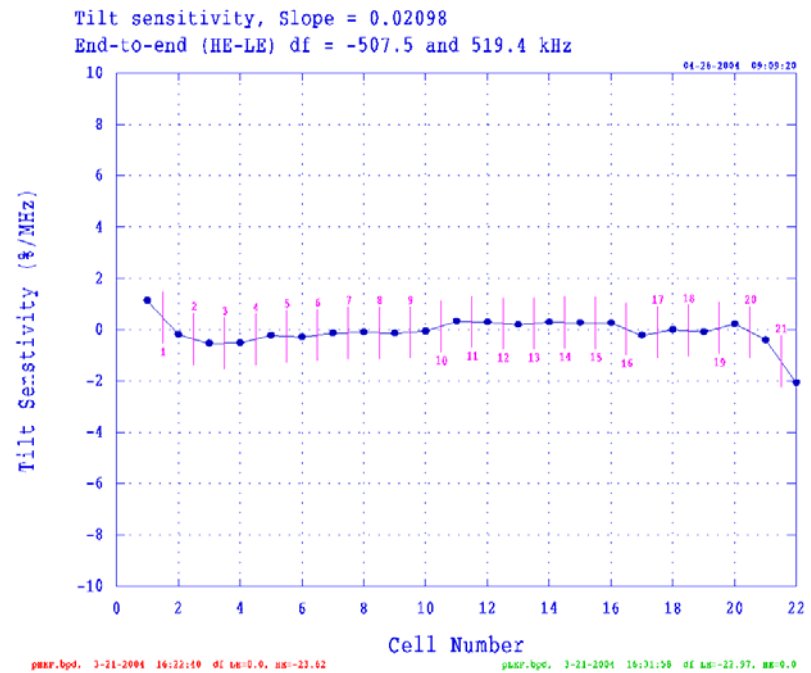
# Measurement of Post Coupler After Tuning Using Coordinate Measuring Machine

- Locate cylindrical tip relative to flange bolt pattern, then weld and machine copper parts to match.

# Water-Cooled Copper Slug Tuner
# (Not Adjustable)

# RF Power Feed is Through a
# Ridge-Loaded Tapered Waveguide
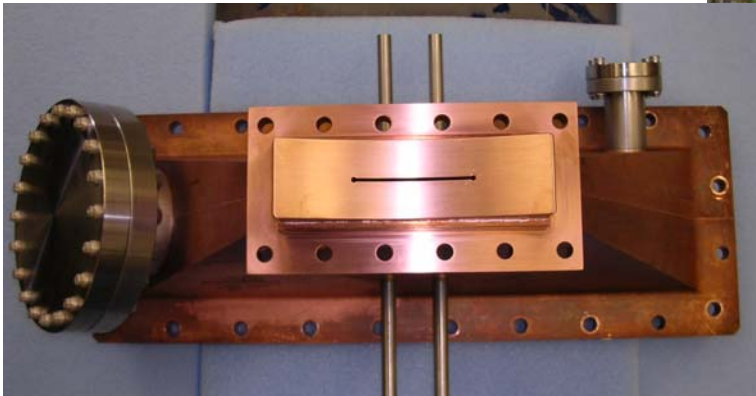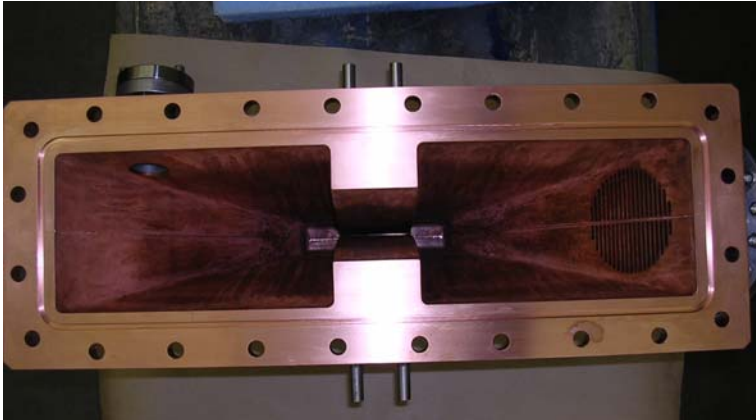
# Waveguide Taper Halves on Milling Machine



1/24/2003 15:57

# DTL Installation as Seen by the Mechanical Engineering Team



- Plan view shows DTL tanks and waveguides, which enter at 45 degrees to vertical from klystron gallery outside and above tunnel.

# Early Tunnel Configuration

- Tank 3 was assembled and tuned first and prepared for RF conditioning while still working on Tank 1.
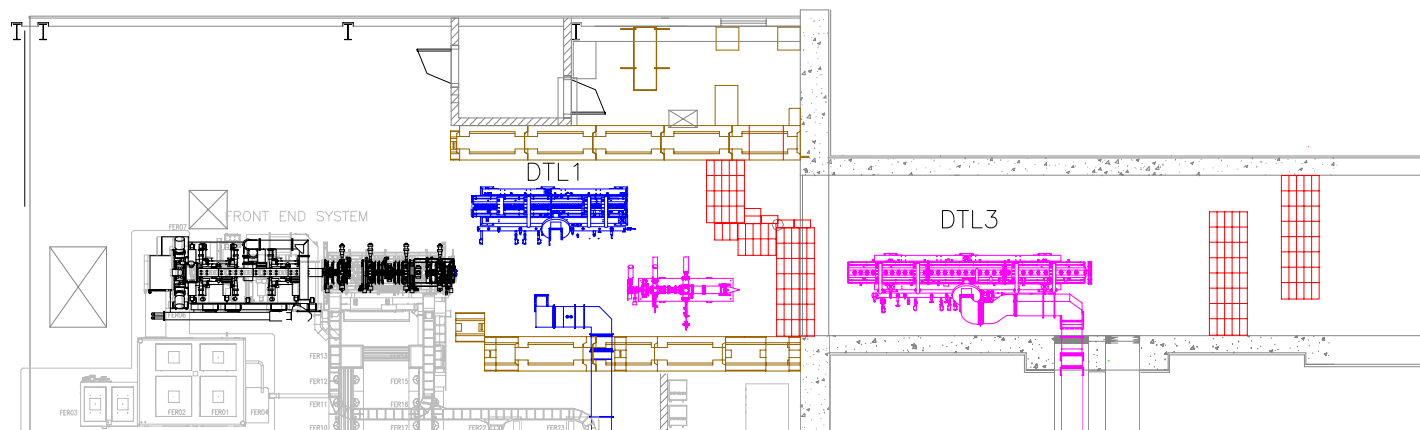
# Drift-Tube Re-Manufacturing
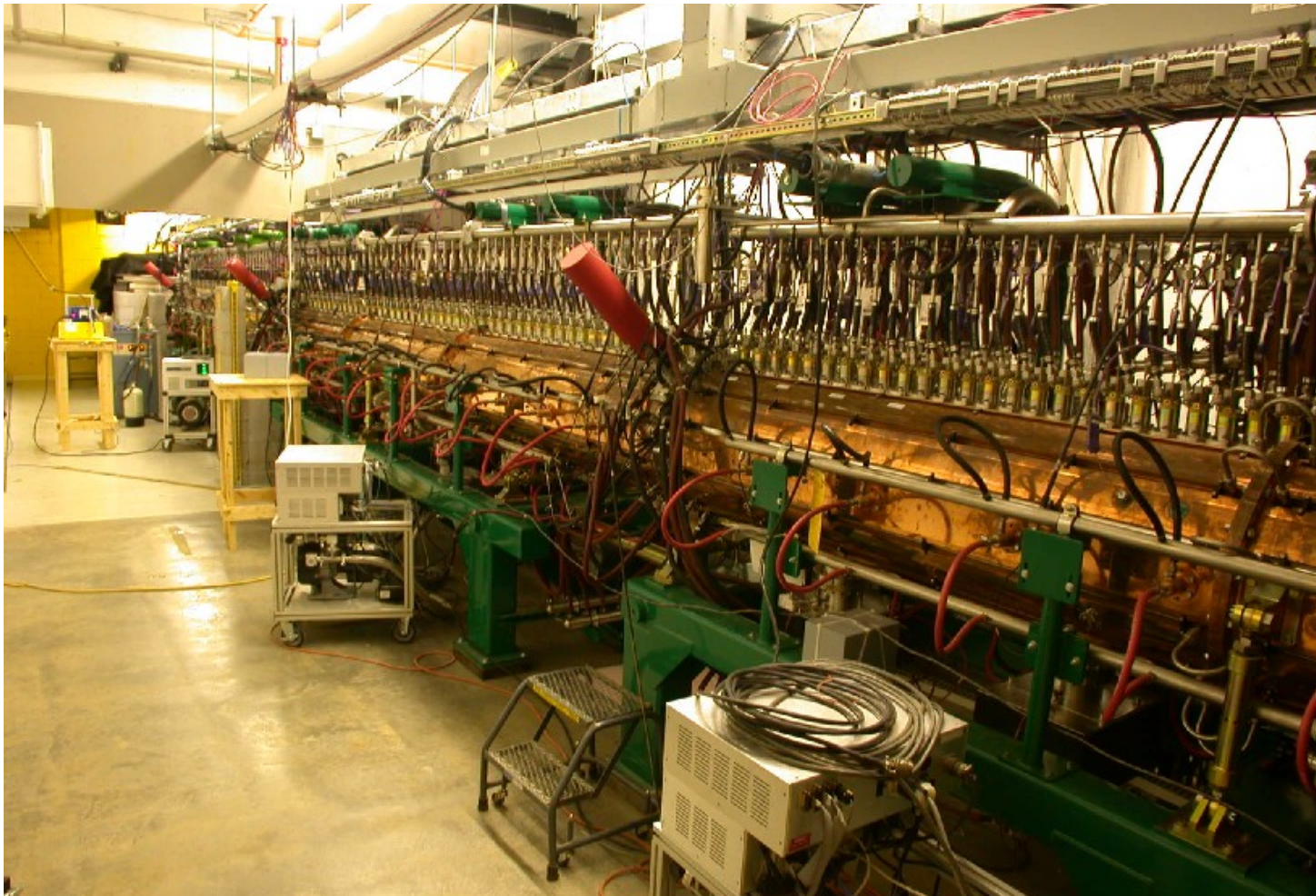
# Serious Problems with Drift Tubes Found During Tank 3 and Tank 1 Assembly

- First indications were leaks found in tank-3 drift tubes.
  - Initial leak testing: Pump on water channels and looked for He leaking in from the outside.
  - New method: Seal drift tube in vacuum chamber, pressurize water channels to 100 psi He, and look for He leaking into vacuum.
- Problems traced to bad e-beam welds.
- All drift tubes already built for tanks 3 and 1 were severely flawed.
- Procurement plan, vendor inexperience, and lack of project oversight were the primary contributors.

# Original Drift-Tube Manufacturing Plan

- Four drift tube types: PMQ, EMD, BPM, and empty.
- Four vendors submitted proposals for drift-tube fabrication.
  - LANL to supply PMQ or EMD components.
- Two vendors selected to submit prototype tank-3 PMQ drift tubes, provide production plan and the demonstrate technology.
  - Diamond machining of copper.
  - Brazing, TIG welding, and e-beam welding of copper.
  - Copper plating and high-vacuum technology.
- Coronado Machine Inc. awarded fixed-price, "deliver-to-print" contract for all drift tubes.
  - LANL provides "statement of work" and "end-product drawings," and specifications for materials, testing, and cleaning.
  - No process drawings and minimal process guidance.

# After Problems Found on Tank 3
# Work Stopped on Tank 1 Drift Tubes

- All but 4 tank-1 drift tubes had been delivered.
- >10% had vacuum leaks.
- ~50% of the PMQs damaged by the electron beam.
- ~15% had been Cu plated to "correct" errors.
- ~15% were damaged by improper handling.
- EMD coil potting was substandard.
- Bore-tube welds completely missed the joint.
- Magnet yokes were corroded by cleaning solution.

# Anatomy of an SNS Drift Tube



Cu plated SS Stem

SS Diverter

PMQ

Vented bore tube

Relieved cavity

Coolant channels

TIG stem weld

Diverter-body braze

Body-sleeve weld

Cap weld

Bore tube weld

Finished contour

"Family-sized" rough machined assy.
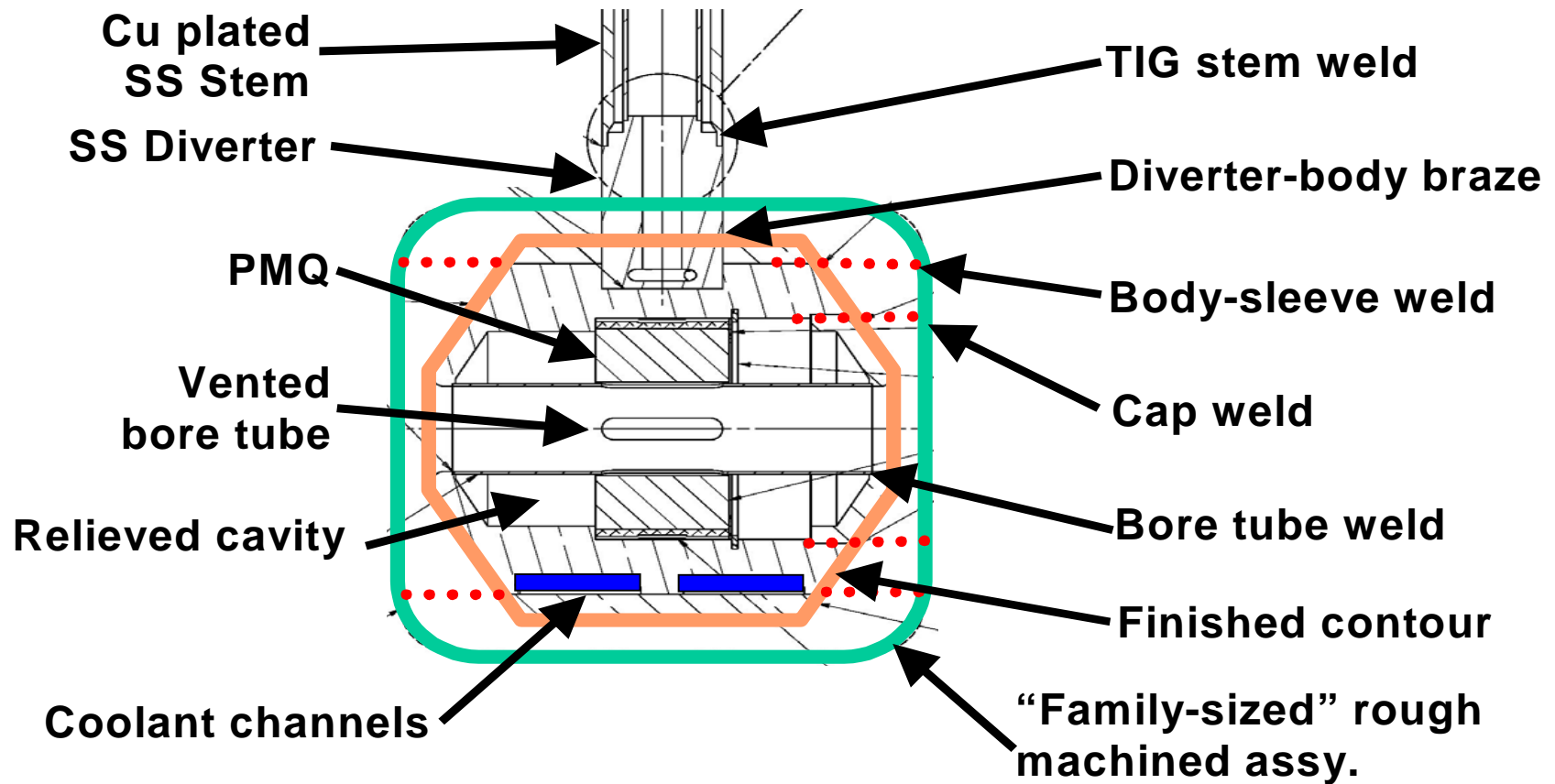
# All e-Beam Welds Were Flawed

- Deep welds were specified for good thermal conductivity.
- CMI changed their design used for the prototype to accommodate "families" of drift tubes.
- Finish machining exposed porosity at the weld root resulting in water-to-vacuum leaks.

Multi-pass deep welds
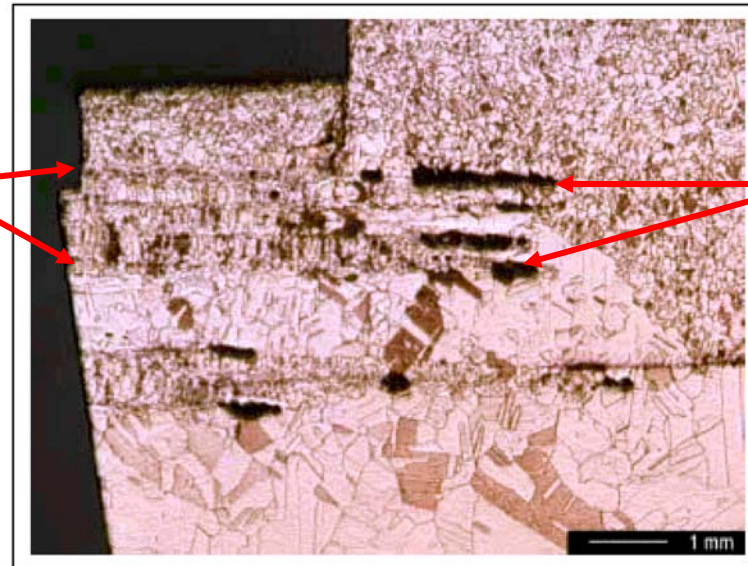
Weld root is porous.

# Tank 1 Drift Tubes Sectioned and Inspected

- Deep welds were porous.

- Insufficient shunting of PMQ field deflected the electron beam, which then missed the intended joint, penetrated the Cu body, and damaged the PMQs.

- Most tank 1 drift tubes were scrapped and rebuilt.
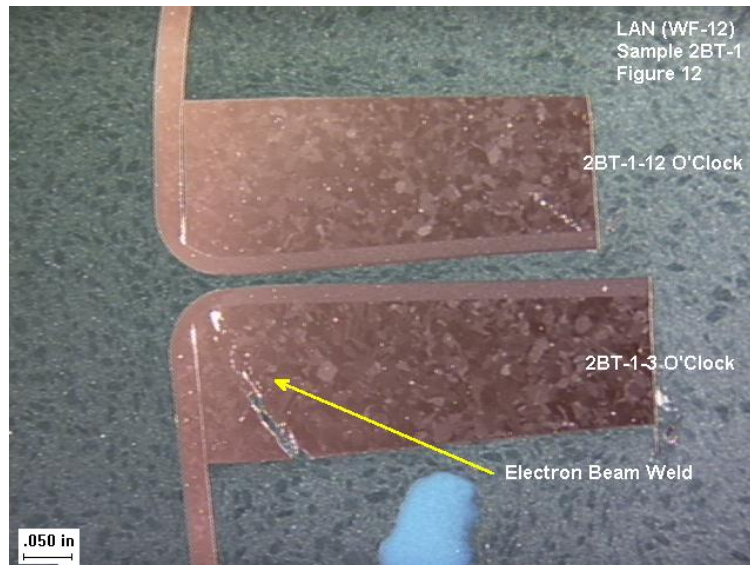
# Intensive Recovery Effort

- 25 experienced staff reassigned to SNS division from other LANL programs.

- Engineering teams were formed for all major components.

- Renegotiated fabrication contracts.

- LANL engineers managed, coordinated, and closely monitored all fabrication tasks.
  - Machining at CMI
  - Brazing at LANL
  - e-beam welding at ESCO
  - Copper plating at Kaehr

- All vacuum, pressure, and flow testing done at LANL.

# Designs Simplified for Rebuilt Drift Tubes and Those for Tanks 2, 4, 5, and 6.
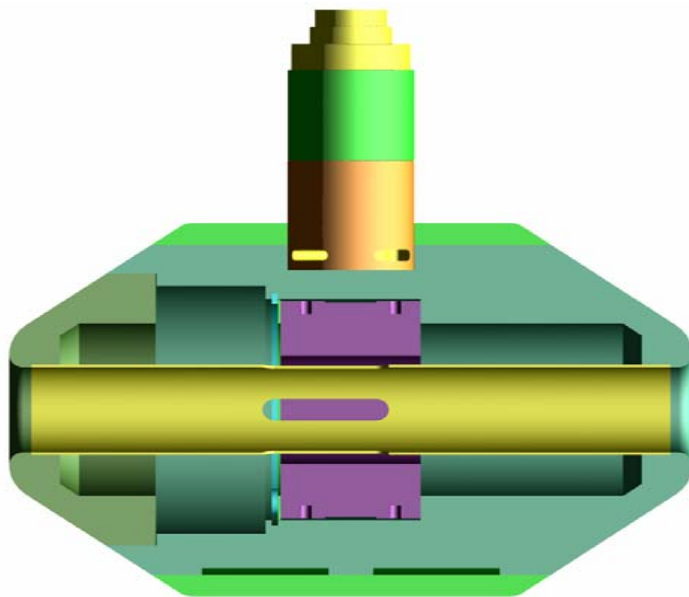


Old design
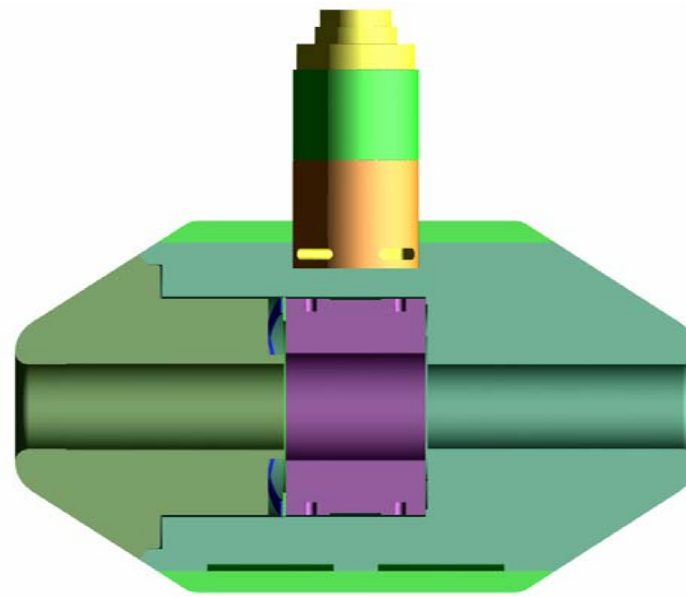
New Design

# Tank 1 Body-Sleeve Assemblies are Rough Machined to Length (no "Families")



1/30/2003 16:46

# Tank-3 Drift Tubes Repaired Using The Ring Weld Repair Process

Magnets were not damaged in tank 3 drift tubes because they are longer than drift tubes in tank 1.
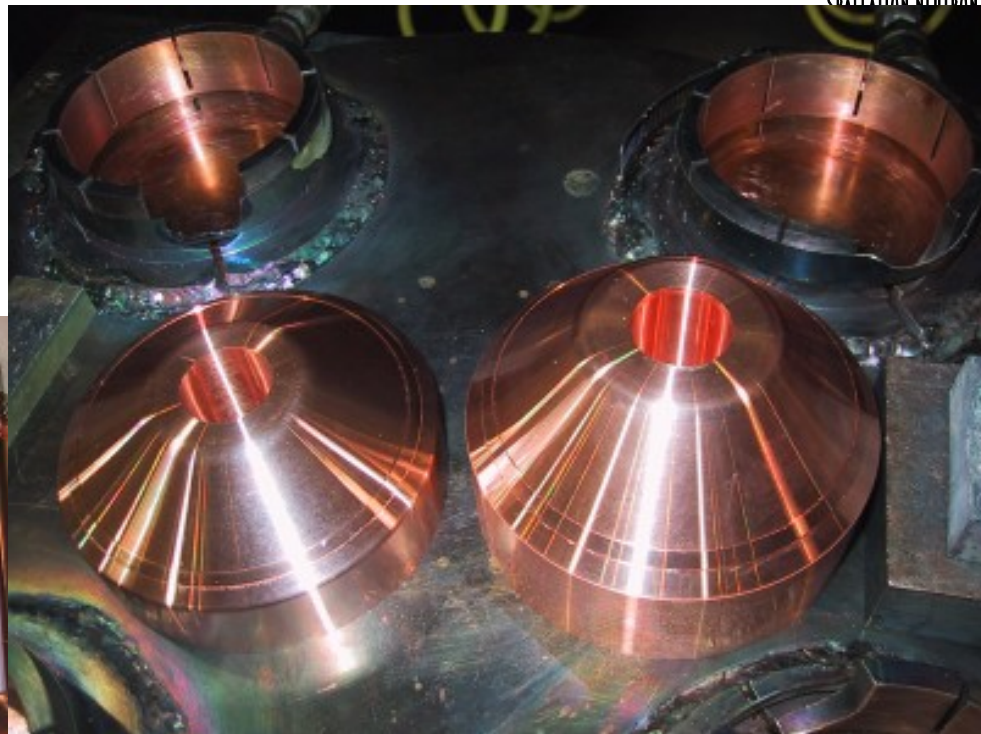
# Some Drift Tubes Repaired by Welding a Ring into Machined Groove
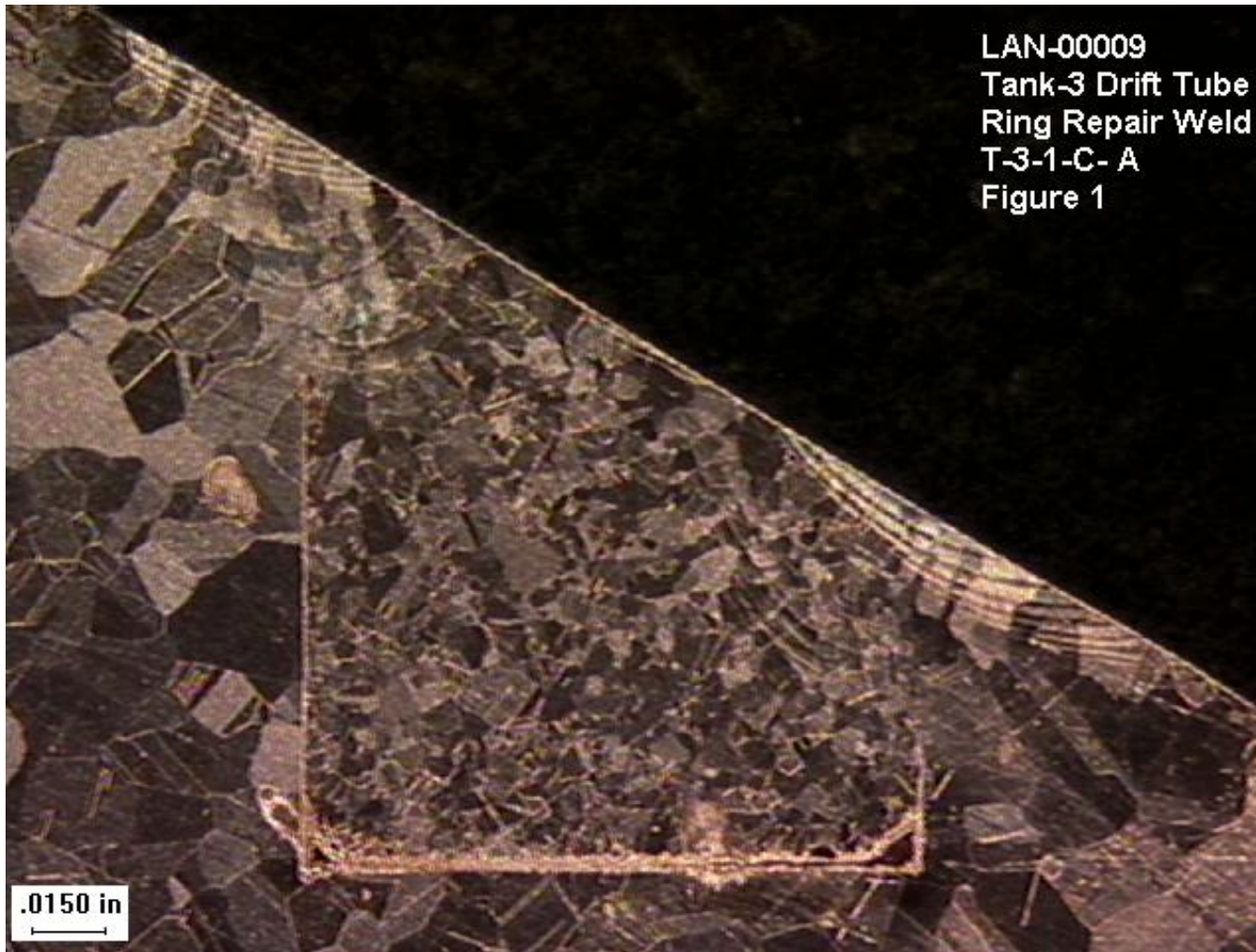


LAN-00009
Tank-3 Drift Tube
Ring Repair Weld
T-3-1-C- A
Figure 1

.0150 in

# Weld Repairs Before Finish Machining

# Finish Profile is Diamond Milled



1/30/2003 16:43
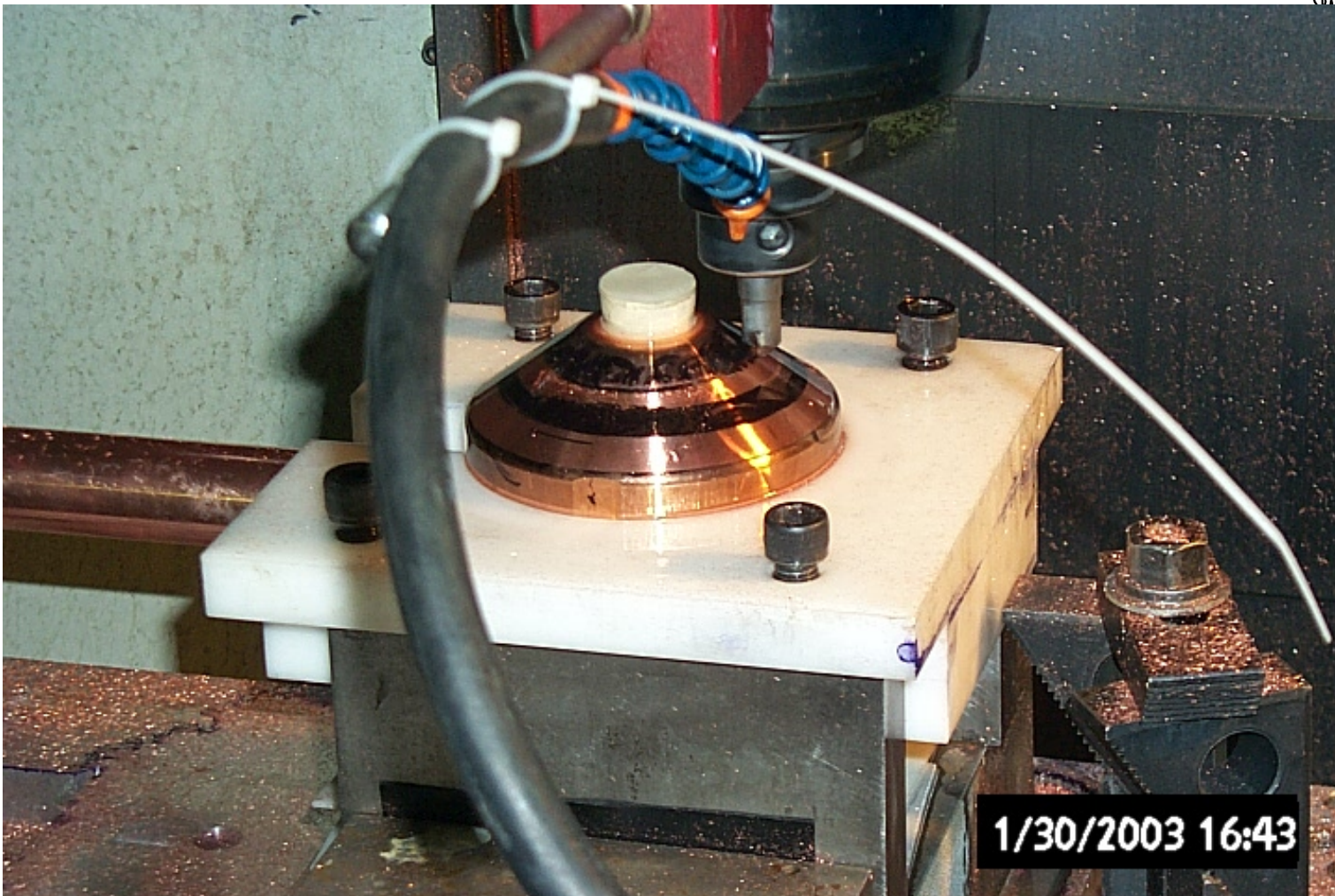
# PMQs are Protected by Cooling Blocks in e-Beam Welder and their Field Shunted
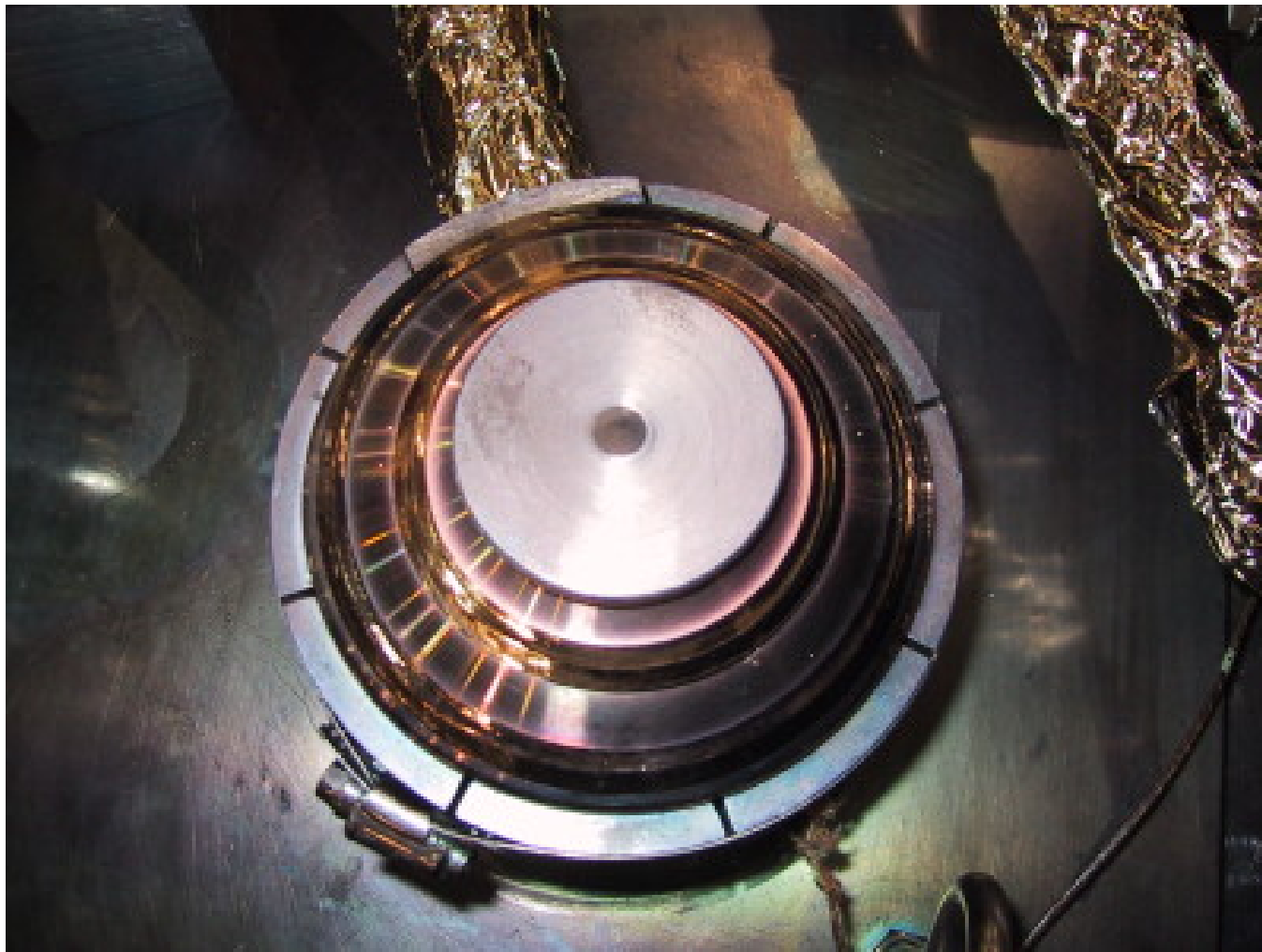
# Repaired Tank-3 Drift Tubes Do Not Look as Good, but Perform Well

Before
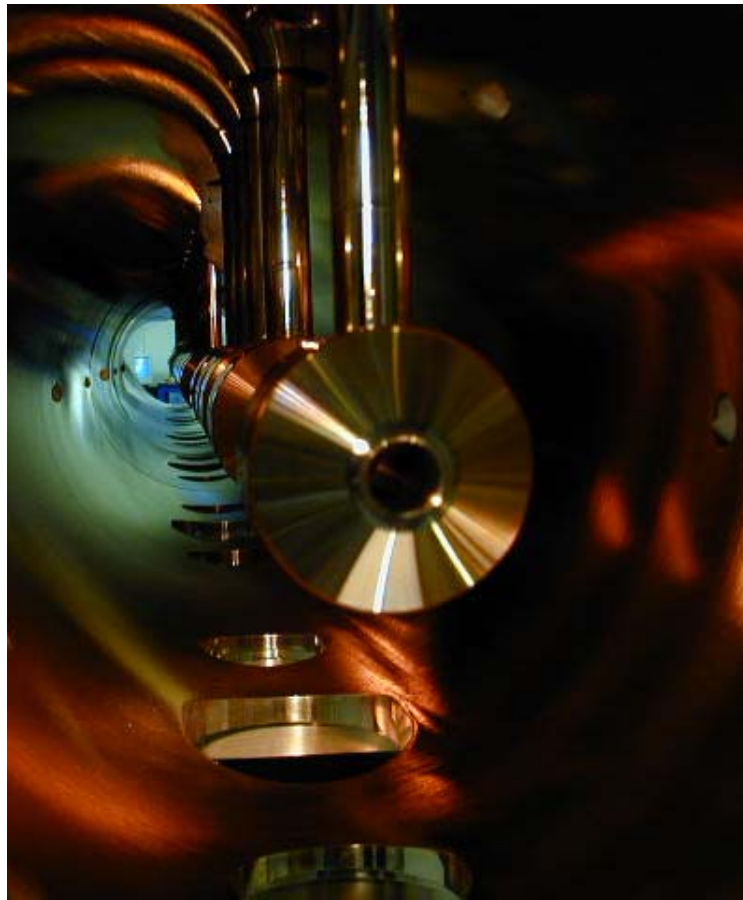
After
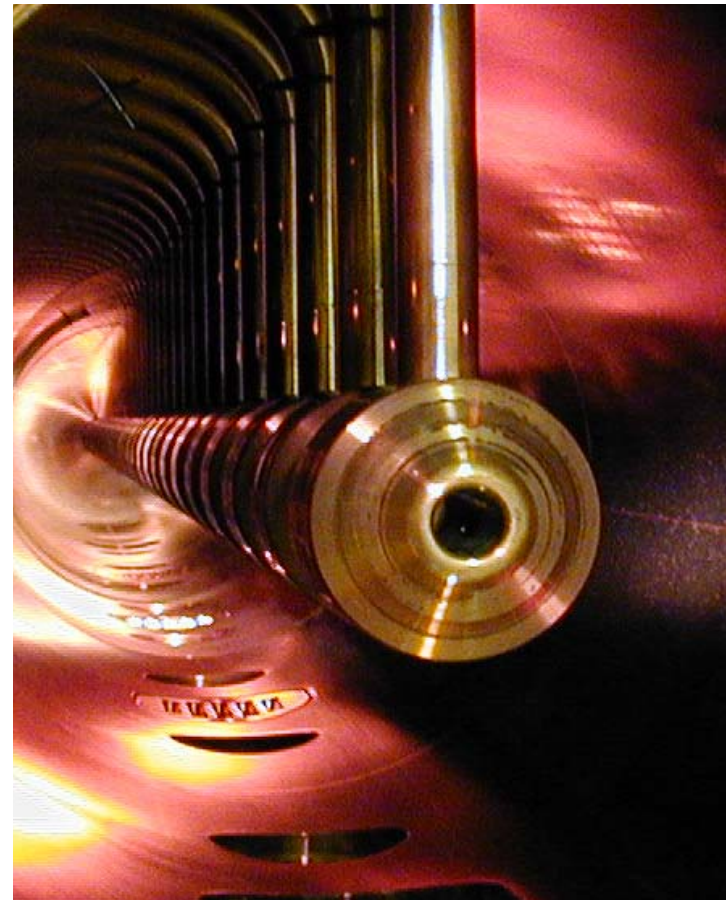
# New Finished Tank-1 Drift Tubes
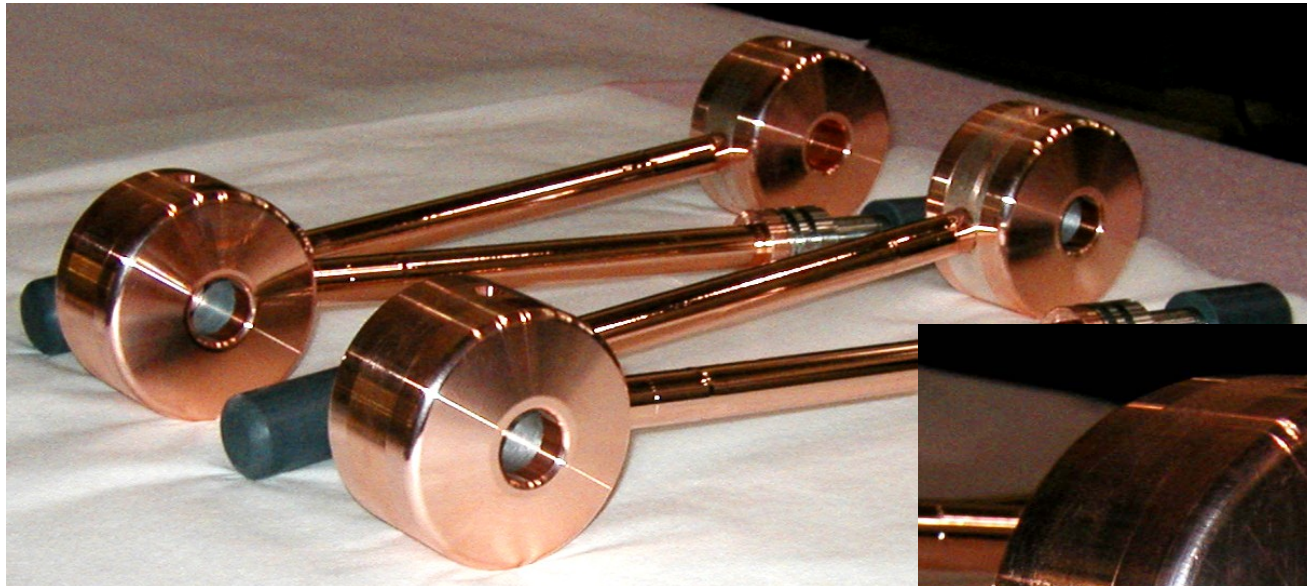
# Good Field Distribution Achieved in Tank 3 After All the Rework
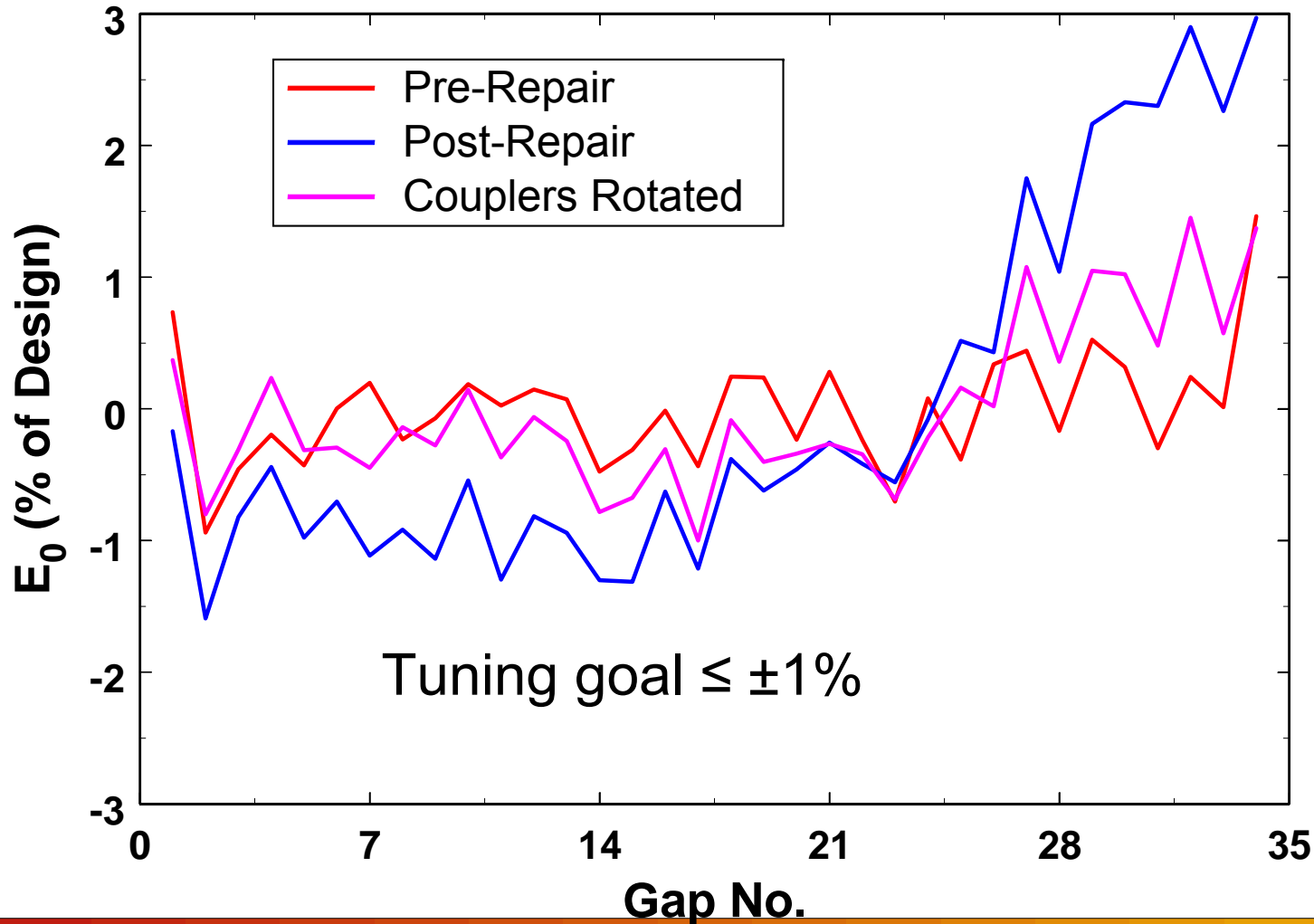
# Tank 3 Conditioned to Full Field in 30 hr

SNS
SPALLATION NEUTRON SOURCE

←Increase $P_{peak}$ →  ←Increase $P_{ave}$ →

$P_{forward}$

$P_{reflected}$

rf Power (kW)



*SNS Linac*                                                                 *Los Alamos*
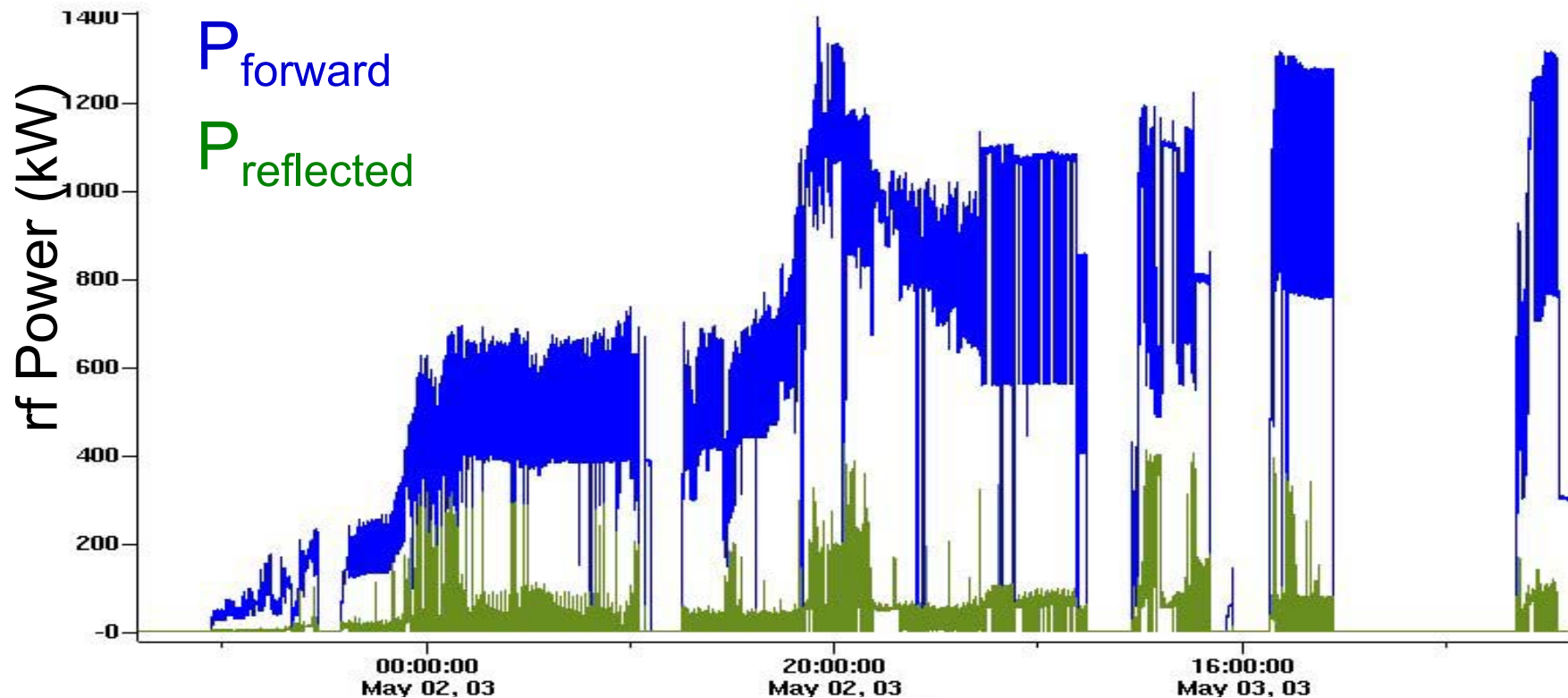
# For high current, DTL efficiency is insensitive to the RF frequency choice

- Consider increasing frequency, holding $E_0$ and L fixed.
- Scale all other dimensions by 1/f. ($ZT^2$ increases as $f^{0.5}$)
- Beam dynamics usually requires a minimum bore radius.
  - If the bore radius R remains fixed, T decreases at higher frequencies as $1/I_0(kR)$, where $k = 2\pi/\beta\lambda$, thus reducing $ZT^2$.
- Electric-field holding capability improves at higher frequency.
  - Kilpatrick factor increases with frequency.
- Redesign of cells for similar Kilpatrick factor recovers $ZT^2$ lost by fixing the bore radius.
- Conclusion: the frequency choice most often comes from factors other than efficiency, typically availability of RF power supplies.

# Shunt impedance and peak surface field



**Shunt impedance comparison for fixed E0 and fixed length**
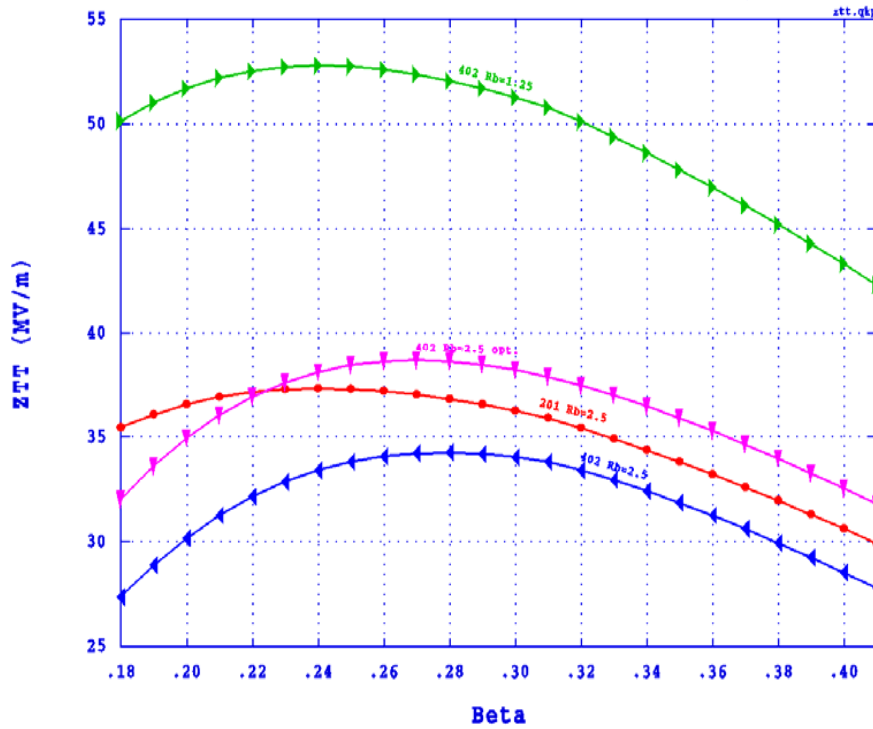
**Peak surface electric field (Kilpatrick factor)**
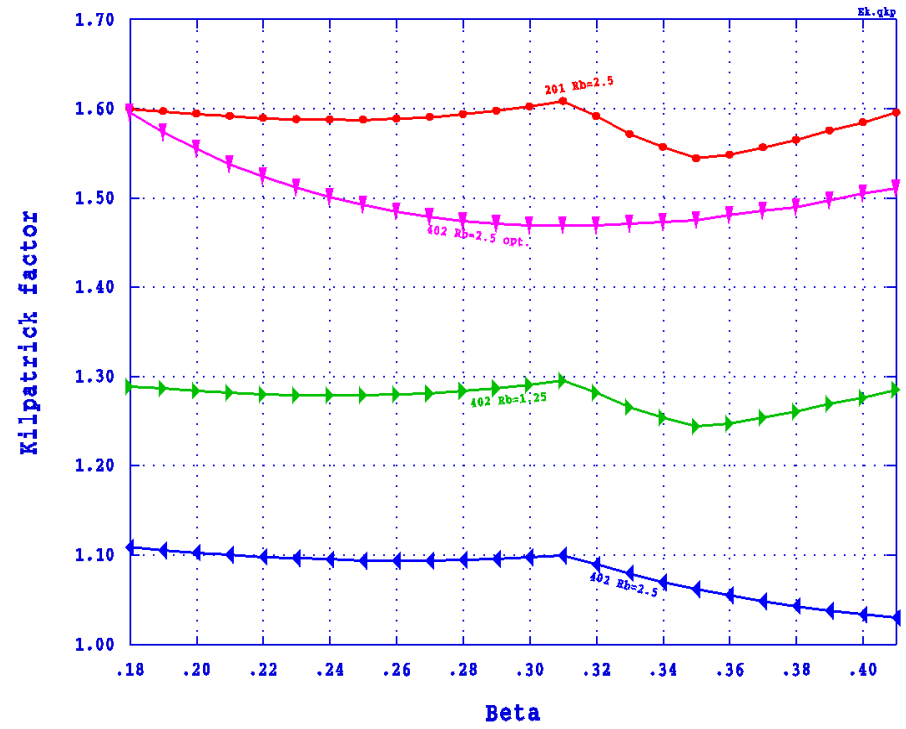
# CCL Design

# Some CCL Terminology



SNS

SPALLATION NEUTRON SOURCE

Coupling cell

Bore

8-Cavity Segment

Segment
End cell

Dimpling ports

Slug
tuner

Bridge coupler

# CCL Components



Coupling cavity

Bridge coupler

Coupling slot formed where two cavities intersect.

Beam axis

Accelerating cavity

Segment (4 cells)

Bridge coupling cell
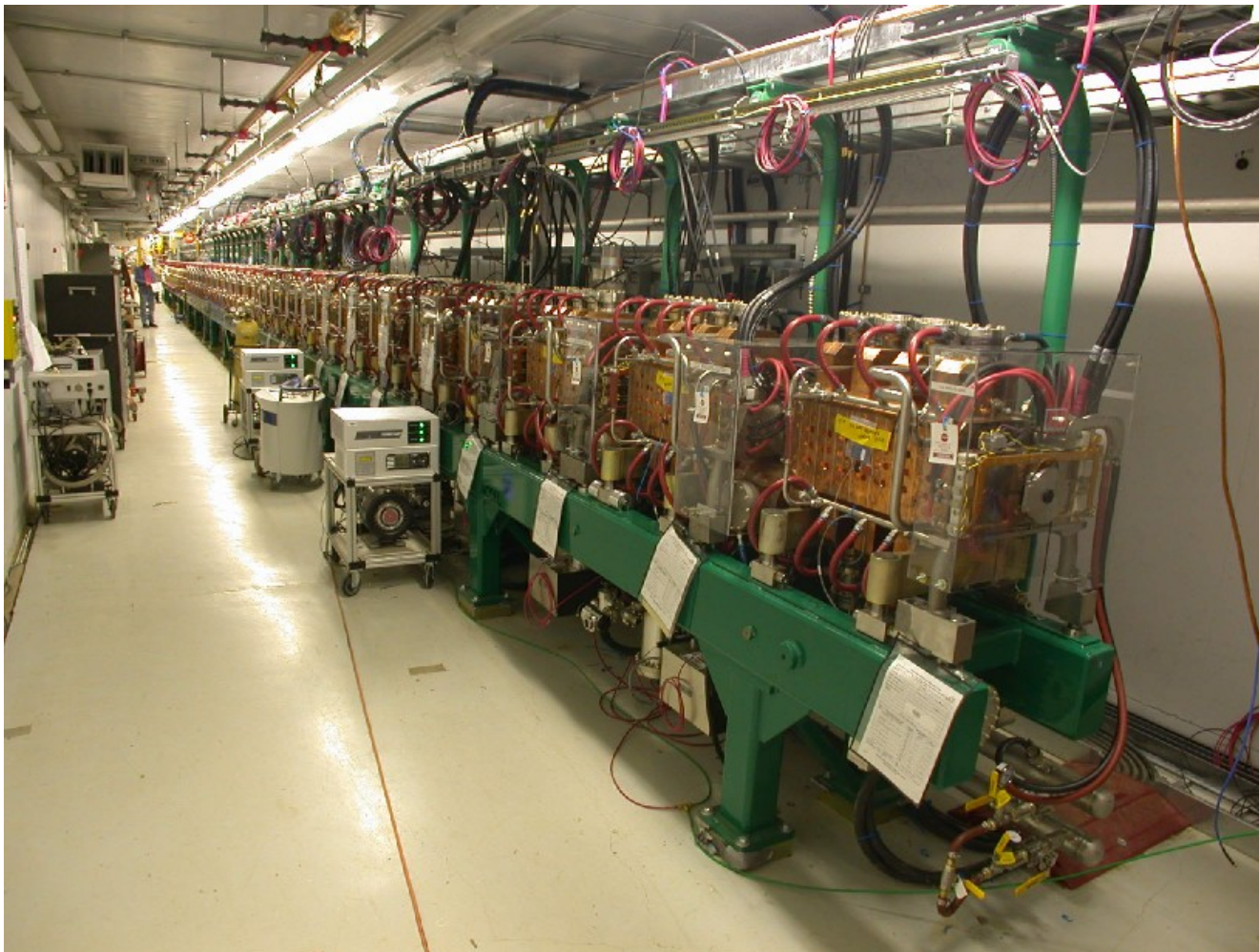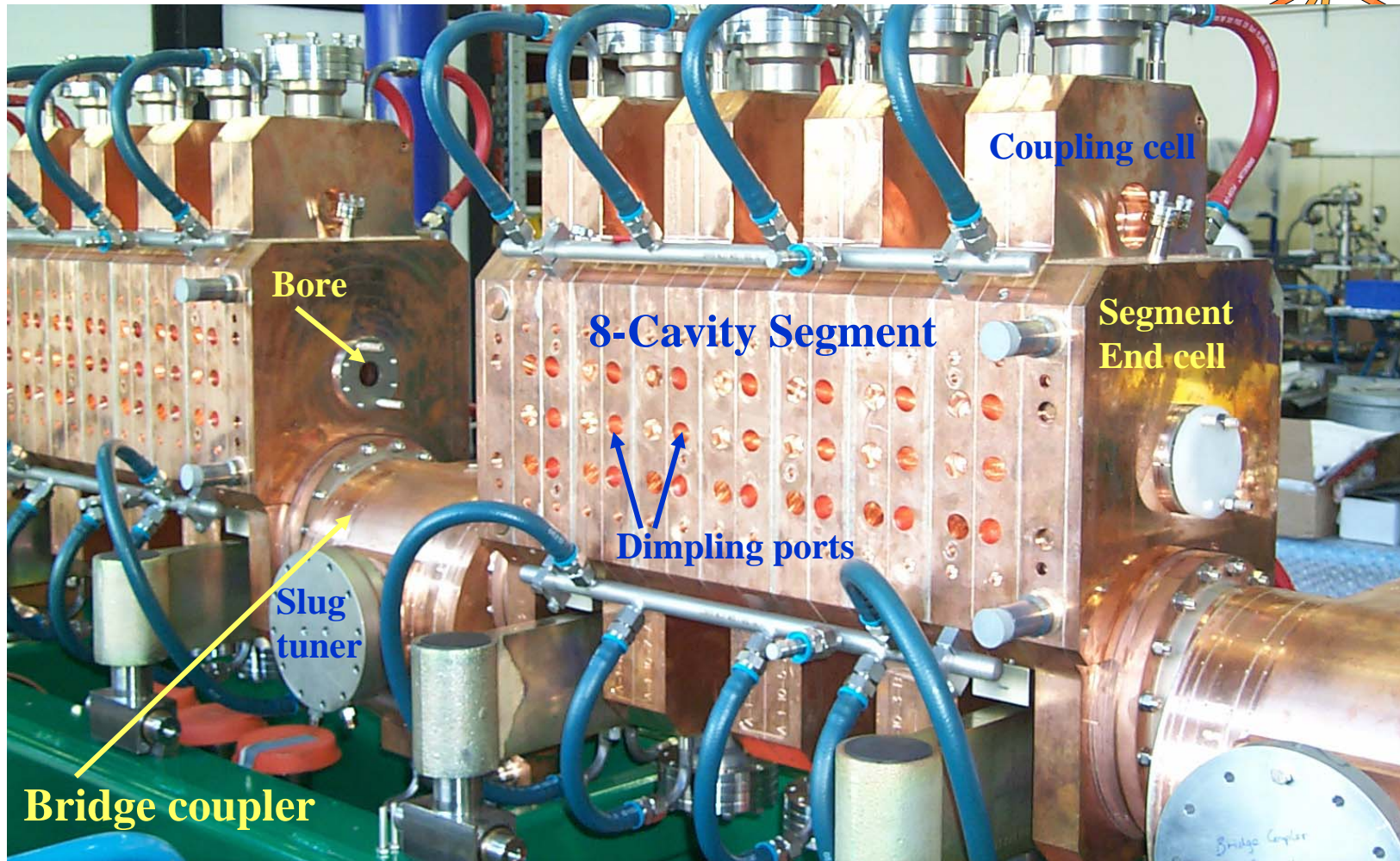
Waveguide iris
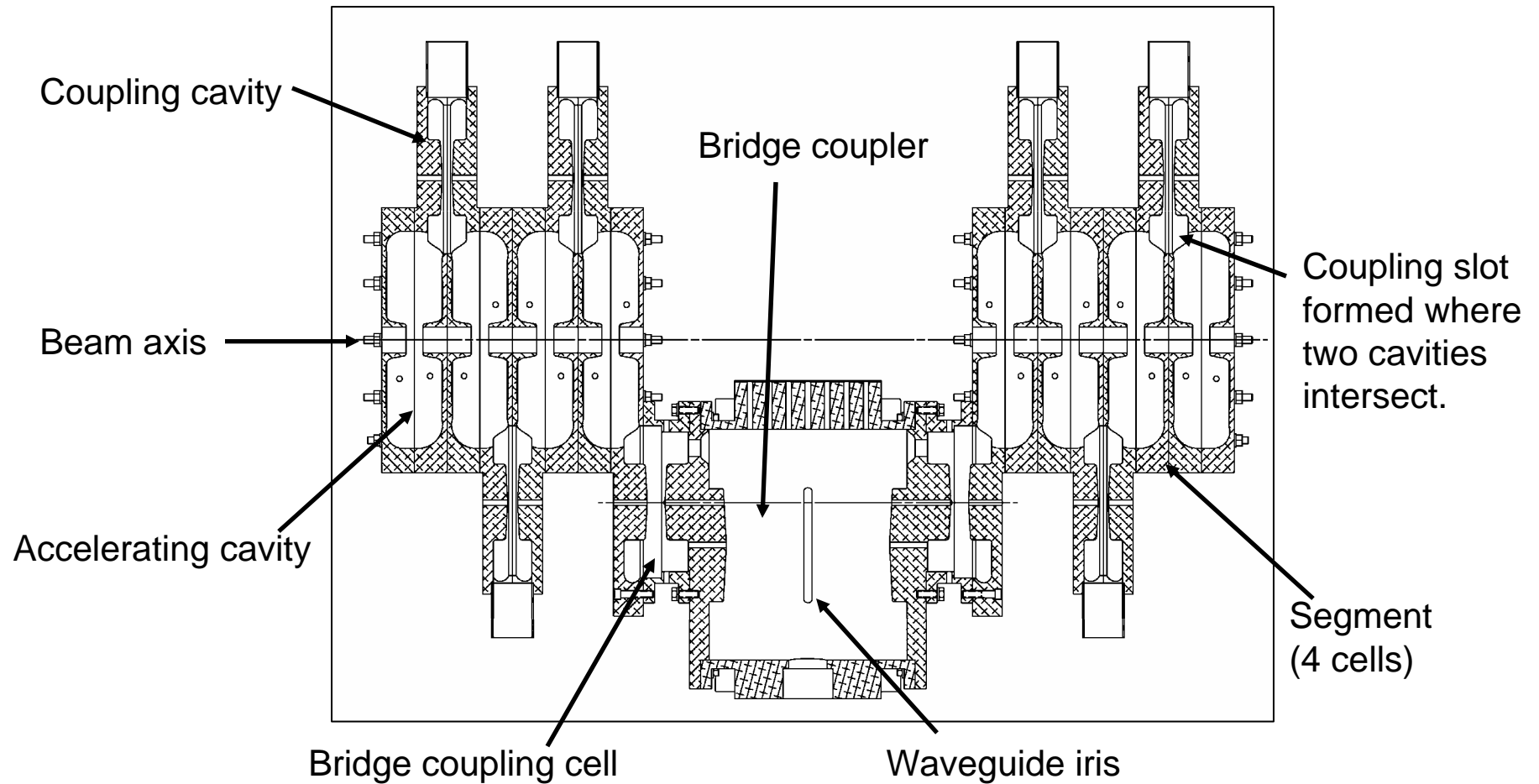
# Steps in CCL Design

- Physics design of representative cells (much like DTL cells).
- Engineering design studies (thermal and structural analysis).
- Beam dynamics design and simulations using transit-time factor data from representative cells.
  - Choose $E_0$ and number of cells per <u>segment</u> (short section of accelerating structure between quadrupole magnets).
- Design each segment from the beam-dynamics design.
  - Geometry tables for engineering design.
  - Compute power, Q, stored energy.
  - $E_z$ data for tuning the structure.
- Bridge coupler design.
- Aluminum cold models for $\beta = 0.4$ and 0.55.

# CCL Cell Geometry
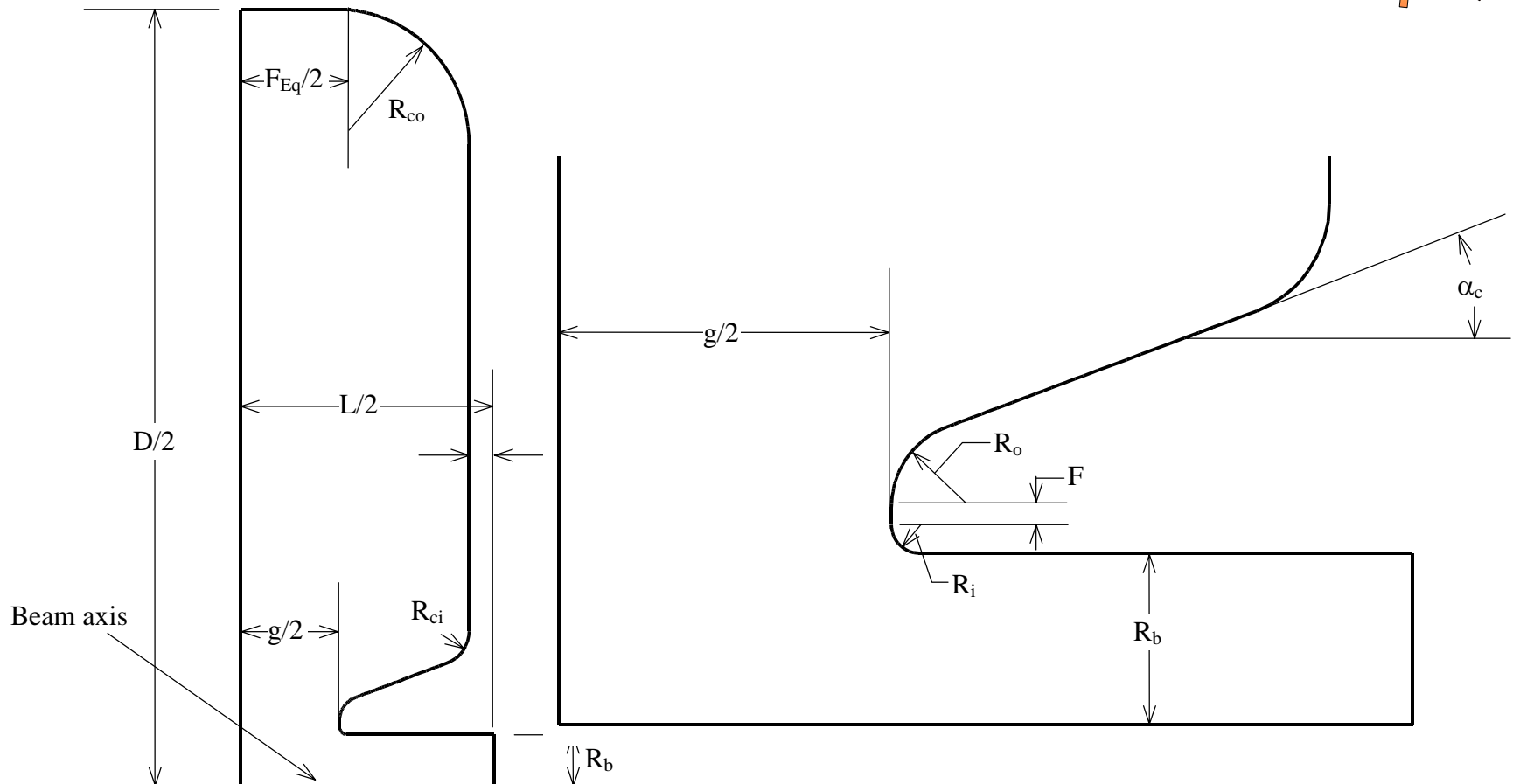
# Tuning Ring Feature Added on Both Sides of a Cell

- Tuning ring is machined to tune cells during assembly.

- Removal of both rings lowers frequency 5 MHz.
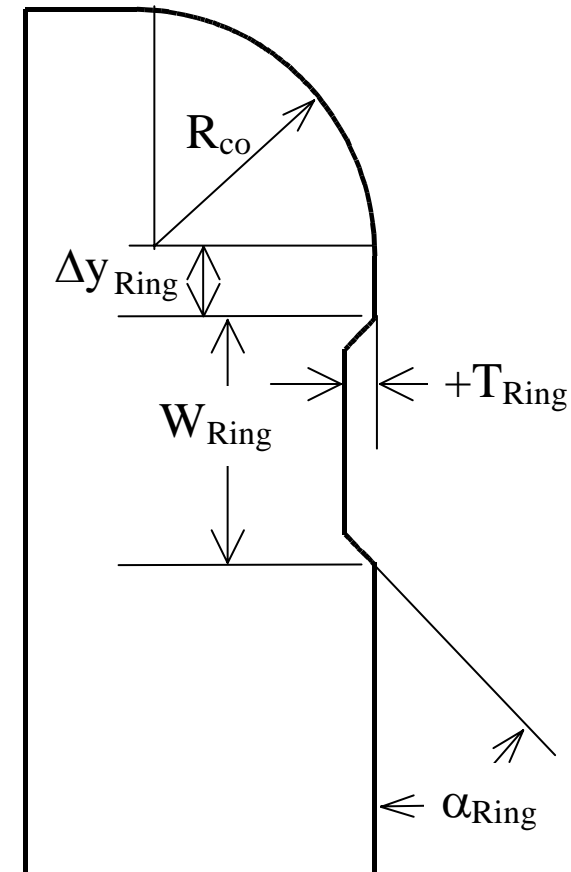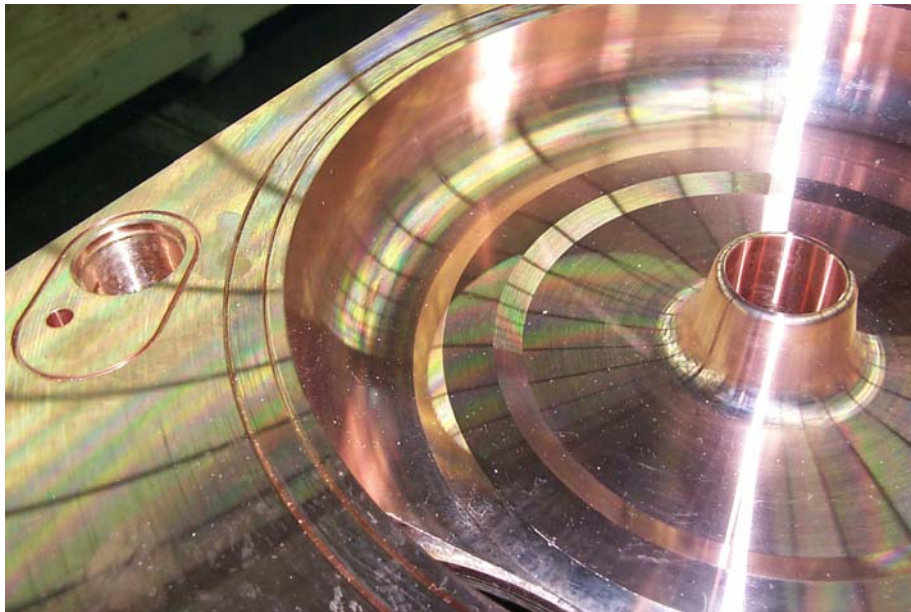
# Parmila code uses transit-time-factor data to design the detailed cell layout

- All cells in a segment are identical (synchronous phase = -90°), but each segment is longer than the previous segment.

- Parmila chooses the segment length to make the design particle's average phase at the gap centers equal to a design "synchronous phase" for the segment.

SNS has 8 cavities per segment ($4\beta\lambda$) and $5\beta\lambda/2$ spaces between segments, which makes the magnetic focusing lattice length $13\beta\lambda$ at 805 MHz. This is nearly the same physical length as the DTL lattice: $6\beta\lambda$ at 402.5 MHz.
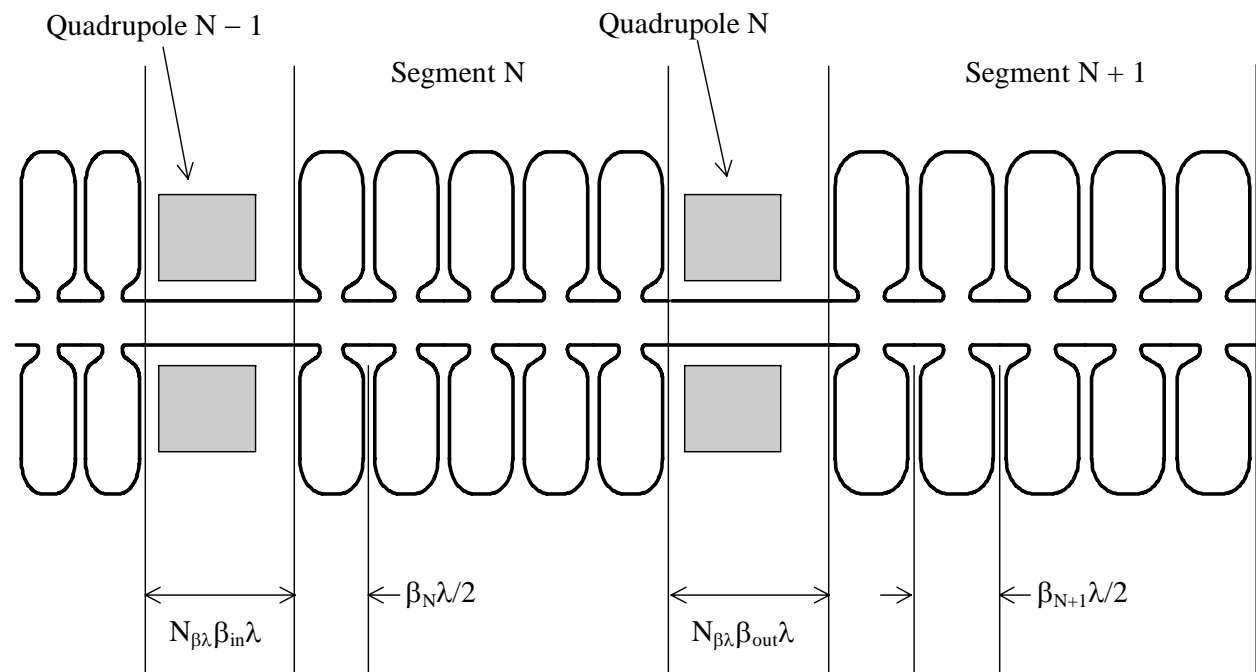


Quadrupole N − 1

Quadrupole N

Segment N

Segment N + 1

$\beta_N\lambda/2$

$\beta_{N+1}\lambda/2$

$N_{\beta\lambda}\beta_{in}\lambda$

$N_{\beta\lambda}\beta_{out}\lambda$

# Poisson Superfish Codes

- Static magnetic and electric fields and radio-frequency electromagnetic fields in either 2-D Cartesian coordinates or axially symmetric cylindrical coordinates.

- Uses triangular mesh fitted to the boundaries of different materials in the problem geometry.

- Original development in the 1960s by Ronald Holsinger and Klaus Halbach.

- Major improvements and additions in the mid 1990s by Lloyd Young and James Billen.

- Windows version now supported by Los Alamos Accelerator Code Group (laacg@lanl.gov).

# Program CCLfish

- Single program incorporates several Poisson Superfish codes to tune CCL cells.
  - Automesh - Triangular mesh generator
  - Fish – RF field solver
  - SFO – Postprocessor, cavity figures of merit, transit-time factors
- CCLfish runs Superfish repetitively to tune each cell to target frequency.
  - Can adjust cavity diameter, gap, or cone angle.
  - Up to 100 jobs per input file.
  - Also adjust the tuning ring for a particular frequency effect.
- CCLcells – Companion program generates CCLfish input file containing all cells from Parmila design table.

# Properties of SNS CCL Module 1

- Length = 11.84 m
- 96 accelerating cells, 213 cavities
- 11 bridge couplers (2 with irises)
- Energy gain = 20.334 MeV
- Stored energy = 7.035 J
- Cavity power = 2.136 MW
- Beam power = 0.525 MW
- $ZT^2$ = 21.8 MW/m
- Unloaded Q = 16,660
- Loaded Q = 7,420
- Cavity-to-cavity coupling = 5.3%
- Waveguide coupling = 0.623 (each iris)
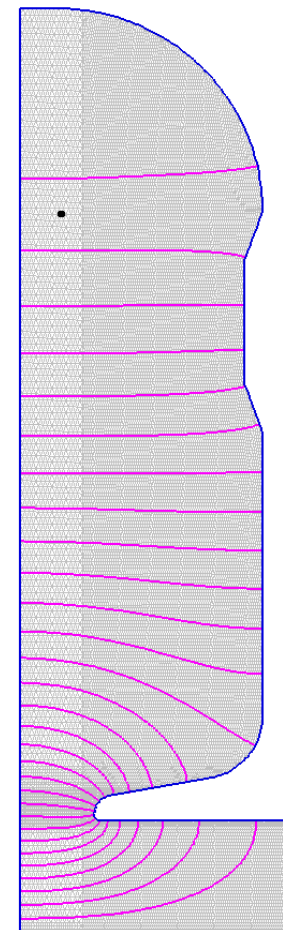
Segment 1

# Properties of SNS CCL Module 2

- Length = 12.95 m

- 96 accelerating cells,213 cavities

- 11 bridge couplers (2 with irises)

- Energy gain = 23.979 MeV

- Stored energy = 8.708 J

- Cavity power = 2.476 MW

- Beam power = 0.620 MW

- $ZT^2$ = 23.9 MW/m

- Unloaded Q = 17,790

- Loaded Q = 7,900

- Cavity-to-cavity coupling = 5.1%

- Waveguide coupling = 0.625 (each iris)
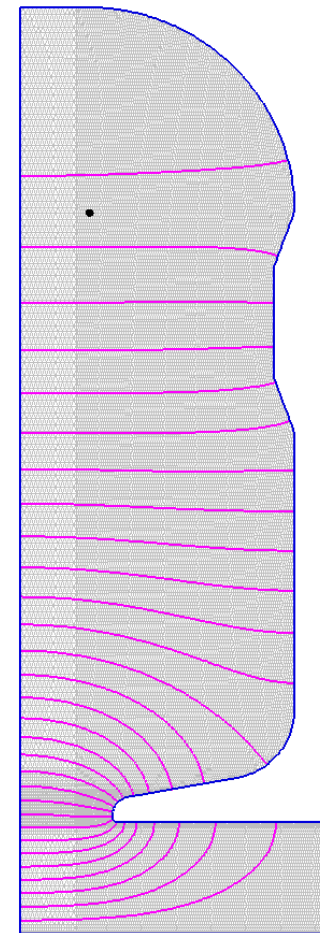
Segment 3

# Properties of SNS CCL Module 3

- Length = 14.00 m
- 96 accelerating cells, 213 cavities
- 11 bridge couplers (2 with irises)
- Energy gain = 26.074 MeV
- Stored energy = 9.320 J
- Cavity power = 2.504 MW
- Beam power = 0.674 MW
- $ZT^2$ = 25.6 MW/m
- Unloaded Q = 18,830
- Loaded Q = 8,300
- Cavity-to-cavity coupling = 4.8%
- Waveguide coupling = 0.634 (each iris)

Segment 9

# Properties of SNS CCL Module 4

- Length = 15.00 m

- 96 accelerating cells, 213 cavities

- 11 bridge couplers (2 with irises)

- Energy gain = 28.412 MeV

- Stored energy = 9.909 J

- Cavity power = 2.541 MW

- Beam power = 0.734 MW

- $ZT^2$ = 27.2 MW/m

- Unloaded Q = 19,730

- Loaded Q = 8,620

- Cavity-to-cavity coupling = 4.6%

- Waveguide coupling = 0.644 (each iris)
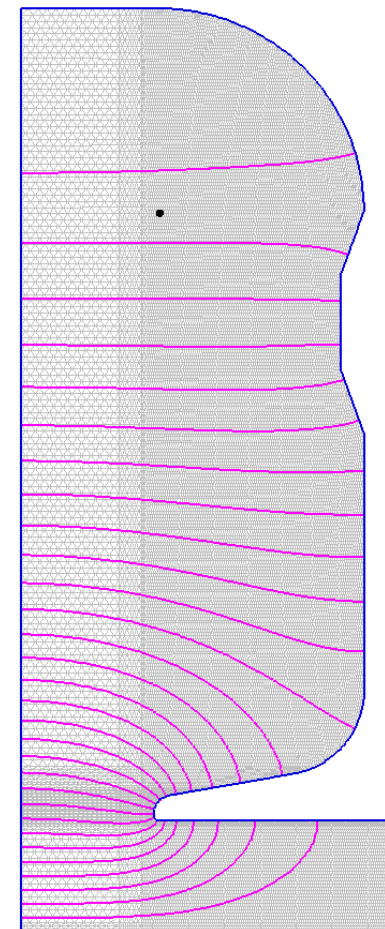
Segment 12

# CCL Cell Geometry Selections
# General Guidelines

- Cell length is $\beta\lambda/2$ (fields change sign between cavities).
  - Unlike in the DTL, there is no need to shield the beam from decelerating fields.
  - Noses increase efficiency by shortening the gap and increasing the transit-time factor.
- Beam-dynamics studies define required bore radius.
- Spherical shaped cavity wall reduces surface to volume ratio.
- Module length set by RF power supply (including beam power)
- Vary other parameters systematically to maximize $ZT^2$ .
  - Optimize cells at ends of a velocity range, interpolate in between.

# CCL Cell Design Procedure

- First, optimize for highest $ZT^2$ at both ends of a range of velocity $\beta$ by varying nose shape, gap length, corner radii.
  - For this study, vary the cavity diameter varied to tune cells.
- Bore radius = 1.5 cm fixed by beam-dynamics design criteria.
- Septum thickness = 1.0 cm set by cooling requirements.
- To simplify the manufacturing, we make some compromises.
  - All eight accelerating cells in a segment are identical.
  - Fix the cavity diameter, outer corner radius, and coupling slot dimensions over the entire CCL, using average dimensions from the optimization exercise.
  - All side coupling cavities are identical.
- Tune one cavity for each segment by slightly adjusting the gap.

# A Few Characteristics of the SNS CCL
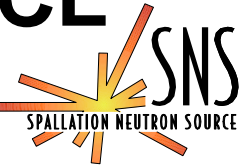
- Energy range: 86.8 MeV ($\beta$ = 0.403) to 185.6 MeV ($\beta$ = 0.550)
- Four rf modules, each with a 805-MHz, 5-MW klystron (2 irises).
- Bridge couplers span the 2.5 $\beta\lambda$ magnet/diagnostic spaces between 8-cavity segments, 12 segments/module.
- Total length = 54.3 m. Bore radius = 1.5 cm.
- Nominally 5% cell-to-cell coupling.
- Peak surface electric field > 33.9 MV/m (1.3 Kilpatrick).
- Nominal accelerating field $E_0$ = 3.77 MV/m. (Field ramps up over the first 9 segments, starting from 3.06 MV/m.)
- $ZT^2$ = 25 M$\Omega$/m (real-estate length), 40 M$\Omega$/m (cavity length)

# CCL Tuning Plan is an Integral Part of the Manufacturing and Assembly Process

- Goal is $f_{\pi/2} = 805.00 \pm 0.01$ MHz, ~5% coupling, and closed stop band under operating conditions.

- Accelerating cavities include two features for tuning at different stages:

  – Pre-braze stack up, machining the tuning-ring has 2.5 MHz range.

  – Post-braze tuning, "dinging" tuning holes has 400-kHz range.

- Coupling cavities are tuned by squeezing or pulling apart the noses.

- Bridge-couplers (total length 2.5 $\beta\lambda$) make room for EMQs while making a continuous rf structure.

  – Slug tuner in powered cell has ~5-MHz range.

  – TE-mode suppressor doubles as tool to adjusts field level in adjacent segments.

# 5% Coupling Produces <0.1% Power Flow Droop for a Perfectly Tuned Linac

Field in cavity n=0 for drive in cavity m=24, $Q_a \sim 16{,}800$, $Q_c \sim 8000$, Stop band $\delta f \sim 50$ kHz, no other frequency errors:

$$X_{2n} = (-1)^{n-m} X_{2m} \left[ 1 - \frac{2(m^2 - n^2)}{k^2 Q_a Q_c} + j \frac{4(m^2 - n^2)}{k^2 Q_a} \frac{\delta f}{f} \right]$$

Making droop and phase shift negligibly small with perfect tuning allows room for effects of frequency errors, beam loading, and chopping.

| k(%) | Droop(%) | Phase shift(deg) |
|------|----------|------------------|
| 1    | 8.5      | 0.049            |
| 2    | 2.1      | 0.024            |
| 3    | 0.24     | 0.016            |
| 4    | 0.13     | 0.012            |
| 5    | 0.086    | 0.010            |

# A CCL Aluminum Model

# Half Cell Assembly Includes Pre-braze and Post-Braze Tuning Features
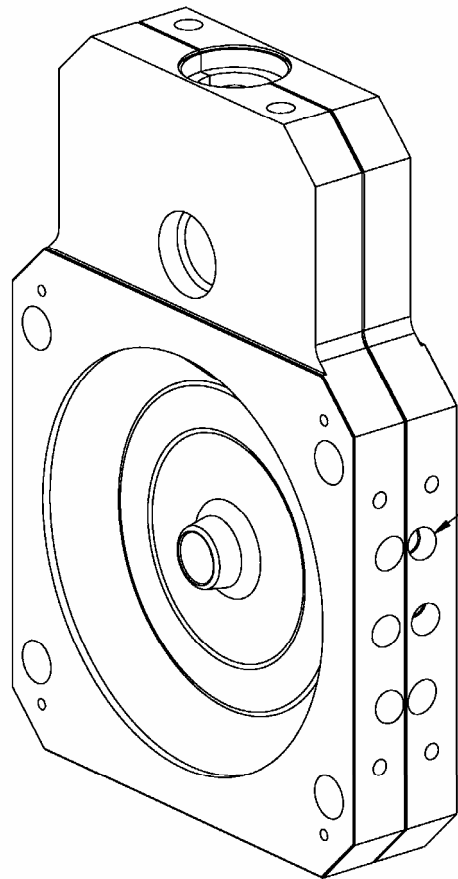


Post-braze tuning by "dinging" on thinned areas
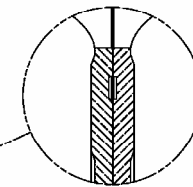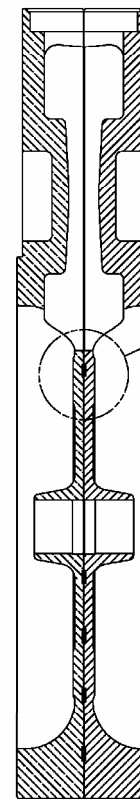
Pre-braze tuning by machining on tuning ring

# Early Bridge Coupler Design Magnetically to Coupling Cells

Waveguide taper to coupling iris

Coupling slot

Slug tuner
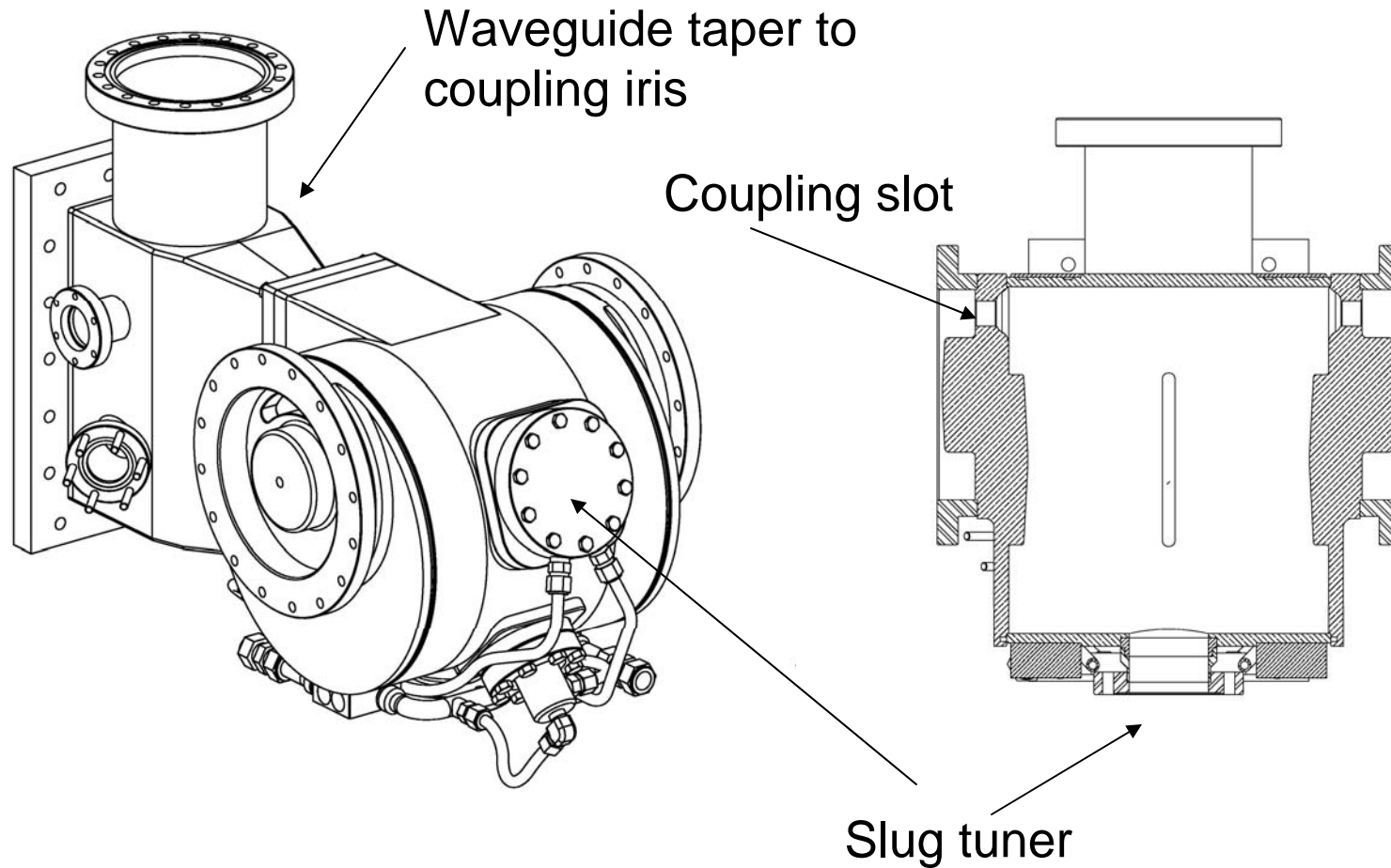
# We Use Low-Power Measurement Results to Analyze the Entire RF Module

- We supply to coupled-circuit code LOOP:
  - Superfish-calculated stored energies for all 12 segments' accelerating cells, all coupling cells, and center bridge cells
  - Measured nearest neighbor and 2nd nearest neighbor couplings
  - Measured accelerating-cell frequencies (internal and end cells)
  - Measured coupling constants for bridge cells
- Program LOOP computes 213 modes of the $TM_{010}$ band
- Fitted dispersion curves to these modes (for biperiodic structure, an approximation) gives coupling and stop band.
  - Red curve (see next slides): all modes
  - Green curve: 23 modes centered on $\pi/2$ mode

# Dispersion Curve Computed Using Coupled Circuit Analysis

- Blue crosses: mode frequencies from coupled circuit analysis using measured cavity data.

- Green curve: fit to 23 modes centered on $\pi/2$ mode.

- The asymmetry in the dispersion curve is the result of second neighbor coupling (between accelerating cells).
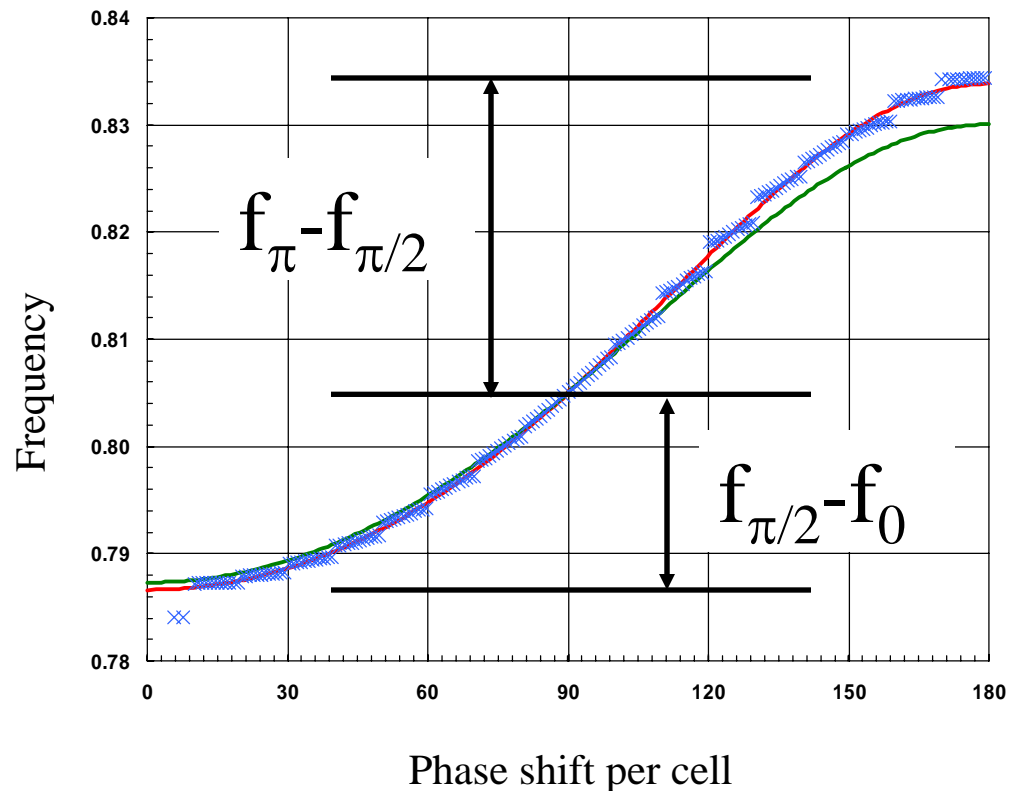
# Cold Model Measurements on Short Segments (No Bridge Couplers)
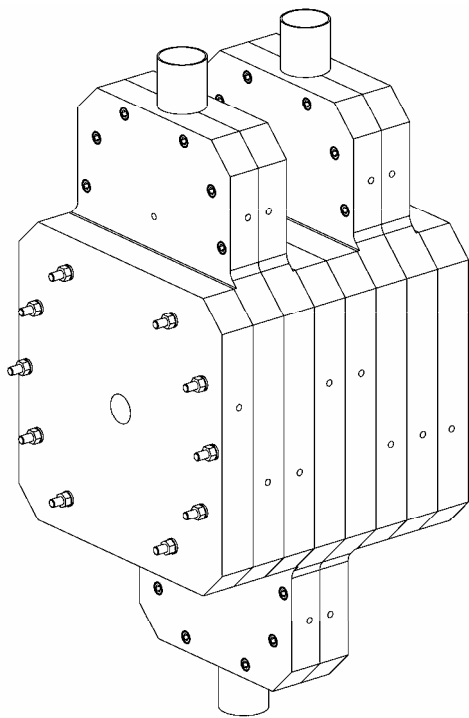


End-of-module termination
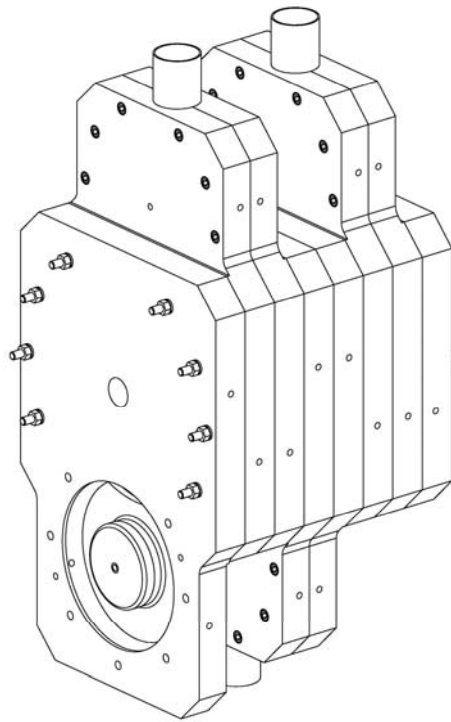


Bridge coupler termination

Measure the individual cavity frequencies.

Measure structure modes and fit the dispersion curve to determine coupling.

Tune the accelerating cavities to make $\pi/2$ mode frequency 805 MHz.

Tune the coupling cavities to close the stop band.

# More Measurements Use Two Tuned 4-Cell Segments and the Bridge Coupler
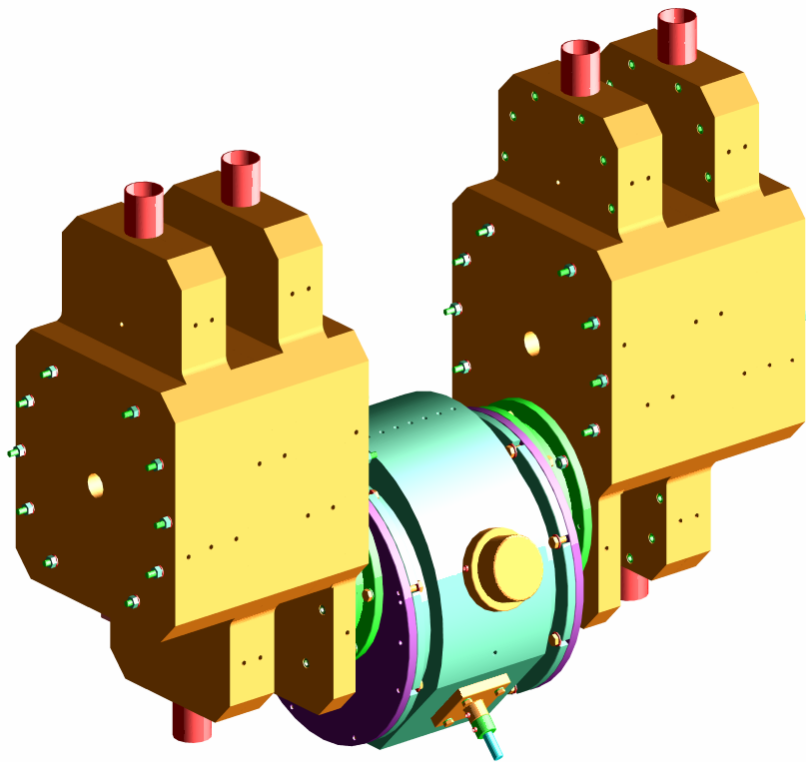


Tune the bridge coupling cells and the center bridge cell.

Measure dispersion curve for the entire structure.

Directly measure 2nd neighbor couplings.

Measure fields on axis and near slots.

# Cells Frequencies and Coupling Factors From Cold Model Measurements

- Frequencies
  - $\pi/2$ mode: 805.0 MHz
  - Coupling cell (average): 805 MHz
  - Internal accelerating cell (average): 809.8 MHz
  - End accelerating cell (average) 807.4 MHz
- Coupling constants
  - Nearest neighbor within segment: 5.5%
  - Accelerating cell 2nd nearest neighbor: 1.1%
  - Accelerating cell to center bridge cell: ~0.5%
  - End accelerating cell to bridge coupling cell: 4%
  - Bridge coupling cell to center bridge cell : 7%

# CCL Manufacturing and Tuning
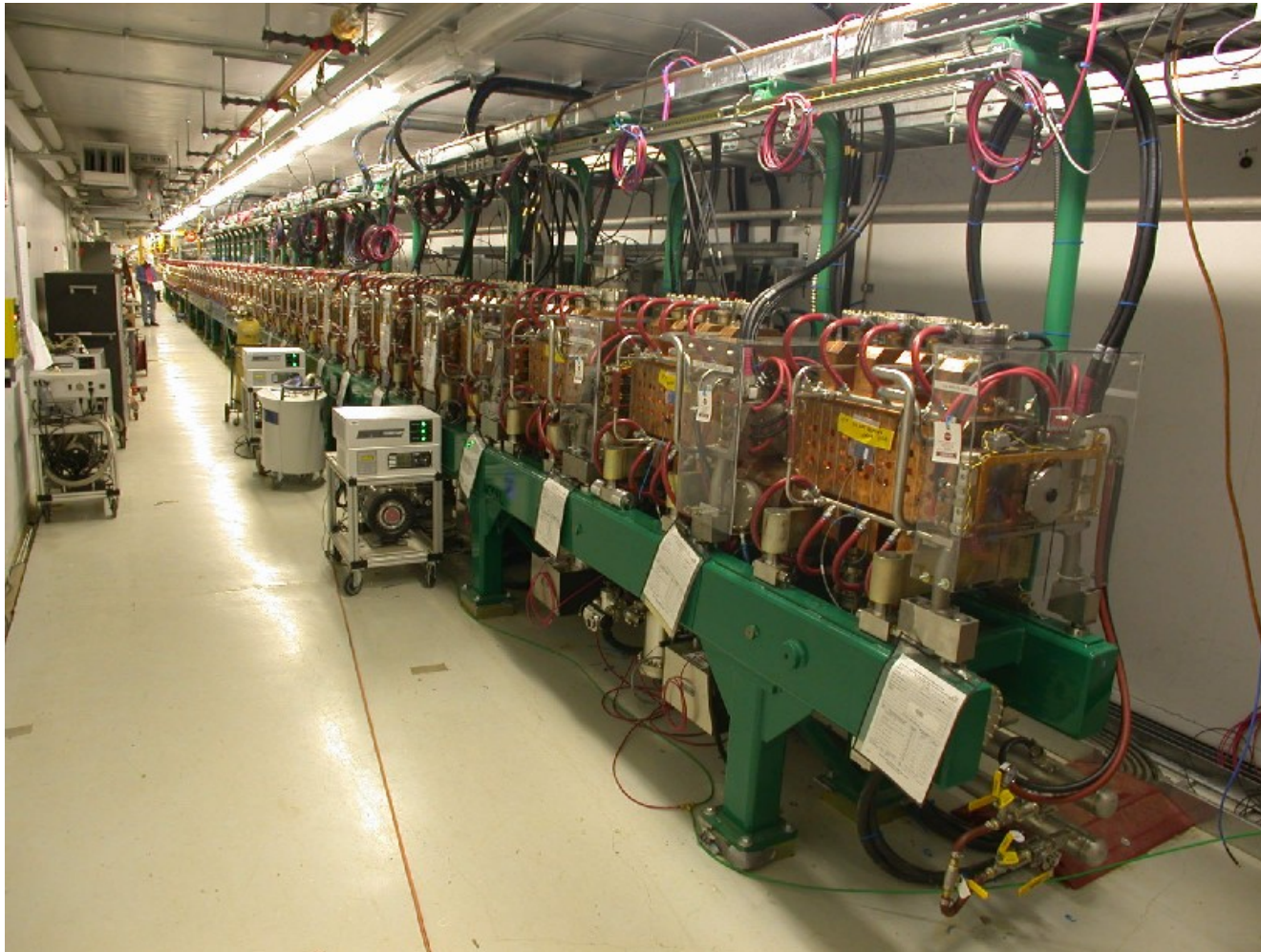
# Fabrication Steps for Building a Segment (Photos from Hot Model)


End wall machining


Waiting for next step in shop


Mechanical Inspection
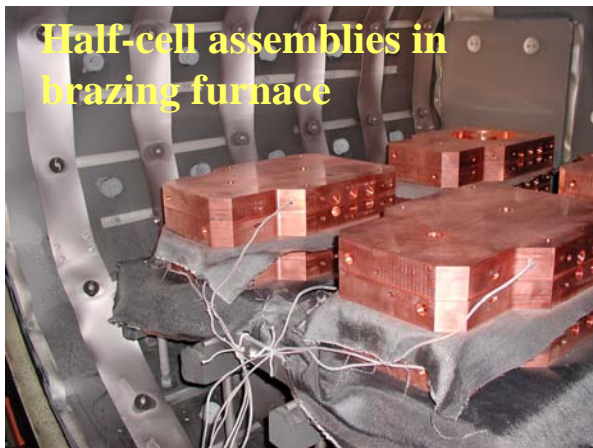

Half-cell assemblies in brazing furnace


Segment stacking
6/17/2001


In handling fixture

*SNS Linac*

# Preparing Half-Cell Assemblies for the Segment Stack Braze
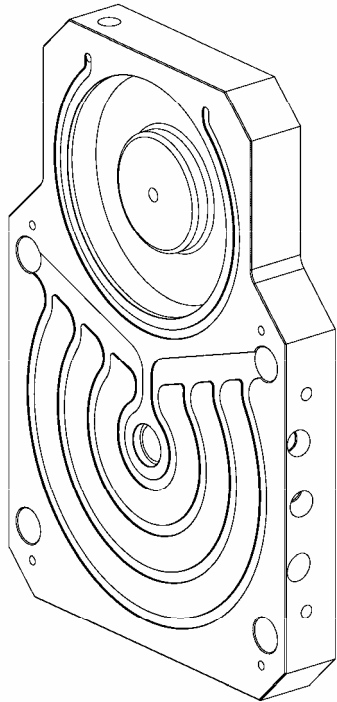


Half cell with finished septum side features, ready to braze
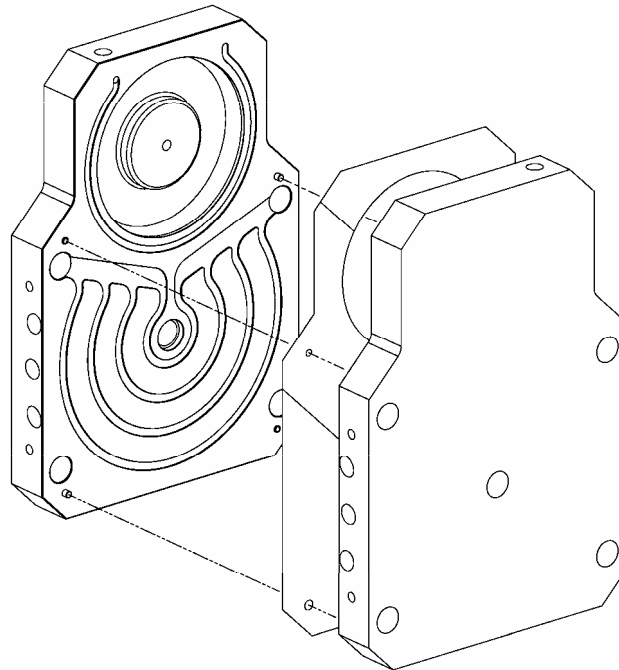
Half-cell plates assembled with the brazing foil and locating pins
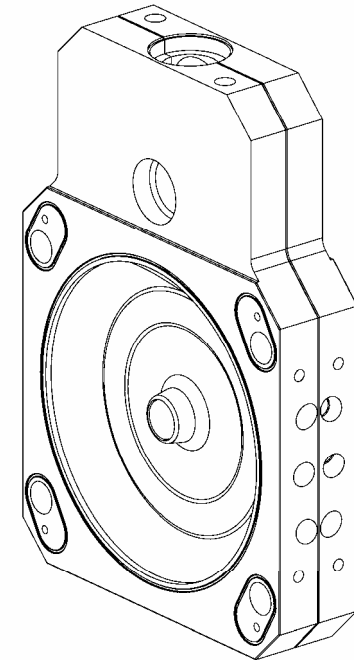
Brazed unit with machined equator surface, ready for the stack braze.

# Half Cells Start Out as Copper Plate



Hot-model stock

On milling machine

CCL production stock
at Los Alamos

8/27/2001

*SNS Linac*
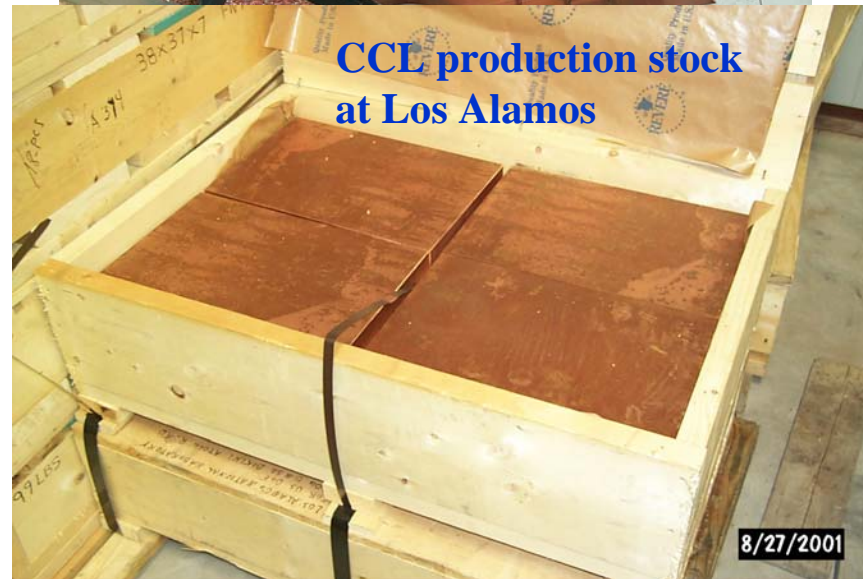
# Half-Cells are Turned to a Fixed Geometry
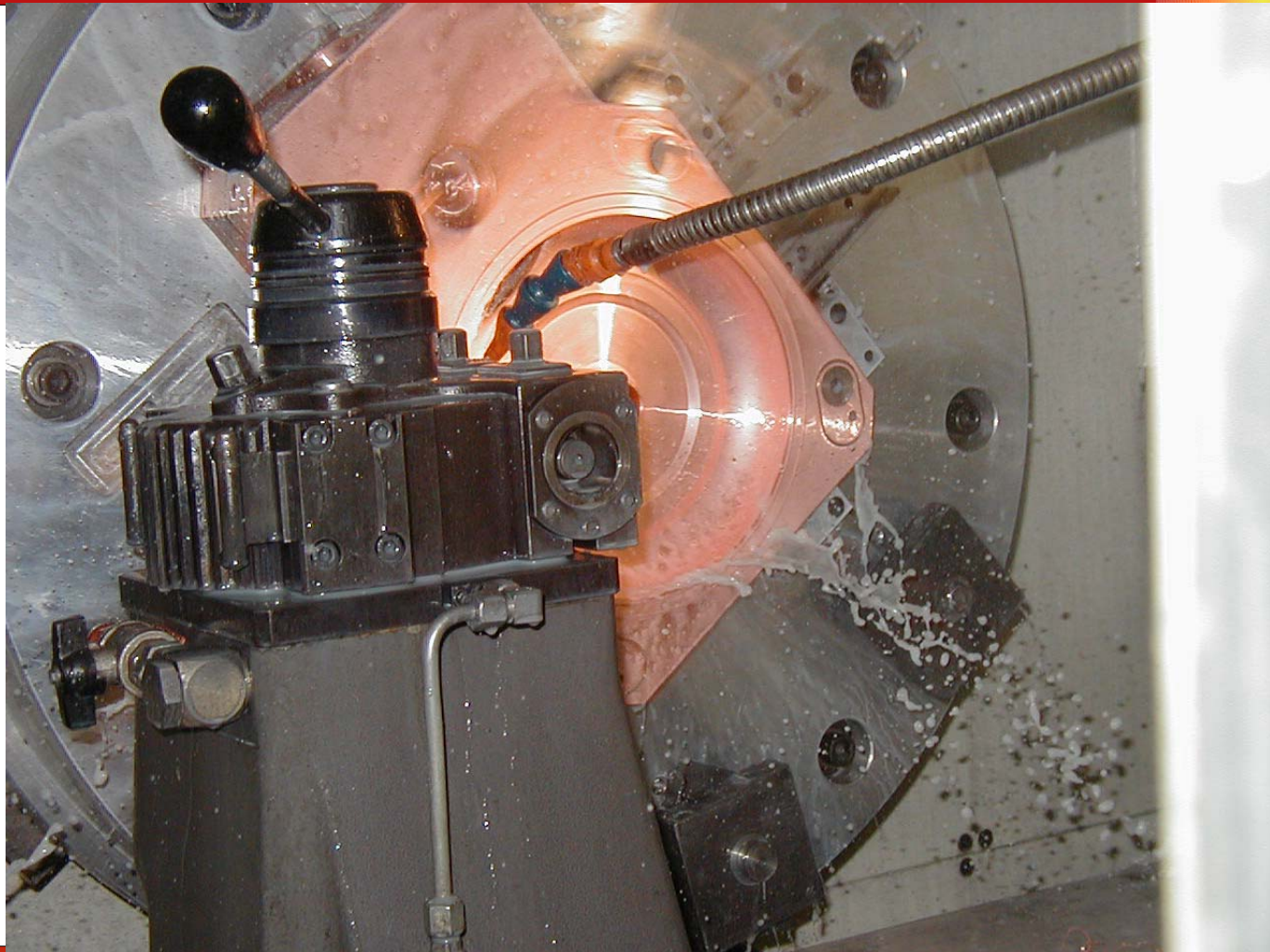
# Segment End Wall
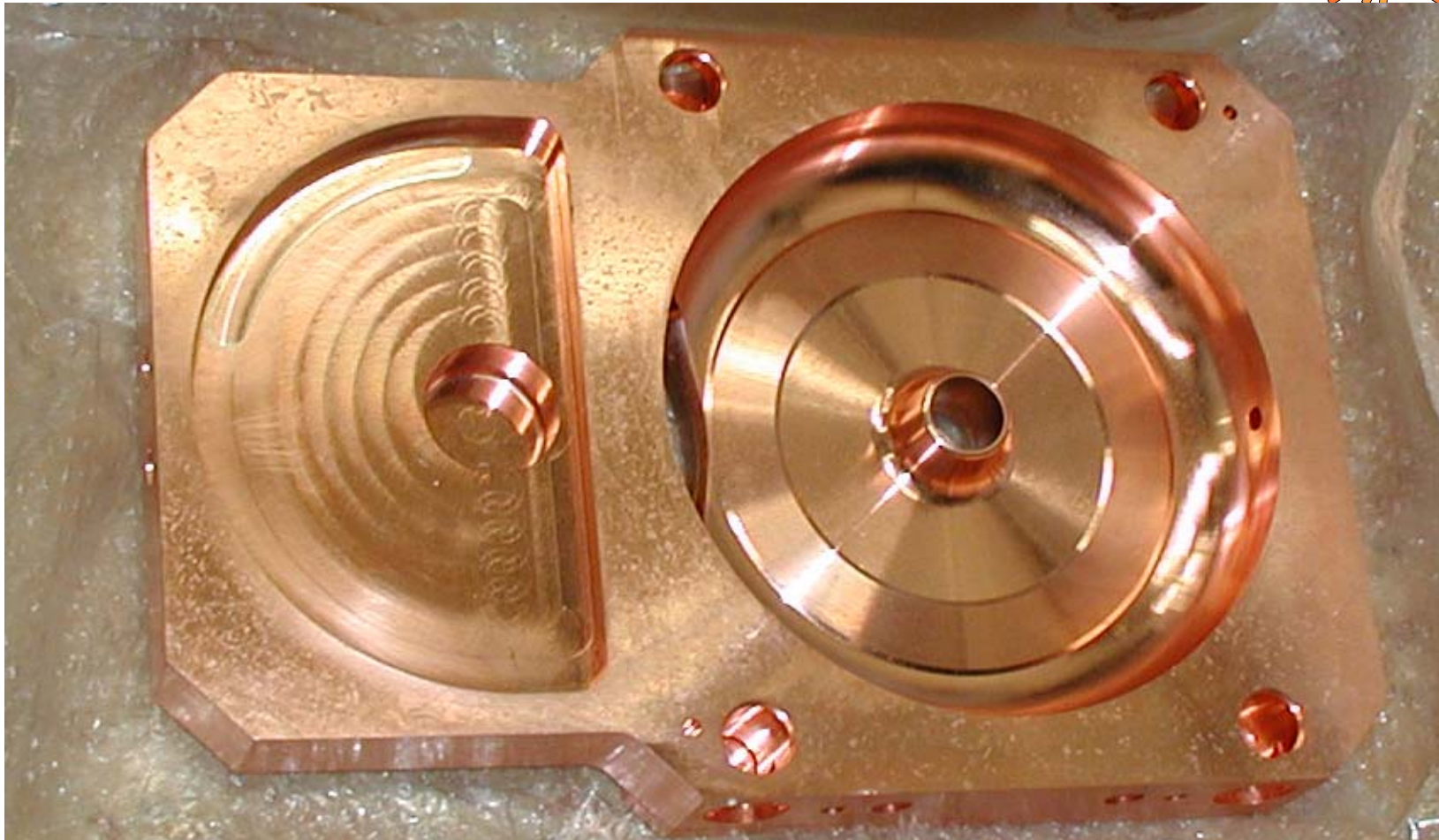
# Half Cell Assemblies Ready for Brazing

- The septum braze uses alloy of 50% gold and 50% copper.
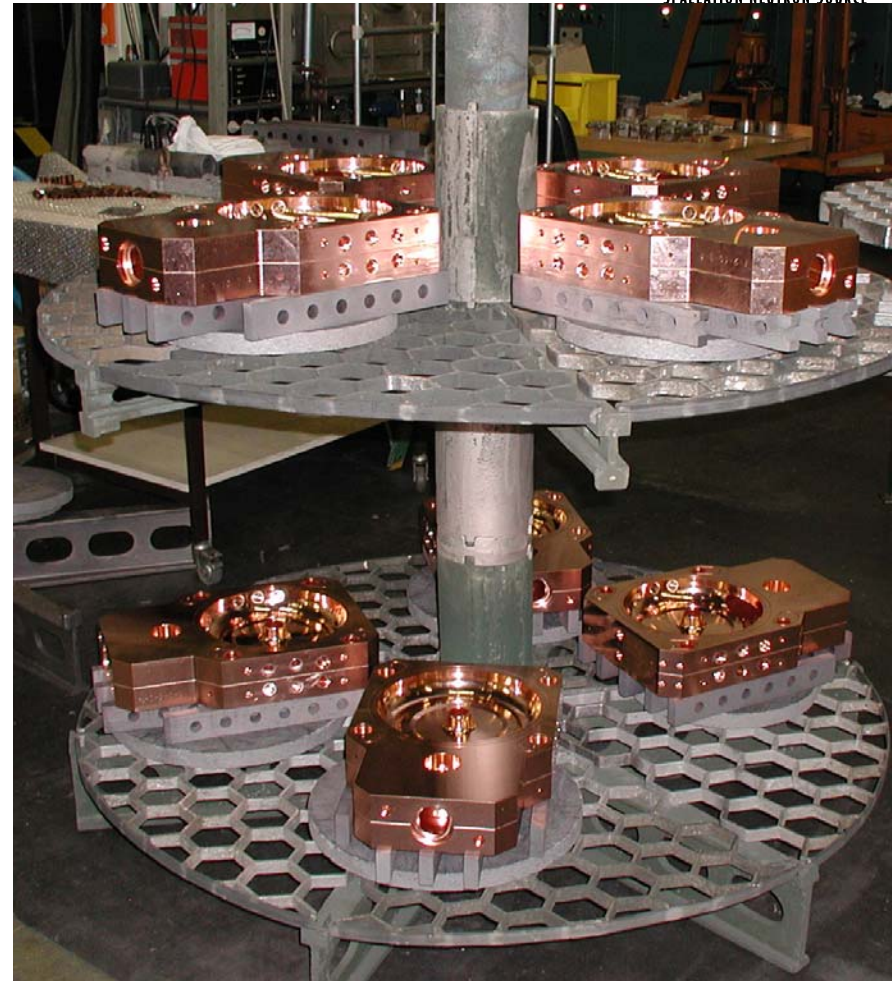
# Pre-Braze Segment Tuning Steps

- With segment stacked, find the frequency offset between the segment $\pi/2$ mode and the frequency of the 6 internal accelerating cells.
  - Second neighbor coupling is the origin of this offset, which causes distortion of the dispersion curve.
  - For SNS with 5% coupling, the offset is about +4.5 MHz (i.e., accelerating-cell frequency of 809.5 MHz.)
- Unstack, and measure the frequency of all 14 internal half cells.
- Compute the frequency change needed for each half-cell and machine the tuning rings to make the $\pi/2$ mode ~150 kHz below its final value.
  - After brazing, dimple tuning will raise accelerating-cell frequencies.
- Restack, and check the $\pi/2$ mode before brazing.

# Pre-Braze Measurements of Segment $\pi$/2 Mode and Individual Accelerating Cells
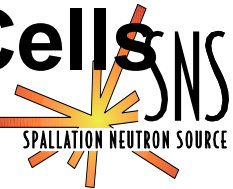
- Find the <u>frequency offset</u> between individual accelerating cells and the $\pi$/2 mode, (about +4.5 MHz).

- Measure $\pi$/2 mode.

- Find average frequency of individual accelerating cells, with nearby cavities shorted.

- Coupling cavities are not tuned at this time. They contain no significant field in the $\pi$/2 mode, so even if badly mistuned then do not influence this procedure.

Coupling-cell short
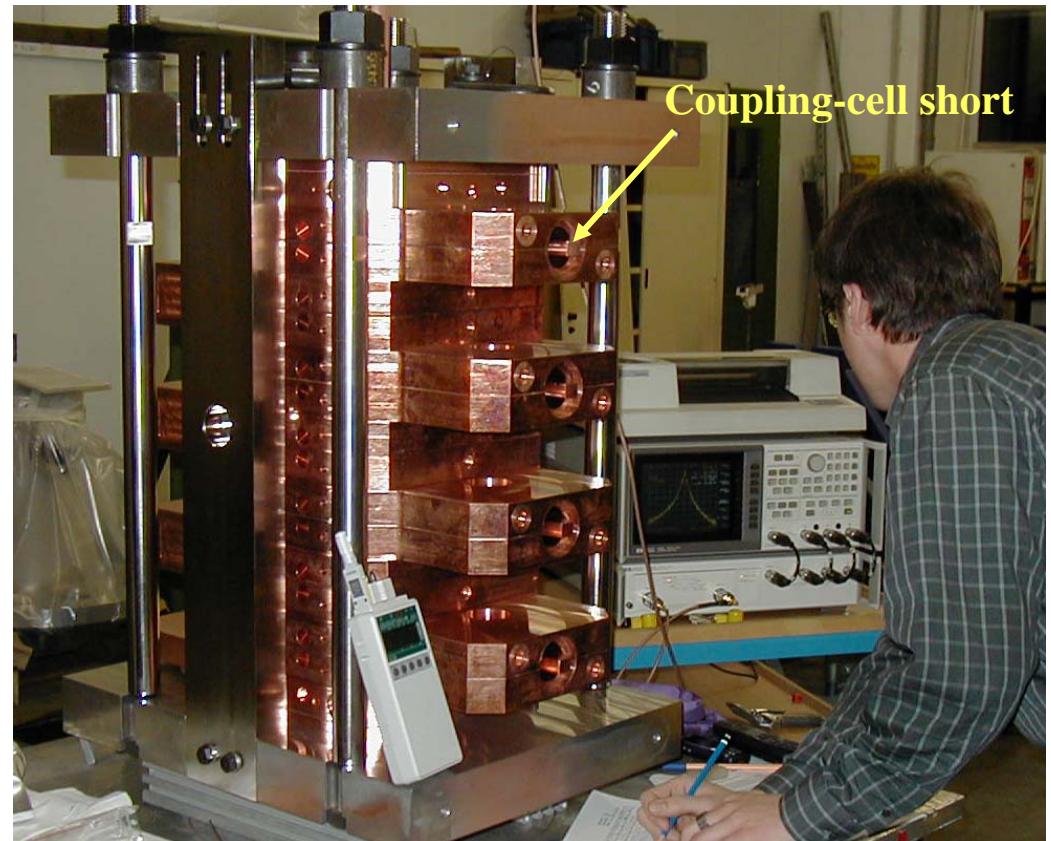
# Measuring Individual Half-Cell Frequency
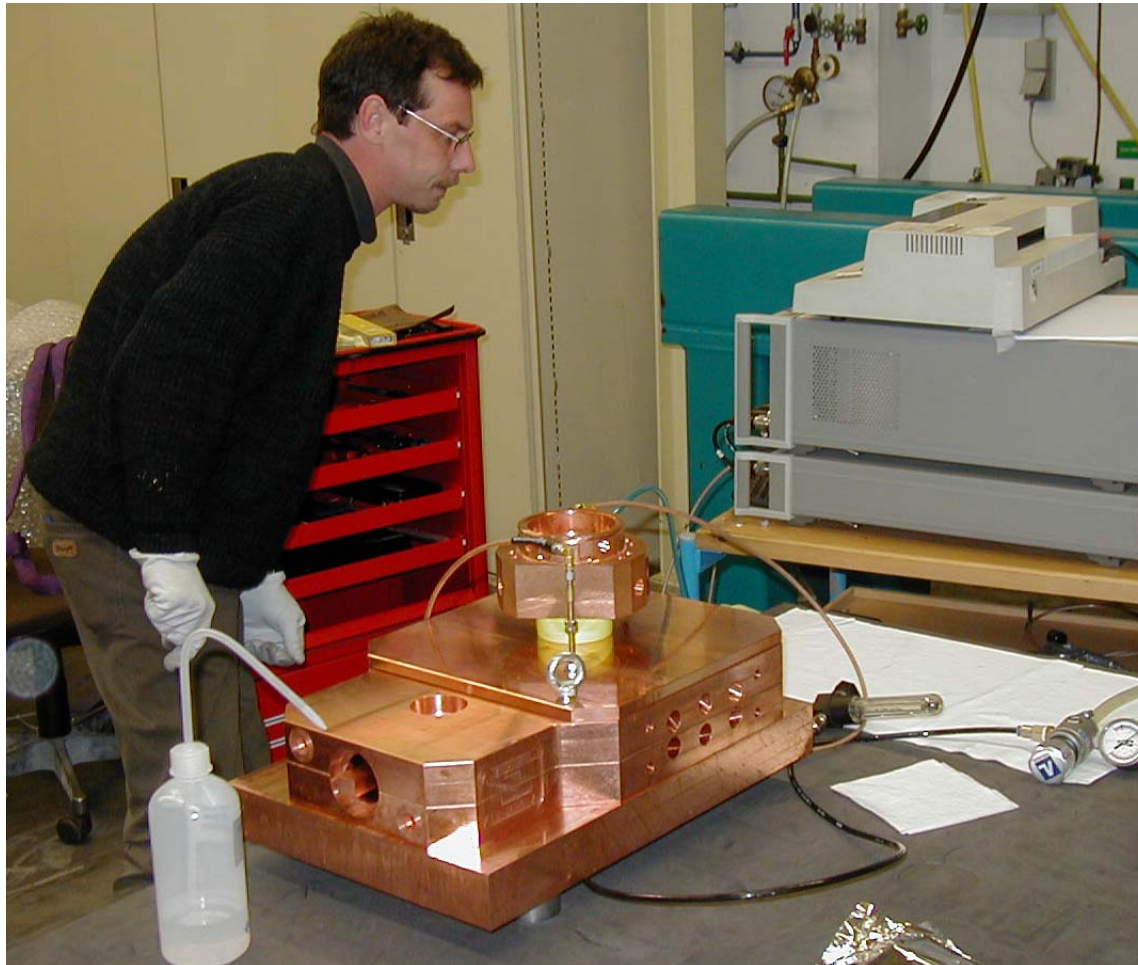
# Milling the Tuning Ring at ACCEL
# to Correct the Half-Cell Frequency
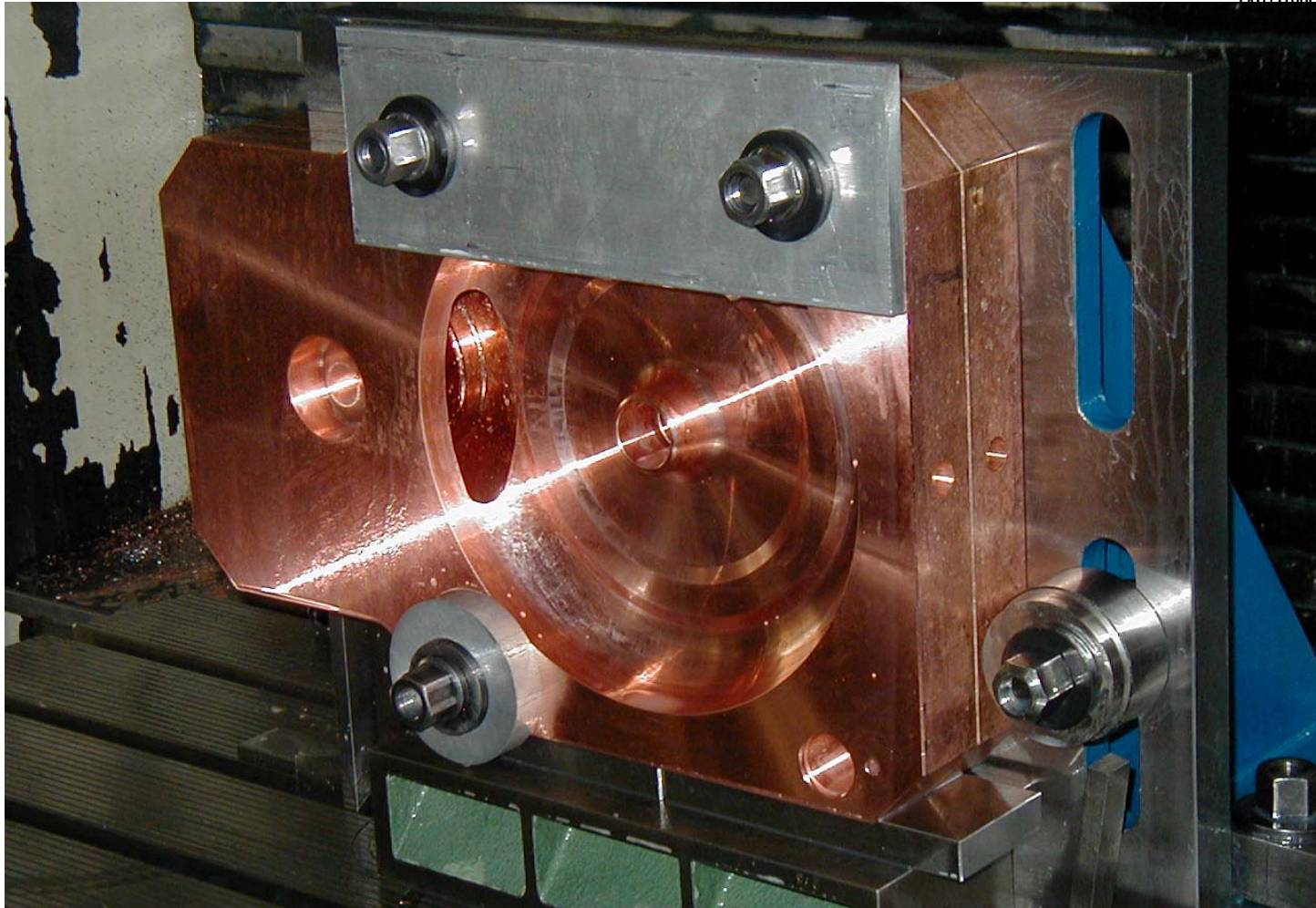
# Segment Ready for Brazing in Vacuum Furnace
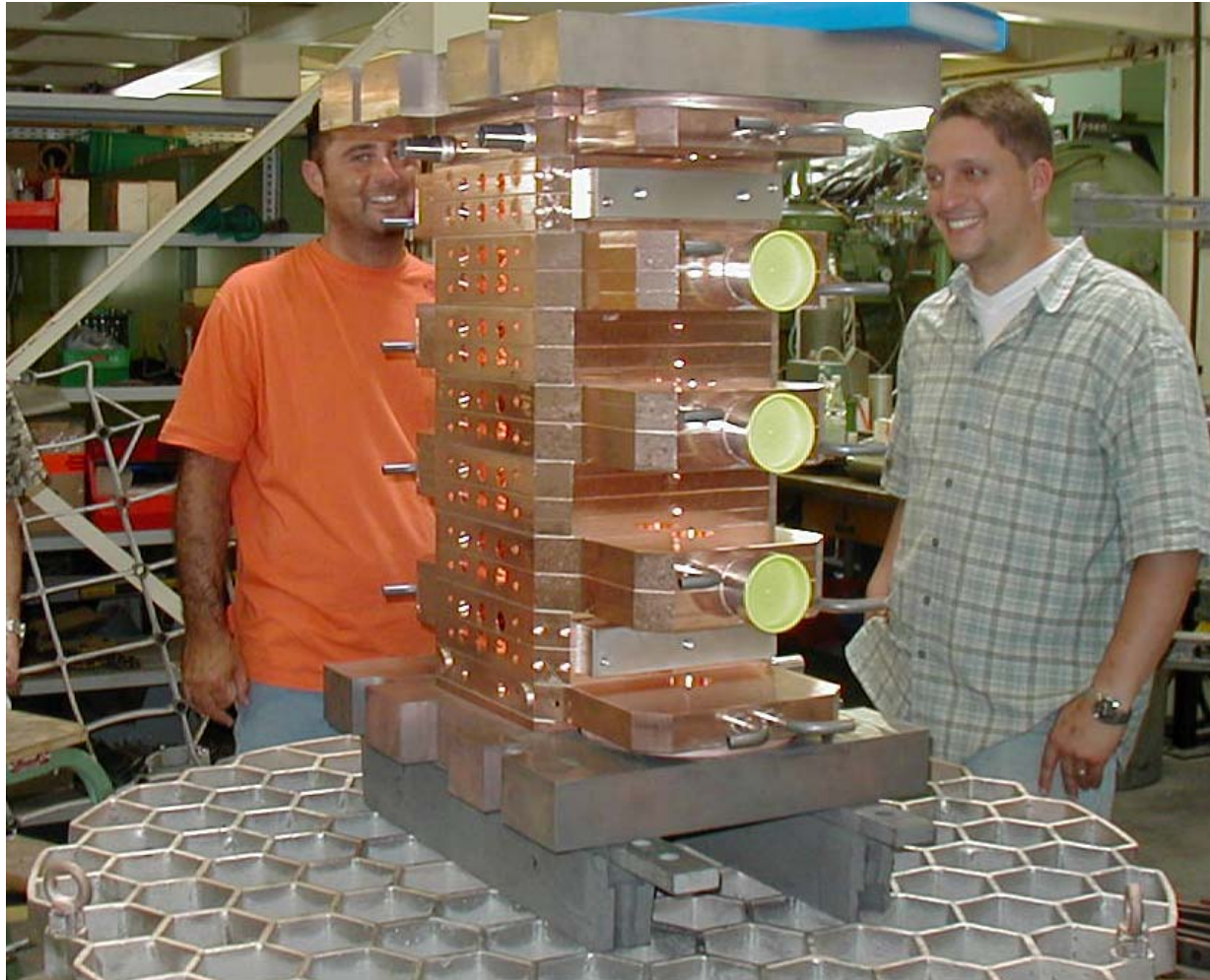
# Post-Braze Tuning Methods for Three Cell Types on Individual Segments

- Six internal accelerating cells.
  - Pre-braze tuning left these cells low by ~200 kHz.
  - Raise frequency by dimpling the cavity wall (12 locations).
- Two end accelerating cells per segment.
  - Tune these cavities to properly terminate the structure ($f_{\pi/2}$ + half the accelerating-cell offset), by pulling or pushing on the end wall.
  - In the module configuration, the require a different frequency.
- Seven internal coupling cells.
  - Tune by squeezing noses together with a hydraulic tool, or by spreading noses apart.

# First Step: Tune Internal Coupling Cavities to the Target Frequency of the Module
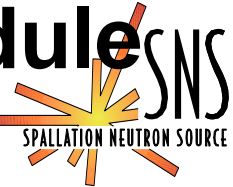
- Target frequency for $\pi/2$ mode is 805 MHz plus offset expected from thermal gradient at full rf power.
  - Correct for air temperature, pressure, and humidity, and copper temperature. (Dry nitrogen eliminates need for humidity correction.)
  - For module-1 segments: 805.110 MHz.
  - Based on module-1 experience, we chose a slightly lower frequency for segments of modules 2, 3, and 4.
- Short all cavities except the one under test.
- To lower frequency, squeeze noses while observing mode on network analyzer.
- To raise frequency, remove probes, spread noses with steel wedge, then return to squeezing method.

# Pre-Tune Accelerating Cavities to the Same Frequency

- More accurate $\pi/2$ mode measurements possible when all accelerating cells have equal frequency.
- Chose a frequency slightly above the present highest frequency.
- Short all cavities except the one under test.
- Dimple the wall using spherical-end rod and large hammer (12 dimpling locations available on each cavity).
- Observe frequency while hammering until close to target (easy to achieve ± 10 kHz).

# "Dimple Tuning" Reduces Cavity Volume in Predominantly Magnetic Field Region

# Dimpling Port Manufacturing Problem Solved by Brazing in New Ports

- Datum for the port location was moved from the septum surface to the cavity mid-plane surface.
- The new dimension is not constant as cavity length changes!
- Affected 18-20 segments.



This area became too thin as cavities got longer

Cavity mid-plane

Septum

# Tune End Accelerating Cavities

- Tune the end cavity to minimize the stored energy in the adjacent internal coupling cell (not visible in picture).

- This is a temporary setting for the individual segments.

  – Re-tune when later connected to the bridge coupler.

- Procedure

  – Excite the $\pi/2$ mode.

  – Observe the coupling-cell field amplitude.

  – Pull on the end wall (or tap the wall in) to minimize amplitude.



End wall pulling fixture
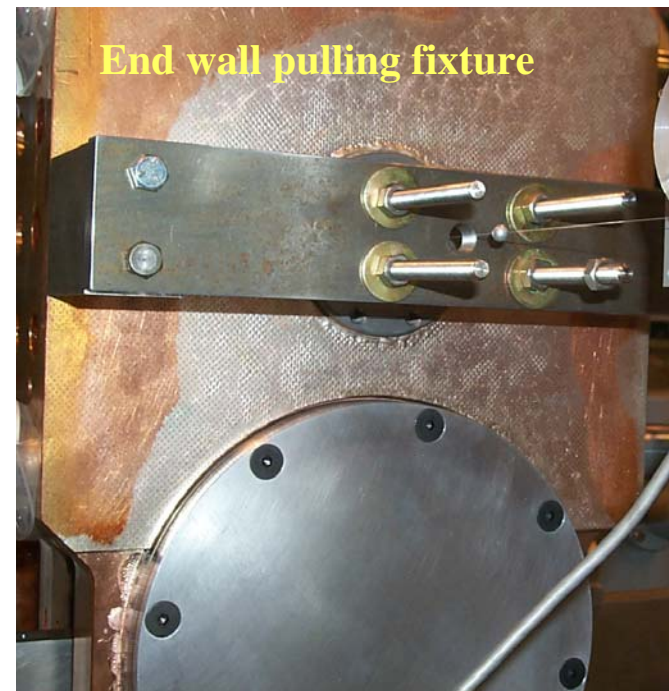
# Complete the Segment Tuning

- Measure the $\pi/2$ mode frequency and compute the change needed to achieve the module's target frequency.
- Raise the frequency (individually) of the 6 internal accelerating cells by dimpling the walls, and retune the end cells for minimum stored energy in the adjacent coupling cells.
  - On the first iteration after initial tuning of accelerating cells to a common value, stop ~100 kHz short of the target because large changes may distort the septum and detune adjacent cavities.
- Repeat until $\pi/2$ mode frequency within tolerance ($\pm10$ kHz).
- No further coupling-cell tuning until module tuning.
  - On module 1, we closed the stop band, but ended up re-tuning the coupling cells to nearly their initial setting.

# Segment Flow Testing

# Segment Vacuum Testing

# Milling Segment to Design Length
# Also Makes End Flanges Parallel



Copper-plated
steel flange

SNS Linac
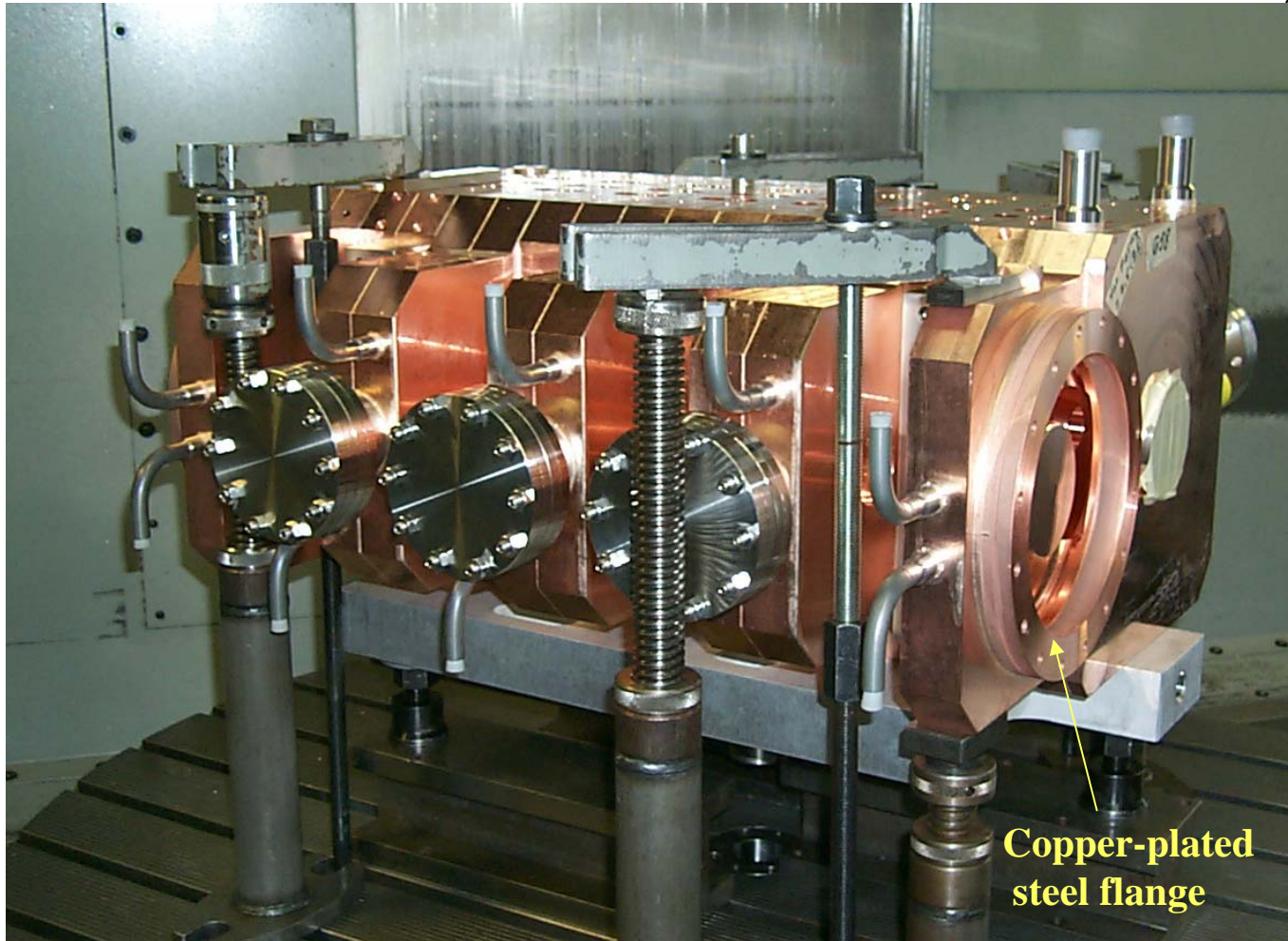
# Installing a Segment on the Support Stand



SNS Linac

# Half the Segments Installed

# Bridge Coupler Manufacturing and Tuning
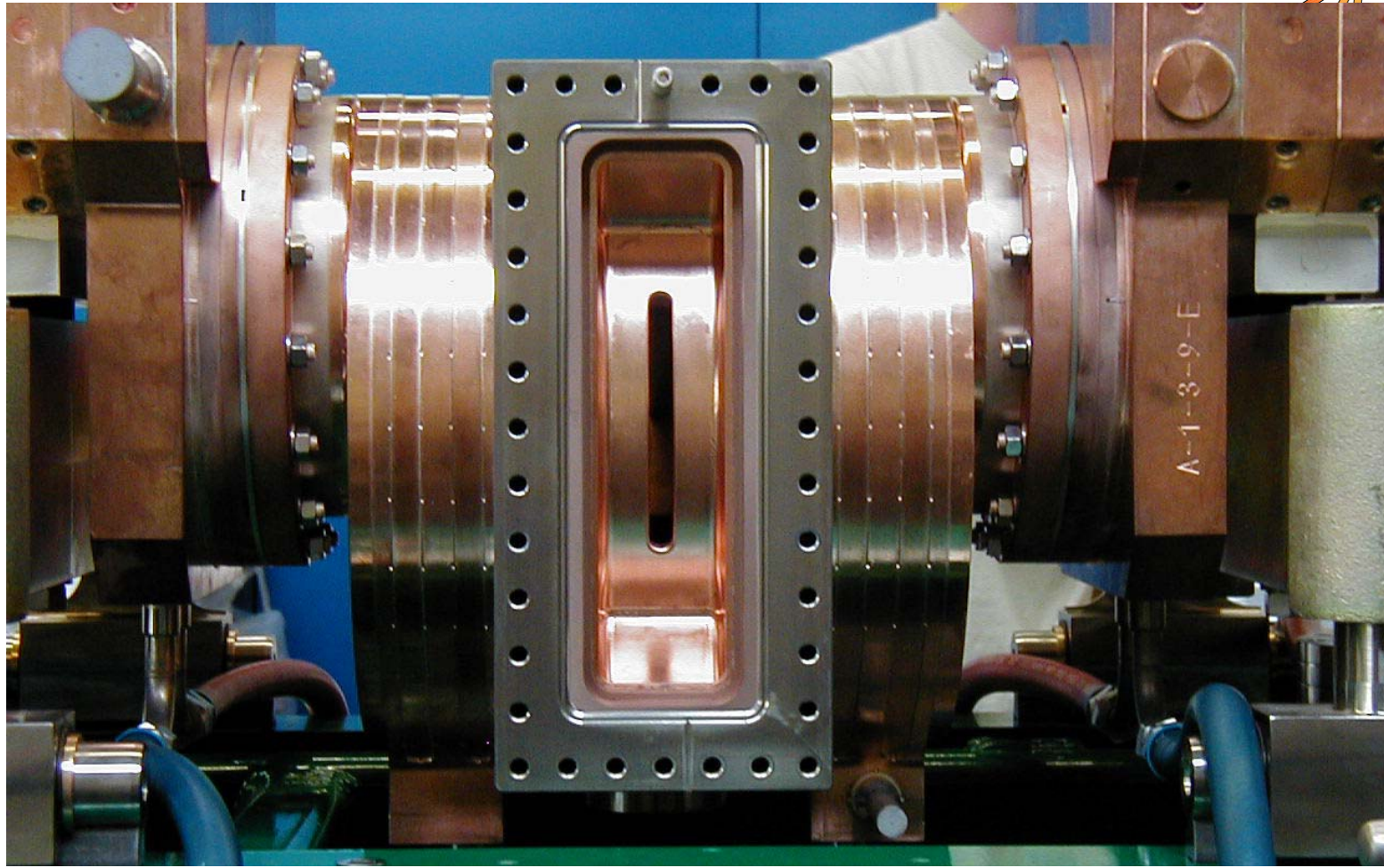
# Machining the Hot Model Bridge Coupler
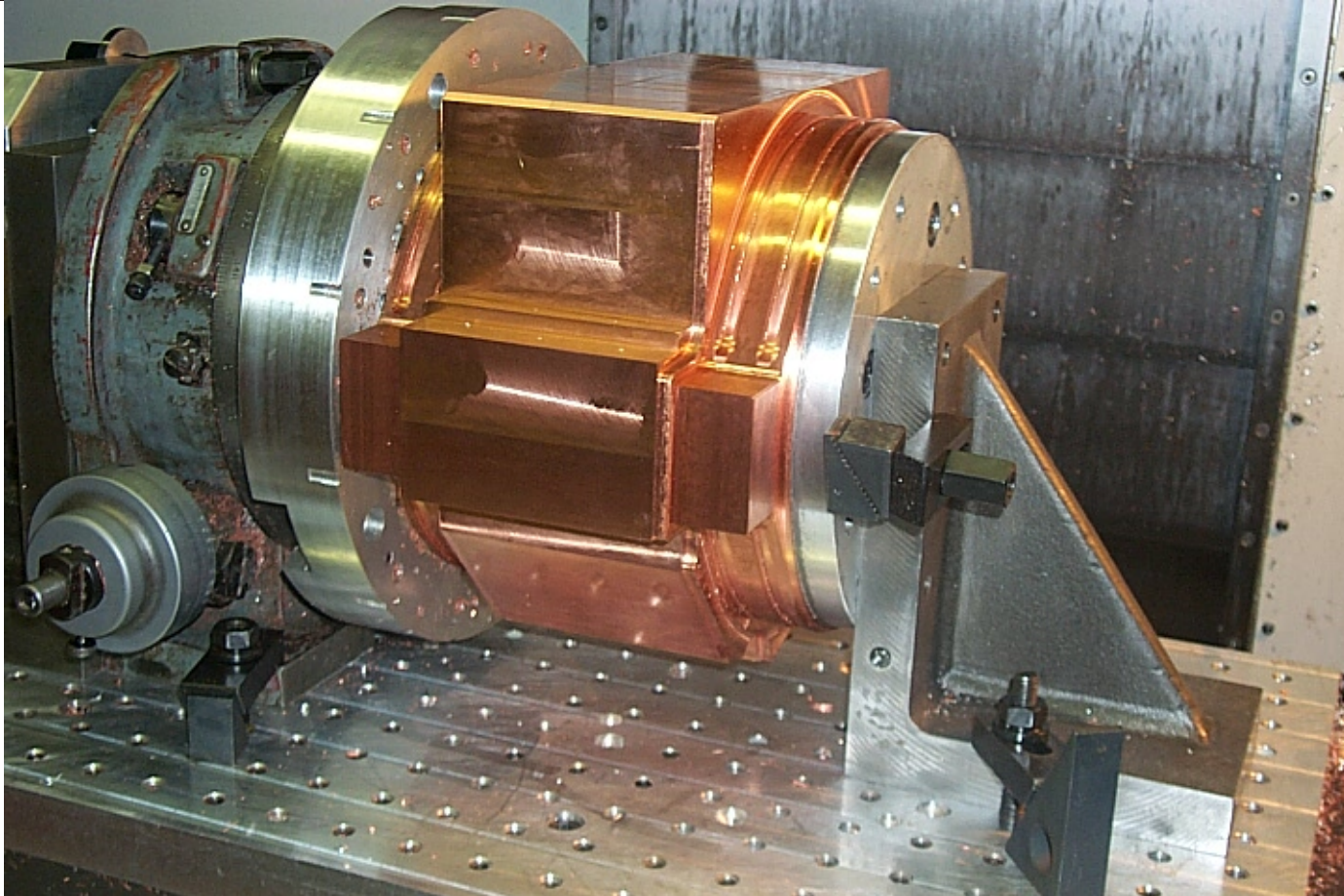
# Hot Model Bridge Coupler Body
# with TE-mode Tuner
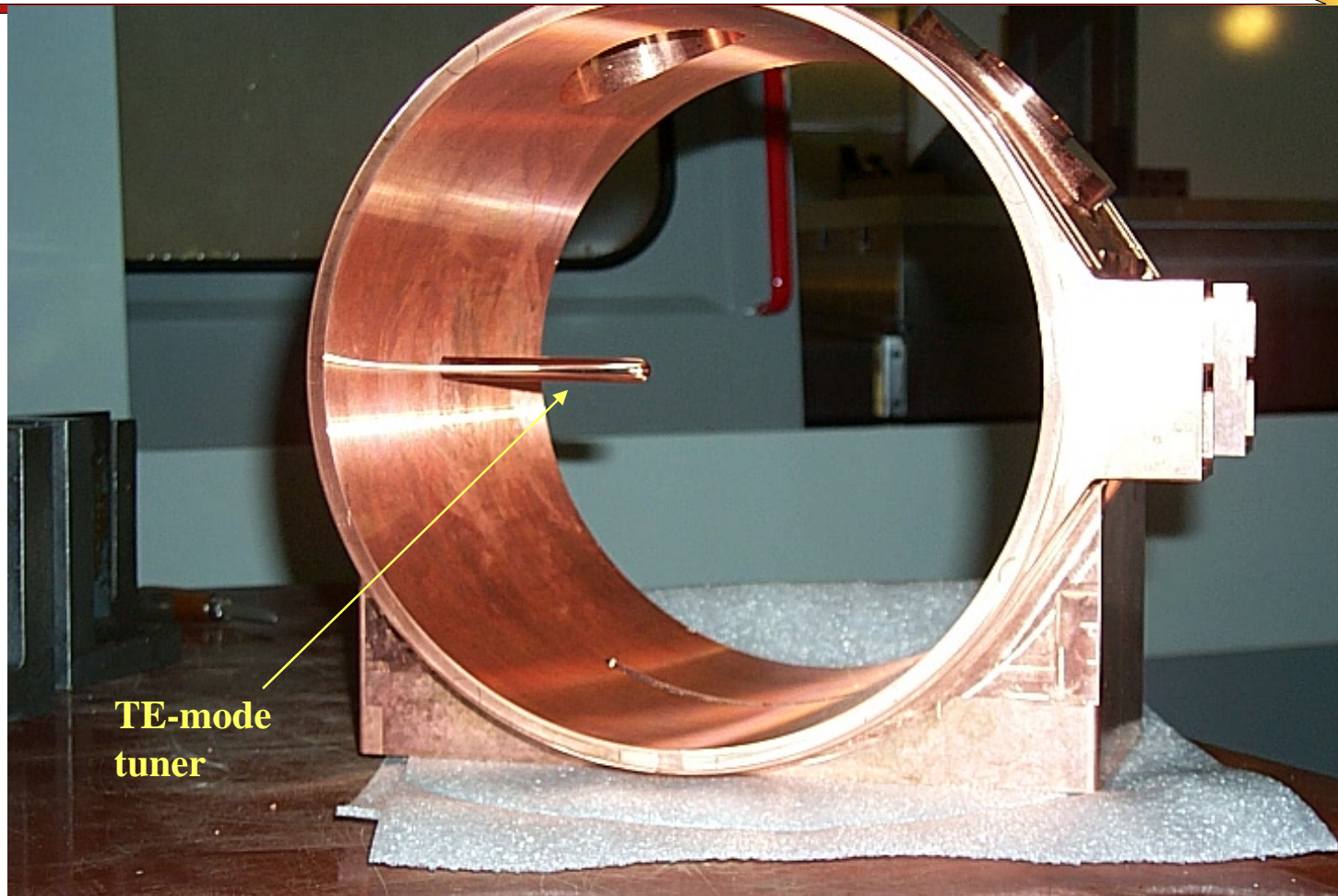


TE-mode tuner

# Bridge Coupler Parts Ready for Welding (ACCEL will use brazed assembly.)



"Smiley-face" coupling slot
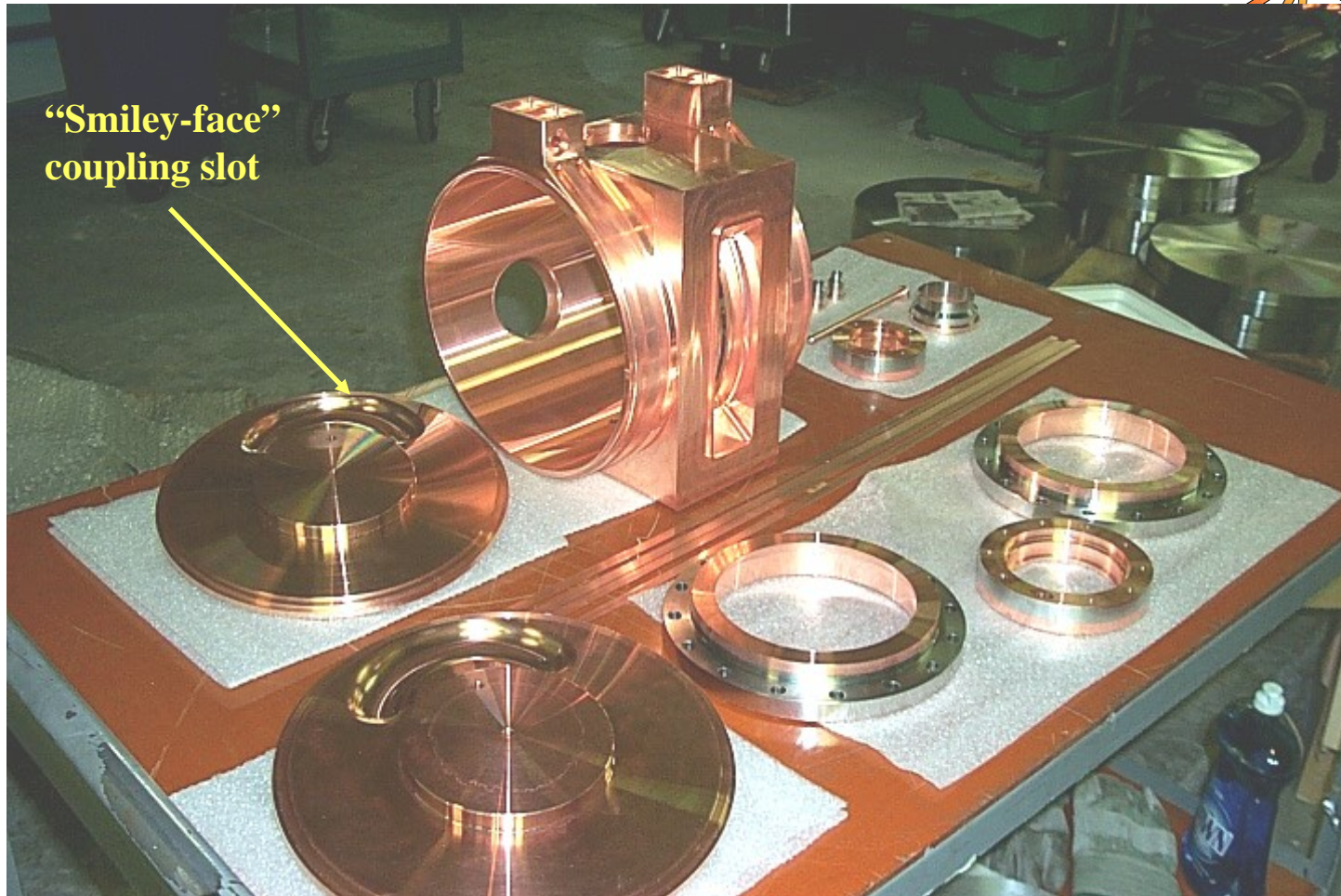
# Completed Hot Model Bridge Coupler
# (Some details changed for production)
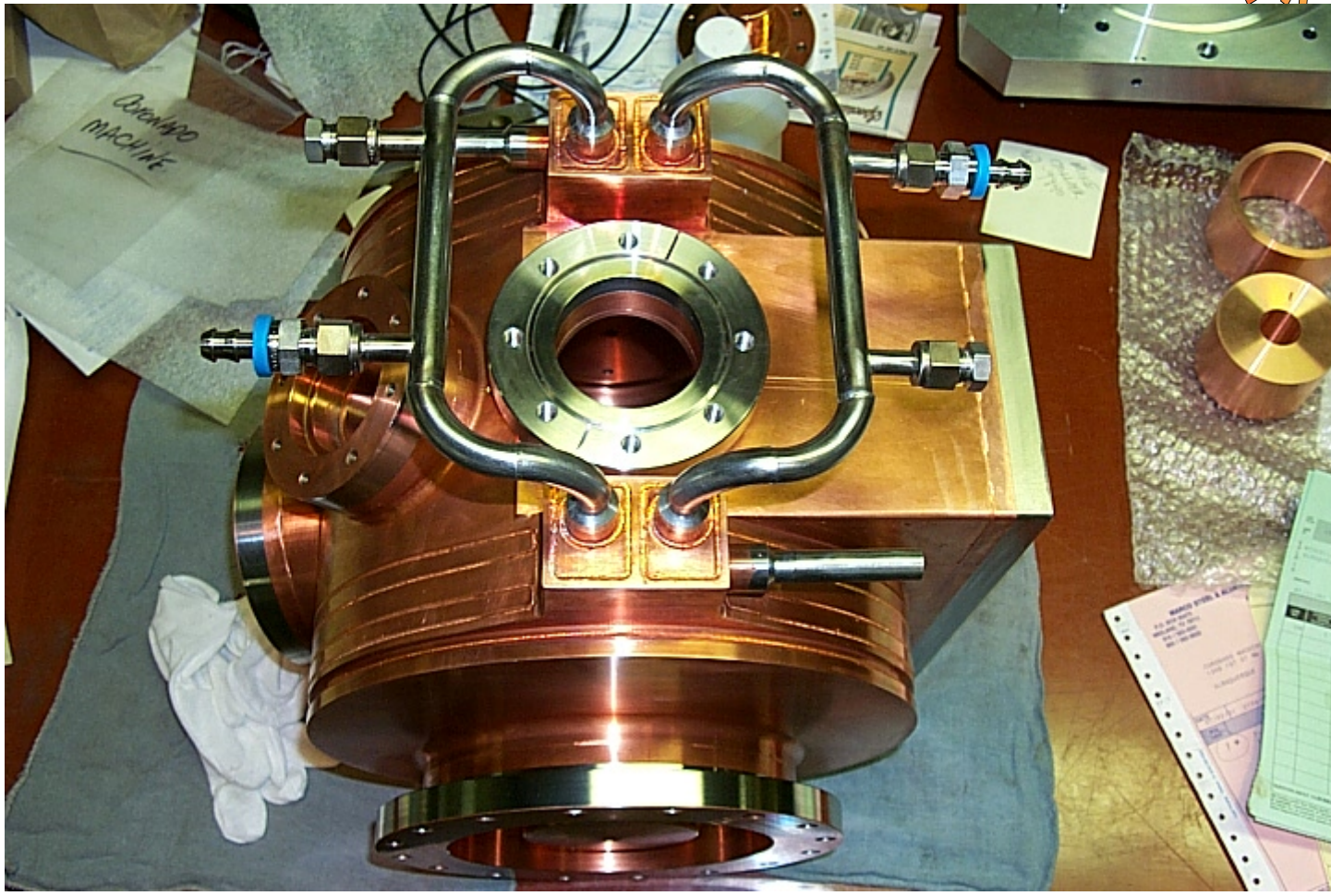
# Bridge Coupler Body Machined to Size

# The "Smiley-Face" Slot Between Center Cell and Coupling Cells
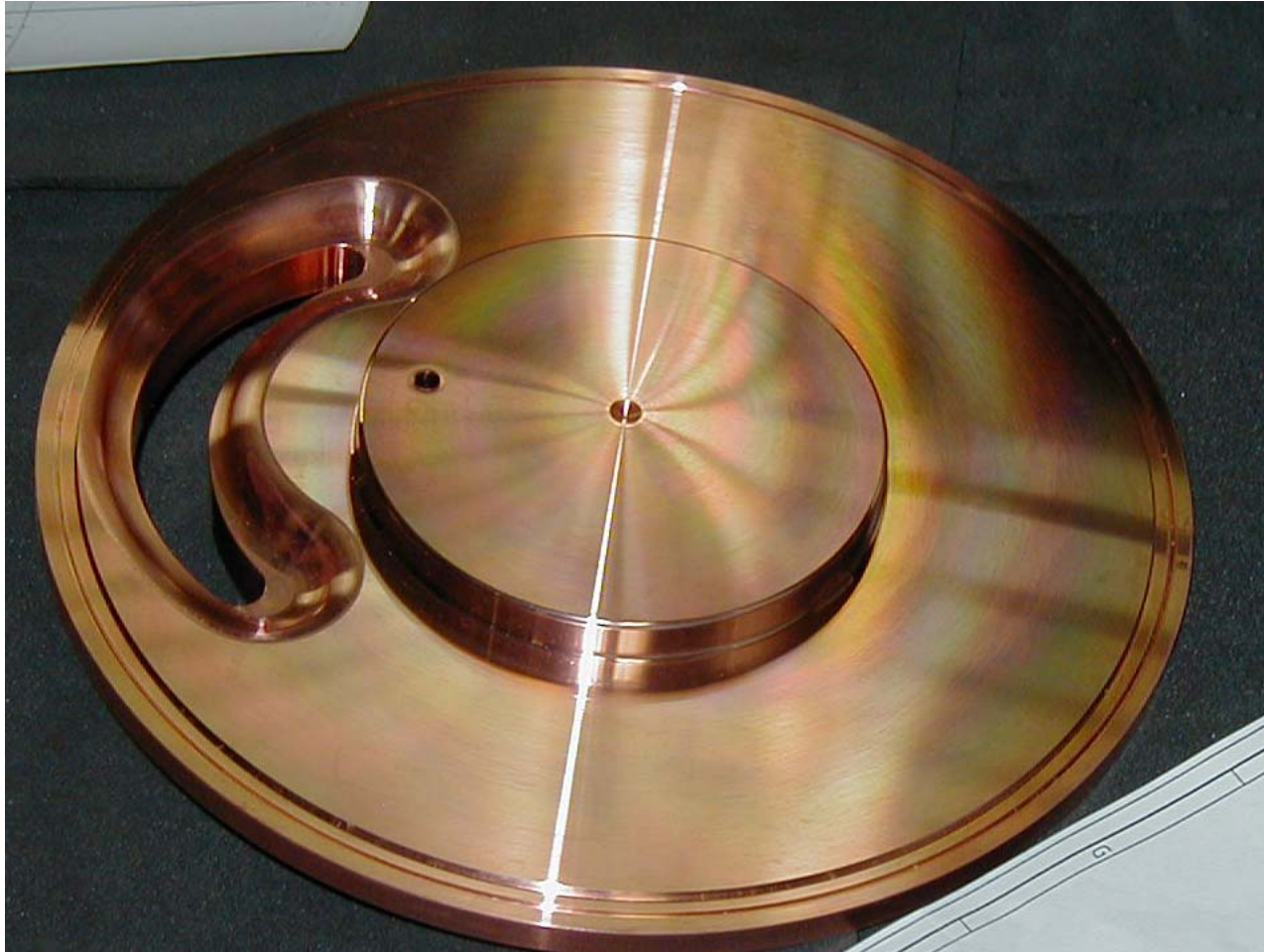
# Bridge Coupler After Brazing
# (Pumping port at bottom when installed)



Slug tuner port

Copper-plated steel flange

Water fittings

Pumping port

Traveler
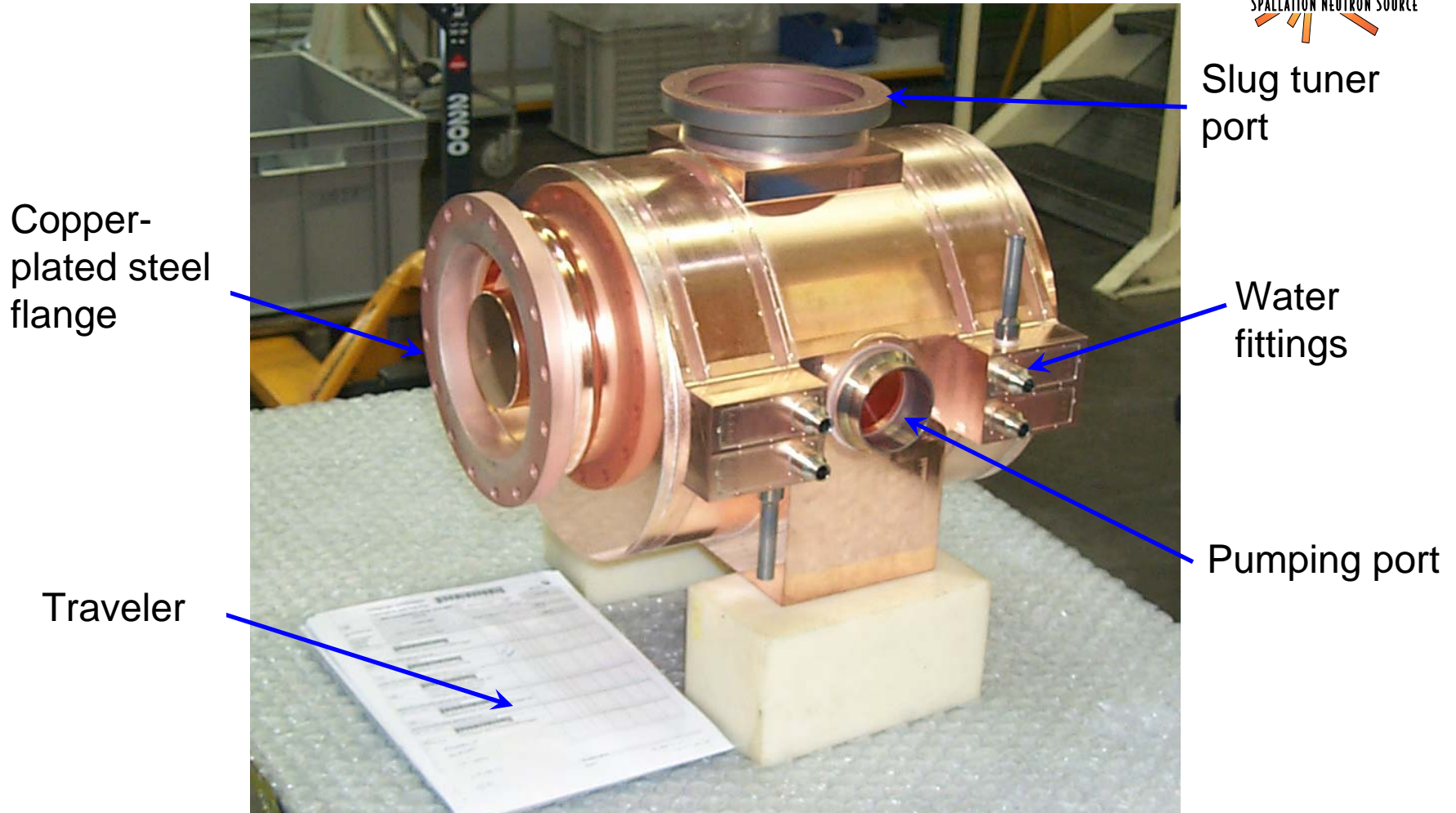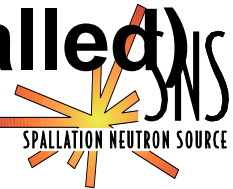
# Bridge Coupler Tuning Fixture
# A 5-Cavity RF Structure
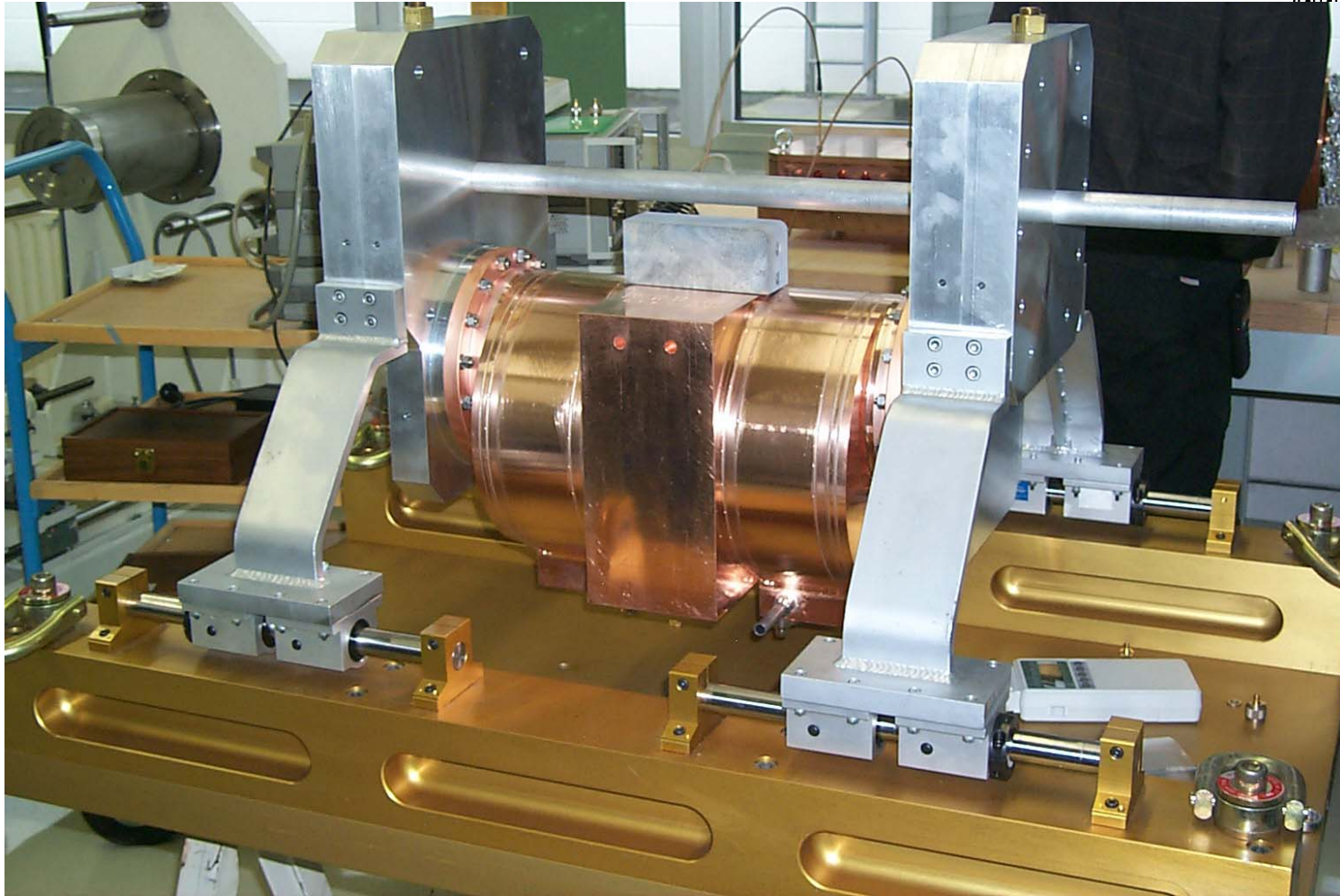
# Why a Special Fixture for Tuning the Bridge Coupler Center Cell?

- The center cell must have the "correct" frequency to make the the $\pi/2$-mode frequency 805 MHz.
  - It is not possible to measure the center-cell frequency directly.
  - Because of the large slots, its field appears in nearby cavities.
  - We don't know what its individual cavity frequency should be even if we could measure it.
- The center cell has reduced field because of the relative coupling factors and contains only 15% of the stored energy of a single accelerating cavity.
  - Between two isolated segments, the cell has <1% of the stored energy, making it very difficult measure the effects of tuning it.

# One Side of the
# Bridge Coupler Tuning Fixture

**Permanent
rf probes**

Los Alamos
NATIONAL LABORATORY
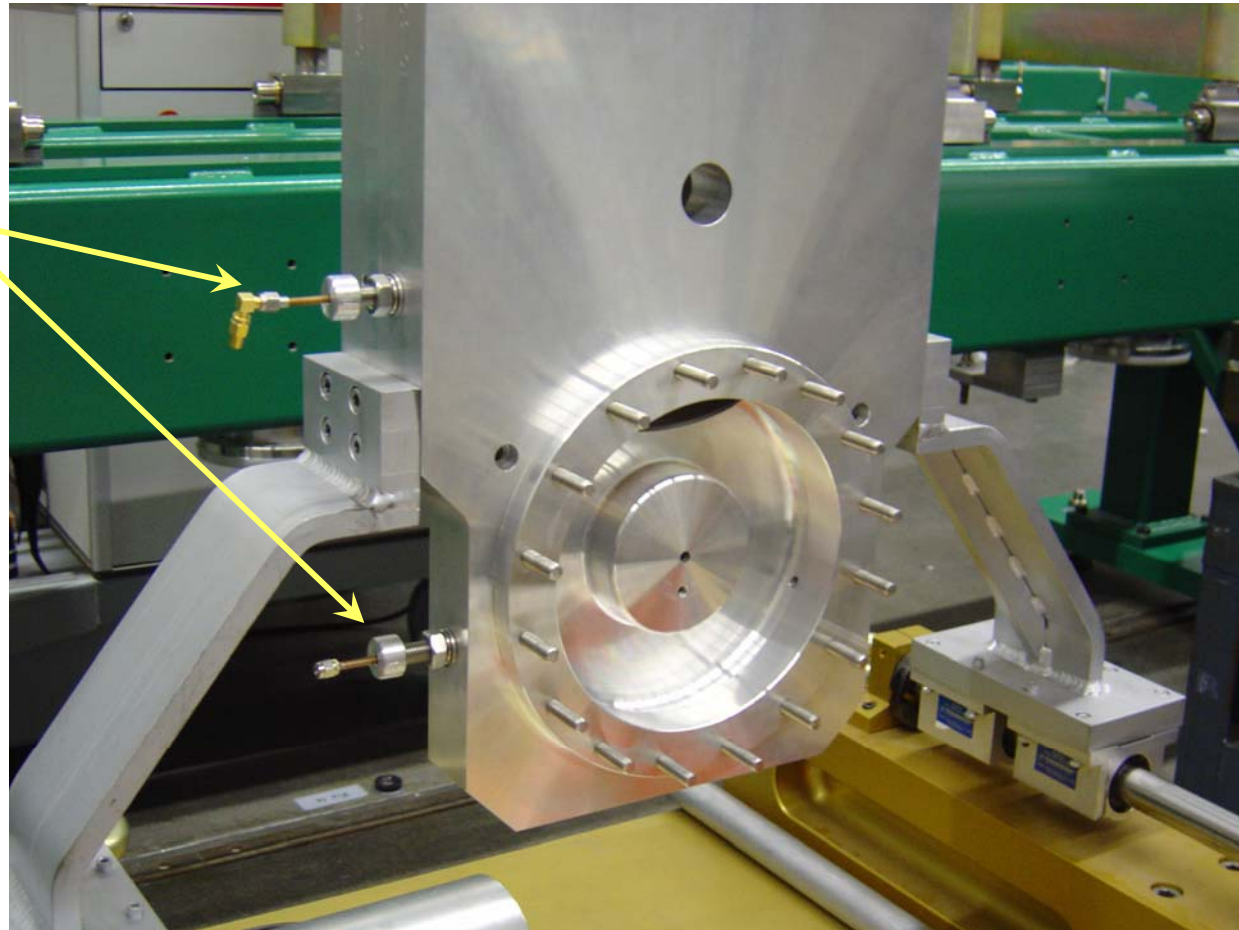
# Bridge-Coupler Center Cell Tuning

- A bridge coupler in the fixture makes a 5-cavity rf structure.
- In the $\pi/2$ mode, if cells 1, 3, and 5 have the same frequency, then cells 2 and 4 contain no stored energy.
  - This property defines proper tuning of the center cell.
  - Coupling-cell frequencies need only be approximately correct.
- Moving probes (magnetic loops) from one cavity to another changes the cavity frequencies.
  - Changing a coupling-cavity probe detunes the end resonator!
  - To avoid this effect, use 4 dedicated probes with strong coupling, one in each end resonator and one in each coupling cavity.
  - We need strong coupling in cavities 2 and 4 because we will be looking for a null signal.

# Bridge-Coupler Center Cell Tuning Procedure

- All unused fixed probes are terminated in 50 $\Omega$.

- Tune the fixture end resonators to the same frequency.

  - Short other cavities in a consistent manner for this adjustment.

- Drive the 5-cavity system in the $\pi/2$ mode.

- Adjust the center-cell slug tuner to minimize stored energy in the coupling cells.

- Measure the $\pi/2$ mode frequency of the 5-cavity system and retune end cells to correct to 805 MHz.

- Readjust the slug tuner to minimize stored energy again, then machine the copper slug to this length.

# Installing a Tuned Bridge Coupler
# (Only the center cell has been tuned.)

# Module Tuning

# Module Tuning Goals

- Frequency 805.12 ± 0.01 MHz @ 20C, vacuum.

- Fields within ±2% of design, to be fine tuned after reassembly at SNS.

- Stable: One segment +10 C too hot causes <1% field error.

- Slight positive slope of tilt sensitivity prevents thermal runaway.
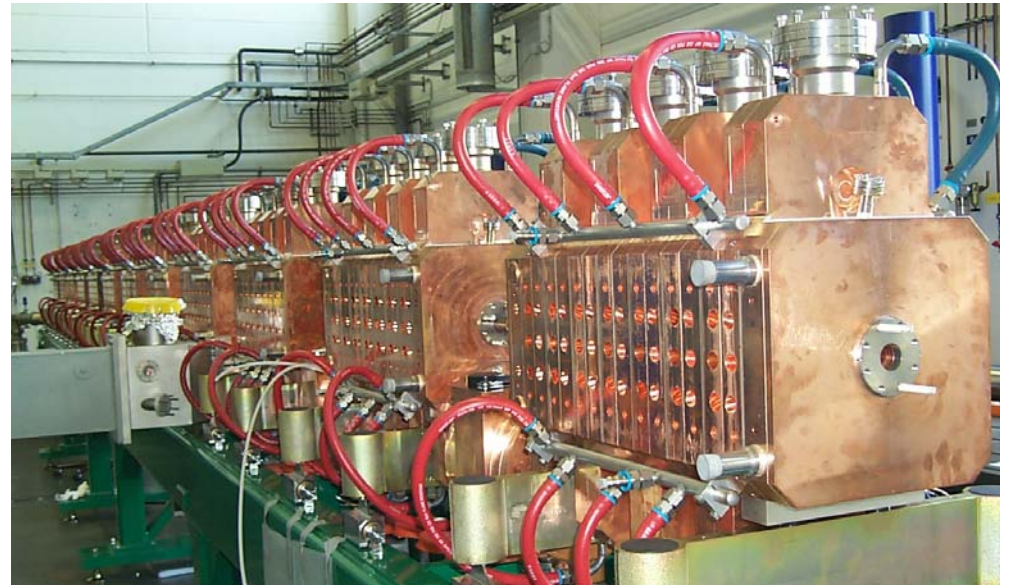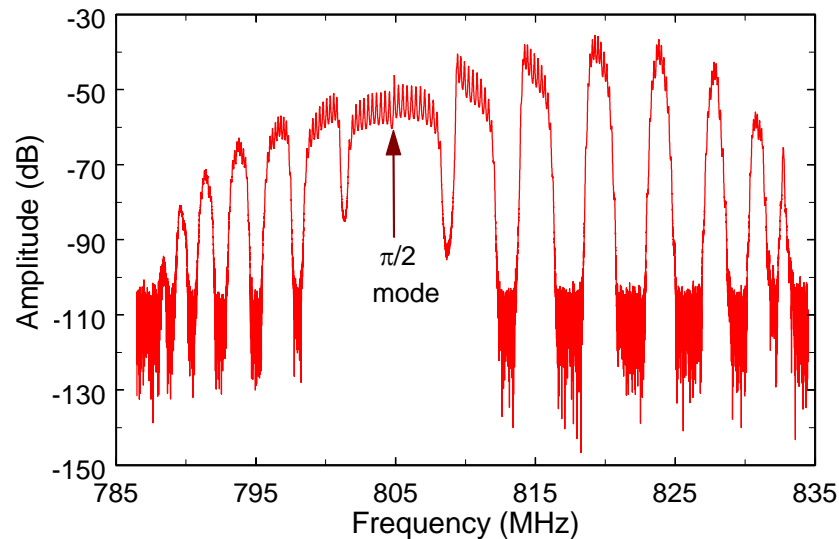
# Major Activities During Module Tuning

- Retune the 22 accelerating cavities at internal ends of segments to achieve the design $\pi/2$ mode frequency.

- Adjust the field distribution.

  - Axial bead-perturbation ("beadpull") measurements.

- Tune the 22 bridge coupling cavities to stabilize fields across a segment pair.

  - Tilt sensitivity measurements (two beadpulls with perturbations on opposite ends).

- Mode spectrum determines stop band gap.

- Cut irises in bridge couplers 3 and 9 to set waveguide coupling.

# Tuning Bridge Coupling Cavities

- When the module is first assembled, the only cavities that have had no previous tuning work are the 22 bridge coupling cavities.

- Like the center bridge cell, it is not possible to directly measure the frequency of an individual bridge coupling cell.

- Measure the $\pi/2$ mode frequency of a three-cavity system consisting of the center cell and both bridge coupling cells.
  - This is the average frequency of the two coupling cells.
  - Center cell contains no stored energy is the $\pi/2$ mode.

- Find their frequency difference by measuring each cavity individually, isolated from nearby cavities.
  - Blocking the "smiley-face" slot isolates the coupling cavity from the center cell, but raises the coupling-cell frequency ~45 MHz.

# Full Module Mode Spectrum

~160 of 213 modes observed with probes in end cavities
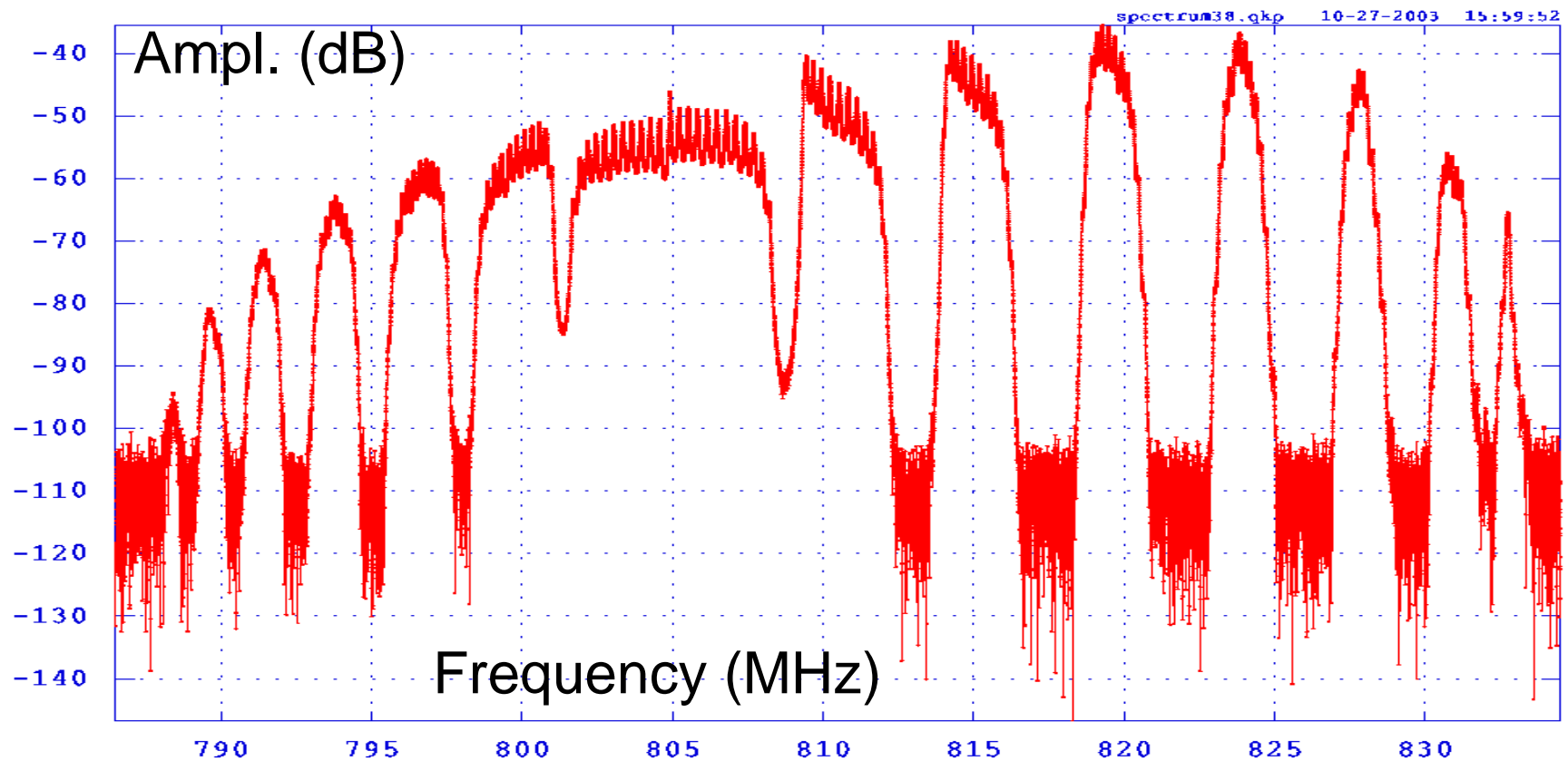
# Comparison of Central 23 Modes Before and After Module Tuning

Upper curve: Initial mode spectrum
Lower curve: 22 end accelerating cells up 1.1 MHz, 70 (of 106) coupling cells (48 upper internal cells plus 22 bridge cells) down 0.21 MHz



$\pi/2$ mode

# Special Tools Used for Tuning



SNS

Axial shorting rods

Waveguide short

Coupling cell shorts

Bead aligner

Lifting fixtures for bridge coupler

End-cell perturbation

End wall puller

Temperature, pressure, humidity meters

*SNS Linac*

Los Alamos
NATIONAL LABORATORY
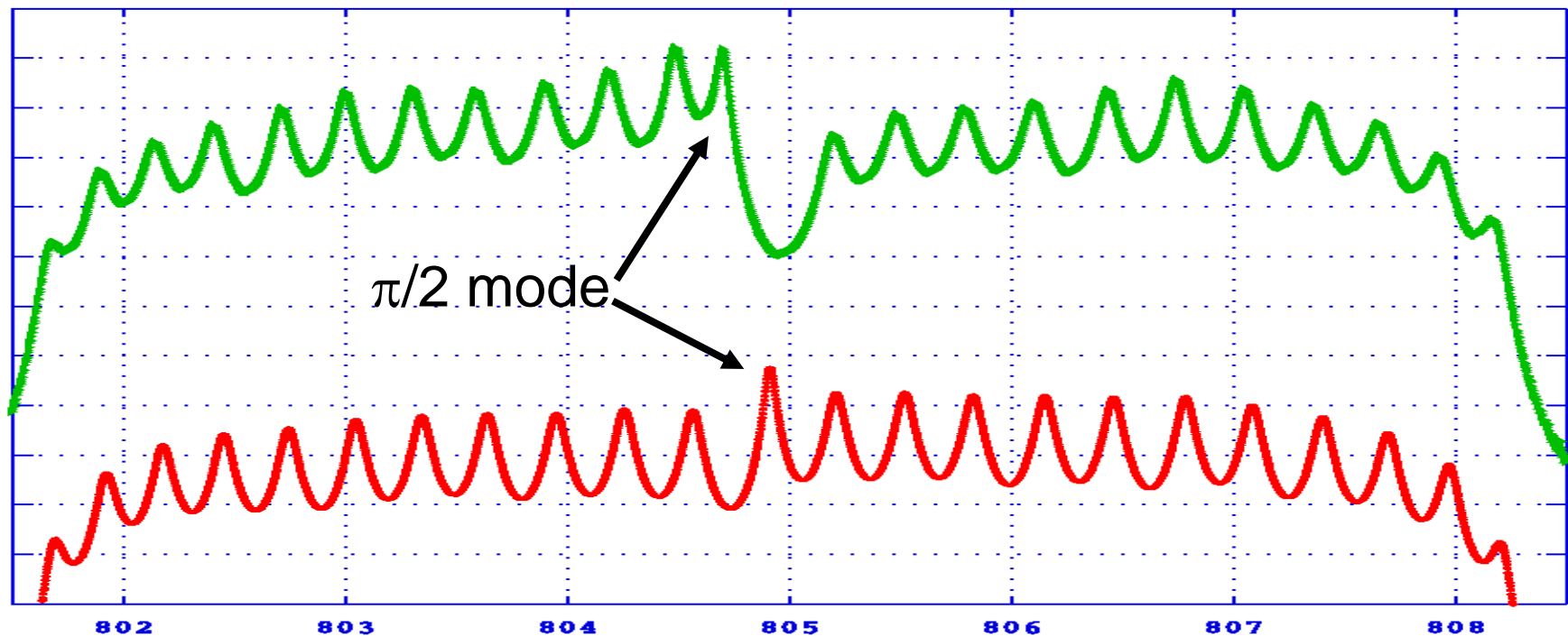
# A Few More Tuner's Tools

# The "Smiley Face" Tool



- This tool is inserted in the slot between the center bridge cell and coupling cavity by reaching in through the slug tuner port.

- Increases coupling cavity frequency ~45 MHz, but makes relative changes easy.

- Contains a magnetic loop.

- Also used as a probe to tune end accelerating cavities.
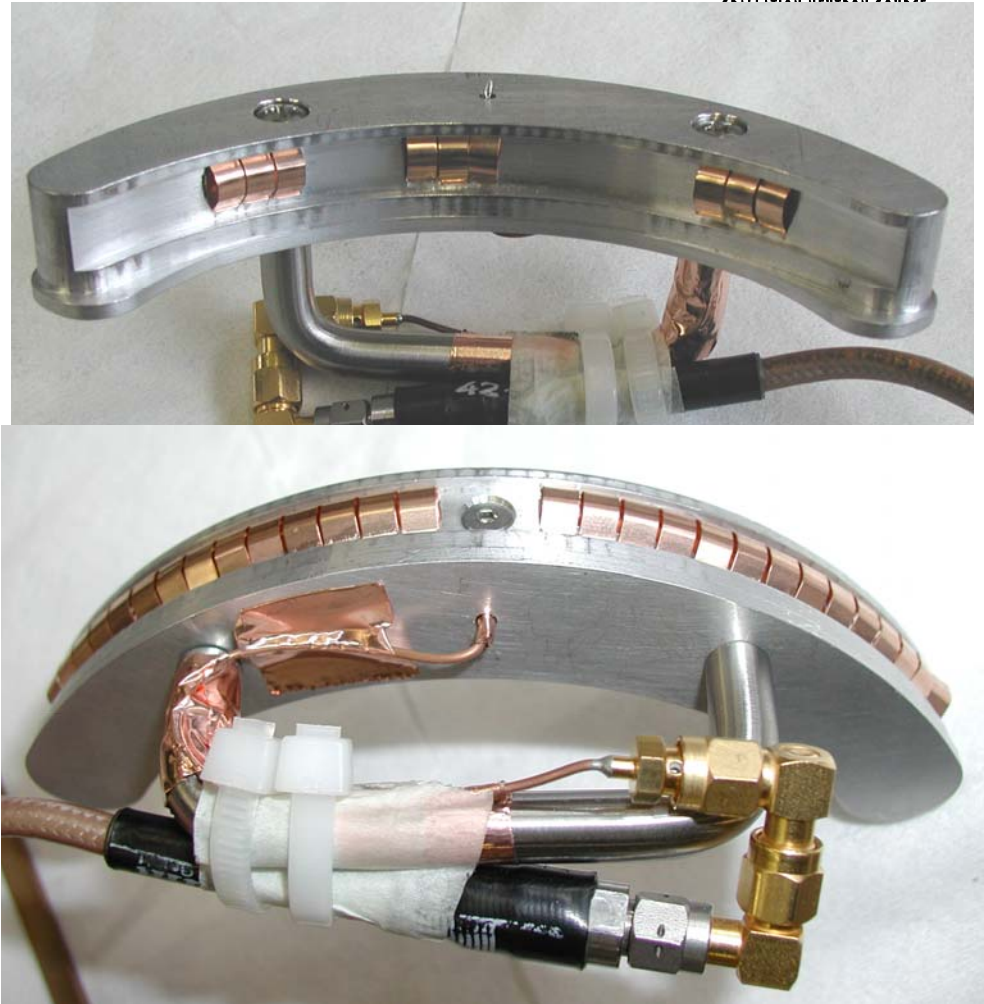
# Another View of the "Smiley Face" Tool
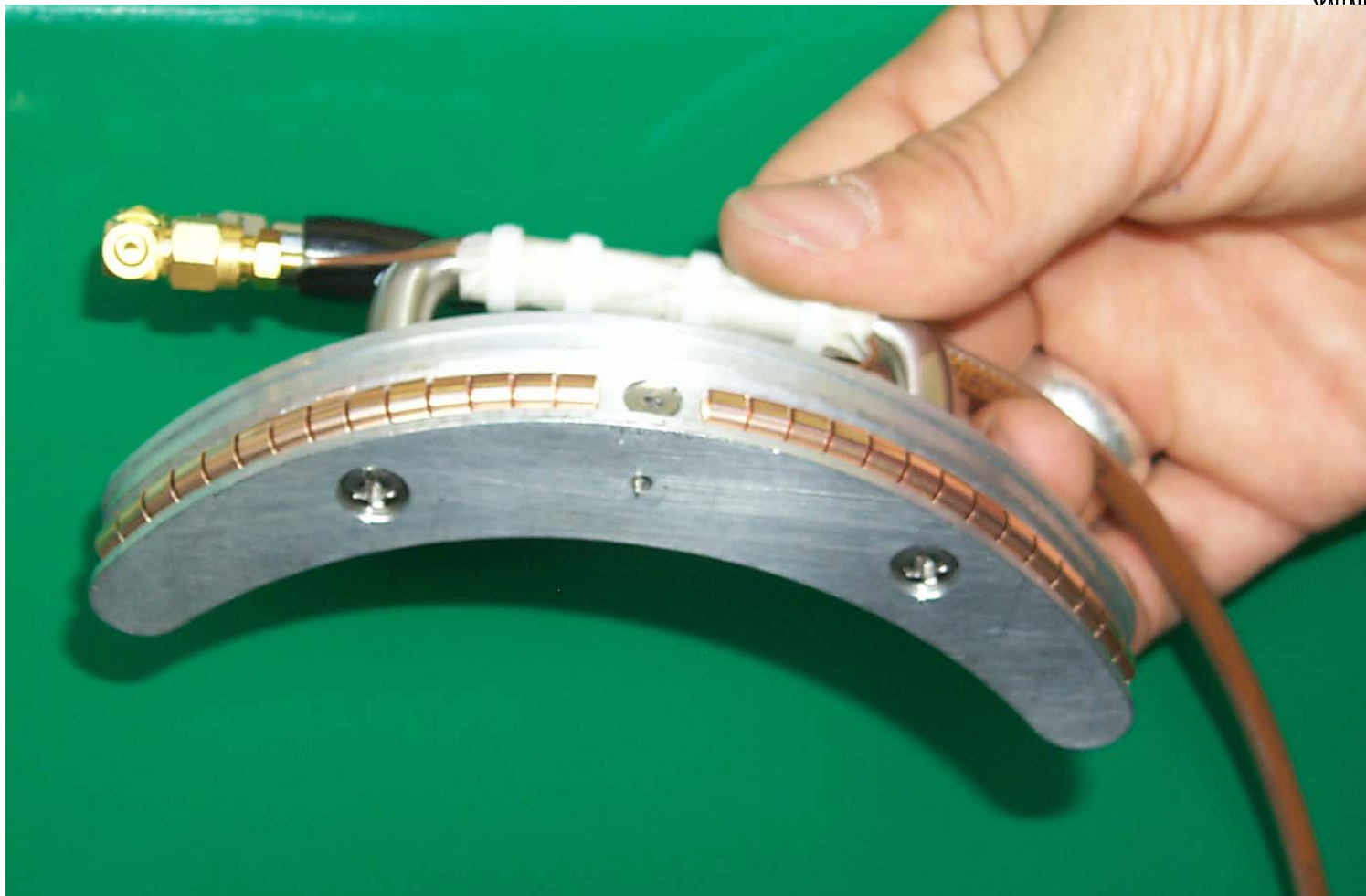
# The "Yoon Probe" Tool



- This combination shorting rod and magnetic probe was suggested by Yoon Kang of SNS.

- It detects fields from an adjacent coupling cell from inside the shorted accelerating cell.

- On module 1, we used two Yoon probes for 3-cell and 2-cell mode measurements on bridge couplers.
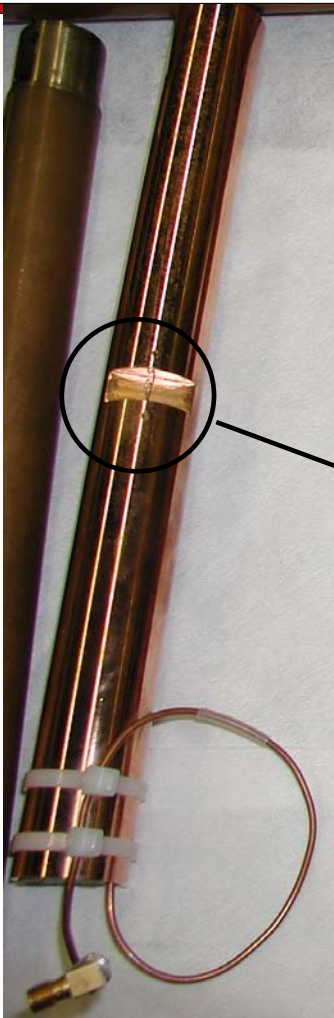
# End-Cell Perturbation Tool



- Split tube with handle inserted down the bore of an end cell lowers module frequency ~25 kHz for tilt-sensitivity measurements.

- Split to slip past nylon beadpull line.

- Hollow to allow bead to pass through.
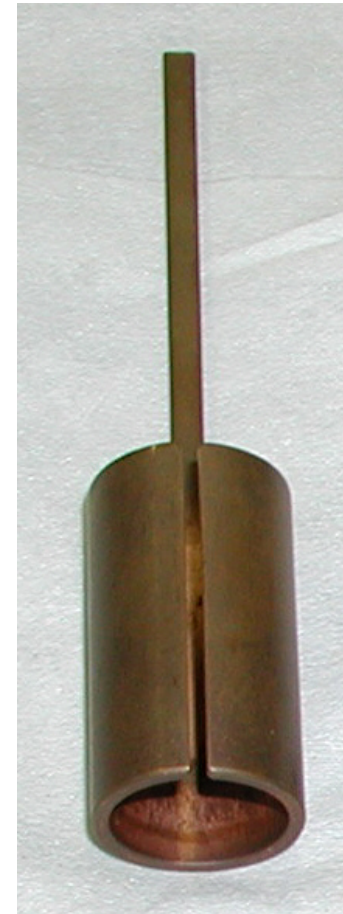
# Pulling the End Wall to Raise Frequency

- At segment tuning, we tune each end accelerating cavity to minimize stored energy in the adjacent coupling cavity.

- When part of the module, the initial end-cavity frequency is ~1.9 MHz too high.

- Tap on the end wall to lower frequency, pull to raise it.

- Uses axial electric antenna in the shorting rod and magnetic loop in port at top of cavity.
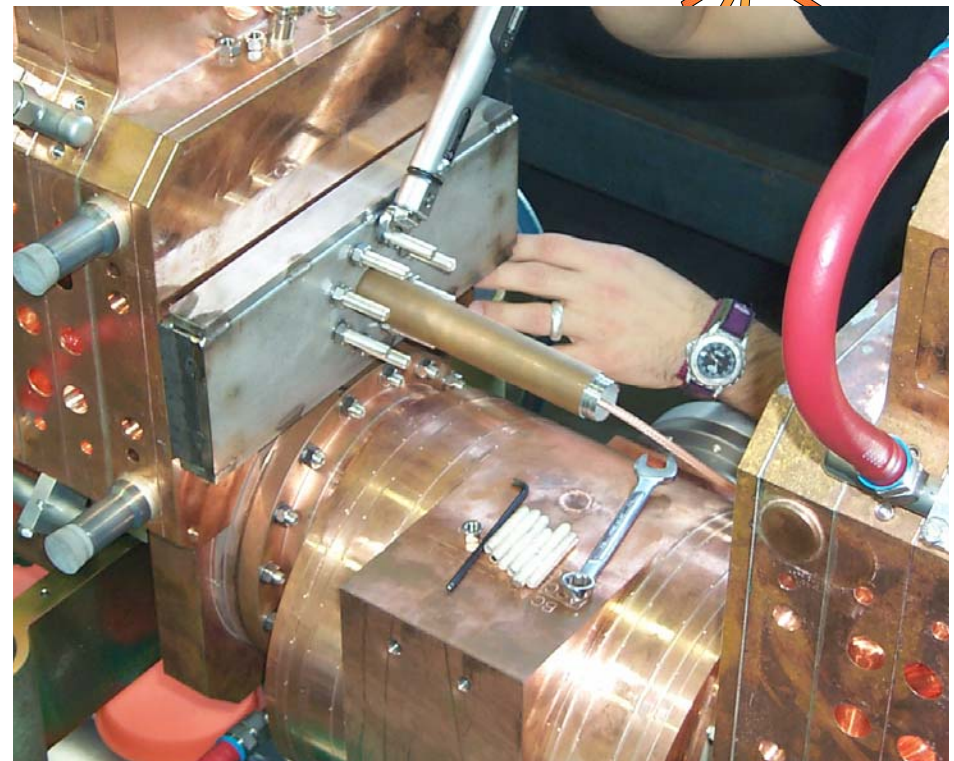
# Tapping the End Wall to Lower Frequency
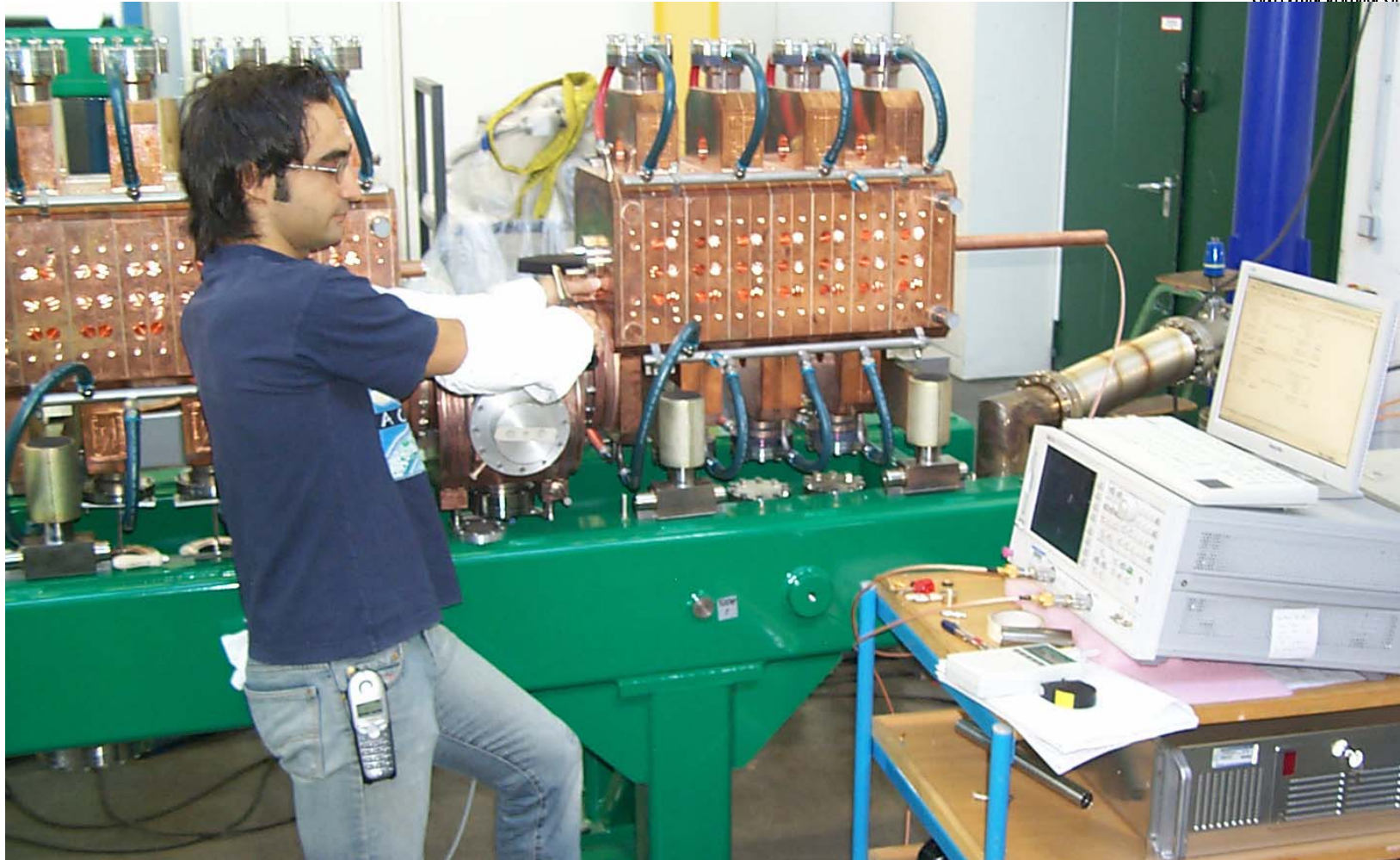
# If Necessary to Reduce Tilt Sensitivity Re-tune Internal Coupling Cavities

- Hydraulic cylinder squeezes cavity, lowering frequency.
- Spreader bar between noses raises frequency.
- Uses loop on flange and Yoon Probe in adjacent accelerating cell.
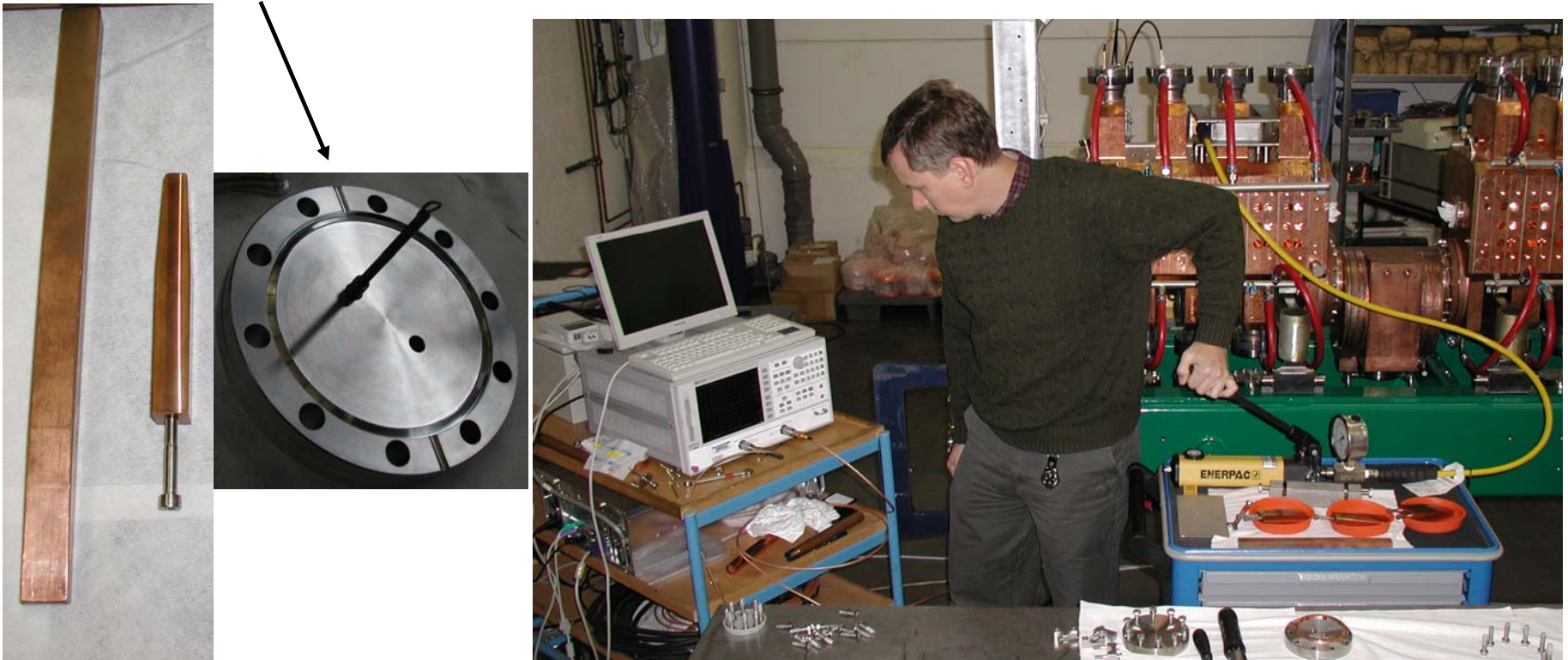
# Tuning Bridge Coupling Cavities

- Adjusted from the bridge center cavity, the screw provides >5 MHz tuning range for coupling cells.

- Power losses are not a problem because the screw is in primarily electric field region of a nominally unexcited cavity.

- Contacts are well inside the tapped hole.

- After final adjustment, another screw inserted behind the tuner locks it in place.

- Both screws include vacuum relief.
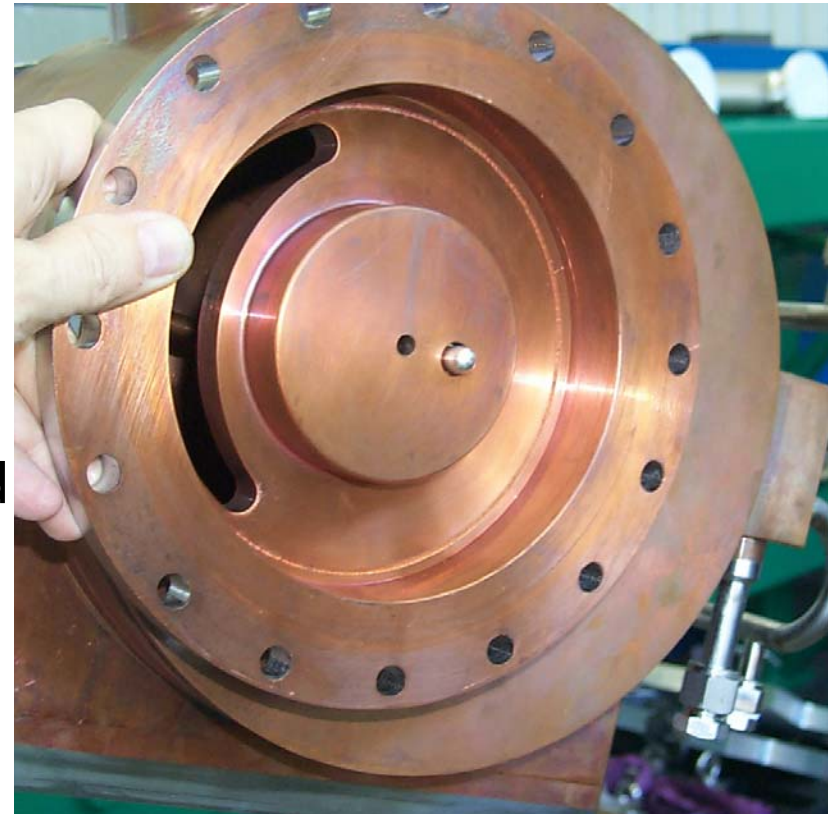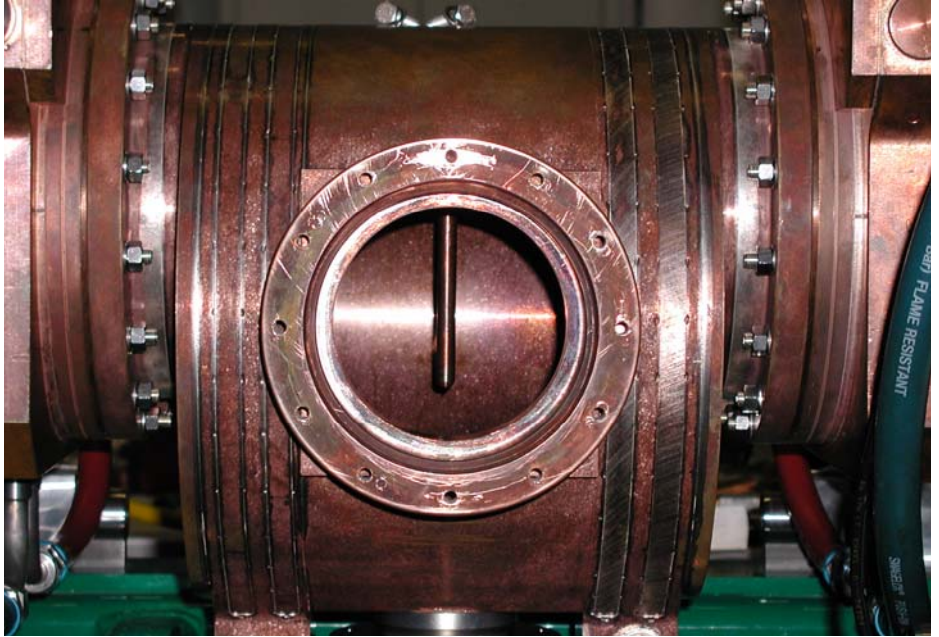
# 5-Mode Measurements Determine Bridge Coupling Cavity Frequencies

- Different length slots in bridge couplers 1-8 establish a field ramp in module 1.

- Also produces a ~1.5-MHz frequency difference in the adjacent coupling cavities.

- The $\pi/2$-mode frequency of the isolated 3-cavity bridge coupler is the average frequency of the coupling cavities.

- To find the frequency difference between coupling cavities, we measure 2 modes of each 2-cavity pair consisting of the center cell and one coupling cell with the other cell shorted.

- All 5 measurements use two Yoon Probes in the adjacent accelerating cells.

- This time-consuming operation is replaced by single-mode "Smiley-Face" measurements where the slots are identical.

# Adjusting the Field Distribution



- The vertically oriented $TE_{111}$ mode couples very strongly to adjacent coupling-cavity fields.

- A rod in all bridge cells moves this mode below 700 MHz.

- A small left-right asymmetry mixes a $TE_{111}$ component with bridge-cell $TM_{010}$ mode.

- The TE mode magnetic field is in opposite directions near the two slots, adding to TM field on one side, subtracting on the other.

- Whack the rod with a steel pipe toward the segment whose field is too high, then check with a 2-segment beadpull.

# Axial Bead-Perturbation Measurements

- LabView code controls a network analyzer, records ~2000 frequency measurements as a 1-cm-diameter bead traverses each segment.

- Separate code computes relative $E_0$ by analyzing peak heights and comparing to Superfish field data for each cavity.
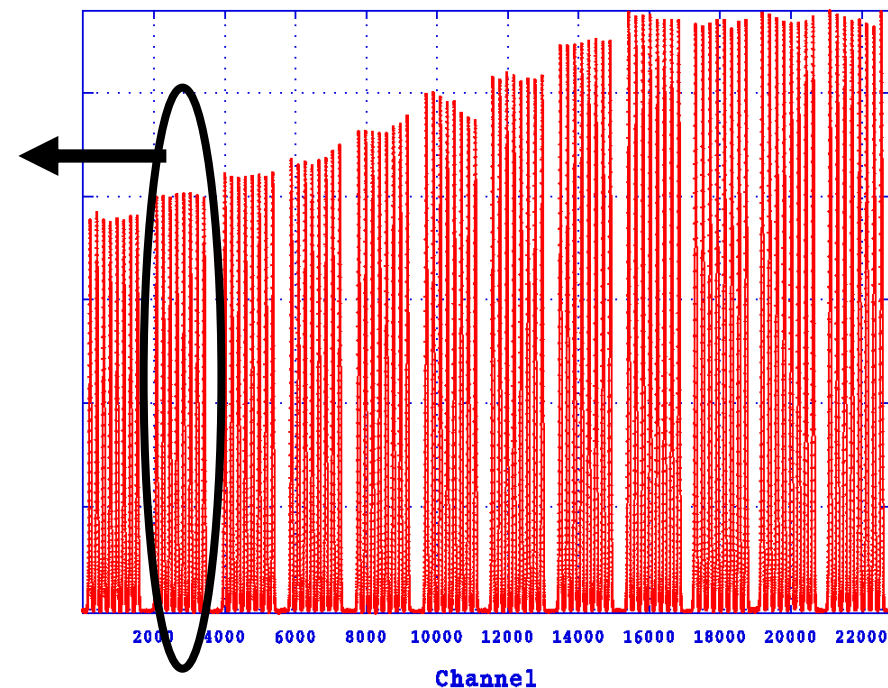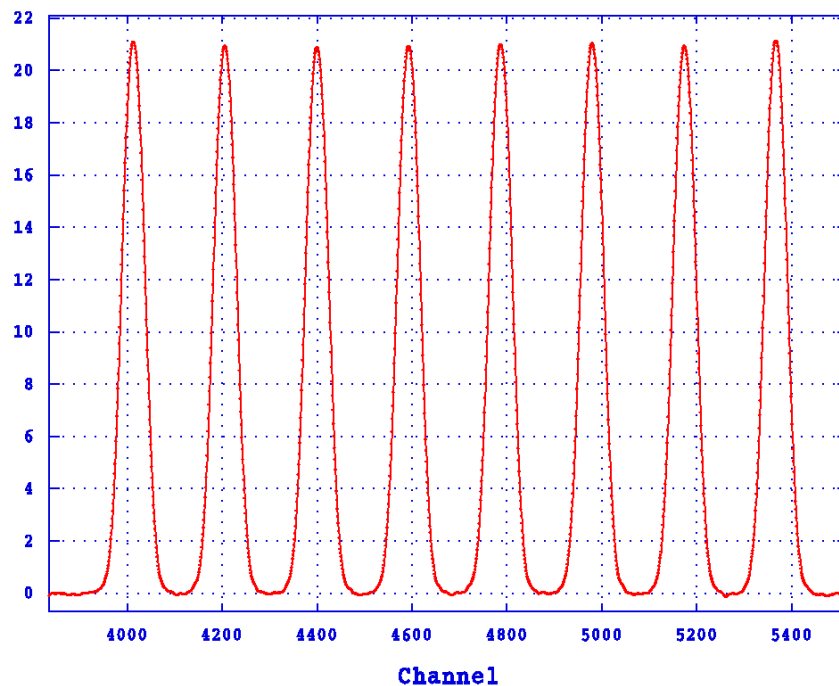
# Tilt sensitivity consists of two beadpulls with perturbations on opposite ends

- Plot shows working data from CCLplot code.
- Displays segment averages and ratios between adjacent segments at top.
- Tilt sensitivity (next screen) is cell-by-cell field difference per average perturbation.



**First cavity detuned –2 MHz**

**Last cavity detuned –2 MHz**

**Thermal run away prevented because field on both ends drops in response to a negative frequency perturbation.**
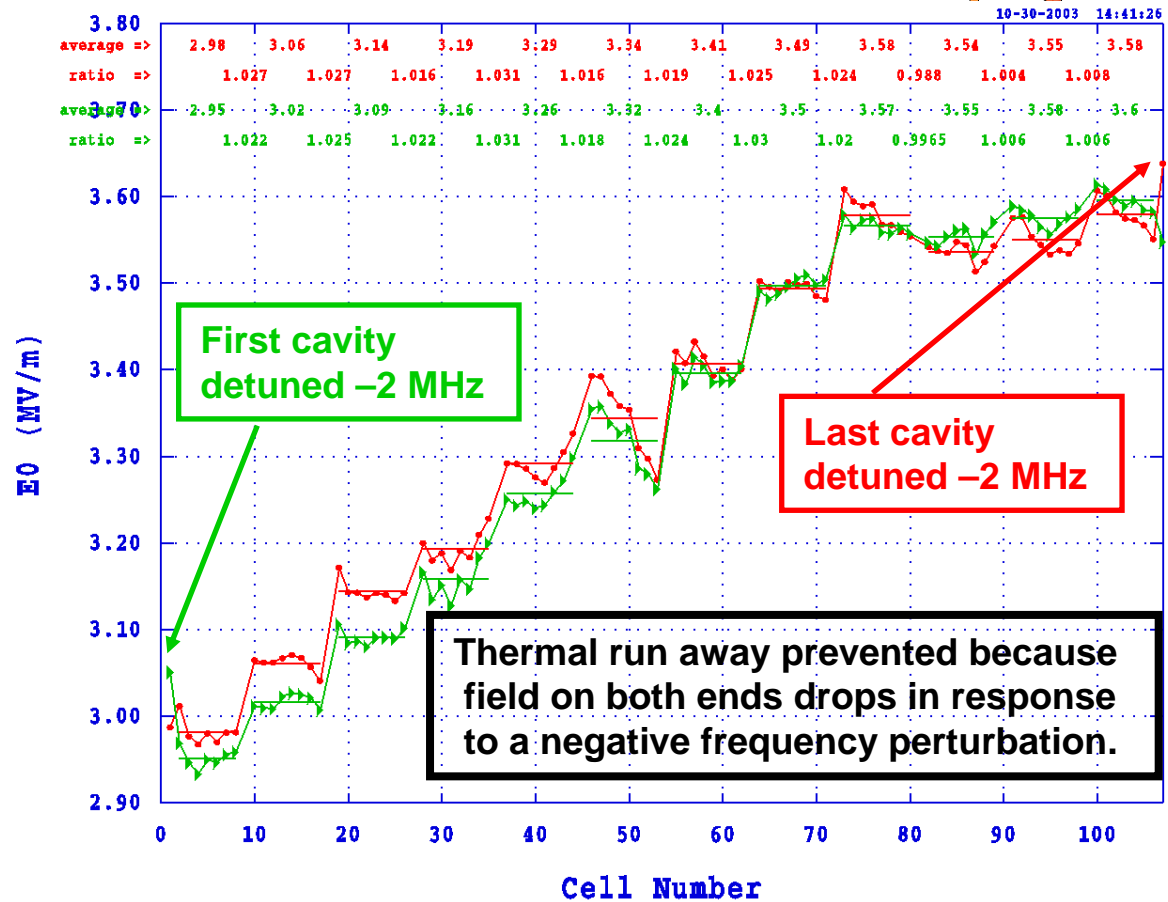
# Module 1 Pre-Shipment Tilt Sensitivity

- Retuning at SNS (needed for modules 1 and 2) took 1 day.
- Reduces segment slopes and steps at bridge coupler locations.
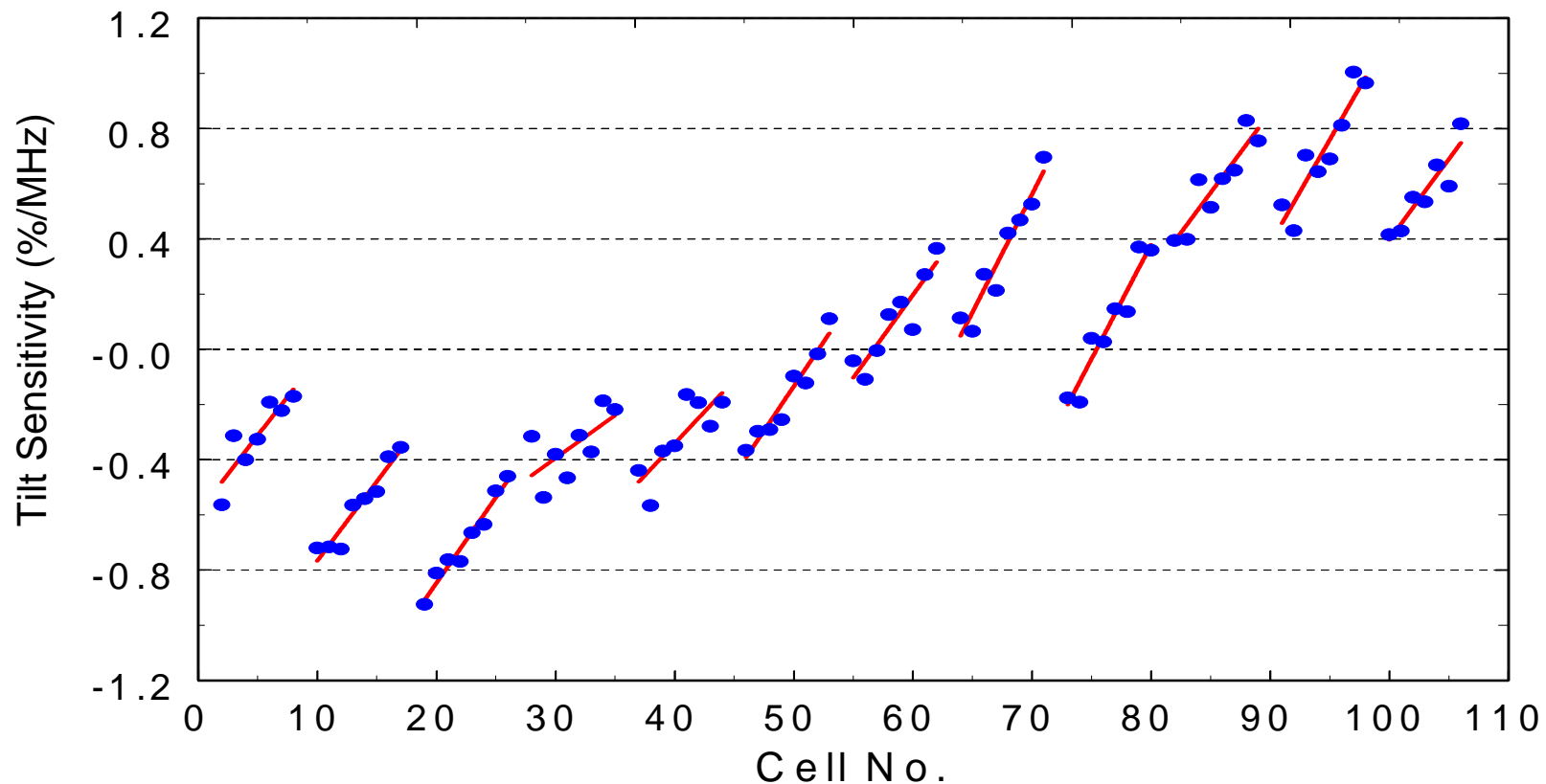
# Pre-Shipment Field Distribution



SNS / SPALLATION NEUTRON SOURCE

Chart: E$_0$ (MV/m) vs Cell No. showing E$_{0, design}$ (red) and E$_{0, measured}$ (blue).

• Los Alamos
NATIONAL LABORATORY
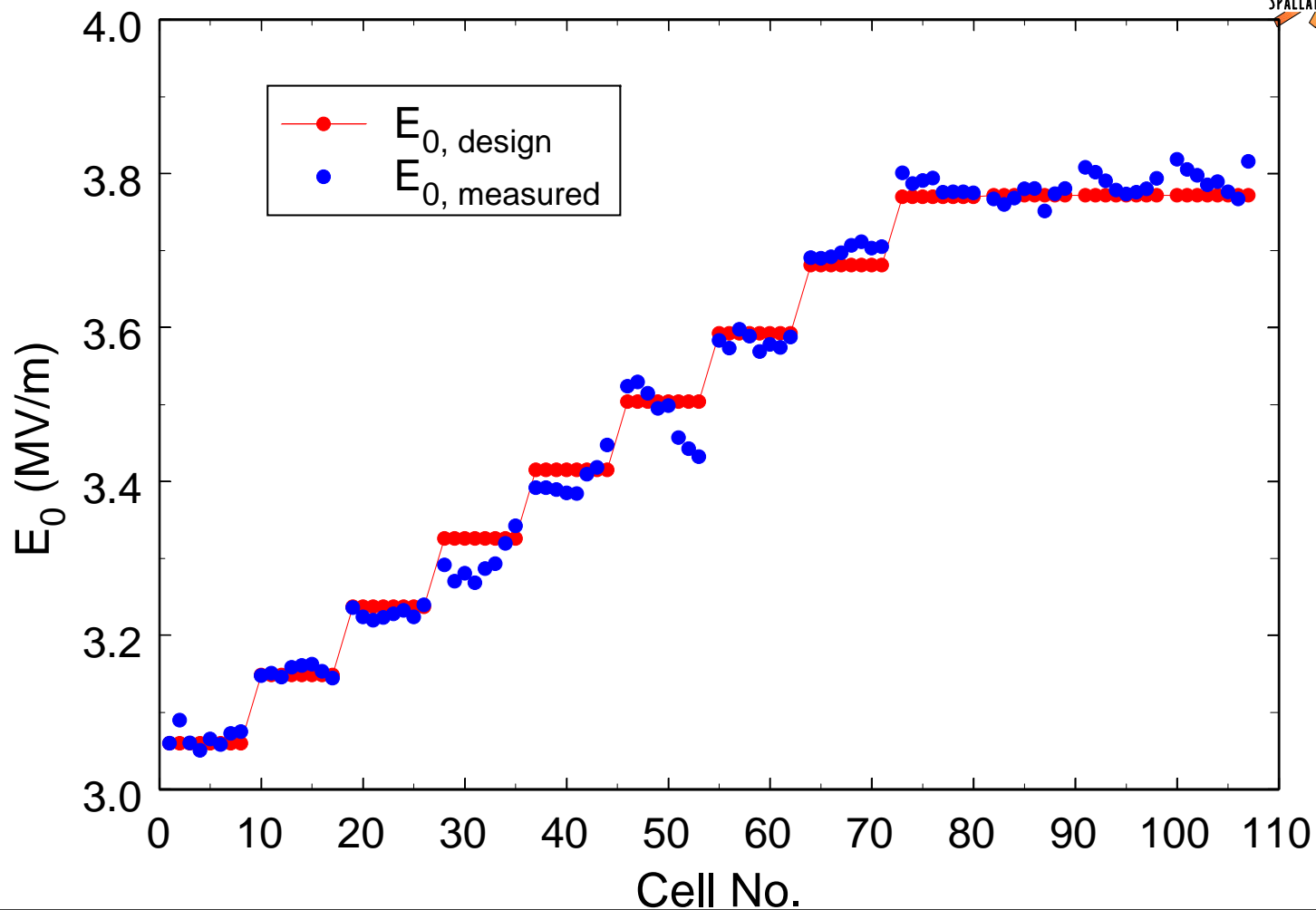
# Ratio of Measured Field to Design Field



SNS Linac
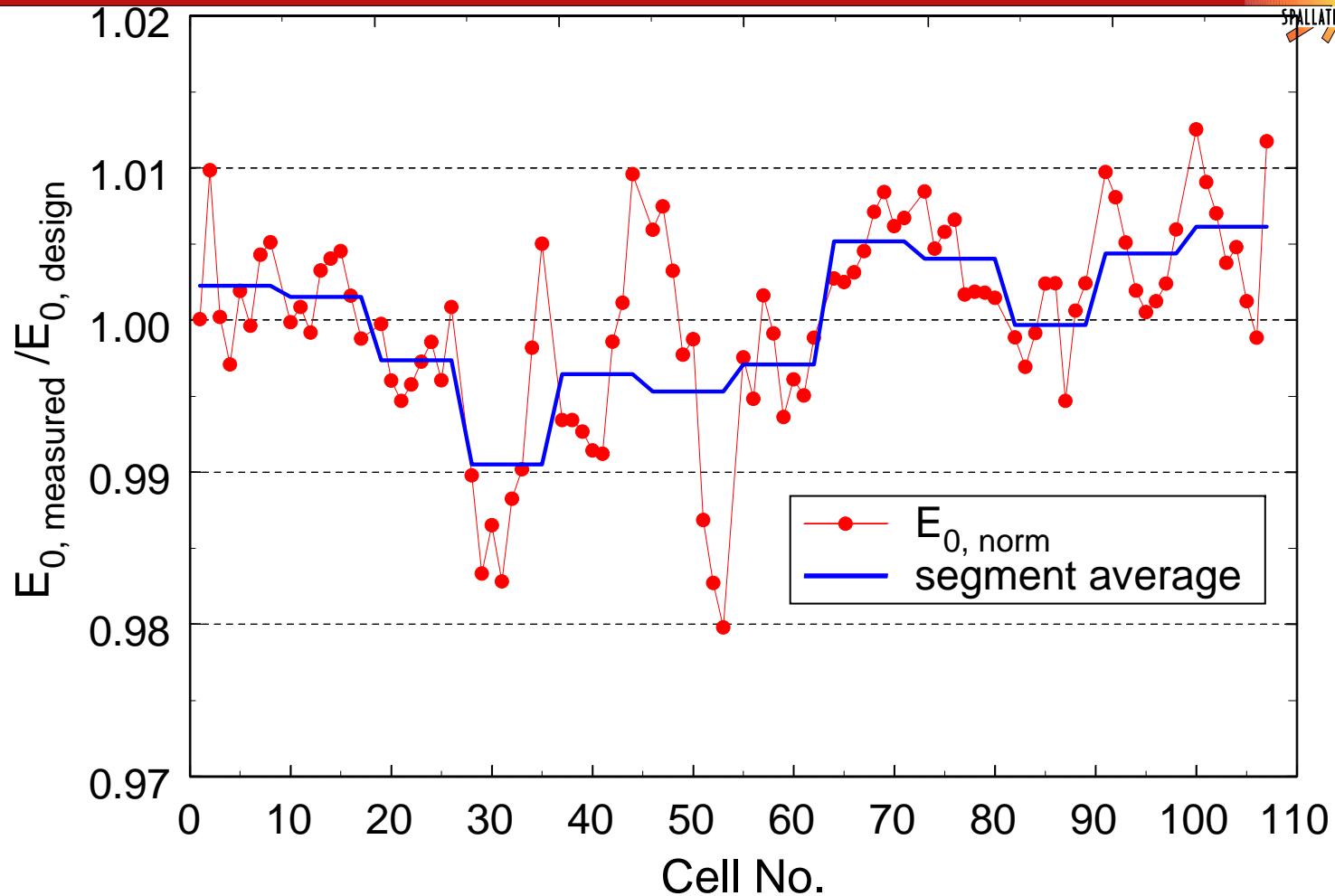
# Bridge Coupler 3 and 9 Waveguide Slots Matched for Full Beam Loading



>23 mm filed from both ends
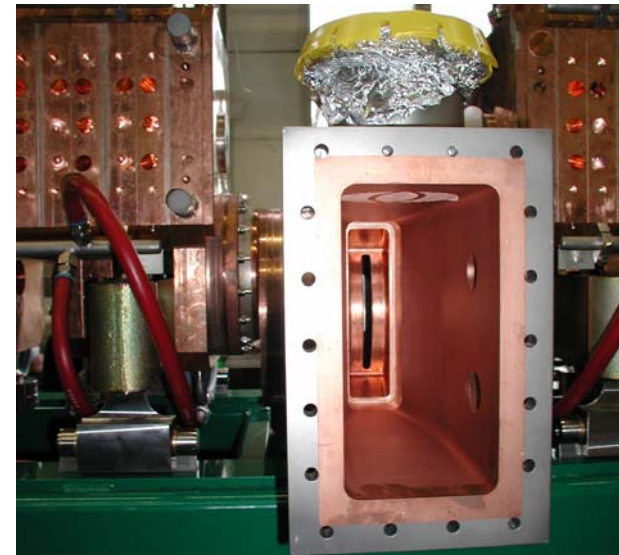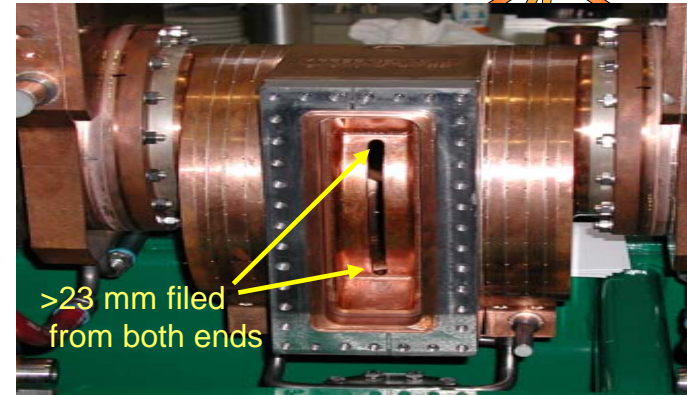
# Module 2, 3, 4 Tuning Went Faster Using Module-1 Experience

- The tuning-plan document underwent nearly constant revision as we invented better procedures and tooling for module 1.

- The updated plan benefited from module 1 experience.
  - Two-segment beadpulls are not needed to tune individually the bridge coupling cavities: all 22 tuned to a common frequency.
  - After segment tuning, end accelerating cavities re-tuned to a common frequency.
  - Time-consuming 5-mode measurements to determine bridge coupling cavity frequencies are not needed in modules without a field ramp.

# ACCEL's SNS Team
# Just Before Shipping Module 4

# CCL Installation and Tuning Team
# in the SNS Tunnel at Oak Ridge



*SNS Linac*

# Retuning the Bottom Coupling Cells During Segment Installation
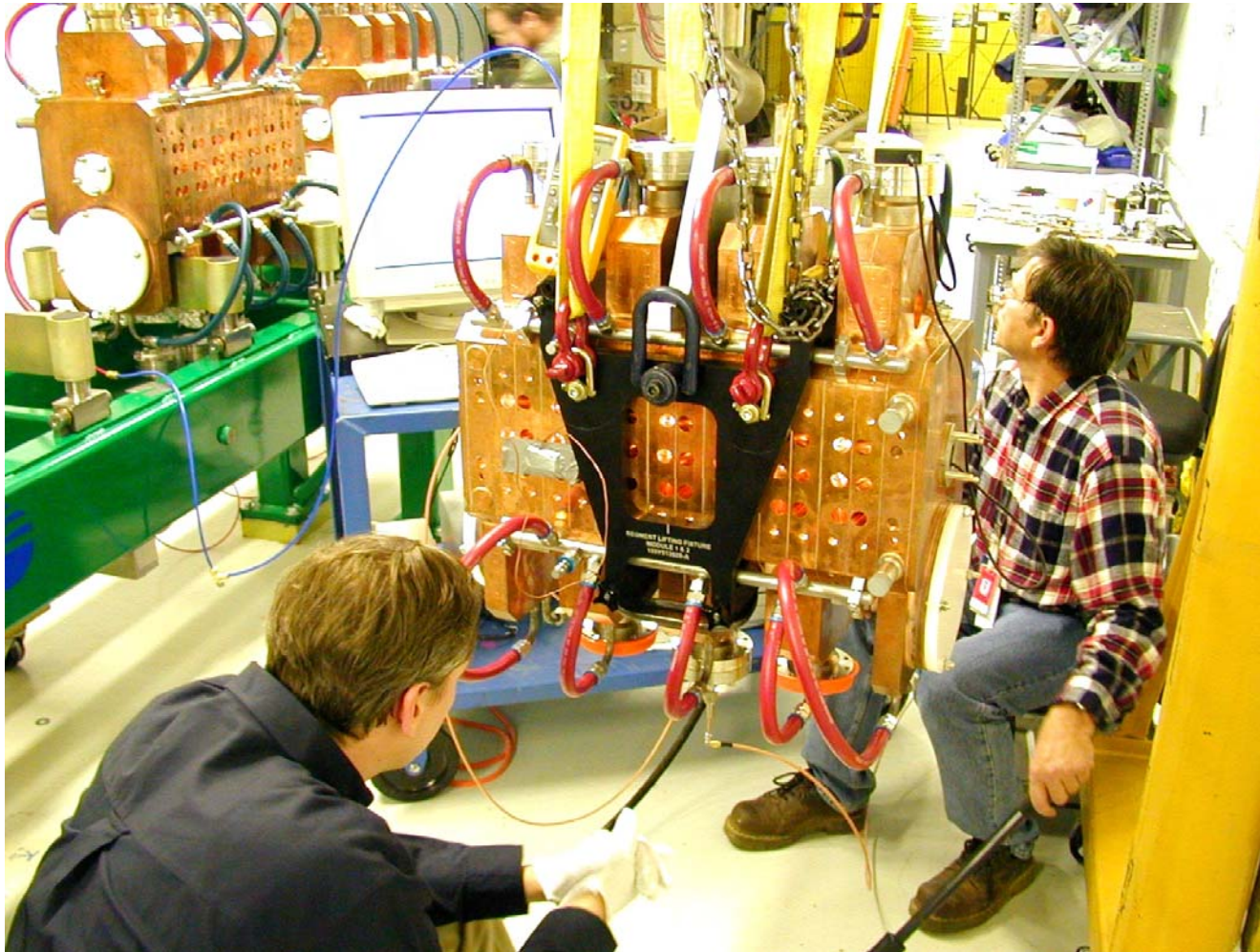
# Removing Flanges on the Next Segment

# Aligning Segments and Preparing to Install Bridge Couplers
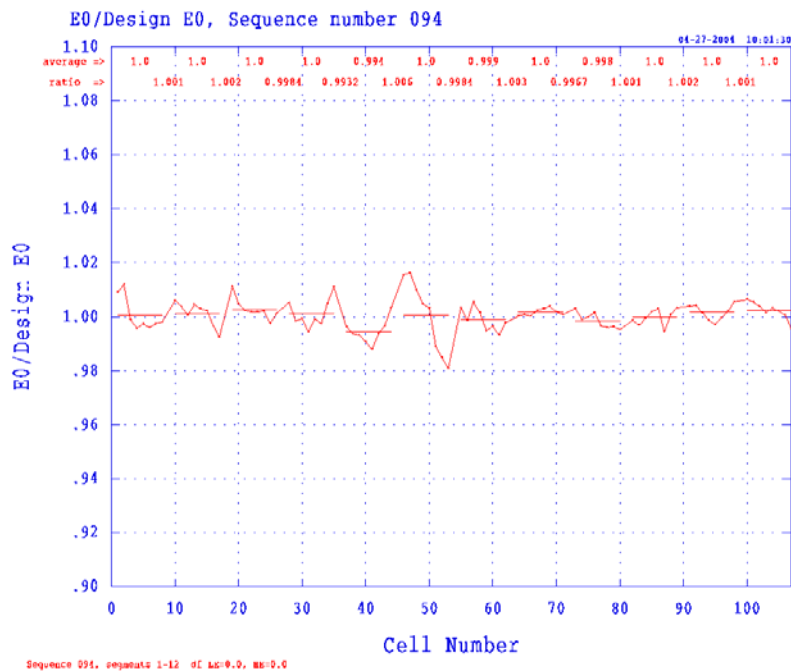
# Installing the Last Bridge Coupler on Module 1

# CCL Module 1
# Arrived at SNS November 24, 2003

$E_o/E_{design}$

Stability
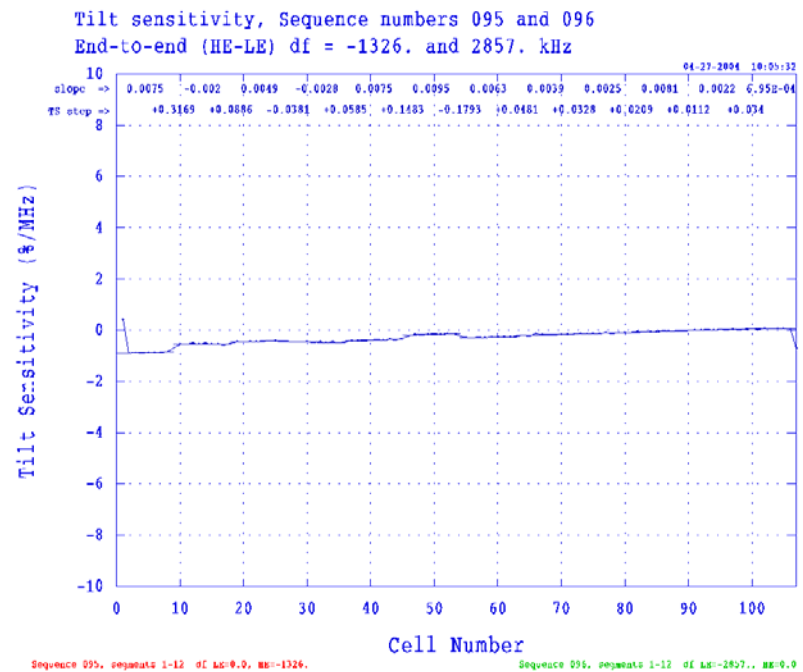


Coupling=0.728+0.826=1.554, $f_o$=805.100 at 20C, $Q_o$=16,000

# CCL Module 2
# Arrived at SNS February 16, 2004

$E_o/E_{design}$

Stability
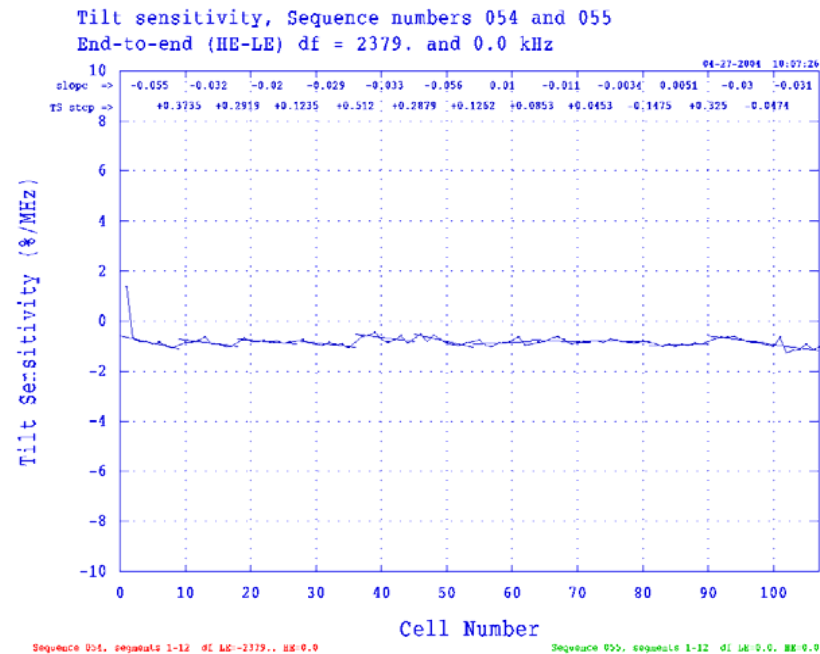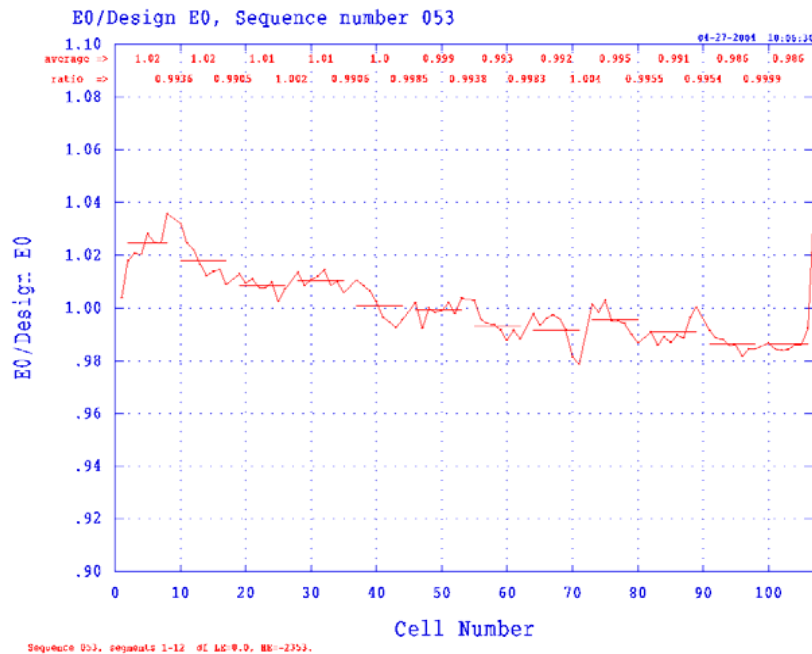


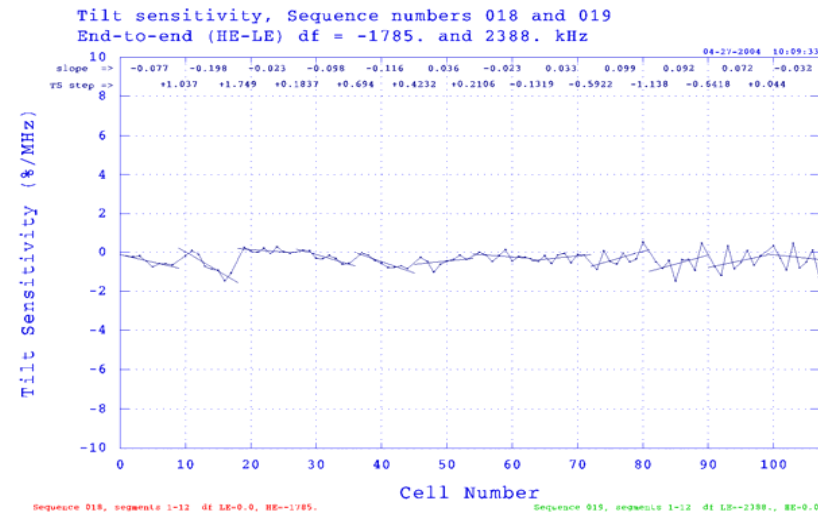Coupling=0.728+0.826=1.554, $f_o$=805.100 at 20C, $Q_o$=16,000

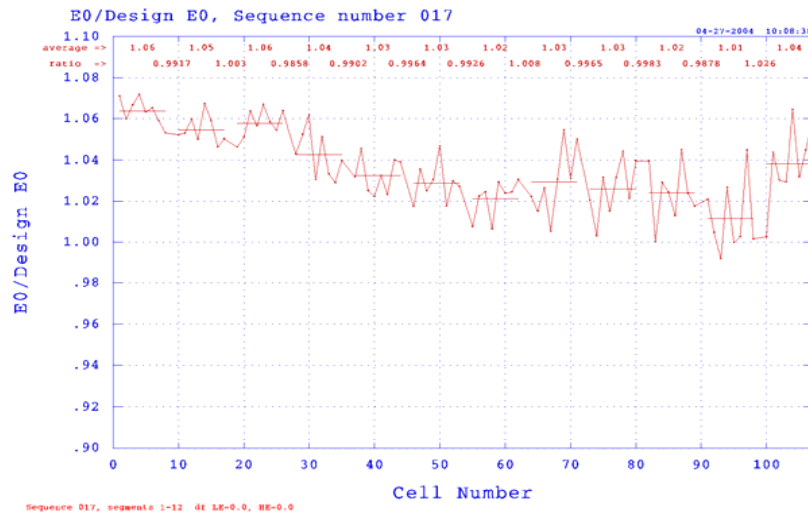# CCL Module 3
# Arrived at SNS April 14, 2004

$E_o/E_{design}$

Stability



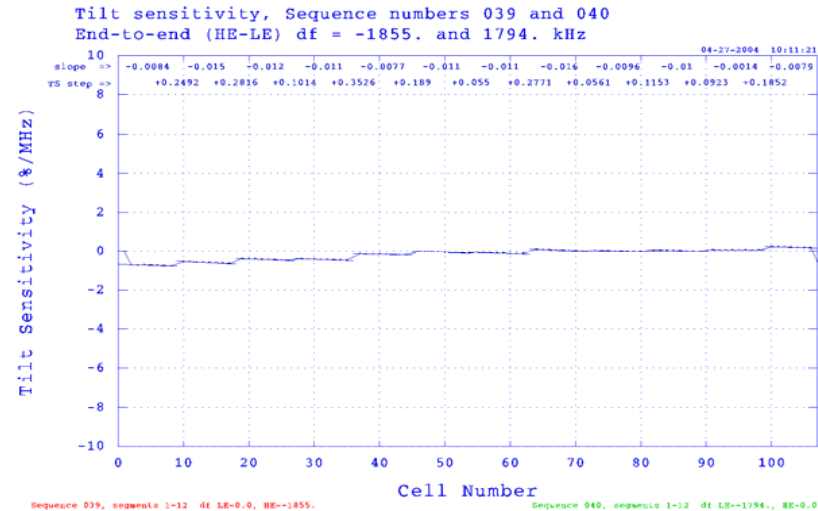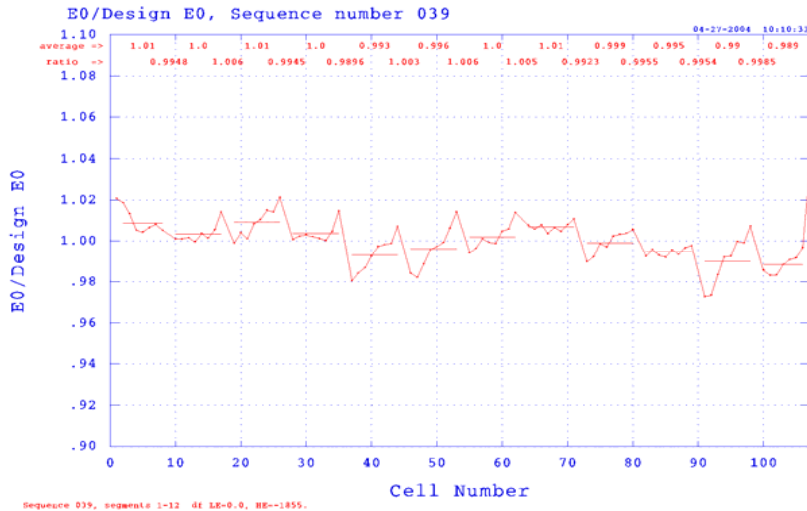Coupling=0.621+0.626=1.247, $f_o$=805.100 at 20C, $Q_o$=16,000

# CCL Module 4
# Arrived at SNS May 6, 2004

$E_o/E_{design}$

Stability



Coupling=0.618+0.612=1.220, $f_o$=805.100 at 20C, $Q_o$=16,000